

Reprints

REPORT DOCUMENTATION PAGE		READ INSTRUCTIONS BEFORE COMPLETING FORM
1. REPORT NUMBER AFFDL-TR	2. GOVT ACCESSION NO.	3. RECIPIENT'S CATALOG NUMBER
4. TITLE (and Subtitle) TRANSIENT THERMAL EFFECTS IN DISC BRAKES		5. TYPE OF REPORT & PERIOD COVERED Technical - Final Oct 77 - Apr 79
		6. PERFORMING ORG. REPORT NUMBER
7. AUTHOR(s) BEN J. BROOKMAN, JR.		8. CONTRACT OR GRANT NUMBER(s)
9. PERFORMING ORGANIZATION NAME AND ADDRESS Mechanical Branch (FEM) Air Force Flight Dynamics Laboratory Wright-Patterson AFB, OH 45433		10. PROGRAM ELEMENT, PROJECT, TASK AREA & WORK UNIT NUMBERS 2402-01-19
11. CONTROLLING OFFICE NAME AND ADDRESS Air Force Flight Dynamics Laboratory Wright-Patterson AFB, OH 45433		12. REPORT DATE November 1979
		13. NUMBER OF PAGES 464
14. MONITORING AGENCY NAME & ADDRESS (if different from Controlling Office)		15. SECURITY CLASS. (of this report) Unclassified
		15a. DECLASSIFICATION DOWNGRADING SCHEDULE
16. DISTRIBUTION STATEMENT (of this Report) Approved for Public Release; Distribution Unlimited		
17. DISTRIBUTION STATEMENT (of the abstract entered in Block 20, if different from Report)		
18. SUPPLEMENTARY NOTES		
19. KEY WORDS (Continue on reverse side if necessary and identify by block number) Brakes, Landing Gear, Finite Difference, Thermal Analysis		
20. ABSTRACT (Continue on reverse side if necessary and identify by block number) An investigation was undertaken with the ultimate objective being to develop a general theoretical model for predicting temperatures within the stators, rotors, rim, torque tube, tire, fuse plug and bead seat of a typical disc brake assembly. The effort was divided into four phases: I. Temperature Measurement Analysis, II. Theoretical Analysis of Brake and Component Parts, III. Full Scale Brake Tests, and IV. Correlation of Results.		

Block 20 Continued

Phase I contained both theoretical development and experimental tests designed to answer questions in the application of thermocouples for brake temperature measurement. A theoretical model was developed containing conduction, convection, and radiation heat transfer to a thermocouple bead placed in a hole at the bottom of which the temperature was desired. The effects of thermocouple lead wire diameter, bead diameter and distance from the hole bottom were explored. Experimentally, nineteen tests were conducted on ten type K thermocouple configurations in a bench test apparatus consisting of a block of carbon approximately .45 x 2. x 3. in. The carbon block was heated from each side by a bank of high intensity tungsten-filament quartz lamps. Each test consisted of heating the thermocouple to 1500^oF in approximately 50 seconds. The best two thermocouple configurations were the sheathed type, one of which had a grounded junction, and the other of which had an exposed junction.

Phase II, the brake theoretical analysis, contained the development of a transient finite difference theoretical model to predict the temperature within the stators, rotors, and brake housing of a typical disc brake. The model contains provisions for predicting temperature within the wheel, rim, and tire. The effort included development of one dimensional, two dimensional and three dimensional heat transfer models. The effort is unique in that it combines variable thermal conductivity, variable heat capacity, rotor-stator interface contact resistance, experimentally determined radiative/convective heat transfer coefficients, and allowable temperature variation from stator to stator and rotor to rotor. The inclusion of variable thermal conductivity is especially important with the use of carbon composite brakes because the conductivity is variable not only with temperature, but also with direction. This added variable is due to the carbon disc build-up by ply direction or random fiber orientation. In addition to the multidisc theoretical development, a caliper type brake is analyzed, and a finite difference model including all required equations is developed.

Phase III, the full scale brake tests, employed an F-14 size, four rotor, multidisc brake tested with a 192 inch diameter inertial dynamometer. Two heat sink materials were tested, beryllium and carbon composite, so that different thermal conductivities, densities, and heat capacities could be used. Tests were conducted at approximately 6.7 and 11.2 million ft-lbs of energy with decelerations ranging from about 2. to 8. ft/sec² and initial velocities ranging from 207. to 274. ft/sec. Test results were used to calculate convective/radiative heat transfer coefficients, and for comparison to theory.

The correlation of results, Phase IV, showed that the one dimensional axial, and the one dimensional radial models predict peak temperatures during a brake stop that are up to 31% and 16% higher than experiment, respectively. The two dimensional model predicts peak temperatures within 5% of experiment in three out of four cases considered, with the fourth case less than 8%. The peak temperature predictions within the torque tube, fuse plug, drive lug, bead seat and contained air were within 10% of experiment for most cases.

FOREWORD

The work contained herein was conducted under the in-house Job Order Number 24020119 with the title "Carbon Brake Performance." The effort concerned brake temperature prediction analysis resulting in computer programs, the results of which were compared to in-house conducted experiments. The work was accomplished in the Mechanical Branch (FEM), Vehicle Equipment Division, Air Force Flight Dynamics Laboratory, Wright-Patterson Air Force Base, Ohio.

The author wishes to thank the following persons for running computer programs, plotting curves and making computations: M. Jaramillo, D. Smith, D. Breslin, and J. Putman. Also the continued support of the effort by Dr. H. K. Brewer, A. V. Petersons, and D. J. Perez kept the total project constantly moving forward.

Contrails

Contrails

TABLE OF CONTENTS

FOREWORD	iii
TABLE OF CONTENTS	v
LIST OF TABLES	viii
LIST OF ILLUSTRATIONS	ix
LIST OF SYMBOLS	xvii

CHAPTER

I. INTRODUCTION	1
Background	1
Statement of the Problem	4
II. REVIEW OF THE LITERATURE	6
Overall	6
Class One--Caliper	6
Class Two--Multidisc	8
Summary	9
III. TEMPERATURE MEASUREMENT ANALYSIS	14
Introduction	14
Theoretical Model	14
Bench Tests	33
IV. FULL-SCALE BRAKE TESTS	63
Introduction	63
Test Apparatus	64
Test Plan	77
Instrumentation	81
Results	91
V. THEORETICAL DEVELOPMENT	113
Introduction	113
Numerical Solution Technique Selection	114
One-Dimensional Radial	134
One-Dimensional Axial	145
Two-Dimensional Radial/Axial (R/S Pair)	156
Three-Dimensional (R/S Pair)	168
Three-Dimensional Caliper	182
Two-Dimensional (Entire Brake/Wheel/Tire)	193

Contrails

TABLE OF CONTENTS continued

CHAPTER		
VI.	CORRELATION OF RESULTS	199
	Introduction	199
	Temperature-Time History, Experiment, 1-DA, 1-DR, 2-DRA	202
	Temperature-Time History, Constant/Variable Torque, and Pads/No Pads	210
	Temperature-Time History, 2-DRA, and 3-D Circumferential Direction Temperature Gradient, 3-D	215
	Disc, Torque Tube, Rim and Contained Air Temperatures, 2-D	216
	Conclusions	220
VII.	UNIQUENESS AND OVERALL CONCLUSIONS	237
	Uniqueness	240
	Overall Conclusions	241
VIII.	MODEL LIMITATIONS AND RECOMMENDATIONS	243
	Model Limitations	243
	Recommendations	244
REFERENCES	246
APPENDIX		
A	Program Listing for One-Dimensional Transient Temperature Distribution of Chapter III	251
B	Program Listing for Two-Dimensional Transient Temperature Distribution of Chapter III	253
C	Program Listing for Thermocouple Bead Temperature Analysis of Chapter III	256
D	Thermocouple Calibration, Calibration Certificate and Checklist for Running Thermocouple Tests of Chapter III	259
E	Recorded Test Parameters vs Time from Chapter IV	264
F	Temperature versus Time Plots for Stator 2, Rotor 2 and Torque Tube	275

Contrails

TABLE OF CONTENTS continued

APPENDIX

G	Temperature versus Axial Position Plots at Various Times	286
H	Temperature versus Time Plots for Radially Located Thermocouples	297
I	Temperature vs Radial Position Plots at Various Times	303
J	Convective/Radiative Heat Transfer Calculation Procedure	309
K	Heat Capacity and Thermal Conductivity Curves	315
L	Program Listing for One-Dimensional Radial (IDR) Temperature Prediction Model	320
M	Contact Resistance Values and Calculation Procedure	329
N	Program Listing for One-Dimensional Axial (IDA) Temperature Prediction Model	332
O	Boundary Condition Equations for Two-Dimensional Radial/Axial (R/S Pair) Model	341
P	Program Listing for Two-Dimensional Radial/Axial (R/S Pair) (IIDRA) Temperature Prediction Model	353
Q	Boundary Condition Equations for Three-Dimensional (R/S Pair) Model	371
R	Program Listing for Three-Dimensional (R/S Pair) Temperature Prediction Model	381
S	Equations for Two-Dimensional (Entire Brake/Wheel/Tire) Model	407
T	Program Listing for Two-Dimensional (Entire Brake/Wheel/Tire) Model	413

Contrails

LIST OF TABLES

TABLE		PAGE
1.	Literature Search Summary	11
2.	Thermocouple Description	38
3.	Test Temperature at Various Baseline Temperatures	44
4.	Percent Difference of Test Thermocouple from Thermocouple Numbers 47	47
5.	Peak Temperature Comparison	57
6.	F-14 Brake Test Plan	79
7.	Typical Test Data	93
8.	Exact, Finite Difference and Finite Element Comparison	132
9.	Selected Computer Program Input Values	200
10.	Experiment vs Theory Peak Temperature Comparison	236

Contrails

LIST OF ILLUSTRATIONS

FIGURE		Page
1.	Brake Assembly	2
2.	Actual Hardware	3
3.	Temperature Measurement Analysis Theoretical Model	15
4.	One-Dimensional Axial Temperature Distribution Model	16
5.	Temperature Lag versus Dimensionless Distance . .	19
6.	Two-Dimensional Air Cavity Temperature Distribution Model	21
7.	Air Cavity X-Direction Centerline Temperature . .	24
8.	Thermocouple Model-Radius Effect	29
9.	Thermocouple Model-Conduction Effect	30
10.	Sketch of Thermocouple Test Apparatus	35
11.	Test Specimen Photograph	36
12.	Sketch of Thermocouple Circuit	37
13.	Grounded, Ungrounded, and Exposed Thermocouples . .	41
14.	Typical X-Y-Y' Plotter Output	43
15.	Accuracy of Different Thermocouple Types	49
16.	Accuracy of Glass Insulation Thermocouples	51
17.	Thermocouple Comparison/Welding Method	52
18.	Effect of Thermocouple Distance from Hole Bottom .	54
19.	Temperature vs Time, Thermocouple Comparison . . .	55
20.	Typical Tire-Brake Test Dynamometer	65
21.	Typical Beryllium Rotor	68
22.	Typical Beryllium Stator	69

Contrails

LIST OF ILLUSTRATIONS continued

FIGURE		PAGE
23.	Typical Carbon Composite Rotor	70
24.	Typical Carbon Composite Stator	71
25.	Beryllium Brake Exploded View	72
26.	Assembled Beryllium Brake	74
27.	Beryllium Brake on Test Mandrel	75
28.	Beryllium Brake with Tire and Wheel Assembly	76
29.	Beryllium Heat Sink Thermocouple Locations	82
30.	Carbon Heat Sink Thermocouple Locations	83
31.	Carbon Rotor 3 Thermocouple Locations	85
32.	Carbon Stator 1 and 2 Thermocouple Locations	86
33.	Overall Thermocouple Locations	87
34.	Data Recording Test Center	90
35.	Brush Recorder Instruments	92
36.	Recorded Test Parameters vs Time	94
37.	Temperature vs Time for Stator 2, Rotor 2 and Torque Tube	96
38.	Temperature vs Axial Position	98
39.	Temperature vs Time for Radial Thermocouples	100
40.	Temperature vs Radial Position	101
41.	Stator 1 Radial Temperature (Test 1.1-3)	103
42.	Stator 1 Radial Temperature (Test 4.2-3)	104
43.	Stator 1 Axial Temperature, Radius = 4.44 in. (Test 1.1-3)	105
44.	Stator 1 Axial Temperature, Radius = 4.44 in. (Test 4.2-3)	106

Contrails

LIST OF ILLUSTRATIONS continued

FIGURE		PAGE
45.	Temperature vs Time-Tire/Wheel Assembly (Test 1.1-3)	107
46.	Temperature vs Time-Tire/Wheel Assembly (Test 4.2-3)	109
47.	Temperature vs Time-Tire/Wheel Assembly (Test 7.2-3)	110
48.	Temperature vs Time-Tire/Wheel Assembly (Test 8.1-2)	111
49.	Theoretical Model	115
50.	Temperature Difference vs Position, Finite Difference, Time = .5	121
51.	Temperature Difference vs Position, Finite Difference, Time = 1.0	122
52.	Temperature Difference vs Position, Finite Element, Time = .5	123
53.	Temperature Difference vs Position, Finite Element, Time = 1.0	124
54.	Temperature Difference vs Position, Finite Difference and Element, Time = .5	125
55.	Temperature Difference vs Position, Finite Difference and Element, Time = 1.0	127
56.	Temperature Difference vs Time, DT = .00390625 . .	128
57.	Temperature Difference vs Time, DT = .0078125 . .	129
58.	Time Increment vs Computer Time Required	131
59.	One-Dimensional Radial Model	135
60.	Rotor/Stator Interface	143
61.	One-Dimensional Axial Model	146
62.	Expanded Rotor/Stator Interface (1-D Axial) . . .	150

Contrails

LIST OF ILLUSTRATIONS continued

FIGURE		PAGE
63.	Two-Dimensional Radial/Axial Model (Rotor/Stator Pair)	157
64.	Expanded Rotor/Stator Interface (2-D Radial Axial)	161
65.	Typical Rotor and Stator	170
66.	Isometric View of Rotor and Stator Sectors	171
67.	Rotor Sector Positions vs Time Increment	176
68.	Caliper Brake Model	183
69.	Caliper Brake Node Arrangement	184
70.	Expanded Lining/Rotor Interface	188
71.	Multidisc Brake Model	194
72.	Node 12 Heat Transfer Rates	196
73.	Temperature vs Time at R = 5.5 in., Test 1.1-3, 1-D vs 2-DRA)	203
74.	Temperature vs Time at R = 5.5 in. (Test 4-2-3, 1-D vs 2-DRA)	206
75.	Temperature vs Time at R = 4.4 in. (Test 7.2-3, 1-D vs 2-DRA)	207
76.	Temperature vs Time at R = 4.4. in. (Test 8.1-2, 1-D vs 2-DRA)	208
77.	Torque and Flywheel Energy vs Time	211
78.	Temperature vs Time at R = 5.5 in. (Test 1.1-3, Constant Torque Effect)	213
79.	Temperature vs Time at R = 4.4 in. (Test 7.2-3, Wear Pad and Constant Torque Effect)	214
80.	Temperature vs Time at 5.5 in. (Test 1.1-3, 2-DRA vs 3-D)	217

Contrails

LIST OF ILLUSTRATIONS continued

FIGURE		PAGE
81.	Temperature v Time at 4.4 in. (Test 7.2-3, 2-DRA vs 3-D)	218
82.	Temperature vs Circumferential Direction (Test 1.1-3)	219
83.	Temperature vs Circumferential Direction (Test 7.2-3)	221
84.	Temperature vs Time, Stator-Torque Tube (Test 1.1-3)	222
85.	Temperature vs Time, Stator-Torque Tube (Test 4.2-3)	223
86.	Temperature vs Time, Stator-Torque Tube (Test 7.2-3)	224
87.	Temperature vs Time, Stator-Torque Tube (Test 8.1-2)	225
88.	Temperature vs Time, Fuse Plug-Drive Lug (Test 1.1-3)	227
89.	Temperature vs Time, Fuse Plug-Drive Lug (Test 4.2-3)	228
90.	Temperature vs Time, Fuse Plug-Drive Lug (Test 7.2-3)	229
91.	Temperature vs Time, Fuse Plug-Drive Lug (Test 8.1-2)	230
92.	Temperature vs Time, Bead Seat-Contained Air (Test 1.1-3)	232
93.	Temperature vs Time, Bead Seat-Contained Air (Test 4.2-3)	233
94.	Temperature vs Time, Bead Seat-Contained Air (Test 7.2-3)	234
95.	Temperature vs Time, Bead Seat-Contained Air (Test 8.1-2)	235

LIST OF ILLUSTRATIONS continued

FIGURE		PAGE
APPENDIX		
E-1.	Test Parameters vs Time (Test 1.1-3)	265
E-2.	Test Parameters vs Time (Test 2.1-2)	266
E-3.	Test Parameters vs Time (Test 2.2-3)	267
E-4.	Test Parameters vs Time (Test 3.1-2)	268
E-5.	Test Parameters vs Time (Test 4.2-3)	269
E-6.	Test Parameters vs Time (Test 6.1-3)	270
E-7.	Test Parameters vs Time (Test 7.1-2)	271
E-8.	Test Parameters vs Time (Test 7.2-3)	272
E-9.	Test Parameters vs Time (Test 8.1-2)	273
E-10.	Test Parameters vs Time (Test 9.2-2)	274
F-1.	Temperature vs Time for Stator 2, Rotor 2, Torque Tube (Test 1.1-3)	276
F-2.	Temperature vs Time for Stator 2, Rotor 2, Torque Tube (Test 2.1-2)	277
F-3.	Temperature vs Time for Stator 2, Rotor 2, Torque Tube (Test 2.2-3)	278
F-4.	Temperature vs Time for Stator 2, Rotor 2, Torque Tube (Test 3.1-2)	279
F-5.	Temperature vs Time for Stator 2, Rotor 2, Torque Tube (Test 4.2-3)	280
F-6.	Temperature vs Time for Stator 2, Rotor 2, Torque Tube (Test 6.1-3)	281
F-7.	Temperature vs Time for Stator 2, Rotor 2, Torque Tube (Test 7.1-2)	282
F-8.	Temperature vs Time for Stator 2, Rotor 2, Torque Tube (Test 7.2-3)	283

Contrails

LIST OF ILLUSTRATIONS continued

FIGURE		PAGE
APPENDIX		
F-9.	Temperature vs Time for Stator 2, Rotor 2, Torque Tube, 8.1-2	284
F-10.	Temperature vs Time for Stator 2, Rotor 2, Torque Tube (Test 9.2-2)	285
G-1.	Temperature vs Axial Position (Test 1.1-3)	287
G-2.	Temperature vs Axial Position (Test 2.1-2)	288
G-3.	Temperature vs Axial Position (Test 2.2-3)	289
G-4.	Temperature vs Axial Position (Test 3.1-2)	290
G-5.	Temperature vs Axial Position (Test 4.2-3)	291
G-6.	Temperature vs Axial Position (Test 6.1-3)	292
G-7.	Temperature vs Axial Position (Test 7.1-2)	293
G-8.	Temperature vs Axial Position (Test 7.2-3)	294
G-9.	Temperature vs Axial Position (Test 8.1-2)	295
G-10.	Temperature vs Axial Position (Test 9.2-2)	296
H-1.	Temperature vs Time for Radial Thermocouples (Test 1.1-3)	298
H-2.	Temperature vs Time for Radial Thermocouples (Test 2.1-2)	299
H-3.	Temperature vs Time for Radial Thermocouples (Test 2.2-3)..	300
H-4.	Temperature vs Time for Radial Thermocouples (Test 3.1-2)	301
H-5.	Temperature vs Time for Radial Thermocouples (Test 4.2-3)	302
I-1.	Temperature vs Radial Position (Test 1.1-3)	304

LIST OF ILLUSTRATIONS continued

FIGURE		PAGE
APPENDIX		
I-2.	Temperature vs Radial Position (Test 2.1-2)	305
I-3.	Temperature vs Radial Position (Test 2.2-3)	306
I-4.	Temperature vs Radial Position (Test 3.1-2)	307
I-5.	Temperature vs Radial Position (Test 4.2-3)	308
J-1.	Carbon Combined Heat Transfer Coefficient	311
J-2.	Beryllium Combined Heat Transfer Coefficient	312
K-1.	Heat Capacity vs Temperature	317
K-2.	Thermal Conductivity vs Temperature	318
K-3.	Thermal Diffusivity vs Temperature	319
O-1.	Two-Dimensional Grid Numbering Scheme	342
O-2.	Two-Dimensional Grid Numbering Scheme (with wear pads)	349
Q-1.	Wear Surface Element Identification	379

LIST OF SYMBOLS

a	Air Cavity y-Direction Dimension
a_1	Stator Thickness
A	Ratio of x to y Direction Dimensions
A_b	Thermocouple Bead Surface Area
A_c	Area of Carbon Radiating Heat to Bead
A_e	Element Area
A_k	Heat Conduction Cross-Sectional Area
\bar{A}	Matrix in One-Dimensional Finite Difference Analysis
b	Air Cavity x-Direction Dimension
\bar{B}	Combination of Capacitance and Conduction Matrices
C	Heat Capacity
C_1	Constant Associated with Pressure Profile
C_a	Average Heat Capacity
\bar{C}	Global Capacitance Matrix
D	Distance Through Which Force Acts
DT	Incremental Time
DX	Incremental x-Distance
DXA	Average of DXR and DXS
DXR	DX of Rotor
DXS	DX of Stator
DY	Incremental y-Distance

Contrails

E	Total Energy of Elemental Mass
EL	Element
$f(r)$	Function of Radius
F_{c-b}	Radiation Shape Factor From Carbon Boundary to Thermocouple Bead
F_e	Force Pushing Rotor Element Past Stator Element
FD	Finite Difference
FE	Finite Element
h	Convective/Radiative Heat Transfer Coefficient
h_1	2 Times the Disc Thickness
\bar{h}	Average Convection Heat Transfer Coefficient
I	Node Index
I_n	Flywheel Inertia
I_v	Variational Statement Integral
IE	Inertia Equivalent
J	Node Index
K	Thermal Conductivity
K_r	Thermal Conductivity in r-Direction
K_x	Thermal Conductivity in x-Direction
K.E.	Kinetic Energy
\bar{K}	Global Conductance Matrix
L	x-Direction Length
M	Mass of Vehicle
n	Summation Index
N	The Number of Rotor/Stator Interfaces
P_e	Normal Pressure Exerted on Element

Contrails

$\dot{q}_{\text{conduction}}$	Conduction Heat Transfer Rate
$\dot{q}_{\text{convection}}$	Convection Heat Transfer Rate
\dot{q}_{in}	Heat Transfer Rate In
\dot{q}_{out}	Heat Transfer Rate Out
$\dot{q}_{\text{radiation}}$	Radiation Heat Transfer Rate
r	Radial Coordinate
R	Bead Radius
R_f	Flywheel Outer Radius
R_r	Tire Rolling Radius
RE	Contact Resistance
RE_r	Rotor Contact Resistance
RE_s	Stator Contact Resistance
RIR	Rotor Inside Radius
ROR	Rotor Outside Radius
RT	Rotor Half Thickness
SIR	Stator Inside Radius
SOR	Stator Outside Radius
ST	Stator Half Thickness
t	Time
t_s	Stop Time
t_T	Time of Occurrence of Adjusted Peak Temperature of Test Thermocouple
t_{47}	Time of Occurrence of Peak Temperature of Test 47 Thermocouple
t'	Dimensionless Time

Contrails

t'_{sn}	Dimensionless Stop Time
T	Temperature
T_{air}	Temperature of Air Cavity at the Bead
T_b	Current Temperature of Baseline Thermocouple
T_{bc}	Temperature of Thermocouple Bead
T_{b47}	Baseline Temperature of Test 47
T_c	Carbon Temperature
T_{exact}	Dimensionless Temperature from Exact Analysis
T_m	Rotor/Stator Interface Temperature
T_o	Initial Temperature
T_{rs}	Torque Generated at Rotor/Stator Interface
T_s	Starting Temperature
T_t	Total Torque Transmitted by the Brake
T_{ta}	Adjusted Temperature of Test T/C
T_{tc}	Current Temperature of Test T/C
T_{test}	Temperature of Test Thermocouple
T_{∞}	Ambient Temperature
T_{47}	Temperature of Test 47 T/C
T^t	Temperature at Time t
T'	Dimensionless Temperature (In cases where dimensionless temperature is not used, this T' symbol indicates the temperature one time step advanced from T^t . This is noted within the text.)
\bar{T}	Temperature Matrix
T/C	Thermocouple
TP	Peak Temperature

Contrails

U	Internal Energy
U_o	Constant Reference Internal Energy
V	Volume
V_o	Initial Velocity of Flywheel Outer Radius
V_v	Vehicle Velocity
\dot{W}_e	The Rate Work Crosses the Elemental Boundary
\dot{W}''	Work Rate per Unit Area
x	Axial Coordinate
x'	Dimensionless Axial Coordinate
y	Coordinate Perpendicular to X
y'	Dimensionless y-Coordinate

GREEK

α	Thermal Diffusivity
Δ	Increment
θ	Angular Position
μ	Coefficient of Friction
π	Constant - 3.14159
ρ	Density
σ	Stefan-Boltzmann Constant
ω	Rotor Angular Velocity
ω_f	Flywheel Angular Velocity

CHAPTER I

INTRODUCTION

Background

The primary function of a brake system is to convert the kinetic energy of vehicle motion into internal energy while the vehicle is being stopped. In addition to this primary function, the brake must store the absorbed heat for a finite amount of time so that overheating of surrounding vehicle hardware will not occur. Two methods for accomplishing these functions are the use of drum brakes and disc brakes. Disc brakes are used in aircraft, trucks, and many automobile braking systems.

A typical disc brake assembly as used in numerous car, truck, and aircraft applications consists of two basic parts, the brake heat sink and the brake housing (Figure 1). The heat sink is built up of alternating stators and rotors which take the shape of annuli. A photograph of actual hardware from an aircraft is shown in Figure 2. The rotors are keyed to the rotating wheel while the stators are keyed to the fixed vehicle axle. The number of keys is dependent upon the particular application. During vehicle stopping, the rotors and stators are pushed together using hydraulically actuated pistons such that the vehicle kinetic energy is transformed into heat due to the friction between the stators and rotors. The contact pressure is normally

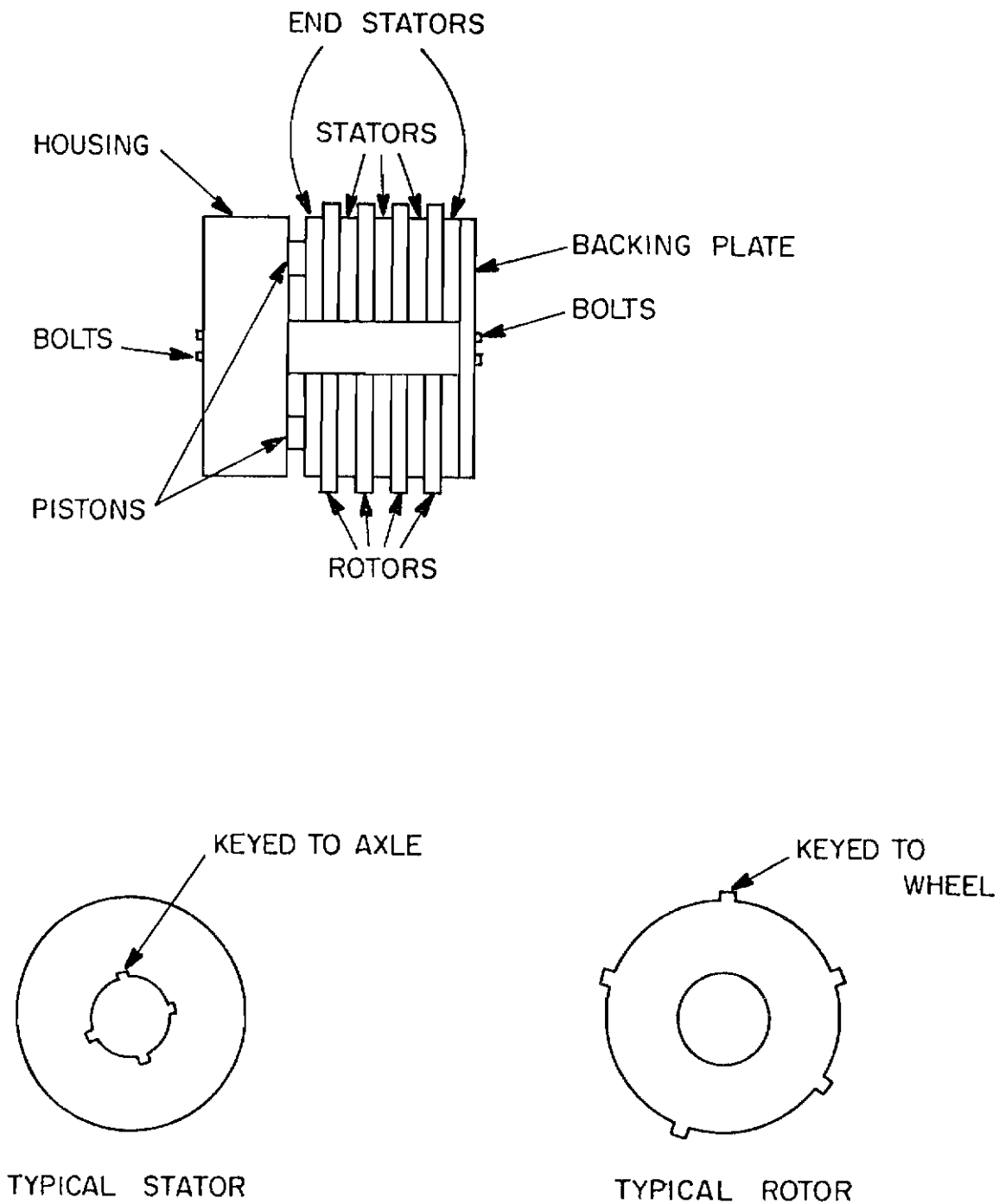


Figure 1. Brake Assembly

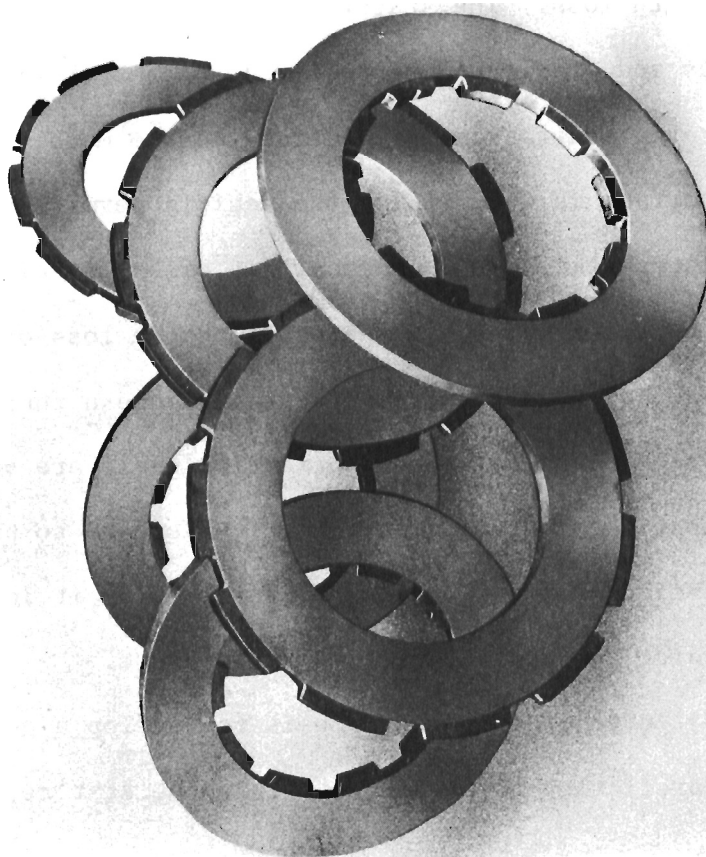
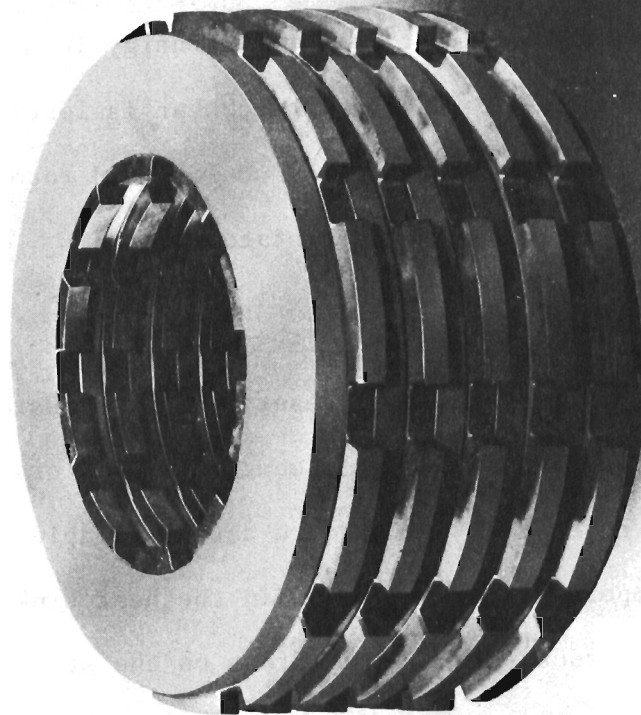


Figure 2. Actual Hardware

Contrails

maintained at a relatively constant value as the vehicle is brought to a stop. This results in a time-varying energy input into the stators and rotors. During this energy input, heat is lost due to convection and radiation from the edges of the stators and rotors and by conduction at the key locations and end stators.

Statement of the Problem

The disc brake arrangement described above must be designed to meet the two functions previously mentioned. In order to do this, the designer must have brake temperature data available to him. Specifically, the temperature distribution in the heat sink is required to determine the structural heating effect on the stators, rotors, brake housing, wheel, and tire. The tire peak temperature is required to prevent deterioration of the rubber properties and subsequent failure due to strength loss. The stator, rotor, brake housing and wheel temperatures and gradients are required so that thermally induced stress patterns and fatigue predictions can be made. The cooling rate is also important in determining the vehicle permissible "time between stops." Since brake wear in common heat sinks is related to heat sink rubbing area and since high temperatures cause loss of material through oxidation, actual heat sink temperatures become a function of brake life. In order that the brake lubrication seals are protected, it is necessary that the hydraulic fluid, which is used to pressurize the pistons, remain below a given temperature. Thus it is important to be able to predict the hydraulic fluid temperature.

The objective of this research is to develop a general model for accurately predicting temperatures within the stators, rotors, and

Contrails

brake housing of a typical disc brake. The model will contain provisions for the calculation of temperature within the wheel, axle, and tire. One-, two-, and three-dimensional models are needed for comparison with each other, as well as with experiment. More than one theoretical model is required so that the most accurate and most expedient model for a particular application can be identified. This research is to apply equally well to caliper type brakes (single-rotor) and to multidisc type brakes. Separate theoretical models are required to accomplish this generality. Experiments for comparison to the theory are an extremely important part of this effort since the validity of the theoretical models will ultimately be judged by how close the experimental curves are matched.

CHAPTER II

REVIEW OF THE LITERATURE

Overall

Efforts at obtaining the temperature distribution in a brake and adjacent hardware can be divided into two classes depending upon the particular style brake analyzed. The first is a single-rotor type brake in which the stators are replaced by a pair of sector-shaped calipers. Energy is then transferred from the rotor into the calipers. The second differs from the first in that the stator is always a complete annulus. While class one is limited to a single rotor, class two can have any number of rotors and corresponding stators. Clearly, class one is a special case of class two.

Class One--Caliper

The class one type brake has been analyzed by Evans and Newcomb.^{1*} They assume that temperature is not a function of the radial or angular directions within the brake. Newcomb and El-Sherbiny² used a similar analytical model but added in a liquid cooling boundary condition and assumed a constant value for thermal conductivity. Secrist and Hornbeck³ assumed that temperature varied in the radial direction but remained constant in the axial and angular directions. They employed a finite difference technique to obtain a solution. An experimental as well as analytical analysis was conducted by Limpert⁴ in which temperature was assumed to vary in the axial direction only. He

Contrails

assumed a constant thermal conductivity and used a finite difference technique. Hartter, Schwartz, and Rhee⁵ conducted tests on a heavy truck brake and used the results to refine their finite difference theoretical analysis. One-dimensional conduction in the axial direction was modeled assuming constant thermal conductivity. Limpert⁶ again assumed that temperature varied in the axial direction only, but included within his finite difference technique a method for calculating the stress in the rotor. Rusnak, Schwartz, and Coleman⁷ numerically analyzed the axial direction allowing for variable thermal conductivity with the intent of rating several different materials. A study was conducted by Dike⁸ that solved the heat conduction equation in the radial and axial directions, but this study assumed that the heat into the brake at the sliding surface was independent of radius. Santini and Kennedy⁹ conducted an entirely experimental effort in which the caliper part of the brake was imbedded with thermocouples. They pointed out the lack of published brake experimental data. These two authors, along with Ling,¹⁰ conducted constant speed experiments with the intent of evaluating external cooling and rotor design modifications. Schwartz¹¹ used the finite difference technique for looking at the radial and axial directions. The caliper was not analyzed and the convection heat transfer coefficients were entirely theoretical. Sinclair and Gulick¹² performed no analyses but discussed the advantages of using a dynamometer for testing rather than a vehicle. Morgan and Dennis¹³ used the finite element technique in the radial and axial directions to predict temperature. Parker and Newcomb¹⁴

Contrails

developed an exact procedure for predicting the surface temperature of a caliper rotor as a function of time.

Class Two--Multidisc

The class two type of brake (annular stators) has been studied by Anderle¹⁵ with the assumption of axial heat transfer only. He analyzed a rotor-stator pair and assumed that all other pairs would have the same temperature profile. A finite difference approach was used in which half of the input energy at the sliding surface was assumed to go into the stator with the remaining half going into the rotor. Claridge¹⁶ developed a brake model that considered the axial direction only. His main objective was to show how a computer could be used in the design of the complete braking system. Scaringe, Ho, and Peterson¹⁷ conducted a primarily experimental effort to evaluate an air-cooling scheme. The theoretical model alluded to assumed no heat conduction in the radial or angular directions. Assumptions of constant thermal conductivity and constant heat input were also made. Kennedy, Wu, and Ling¹⁸ analyzed a stator-rotor pair employing the finite element approach with assumptions of heat transfer in the axial direction only. The results were compared to experiments. Mercer¹⁹ has used a finite difference approach to analyze a rotor-stator pair, allowing heat transfer in the radial as well as axial directions. The energy input is varied with radius as well as time. The angular direction is ignored, as well as any losses to surrounding components. Experimental studies have been accomplished by Ho and Peterson^{20, 21} in which sliding tests were used to simulate braking. These tests were aimed at materials development. Unfortunately, it has been

Contrails

found, sliding-type tests do not adequately simulate the conditions within the brake due to different geometry and cooling conditions. Ho, Kennedy, and Peterson²² conducted two-rotor tests in which the temperature at locations within the stators was monitored. Wagner²³ reports an experimental comparison of two materials run within a two-rotor brake. Results consistently show both radial and axial (stator-to-stator and rotor-to-rotor) temperature variations that are significant (up to 40%). Bender and Han²⁴ used a finite difference model to look at brake temperatures but lumped each stator and rotor so that no temperature variation was allowed within the stator or rotor. Brewer²⁵ analyzed one rotor using a one-dimensional finite difference approach with constant properties. Donaldson, Stocks, Teter, and Rebholz²⁶ also used finite differences but looked at the radial as well as the axial direction. They analyzed a single rotor and stator and assumed that the others were identical. They also found a theoretical convective heat transfer coefficient. Lee²⁷ analyzed all three directions but performed no experiments, assumed an energy split between the rotor and stator, used theoretical convection heat transfer coefficients, and looked at only one pair of discs. Nemeth and Wieter²⁸ employed a finite difference approach but used a lumped system that resulted in only one temperature for the rotor and one for the stator. Stout²⁹ conducted tests on a brake system designed for a space application in which the ambient temperature was 800°F.

Summary

In summary, past analyses have assumed that all rotors behaved the same and that all stators behaved the same. This ignores heat

Contrails

loss through the end stators. No theoretical model is currently available that accounts for the experimentally measured axial temperature variation from disc to disc. With such an analytical model, a brake heat sink could be designed such that it would have a minimum axial temperature gradient at the most used stopping conditions. This would reduce the high wear oxidation rate at the present heat sink high temperature area. Past efforts have assumed constant thermal properties which could result in significant error, especially at the high temperatures that are being routinely encountered in present-day heat sink materials (1500°F). Often an estimate is made of the fraction of generated heat that goes into a rotor and stator. This estimate is not required. Also, it is apparent that no comparison of model complexities has been reported. Thus, it is unclear which model should be used in a particular application. Extensive testing is also sketchy in the literature. When tests are conducted, they are usually not accompanied by a theoretical development. Table 1 is a summary table that lists authors, brake type, whether effort was experimental or theoretical, and whether thermal properties were varied with temperature.

TABLE 1

LITERATURE SEARCH SUMMARY

	Author	Caliper	Multi-disc	Theory ^a	Dimensions ^b	Experiment	Properties Variable ^c	Remarks ^d
1.	Evans ^e			F.D.	x	no	K-only	Oil used, energy split guessed
2.	Newcomb			Exact	x	no	no	
3.	Secrist			F.D.	r	no	no	
4.	Limpert			F.D.	x	yes	no	
5.	Hartter			F.D.	x, r	no	no	
6.	Limpert			F.D.	x	yes	no	Energy split by experiment
7.	Rusnak			F.D.	--	no	yes	Rotor lumped, pad lumped
8.	Dike			F.D.	x, r	no	no	Heat Input = f (r)
9.	Santini			no	--	yes	--	
10.	Santini			no	--	yes	--	External cooling
11.	Schwartz			F.D.	x, r	yes	yes	Caliper ignored, \bar{h} theoretical
12.	Sinclair			--	--	---	--	Discussed Dynamometer Advantage
13.	Morgan			F.E.	x, r	no	yes	
14.	Parker			Exact	none	no	no	Surface temperature = f(t)

11

TABLE 1--continued

Author	Caliper	Multi-disc	Theory ^a	Dimensions ^b	Experiment	Properties Variable ^c	Remarks ^d
15. Anderle		✓	F.D.	x	no	yes	Assumes 50-50 energy split
16. Claridge		✓	--	x	no	--	No results shown
17. Scaringe		✓	--	x	no	no	
18. Kennedy		✓	F.E.	x	yes	yes	Single Disc
19. Mercer		✓	F.D.	x, r	yes	yes	Single disc, energy split assumed
20. Ho		✓	no	--	yes	--	Two rotor brake
21. Peterson		✓	no	--	yes	--	
22. Ho		✓	no	--	yes	--	Two rotor brake
23. Wagner		✓	no	--	yes	--	Two rotor brake
24. Bender		✓	F.D.	--	no	yes	Rotor lumped, stator lumped
25. Brewer		✓	F.D.	x	no	no	Experiments excluded brake
26. Donaldson		✓	F.D.	x, r	yes	yes	h theo., single rotor and stator
27. Lee		✓	F.D.	x, r, θ	no	yes	h theo., 1 disk, en. split assumed
28. Nemeth		✓	F.D.	--	no	yes	Rotor lumped, stator lumped
29. Stout		✓	no	--	yes	--	Ambient temperature = 800°F

TABLE 1--continued

^aF.D. stands for Finite Difference.

F.E. stands for Finite Element.

no indicates No Theory Included.

-- indicates Theoretical Technique Unclear.

^bx is axial position, r is radial position, θ is angular position.

^cProperties refer to heat capacity and thermal conductivity.

^d \bar{h} refers to average convective heat transfer coefficient. Energy split refers to amount of energy going into the rotor at a sliding surface as opposed to amount of energy going into the stator at the same sliding surface.

^eIn the case of multiple authors, only the first is listed. The numbering system in this table is coincident with that used in the list of references.

CHAPTER III

TEMPERATURE MEASUREMENT ANALYSIS

Introduction

In any experimental program it is important to know the limitations of the equipment being used. In this research the measurement of temperature of brakes and their surrounding hardware is a major consideration. Different types and sizes of thermocouples are routinely used interchangeably by many organizations with little thought given to the resulting accuracy or response time of the thermocouple being used. Thermocouple manufacturers often give time constant data, but this is only valid for a particular application. The problems inherent in thermocouple temperature measurement are discussed in the literature along with recommended methods to construct, locate, and use thermocouples. Although this information is important, the deviations that could result from compromises that may have to be made as a result of geometry, availability, time, resources, or durability are not discussed in the literature. Clearly, a need exists in a particular application for answers to some of these thermocouple unknowns in order to obtain the best results.

Theoretical Model

A model is used to determine the temperature reached within a thermocouple bead (the welded junction of the two dissimilar metals of the thermocouple) as a function of the temperature of the material

surrounding the bead. In order to accomplish this analysis, a typical temperature distribution in a disc of a brake must be found, as well as the temperature distribution in the air within the hole into which the thermocouple is embedded. This model is shown in Figure 3.

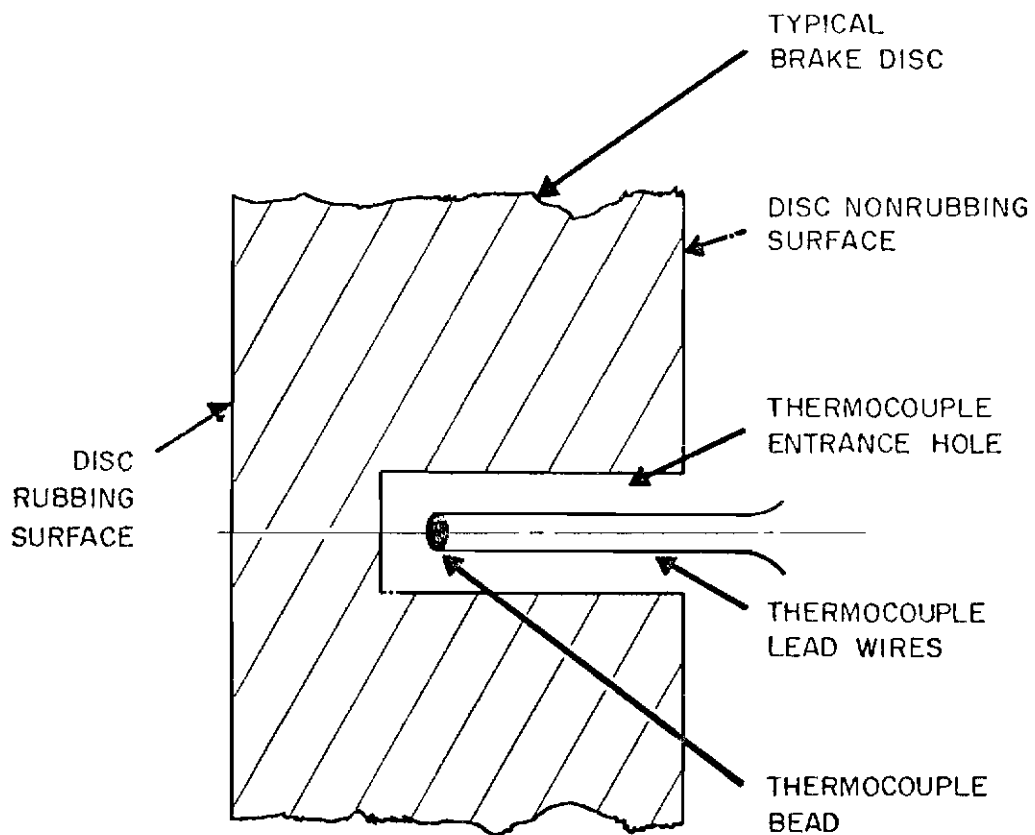


Figure 3. Temperature Measurement Analysis Theoretical Model

One-Dimensional Brake Material Analysis

As a first step, the one-dimensional temperature distribution is needed. Figure 4 shows the model used for obtaining this temperature

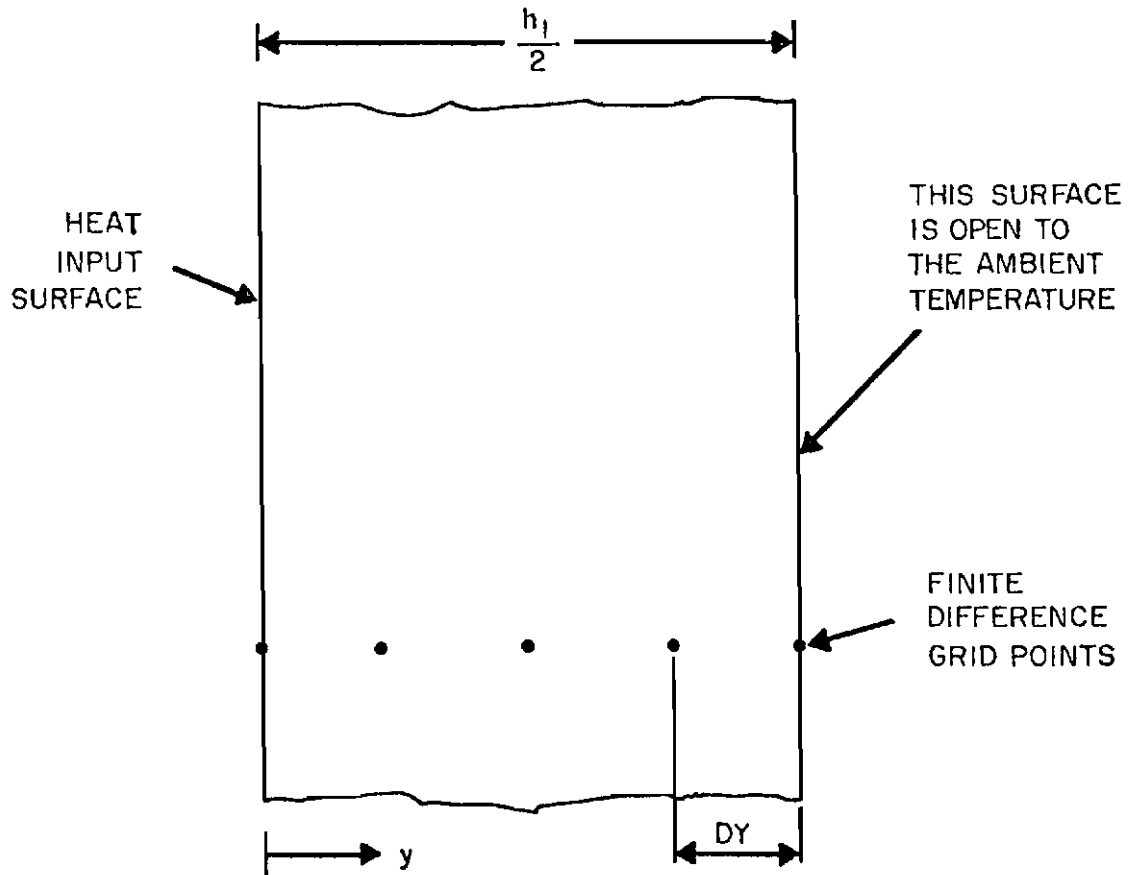


Figure 4. One-Dimensional Axial Temperature Distribution Model

distribution in the brake material. The governing one-dimensional transient equation³⁰ in dimensionless form is:

$$\frac{\partial^2 T'}{\partial y'^2} = \frac{\partial T'}{\partial t'} \quad (1)$$

Contrails

where T' is temperature, y' is distance and t' is time. [See Equation (4) for definition.] The initial condition is:

$$T'(y', 0) = 0 \quad (2)$$

One boundary condition is:

$$T'(0, t') = \frac{t'}{t'_{sn}} \frac{TP - T_0}{T_0} \quad (3)$$

where t'_{sn} is the dimensionless stop time (time required for the brake to come to rest), T_0 is the initial temperature and TP is the peak temperature during the stop. Equation (3) was selected as the boundary condition at $y' = 0$ since experiment showed that a linear surface temperature increasing to a peak at the stop time was a good approximation to the actual temperature rise. In terms of dimensional variables (depicted without primes), the above are:

$$y' = \frac{2y}{h_1}, \quad t' = \frac{\alpha t}{\left(\frac{h_1 \bar{h}}{2}\right)^2}, \quad T' = \frac{(T - T_0)}{T_0} \quad (4)$$

where α is the thermal diffusivity and T_0 is the initial temperature.

The second boundary condition is:

$$\left. \frac{\partial T'}{\partial y'} \right|_{y' = 1} = -\left(\frac{h_1 \bar{h}}{2K}\right) T'(1, t') \quad (5)$$

where $h_1/2$ is the disc thickness as seen in Figure 4, K is the thermal conductivity and \bar{h} is the average convective heat transfer coefficient.

Contrails

With the use of standard finite difference techniques and the Euler time marching technique, Equation (1) becomes:

$$T^{t+\Delta t}(I) = T^t(I) \times \left[1 - \frac{2 DT}{(DY \times DY)} \right] + \left[T^t(I + 1) + T^t(I - 1) \right] \times \frac{DT}{(DY \times DY)} \quad (6)$$

where t indicates time, $t + \Delta t$ is one time increment advanced from t , I is the I th node in the finite difference network shown in Figure 4, DY is the distance between two nodes, and DT is the time increment. The primes have been omitted from (6) for clarity. The computer program solving Equations (2) through (6) is shown in Appendix A. The material constants used in this program were for a carbon composite brake material. Carbon was selected at this point since full-scale tests (discussed in Chapter 4), employed carbon and beryllium, and the carbon material provided the highest temperature gradients. The time-varying boundary condition was selected because it was indicative of the rubbing surface temperature rise of past full-scale test results. Specific numbers were chosen from a typical carbon brake test. Results showed that for a peak temperature of 1170°F and an input rate of 40°F/sec, the actual temperature at each node was lower at each time step by an amount independent of the time step. This is shown in Figure 5 as a plot of temperature lag from the heat input surface versus the dimensionless distance.

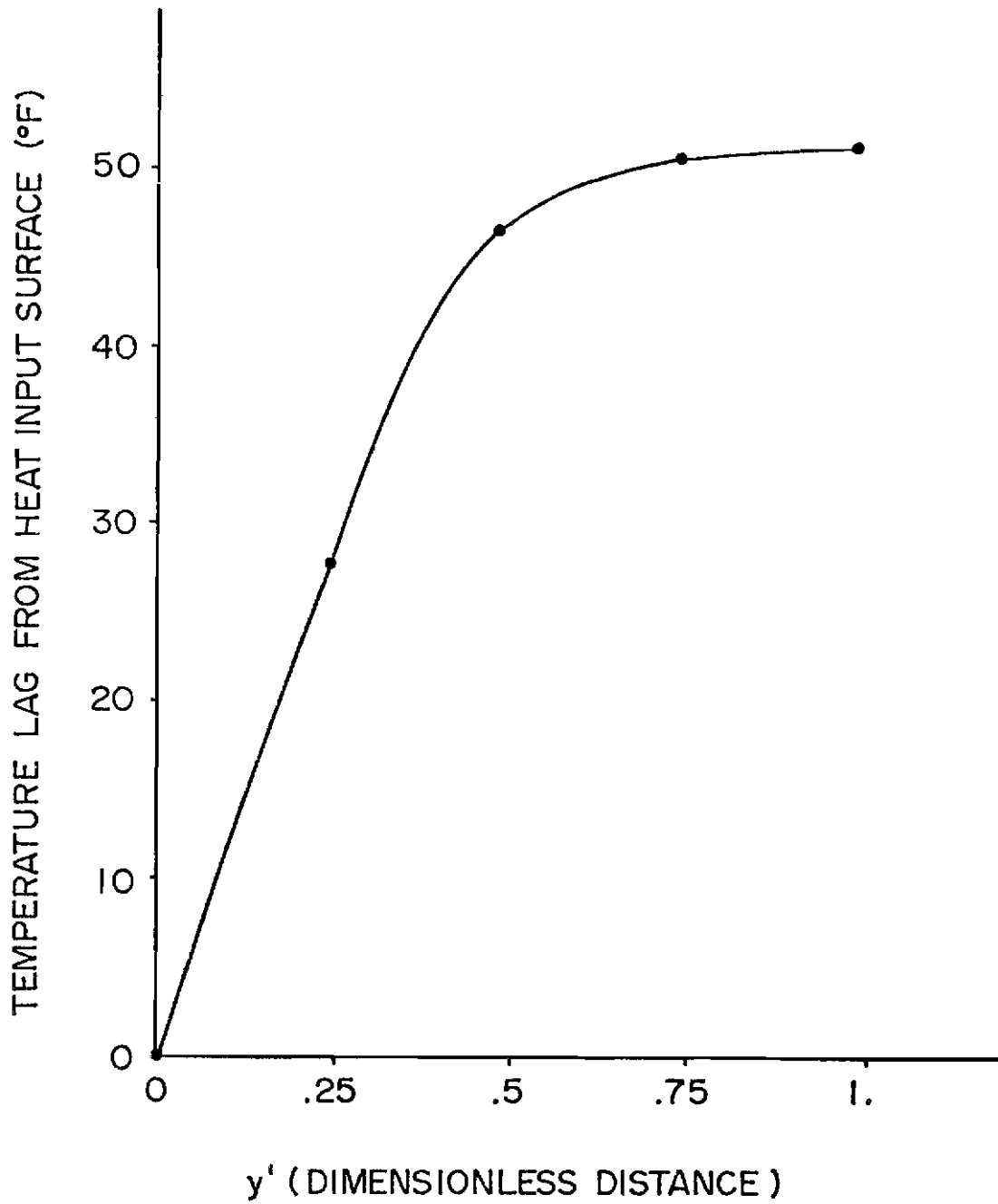


Figure 5. Temperature Lag Versus Dimensionless Distance

Two-Dimensional Air Cavity Analysis

The temperature distribution within the hole shown in Figure 3 is needed to evaluate the heat transfer to the thermocouple bead due to convection. The boundary temperatures for this problem were obtained from the previous one-dimensional analysis. Figure 6 shows the model to be analyzed including the finite difference grid points and the grid numbering system. The two-dimensional transient equation in dimensionless form is:

$$\frac{\partial^2 T'}{\partial x'^2} + A^2 \frac{\partial^2 T'}{\partial y'^2} = \frac{\partial T'}{\partial t'} \quad (7)$$

where x' and y' are coordinates shown in Figure 6, T' is temperature, t' is time, and A is the ratio of the length to height of the model, as shown in Figure 6. In terms of dimensional variables (depicted without primes), the above are:

$$x' = \frac{x}{b}, \quad y' = \frac{y}{a}, \quad t' = \frac{t\alpha}{b^2}, \quad T' = \frac{(T - T_o)}{T_o} \quad (8)$$

where α is thermal diffusivity and T_o is the initial temperature. The initial condition is:

$$T'(x', y', 0) = 0 \quad (9)$$

The boundary condition of all nodes on the right face is assumed:

$$T'(1, y', t') = 0 \quad (10)$$

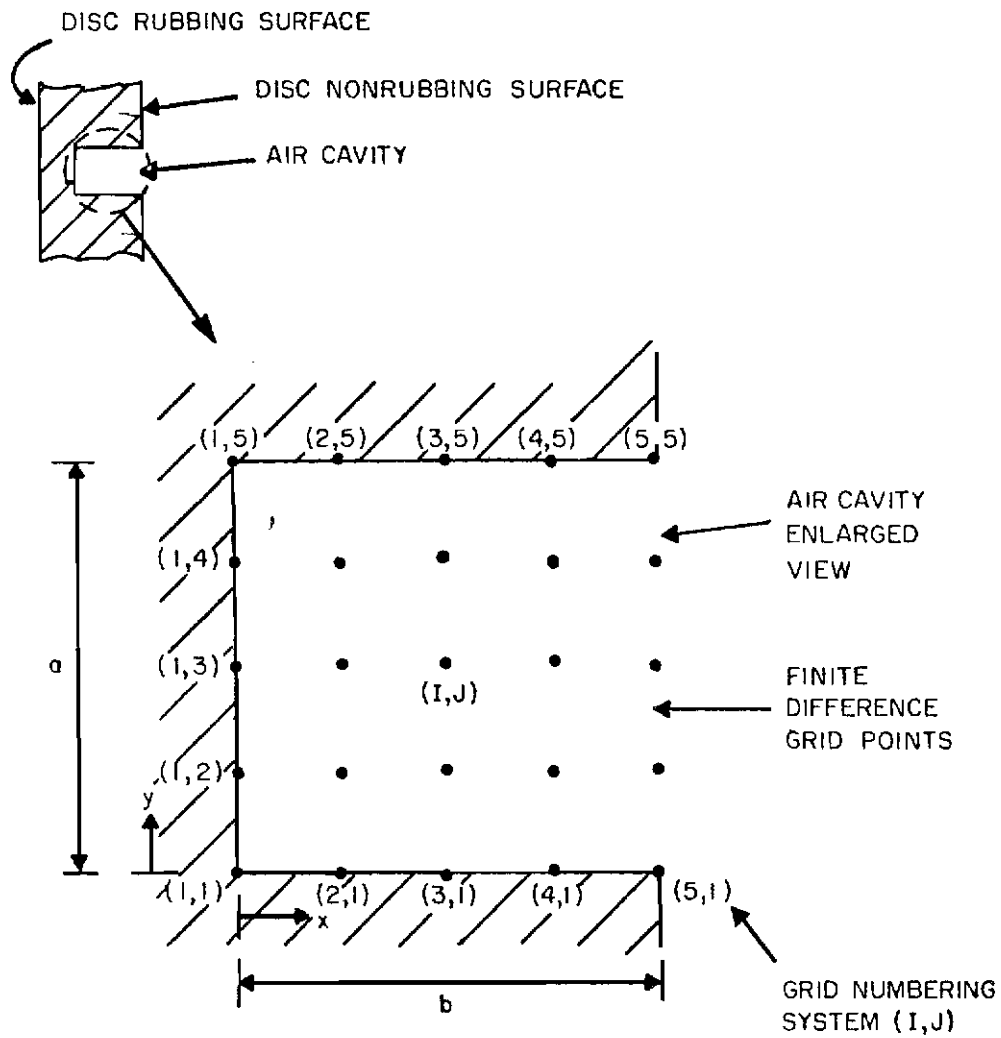


Figure 6. Two-Dimensional Air Cavity Temperature Distribution Model

Contrails

The boundary condition of all nodes on the left face was again selected to be:

$$T'(0, y', t') = \frac{t'}{t'_{sn}} \frac{TP - T_o}{T_o} \quad (11)$$

where t'_{sn} is the dimensionless stop time and TP is the peak temperature during the stop. The remaining three points on the upper boundary and the remaining three points on the lower boundary are assigned temperatures based on values taken from Figure 5, i.e.:

$$T'(2, 5, t') = T'(2, 1, t') = T'(0, y', t') - 27.5/T_o \quad (12)$$

$$T'(3, 5, t') = T'(3, 1, t') = T'(0, y', t') - 46.1/T_o \quad (13)$$

$$T'(4, 5, t') = T'(4, 1, t') = T'(0, y', t') - 49.9/T_o \quad (14)$$

With the use of standard finite difference techniques and the Euler time marching technique, Equation (7) becomes:

$$\begin{aligned} T^{t + \Delta t}(I, J) = T(I, J) + \frac{DT}{DX^2} [T(I-1, J) - 2T(I, J) \\ + T(I+1, J)] + \frac{(DT) A^2}{DY^2} \\ [T(I, J-1) - 2T(I, J) + T(I, J + 1)] \quad (15) \end{aligned}$$

where t indicates time, $t + \Delta t$ is one time interval advanced from t , I is the I th node in the x direction, and J is the J th node in the y direction (Figure 6). For clarity, the primes in (15) have been omitted. The computer program for solving Equations (9) through (15) is given in Appendix B. The material of concern in this part of the

Contrails

analysis was air. It was assumed that conduction was the only heat transfer mechanism, i.e., convection and radiation were neglected. The results showed for $y' = .5$, that the first two nodes to the right of the left-hand boundary differed from that boundary by a constant amount which was independent of time. Figure 7 gives the temperature ($^{\circ}\text{F}$) at $y' = .5$ as a function of x' and t' . The $x' = 0$ value is the bottom of the hole or the carbon temperature. From Figure 7 it can be seen that at $x' = .25$ the temperature is 27°F less than the carbon temperature. This information is used in the following:

Thermocouple Bead Temperature Analysis

The final step in analyzing the thermocouple embedded in a hole (Figure 3) was to use the previously developed carbon temperature and air cavity temperature as boundary conditions for the bead inserted in the hole. The first law of thermodynamics can be applied to the bead of the inserted thermocouple shown in Figure 3. Since no work crosses the bead boundary and no kinetic energy or potential energy changes are involved, the only energy change mechanisms are heat transfer and internal energy. The first law then takes the form:

$$\dot{q}_{\text{total}} = \frac{d}{dt} (U - U_0) = \frac{dU}{dt} \quad (16)$$

where \dot{q}_{total} is the total heat transfer to the bead per unit of time, $U - U_0$ is the bead internal energy, U_0 is a constant reference internal energy, and t is the time. The value \dot{q}_{total} can be expressed as the sum of three separate heat transfer rates as follows:

$$\dot{q}_{\text{total}} = \dot{q}_{\text{conduction}} + \dot{q}_{\text{convection}} + \dot{q}_{\text{radiation}} \quad (17)$$

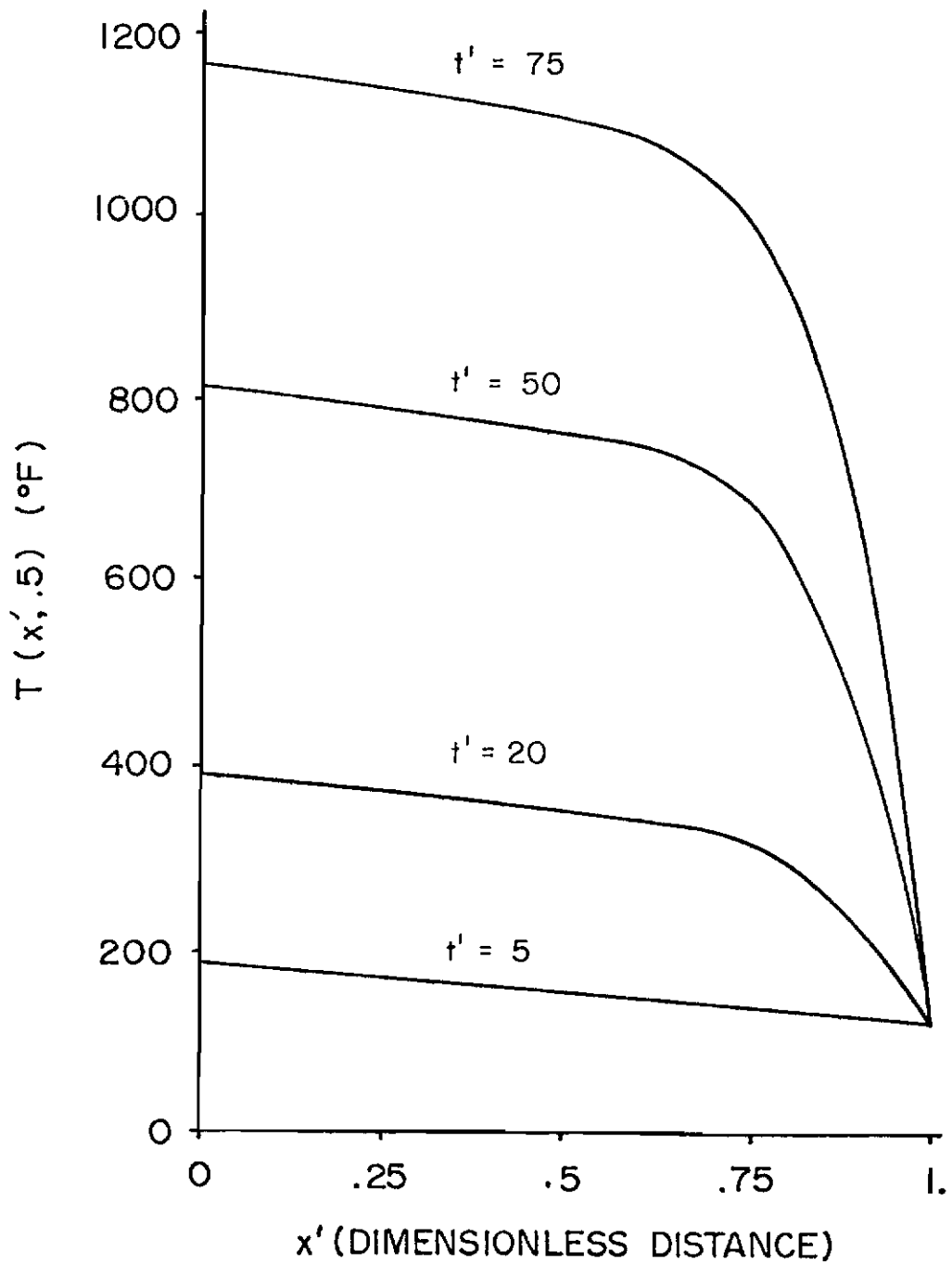


Figure 7. Air Cavity X-Direction Centerline Temperature

Contrails

The conduction term is the rate of heat conducted away from the bead through the thermocouple lead wires due to the temperature gradient along the wires. For this analysis the worst case of thermocouple insertion is assumed, namely, that the bead does not touch the bottom of the hole. It is thus assumed that the thermocouple bead rests approximately 1/16 in. from the bottom of the hole. This allows application of specific boundary conditions specified by the previous models. Further, it was assumed that the temperature gradient in the wires was the same as that in the air. In actual fact, the temperature gradient will be less than that of the air due to the lead wire thermal properties as compared to those of air. The equation³¹ for finding the conduction heat transfer rate was:

$$\dot{q}_{\text{conduction}} = -KA_k \frac{\partial T}{\partial x} \quad (18)$$

where $\frac{\partial T}{\partial x}$ is the temperature gradient along the wires, A_k is the wire cross-sectional area and K is the thermal conductivity of the wires. The thermal conductivity used was the average of that for chromel and alumel³² since type K chromel-alumel thermocouples were to be used in testing. The cross-sectional area was written as a function of wire radius so that a program could be written leaving radius as a variable.

The convection heat transfer rate term arises due to the heat transferred from the surrounding air to the thermocouple bead. To determine the convection heat transfer rate, Newton's law of cooling

$$\dot{q}_{\text{convection}} = \bar{h} A_b (T_{\text{air}} - T_b) \quad (19)$$

was used, where \bar{h} is the average convection heat transfer coefficient, A_b is the thermocouple bead surface area, T_{air} is the temperature of the air in the air cavity at the location of the thermocouple bead, and T_b is the thermocouple bead temperature. In order to be conservative, the average convection heat transfer coefficient was taken to be the upper limit free-convection value given by Kreith.³³ The radius of the bead was selected to be twice the lead wire radius and the bead surface area was then reduced to a function of radius.

The radiation heat transfer rate contribution in Equation (17) arises from the heat transferred from the air cavity sides (carbon) to the thermocouple bead. Assuming blackbody radiation, the equation for the radiation contribution is:

$$\dot{q}_{\text{radiation}} = A_c F_{c-b} \sigma (T_c^4 - T_b^4) \quad (20)$$

where A_c is the area of the carbon that is radiating heat to the bead, F_{c-b} is the radiation shape factor from the carbon boundary to the thermocouple bead, and σ is the Stefan-Boltzmann constant, T_c is the carbon temperature, and T_b is the thermocouple bead temperature. The reciprocity theorem³³ in this application is:

$$A_c F_{c-b} = A_b F_{b-c} \quad (21)$$

where A_b is the bead surface area and F_{b-c} is the radiation shape factor from the thermocouple bead to the carbon boundary. Substituting Equation (21) into Equation (20) gives:

$$\dot{q}_{\text{radiation}} = A_b F_{b-c} \sigma (T_c^4 - T_b^4) \quad (22)$$

This form of the equation is desirable since A_b can be reduced to a function of radius and since F_{b-c} can be readily approximated as the value 1; all radiation leaving the bead reaches the carbon boundary. This relation along with Equations (17), (18), and (19) can be substituted into Equation (16) to yield:

$$\begin{aligned} -KA_k \frac{\partial T}{\partial x} + \bar{h} A_b (T_{\text{air}} - T_b) + A_b F_{b-c} \sigma (T_c^4 - T_b^4) \\ = \frac{dU}{dt} \end{aligned} \quad (23)$$

As shown in Equation (16), the time derivative of the internal energy can be written for a solid as:

$$\frac{dU}{dt} = \frac{d}{dt} \rho V u; \quad du = C dT_b \quad (24)$$

where ρ is the bead density, V is the bead volume which is reducible to a function of radius, C is the bead heat capacity, and T_b is the bead temperature. The values of ρ and C were taken as average values of chromel and alumel and obtained from Benedict.³² With the assumption of constant ρ , V and C , the time derivative of U becomes:

$$\frac{dU}{dt} = \rho V C \frac{dT_b}{dt} \quad (25)$$

Using the Euler time marching technique along with Equations (23) and (25) yields:

Contrails

$$\rho VC \frac{T_b^{t+\Delta t} - T_b^t}{\Delta T} = -kA_k \frac{\partial T}{\partial x} + \bar{h} A_p (T_{\text{air}} - T_b) + A_b F_{b-c} \sigma (T_c^4 - T_b^4) \quad (26)$$

The carbon temperature, T_c , was represented by an average of the first node and second node temperatures resulting from the one-dimensional carbon model. The air temperature was given as the midline node temperature next to the heated surface using the two-dimensional air cavity model [Node (2, 3) in Figure 6]. Equation (26) was programmed on a digital computer to give the thermocouple bead temperature as a function of time. The resulting program is shown in Appendix C.

Figure 8 shows the effect of the variation of the radius of the thermocouple lead wires. The results shown in this figure were obtained assuming no heat conduction along thermocouple leads. This would be the case if a thermocouple hole were placed so that no temperature gradient existed along the lead wires of the thermocouple. This situation is approximated by entering a brake disk in the radial direction with the thermocouple. It should be reiterated that this analysis assumes that the thermocouple is placed 1/16 in. from the bottom of the hole.

Figure 9 shows the effect if conduction heat transfer along the lead wires is taken into account. It should be recalled, as discussed under Equation (19), that at all times the bead radius was twice the lead wire radius. It is noted that at large lead wire radii, the effect of conduction out of the lead wires is not nearly as important as the fact that the mass of the bead has increased significantly. On

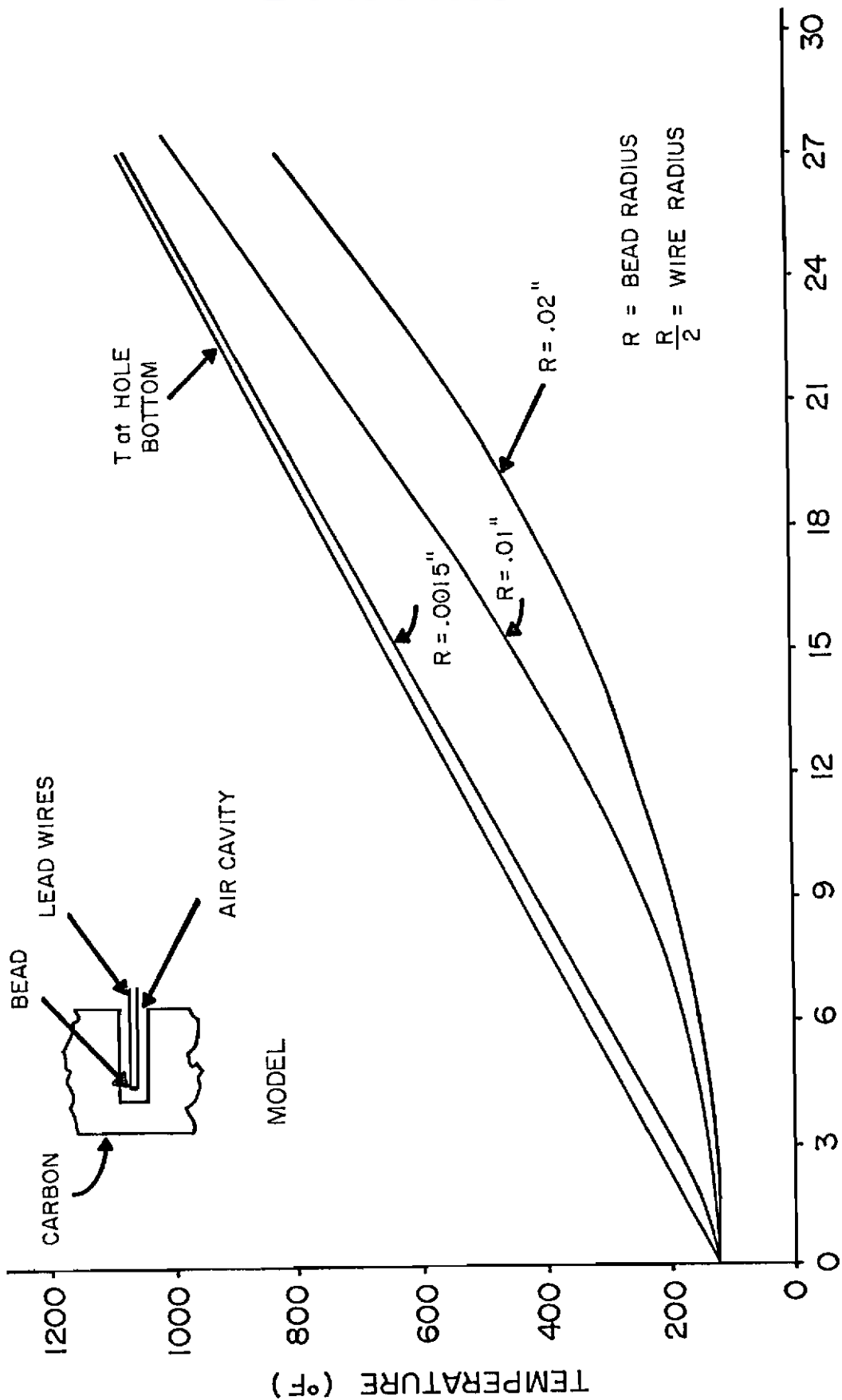


Figure 8. Thermocouple Model-Radius Effect

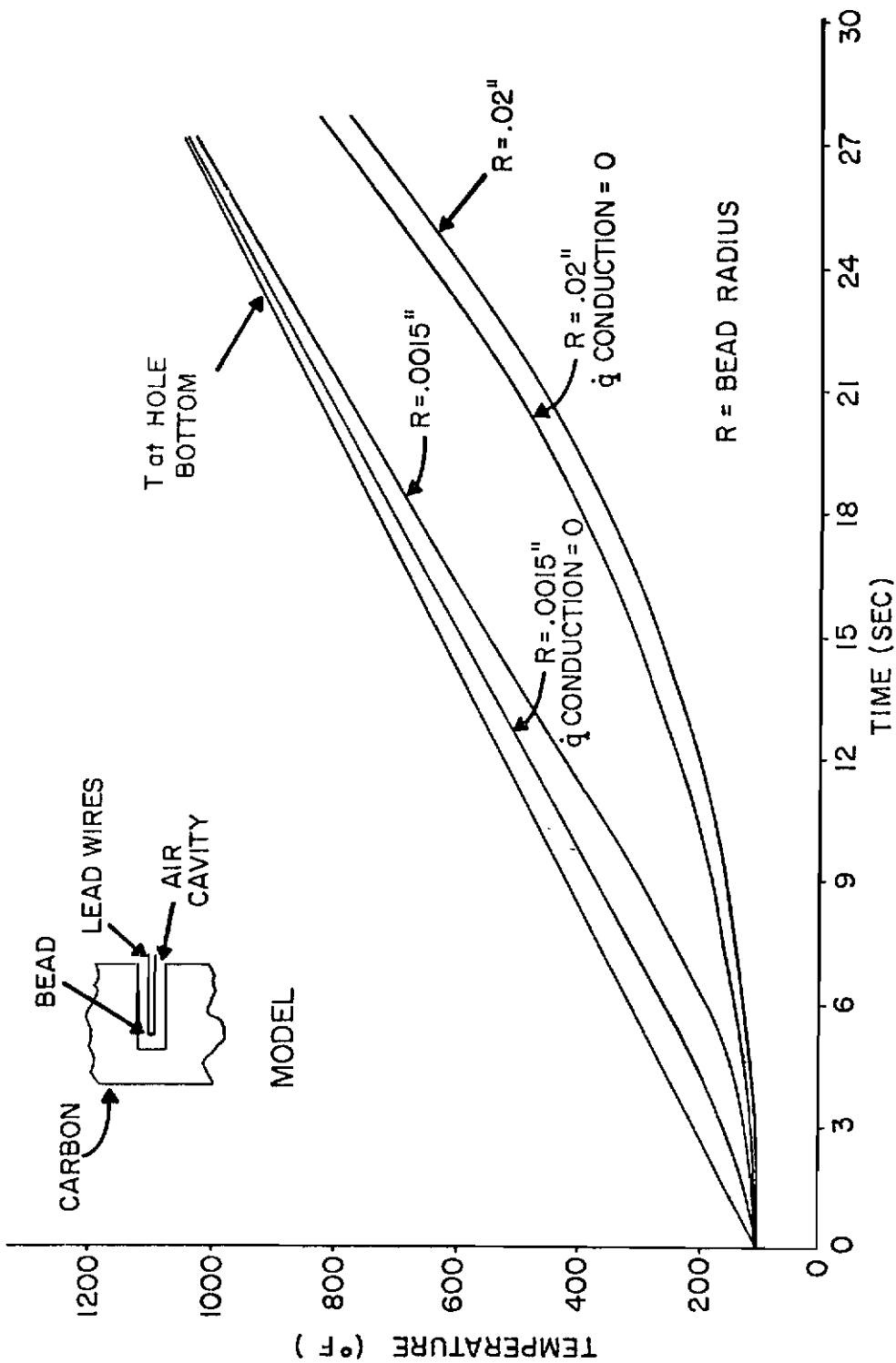


Figure 9. Thermocouple Model-Conduction Effect

the other hand, at low lead wire radii the conduction effect is significant, especially at the lower temperatures. At high temperatures the radiation effect allows the bead temperature to asymptotically approach the temperature at the bottom of the hole.

Conclusions From Theoretical Model

Conclusions that can be drawn from this section of the temperature measurement analysis chapter are summarized below.

1. In the end stator of a brake with a thermocouple entering in the axial direction, a thermocouple placed 1/16 in. from the bottom of the hole can have an error of 370°F out of 840°F. This occurs when a .02 in. radius lead wire is used. This error decreases at higher temperature due to radiation effects (300°F error at 1050°F).
2. If the lead wire radius is reduced to .0015 in., even with the bead not touching the parent material, the error can be reduced to 40°F at low temperature (200°F) and to a minimum error of 18°F at high temperature (1050°F) for the model considered.
3. In case 2, radiation effects insure that the bead temperature is higher than the air temperature, but the conduction through the lead wires and the convection to the air, both of which remove heat from the bead, insure that the parent material temperature can never be reached.
4. The three conclusions above are based on a properly made thermocouple junction. If the junction is twisted a few times at the end, the temperature measured is affected in two

Contrails

ways. First, the EMF passing through the thermocouple system does so partially at each contact point of the twist, the highest EMF fraction being at the point of contact of least resistance. This point is unknown so the temperature measured will probably not be at the thermocouple end. Second, the thermocouple standard EMF tables are listed for welded contact at the thermocouple wire junction. If contact occurs at other locations, as in a twist, the EMF passes through an oxide layer on the lead wires, rather than through only pure metal.

5. The radial temperature gradient in the discs is less than the axial gradient in the end stator. Thus, the error in measurement is less in that case since the conduction loss is negligible.
6. A standard Type K thermocouple error at 1000°F is $\pm 7.5^\circ\text{F}$ and 2000°F is $\pm 15^\circ\text{F}$. If this error is added to those discussed above (twists instead of beads, improper placement, large wire diameter), the overall error would, of course, be even greater. The .75% error of above can be reduced by purchasing special wire. This decreases this type of error to no more than .375%. Calibration should also be accomplished.
7. The fact that no bead is formed in some applications (twists only are sometimes used) probably helps the situation from the standpoint of response time. The main factor in decreasing the lead wire diameter is to decrease the bead size; then the response time is less. Thus, if no bead is formed and EMF is

Contrails

still transmitted, the results could be better than if a bead were formed, if a large radius lead wire is used. This is not recommended due to other errors, as stated above.

Bench Tests

Objective

Bench tests were conducted to experimentally determine the differences that exist between various types and sizes of test thermocouples when all were subjected to the same heat input within the same amount of time, utilizing the same test specimen. The results were to be used in related tests. It was desired to know the accuracy of current brake laboratory thermocouple practice so that changes could be made if required for conducting the full-scale brake tests. It is desirable to have the best experimental data practical to eliminate that possible unknown prior to the comparison with the computer model.

Test Apparatus

Test Specimen and Heat Lamps. A test apparatus with banks of quartz lamps was used for heating the first specimen. The lamp control is such that the lamps can be maintained at a constant temperature automatically or varied manually. For these tests the control was manually set to the maximum heat rate and maintained there throughout all but one of the 48 tests conducted. The material selected for heating was allowed to attain 1500°F at which point the lamps were manually turned off.

In order to approximate the heat input to a piece of material within an actual brake without conducting a brake test, a small piece

Contrails

(.45 in. × 1.9 in. × 3.0 in.) of carbon composite brake material was suspended between two high-density radiant heaters containing quartz lamps. This arrangement is shown in Figure 10. A carbon composite material was selected as the test specimen since carbon is being used in more and more brakes for Air Force aircraft. Since the carbon composites of interest are about one-fourth the density of steel, the temperature gradients in the carbon will be higher. Also shown in Figure 10 is the rod that supported the carbon, the test thermocouple, and the baseline thermocouple. The thermocouple holes in the carbon were 1.0 in. deep. The holes were located in the middle of the thickness direction and were 0.7 in. inward from the edge in the 1.9 in. dimension direction, making the thermocouples 0.5 in. apart. The lamp and thermocouple arrangement simulates the brake condition in which energy is input from each rubbing surface due to friction, while the thermocouples enter from the outside or inside radius of the brake disc. The baseline thermocouple was cemented into place with Omega CC high temperature sodium silicate cement that would withstand temperatures up to 2000°F. The maximum temperature encountered during any test was 1602°F. This baseline thermocouple was installed so that it could be assured, after each test, that the same maximum temperature occurred in the carbon block during each test. A photograph of the carbon block with the supporting rod and two thermocouples is shown in Figure 11.

Data Recording Equipment. The temperatures of interest were recorded using thermocouples in an arrangement as shown in Figure 12. The copper/alumel junction and the copper/chromel junction were made using

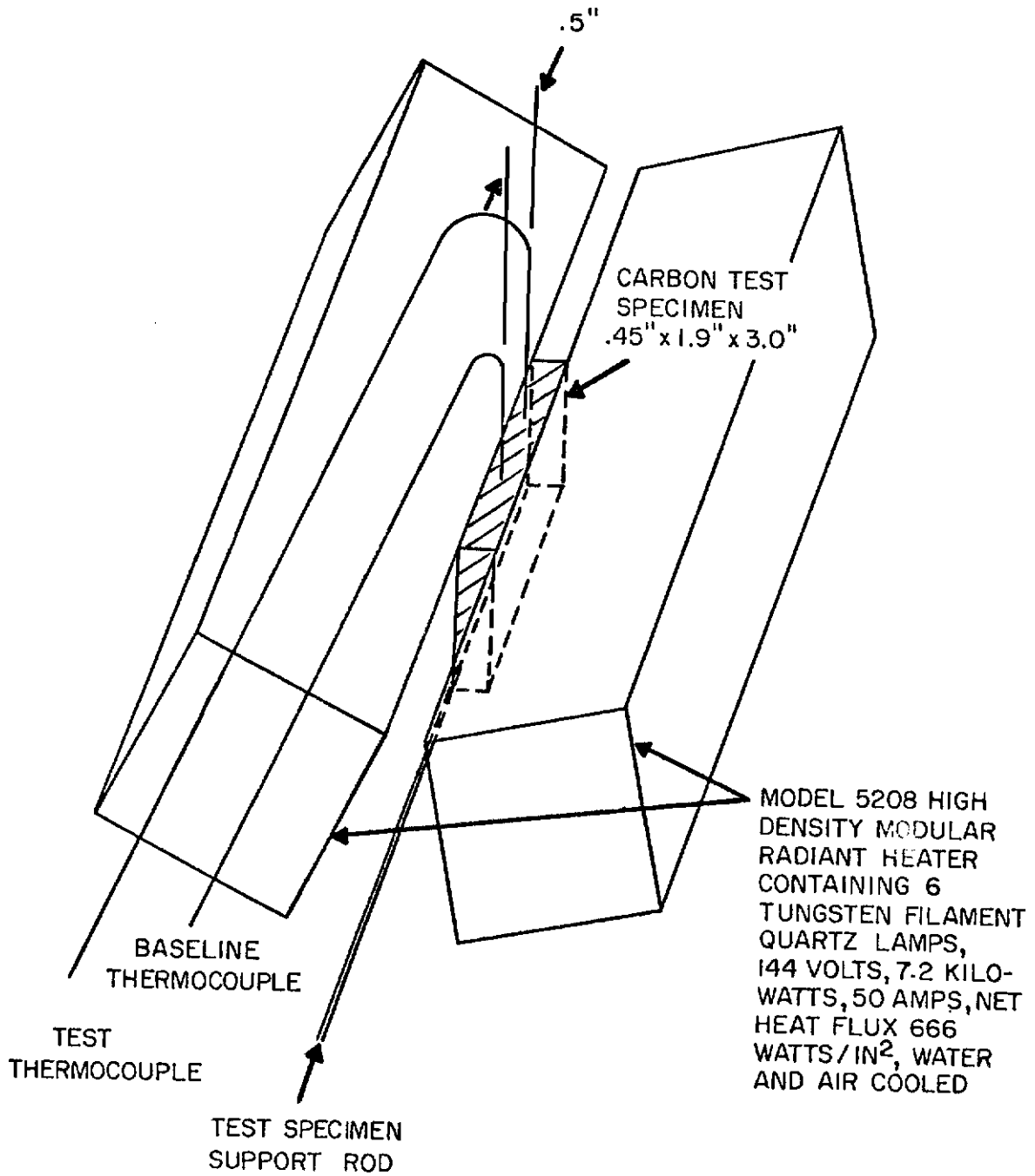


Figure 10. Sketch of Thermocouple Test Apparatus

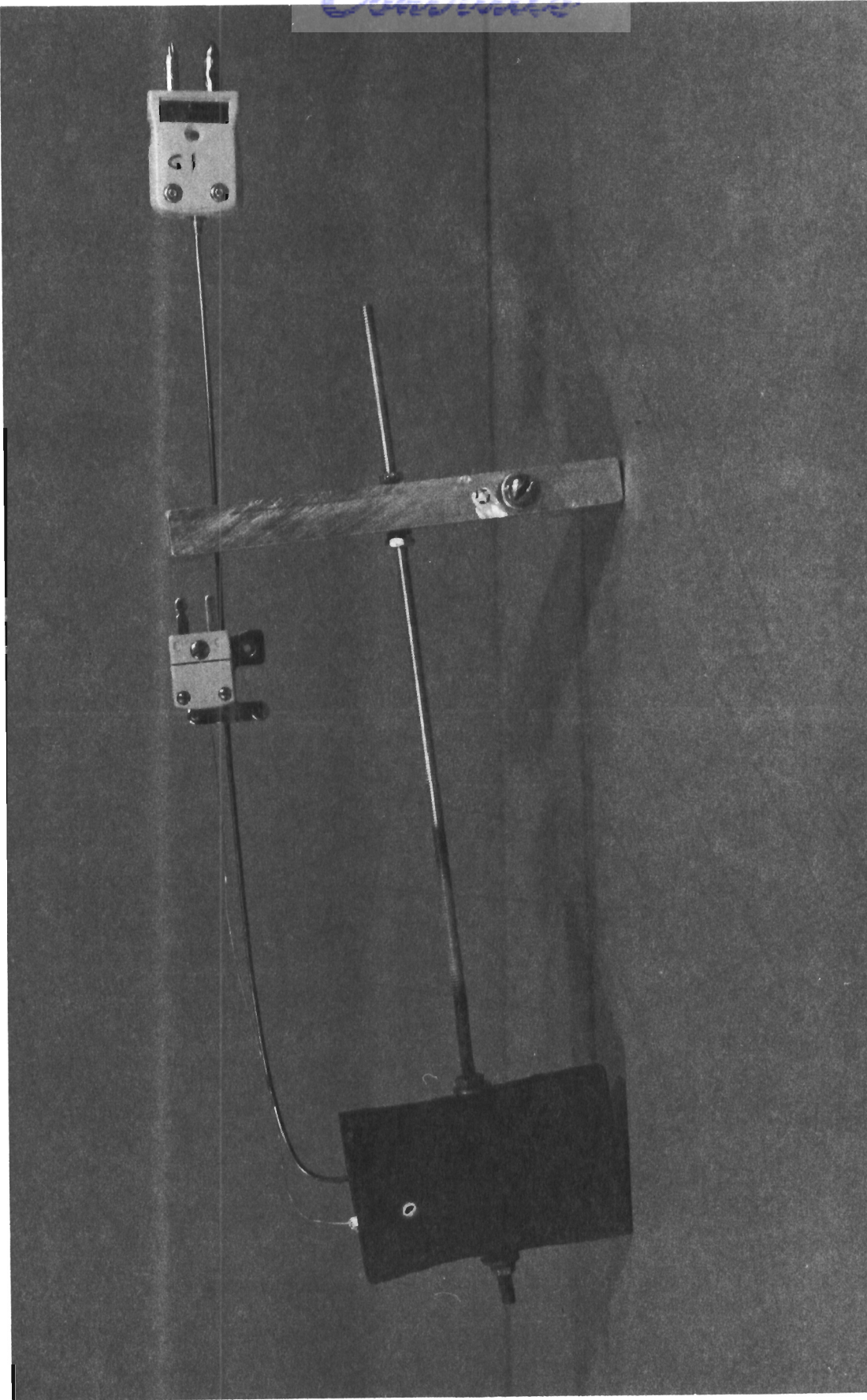


Figure 11. Test Specimen Photograph

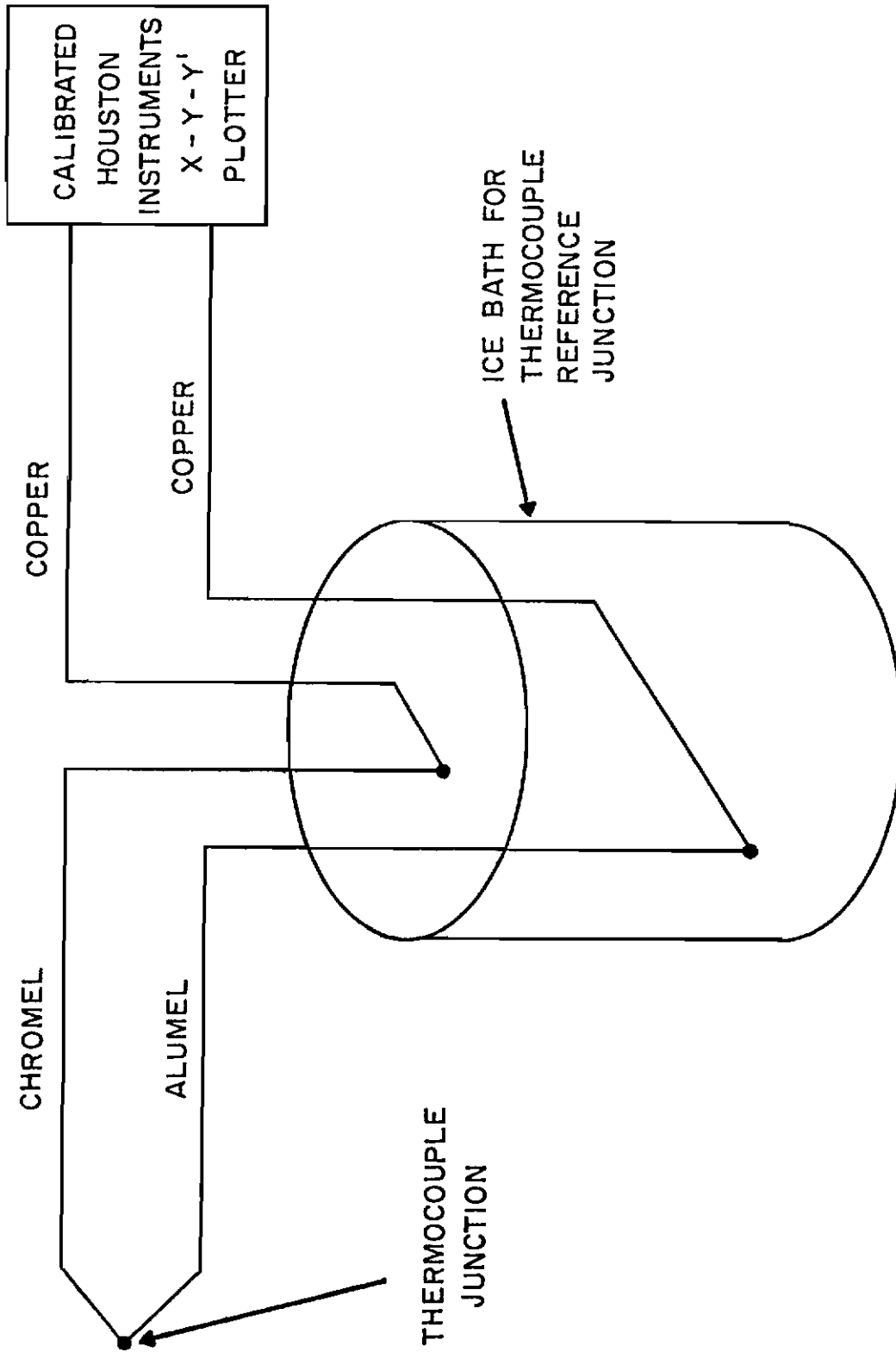


Figure 12. Sketch of Thermocouple Circuit

terminal blocks. The thermocouple junction was a variable and is discussed in the next section. A Houston Instruments X-Y-Y' plotter was used to record the thermocouple voltage output. The plotter was calibrated using a Brown Portable Potentiometer, Model 126W3, from Minneapolis-Honeywell Regulator Company. Calibration data points were at every two millivolts to a full scale of 50 millivolts. The millivolts were converted to °F by using a table of temperature versus millivolts published by the National Bureau of Standards.

Thermocouple Description. Thermocouples in these tests were all type K, chromel-alumel. The variations were in diameter, configuration, type of junction, and distance from bottom of the hole in the carbon block. Table 2 shows the variation in diameter, configuration, and

TABLE 2

THERMOCOUPLE DESCRIPTION

Test No. (Code)	Description
15, 47, 48	.01 in. dia. stainless sheath, magnesium oxide insulation, .0015 in. wire dia., grounded junction, Omega No. SCASS-010G-6
18, 19, 23 (E1)	.0625 in. dia. stainless sheath, magnesium oxide insulation, .01 in. wire dia., exposed junction, Omega No. CASS-116E-12
24, 27 (U1)	.0625 in. dia. stainless sheath, magnesium oxide insulation, .01 in. wire dia., ungrounded junction, Omega No. CASS-116U-12

Contrails

TABLE 2-continued

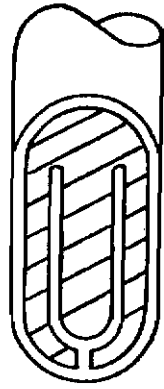
Test No. (Code)	Description
29, 30 (G2)	.0625 in. dia. stainless sheath, magnesium oxide insulation, .01 in. wire dia., grounded junction, Omega No. CASS-116G-12
32, 34 (3)	.01 in. wire dia. unsheathed T/C installed in .0625 in. dia., .25 in. LG two-hole magnesium oxide insulators
36, 38, 41	.045 in. × .078 in. size, glass braid insulation, .02 in. wire dia. also covered with glass braid insulation, junction twisted 3 times.
40B	Same as above glass braid except junction twisted 10 times
42	Same as above glass braid except junction twisted once
44	Same as above glass braid except junction spot welded
45	.030 in. × .053 in. size, glass braid insulation, .012 in. wire dia. also covered with glass braid insulation, junction spot welded

type of junction. Five basic types are shown, i.e., .01 in. diameter stainless steel sheath, .0625 in. diameter stainless steel sheath, .045 in. × .078 in. diameter glass braid, .030 in. × .053 in. diameter glass braid and an unsheathed thermocouple installed in a two-hole magnesium oxide insulator. The .01 in. diameter stainless steel sheathed thermocouple had a grounded junction as opposed to ungrounded and exposed junctions. These three junction types are shown in

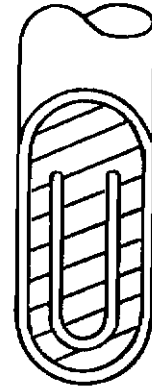
Contrails

Figure 13. The .0625 in. diameter stainless steel sheathed thermocouples were tested with exposed, grounded, and ungrounded junctions. The unsheathed thermocouple was installed in a .0625 in. outside diameter, two-hole magnesium oxide insulator. The insulator was one inch long at the end placed within the carbon block, while the remainder of the 6 in. thermocouple was covered with .25 in. long pieces of the two-hole magnesium oxide insulator. The remaining thermocouples were such that the individual wires were insulated with glass braid insulation and the two insulated wires were then insulated and held together with the same type glass braid insulation. The spot-welded thermocouples were constructed by overlapping the lead wires, using a hand-held spot welding tool and cutting off the remaining wire ends. Several thermocouples were joined by twisting the leads to form a junction. One twist is defined as turning the leads through 180 degrees while holding the main thermocouple stationary. The twisted area was void of insulation but insulation started immediately at the spot where the twists stopped.

Five of the thermocouples tested were independently calibrated at two temperatures, 750°F and 1100°F. Appendix D shows the percent deviation from a National Bureau of Standards tested platinum, 10% rhodium versus platinum thermocouple. Also shown are the thermocouple codes used and a list of tests during which the various thermocouples were used. In addition, Appendix D shows the calibration of the same ten thermocouples but gives millivolts and °F instead of percent. Also included are the conditions at which the thermocouples were calibrated, as well as the equipment used and the accuracy of the results.



GROUNDED



UNGROUNDED



EXPOSED

Figure 13. Grounded, Ungrounded, and Exposed Thermocouples

Contrails

Test Procedure

The basic test procedure was to subject the carbon block with embedded thermocouples to the maximum lamp output, raising the baseline thermocouple temperature from 100°F to 1500°F. The method of obtaining the 100°F starting temperature for all tests was either to heat the block to about 150°F and allow it to cool down to 100°F or to allow the block to cool down to 100°F from the previous test. The heat input of each test was manually terminated at 1500°F. Due to this manual control the peak temperature varied slightly. The temperatures during the heat up and cool down periods were recorded on the X-Y-Y' plotter. A detailed list of the steps involved in running a particular thermocouple test is given in Appendix D.

Results and Discussion

The specific baseline and test thermocouple output in the form of millivolts versus time is depicted in Figure 14 for a typical test. The particular test from which this data was generated was Test 27. The tests were run in numerical order. Not all tests run are reported since many tests were duplicates of those reported and produced exactly the same results. These tests were run specifically to assure repeatability from test to test. Table 3 shows test temperatures at various baseline temperatures. The particular thermocouples associated with each test number are given in Table 2. Table 3 shows that five tests were run in which the thermocouple was placed 1/16 in. from the bottom of the 1.0 in. deep hole in the carbon block. Table 2 shows that Tests 15, 47, and 48 were conducted with the same thermocouple. Test 15 utilized a .02 in. diameter hole in the carbon block. Test 47 used the

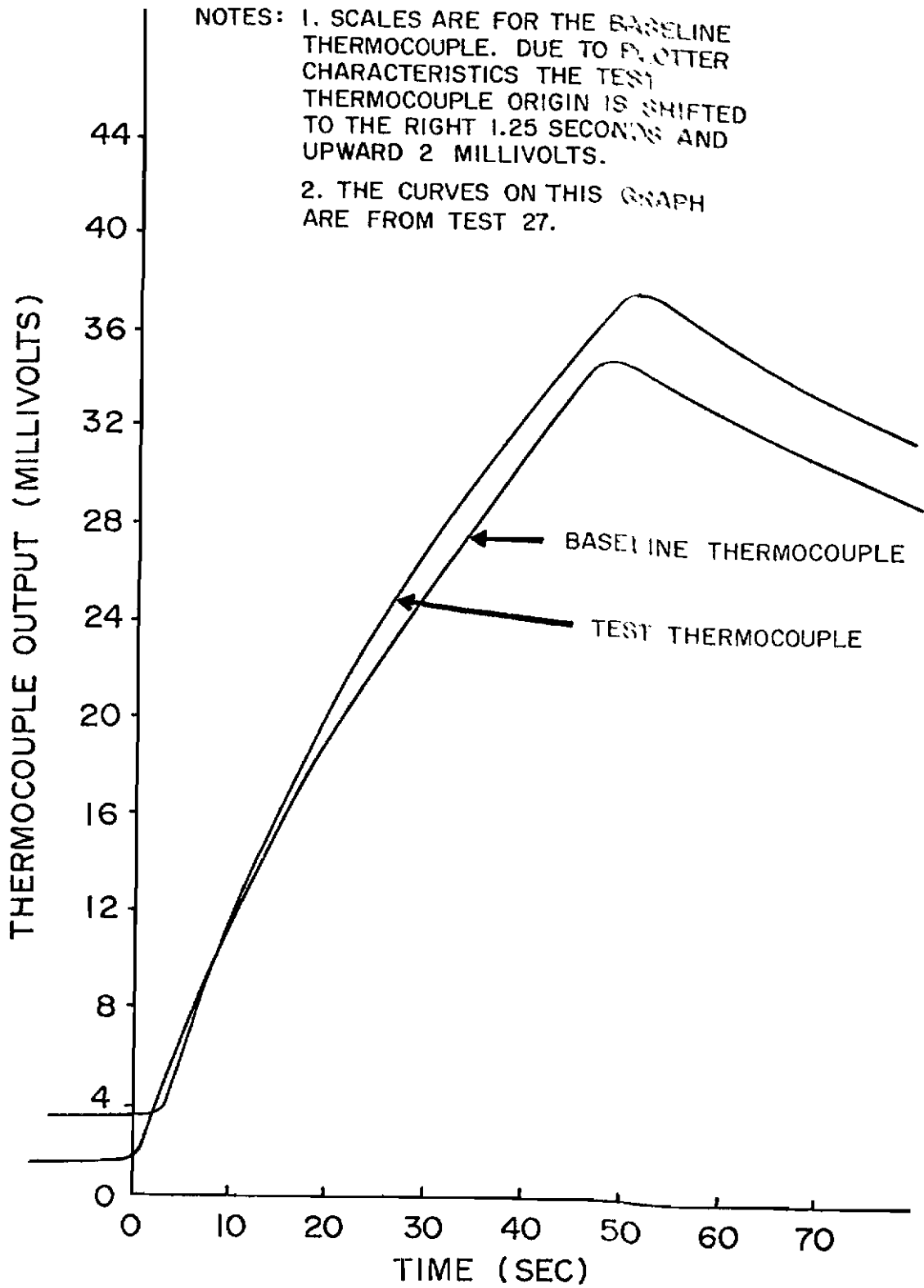


Figure 14. Typical X-Y-Y' Plotter Output

TABLE 3

TEST TEMPERATURE AT VARIOUS BASELINE TEMPERATURES

TEST NO	BASELINE						
	TEMP (°F)	300	450	750	1,100	1,350	1,500
15		316	468	778	1,130	1,381	1,521
18 ^a		223	377	725	1,105	1,361	1,505
19		286	448	777	1,144	1,402	1,539
23		274	448	777	1,146	1,402	1,540
24 ^a		212	388	736	1,112	1,366	1,503
27		221	395	745	1,124	1,381	1,519
29 ^a		225	412	751	1,133	1,386	1,524
30		283	444	777	1,152	1,408	1,538
32 ^a		217	369	731	1,116	1,374	1,517
34		260	423	762	1,147	1,407	1,542
36 ^a		143	241	555	985	1,257	1,396
38		160	265	602	1,019	1,278	1,429
40B		139	230	537	935	1,187	1,320
41		145	245	581	1,019	1,281	1,425
42		207	314	640	1,052	1,306	1,473
44		225	363	697	1,089	1,359	1,486
45		232	384	733	1,120	1,385	1,521
47		318	469	775	1,136	1,377	1,516
48		323	478	778	1,133	1,366	1,512

NOTE: a. This thermocouple was placed 1/16 in. from hole bottom. All others were placed at the hole bottom.

Contrails

same small thermocouple but it was cemented inside a .0625 in. x 1.0 in. long stainless steel sheath and cemented into the bottom of the .07 in. diameter hole in the carbon block. This was done to negate the possible influence of the metal sheaths of other thermocouples when making comparisons. Comparison of values from Table 3 for Tests 15 and 47 shows very little sheath effect. Test 48 differed from 47 in that 48 had a heat input rate approximately one-half that of Test 47. All heating rates were the same except for Test 48. To reach 1500°F each test required approximately 45 to 50 seconds except for Test 48, which required 65 to 70 seconds. This heating rate is representative of that of a typical 3 or 4 rotor aircraft brake with a carbon heat sink and a deceleration of about 9 ft/sec² with an absorbed energy of about 11 million ft-lbs. Table 2 shows that Tests 18, 19, and 23 were conducted with the same thermocouple. Tests 19 and 23 were identical runs; Test 18 was conducted with the thermocouple 1/16 in. from the bottom of the hole in the carbon. Tests 36 and 38 used the same thermocouple, while Test 41 used a physically different thermocouple but one configured the same as for Test 38. This was accomplished due to the large differences observed between these tests and other tests of thermocouples enclosed in metal sheaths. Table 3 shows that temperatures in Tests 38 and 41 are close, especially at the higher three temperatures.

As previously discussed, the baseline thermocouple was installed to insure that the same temperature was reached in the carbon block from test to test. However, due to (1) room temperature and humidity changes from day to day, (2) the overall test apparatus heating up

Contrails

slightly during a test, and (3) specimen weight loss from test to test (9 grams were lost of the total specimen weight of 64 grams over the last 32 tests due to oxidation of the carbon), the baseline temperature was not strictly constant over all tests. The variation was as high as 3% near the peak temperature. To determine the effect of this variation on test thermocouple temperatures, Tests 19 and 23 can be compared. The baseline temperature difference was the only variable between the two tests. As shown in Table 3 or Table 4, this effect is extremely small. The maximum difference was at a baseline temperature of 300°F. In this area the slope of the temperature versus time curve is the greatest, which adds inaccuracy to reading the temperature in this area. Since all of the other five readings are so close and the possibility of resolution error at low temperatures is high, it is reasonable to conclude that the effect of a slight baseline temperature change from test to test is negligible.

Since Test 47 was accomplished with the smallest thermocouple wire combined with a .0625 in. x 1.0 in. long stainless steel sheath and a cemented junction, this test was judged to be the most accurate of all those conducted. Due to this, results are tabulated and graphed showing the percent difference of the test thermocouple from thermocouple Number 47. Table 4 gives such values for each test reported. Also shown is the calculation procedure. The numbers range from -56.3% to +2.3%. A positive deviation indicates that the test thermocouple associated with that positive deviation responds faster than the Test 47 thermocouple, or that it is more accurate than the Test 47 thermocouple or a combination of both. Test 47 was selected for the

Contrails

TABLE 4

PERCENT DIFFERENCE OF TEST THERMOCOUPLE
FROM THERMOCOUPLE NUMBER 47

TEST NO T ₄₇ (°F)	318	469	775	1136	1377	1516
15	-.6	-.2	.4	-.5	.3	.3
18 ^b	-29.9	-19.6	-6.4	-2.7	-1.2	-.7
19	-10.1	-4.5	.30	.70	1.8	1.5
23	-13.8	-4.7	.26	.88	1.8	1.5
24 ^b	-33.3	-17.3	-5.0	-2.1	-.8	-.9
27	-30.5	-15.8	-3.9	-1.1	.3	.2
29 ^b	-29.2	-12.1	-3.1	-.26	.6	.53
30	-11.0	-5.3	.3	1.4	2.3	1.4
32 ^b	-31.8	-21.3	-5.7	-1.8	-.22	.07
34	-18.2	-9.8	-1.7	1.0	2.2	1.7
36 ^b	-55.0	-48.6	-28.4	-13.3	-8.7	-7.9
38	-49.7	-43.5	-22.3	-10.3	-7.2	-5.7
40B	-56.3	-50.9	-30.7	-17.7	-13.8	-12.9
41	-54.4	-47.8	-25.0	-10.3	-7.0	-6.0
42	-34.9	-33.0	-17.4	-7.4	-5.2	-2.8
44	-29.2	-22.6	-10.1	-4.1	-1.3	-2.0
45	-27.0	-18.1	-5.4	-1.4	.6	.3
47	0	0	0	0	0	0
48	1.57	1.88	.38	-.26	-.80	-.26

NOTE(S): a. Table values calculated by $100 \times (T_{\text{test}} - T_{47})/T_{47}$
 b. This thermocouple was placed 1/16 in. from the hole bottom. All others were placed at the hole bottom.

Contrails

comparison test because of its size and insertion technique, therefore this small value (2.3% maximum) is attributed in most cases to small discrepancies in setup, input energy, or plotter characteristics. The exception to this is Test 48 which used the same thermocouple and installation as Test 47. Test 48 is the only test to indicate positive values in Table 4 in the lowest three temperature columns. Since the temperature comparisons of Tables 3 and 4 are based on baseline temperature, the test with a lower heat input rate (Test 48) can give a higher temperature than the test with a higher input rate (Test 47). Although this is noted, the highest temperature difference is only 1.88%. Test 15 varies less than 1% from Test 47, showing the lack of effect of inserting the thermocouple in a .02 in. diameter hole without cement as in Test 15 compared with using the same thermocouple cemented inside a .0625 in. diameter sheath which was, in turn, cemented in the hole in the carbon as in Test 47. This small difference can also be seen in Figure 15 where six different thermocouples are compared. The test numbers are shown along with the thermocouple description. A more complete description is given in Table 2. As noted in Figure 15, all of these thermocouples were placed at the bottom of the hole in the carbon except for Test 36. From Table 4 it is noted that results of Tests 38 and 41 are fairly close, thus only Test 38 is shown on Figure 15. Recall that 38 and 41 used physically different thermocouples but the same configuration. Also from Table 4, Tests 19 and 30 show approximately the same values. Again, only Test 19 is graphed on Figure 15. The difference between the thermocouples of Test 19 and Test 30 is that Test 19 had an exposed junction and Test 30 had a

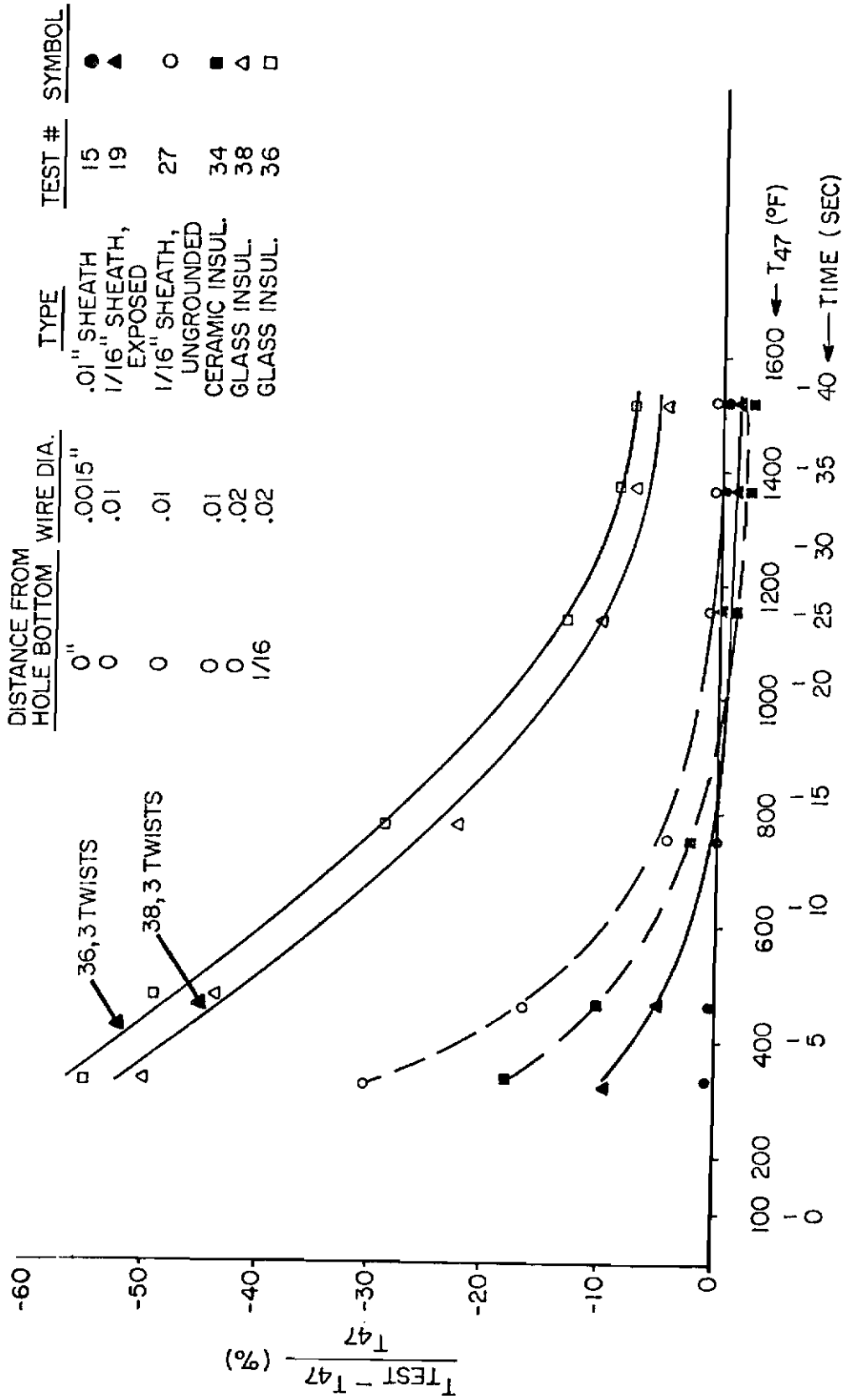


Figure 15. Accuracy of Different Thermocouple Types

Contrails

grounded junction (see Figure 13). One obvious and predictable trend is that the difference increases in absolute value as the thermocouple diameter increases. The exposed junction (and thus the grounded junction) is better than the ungrounded junction.

A graph depicting the differences of Table 4 for thermocouples with glass braid insulation is shown in Figure 16. The graph shows that 10 twists are less accurate than 3 twists which are, in turn, less accurate than 1 twist. The spot-welded thermocouples are most accurate and the smallest diameter one is best. It should be pointed out that the spot welding was done with a hand-held spot welder, and as a result, it was impossible to make a perfect bead. This could account for the up to 25% difference shown at low temperatures. Any better method to form the bead on this type thermocouple was not attempted since it would be time consuming if reduced to everyday practice.

A comparison should be made between Test 45 and Test 19, both of which are shown in Figure 17. The first has glass braid insulation and the second has a stainless steel sheath, but the wire diameters are almost identical. The major difference is in the bead formation. The thermocouple of Test 19 was made under controlled conditions by the manufacturer, whereas the other was made by spot welding. Observing the two graphs (Figures 16 and 17) or the tabular data in Table 4 leads to the conclusion that the differences in test thermocouple 45 are about triple those of Test 19 (or Test 30). The best thermocouple, other than the small diameter one, is the one used in Test 19 or Test 30.

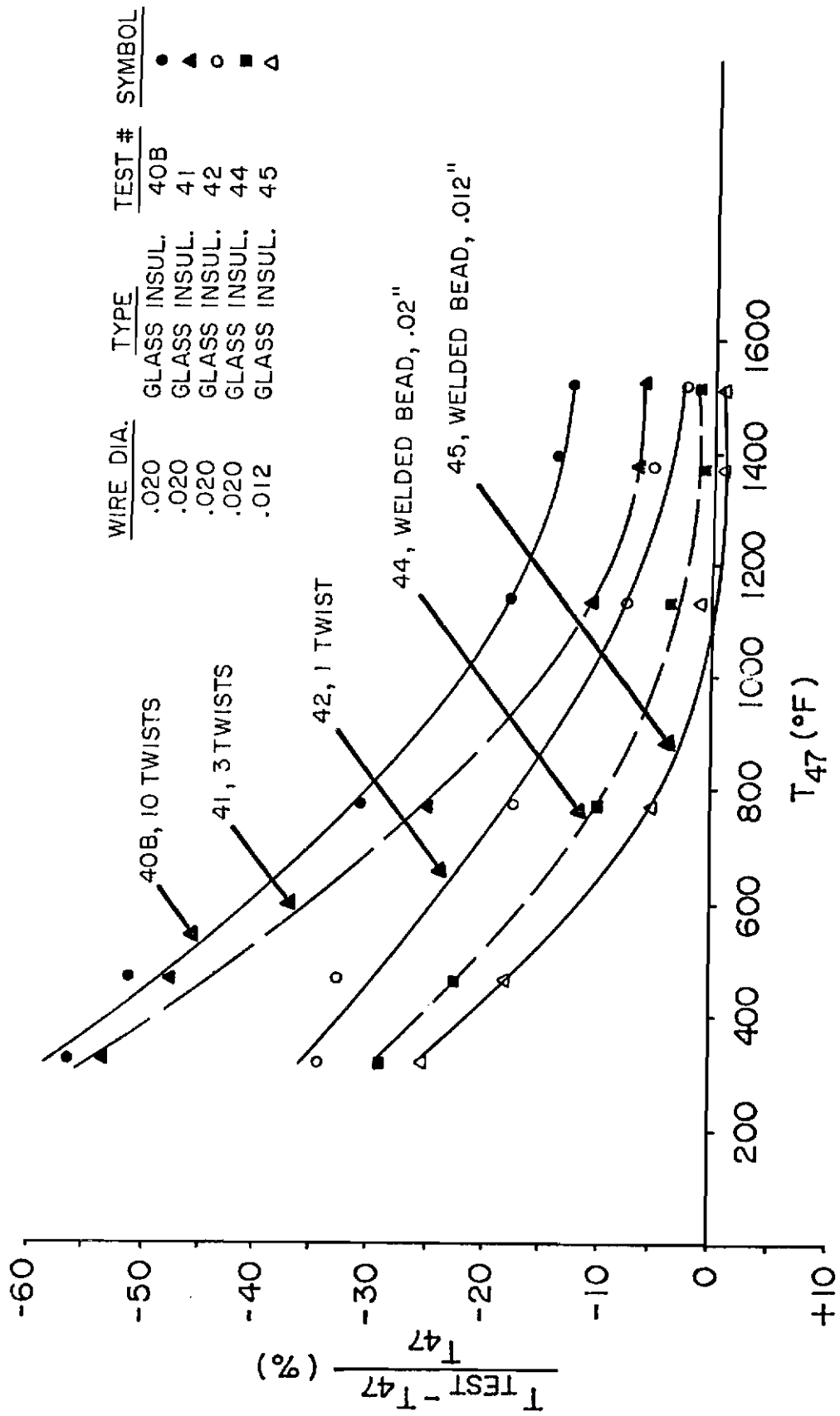


Figure 16. Accuracy of Glass Insulation Thermocouples

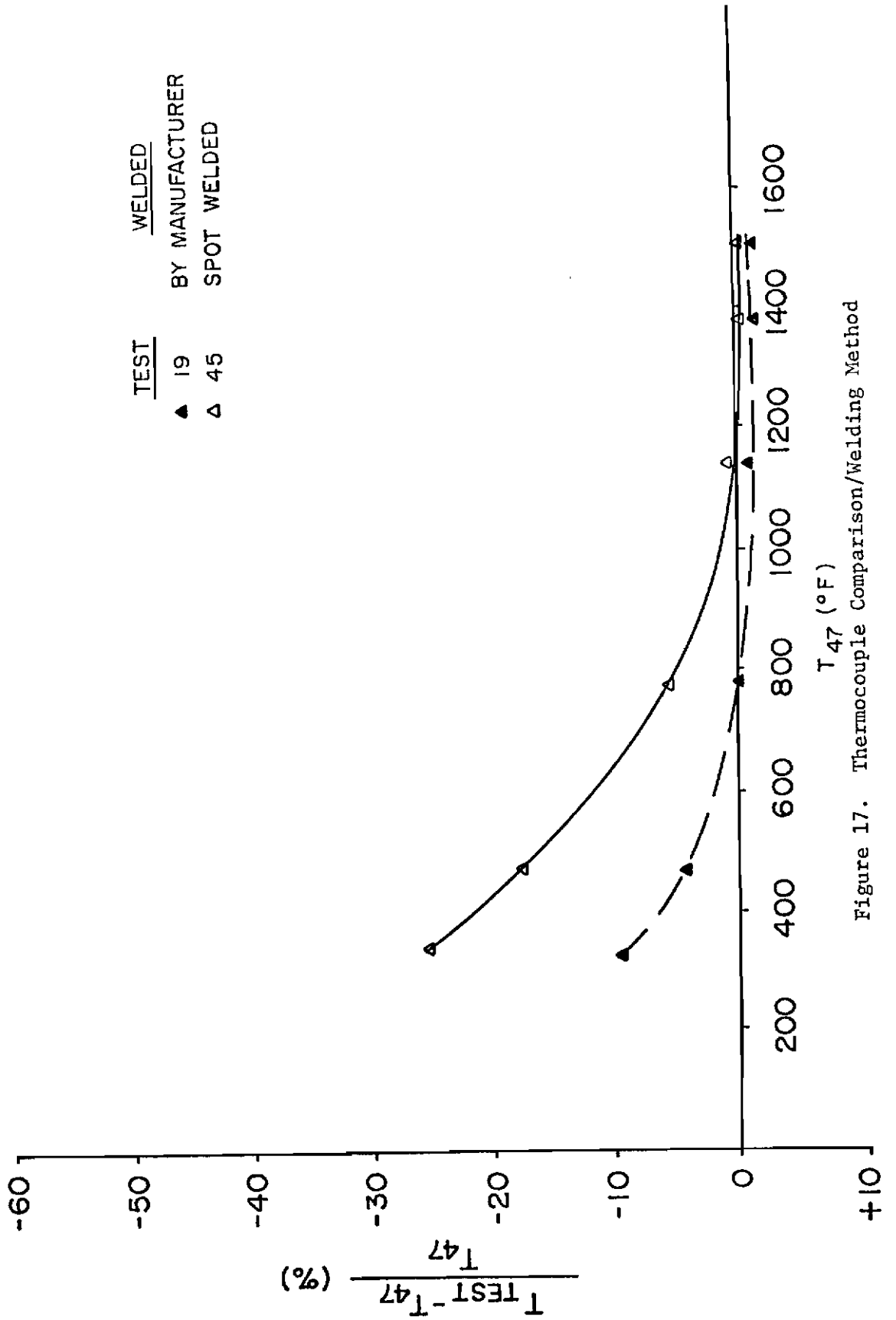


Figure 17. Thermocouple Comparison/Welding Method

Contrails

The effect of placing the thermocouple 1/16 in. from the bottom of the hole can be seen in Figure 18. In each case, as expected, the most accurate is the one at the bottom of the hole. Glass braid insulated ones are least accurate followed by ungrounded and exposed (or grounded, since results of Tests 19 and 30 are almost identical). Note that the glass braid insulated thermocouples have been shown to have higher differences from the Test 47 thermocouple not because of the insulation type, which is merely a categorizing method, but because of the junction on those particular thermocouples. Also of interest in this area is the relative condition of the thermocouples after testing. The metal sheathed thermocouples showed no change but those with glass braid insulation deteriorated significantly. After one exposure to 1500°F during a test, the insulation became white and brittle. Any handling after this one exposure in most cases led to the insulation crumbling and falling off. After about five tests with any one thermocouple the insulation would fall off when the thermocouple was removed from the test specimen. Although nothing irregular was noted in the data, this phenomenon could cause the thermocouple to form a junction in any location along the white brittle area.

A plot of temperature versus time for five thermocouples, including the thermocouple used in Test 47, is shown in Figure 19. A significant lag is seen in Tests 36, 38, and 40B when they are compared to Test 47. The glass braid insulation thermocouple with ten twists is the most dramatic followed by the three-twist tests. The best thermocouple appears to be that of Test 30. It is shown to be above the Test 47 curve at the high temperatures. This, again, is attributed to small

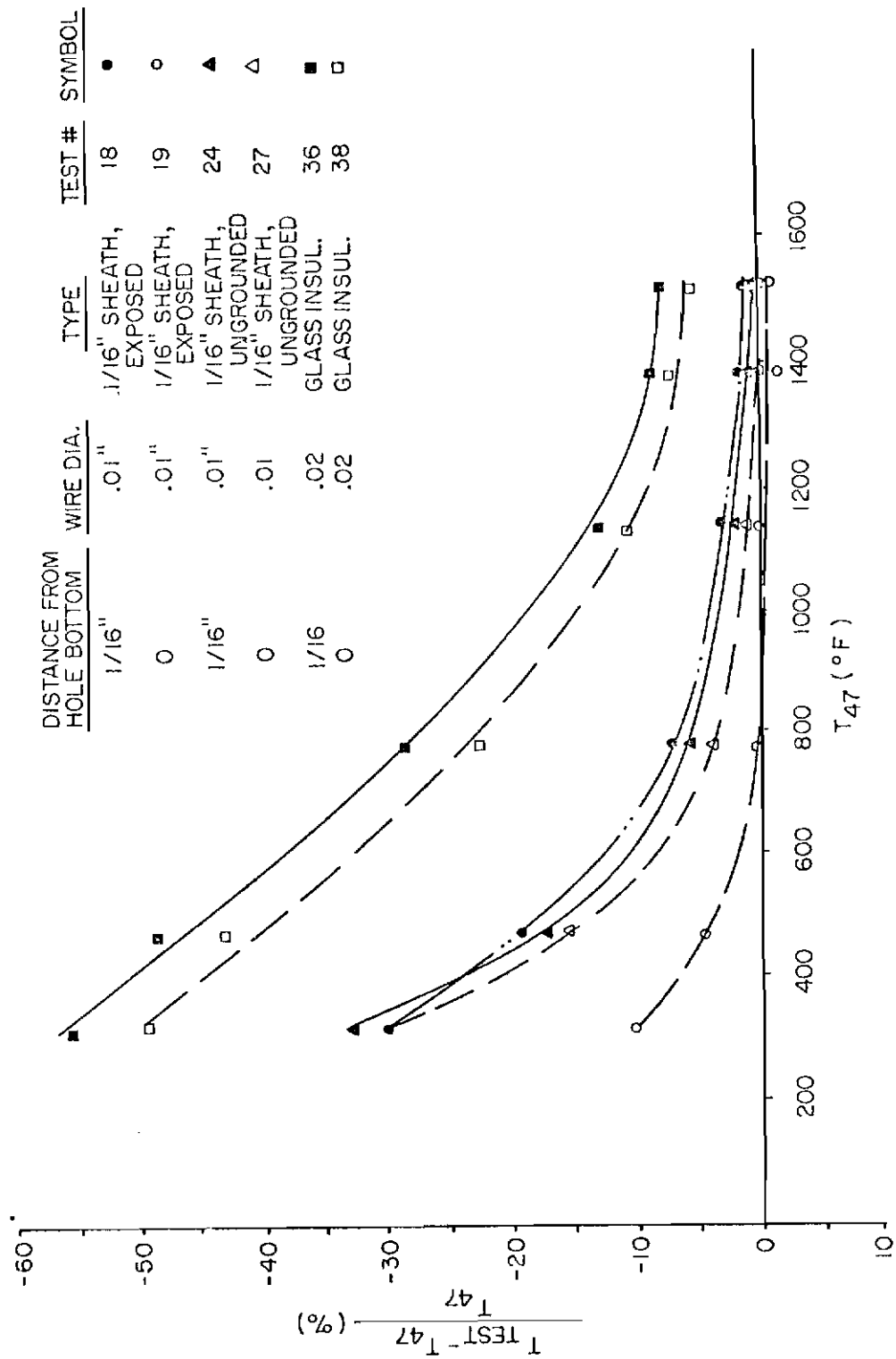


Figure 18. Effect of Thermocouple Distance from Hole Bottom

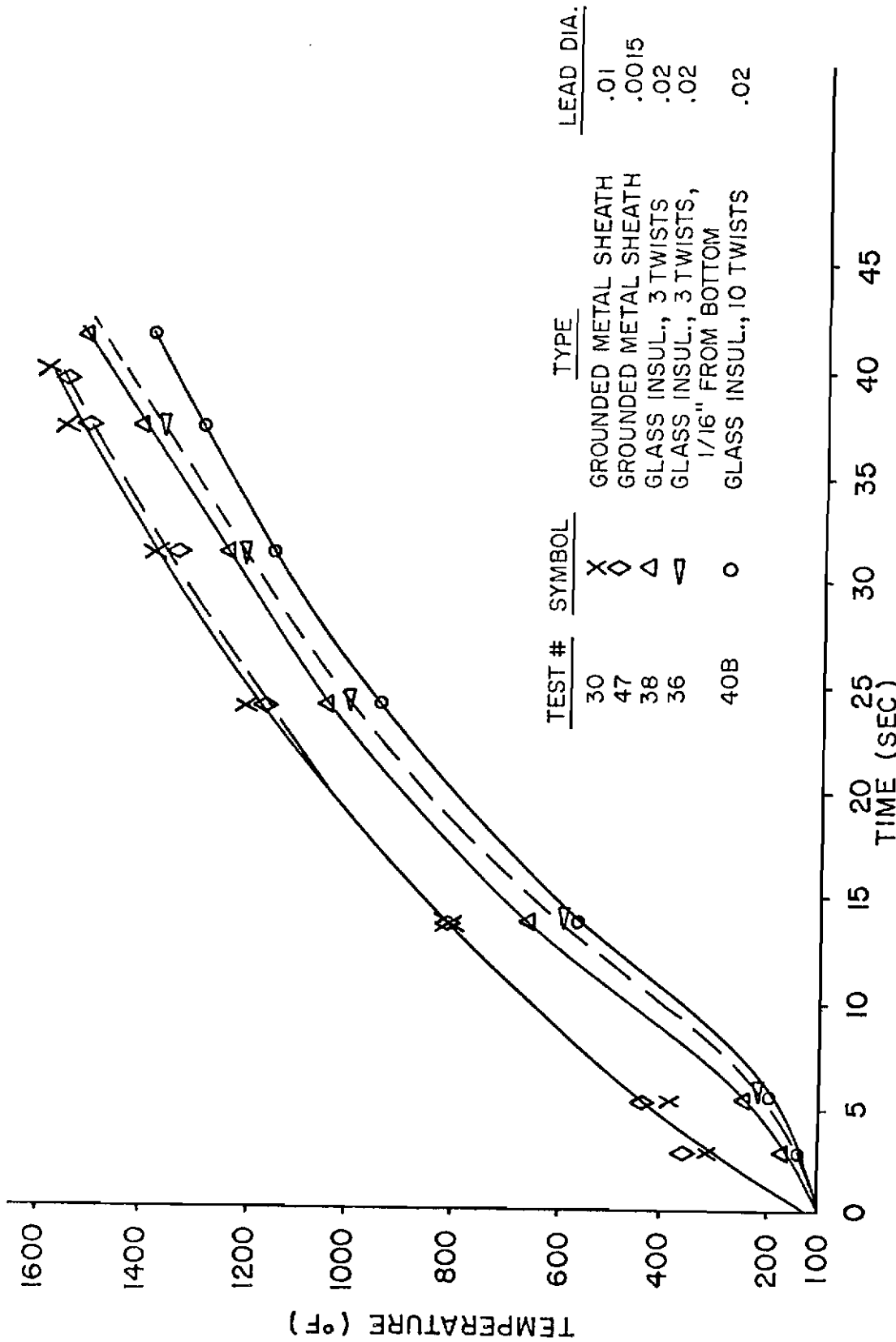


Figure 19. Temperature vs Time, Thermocouple Comparison

Contrails

discrepancies in setup, input energy, or plotter characteristics. Note as before that Test 30 and Test 19 show almost the same results. This shows that either the exposed (Test 19) or the grounded (Test 30) metal sheathed thermocouple is the best tested other than the Test 47 thermocouple. The small diameter (.10 in. sheath diameter) thermocouple used in Test 47 is not recommended for use in actual brake tests due to its size and fragility. The highest temperature plotted in Figure 19 for each curve is the actual peak temperature reached during the test. This is somewhat misleading since baseline peak temperatures for these tests varied slightly.

A comparison of the peak temperatures reached during all reported tests is shown in Table 5. The peak temperatures of the test thermocouples are not directly correlatable since the baseline peak temperatures are not identical. To circumvent this difficulty, the peak temperature of each test thermocouple was adjusted by multiplying it by the ratio of the Test 47 baseline peak temperature to the baseline peak temperature of the particular test in question. This adjustment is shown in the third column of temperatures in Table 5. The column following shows the percent difference between each adjusted test peak temperature and the peak temperature of Test 47. The greatest difference is for Test 40B which shows that the adjusted peak temperature of Test 40B is 11.1% lower than that of Test 47. This is the glass braid insulation thermocouple with 10 twists as the junction. The next highest difference is with Test 36 which is 5.1% low. This thermocouple was of the glass braid insulation type with 3 twists forming the junction and was placed 1/16 in. from the bottom of the hole in the

TABLE 5

PEAK TEMPERATURE COMPARISON

TEST NO.	THERMOCOUPLE DESCRIPTION	BASELINE ^a T/C (°F)	TEST ^a T/C (°F)	T _{TA} (°F) ^d	$\frac{T_{TA} - T_{47}}{T_{47}}$ (%)	LAG (SEC) $t_T - t_{47}$
15	.01" Shth, .0015" Leads, Grnded	1,552	1,572	1,569	.71	0.
18	.0625" Shth, .01 Leads, Exposed ^b	1,556	1,573	1,565	.45	1.
19	.0625" Shth, .01" Leads, Exposed	1,558	1,599	1,589	1.99	.25
23	.0625" Shth, .01" Leads, Exposed	1,552	1,595	1,591	2.12	.25
24	.0625" Shth, .01" Leads, Ungrnded ^b	1,547	1,563	1,564	.38	.75
27	.0625" Shth, .01" Leads, Ungrnded	1,542	1,574	1,580	1.41	1.
29	.0625" Shth, .01" Leads, Grnded ^b	1,532	1,569	1,585	1.73	.75
30	.0625" Shth, .01" Leads, Grnded	1,521	1,575	1,602	2.82	.25

TABLE 5--continued

TEST NO.	THERMOCOUPLE DESCRIPTION	BASELINE ^a T/C (°F)	TEST ^a T/C (°F)	T _{TA} (°F) ^d	$\frac{T_{TA} - T_{47}^d}{T_{47}}$ (%)	LAG (SEC) t _T - t ₄₇
32	.0625" Beads, .01" Leads, Exposed ^b	1,530	1,565	1,583	1.60	1.
34	.0625" Beads, .01" Leads, Exposed	1,537	1,591	1,602	2.82	.25
36	.061" Glass, .02" Leads, 3 Twists ^b	1,567	1,497	1,478	-5.1	2.75
38	.061" Glass, .02" Leads, 3 Twists	1,531	1,502	1,519	-2.5	2.5
40B	.061" Glass, .02" Leads, 10 Twists	1,573	1,407	1,385	-11.1	2.5
41	.061" Glass, .02" Leads, 3 Twists	1,547	1,510	1,511	-3.02	2.75
42	.061" Glass, .02" Leads, 1 Twist	1,611	1,586	1,523	-2.25	2.75
44	.061" Glass, .02" Leads, Welded	1,547	1,548	1,549	-.58	1.25

TABLE 5--continued

TEST NO.	THERMOCOUPLE DESCRIPTION	BASELINE ^a T/C (°F)	TEST ^a T/C (°F)	T _{TA} (°F) ^d	$\frac{T_{TA} - T_{47}^d}{T_{47}}$ (%)	LAG (SEC) t _T - t ₄₇
45	.041" Glass, 012", Welded	1,549	1,577	1,576	1.15	.5
47	.01" Shth, Glued, .0015" Lds, Grnd	1,548	1,558	1,558	0	0.
48	.01" Shth, Glued, .0015" Lds, Grnd ^c	1,510	1,522	1,560	.13	0.

^aApplicable temperatures have been corrected for calibration.

^bThis thermocouple was placed 1/16 in. from the hole bottom. All others were placed at the hole bottom.

^cThis test differed from No. 47 in that a heat input rate of about half that of No. 47 was used.

^dSubscript Terminology: T - Test, B - Baseline, C - Current, A - Adjusted, T_{TA} = $\frac{T_{TC} \times T_{B47}}{T_{BC}}$

Contrails

carbon block. All other adjusted peak temperatures are within 3% of that of Test 47. The last column in Table 5 shows the difference between the time the adjusted peak temperature of each test occurred and the time the peak temperature of Test 47 occurred. This information could only be read accurately to the nearest 1/4 sec. The largest lag occurred with Tests 36, 41, and 42 at 2.75 sec followed closely by Tests 38 and 40B at 2.5 sec. These five tests were all of the .061 in. diameter glass braid insulation type with twisted junctions. The .061 in. diameter glass braid with the welded junction (Test 44) was next at 1.25 sec. Thermocouples placed 1/16 in. from hole bottom, other than the .061 in. diameter glass braid, had lag times of from .75 to 1.0 sec. The three tests (15, 47, 48) conducted with the .01 in. diameter sheath had no lag time. Comparing the two spot-welded thermocouples shows that the smaller diameter lead wire (.012 in. vs .02 in.) gives a smaller lag time, 0.5 vs 1.25 sec. The best thermocouples as far as supplying the least lag time (.25 sec), other than the .01 in. diameter sheath thermocouple, are those of Tests 19, 23, 30, 34. All of these are either grounded or exposed.

Conclusions

These conclusions are based on the particular test configuration employed. If other applications change heating rates or levels or materials, the levels of error could change. Each conclusion is followed by a set of numbers which refers to the tests from which the conclusion was drawn.

Conclusions

1. The difference in temperature caused by increasing the hole in the carbon block from .02 in. diameter to .07 in. diameter and cementing a stainless steel sheath in the larger hole is negligible (15, 47).
2. The difference in temperature caused by decreasing the heat input rate to approximately half is less than 2% for the .01 in. diameter sheath thermocouple (47, 48).
3. The method of creating a junction by twisting the thermocouple end gives temperatures up to 35% low if 1 twist is used and up to 55% low if 10 twists are used (38, 40B, 41, 42).
4. Welding the thermocouple junction reduces that maximum error from the above value of 35% for 1 twist to 29% (42, 44).
5. Using a smaller diameter thermocouple (.012 in. vs .02 in.) reduces the error about 5% (44, 45).
6. The error incurred in moving the thermocouple 1/16 in. from the bottom of the hole in the carbon is approximately 5% (18, 19, 24, 27, 36, 38).
7. The best two thermocouples are the .0625 in. diameter stainless steel sheathed thermocouples, one of which had an exposed junction and the other had a grounded junction. The grounded junction is recommended in the brake application due to the lack of junction protection in the exposed junction thermocouple. The smallest diameter thermocouple (.01 in.) is not recommended due to its size and thus inherent fragility (19, 30). Refer to Table 2, page 38, for lead wire diameters.
8. The use of glass braid insulated thermocouples at temperatures around or above 1500°F should be limited to short-time usage in

Contrails

nonmoving environments due to the insulation brittleness and probable crumbling (36, 38, 40B, 41, 42, 44, 45).

9. As long as an excessive (above 3) number of twists is not used and the thermocouple is located at the bottom of the hole, the error in peak temperature is less than 3% (36, 40B).

10. A lag time of up to 2.75 sec can be expected at the peak temperature for twisted junction thermocouples (36, 38, 40B, 41, 42). This lag time can be reduced to .25 sec for exposed or grounded junction stainless steel sheathed thermocouples (18, 23, 30).

11. All of the ten thermocouples calibrated independently from the manufacturer proved to be more accurate than the tolerance given by the manufacturer.

CHAPTER IV

FULL-SCALE BRAKE TESTS

Introduction

At present, in the evaluation of brakes for automobiles, trucks, and aircraft, a fairly extensive testing program is essential. It is time consuming and expensive to conduct full-scale brake tests on the vehicles they are designed to stop. Although the ultimate evaluation must occur on the particular vehicle, much laboratory testing is necessary first. Two basic test methods are generally used to evaluate brakes in the laboratory. The first and most common method used to test brakes uses a flywheel to provide the relative speed between the brake-axle assembly and the flywheel. Thus, the brake-axle assembly remains stationary and the flywheel turns. The speed at the flywheel's outer diameter is equal to that speed required between the test vehicle and the ground. The inertia of the flywheel is usually variable to allow the vehicle mass to be simulated. This testing method¹² is universally used within the brake industry. In the second method, a machine employing a flat plate creates relative motion between the plate and the brake-axle assembly. This test method is seldom used since speeds attainable are limited due to power requirements, moving plate weight and plate length. Additionally, the plate dimension in the moving direction can restrict the duration of the brake test. If the plate is made longer, available space becomes a primary

concern. The first method discussed eliminates many of these problems. On the other hand, test flywheels or dynamometers are expensive to procure and maintain and are thus found mostly in large corporations or governmental facilities. This is the primary reason that many efforts dealing with brake theoretical models are void of experimental verification data.

Test Apparatus

Dynamometer

A typical dynamometer is shown in Figure 20. The flywheel is in three sections. The center section rotates and the outer two sections remain stationary. Each of the outer sections is a series of discs that can be transferred to the center rotating section prior to a test. This allows different weights of vehicles to be simulated from test to test. The wheel assembly, as shown in Figure 20, is installed on the axle which is, in turn, fastened rigidly to a structure reaching to the floor and supported by large rollers. This structure, as well as the wheel assembly is pneumatically moved toward the flywheel during a test. All of the full-scale brake tests were conducted on a 192 in. diameter dynamometer located within the Landing Gear Test Facility, Building 31, in Area B of Wright-Patterson Air Force Base. This is the largest dynamometer in the world. The size of the flywheel is important to more adequately simulate a flat road surface (which has an infinite radius of curvature) and in being able to have large mass capabilities. This 192 in. dynamometer has the capability to test wheel assemblies on both sides and the small, or north side, carriage was used in

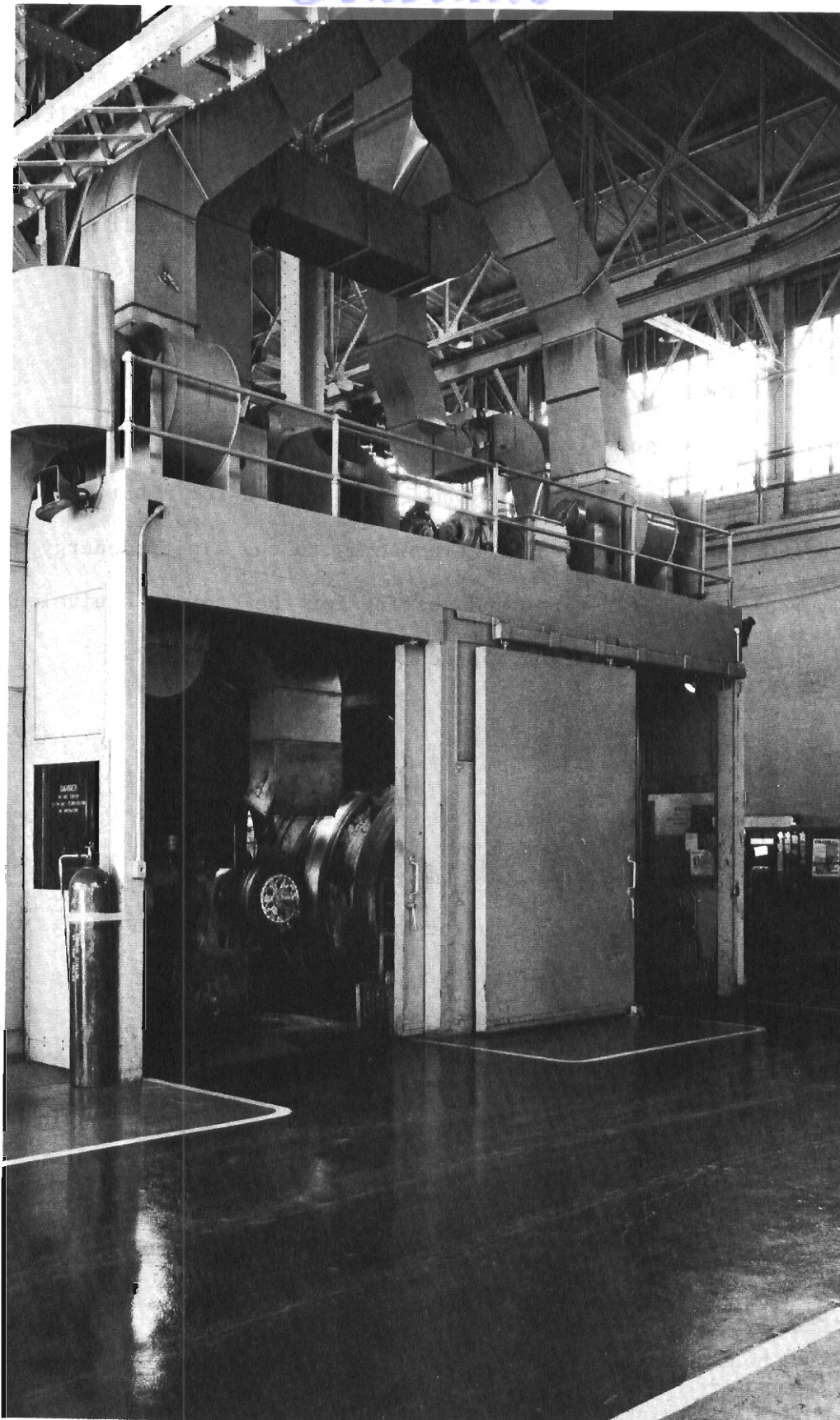


Figure 20. Typical Tire Test Dynamometer

this research. This carriage has the following maximum capabilities:

- (1) 40,000 lbf normal load between the tire and flywheel
- (2) 200 miles/hour tangential velocity at the flywheel maximum radius
- (3) 205×10^6 ft-lbf kinetic energy
- (4) 80 in. tire diameter,
- (5) inertia equivalent of 162,987 lbm

The inertia equivalent of the flywheel is obtained for a particular test by equating the desired kinetic energy to the kinetic energy of the flywheel in angular terms and solving for the inertia equivalent term. The following equation applies.

$$\frac{1}{2} M V_v^2 = \frac{1}{2} I_n \omega_f^2 = \frac{1}{2} IE R_f^2 \omega_f^2 \quad (27)$$

where M is the mass of the vehicle to be tested, V_v is the velocity at which the vehicle is traveling, I_n is the flywheel inertia, ω_f is the flywheel angular velocity, IE is the inertia equivalent and R_f is the flywheel outer radius. Solving for the inertia equivalent gives:

$$IE = M V_v^2 / R_f^2 \omega_f^2 \quad (28)$$

Full-Scale Brakes

The brake selected for the experimental tests is also used in the F-14 aircraft. A four-rotor brake was primarily selected because two sets of rotors and stators were readily available that would fit into the brake housing. One complete set of rotors and stators for a brake is called a heat sink. The above heat sink selection allowed the testing of two heat sink materials without the effects of a different

Contrails

housing, tire, and wheel. The two heat sink materials used were carbon composite and beryllium. This choice allowed a variation in density, heat capacity, and thermal conductivity. A typical beryllium rotor is shown in Figure 21. The keyways are located at the outside diameter of the rotor. The rotor keys to the rotating wheel through these keyways and thus rotates with the wheel. Wear pads are bolted to the beryllium core as shown. The wear pad thickness is about 3% of the total disc thickness. Figure 22 shows a typical beryllium stator. Here the keyways are at the inside diameter since the stator is keyed to the nonrotating axle. Note that the force must be greater at a stator keyway than at a rotor keyway since both support the same torque during a test. Thus, in order to have a more even force distribution, the stator has ten keyways compared to eight for the rotor. Figures 23 and 24 are photographs of a typical carbon composite rotor and stator, respectively. Other than the material, the main difference between the carbon and beryllium is that the carbon requires no separate wear pads, as does the beryllium. The separate wear pads are required on beryllium since any rubbing on beryllium itself creates a toxic dust.

Figure 25 shows a photograph of the beryllium heat sink ready to be assembled. The brake housing is shown on the left, the heat sink (all rotors and stators) is on the right, and the torque tube, through which the stators are keyed to the axle, is in the middle. At assembly the housing is bolted to the left side of the torque tube, and the stator on the far right is bolted to the right end of the torque tube. This allows the hydraulic pressure to push the pressure plate (plate at the right of the housing) to the right, engaging the stators and

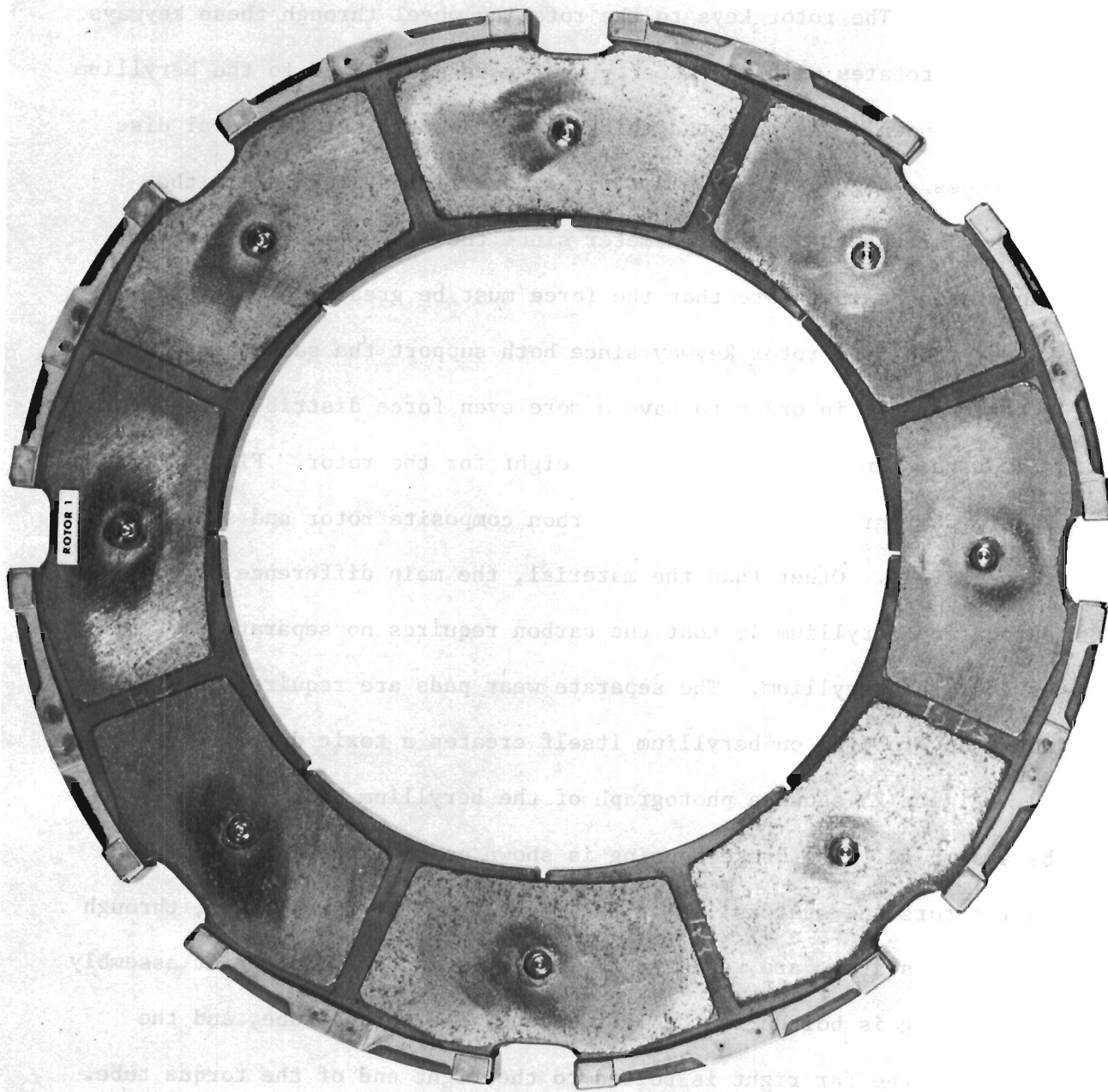


Figure 21. Typical Beryllium Rotor

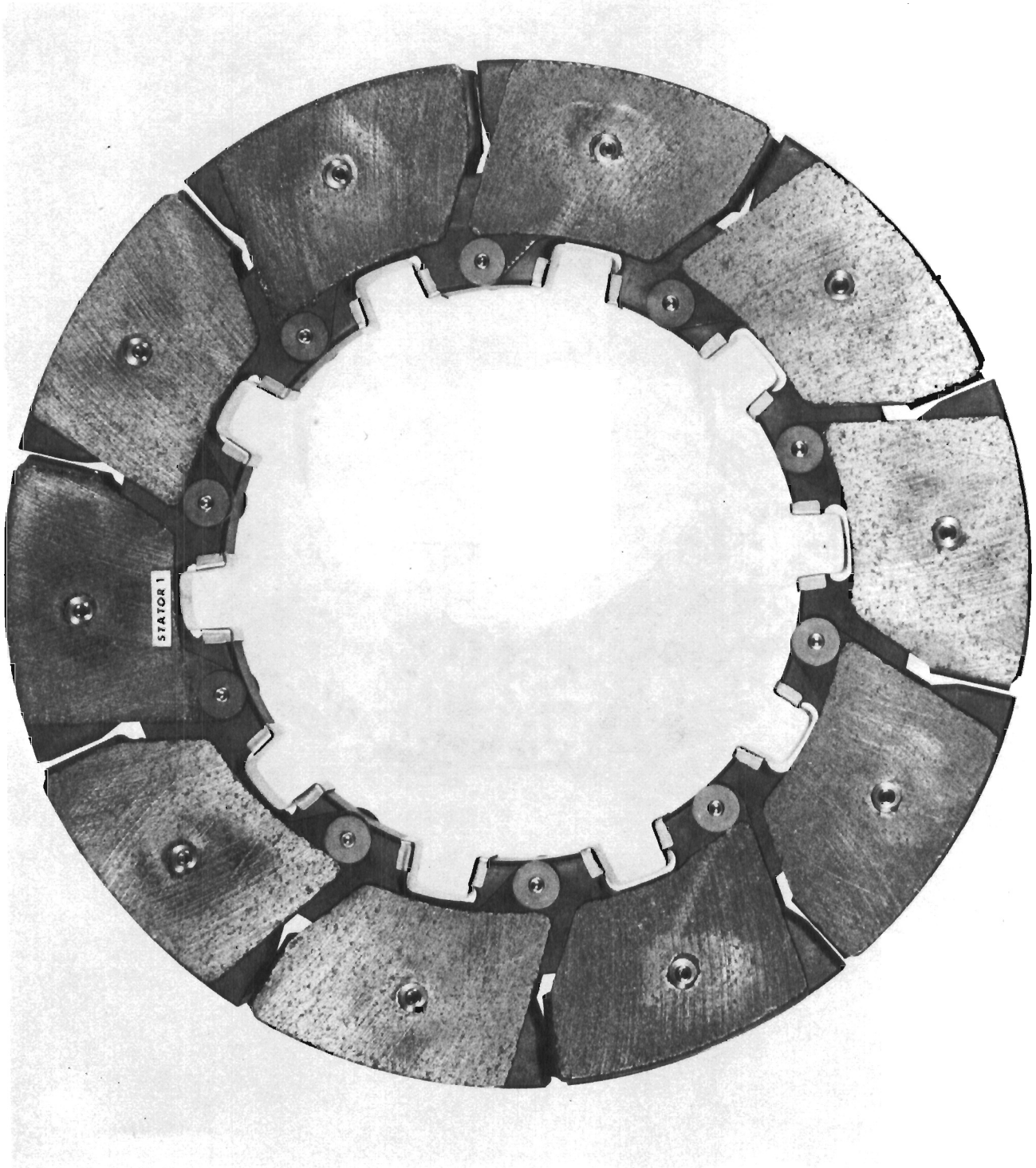


Figure 22. Typical Beryllium Stator

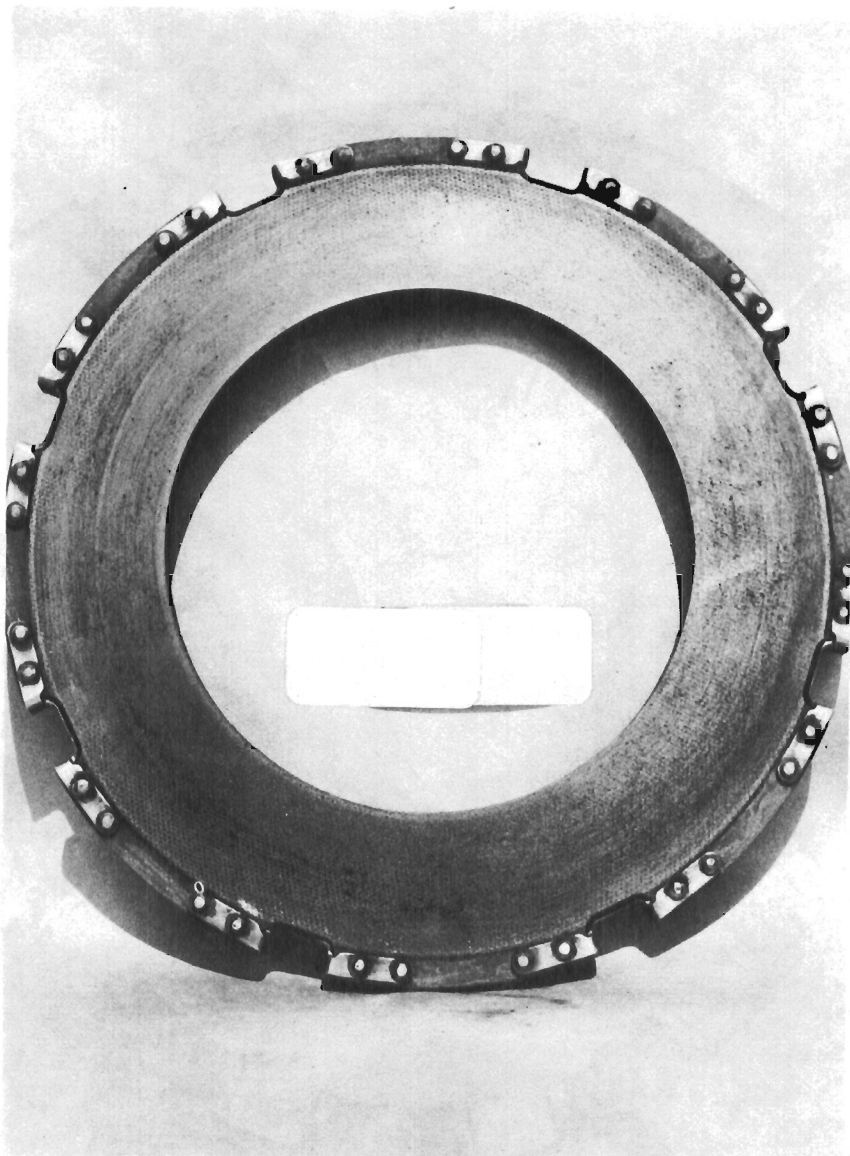


Figure 23. Typical Carbon Composite Rotor

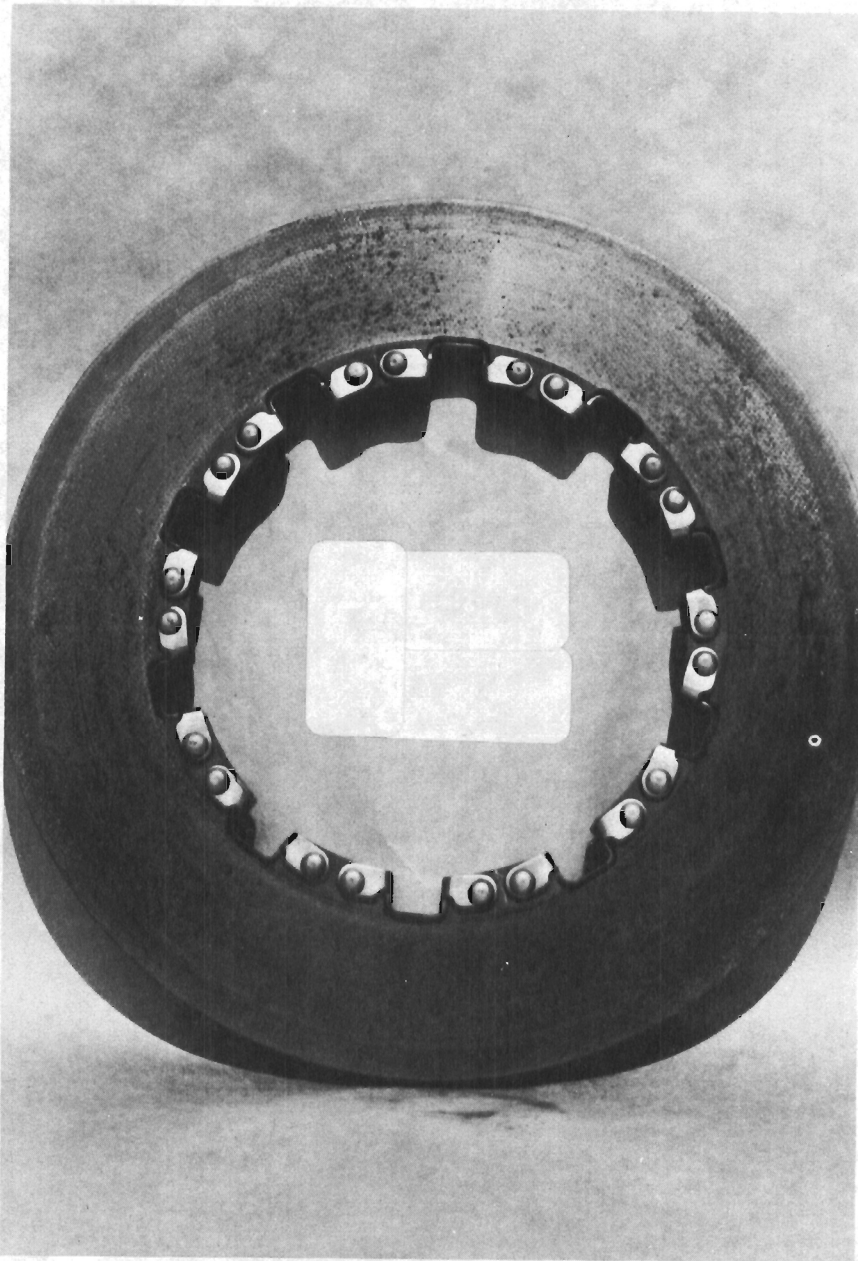


Figure 24. Typical Carbon Composite Stator

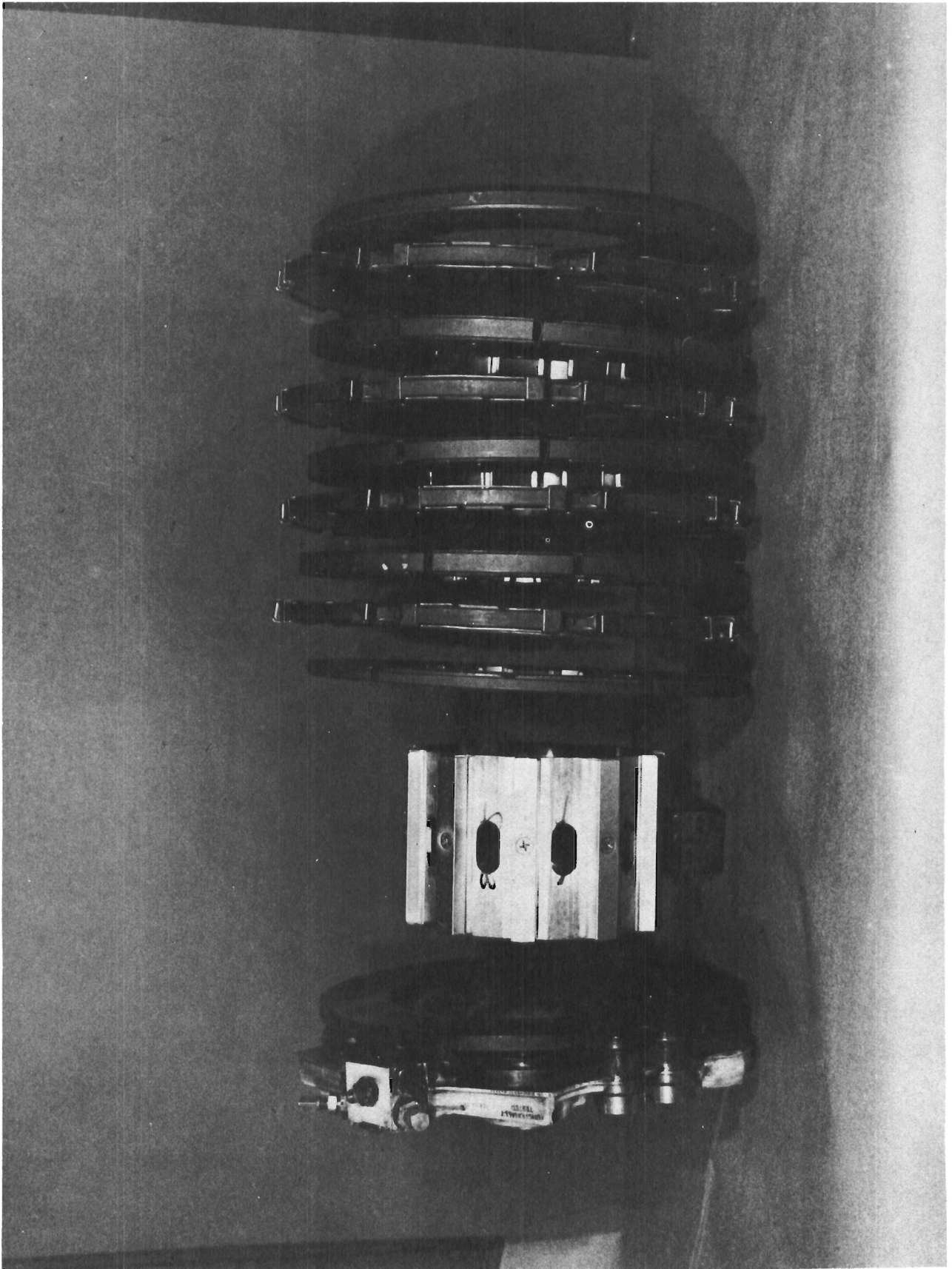


Figure 25. Beryllium Brake Exploded View

Contrails

rotors. The carbon heat sink is assembled similarly using the same housing and torque tube. The assembled brake is shown in Figure 26. The torque tube can be seen at the housing inside diameter. The ten cylindrical objects arranged in sets of two, placed symmetrically within the housing, are the return springs. They insure that the pressure plate will be pulled away from the stators and rotors when the brake hydraulic pressure is not applied. This allows the stators and rotors to separate from one another when no braking is desired. The five lighter colored cylindrical shapes (Figure 26) evenly spaced between the sets of return springs are the pistons to which the hydraulic fluid is fed to apply the pressure required during vehicle braking. The hydraulic fluid enters the housing through the fluid port shown on the extreme left of Figure 26. The fluid is channeled to each piston through the raised channels shown between each pair of pistons.

Next, the brake is mounted on the axle or mandrel in front of the dynamometer as shown in Figure 27. The rotating portion of the flywheel is shown in the background on the right with the nonrotating portion on the left. The structure into which the mandrel fits is mounted on large rollers and, as mentioned earlier, will move toward the flywheel during a test. The hydraulic pressure line is shown at the top of the brake. The wires with the connectors are the thermocouples used for temperature measurement and will be described in more detail later.

The last step in assembling the test setup is to install the tire and wheel over the brake and to attach the end axle nut as shown in Figure 28. The assembly in front of the wheel including the wires is

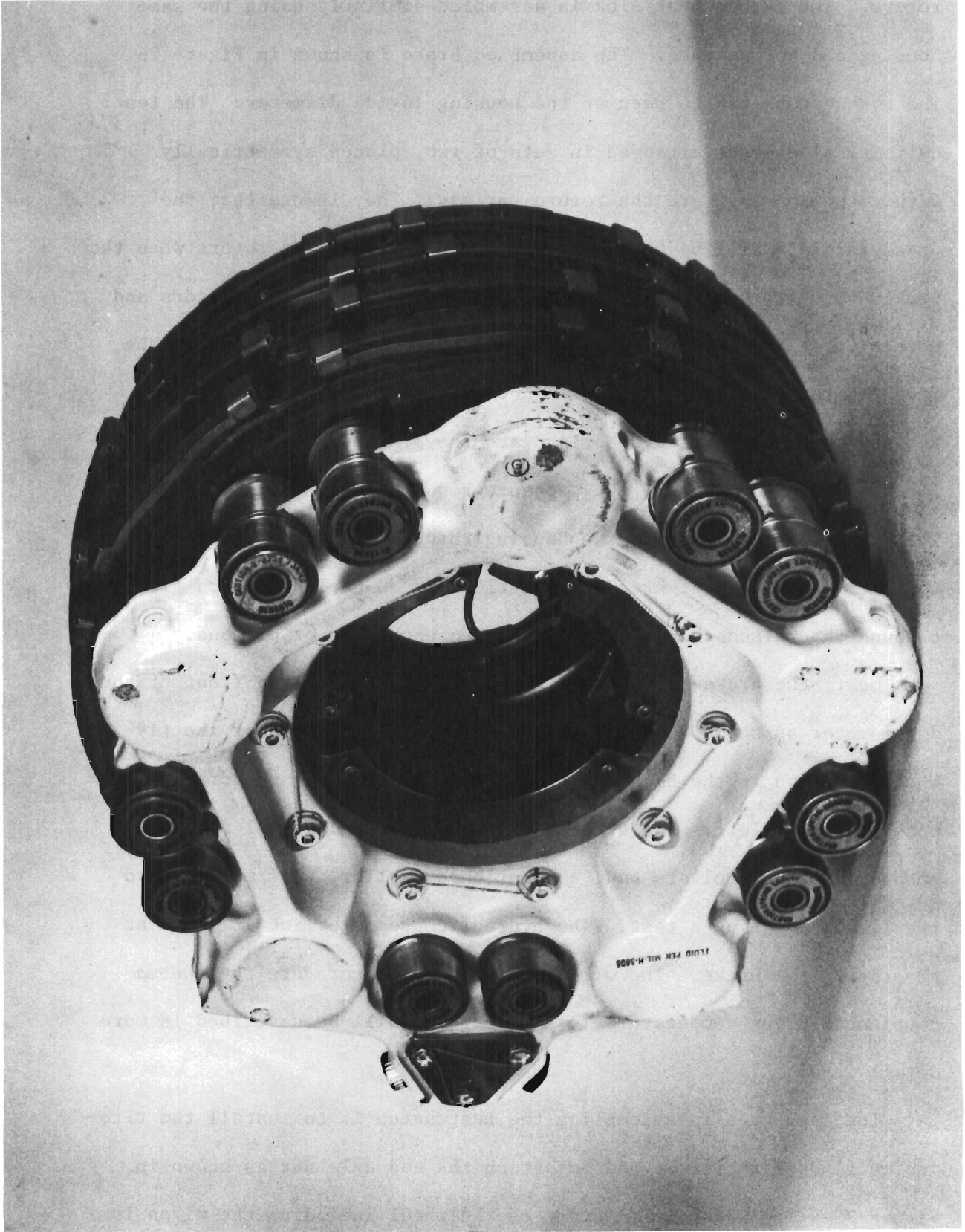


Figure 26. Assembled Beryllium Brake

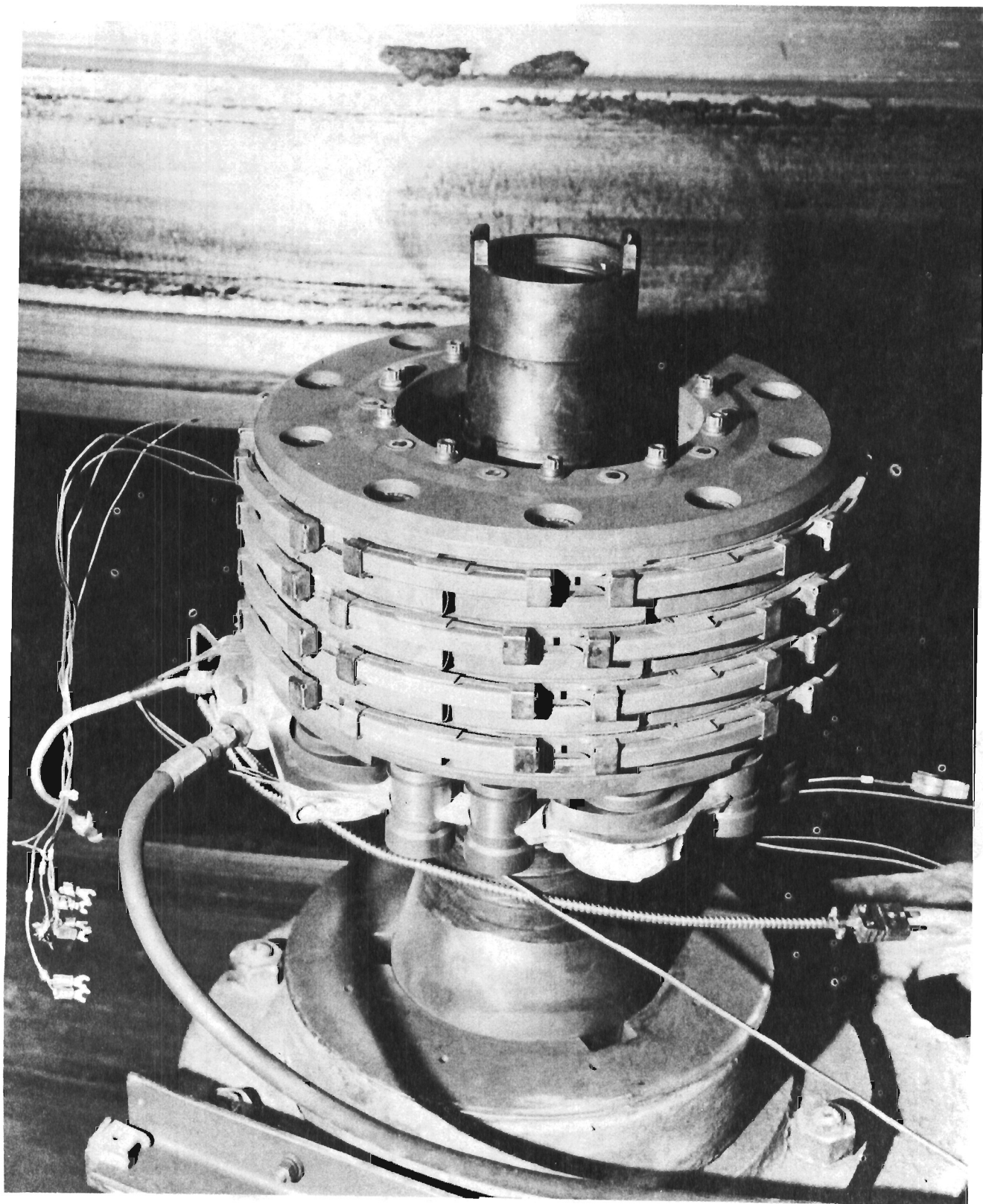


Figure 27. Beryllium Brake on Test Mandrel

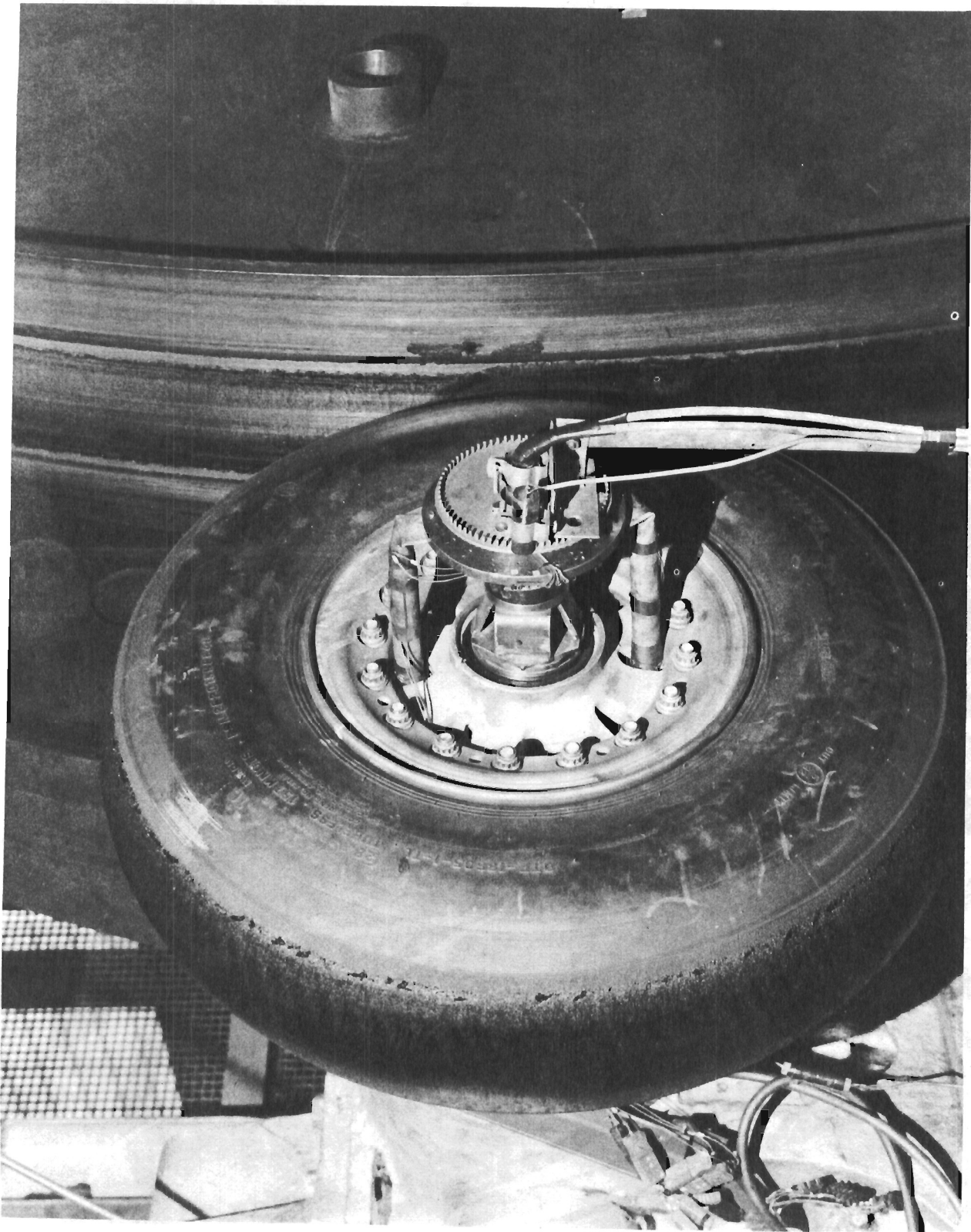


Figure 28. Beryllium Brake With Tire and Wheel Assembly

Contrails

part of the instrumentation used and will be described in the instrumentation section.

Test Plan

The basic objective was to test both the carbon and beryllium brakes to the same set of conditions. The inertia equivalent, normal load, rolling radius (distance from flywheel outer surface to the mandrel centerline), kinetic energy, and the inflation pressure were selected to be approximately those of the F-14 aircraft. The inertia equivalent was 10,147 lbm and was calculated as described earlier. The normal load for all stops was 20,000 lbf, and the rolling radius was 16.5 in. The inflation pressure was not an independent parameter and was selected so that the 20,000 lbf normal load would result in a rolling radius of 16.5 in. as specified. Tests were run at two kinetic energies, i.e., 11.23×10^6 ft-lbf and 6.74×10^6 ft-lbf. These are subsequently referred to as 100% and 60% conditions, respectively. Since the kinetic energy and mass were specified, the initial velocity was calculated. This resulted in 141 mph for the 60% kinetic energy tests and 182 mph for the 100% kinetic energy tests. The brake pressure was maintained at a constant value during a particular test and was selected based upon a desired flywheel deceleration. Two decelerations were selected in order to have two heating rates for the brake. Since the deceleration is dependent on the wearing surface coefficient of friction characteristics, the actual deceleration varies somewhat from the desired values. The first value selected was 3.0 ft/sec^2 and was selected based on a smooth routine F-14 landing. The second was 7.0 ft/sec^2 and was selected based on a more severe braking condition

Contrails

but not at the maximum capability of the brake. Based on previous test experience, the brake pressures could now be specified since the dynamometer operator must have a pressure value rather than a deceleration. For the beryllium brake the pressures required to give approximately 3.0 and 7.0 ft/sec² deceleration were 270 psig and 400 psig, respectively. The carbon brake required 240 and 425 psig to attain the desired decelerations.

Basically two types of tests were conducted. The first was a constant pressure stop at the various conditions described above. At the completion of this stop the brake heat sink was allowed to cool to 150°F before beginning the next stop. This cooling was accomplished either by forced convection using external air blowers (shown as rectangular ducts above the tire in Figure 20) or by natural convection. The second test was accomplished to allow calculation of convection-radiation heat transfer coefficients at various brake rotation speeds without the brake being actuated during the rotation. This calculation procedure is discussed later. Thus, the procedure was to complete a brake stop as described above, but to rotate the brake using the dynamometer at a constant speed during the cooling process. This was accomplished with the blowers as previously described and also without the blowers. In each type of test the procedure was to bring the flywheel to the desired speed, shut off the motor, bring the tire into contact with the flywheel, apply a constant pressure to the brake until the flywheel stopped and then to bring the test wheel away from the flywheel. Table 6 summarizes all tests conducted as described above. It should be noted that all tests, except the

TABLE 6

F-14 BRAKE TEST PLAN

Brake: Paragraphs 1 - 5 -- Carbon
Paragraphs 6 - 10 -- Beryllium

I.E. -- 10,147 lbm - North (Small) Carriage 192 in. Diameter
Dynamometer

Normal Load -- 20,000 lbf

Rolling Radius -- 16.5 in.

Inflation Pressure -- that required to get 16.5 in. rolling
radius at 20,000 lbf load

1. 60% K.E., 141 mph, brake pressure = 240 psi
 - 1.1 3 stops using blowers after stators peak
 - 1.2 3 stops with blowers off continuously
2. 60% K.E., 141 mph, brake pressure = 425 psi
 - 2.1 3 stops using blowers after stators peak
 - 2.2 3 stops with blowers off continuously
3. 100% K.E., 182 mph, brake pressure = 240 psi
 - 3.1 3 stops using blowers after stators peak
 - 3.2 3 stops with blowers off continuously
4. 100% K.E., 182 mph, brake pressure = 425 psi
 - 4.1 3 stops using blowers after stators peak
 - 4.2 3 stops with blowers off continuously
5. 100% I.E., 182 mph, brake pressure = 425 psi

Make complete stop but immediately following the stop (no cooling time), let the brake cool by landing the tire at about 1,000 lbs normal load, maintaining speed in table below until the stators reach approximately 200°F (no brake pressure).

Contrails

TABLE 6-continued

Stop Number	Velocity at which to keep flywheel during brake cooling (mph)	Blowers turned on during const. speed cooldown
5.1	50	Yes
5.2	50	No
5.3	150	Yes
5.4	150	No
5.5	100	Yes
5.6	100	No
6.	60% K.E., 141 mph, brake pressure = 270 psi	
6.1	3 stops using blowers after stators peak	
6.2	3 stops with blowers off continuously	
7.	60% K.E., 141 mph, brake pressure = 400 psi	
7.1	3 stops using blowers after stators peak	
7.2	3 stops with blowers off continuously	
8.	100% K.E., 182 mph, brake pressure = 270 psi	
8.1	3 stops using blowers after stators peak	
8.2	3 stops with blowers off continuously	
9.	100% K.E., 182 mph, brake pressure = 400 psi	
9.1	3 stops using blowers after stators peak	
9.2	3 stops with blowers off continuously	
10.	100% K.E., 182 mph, brake pressure = 400 psi	

Make complete stop but immediately following the stop (no cooling time), let the brake cool by landing the tire at about 1,000 lbs normal load maintaining speed in table below until the stators reach approximately 200°F (no brake pressure).

TABLE 6-continued

Stop Number	Velocity at which to keep flywheel during brake cooling (mph)	Blowers turned on during const. speed cooldown
10.1	50	Yes
10.2	50	No
10.3	150	Yes
10.4	150	No
10.5	100	Yes
10.6	100	No

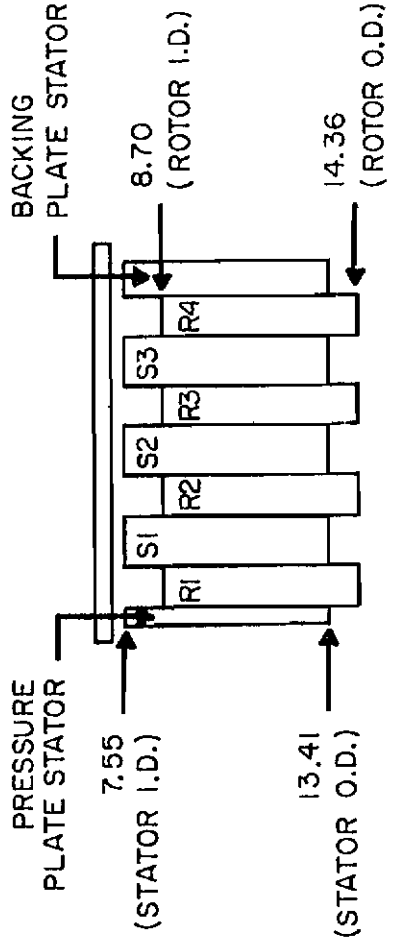
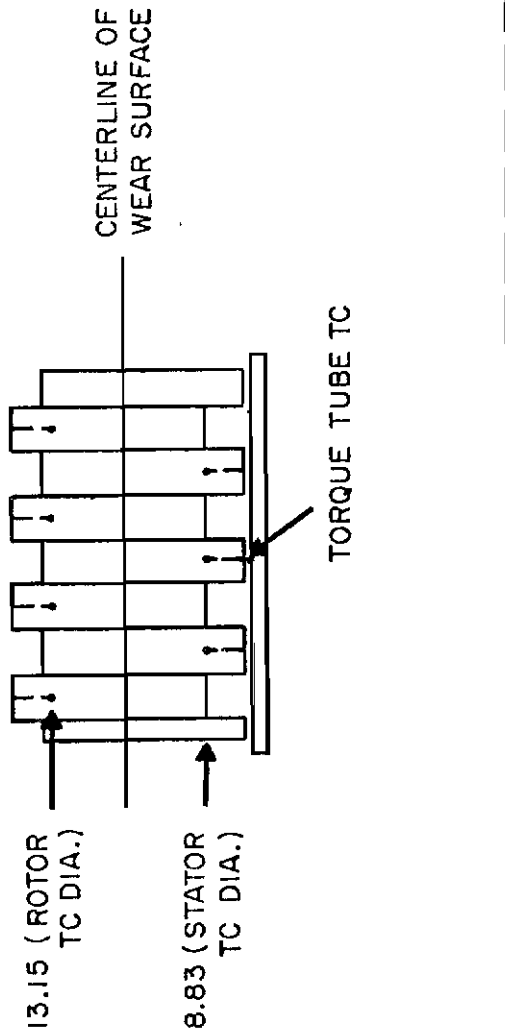
assisted cooling tests, were repeated three times to insure adequate repeatability of both the test conditions and the instrumented parameters.

Instrumentation

The purpose of this experimental portion of the investigation was to determine temperatures within the brake as a function of time for correlation with the theoretical developments. To accomplish this, 14 thermocouples were installed in the beryllium brake and 24 in the carbon brake. Based on the temperature measurement analysis in Chapter III, type K thermocouples with a stainless steel sheath and a grounded protected junction were used. The location of the thermocouples in the beryllium is shown in Figure 29. The dashed line indicates the direction of the thermocouple leads and the darkened circle indicates the location of the thermocouple junction. Figure 30 shows the location of thermocouples for the carbon heat sink. The placement of thermocouples, as well as the number of thermocouples in the carbon, is somewhat different than that in the beryllium. This is primarily

THERMOCOUPLE NUMBERS

2. STATOR # 1
3. STATOR # 2
4. STATOR # 3
5. TORQUE TUBE
6. TIRE BEAD SEAT
7. WHEEL LUG
8. FUSE PLUG
9. ROTOR # 1
10. ROTOR # 2
11. ROTOR # 3
12. ROTOR # 4
13. HYDRAULIC FLUID
14. CONTAINED AIR
15. WHEEL



- NOTES:
1. T/C ENTRANCE HOLE DIA. .08 IN.
 2. ALL DIMENSIONS ARE IN INCHES.
 3. THERMOCOUPLES 2-4 AND 9-12 ARE METAL SHEATHED.

Figure 29. Beryllium Heat Sink Thermocouple Locations

THERMOCOUPLE NUMBERS

- 2. STATOR #1
- 3. STATOR #2
- 4. STATOR #3
- 5. TORQUE TUBE
- 6. TIRE BEAD SEAT
- 7. WHEEL LUG
- 8. FUSE PLUG
- 9. ROTOR #1
- 10. ROTOR #2
- 11. ROTOR #3
- 12. ROTOR #4
- 13. HYDRAULIC FLUID
- 14. CONTAINED AIR
- 15. WHEEL
- 16. BACK PLATE #1 (O.D.)
- 17. BACK PLATE #2
- 18. BACK PLATE #3
- 19. BACK PLATE #4 (I.D.)
- 20. STATOR #1 SHALLOW
- 21. STATOR #1 ANGLED
- 22. STATOR #2 SHALLOW
- 23. STATOR #2 ANGLED
- 24. ROTOR #3 SHALLOW
- 25. ROTOR #3 ANGLED

NOTES: 1. T/C ENTRANCE HOLE DIAMETER .08 IN.

2. ALL DIMENSIONS ARE IN INCHES.

3. T/C 2-4, 9-12, 16-25 ARE METAL SHEATHED.

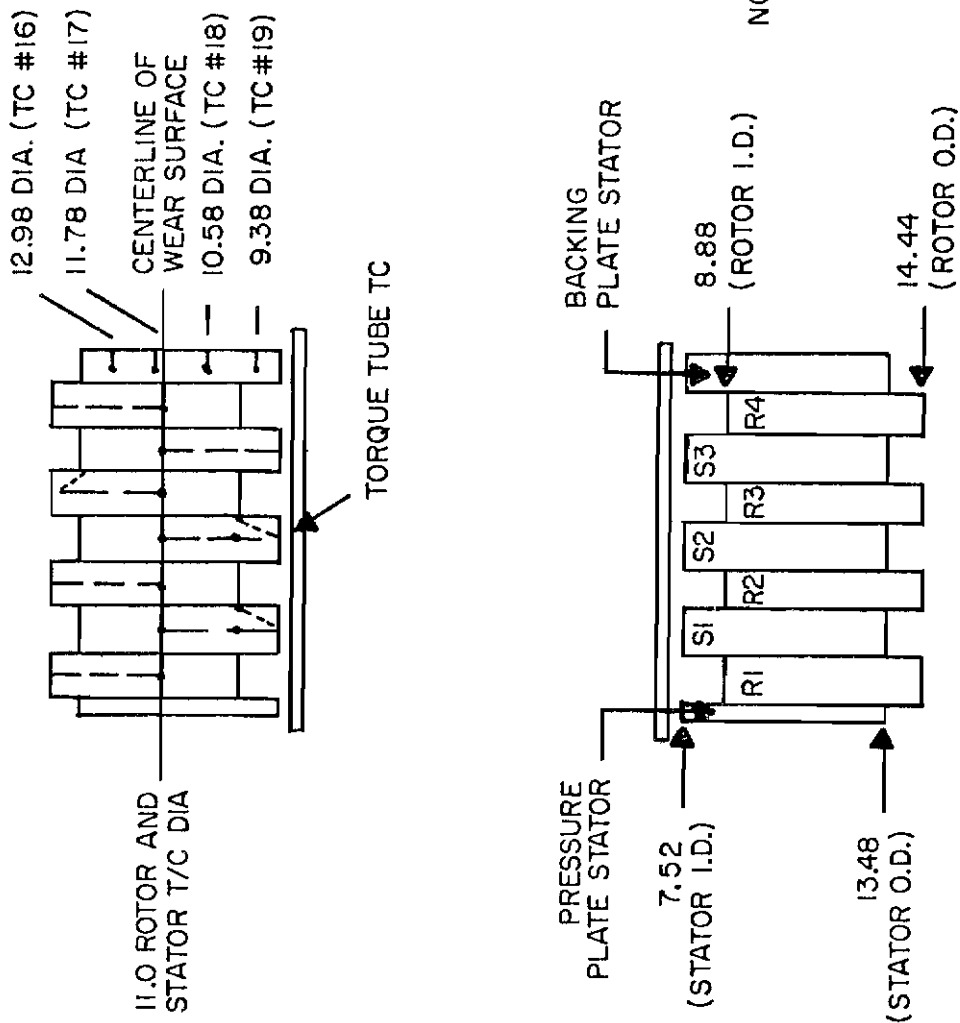


Figure 30. Carbon Heat Sink Thermocouple Locations

Contrails

due to the difficulty of drilling holes in the beryllium. The carbon composite used appeared to be of the consistency similar to ordinary pencil lead. It was readily machinable in a lathe or drill press. The excellent machinability of the carbon facilitated drilling holes at angles (No. 21, 23, 25 on Figure 30) with precise depth control and to controlled short depths (No. 16-19) and long depths (No. 2-4, 9-12) as well. On the other hand, the holes in the beryllium could not be drilled or controlled nearly as well. The beryllium material, when machined, emits a toxic beryllium dust that can accumulate within the human body and can ultimately cause death. Thus, machining of beryllium must be conducted within a special clean room and all operators must be protected such that beryllium dust cannot come in contact with any part of the body. This includes the wearing of gloves, hats, face masks, goggles, and a special mask for filtering the breathing air.

These machine operator hinderances, plus the fact that the holes were chemically etched into the beryllium, resulted in limited control compared to that in the carbon. Therefore, it was decided to use only shallow holes in the beryllium and not complicate the procedures with critical angles or depths. The specific holes in Rotor 3 and Stators 1 and 2, including the angled holes, all of which are shown in Figure 30, are more explicitly defined in Figure 31 for Rotor 3 and in Figure 32 for Stators 1 and 2. All thermocouples other than those in the heat sinks are shown in Figure 33. Due to the lower temperature gradients in the brake parts of Figure 33, glass insulation-type thermocouples were selected for those areas. All thermocouple outputs were recorded

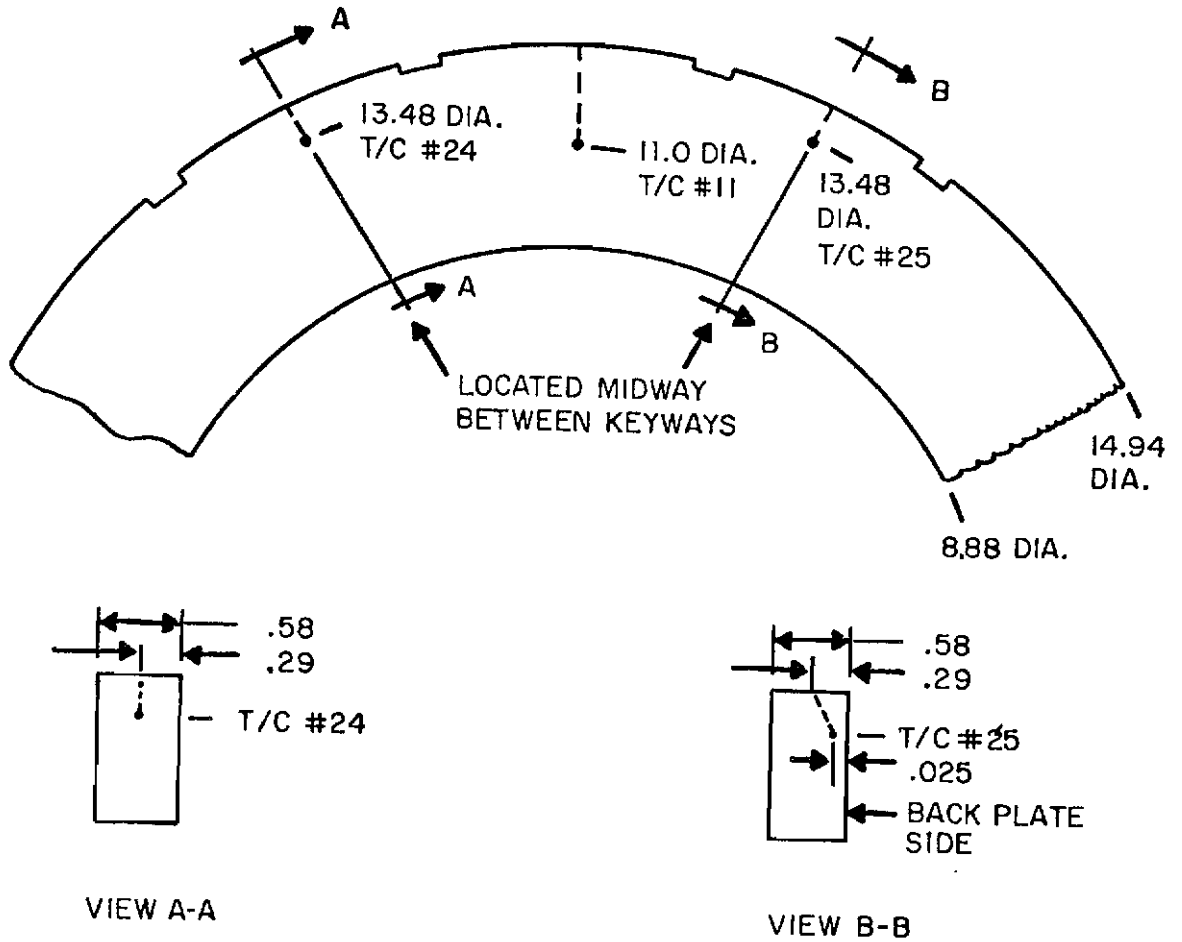


Figure 31. Carbon Rotor 3 Thermocouple Locations

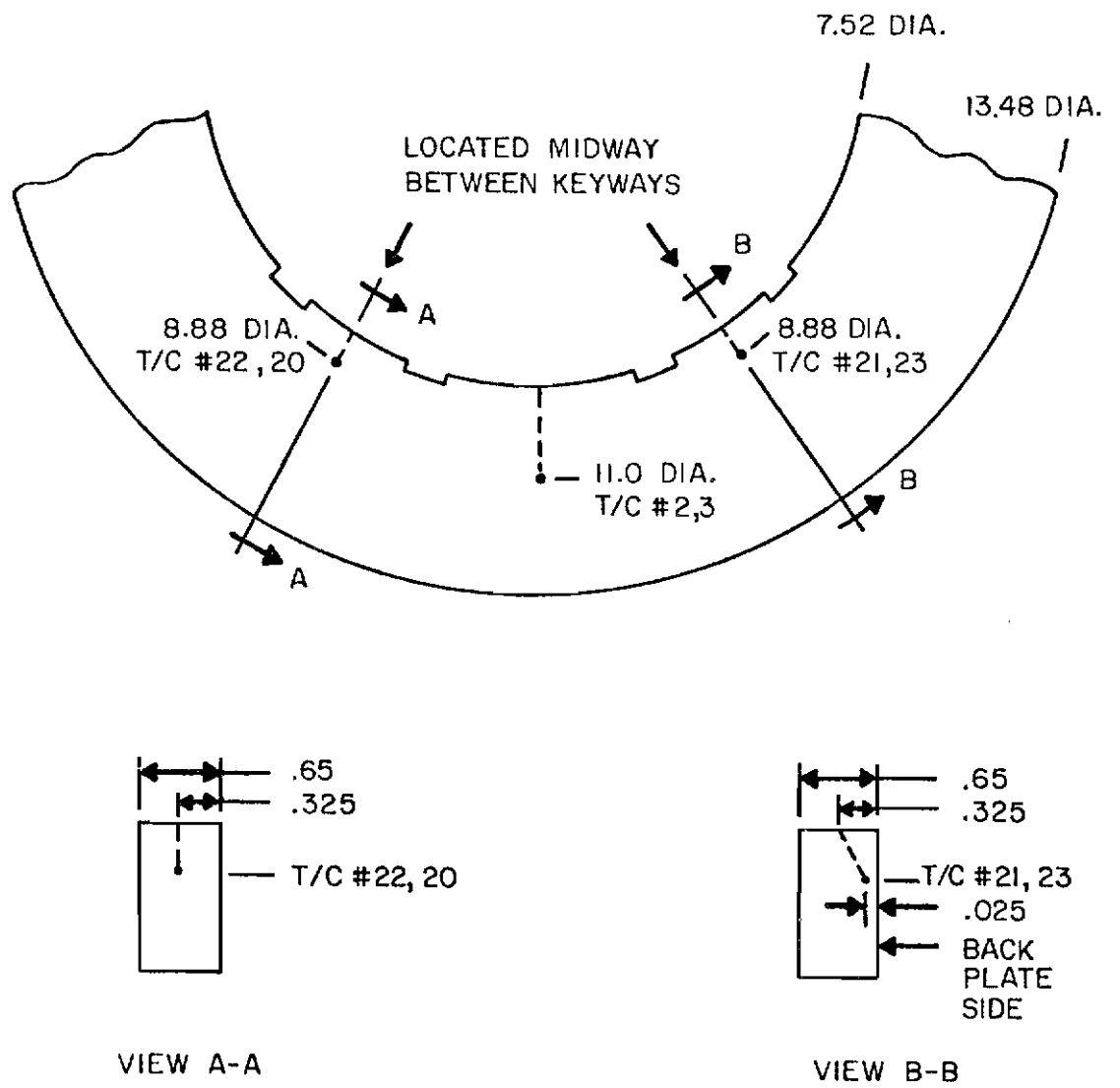
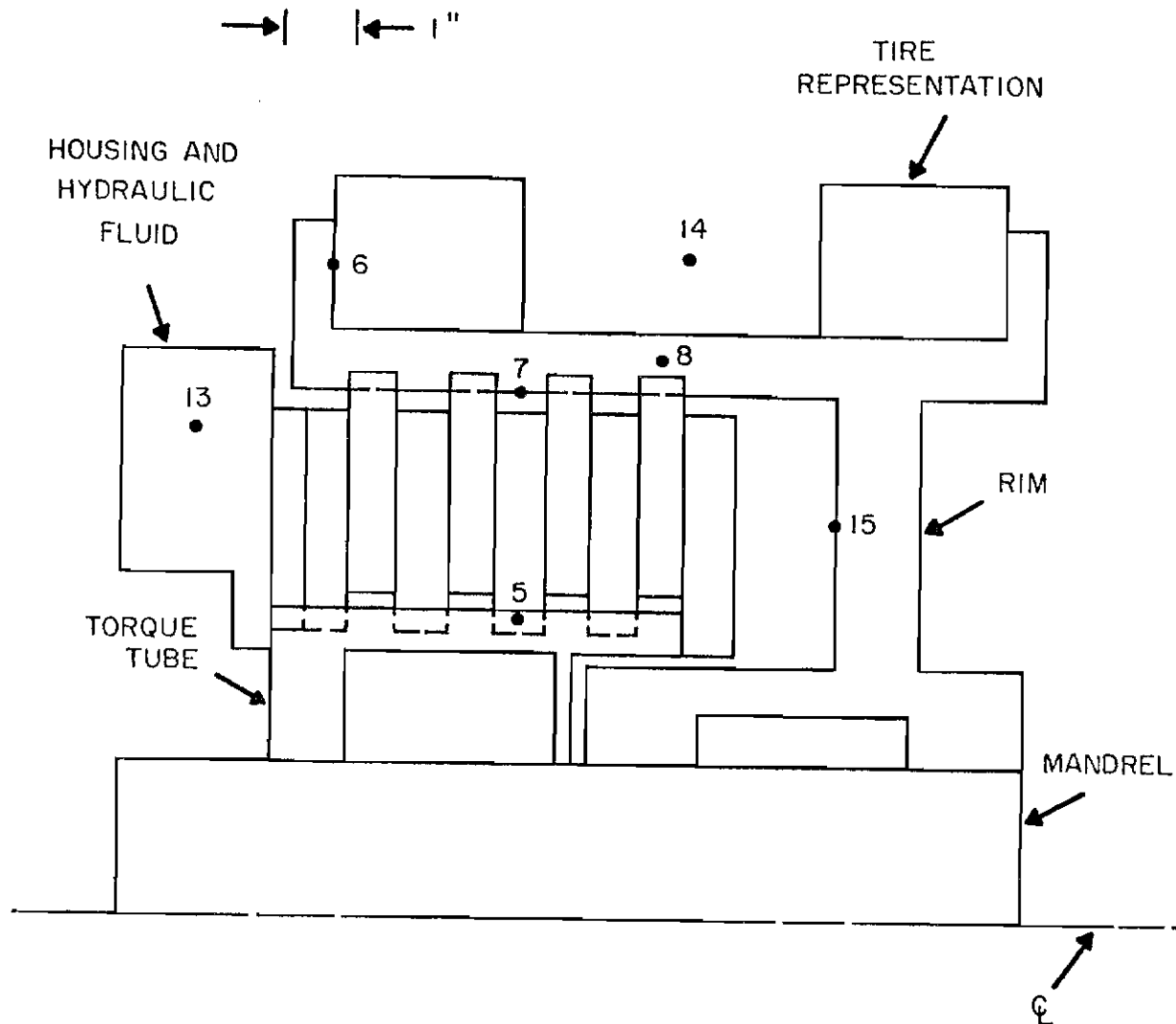


Figure 32. Carbon Stator 1 and 2 Thermocouple Locations



<u>THERMOCOUPLE NUMBER</u>	<u>LOCATION</u>
5	TORQUE TUBE
6	TIRE BEAD SEAT
7	WHEEL DRIVE LUG
8	FUSE PLUG
13	HYDRAULIC FLUID
14	CONTAINED AIR
15	WHEEL

Figure 33. Overall Thermocouple Locations

Contrails

on digital recorders. To increase the sampling rate, two recorders were used during each test. A Digitrend 220 Doric recorder and a Kaye Model 8000 recorder were used for all tests. For the carbon brake tests, Thermocouples 2-13 were recorded on the Kaye recorder while Thermocouples 14-25 were recorded on the Doric. For the beryllium, Thermocouples 2-8 were recorded on the Kaye and 9-13 on the Doric. This arrangement increased the sampling rate to 12 samples per minute. To insure that the start of a brake stop could be synchronized with the temperature information, at least one channel of each temperature recorder was, in addition to being recorded on the temperature recorder, recorded on magnetic tape along with brake pressure. This permitted comparison of the two temperatures from the same channel and provided the desired time reference. Rotor thermocouple output was channeled through a commutator (Figure 28) in order to record the outputs. The commutator longitudinal axis is in line with the mandrel axis.

Also shown in Figure 28 is the instrument used to measure the test wheel speed. A light source is located just to the left of the commutator that, during tire rotation, is continually interrupted by a series of small bolts at the outer diameter of the small plate in Figure 28. The corresponding pulse signals are fed into a digital-to-analog converter and the resulting analog signal is recorded on magnetic tape. Thus, it is a relatively simple matter to accurately determine the test wheel speed.

Contrails

Flywheel speed is measured similarly and is also recorded on magnetic tape. In this case the speed at the flywheel outer diameter is found in feet per second.

The torque developed during a brake stop is of primary interest in determining the energy absorbed by the brake as a function of time. The torque was obtained by mounting a temperature compensated strain gauge circuit to the mandrel and calibrating it using a torque arm applied to the mandrel when the wheel-brake assembly was removed. This signal was also recorded on tape for subsequent analysis.

Brake pressure was obtained using a pressure transducer upstream of the hydraulic inlet line as depicted in Figure 27. The pressure measured in this way is the pressure applied to the brake and includes not only the pressure forcing the discs together but also that pressure required to overcome the force of the return springs.

Normal load was found by measuring the pressure within the pneumatic loading system and multiplying it by the applicable area. This was recorded on tape in pounds force.

The deflection of the tire was also monitored and recorded. A linear velocity-displacement transducer was used in this case and similarly recorded on magnetic tape.

Each of the above mentioned parameters, including the two temperature channels, was recorded on a Bell and Howell VR-3700B Datatape unit. The specific units used are shown in Figure 34. Also shown in Figure 34 is the signal conditioning equipment which contains the capability of recording an audible signal describing each brake stop as to the test number and test conditions. This was accomplished for all

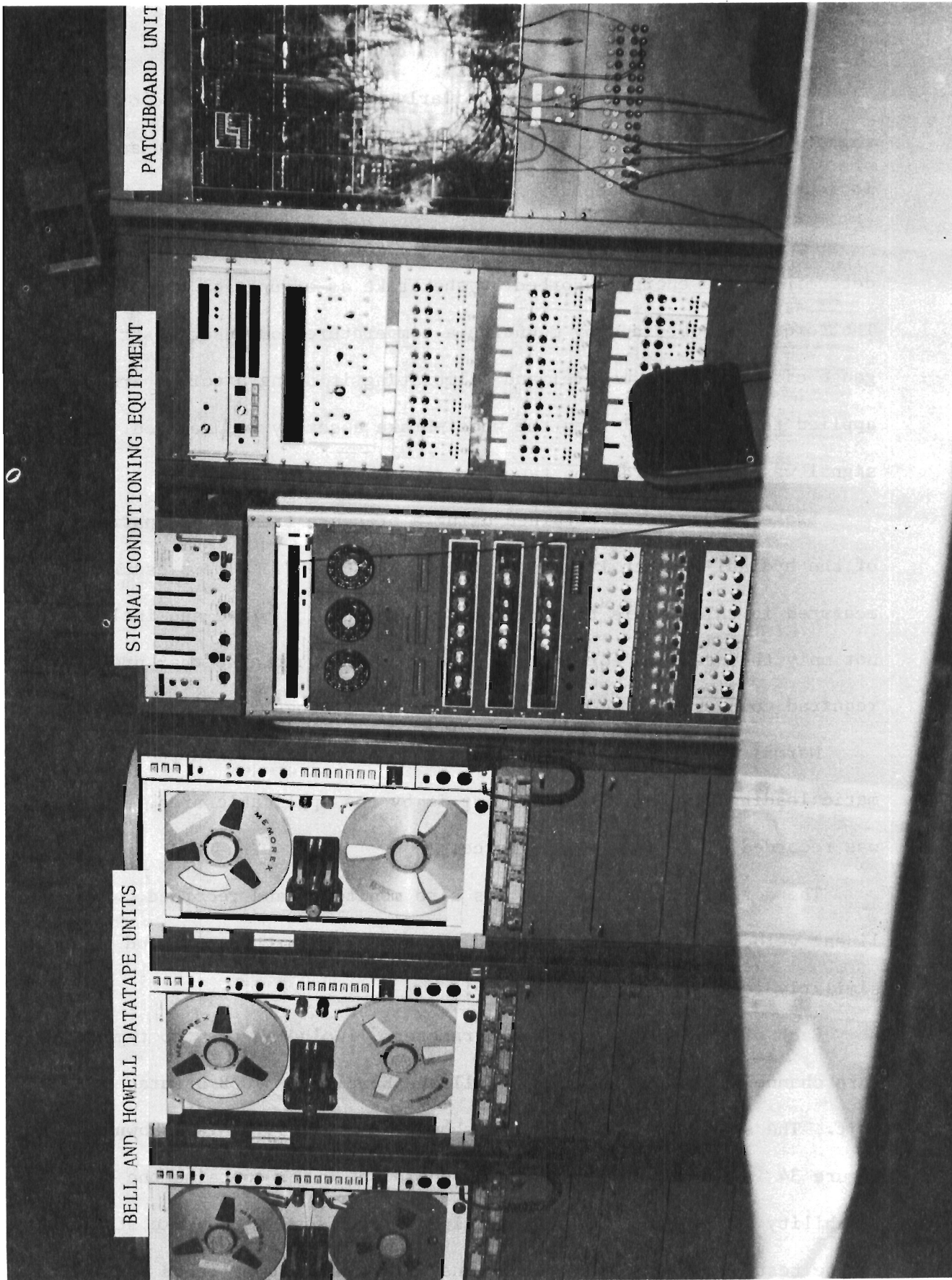


Figure 34. Data Recording Test Center

tests. The unit on the far right of Figure 34 is the patchboard where all signals from the dynamometer station are patched into the signal conditioning equipment. Once the data is recorded, or even while it is being recorded, it may also be channeled into a brush recorder so that a hard copy output of each parameter can be displayed as a function of time. Figure 35 shows the brush recorders used. Sample output from these recorders is shown and discussed in the test results section.

Results

A total of 60 tests was conducted. Of these, 48 were conducted for comparison with theoretical models. The remaining 12 were run specifically to determine the convective-radiative heat transfer coefficients for use in the theoretical models. Since the theoretical models are described in Chapter V, the discussion of these 12 tests will be deferred until Chapter V where boundary conditions are developed.

Recorded Parameters Versus Time

Ten tests were selected for detailed study and temperature plotting. Table 7 shows the particular ten stops selected. The tests can be identified by the test number which corresponds to the paragraph numbers shown in Table 6, the test plan. The third digit in the test number is the particular stop of the three conducted at that paragraph. The ten stops were selected to encompass a range of kinetic energies and decelerations. In addition, six tests were selected with cooling blowers on and four tests were selected with cooling blowers off. Figure 36 shows typical data recorded during each test as a function of

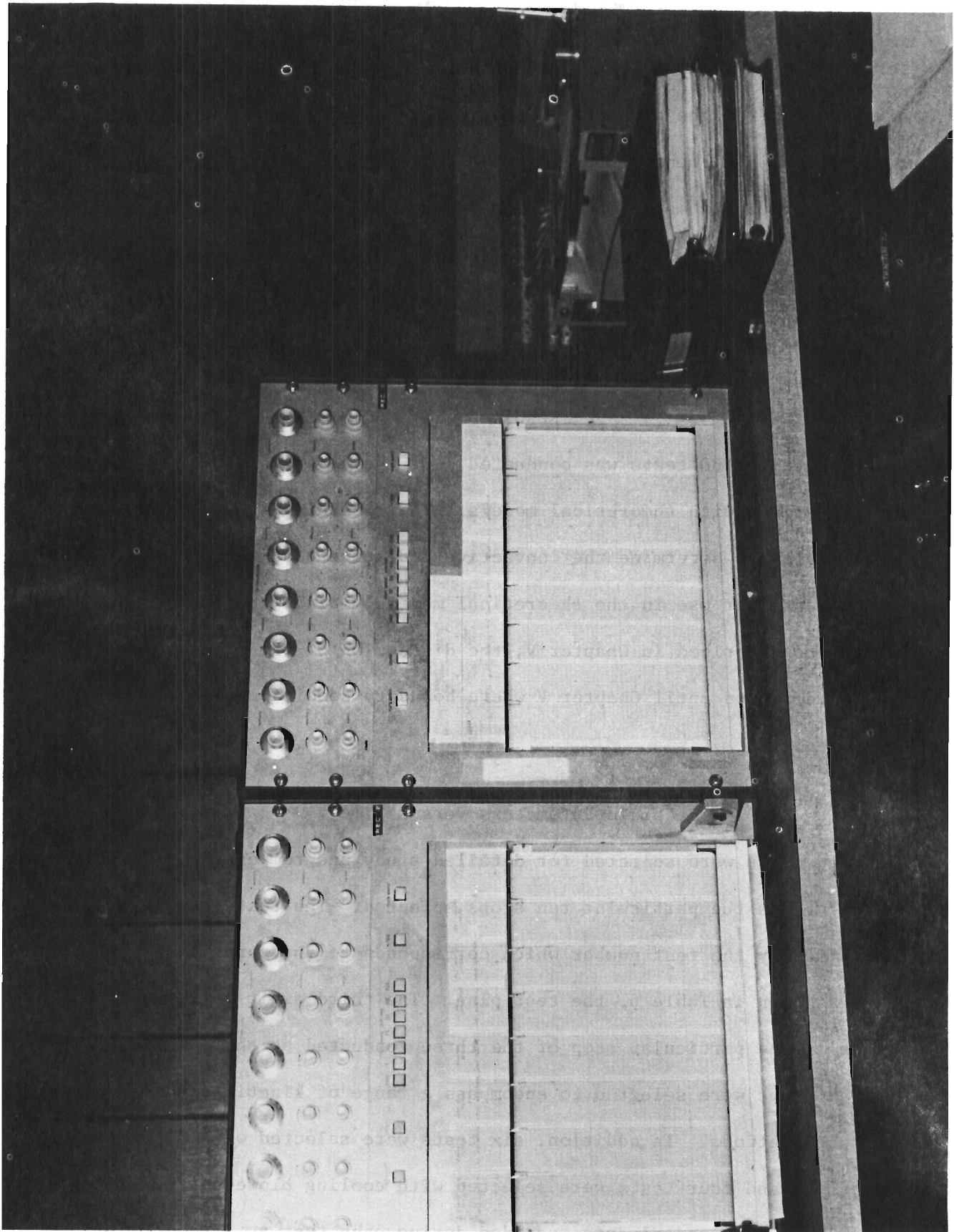


Figure 35. Brush Recorder Instruments

TABLE 7

TYPICAL TEST DATA

Test No.	Kinetic Energy (%)	Stop Time (sec)	Decel (Ft/sec ²)	Average Torque (Ft-lb)	Initial Speed (Ft/sec)	Ambient Temp (°F)	Start Temp (°F)	Blowers
1.1-3	60	58	3.58	1554	207	80	129	ON
2.1-2	60	26	7.98	3735	207	80	142	ON
2.2-3	60	30	6.91	3133	207	86	86	OFF
3.1-2	100	107	2.50	959	267	86	100	ON
4.2-3	100	41	6.68	2967	274	83	120	OFF
6.1-3	60	95	2.21	868	210	84	110	ON
7.1-2	60	31	6.93	3139	215	85	132	ON
7.2-3	60	36	5.89	2551	212	76	127	OFF
8.1-2	100	124	2.19	757	271	85	127	ON
9.2-2	100	48	5.71	2436	274	84	98	OFF

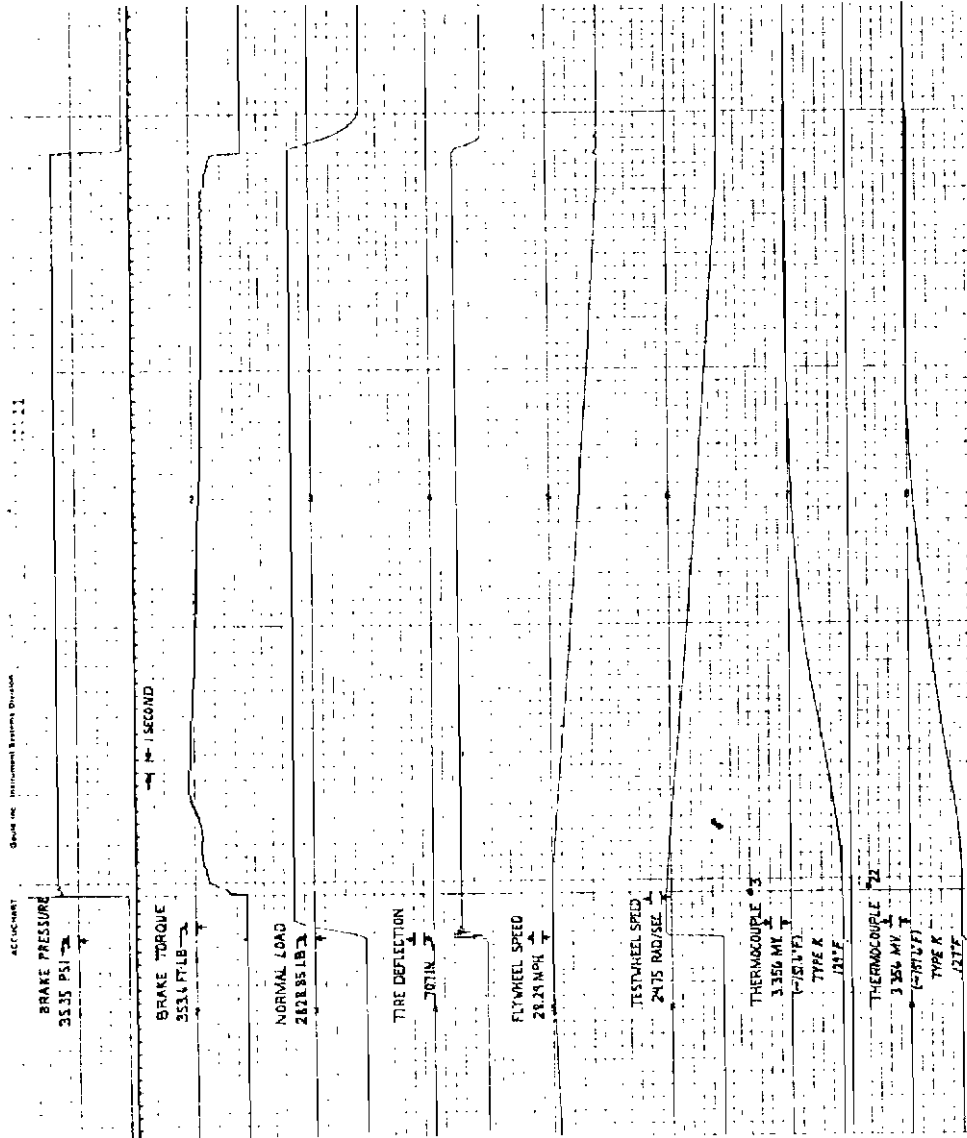


Figure 36. Carbon Brake Test 1.1-3, Blowers on, Deceleration = 3.58 ft/sec², 60% of Normal K.E.

Contrails

time. The graph shown is for Test 1.1.3, the first listed on Table 7, but is typical of all the tests. The scale for each recorded parameter is given under that parameter. The time divisions are shown as one-second intervals and are located between the pressure and torque traces. The complete brake stop can be followed by considering Figure 36. The first thing to note is that the flywheel has been brought up to the required speed. The tire is moved into contact with the flywheel at this point. As noted in Figure 36, the test wheel speed, tire deflection, and normal load all rise simultaneously. About three and one-half seconds later the brake pressure is applied. The torque then increases immediately and the flywheel begins to slow down. At this point the brake is starting to heat up. This is evident from the rise noted in the two temperature traces.

Approximately one minute later, the flywheel is stopped and the pressure and load are returned to zero. The first six traces are now zero and the cooling period begins. Another stop is not made until the brake has cooled to 150°F. Table 7 lists data that have been extracted from the traces of Figure 36. The average deceleration was calculated by dividing the initial speed by the stop time. The average torque was obtained by approximating the average torque during each second, adding these values for the entire stop and dividing by the stop time of the stop. Appendix E contains the data recorded during each test, as shown in Figure 36, for each of the ten stops of Table 7. Unfortunately, due to instrumentation difficulties, two stops do not have test wheel speed shown but do contain all of the other more important parameters.

Temperature Versus Time

The temperature in Rotor 2, Stator 2, and the torque tube is shown as a function of time for Stop 1.1-3 in Figure 37. The exact thermocouple locations are given in Figure 30. The left side of Figure 37 has an expanded time scale to allow observation of the initial high temperature gradients. The curves on the right show the cooling that takes place over the next 70 minutes. The point at which the brake stopped the flywheel is seen to be at 58 seconds and slightly after the peak temperature occurs in the stator and rotor. The heat from the stators and rotors flows into the surrounding brake hardware, including the torque tube. The peak temperature in the torque tube occurs later than the peak temperatures of the heat sink. Appendix F contains curves of this type for each test in Table 7.

Temperature Versus Axial Position

The way in which the temperature varies in the axial direction during a stop is depicted in Figure 38. Here the temperature plotted is from the thermocouples at the bottom of the graph. They are located in the disc shown above the thermocouple number on Figure 38, and the exact location can again be found on Figure 30. The data points were connected by straight lines since the information between the data points does not indicate the brake temperatures in that area. As can be seen in the graph, the rotors tend to be hotter than the stators at early time, but this difference decreases as time increases. Also, it is evident that the temperature is less near the left end or brake housing. Appendix G gives these axial position plots for all ten of

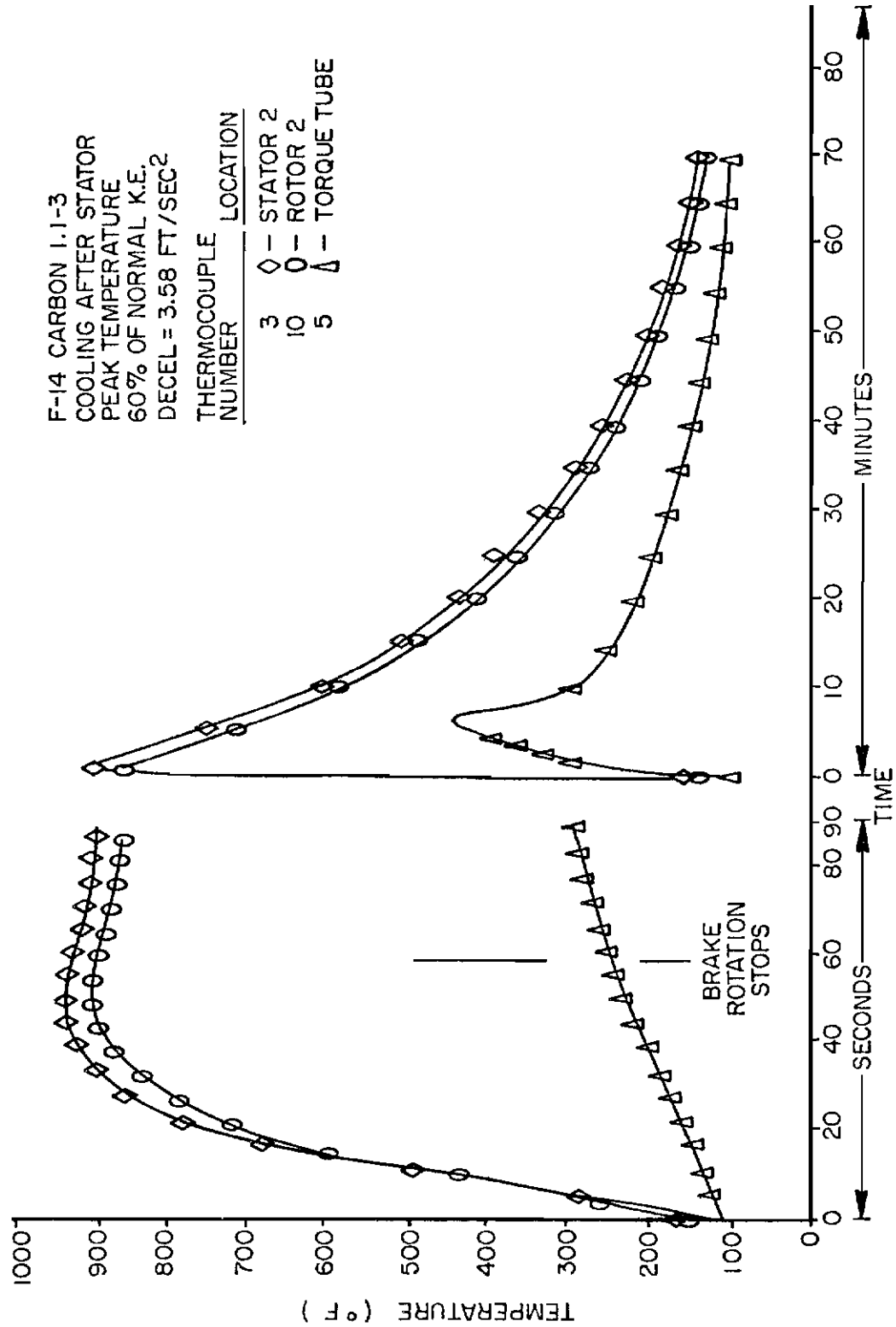


Figure 37. Temperature vs Time; Stator 2, Rotor 2, and Torque Tube

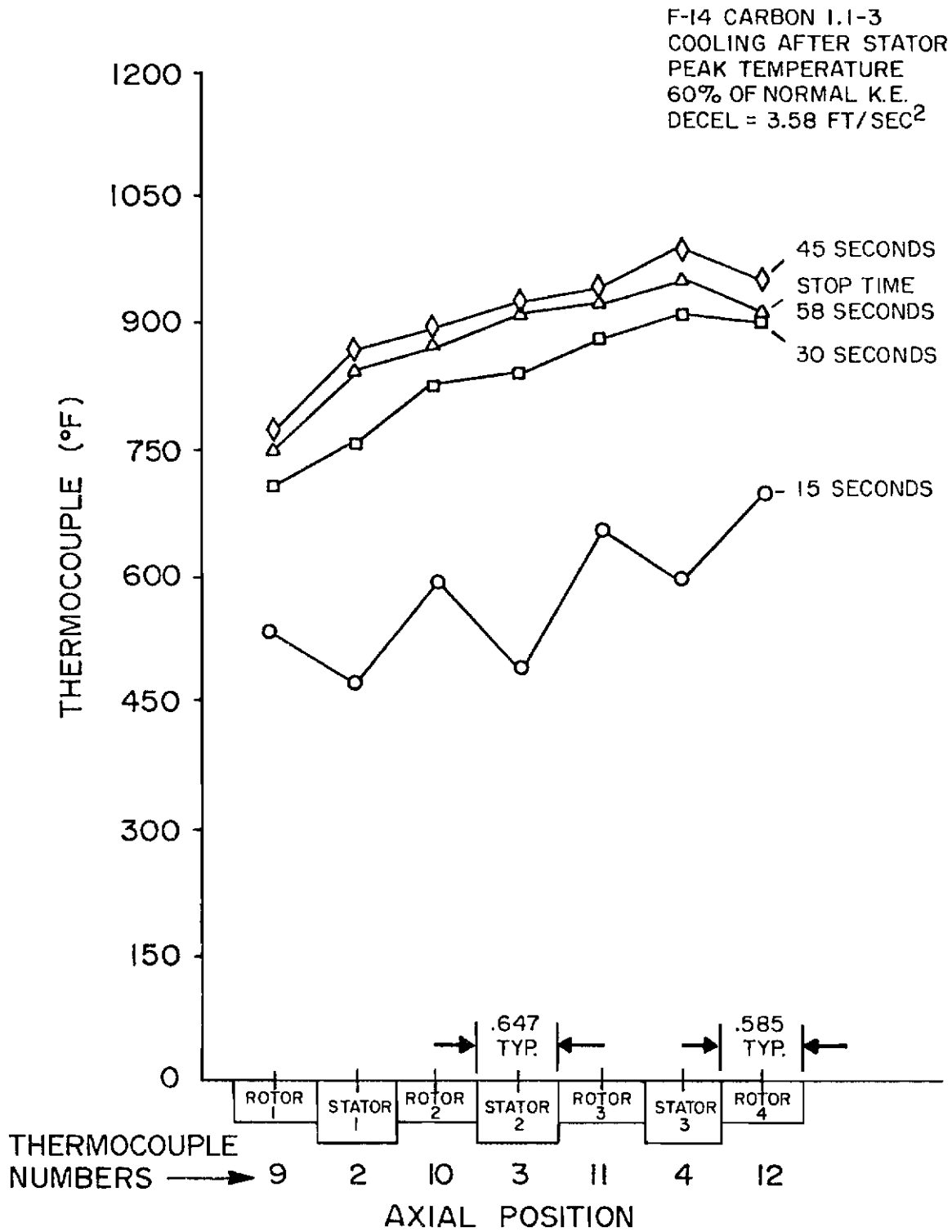


Figure 38. Temperature vs Axial Position

the stops of Table 7. The beryllium curves are plotted somewhat differently than the carbon since the thermocouples in the beryllium were not in a straight axial line. Due to this, at each time points are plotted, the stator points are connected to stator points and the rotor points are connected to rotor points. Figure 29 gives the exact beryllium thermocouple locations.

Temperature Versus Radial Position

Figure 39 shows a plot of temperature versus time for the four thermocouples located in a radial line in the backing plate of the carbon heat sink. The exact location of the thermocouples is shown in Figure 30. The inner and outer thermocouple locations appear to be cooler than the other two at early times, but all four cooling curves coincide at later times. The radial position plots for each of the five carbon brake tests identified in Table 7 are given in Appendix H.

To more clearly understand the temperature pattern in the radial direction for early times, Figure 40 was plotted. This figure shows temperature versus radial position at various times up until the stop time. Here the particular radial temperature is seen at each time increment. The thermocouple position is shown on the graph, as is the wearing surface location. At early time the middle two thermocouples are higher in temperature than the other two. The curve is fairly flat by the time the stop time is reached. Also, the peak temperature occurs earlier than at the stop time. Appendix I contains similar temperature versus radial position plots for the five carbon brake stops of Table 7.

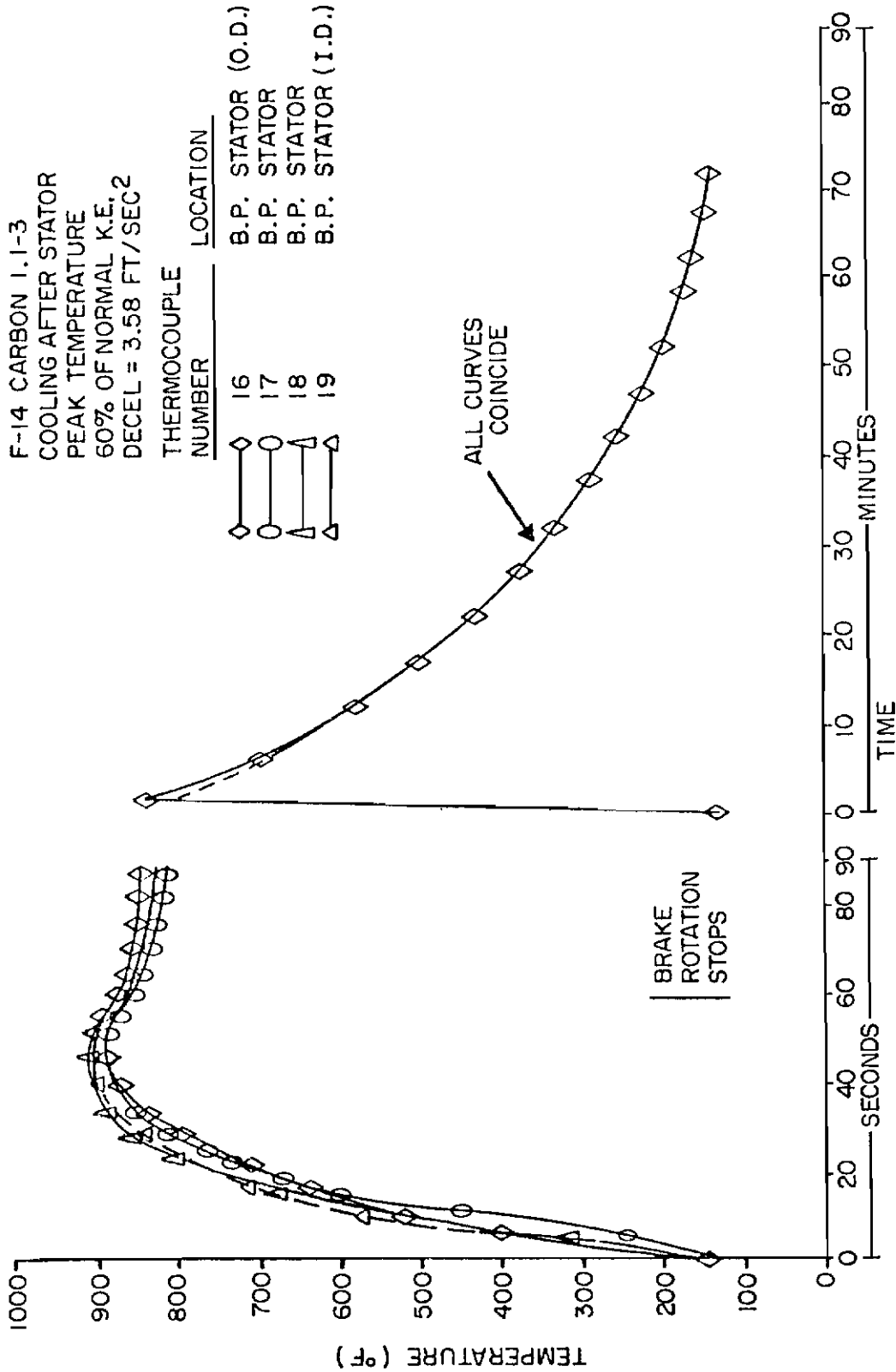


Figure 39. Temperature vs Time for Radial Thermocouples

F-14 CARBON 1.1-3
 COOLING AFTER STATOR
 PEAK TEMPERATURE
 60% OF NORMAL K.E.
 DECEL = 3.58 FT/SEC²

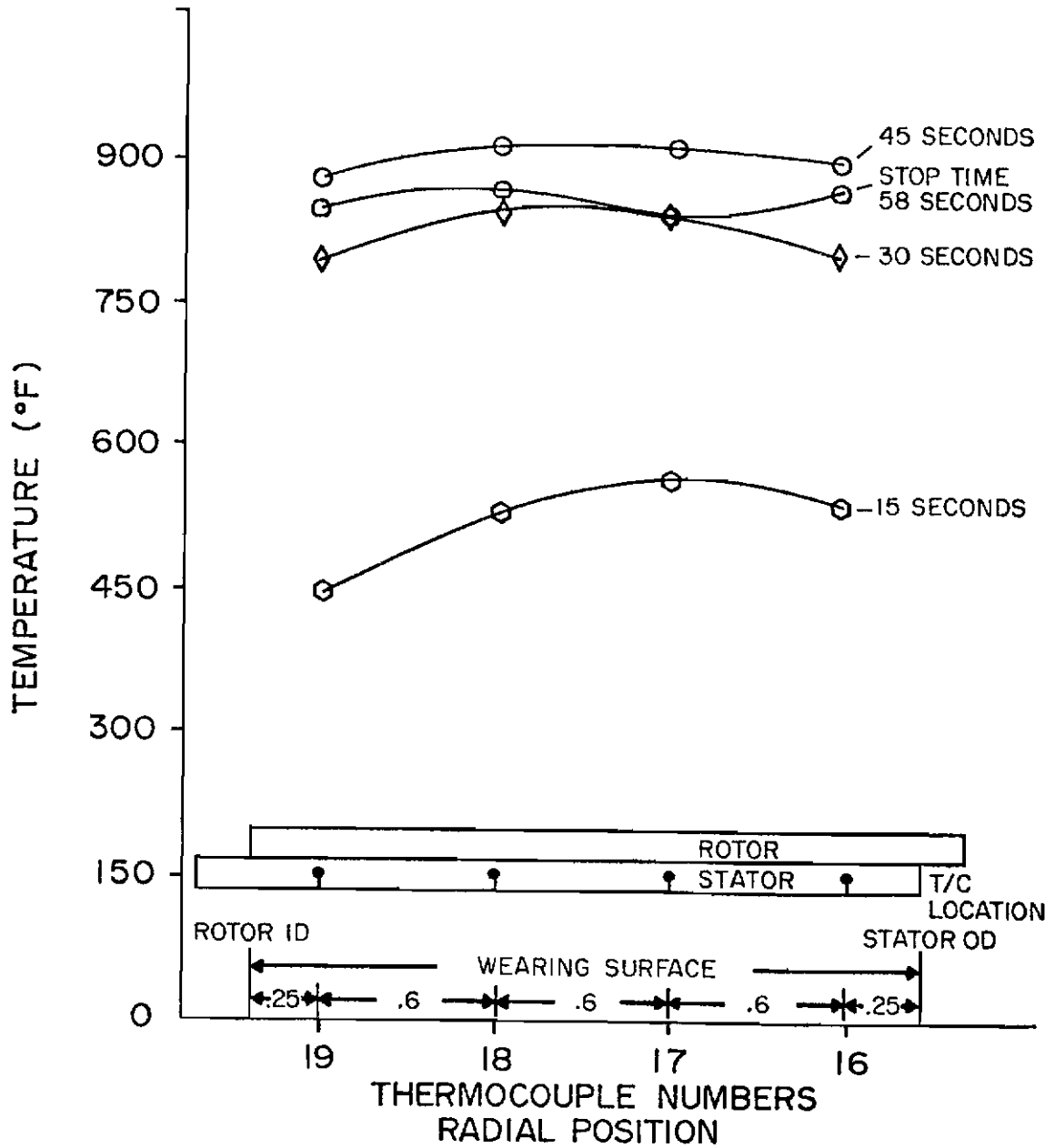


Figure 40. Temperature vs Radial Position

In order to observe the radial temperature variation in Stator 1, Figure 41 was plotted. The two thermocouples plotted are both at the axial center of Stator 1 but are at different radii, 4.4. in. and 5.5 in. The thermocouple at the largest radius has a higher gradient but reaches about the same peak temperature as the other thermocouple. Figure 42 shows the same characteristics; however, the test was conducted with a higher energy input and deceleration. Figure 41 shows a peak temperature of about 900°F while Figure 42 shows a peak of about 1500°F.

Figure 43 is a plot of temperature versus time for two thermocouples at the same radial position in Stator 1. The difference between the two is that one is located in the axial center of the stator and the other is very close to the wearing surface (Figure 30). The temperature measured close to the wearing surface is slightly higher than that of the other. The difference would probably have been higher if the radius were increased so that the angled thermocouple would not be at the radial edge of the rubbing surface. At a higher energy and deceleration, this temperature difference is higher (see Figure 44). It is also seen that during cooling the curves are coincident in the first case and almost so in the second.

Brake Hardware Temperature Versus Time

Four stops were selected to show the temperatures reached in the tire-wheel assembly other than in the heat sink. Figure 45 shows such a plot for the carbon brake at a low deceleration (3.58 ft/sec²) and at 60% of normal kinetic energy. The thermocouple numbers and locations are specified on the graph. Figure 33 gives a pictorial view of

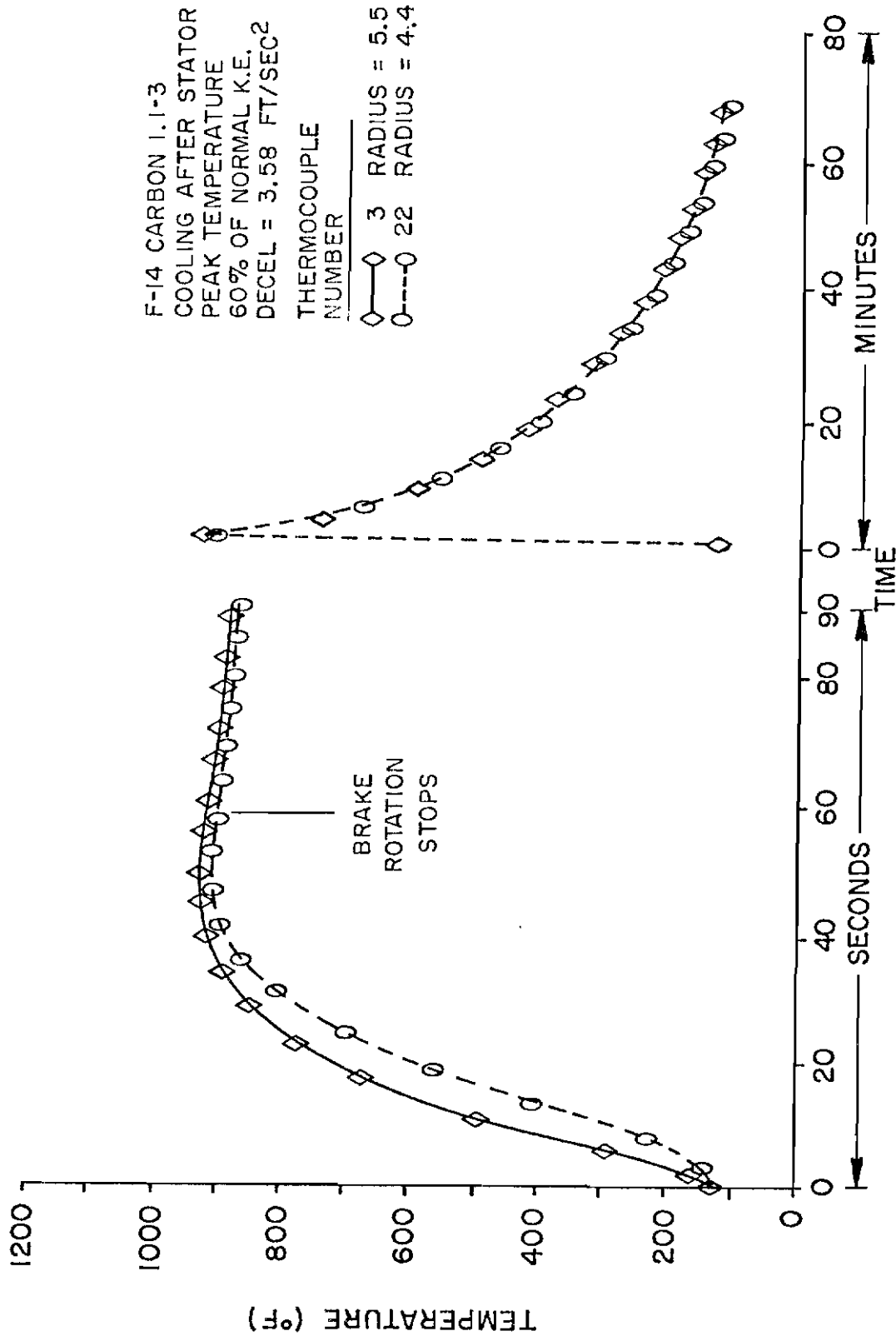


Figure 41. Stator 1 Radial Temperature (Test 1.1-3)

Contrails

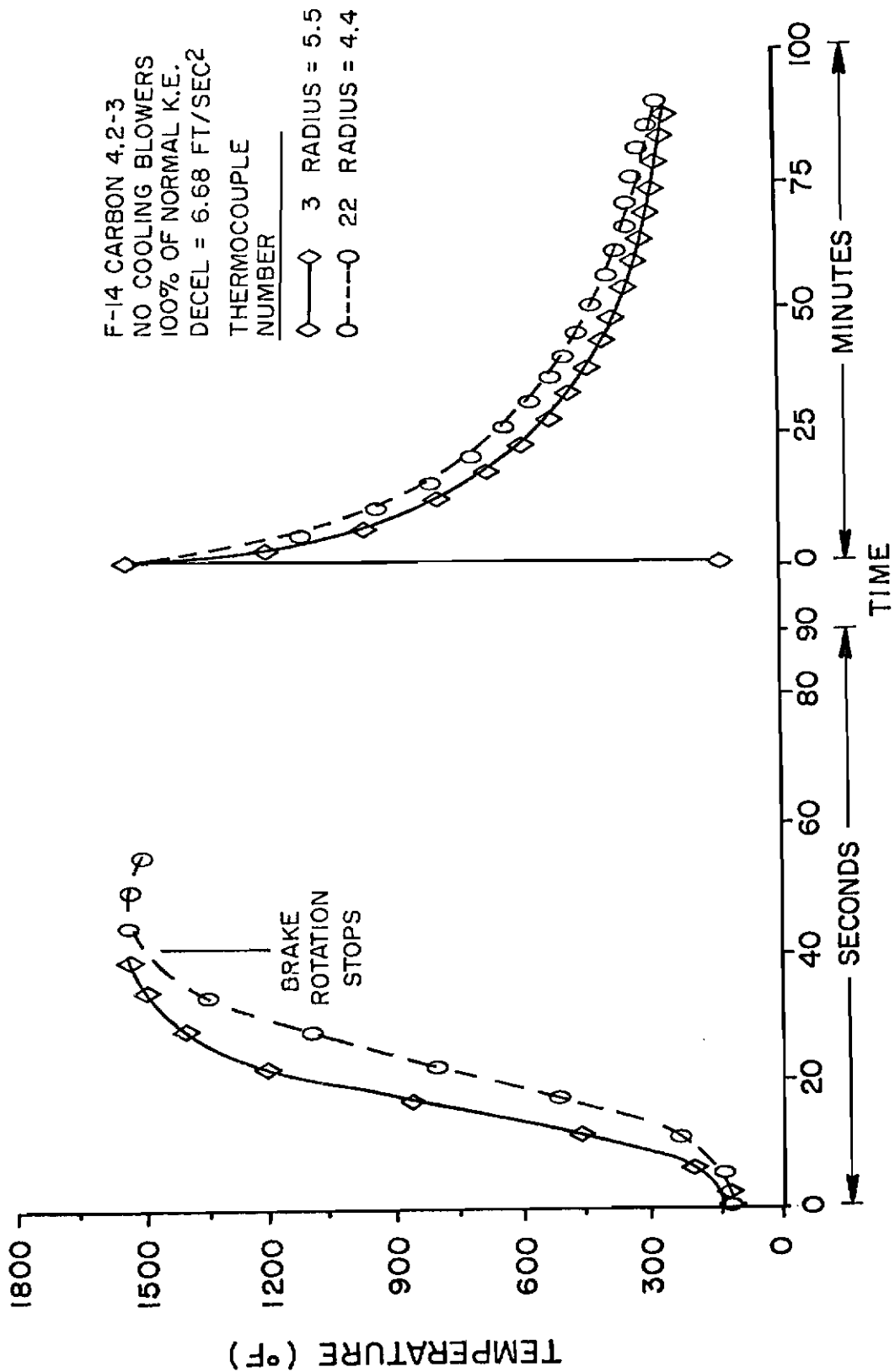


Figure 42. Stator 1 Radial Temperature (Test 4.2-3)

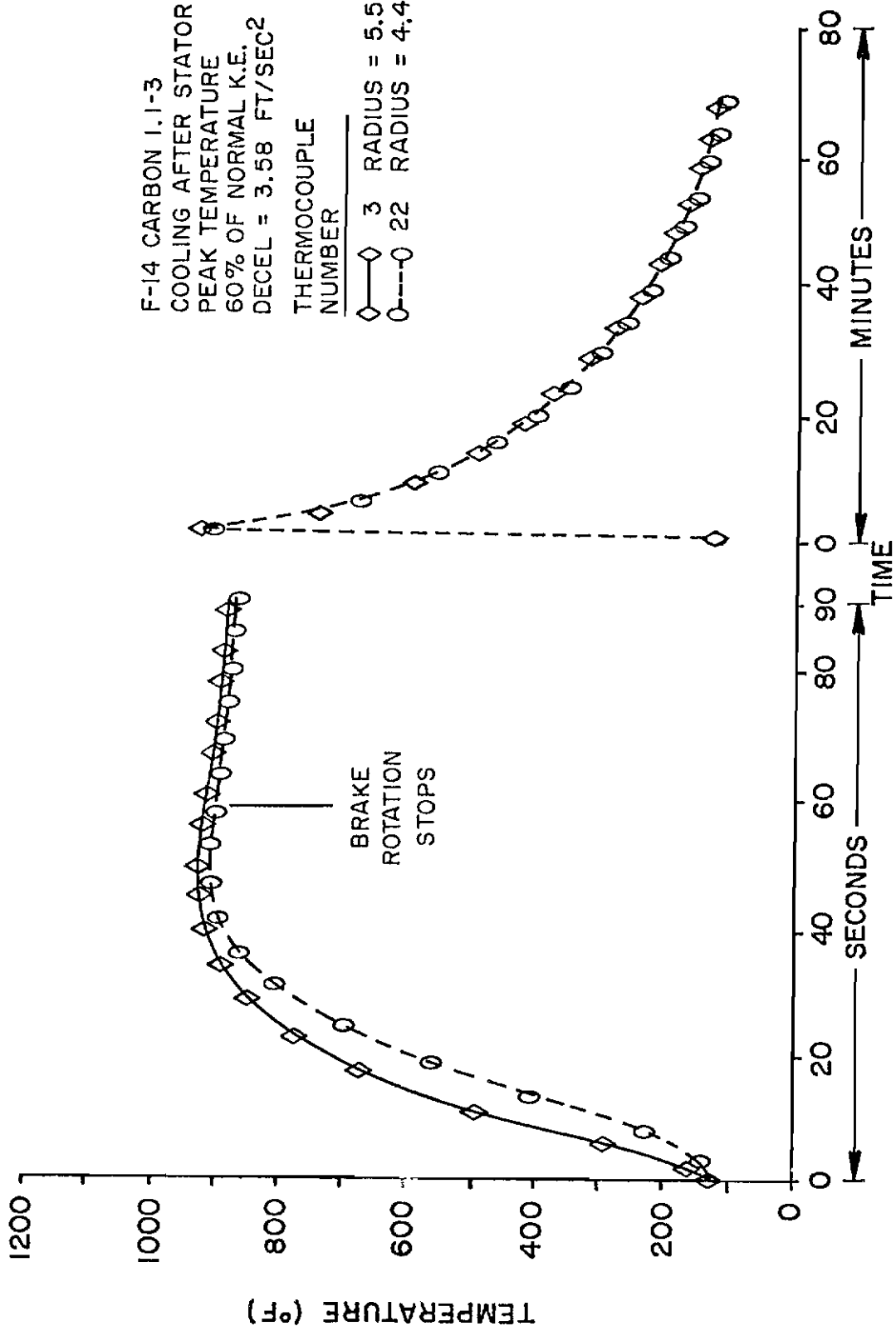


Figure 43. Stator 1 Axial Temperature, Radius = 4.44 in. (Test 1.1-3)

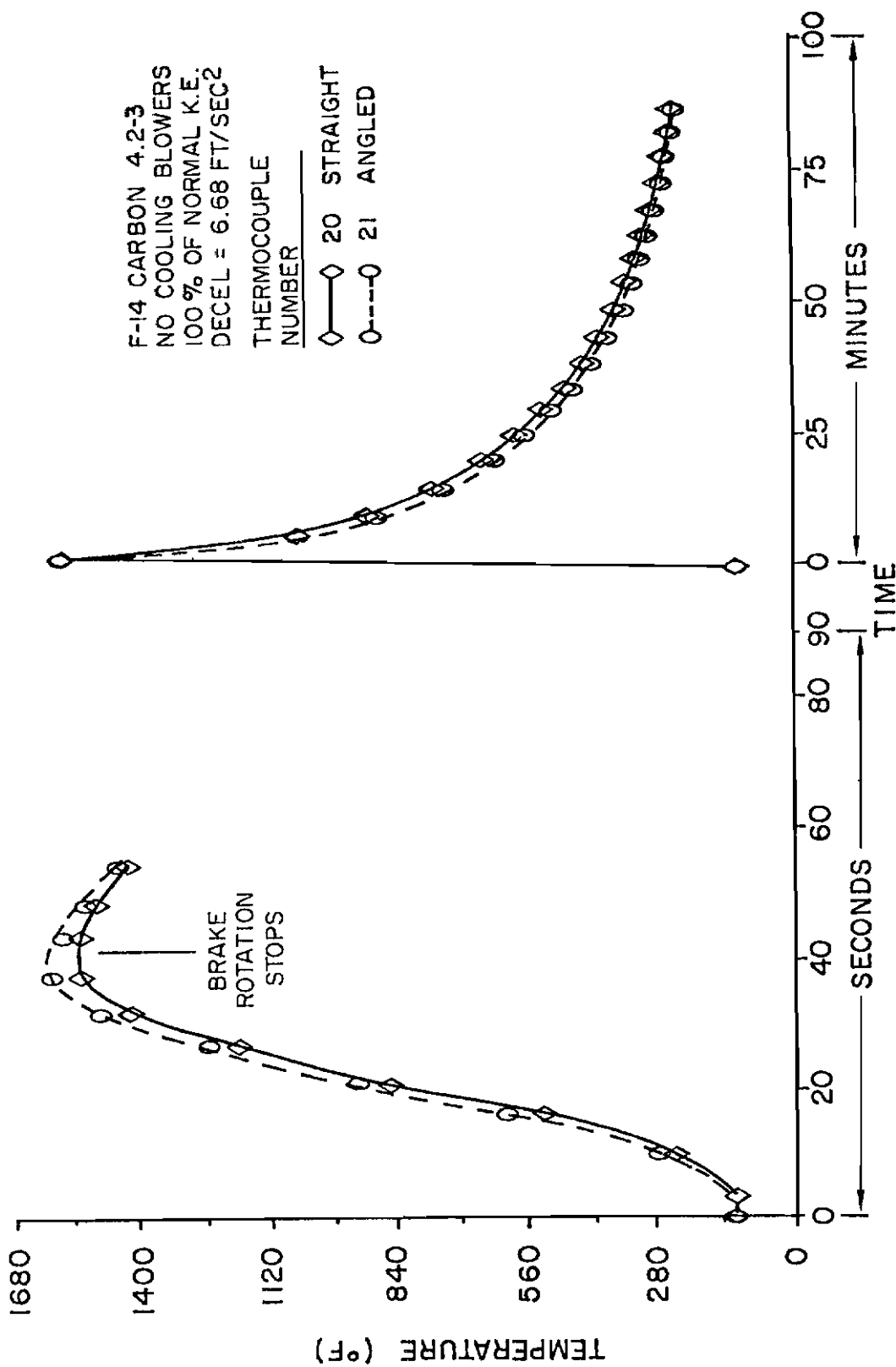


Figure 44. Stator 1 Axial Temperature, Radius = 4.44 in. (Test 4.2-3)

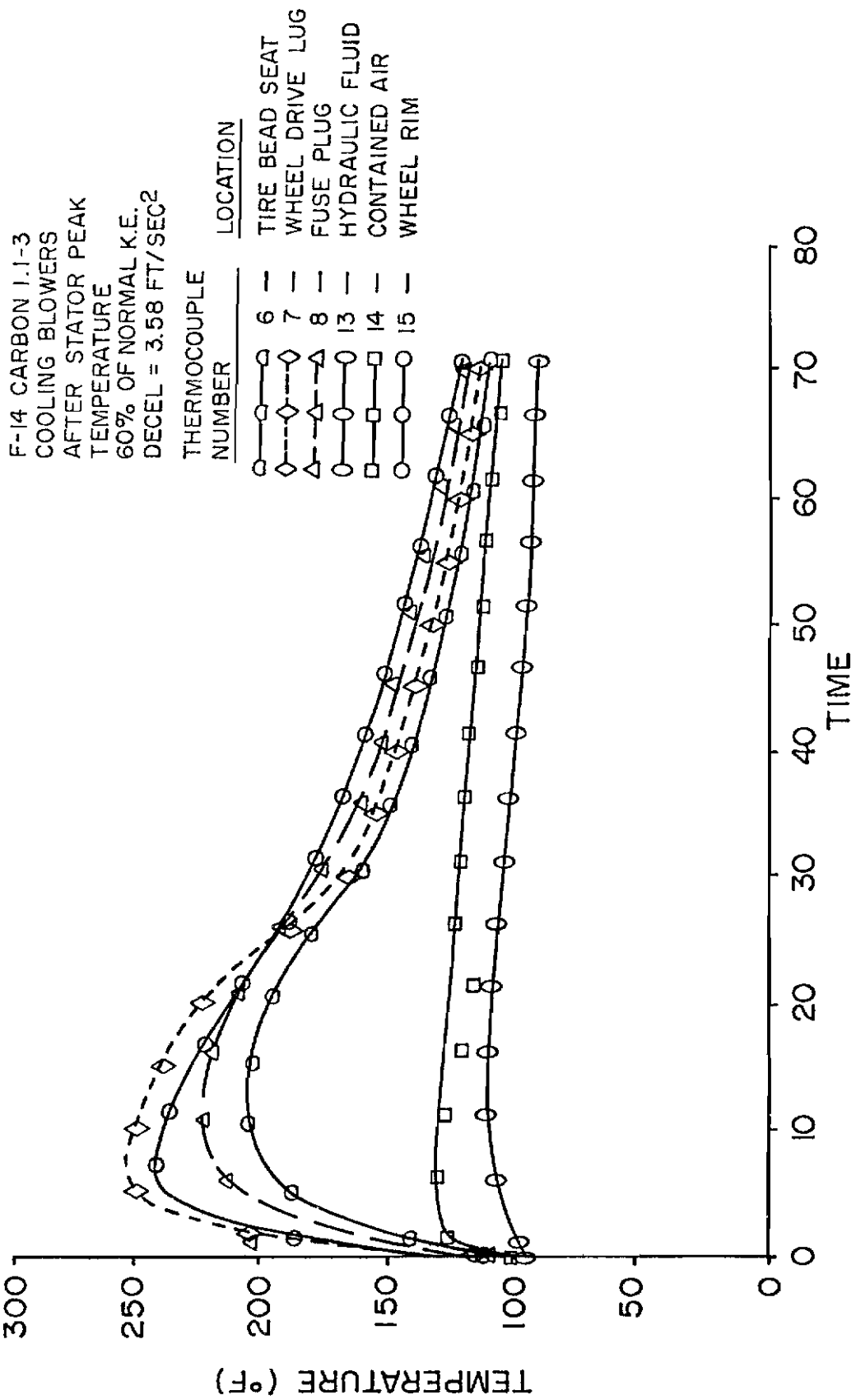


Figure 45. Temperature vs Time-Tire/Wheel Assembly (Test 1.1-3)

Contrails

these particular thermocouple locations. The wheel drive lug attains the highest temperature while the hydraulic fluid is the lowest. The air temperature in the tire is also low and only slightly above the hydraulic fluid temperature. For a higher deceleration and kinetic energy, Figure 46 shows that the air temperature in the tire remains low but that the hydraulic fluid temperature rises significantly over the test previously described. The highest temperature is again attained in the wheel drive lug. Another difference in the two graphs is the relative position of the temperature of the wheel rim. For the low energy and low deceleration, the wheel rim temperature is the second highest of the six curves; in the other case, the wheel rim is the fourth highest in temperature.

Figures 47 and 48 show similar plots for the beryllium brake. The large jump in the hydraulic fluid temperature from the low to high deceleration can again be noticed. On the high deceleration stop (Figure 47), the temperature of the air in the tire did not rise significantly, while on the low deceleration stop the air temperature did rise significantly. Although cooling blowers were used in the low deceleration case, the air temperature increase for this case is attributed to the higher energy input (100% vs 60%). For the beryllium brake it is noted that although the wheel rim temperature is close to the highest temperature in Figure 48, it is the next to lowest in Figure 47. The apparent discrepancy in the results is probably due to two factors. The first is that the combination of low deceleration, low energy input found in the carbon brake stop of Figure 45 is not found in either of the two beryllium brake stops. The conditions of

F-14 CARBON 4.2-3
 NO COOLING BLOWERS
 100% OF NORMAL K.E.
 DECEL = 6.68 FT/SEC²

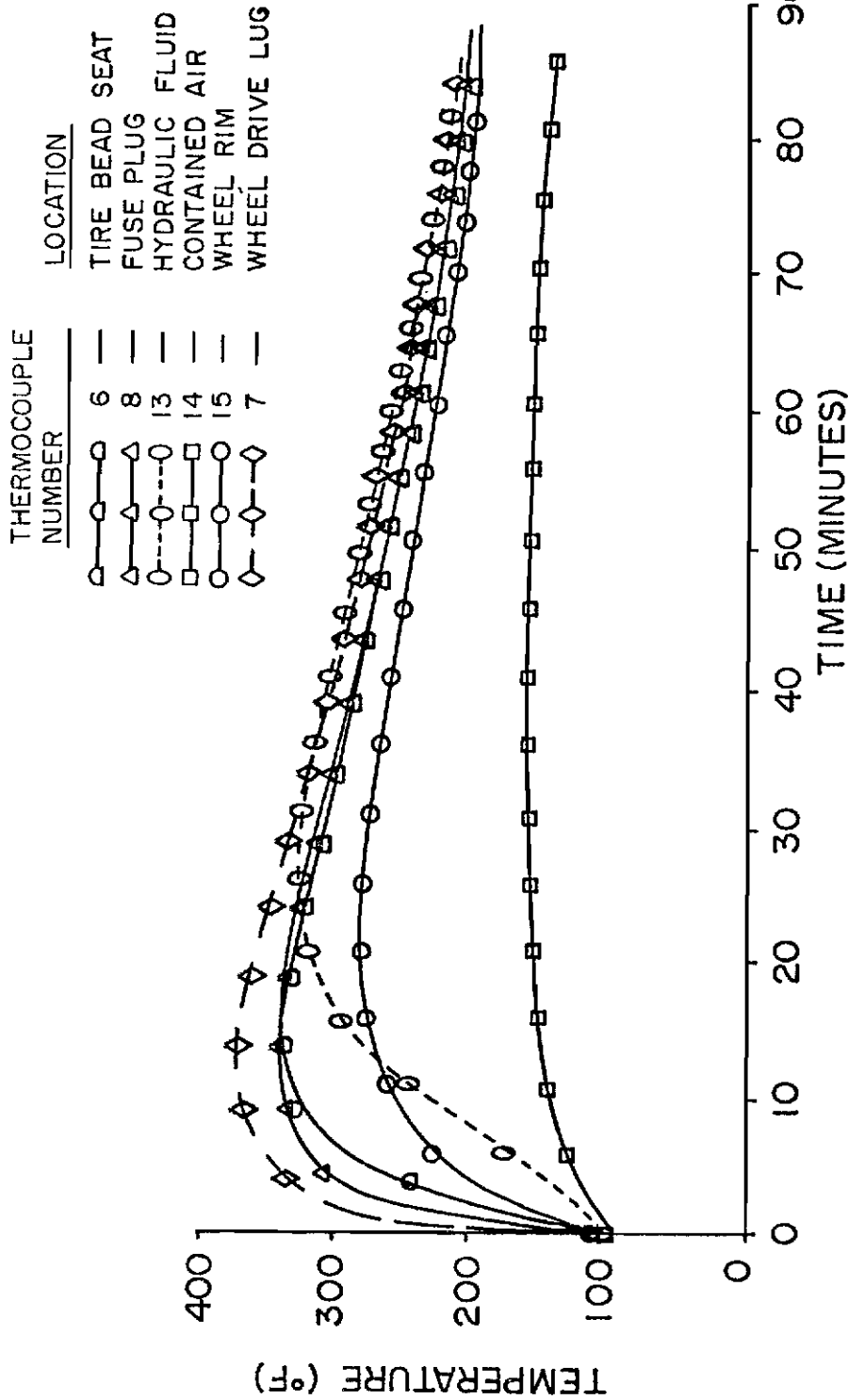


Figure 46. Temperature vs Time-Tire/Wheel Assembly (Test 4.2-3)

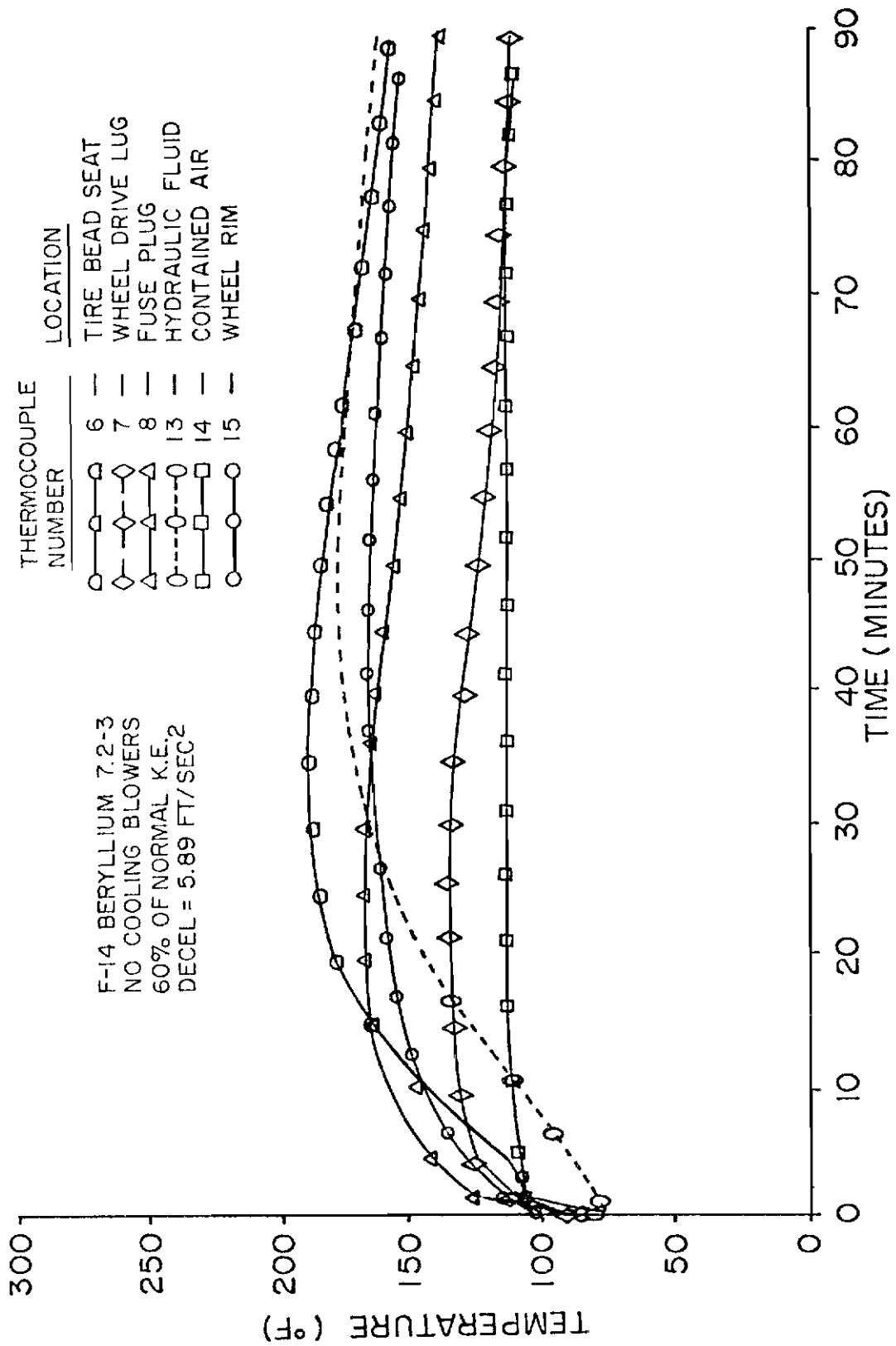


Figure 47. Temperature vs Time-Tire/Wheel Assembly (Test 7.2-3)

F-14 BERYLLIUM 8.1-2
 COOLING BLOWERS
 100% OF NORMAL K.E.
 DECEL = 2.19 FT/SEC²

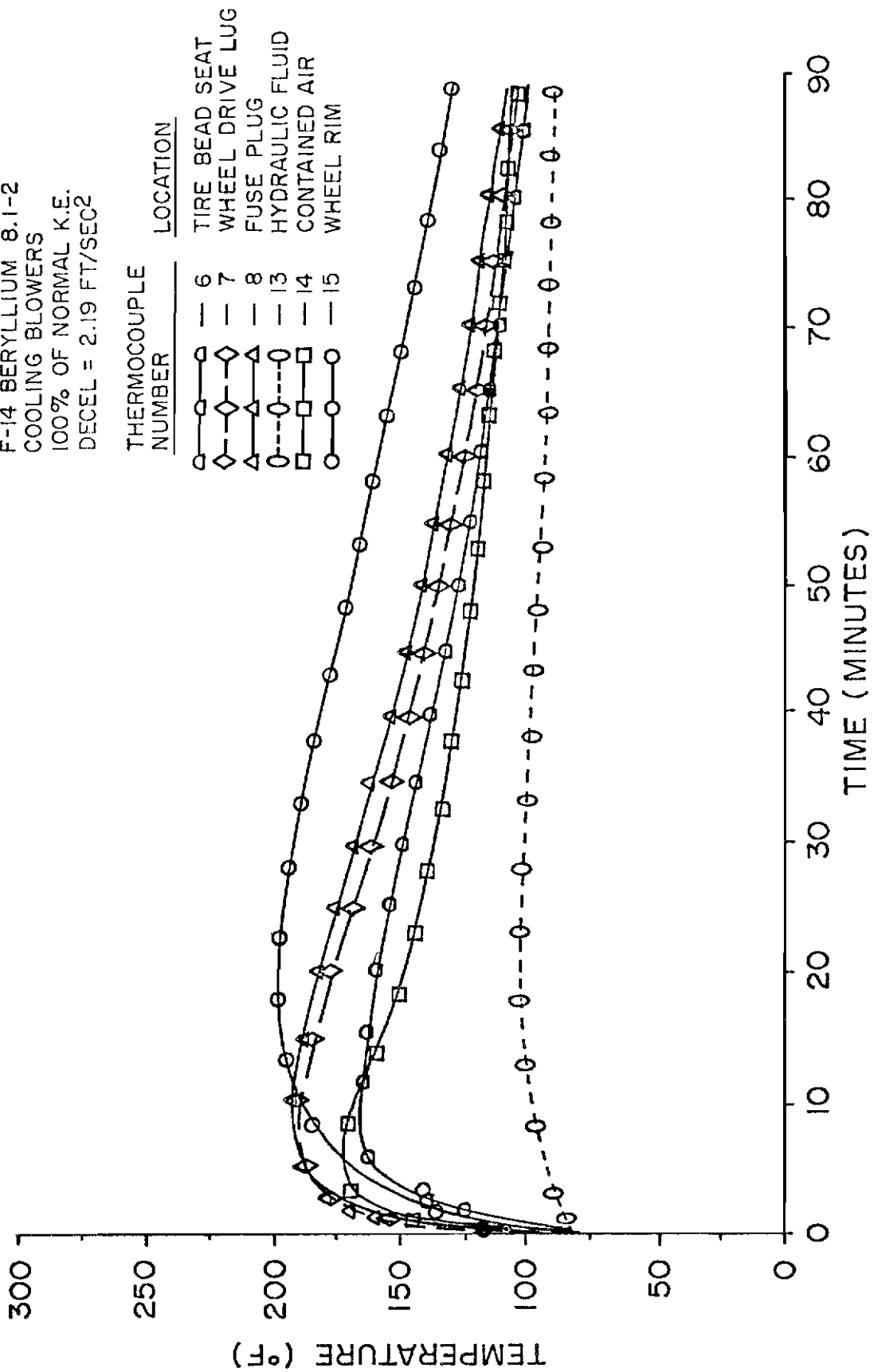


Figure 48. Temperature vs Time-Tire/Wheel Assembly (Test 8.1-2)

Contrails

Figure 46 were also not duplicated by either of the two beryllium brake stops shown. The second reason is that the carbon brake was equipped with heat shields that were placed circumferentially between the wheel rim inside diameter and the heat sink outer diameter. These were inserted to keep the wheel rim from obtaining a high temperature when the carbon heat sink obtained a high temperature. Due to the low temperatures in the beryllium heat sink, the heat shields were not used for the beryllium brake tests.

CHAPTER V

THEORETICAL DEVELOPMENT

Introduction

The theoretical models described in this chapter are all concerned with the multidisc brake except the last which deals with a single rotor caliper type brake. The analysis is most directed toward the multidisc brake because of the extensive testing that was accomplished on the multidisc brakes as reported in Chapter IV. Within the multidisc brake analysis, several models employing different assumptions were developed. These allowed a gradual buildup to the most extensive model. In addition, the validity of less complicated models is shown since all are compared to experiment. This approach has seldom, if ever, been reported for the brake application before.

During the course of the theoretical development, the term "R/S Pair" is used. This refers to a commonly made assumption within multidisc brake analysis. The assumption is that, if the area between the radial centerlines of an adjacent rotor and stator is analyzed, all other such areas within the brake are the same and need not be analyzed. This greatly simplifies the analysis but has the drawback of ignoring the axial temperature gradient within the heat sink that has been shown experimentally to exist (see Figure 38).

In several of the multidisc analyses, a boundary condition resulting from convection and radiation at the brake, wheel, and tire

exposed boundaries is utilized. The actual values of the convective/radiative heat transfer coefficients have been calculated from the experimental results. The values calculated and the calculation procedure are described in Appendix J.

Numerical Solution Technique Selection

The equations to be developed in subsequent sections of this chapter prove to be nonlinear due to the inclusion of variable thermal conductivity and heat capacity. Also, the boundary condition at the rotor/stator interface contains a work term that varies with radius as well as time. Due to these facts, a numerical solution technique was necessary. The objective of this section of the research is to select a simple, one-dimensional, theoretical model simulating an aircraft brake that will enable comparison of an exact, finite difference and finite element solution in the areas of accuracy, computer storage and computer time required. It should be noted that the results indicated herein are equally applicable to any disc type brake, aircraft, truck or car.

Theoretical Model

The problem selected simulates a rotor or stator disc in a brake in that the entire piece of material is initially at a constant temperature, one edge is adiabatic which is the disc centerline and at time equal zero, heat crosses the face opposite the adiabatic face. In the brake disc, heat is added due to the friction between the discs. In the model selected, heat is taken from the material by keeping the face at a constant temperature which is lower than the initial

temperature. The model selected is shown in Figure 49. The face at

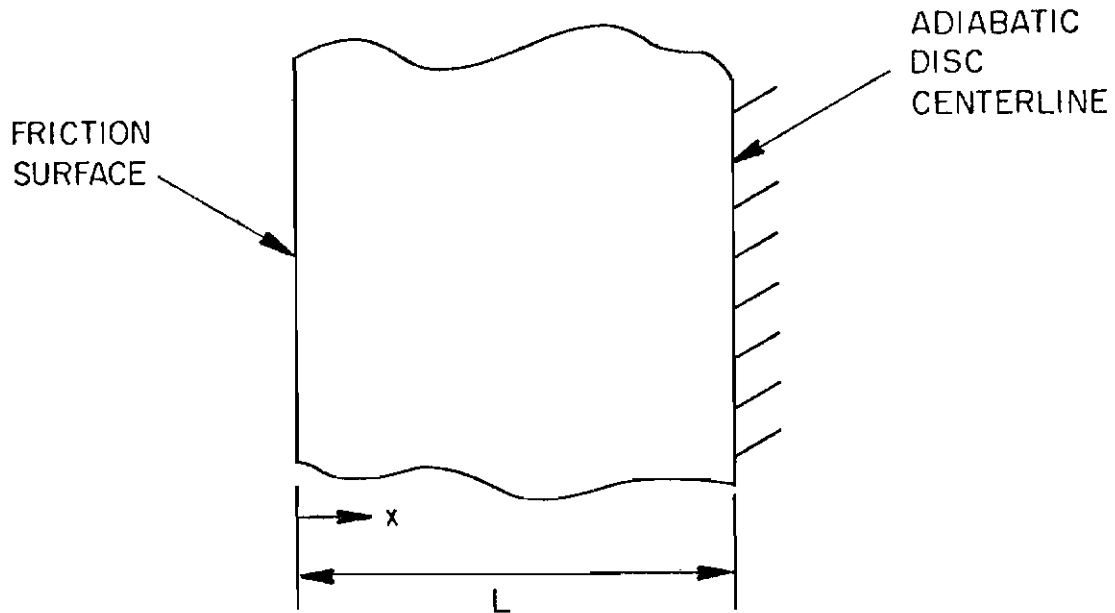


Figure 49. Theoretical Model

$x = L$ is insulated and the entire piece of material is initially at temperature T_0 . The face at $x = 0$ is suddenly changed to temperature T_s . The governing equation using constant properties and one spatial dimension is

$$\frac{\partial^2 T}{\partial x^2} = \frac{1}{\alpha} \frac{\partial T}{\partial t} \quad (29)$$

where α is the thermal diffusivity.

Contrails

Boundary and initial conditions are:

$$T(x,0) = T_o, \frac{\partial T}{\partial x}(L,t) = 0, T(0,t) = T_s \quad (30)$$

Define nondimensional quantities as follows:

$$T' = \frac{T - T_s}{T_o - T_s}, \quad x' = \frac{x}{L}, \quad t' = \frac{\alpha t}{L^2} \quad (31)$$

Then equation (29) becomes:

$$\frac{\partial^2 T'}{\partial x'^2} = \frac{\partial T'}{\partial t'} \quad (32)$$

and the initial and boundary conditions are:

$$T'(x',0) = 1, T'(0,t') = 0, T'_x(1,t') = 0 \quad (33)$$

where the x' subscript denotes differentiation with respect to x' .

Analysis

Exact Solution. Assuming that the solution to the above equation consists of the product of a function of x' and a function of t' , two ordinary differential equations can be obtained, the solutions of which can be combined to give the solution to the original equation. With the initial and boundary conditions applied, the exact solution³³ is:

Contrails

$$T(x,0) = (2/\pi) \sum_{n=0}^{\infty} \exp \left[- \left(n + \frac{1}{2} \right)^2 \pi^2 t \right] \cos \left[\left(n + \frac{1}{2} \right) \pi (1-x) \right] \frac{(-1)^n}{n + \frac{1}{2}} \quad (34)$$

where the primes have been omitted for convenience.

Finite Difference Solution. Equation (32) written in finite difference form is

$$T^{t+\Delta t} = T^t(I) \left[1 - \frac{2\Delta t}{(\Delta x)^2} \right] + \frac{\Delta t}{(\Delta x)^2} [T(I+1) + T(I-1)]^t \quad (35)$$

This equation can be programmed directly using an iterative scheme within the computer. It can also be written in matrix form.

$$\bar{T}^{t+\Delta t} = \bar{A} \bar{T}^t \quad (36)$$

In this case, operations within the computer would involve matrices. For comparison of storage and time requirements both methods were used and are referred to as "Finite Difference Equation" and "Finite Difference Matrix," respectively.

For stability and compliance with the second law of thermodynamics, the quantity multiplying $T^t(I)$ must be greater than zero. Since the number of modes was taken to be five, the nondimensional Δx value becomes .25 and the following equation results:

$$1 - \frac{2\Delta t}{(.25)^2} > 0 \quad (37)$$

This equation yields a Δt of .03125. This is a conservative value and for this problem a value of .031967 was found by trial and error to be the maximum value allowable for a stable solution.

Finite Element Solution. The first step in the Finite Element Solution³⁴ is to find the variational statement from the second order differential equation given earlier. This statement is

$$I_v = \frac{1}{2} \int_0^1 \left[\left(\frac{\partial T}{\partial x} \right)^2 + \frac{\partial (T^2)}{\partial t} \right] dx \quad (38)$$

This integral is then manipulated to obtain equations to solve for temperature. This manipulation leads to the matrix equation

$$\bar{K} \bar{T} + \bar{C} \dot{\bar{T}} = 0 \quad (39)$$

where the bars indicate matrices and the dot indicates differentiation with respect to time. \bar{K} is the global conduction matrix and \bar{C} is the global capacitance matrix. The solution is advanced in time by using the Euler numerical solution technique:

$$\bar{T}^{t+\Delta t} = \bar{T}^t + \dot{\bar{T}}^t \Delta t \quad (40)$$

Evaluating Equation (39) at time t and substituting into Equation 40 yields:

$$\bar{C} \bar{T}^{t+\Delta t} = \bar{B} \bar{T}^t \quad (41)$$

where

$$\bar{B} = \bar{C} - \Delta t \bar{K}$$

Solving for

$$\bar{T}^{t+\Delta t}$$

yields

$$\bar{T}^{t+\Delta t} = \bar{C}^{-1} \bar{B} \bar{T}^t \quad (42)$$

This equation can now be solved at each time step to obtain the solution to the differential equation as long as initial conditions, boundary conditions, \bar{C} , and \bar{B} are known. The number of nodes in this one-dimensional problem was again five, which results in four elements.

For comparison with the finite difference technique, a method of solving the finite element equations without using matrices was desired in addition to the above described procedure. The method employed was to write Equation (39) as a series of equations and then solve them algebraically for the required time derivatives. This practice is cumbersome and not recommended, but it does allow a direct comparison with the other methods. The two finite element computer solutions are referred to as "Finite Element Matrix" and "Finite Element Equation," respectively. The one-dimensional finite element critical time step³⁵ was found to be:

$$1 - \frac{6\Delta t}{(.25)^2} > 0 \quad (43)$$

This gives the conservative value of .01042. Trial and error produced the value of .0115 for the maximum value allowable for a stable solution.

Comparison of Finite Element Method to Finite Difference Method

The exact, finite difference, and finite element solutions were numerically evaluated for various time increments, elapsed time values, and at five spatial locations. Figures 50 and 51 show plots of $T - T_{\text{exact}}$ versus position, where T is the temperature predicted by the finite element or finite difference technique and T_{exact} is the temperature as given by the exact analysis at the same time and position as the approximate analyses. As shown in Figure 50 at time equal .5, the error in using the finite difference techniques increases with increasing x and with increasing time increment. Recall that T , T_{exact} , x , and time are nondimensional as defined in the Theoretical Model Section. It is interesting to note that results with the finite difference technique show increasing error with increasing x in Figure 51 also, but show just the opposite effect of that in Figure 50 with respect to the time increment; the error decreases with increasing time increment. The difference between the two figures other than the results is that Figure 50 is plotted for time = .5 while Figure 51 is plotted for time = 1.0.

Figure 52 shows, for time = .5, the absolute value $\left| T - T_{\text{exact}} \right|$ versus x for the finite element technique. Error increases with increasing x , but no trend is evident of error change with time increment. Figure 53 gives the same information as Figure 52 but at time = 1.0. In this case, error increases with increasing x and increasing time increment. This time increment trend from time = .5 to time = 1.0 is opposite to that found using the finite difference technique. Figure 54, for time = .5, compares finite difference and finite element

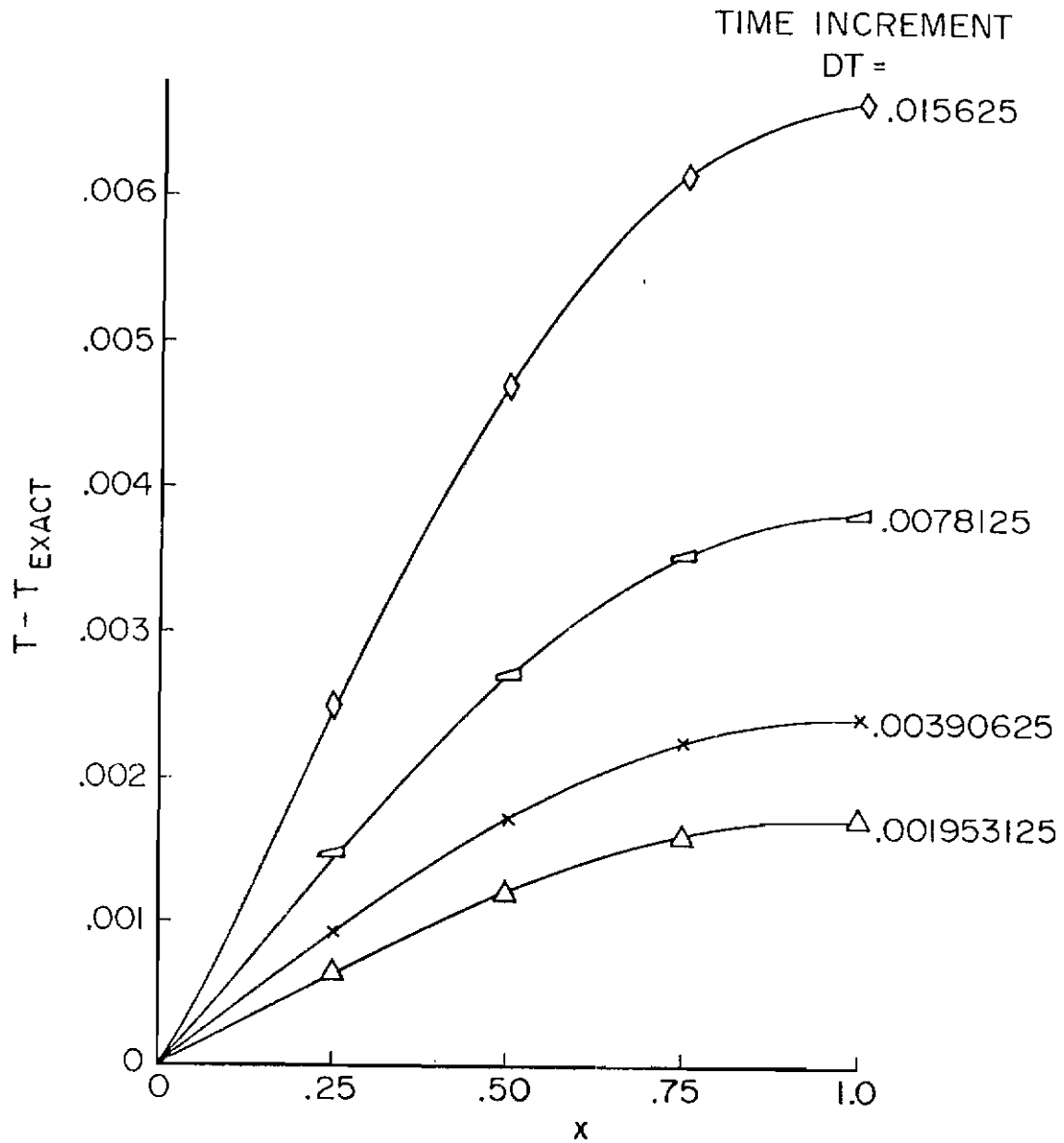


Figure 50. Temperature Difference vs Position, Finite Difference, Time = .5

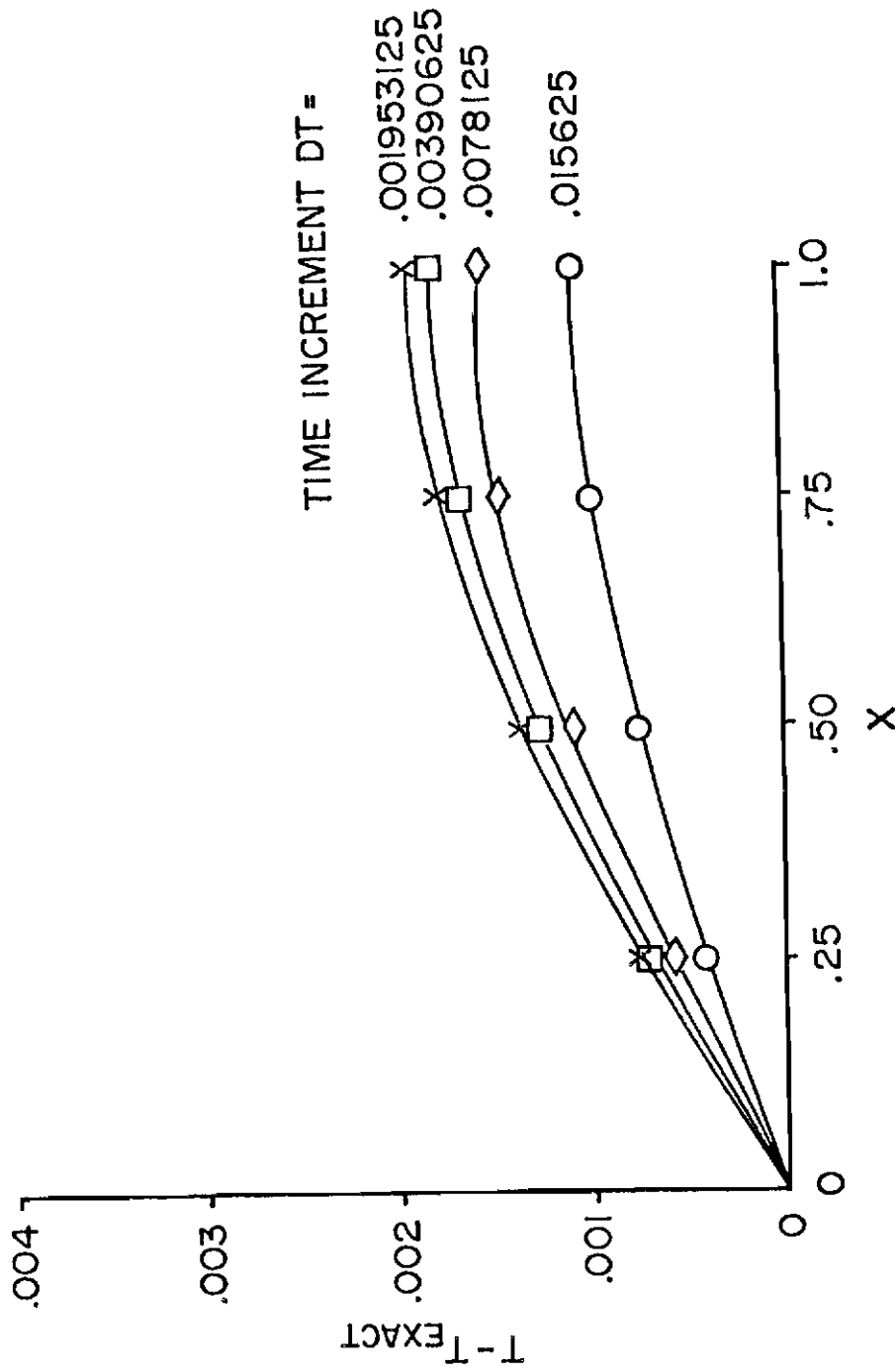


Figure 51. Temperature Difference vs Position,
Finite Difference, Time = 1.0

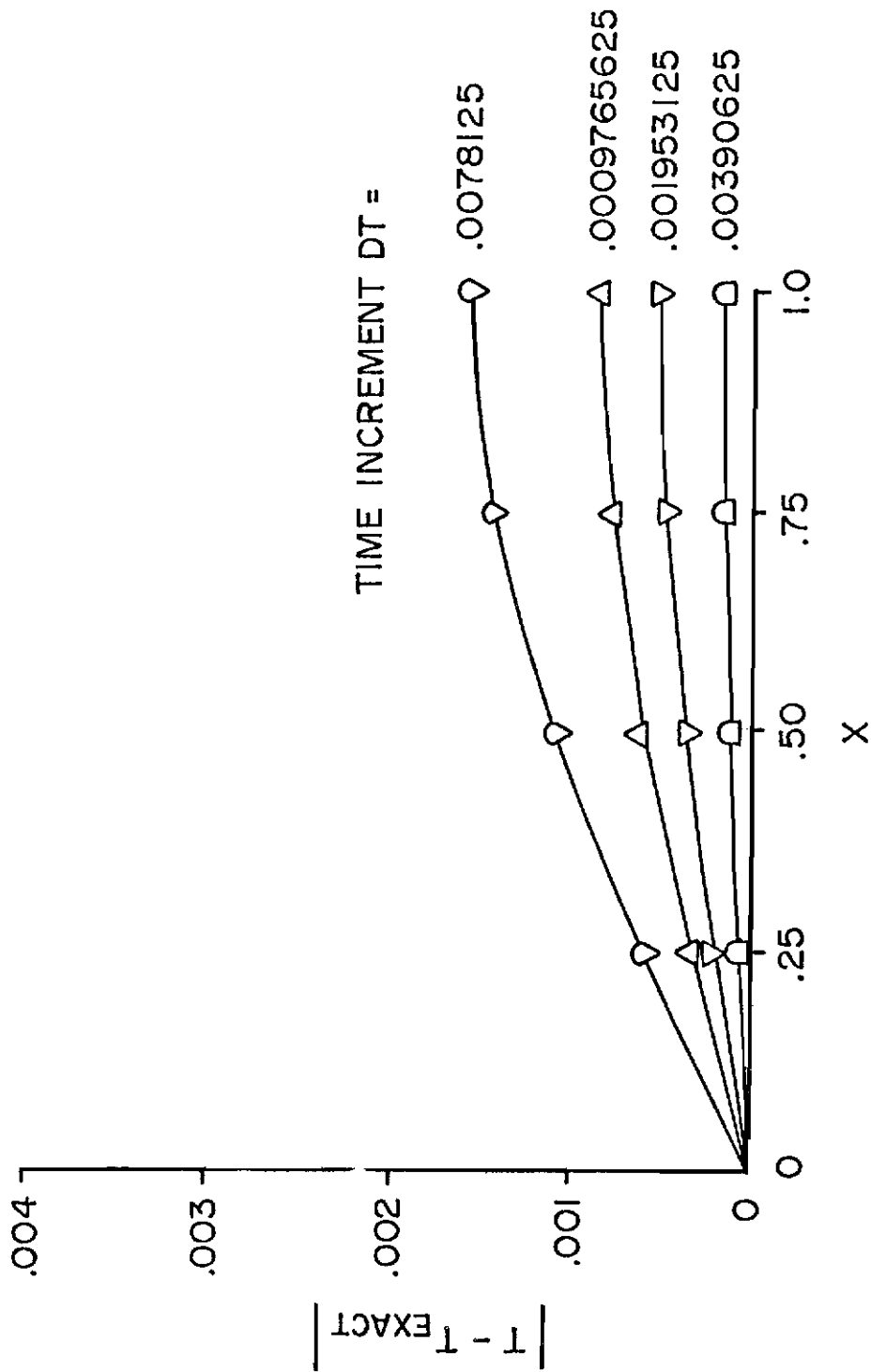


Figure 52. Temperature Difference vs Position
Finite Element, Time = .5

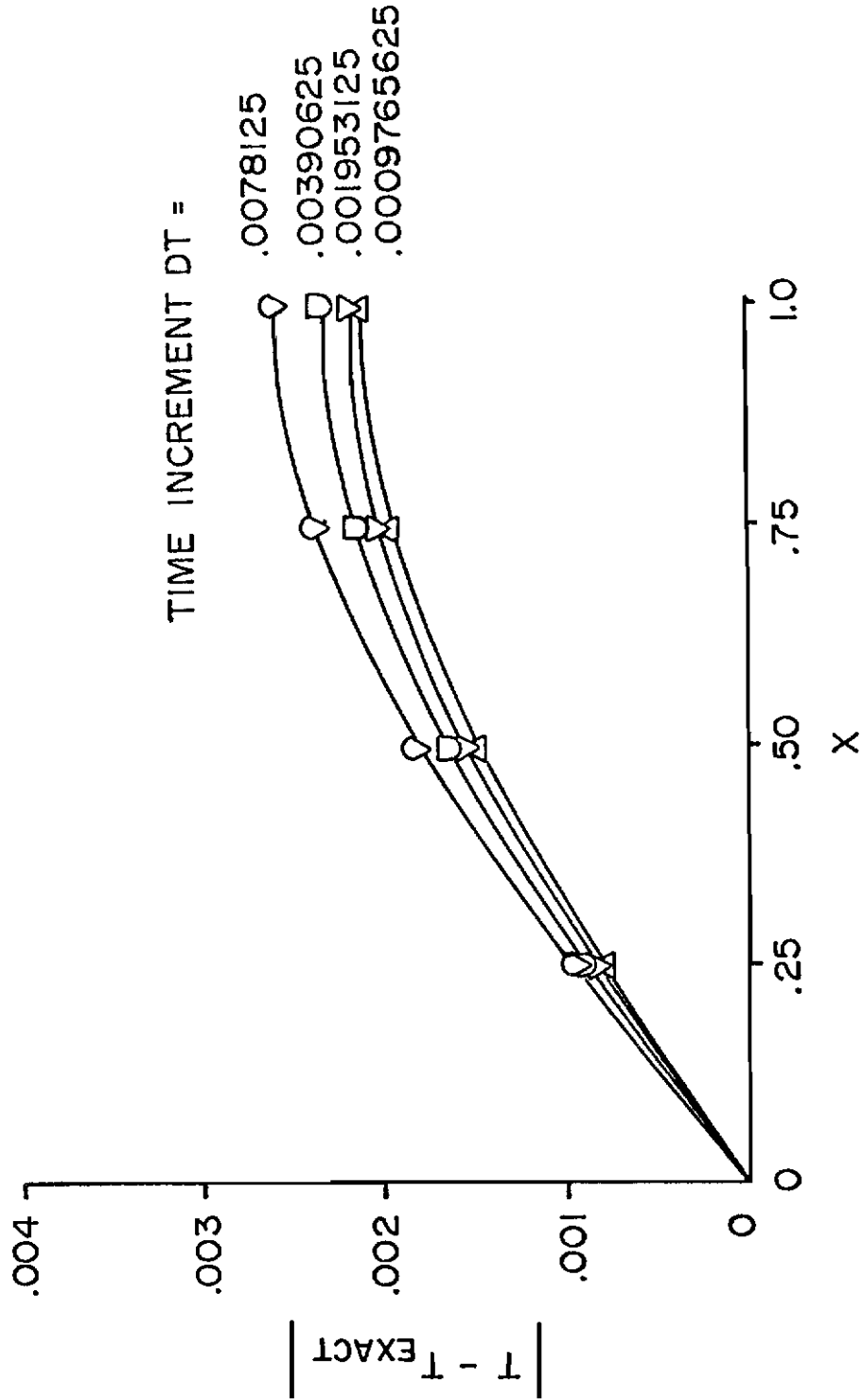


Figure 53. Temperature Difference vs Position, Finite Element, Time = 1.0

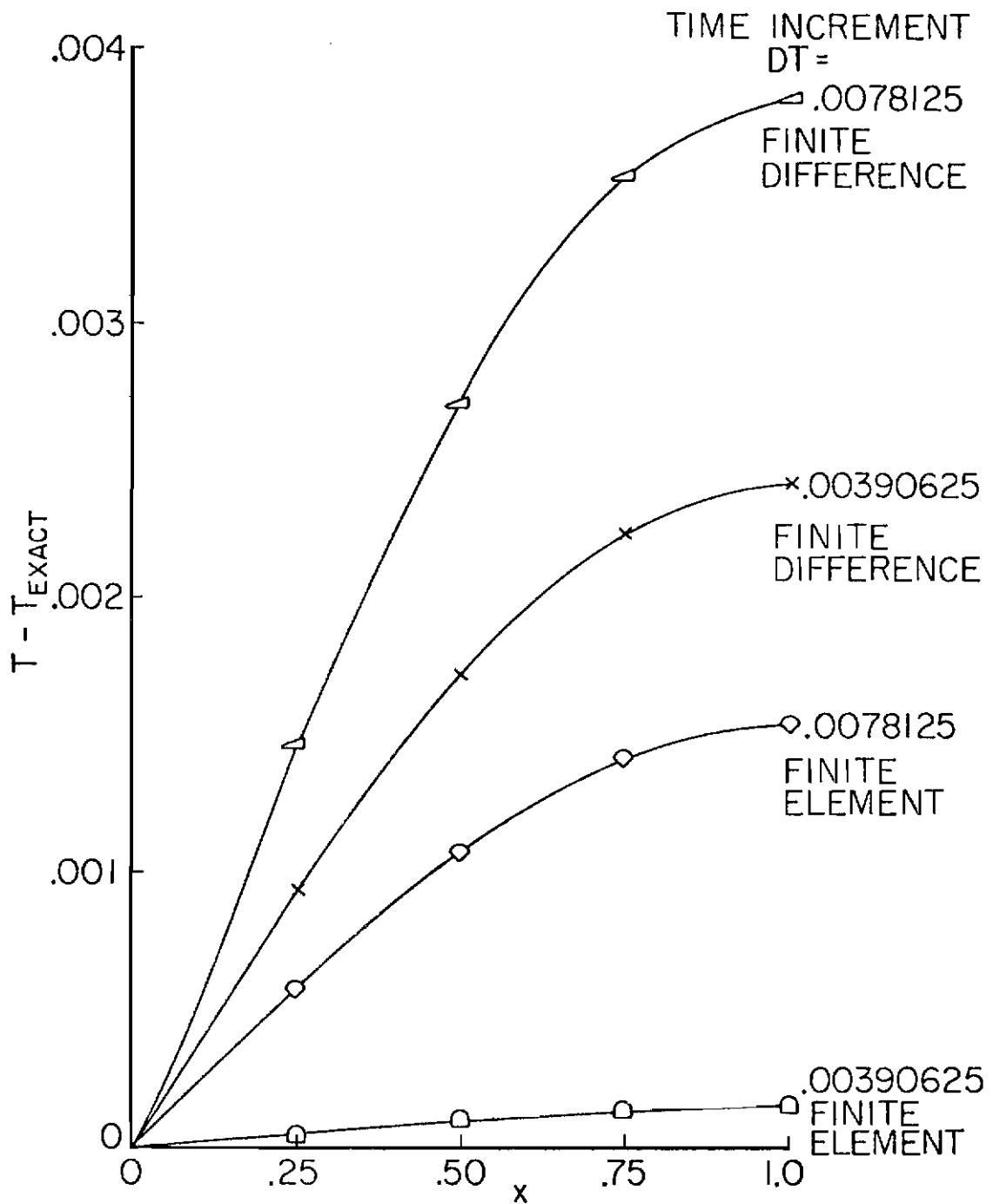


Figure 54. Temperature Difference vs Position, Finite Difference and Element, Time = .5

techniques for two time increments. As can be seen, the larger time increments show larger error than the smaller time increments and at a given time increment the finite difference technique has greater error than the finite element technique. The same information is shown in Figure 55 for time = 1.0. Here the finite element technique error is larger than the finite difference error. For the finite element technique the larger time increment gives the higher error while within the finite difference technique, the higher error is produced by the smaller time increment. These results do not appear conclusive and must be looked at in another way to provide meaningful results. A plot of $T - T_{\text{exact}}$ versus time is given in Figure 56 for $DT = .00390625$. This shows a comparison of the finite element and the finite difference techniques. Each point represents an average of four $T - T_{\text{exact}}$ values at that time. The four points averaged are those at $x = .25, .50, .75,$ and 1.0 . At small times the finite element technique has much greater error than the finite difference technique. The finite element error at time = $.03125$ is about three and one-half times greater than the finite difference error at the same time. The maximum error at time = $.03125$ for the finite element technique is 4.7% compared with 1.1% for the finite difference technique. These values change to 2.2% and 1.7% respectively at time = 1.0. Figure 57 is comparable to Figure 56 and is plotted for $DT = .0078125$. Here the maximum error in the finite element technique at time = $.03125$ is 7.5% compared to 3.8% for the finite difference technique. At time = 1.0 these values reduce to 2.4% and 1.7%, respectively.

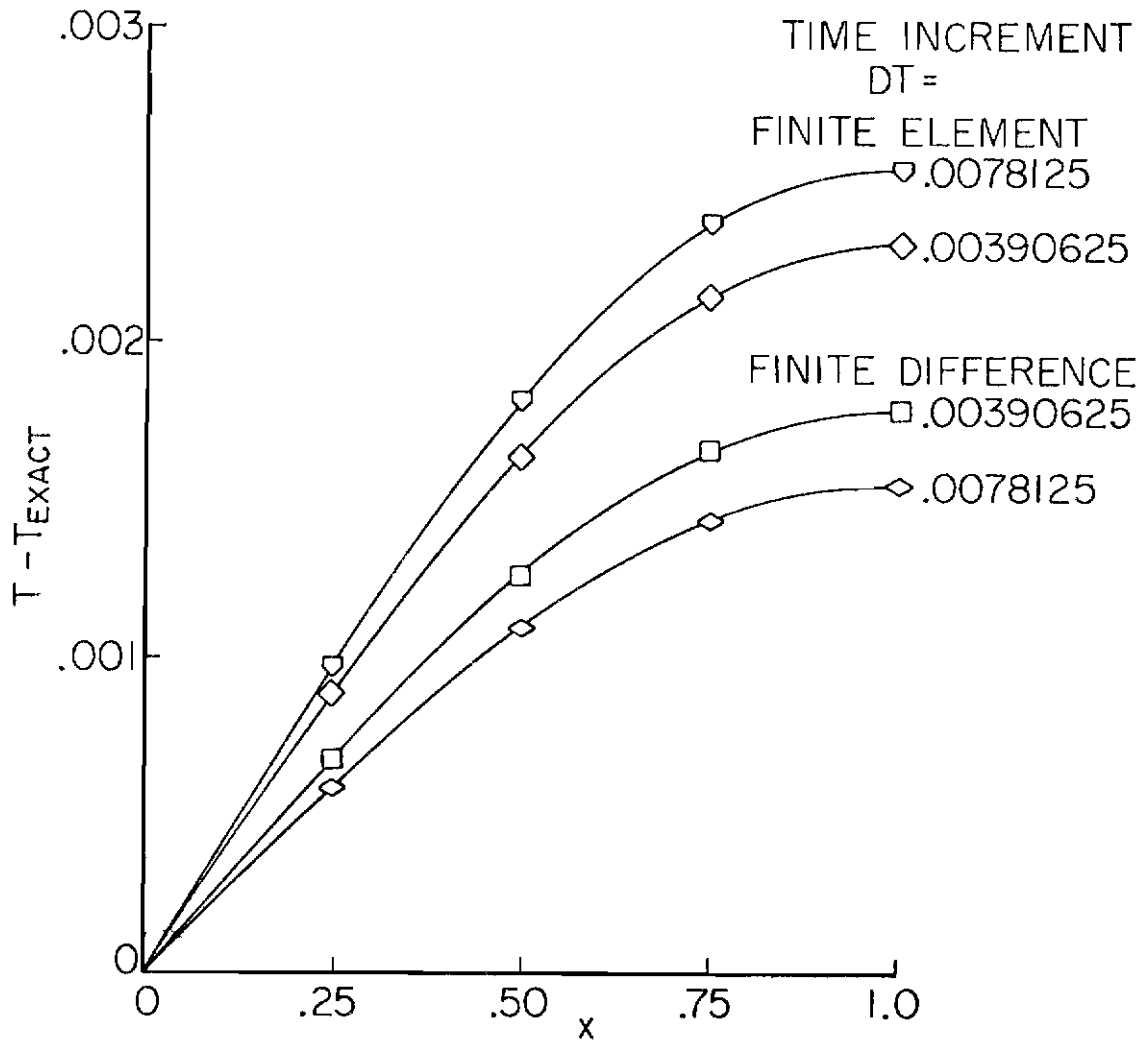


Figure 55. Temperature Difference vs Position, Finite Difference and Element, Time = 1.0

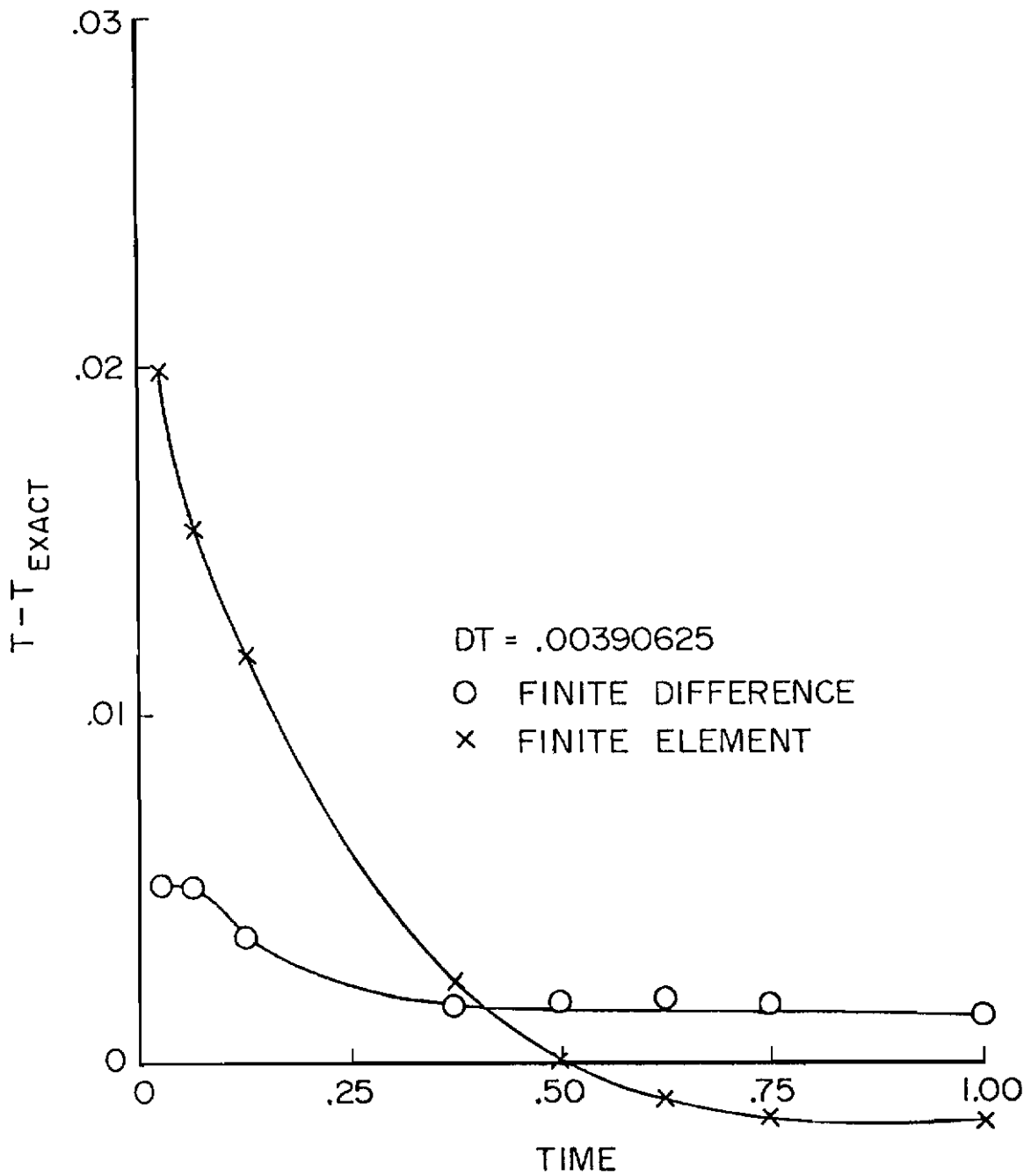


Figure 56. Temperature Difference vs Time,
DT = .00390625

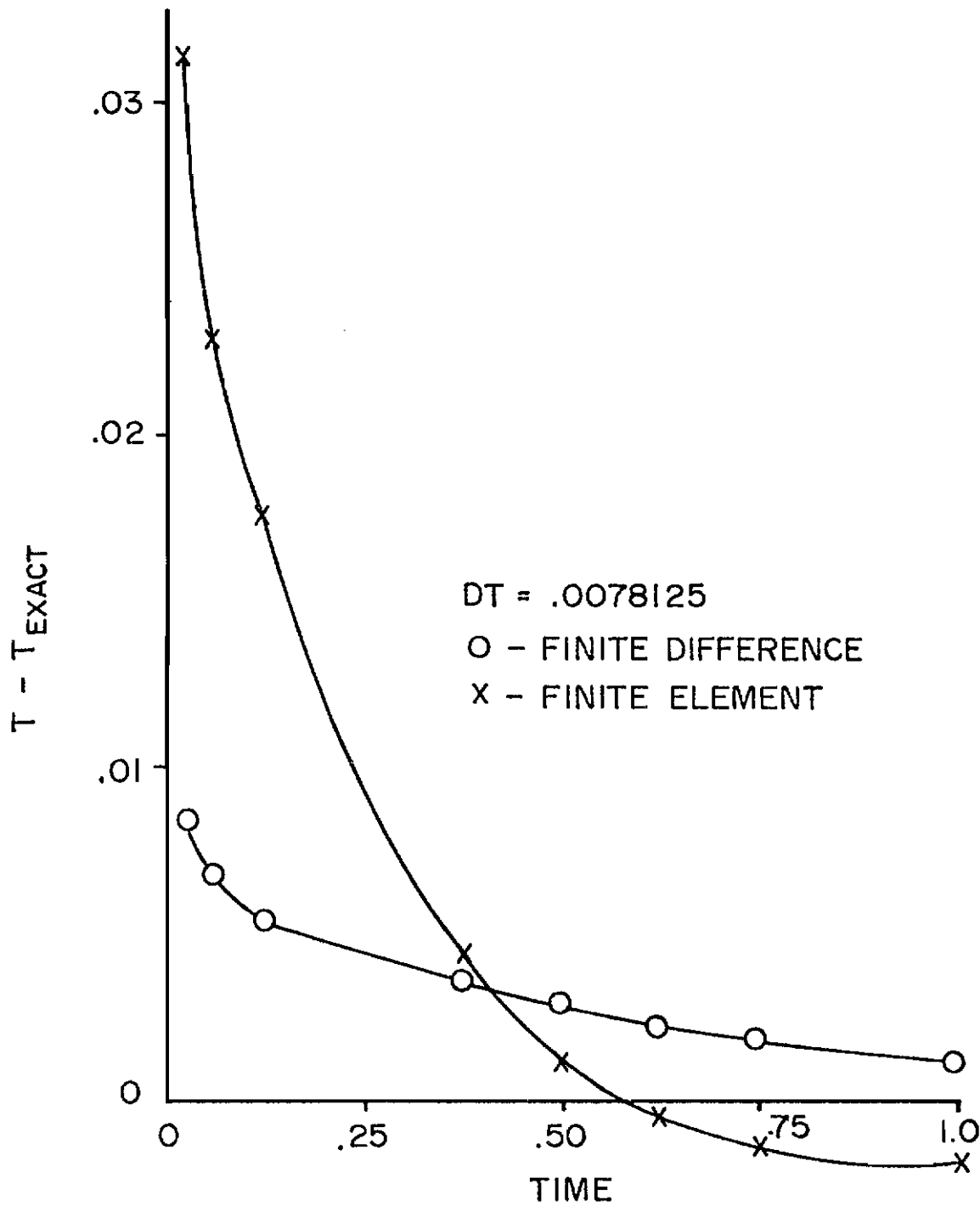


Figure 57. Temperature Difference vs Time, DT = .0078125

Contrails

In addition to error values, the time required to perform the analyses was recorded. Figure 58 is a plot of the time increment used versus the computer time used, given in CPU seconds on the CDC 6600 computer. It is apparent that the time required is greater for the finite element technique as long as the time increment is the same and the equation formulation within each technique is the same. Note that the upper limit in DT is different for the two techniques. The upper limit in DT represents the maximum value that can be used and still maintain a stable solution. Thus, a larger time increment can be used within the finite difference technique and this means that less computer time is necessary to solve the problem.

The fact that the time required is higher in the finite element case is at least partially caused by the fact that more arrays are necessary in that case. Table 8 compares the exact, finite difference and finite element techniques in the areas of storage requirements and computer time necessary. The finite element method requires considerably more time and storage than the finite difference method when using matrices. Also, although array requirements are the same when using the equation formulation, the finite element technique is still more time consuming than the finite difference technique. Note that although the exact method uses no arrays, it takes much more time than any of the others. This suggests that even if the exact solution to a problem exists, it could be more economical to use a numerical solution.

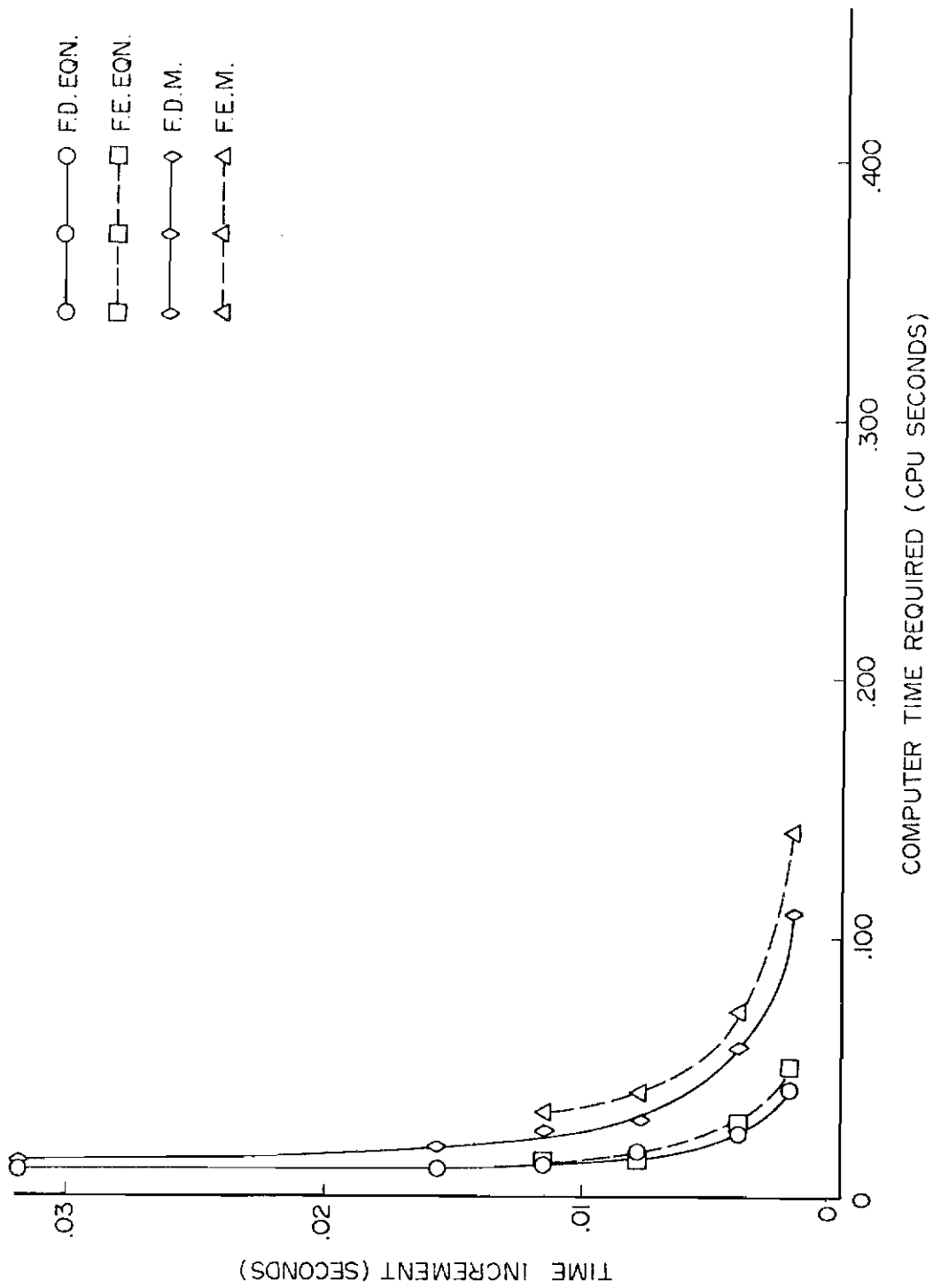


Figure 58. Time Increment vs Computer Time Required

TABLE 8

EXACT, FINITE DIFFERENCE AND FINITE ELEMENT COMPARISON

	Exact With 200 Terms	Finite Difference Equation, DT _{crit} = .031967	Finite Element Equation, DT _{crit} = .0115	Finite Difference Matrix, DT _{crit} = .031967	Finite Element Matrix, DT _{crit} = .0115
Required Arrays					
One-Dimensional	0	1 with 5 EL*	1 with 5 EL	2 with 4 EL	2 with 4 EL
One-Dimensional					2 at 5 EL
Two-Dimensional	0	0	0	2 at (4 × 4)	7 at (5 × 5)
Two-Dimensional				2 at (4 × 1)	
Computation Time (CPU-SEC)	.811				
DT = .031967		.010		.013	
DT = .015625		.010		.019	
DT = .0115		.011	.013	.025	.032
DT = .0078125		.017	.015	.029	.040
DT = .00390625		.024	.027	.057	.071
DT = .001953125		.041	.050	.111	.141

*EL--Elements

Conclusions

Based on a comparison of finite difference, finite element and exact solutions of the one-dimensional model of a brake:

1. The finite element method gives about three times more error at small times as does the finite difference method. At larger times the absolute value of the error is about the same for the two methods.

2. The computer time required at the same time increment is greater for the finite element method than for the finite difference method.

3. The critical time increment as far as stability is concerned is almost three times greater in the finite difference method as compared to the finite element method.

4. Storage requirements are more extensive with the finite element method.

5. The exact solution requires much more time than either of the numerical solutions.

6. Whether or not the finite difference method has less error at a given time and time increment than the finite element method depends on both the particular time and particular time increment.

Discussion

The conclusions of above pointed toward the use of the finite difference technique. Pertinent literature on the subject was also investigated. Most authors seem to choose a technique with no reasons given for the selection. Huebner,³⁶ among others, has pointed out that the finite element method is superior in treating irregular geometries

and that it can be more accurate than finite difference in steady state heat transfer problems. Emery and Carson³⁷ studied the finite element method as used in heat transfer problems. They concluded:

1. An oscillation at early time exists in transient problems within the finite element method. This is not a numerical instability but is inherent within the technique itself.
2. More severe numerical oscillation limits exist in transient problems in the finite element technique.
3. Variable property steady state problems usually require large amounts of computer execution time when the finite element method is used, an order of magnitude more than the finite difference technique.
4. Due to item 3, variable property transient problems will compound the time problem and thus should not be treated by the finite element technique.
5. Problems such as 3 and 4 of above are not only slower using the finite element method but also require an order of magnitude more computer storage.

Due to the results of this section of the research, all models employ the finite difference technique for solution.

One-Dimensional Radial

Interior Node Equation Development

The model selected for this radial analysis is shown in Figure 59. The nodes and typical elements of mass are shown as well as applicable dimensions. The equation for the interior nodes was derived from the first law of thermodynamics:

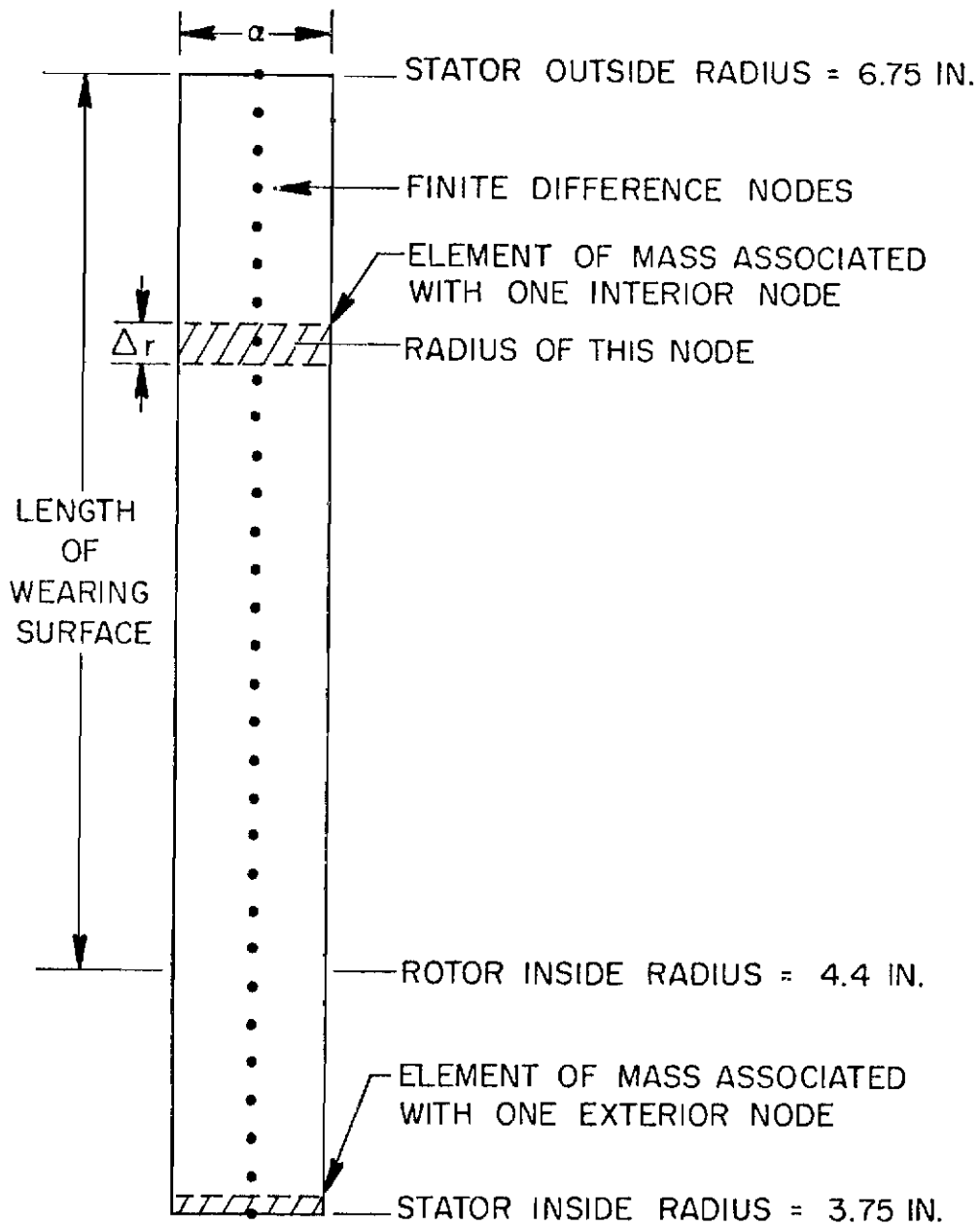


Figure 59. One Dimensional Radial Model

Contrails

$$\dot{q}_{in} - \dot{q}_{out} - \dot{W}_e = \frac{dE}{dt} \quad (44)$$

where \dot{q}_{in} is the heat transfer rate into the elemental mass, \dot{q}_{out} is the heat transfer rate out of the elemental mass, \dot{W}_e is the rate work crosses the elemental mass boundary, E is the total energy of the elemental mass and t is the time. If the kinetic and potential energy changes with respect to time are discarded, the total energy becomes only the internal energy, U or the specific internal energy, u , times the mass, ρV . Since the specific internal energy can be considered a function of temperature, T , and specific volume, v , the differential of u can be expressed as:

$$du = \left(\frac{\partial u}{\partial v} \right)_T dv + \left(\frac{\partial u}{\partial T} \right)_v dT \quad (45)$$

where the subscripts indicate evaluation at constant temperature and constant specific volume, respectively. For a solid, dv is approximately zero so the first term in Equation (45) becomes zero. Also the quantity multiplying dT in Equation (45) is the definition of specific heat at constant volume, C . Thus, Equation (45) substituted into Equation (44) yields:

$$\dot{q}_{in} - \dot{q}_{out} - \dot{W}_e = \rho VC \frac{dT}{dt} \quad (46)$$

An expression for \dot{W}_e in terms of known or measurable quantities is desired. Considering the bigger of the two cross-hatched elements in Figure 59, an expression for the work input to that element is:

$$\dot{W}_e = \frac{-F_e D}{t} \quad (47)$$

Contrails

where \dot{W}_e is the rate work crosses the element boundary, F_e is the force pushing the rotor element past the stator element (Figure 59), D is the distance through which the force, F_e , acts and t is the time interval through which this force acts. The negative sign is included since this work is done on the elemental system. The force on the element can be written as:

$$F_e = \mu P_e A_e \quad (48)$$

where μ is the coefficient of friction between the rotor and stator, P_e is the normal pressure exerted on the element and A_e is the area of the element. The elemental area, A_e , around the disc is

$$A_e = 2\pi r \Delta r \quad (49)$$

where r is the radius associated with the node in question and Δr is the incremental radius. The pressure on the element, P_e , can be obtained by using the condition of constant brake wear with radius. Laboratory testing has shown this to be a good assumption. Using this assumption the pressure on the element, P_e , is:

$$P_e = \frac{C_1}{r} \quad (50)$$

where C_1 is a constant.

Combining (48), (49), and (50) gives:

$$F_e = \mu \left(\frac{C_1}{r} \right) (2\pi r \Delta r) \quad (51)$$

Contrails

The distance, D , through which the force, F_e , acts is given by:

$$D = r \omega t \quad (52)$$

where ω is the angular velocity of the rotor with respect to the stator. This angular velocity at any time, t , can be expressed by:

$$\omega = \left(\frac{V_o}{R_r} \right) \left(1 - \frac{t}{t_s} \right) \quad (53)$$

where V_o is the velocity of the test wheel at its point of contact with the fly wheel, R_r is the tire rolling radius (distance from axle centerline to tire/flywheel contact spot) and t_s is the time required during a particular brake test for the rotors to come to a complete stop.

Equations (47), (51), (52), and (53) can now be combined to give:

$$\dot{W}_e = - \mu C_1 2\pi \Delta r r \left(\frac{V_o}{R_r} \right) \left(1 - \frac{t}{t_s} \right) \quad (54)$$

Consider the torque exerted at the element during a brake stop.

$$T_e = F_e r \quad (55)$$

The total torque can be found by integrating over the entire wearing surface. Substituting (51) into (55) and arranging this in integral form gives:

$$T_{rs} = \int_{RIR}^{SOR} \mu 2\pi C_1 r dr \quad (56)$$

where T_{rs} is the torque generated at the interface of one rotor and one stator, SOR is the stator outside radius, RIR is the rotor inside radius and dr is the result of allowing Δr to become infinitely small.

Upon integration the torque is given by:

$$T_{rs} = \mu\pi C_1 (SOR^2 - RIR^2) \quad (57)$$

The total torque transmitted by the brake is related to the torque at each rotor/stator interface by:

$$T_t = NT_{rs} \quad (58)$$

where T_t is the total torque transmitted by the brake and N is the number of rotor/stator interfaces. Solving (57) for $\mu\pi C_1$, substituting into (54) and incorporating (58) yields the following:

$$\dot{W}_e = - \frac{T_t \ 2r \ \Delta r \ \left(\frac{V_o}{R_r}\right) \left(1 - \frac{t}{t_s}\right)}{N (SOR^2 - RIR^2)} \quad (59)$$

The elemental work term is now in terms of experimentally measurable quantities. This is the total work transmitted into the stator and the rotor element. For this analysis the fraction of work input to the stator was taken to be the same amount as that observed in the one-dimensional axial analysis. The axial analysis is discussed in another section.

Referring back to Equation (46), it is necessary to obtain expressions for \dot{q}_{in} and \dot{q}_{out} . The heat rate input, \dot{q}_{in} , at radius r is expressed by Fourier's Law:

$$\dot{q}_{in} = -KA_k \left(\frac{\partial T}{\partial r}\right)_r \quad (60)$$

where K is thermal conductivity and A_k is the area through which the heat conduction takes place. The subscript r refers to the location at

Contrails

which the subscripted term must be evaluated. Writing A_k as a function of radius and disc thickness, a , gives:

$$\dot{q}_{in} = -Ka2\pi \left(r \frac{\partial T}{\partial r} \right)_r \quad (61)$$

Similarly the rate of heat flowing out of an element at $r + \Delta r$ is:

$$\dot{q}_{out} = -Ka2\pi \left(r \frac{\partial T}{\partial r} \right)_{r+\Delta r} \quad (62)$$

The elemental volume, V , can be expressed as:

$$V = 2\pi r \Delta r a \quad (63)$$

where a is the thickness of the disc being analyzed. The time derivative term is now:

$$\rho V C \frac{dT}{dt} = \rho 2\pi r \Delta r a C \frac{dT}{dt} \quad (64)$$

Combining (46) and (59) through (64) yields:

$$\begin{aligned} & -2\pi a \left(Kr \frac{\partial T}{\partial r} \right)_r - 2\pi a \left(-Kr \frac{\partial T}{\partial r} \right)_{r+\Delta r} + \frac{2 T_t r \Delta r V_o \left(1 - \frac{t}{t_s} \right)}{N R_r \left(\text{SOR}^2 - RIR^2 \right)} \\ & = \rho 2\pi r \Delta r a C \frac{\partial T}{\partial t} \end{aligned} \quad (65)$$

Dividing (65) by $2\pi a \Delta r$ and taking the limit of each term as Δr goes to zero leads to:

$$\frac{\partial}{\partial r} \left(Kr \frac{\partial T}{\partial r} \right) + \frac{T_t r V_o \left(1 - \frac{t}{t_s} \right)}{N R_r \pi a \left(\text{SOR}^2 - RIR^2 \right)} = \rho r C \frac{\partial T}{\partial t} \quad (66)$$

Contrails

The first term can be expanded to give:

$$\frac{\partial}{\partial r} \left(Kr \frac{\partial T}{\partial r} \right) = Kr \frac{\partial^2 T}{\partial r^2} + K \frac{\partial T}{\partial r} + r \left(\frac{\partial T}{\partial r} \right)^2 \frac{\partial K}{\partial T} \quad (67)$$

where the chain rule has been applied in the case of the last term.

With the aid of Equation (67) all terms in Equation (66) can be converted into finite difference approximate expressions. The expressions used here are:

$$\frac{\partial T}{\partial r} = \frac{T(I+1) - T(I-1)}{2\Delta r} \quad (68)$$

$$\frac{\partial^2 T}{\partial r^2} = \frac{T(I+1) - 2T(I) + T(I-1)}{(\Delta r)^2} \quad (69)$$

$$\frac{\partial T}{\partial t} = \frac{T'(I) - T(I)}{\Delta t} \quad (70)$$

where $T(I)$ refers to the temperature of the I^{th} element and $T'(I)$ refers to the temperature of the I^{th} element at the next increment in time. The heat capacity and thermal conductivity used were obtained from the manufacturer in the case of beryllium and were obtained by experiment in the case of carbon. Appendix K gives the properties as a function of temperature. Incorporating (67) - (70) into (66) and solving for $T'(I)$ gives:

Contrails

$$\begin{aligned}
 T'(I) = T(I) + \frac{\Delta t}{r\rho C} & \left\{ \frac{Kr}{[\Delta r]^2} [T(I+1) - 2T(I) + T(I-1)] \right. \\
 & + \frac{K}{2\Delta r} [T(I+1) - T(I-1)] + r \frac{\partial K}{\partial T} \left[\frac{T(I+1) - T(I-1)}{2\Delta r} \right]^2 \\
 & \left. + \frac{T_t V_o r \left(1 - \frac{t}{t_s} \right)}{a \pi R_r N (SOR^2 - RIR^2)} \right\} \quad (71)
 \end{aligned}$$

This is the equation used to predict the interior node temperatures.

Boundary Condition Equation Development

The development to this point could be for a rotor or for a stator. Although Figure 59 shows typical values for a stator, the interior node equation development applies equally well to a stator or a rotor. On the other hand, boundary conditions are dependent on a particular selection. Figure 60 shows a rotor, stator, and the interface between them. The stator was selected for analysis of the boundary conditions. The two elements of interest are shown in Figure 60. Considering the lower element first and applying the first law of thermodynamics as given in Equation (46) yields:

$$K 2\pi r a \frac{\partial T}{\partial r} - h 2\pi r a (T - T_\infty) = \rho \frac{\Delta r}{2} 2\pi r a C \frac{\partial T}{\partial t} \quad (72)$$

where h is the convective/radiative heat transfer coefficient, T is the temperature of the element, the work input is zero and T_∞ is the ambient air temperature. Note that the radial thickness of this element is $\Delta r/2$ as compared with Δr for the interior elements. Dividing

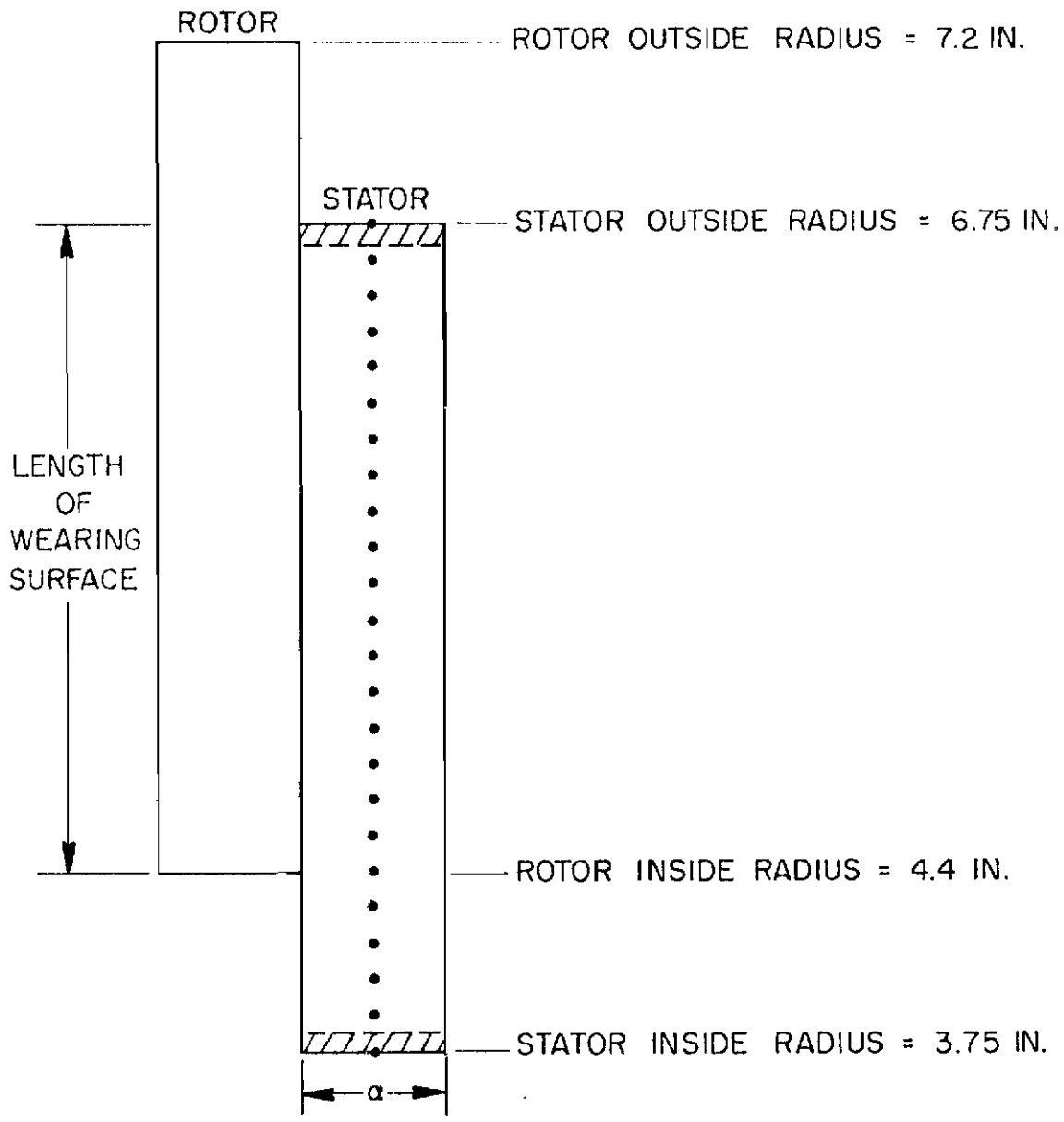


Figure 60. Rotor/Stator Interface

Contrails

(72) by $2\pi r a$, denoting the boundary temperature by $T(1)$, denoting the adjacent element temperature by $T(2)$, and expanding the right most term of the equation yields:

$$K \frac{T(2) - T(1)}{\Delta r} - h \left[T(1) - T_{\infty} \right] = \rho C \frac{\Delta r}{2} \frac{T'(1) - T(1)}{\Delta t} \quad (73)$$

where $T'(1)$ is the temperature of Element 1 at the next increment in time. Equation (73) can now be solved for $T'(1)$ to give:

$$T'(1) = T(1) + \frac{2\Delta t}{\rho \Delta r C} \left\{ K \frac{T(2) - T(1)}{\Delta r} - h \left[T(1) - T_{\infty} \right] \right\} \quad (74)$$

This is the equation used to calculate the temperature at the stator inside radius.

At the stator outside radius the boundary condition is somewhat different due to the work input. Applying the first law of thermodynamics as given in Equation (46) yields:

$$-K 2\pi r a \frac{\partial T}{\partial r} - h 2\pi r a \left(T - T_{\infty} \right) - \frac{\dot{W}_e}{2} = \rho \frac{\Delta r}{2} 2\pi r a C \frac{\partial T}{\partial t} \quad (75)$$

where \dot{W}_e is the expression given by Equation (59). If (75) is now divided by $2\pi r a$, the node at the stator outside radius is denoted by N and the finite difference formulation of each term is indicated, the following equation results:

$$\begin{aligned} & - K \frac{T(N) - T(N-1)}{\Delta r} - h \left[T(N) - T_{\infty} \right] - \frac{\dot{W}_e}{4\pi r a} \\ & = \frac{\rho \Delta r}{2} C \frac{T'(N) - T(N)}{\Delta t} \end{aligned} \quad (76)$$

Contrails

where $T'(N)$ is the temperature of the N^{th} element at the next increment in time. Equation (76) can now be solved for $T'(N)$ to give:

$$T'(N) = T(N) + \frac{2\Delta t}{\rho\Delta r C} \left\{ -\frac{K}{\Delta r} [T(N) - T(N-1)] \right. \\ \left. - h [T(N) - T_{\infty}] - \frac{\dot{W}_e}{4\pi r a} \right\} \quad (77)$$

Equation (77), with the help of Equation (59) for \dot{W}_e , was used for the calculation of the temperature at the stator outside radius. The initial condition requirement was satisfied by initially setting all nodes to a value dictated by the experiment being simulated.

A computer program employing variable heat capacity, variable thermal conductivity, variable convective/radiative heat transfer coefficients and variable work input was written to calculate the temperatures from the equations derived above. The program listing is given in Appendix L. Although employing the equations above for the work input portion of the brake stop, the computer program employs a cooling scheme beginning at 1.25 times the stop time that lumps the entire rotor and stator into one mass at constant temperature and allows that mass to cool. The radiative/convective heat transfer coefficients used are given in Appendix J.

One-Dimensional Axial

Interior Node Equation Development

The model selected for this axial analysis is shown in Figure 61. The nodes and typical elements of mass are shown as well as applicable

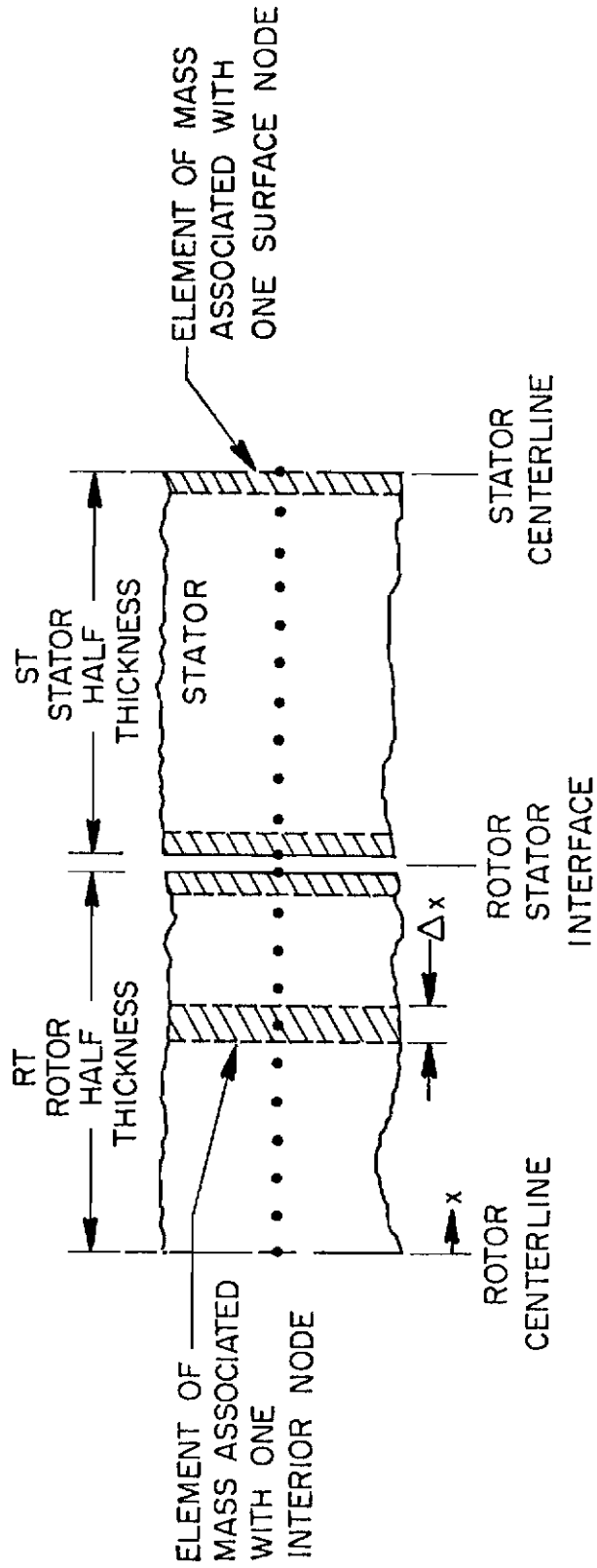


Figure 61. One-Dimensional Axial Model

dimensions. The rotor/stator interface is shown separated and identified with two nodes because the contact resistance of the interface is considered in the boundary condition analysis. The starting point for the interior node equation development is the first law of thermodynamics as expressed in Equation (46) and as shown below with the work term of (46) being zero:

$$\dot{q}_{in} - \dot{q}_{out} = \rho V C \frac{dT}{dt} \quad (78)$$

The heat rate input, \dot{q}_{in} , of a given interior element at axial position x , is expressed by Fourier's Law:

$$\dot{q}_{in} = -\left(K A_k \frac{\partial T}{\partial x}\right)_x \quad (79)$$

where the x subscript indicates the axial position at which the term must be evaluated. Similarly the heat rate output, \dot{q}_{out} , from the element is:

$$\dot{q}_{out} = -\left(K A_k \frac{\partial T}{\partial x}\right)_{x + \Delta x} \quad (80)$$

The volume of the element can be expressed as the area, A_k , times thickness, Δx , which gives

$$V = A_k \Delta x \quad (81)$$

Substituting (79) through (81) into (78) and dividing by $A_k \Delta x$ yields:

$$\frac{\left(K \frac{\partial T}{\partial x}\right)_x + \Delta x - \left(K \frac{\partial T}{\partial x}\right)_{x + \Delta x}}{\Delta x} = \rho C \frac{\partial T}{\partial t} \quad (82)$$

Contrails

If the limit of this equation is taken as Δx approaches zero, the following equation results:

$$\frac{\partial}{\partial x} \left(K \frac{\partial T}{\partial x} \right) = \rho C \frac{\partial T}{\partial t} \quad (83)$$

Expanding Equation (83) and applying the chain rule yields:

$$K \frac{\partial^2 T}{\partial x^2} + \left(\frac{\partial T}{\partial x} \right)^2 \frac{\partial K}{\partial T} = \rho C \frac{\partial T}{\partial t} \quad (84)$$

Equation (84) can be placed in finite difference form by employing Equations (68) through (70) and simply replacing r with x . This yields:

$$\begin{aligned} & K \frac{T(I+1) - 2T(I) + T(I-1)}{(\Delta x)^2} + \frac{\partial K}{\partial T} \left[\frac{T(I+1) - T(I-1)}{2\Delta x} \right]^2 \\ & = \rho C \frac{T'(I) - T(I)}{\Delta t} \end{aligned} \quad (85)$$

Solving Equation (85) for $T'(I)$ gives:

$$\begin{aligned} T'(I) = T(I) + \frac{\Delta t}{\rho C} & \left\{ K \frac{T(I+1) - 2T(I) + T(I-1)}{(\Delta x)^2} \right. \\ & \left. + \frac{\partial K}{\partial T} \left[\frac{T(I+1) - T(I-1)}{2\Delta x} \right]^2 \right\} \end{aligned} \quad (86)$$

This is the equation used to predict the interior node temperatures.

Boundary Condition Equation Development

The boundary condition at the centerlines of the rotor and stator were taken to be adiabatic. This was handled within the finite difference technique by creating an imaginary node just adjacent to the centerline node. In Figure 61 the stator imaginary node was placed to the right of the stator centerline while the rotor imaginary node was placed to the left of the rotor centerline. At each time step the imaginary node of each centerline was set equal in temperature to the temperature of the node just on the opposite side of the applicable centerline. As can be seen from Equation (68), this procedure insures that the temperature gradient at each centerline is zero.

In order to consider the interface boundary condition, it is helpful to expand the rotor/stator interface area of Figure 61 as is shown in Figure 62. Similar to the mathematical development by Schaaf,³⁸ the contact resistance at the interface is broken into two parts, that associated with the stator and that associated with the rotor. The actual contact resistance values and the calculation procedure are shown in Appendix M. The heat resulting from the work input is required to pass through the resistances prior to flowing into the rotor or stator. The actual contact point of the rotor and stator is modeled as some temperature, T_m , that is necessarily higher than either of the two adjacent nodal temperatures. The resistances and T_m are shown in Figure 62. Although the figure shows a separation between the two interface nodes, this is only for discussion purposes. The nodes are allowed to have different temperatures but are required to have no distance between them. This is an approximation to the fact that the

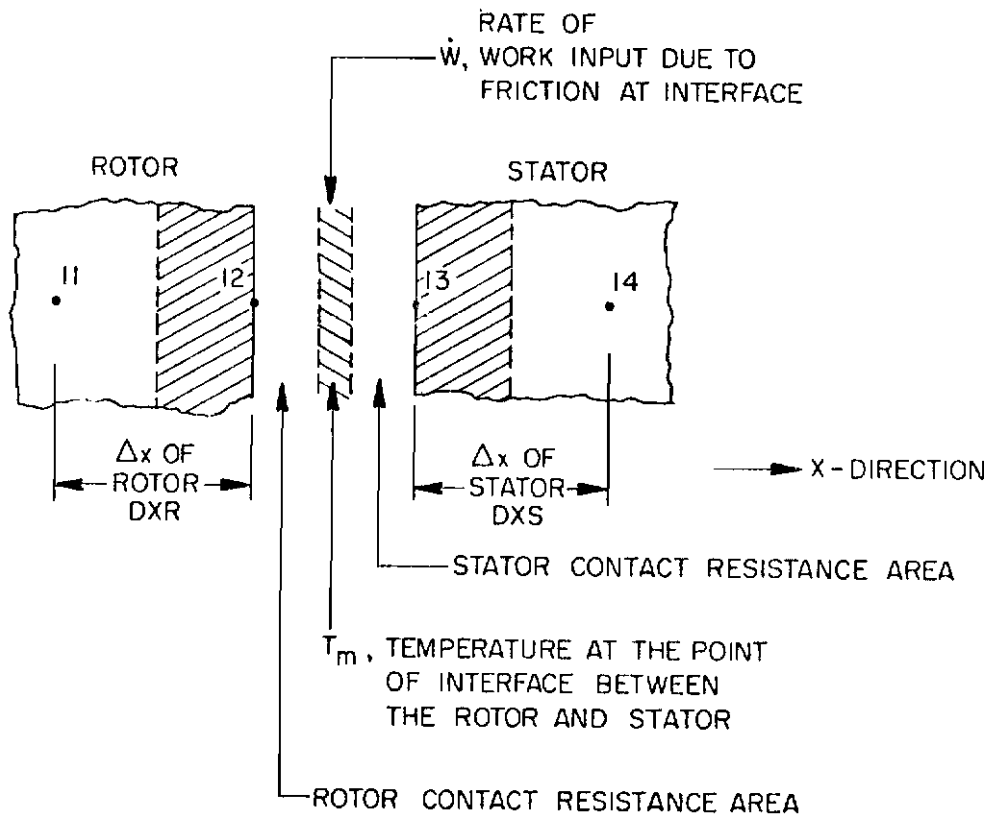


Figure 62. Expanded Rotor/Stator Interface

points would indeed be separated by a small amount but this amount is much smaller than the Δx values between the other nodes. To assist in the equation development, numbers were assigned to the nodes as shown in Figure 62. The first law of thermodynamics as shown in Equation (46) is repeated below for reference:

$$\dot{q}_{in} - \dot{q}_{out} - \dot{W} = \rho V C \frac{dT}{dt} \quad (86)$$

Equation (46) as applied to the crosshatched part of Figure 62 between Nodes 11 and 12 gives:

$$-\left(K A_k \frac{\partial T}{\partial x}\right)_{left} - \frac{A_k}{RE_r} (T(12) - T_m) = \rho A_k \frac{DXR}{2} C \frac{\partial T(12)}{\partial t} \quad (87)$$

where the first term is evaluated at the left face of the element, RE_r is the contact resistance associated with the rotor and DXR is the incremental distance in the x direction associated with the rotor. This distance, DXR, is allowed to vary from the incremental x direction distance within the stator, DXS. Dividing by A_k , expanding the right hand side and putting Equation (87) into finite difference form yields:

$$\begin{aligned} & -\frac{K_{12}}{DXR} [T(12) - T(11)] - \frac{1}{RE_r} [T(12) - T_m] \\ & = \rho \frac{DXR}{2} C_{12} \left[\frac{T'(12) - T(12)}{\Delta t} \right] \end{aligned} \quad (88)$$

where the 12 used as a subscript indicates that the subscripted quantity should be evaluated at T(12). Similarly, applying Equation (46) to the crosshatched part of Figure 62 between Nodes 13 and 14 gives:

Contrails

$$\begin{aligned} & \left(K A_k \frac{\partial T}{\partial x} \right)_{\text{right}} + \frac{A_k}{RE_s} [T_m - T(13)] \\ & = \rho A_k \frac{DXS}{2} C_{13} \frac{\partial T(13)}{\partial t} \end{aligned} \quad (89)$$

where the first term is evaluated at the right face of the element and RE_s is the stator contact resistance. Dividing by A_k , expanding the right-hand side and placing (89) into finite difference form yields:

$$\begin{aligned} & \frac{K_{13}}{DXS} [T(14) - T(13)] + \frac{1}{RE_s} [T_m - T(13)] \\ & = \rho \frac{DXS}{2} C_{13} \left(\frac{T'(13) - T(13)}{\Delta t} \right) \end{aligned} \quad (90)$$

Since the material of the rotor is the same as that of the stator, the contact resistance of each is also identical, i.e.:

$$RE_s = RE_r \quad (91)$$

This would not necessarily be true if the two materials were different, although Equation (91) could still be used if no experimental data were available. Subtracting Equation (88) from (90) while employing Equation (91) gives:

$$\begin{aligned}
 & \frac{K_{13}}{DXS} [T(14) - T(13)] + \frac{K_{12}}{DXR} [T(12) - T(11)] \\
 & + \frac{1}{RE} [T(12) - T(13)] \\
 & = \rho \frac{DXS}{2} C_{13} \left(\frac{T'(13) - T(13)}{\Delta t} \right) \\
 & \quad - \rho \frac{DXR}{2} C_{12} \left(\frac{T'(12) - T(12)}{\Delta t} \right) \tag{92}
 \end{aligned}$$

Applying Equation (46) to the entire element, the two halves of which are shown crosshatched in Figure 62, yields:

$$\begin{aligned}
 & - \left(K A_k \frac{\partial T}{\partial x} \right)_{\text{left}} + \left(K A_k \frac{\partial T}{\partial x} \right)_{\text{right}} - \dot{W} \\
 & = \rho A_k DXA C \frac{\partial T}{\partial x} \tag{93}
 \end{aligned}$$

where W is the rate of work input due to the friction at the interface and DXA is an average between DXR and DXS . Dividing A_k , expanding the right-hand side and putting in finite difference form gives:

$$\begin{aligned}
 & - K_{12} \frac{[T(12) - T(11)]}{DXR} + K_{13} \frac{[T(14) - T(13)]}{DXS} - \dot{W}'' \\
 & = \rho DXA C_a \left(\frac{T'(a) - T(a)}{\Delta t} \right) \tag{94}
 \end{aligned}$$

where W'' is the rate of work input per unit area and the subscript "a" indicates that the subscripted term must be evaluated at the average temperature of Nodes 12 and 13, i.e.,:

$$T(a) = \frac{[T(13) + T(12)]}{2} \tag{95}$$

Contrails

With the inclusion of average temperature definition of (95),
Equation (94) becomes:

$$\begin{aligned}
 & - K_{12} \frac{T(12) - T(11)}{DXR} + K_{13} \frac{T(14) - T(13)}{DXS} - \dot{W}'' \\
 & = \frac{\rho DXA}{\Delta t} C_a \left(\frac{T'(13) + T'(12)}{2} - \frac{T(13) + T(12)}{2} \right) \quad (96)
 \end{aligned}$$

Solving Equation (96) for $T'(12)$ gives:

$$\begin{aligned}
 T'(12) & = T(12) + T(13) - T'(13) \\
 & + \left\{ \frac{\frac{K_{13}}{DXS} [T(14) - T(13)] + \frac{K_{12}}{DXR} [T(11) - T(12)] - \dot{W}''}{\frac{\rho DXA}{2\Delta t} C_a} \right\} \quad (97)
 \end{aligned}$$

Substituting Equation (97) into Equation (92) yields:

$$\begin{aligned}
 & \frac{K_{13}}{DXS} [T(14) - T(13)] + \frac{K_{12}}{DXR} [T(12) - T(11)] + \frac{1}{RE} [T(12) - T(13)] \\
 & = \frac{\rho DXS}{2} C_{13} \left(\frac{T'(13) - T(13)}{\Delta t} \right) - \frac{\rho DXR C_{12}}{2\Delta t} \left\{ T(13) - T'(13) \right. \\
 & \left. + \frac{\frac{K_{13}}{DXS} [T(14) - T(13)] + \frac{K_{12}}{DXR} [T(11) - T(12)] - \dot{W}''}{\left(\frac{\rho DXA C_a}{2\Delta t} \right)} \right\} \quad (98)
 \end{aligned}$$

Contrails

Equation (98) can now be solved for $T'(13)$ to give:

$$\begin{aligned}
 T'(13) = & \left\{ \frac{K_{13}}{DXS} [T(14) - T(13)] + \frac{K_{12}}{DXR} [T(12) - T(11)] \right. \\
 & + \frac{T(12) - T(13)}{RE} + \frac{\rho DXR C_{12}}{2\Delta t} \\
 & \left. \left[\frac{T(13) + \frac{K_{13}}{DXS} [T(14) - T(13)] + \frac{K_{12}}{DXR} [T(11) - T(12)] - \dot{W}''}{\frac{\rho DXA C_a}{2\Delta t}} \right] \right. \\
 & \left. + \frac{\rho DXS T(13) C_{13}}{2\Delta t} \right\} / \left\{ \frac{\rho DXS C_{13}}{2\Delta t} + \frac{\rho DXR C_{12}}{2\Delta t} \right\} \quad (99)
 \end{aligned}$$

Equations (97) and (99) contain the rate of work input term, \dot{W}'' . The work rate is the force pushing the rotor past the stator times the distance through which the force acts divided by the time required to travel the distance. The force can be expressed as the brake torque, T_t , divided by the rolling radius, R_r . The distance divided by time is the angular velocity, ω , given by Equation (53) multiplied by the rolling radius. Thus the work rate is:

$$\dot{W} = \left(\frac{T_t}{NR_r} \right) \left[v_o \left(1 - \frac{t}{t_s} \right) \right] \quad (100)$$

where N is the number of friction pairs. The work rate per unit area is:

Contrails

$$\dot{w}'' = \left(\frac{T_t}{NR_r} \right) \left[v_o \left(1 - \frac{t}{t_s} \right) \right] \frac{1}{\pi SOR^2 - RIR^2} \quad (101)$$

Equations (97), (99), and (101) were used to obtain the rotor/stator interface temperatures when contact resistance was a finite value. To allow comparisons with contact resistance equal zero, the temperatures at Nodes 12 and 13 were set equal and Equation (97) was solved to give:

$$T'(12) = T(12) + \frac{\left\{ .5 \frac{K_{13}}{DXS} [T(14) - T(13)] + \frac{K_{12}}{DXR} [T(11) - T(12)] - \dot{w}'' \right\}}{\frac{\rho DXA C_a}{2\Delta t}} \quad (102)$$

A computer program employing variable heat capacity, variable thermal conductivity, variable work input, variable x direction nodal spacing from rotor to stator, and contact resistance was written using the equations derived above. The program listing is given in Appendix N.

Two Dimensional Radial/Axial (Rotor/Stator Pair)

Interior Node Equation Development

This analysis was accomplished assuming that each rotor was equivalent to every other in temperature and that each stator was equivalent to every other in temperature. Thus, in order to analyze the total heat sink, analysis of only one rotor and one stator was sufficient. The model selected for this analysis is shown in

Figure 63. The nodes are shown as well as the different element types

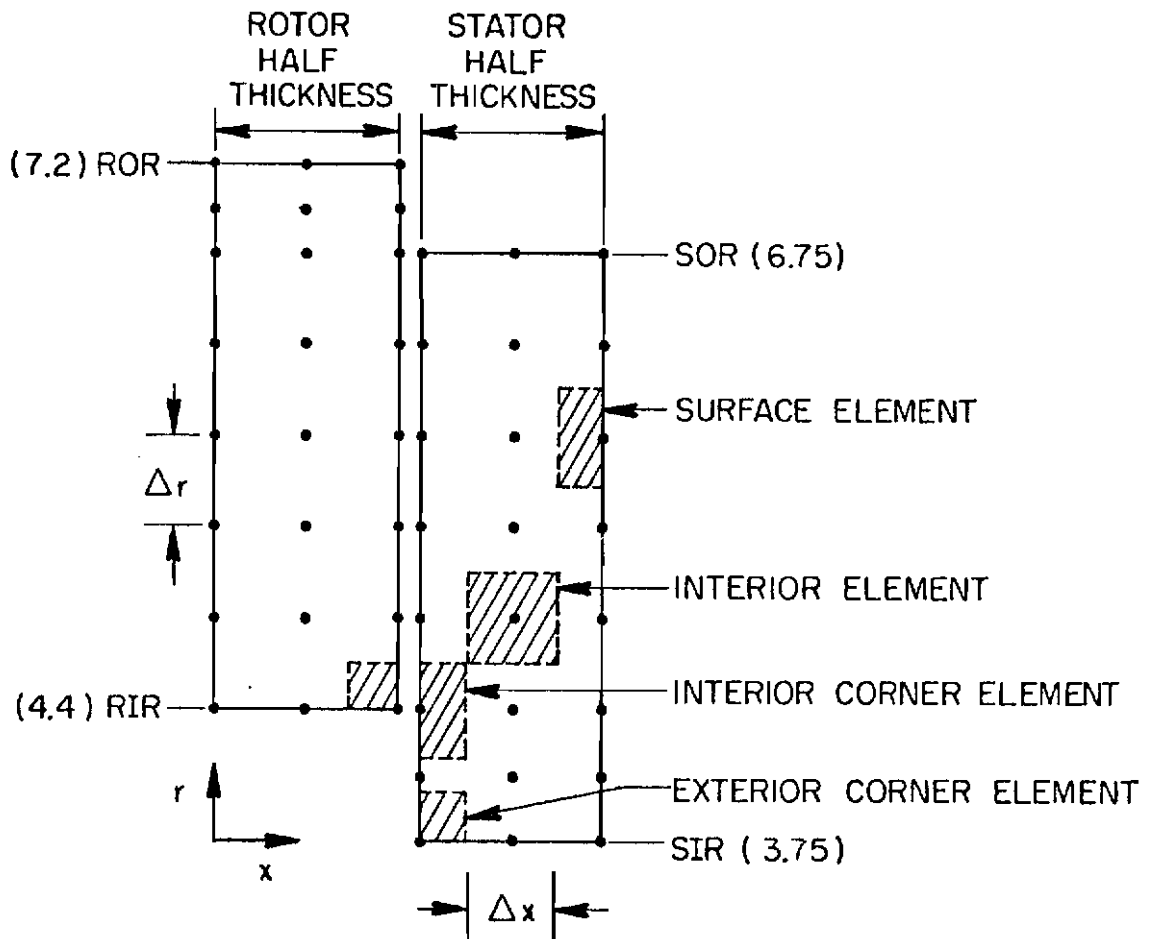


Figure 63. Two-dimensional Radial/Axial Model (Rotor/Stator Pair)

and dimensions. The actual numbers shown are those of the experimental brake discs. As in the previous analysis, the rotor/stator interface is shown separated and identified with two nodes at each radial position because the contact resistance of the interface is considered in the boundary condition analysis. The starting point for the interior

Contrails

node equation development is again the first law of thermodynamics as expressed in Equation (46) and as shown below with the work term of (46) being zero:

$$\dot{q}_{in} - \dot{q}_{out} = \rho V C \frac{dT}{dt} \quad (103)$$

The heat rate input of an interior element is expressed as:

$$\dot{q}_{in} = \left[-K_x (2\pi r \Delta r) \frac{\partial T}{\partial x} \right]_x + \left[-K_r (2\pi r \Delta x) \frac{\partial T}{\partial r} \right]_r \quad (104)$$

where K_x and K_r are the thermal conductivities in the x and r directions, respectively. Similarly the heat rate output is:

$$\begin{aligned} \dot{q}_{out} = & \left[-K_x (2\pi r \Delta r) \frac{\partial T}{\partial x} \right]_{x+\Delta x} \\ & + \left[-K_r (2\pi r \Delta x) \frac{\partial T}{\partial r} \right]_{r+\Delta r} \end{aligned} \quad (105)$$

The volume of the element is:

$$V = 2\pi r \Delta x \Delta r \quad (106)$$

Substituting (104) through (106) into (103) and rearranging yields:

$$\begin{aligned} & \left(K_x 2\pi r \Delta r \frac{\partial T}{\partial x} \right)_{x+\Delta x} - \left(K_x 2\pi r \Delta r \frac{\partial T}{\partial x} \right)_x + \left(K_r 2\pi r \Delta x \frac{\partial T}{\partial r} \right)_{r+\Delta r} \\ & - \left(K_r 2\pi r \Delta x \frac{\partial T}{\partial r} \right)_r = \rho 2\pi r \Delta x \Delta r C \frac{\partial T}{\partial t} \end{aligned} \quad (107)$$

Contrails

Dividing both sides of this equation by $2\pi r \Delta x \Delta r$ and taking the limit as Δx and Δr approach zero gives:

$$\frac{\partial}{\partial x} \left(K_x \frac{\partial T}{\partial x} \right) + \frac{1}{r} \frac{\partial}{\partial r} \left(K_r r \frac{\partial T}{\partial r} \right) = \rho C \frac{\partial T}{\partial t} \quad (108)$$

Expanding this equation and applying the chain rule leads to:

$$\begin{aligned} & K_x \frac{\partial^2 T}{\partial x^2} + \left(\frac{\partial T}{\partial x} \right)^2 \frac{\partial K_x}{\partial T} + K_r \frac{\partial^2 T}{\partial r^2} + \left(\frac{\partial T}{\partial r} \right)^2 \frac{\partial K_r}{\partial T} + \frac{K_r}{r} \frac{\partial T}{\partial r} \\ & = \rho \frac{\partial T}{\partial t} C \end{aligned} \quad (109)$$

Equation (109) can be placed in finite difference form by employing Equations (68) through (70) for the r-direction terms and replacing r with x for the x-direction terms. With these equations and the Euler time marching technique, Equation (109) converts to:

$$\begin{aligned} & K_x \frac{T(I+1,J) - 2T(I,J) + T(I-1,J)}{(\Delta x)^2} + \frac{\partial K_x}{\partial T} \left[\frac{T(I+1,J) - T(I-1,J)}{2\Delta x} \right]^2 \\ & + K_r \frac{T(I,J+1) - 2T(I,J) + T(I,J-1)}{(\Delta r)^2} + \frac{\partial K_r}{\partial T} \left[\frac{T(I,J+1) - T(I,J-1)}{2\Delta r} \right]^2 \\ & + \frac{K_r}{r} \left[\frac{T(I,J+1) - T(I,J-1)}{2\Delta r} \right] = \rho C \left[\frac{T'(I,J) - T(I,J)}{\Delta t} \right] \end{aligned} \quad (110)$$

Solving this equation for $T'(I, J)$ gives:

$$\begin{aligned}
 T'(I, J) = T(I, J) + \frac{\Delta t}{\rho C} & \left\{ K_x \frac{T(I+1, J) - 2 T(I, J) + T(I-1, J)}{(\Delta x)^2} \right. \\
 & + \frac{\partial K_x}{\partial T} \left[\frac{T(I+1, J) - T(I-1, J)}{2\Delta x} \right] \\
 & + K_r \frac{T(I, J+1) - 2 T(I, J-1) + T(I, J-1)}{(\Delta r)^2} \\
 & + \frac{\partial K_r}{\partial T} \left[\frac{T(I, J+1) - T(I, J-1)}{2\Delta r} \right]^2 \\
 & \left. + \frac{K_r}{r} \left[\frac{T(I, J+1) - T(I, J-1)}{2\Delta r} \right] \right\} \quad (111)
 \end{aligned}$$

This is the equation used to predict the interior node temperature.

Boundary Condition Equation Development

As in the previous development the boundary condition at the centerlines of the rotor and stator was taken to be adiabatic. This was accomplished within the finite difference technique by creating imaginary nodes adjacent to the centerline nodes and forcing the temperature of these nodes, at each time step, to be equal to the temperature of the node on the opposite side of the centerline.

In order to consider the interface boundary condition, the rotor/stator interface is expanded as shown in Figure 64. As in the previous development, the contact resistance at the interface is broken up into two parts, that associated with the rotor and that associated with the stator. Appendix M gives the contact resistance values and calculation

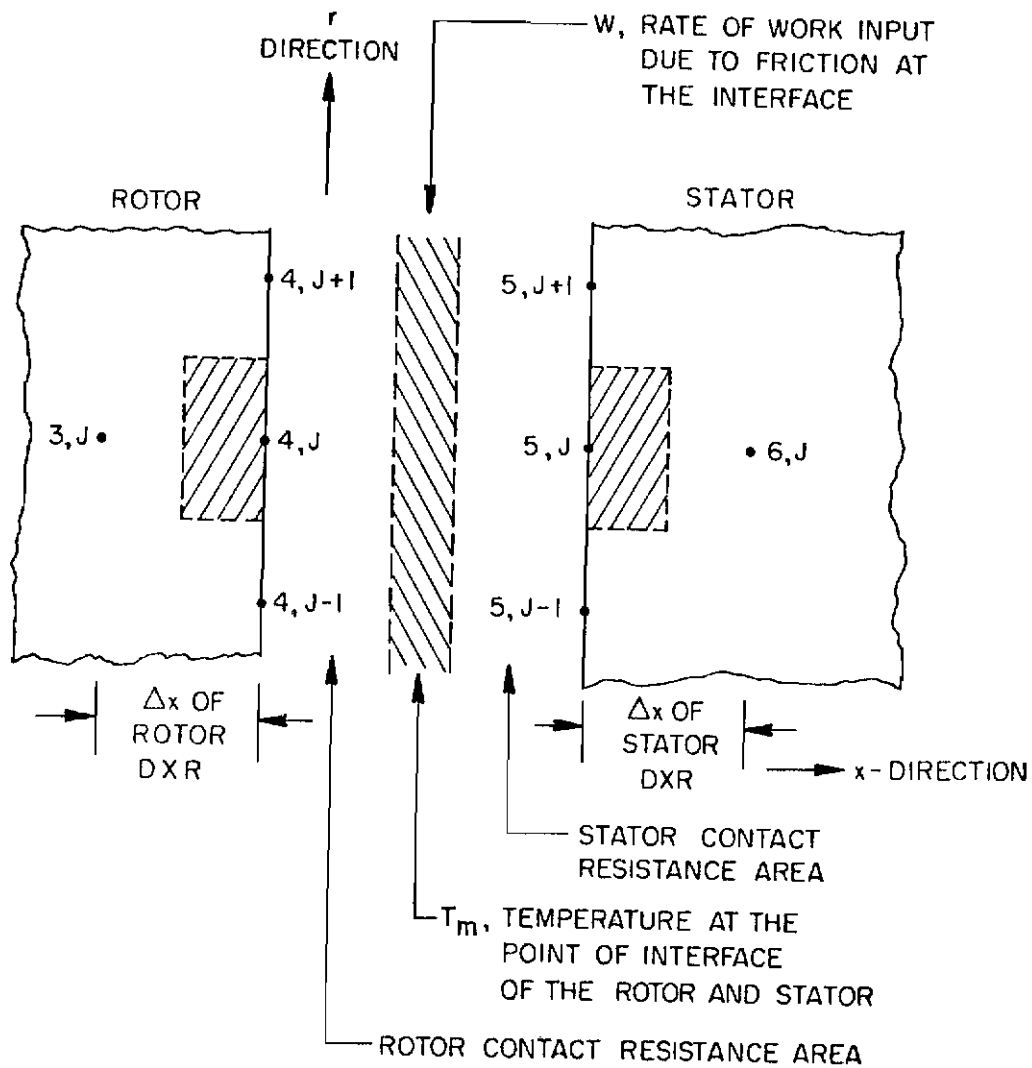


Figure 64. Expanded Rotor/Stator Interface (2D Radial/Axial)

procedure. The actual contact point of the rotor and stator is modeled as some temperature, T_m , that is necessarily higher than either of the two adjacent nodal temperatures. The resistances and T_m are shown in Figure 64. Adjacent interface nodes are shown physically separated for clarity. The nodes are allowed to have different temperatures but are required to have no distance between them. This approximates the fact that the distance between the nodes is actually much less than the Δx value. The node identification shown in Figure 64 is employed to assist in equation derivation. The first law of thermodynamics as shown in Equation (46) is repeated below for reference:

$$\dot{q}_{in} - \dot{q}_{out} - \dot{W} = \rho V C \frac{dT}{dt} \quad (112)$$

Applying Equation (112) to the crosshatched section of Figure 64 between nodes (3, J) and (4, J) yields:

$$\begin{aligned} & \left(KR4J \frac{DXR}{2} 2\pi r \frac{\partial T}{\partial r} \right)_{r+\Delta r} - \left(KR4J \frac{DXR}{2} 2\pi r \frac{\partial T}{\partial r} \right)_r \\ & - KX4J \frac{T(4, J) - T(3, J)}{DXR} (DR2) 2\pi r + \frac{T_m - T(4, J)}{RE_r} (DR2) 2\pi r \\ & = \rho \frac{DXR}{2} 2\pi r C4 \left[\frac{T'(4, J) - T(4, J)}{\Delta t} \right] \end{aligned} \quad (113)$$

where all terms except the first two have been placed in finite difference form, $C4$ is the heat capacity of the (4, J) element, $KX4J/KR4J$ is the thermal conductivity in the axial/radial direction of the 4J element and $DR2$ is the distance between nodes in the radial direction. $DR2$ is a function of the distance between the stator outside radius and

Contrails

the rotor inside radius and of the number of nodes in this area. Thus, referring to Figure 63:

$$DR2 = \frac{(SOR - RIR)}{5} \quad (114)$$

It is possible that the distance between nodes in the radial direction is different in the area where the stator and rotor make contact, as opposed to the areas where the stator or rotor are not in contact.

Divide Equation (113) by $\pi(DR2)$ and consider the case when DR2 approaches zero. This transforms Equation (113) into:

$$\begin{aligned} DXR \frac{\partial}{\partial r} \left(KR4J r \frac{\partial T}{\partial r} \right) - 2(KX4J)r \frac{T(4,J) - T(3,J)}{DXR} \\ + 2 r \frac{T_m - T(4, J)}{RE_r} = \rho (DXR)r C4 \left[\frac{T'(4,J) - T(4,J)}{\Delta t} \right] \end{aligned} \quad (115)$$

The derivative in the first term of Equation (115) can be expanded to give:

$$\begin{aligned} \frac{\partial}{\partial r} \left(KR4J r \frac{\partial T}{\partial r} \right) = KR4J r \frac{\partial^2 T}{\partial r^2} + r \left(\frac{\partial T}{\partial r} \right)^2 \frac{\partial (KR4J)}{\partial T} \\ + (KR4J) \frac{\partial T}{\partial r} \end{aligned} \quad (116)$$

Contrails

Substituting Equation (116) into Equation (115) and dividing the result by r yields:

$$\begin{aligned}
 & \text{DXR (KR4J)} \frac{\partial^2 T}{\partial r^2} + \text{DXR} \left(\frac{\partial T}{\partial r} \right)^2 \frac{\partial (\text{KR4J})}{\partial T} + \frac{\text{KR4J}}{r} \frac{\partial T}{\partial r} \\
 & - 2(\text{KX4J}) \frac{T(4,J) - T(3,J)}{\text{DXR}} + 2 \frac{T_m - T(4,J)}{\text{RE}_r} \\
 & = \rho \text{DXR} C_4 \left[\frac{T'(4,J) - T(4,J)}{\Delta t} \right] \tag{117}
 \end{aligned}$$

The first three terms can now be placed in finite difference form.

This transforms Equation (117) into:

$$\begin{aligned}
 & \text{DXR (KR4J)} \frac{T(4,J+1) - 2 T(4,J) + T(4,J-1)}{\text{DR}^2} \\
 & + \text{DXR} \left[\frac{T(4,J+1) - T(4,J-1)}{2 \text{DR}^2} \right]^2 \frac{\partial (\text{KR4J})}{\partial T} \\
 & + \frac{\text{DXR (KR4J)}}{r} \left[\frac{T(4,J+1) - T(4,J-1)}{2 \text{DR}^2} \right] - 2(\text{KX4J}) \frac{T(4,J) - T(3,J)}{\text{DXR}} \\
 & + 2 \frac{T_m - T(4,J)}{\text{RE}_r} = \rho (\text{DXR}) C_4 \frac{T'(4,J) - T(4,J)}{\Delta t} \tag{118}
 \end{aligned}$$

Contrails

Similarly to the above development, Equation (112) can be applied to the crosshatched section of Figure 64 between nodes (5,J) and (6,J) to give:

$$\begin{aligned}
 & DXS (KR5J) \frac{T(5,J+1) - 2 T(5,J) + T(5,J-1)}{DR^2} \\
 & + DXS \left[\frac{T(5,J+1) - T(5,J-1)}{2 DR^2} \right]^2 \frac{\partial (KR5J)}{\partial T} \\
 & + \frac{DXS (KR5J)}{r} \left[\frac{T(5,J+1) - T(5,J-1)}{2 DR^2} \right] + 2 (KX5J) \frac{T(6,J) - T(5,J)}{DXS} \\
 & + 2 \frac{T_m - T(5,J)}{RE_s} = \rho DXS C_5 \left[\frac{T'(5,J) - T(5,J)}{\Delta t} \right] \quad (119)
 \end{aligned}$$

where KR5J is the thermal conductivity in the r-direction, KX5J is the thermal conductivity in the x direction, and C5 is the heat capacity of the (5,J) element. Apply Equation (112) to the entire crosshatched area of Figure 64. The heat transfer rate terms will be similar to those in Equations (118) and (119) but contact resistance terms will not appear and a work rate term will appear. For compactness, designate all terms on the left-hand side of the equal sign of Equation (118) except the contact resistance term by S4J. Similarly, designate all terms on the left-hand side of the equal sign of Equation (119) except the contact resistance term by S5J. Equation (112) now becomes:

Contrails

$$S4J + S5J - \frac{\dot{W}_e}{\Delta r 2\pi r} = \rho \text{ (DXR) } C4 \left[\frac{T'(4,J) - T(4,J)}{\Delta t} \right] + \rho \text{ (DXS) } C5 \left[\frac{T'(5,J) - T(5,J)}{\Delta t} \right] \quad (120)$$

where \dot{W}_e is the rate at which work crosses the element boundary and is given by Equation (59). Subtracting Equation (118) from Equation (119) and solving for $T'(5,J)$ eliminates T'_m and yields:

$$T'(5,J) = T(5,J) + \frac{\Delta t}{\rho \text{ (DXS) } C5} \left\{ \frac{\rho \text{ DXR } C4}{\Delta t} [T'(4,J) - T(4,J)] + S5J - S4J + \frac{2}{RE} [T(4,J) - T(5,J)] \right\} \quad (121)$$

where it has been noted that $RE_s = RE_r$. Equations (120) and (121) are now two equations with two unknowns, namely $T'(4,J)$ and $T'(5,J)$. If Equation (12) is solved for $T'(4,J)$ and this is substituted into Equation (121), $T'(5,J)$ becomes:

$$T'(5,J) = T(5,J) + \frac{\Delta t}{2\rho \text{ (DXS) } C5} \left\{ 2 S5J - \frac{\dot{W}_e}{\pi r (DR2)} + \frac{2}{RE} [T(4,J) - T(5,J)] \right\} \quad (122)$$

Either Equation (120) or (121) can be used to obtain the $T'(4,J)$ value since $T'(5,J)$ is now known.

In the case that contact resistance is zero, the previous development is inadequate since the contact resistance value appears in the denominator. For this case the rotor/stator interface shown in

Figure 64 can be used as long as it is noted that adjacent surface nodes are required to have the same temperature and that T_m is no longer required. With this in mind, application of Equation (112) yields:

$$\begin{aligned}
 & -K_x 2\pi r DR^2 \frac{T(4,J) - T(3,J)}{DXR} + K_x 2\pi r DR^2 \frac{T(6,J) - T(5,J)}{DXS} \\
 & + \left(K_r 2\pi r \frac{DXR + DXS}{2} \frac{\partial T}{\partial r} \right)_{r+\Delta r} - \left(K_r 2\pi r \frac{DXR + DXS}{2} \frac{\partial T}{\partial r} \right)_r - \dot{W}_e \\
 & = 2\pi r \rho \frac{DXR + DXS}{2} DR^2 C \frac{T'(4,J) - T(4,J)}{\Delta t} \tag{123}
 \end{aligned}$$

Similarly to the previous development, divide Equation (123) by $2\pi r DR^2$ and pass to the limit as DR^2 approaches zero. Solving the result for $T'(4,J)$ gives:

$$\begin{aligned}
 T'(4,J) = T(4,J) + \frac{2\Delta t}{\rho (DXR + DXS)C} & \left\{ -K_x \frac{T(4,J) - T(3,J)}{DXR} \right. \\
 & + K_x \frac{T(6,J) - T(5,J)}{DXS} + \left(\frac{DXR + DXS}{2} \right) \\
 & \left(K_r \frac{T(4,J+1) - 2T(4,J) + T(4,J-1)}{DR^2} \right. \\
 & + \frac{\partial K_r}{\partial T} \left[\frac{T(4,J+1) - T(4,J-1)}{2 DR^2} \right]^2 \\
 & \left. \left. + \frac{K_r}{r} \frac{T(4,J+1) - T(4,J-1)}{2 DR^2} \right) + \frac{\dot{W}_e}{2\pi r DR^2} \right\} \tag{124}
 \end{aligned}$$

Equations (120), (122) and (124) were used to find the interface boundary temperatures.

The remaining boundary condition equations were developed similarly with areas and masses changed as applicable. To account for the fact that some brake rotors and stators have wear pads riveted to the actual heat sink material, a set of wear surfaces boundary conditions was derived that included a mass for the wear pads and a contact resistance between the wear pads and the heat sink material. These equations are shown in Appendix O. In some of these remaining equations, a radiative/convective heat transfer coefficient arises. The values used and the calculation procedure are contained in Appendix J. The thermal conductivity values and heat capacity values are shown in Appendix K.

All of the equations developed here were incorporated into a computer program employing variable heat capacity, variable thermal conductivity, variable radiative/convective heat transfer coefficient and variable work input. Although employing the equations derived above for the work input portion of the brake stop, the program employs a cooling scheme beginning at 1.25 times the stop time that lumps the entire rotor and stator into one mass at constant temperature and allows that mass to cool. The resulting computer program is given in Appendix P.

Three Dimensional (Rotor/Stator Pair)

Interior Node Equation Development

The following analysis again contains the assumption that each stator is the same temperature as every other and that each rotor is

Contrails

the same temperature as every other. This allows analysis of only one stator and rotor. In the circumferential direction symmetry is also utilized such that only a sector of a rotor and stator must be analyzed. A typical rotor and stator are shown in Figure 65. The area of each required for analysis is also shown. An isometric drawing of the sectors selected for analysis is shown in Figure 66. The nodes used for analysis are also shown. The equation derivation for the interior nodes parallels the two-dimensional development given earlier. The basic difference is the inclusion of the terms in the circumferential or theta direction. Considering the theta direction in addition to the other two:

$$\begin{aligned} \dot{q}_{in} = & \left(-K_x r \Delta\theta \Delta r \frac{\partial T}{\partial x} \right)_x + \left(-K_r \Delta x r \Delta\theta \frac{\partial T}{\partial r} \right)_r \\ & + \left(-K_\theta \Delta x \Delta r \frac{1}{r} \frac{\partial T}{\partial \theta} \right)_\theta \end{aligned} \quad (125)$$

$$\begin{aligned} \dot{q}_{out} = & \left(-K_x r \Delta\theta \Delta r \frac{\partial T}{\partial x} \right)_{x+\Delta x} + \left(-K_r \Delta x r \Delta\theta \frac{\partial T}{\partial r} \right)_{r+\Delta r} \\ & + \left(-K_\theta \Delta x \Delta r \frac{1}{r} \frac{\partial T}{\partial \theta} \right)_{\theta+\Delta\theta} \end{aligned} \quad (126)$$

The volume of the interior element is:

$$V = r \Delta\theta \Delta r \Delta x \quad (127)$$

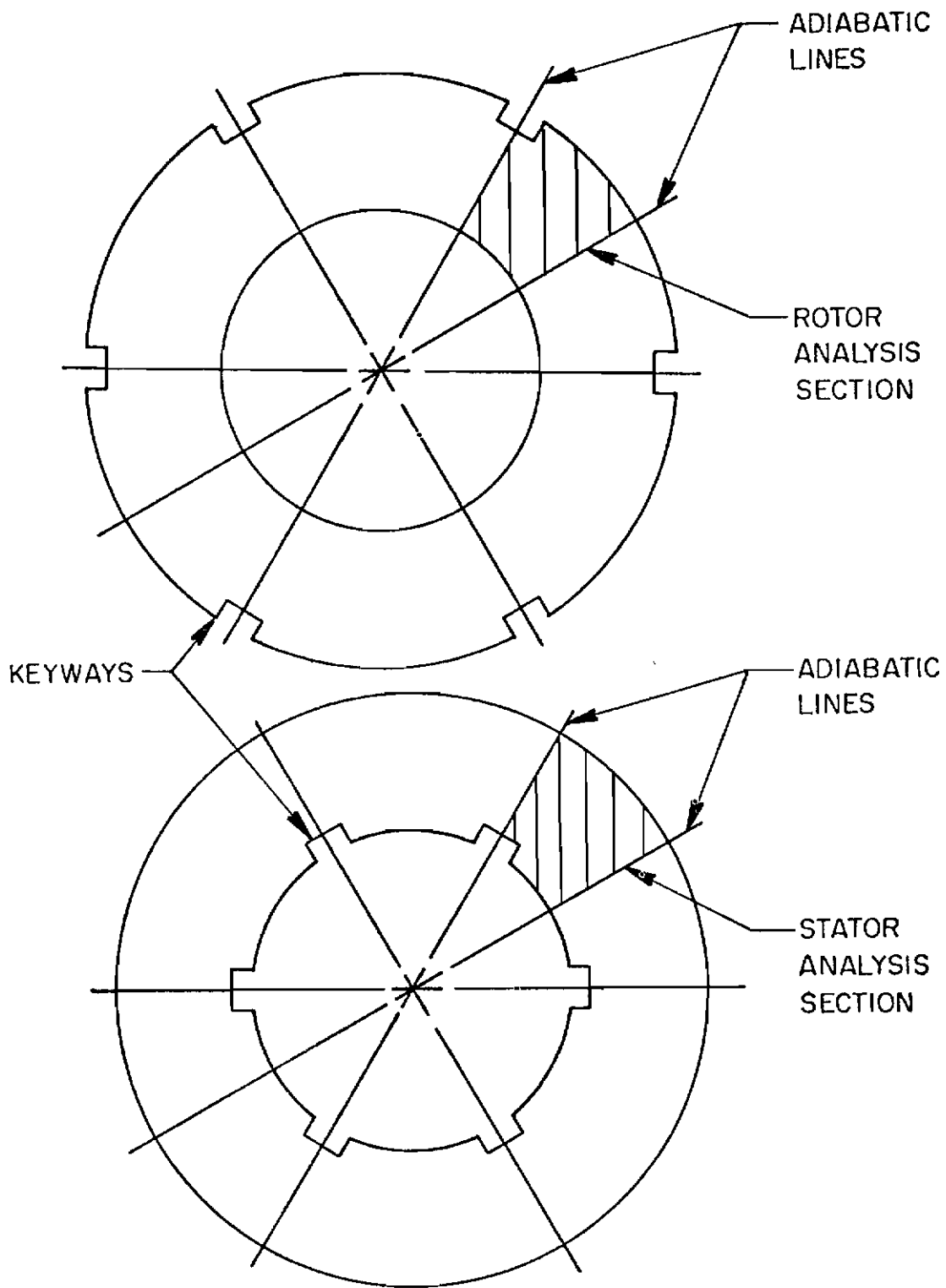


Figure 65. Typical Rotor and Stator

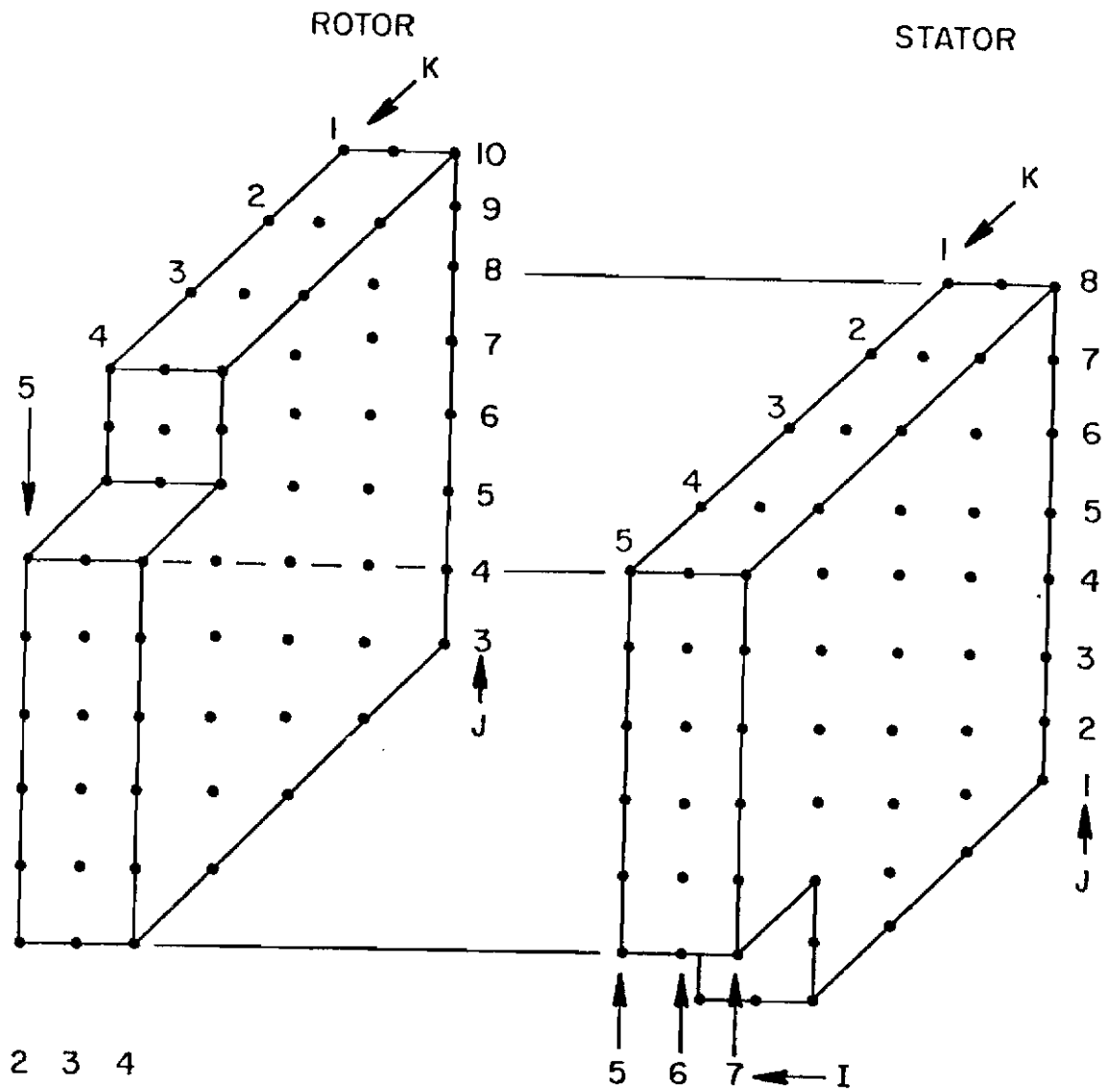


Figure 66. Isometric View of Rotor and Stator Sectors

Contrails

Substituting Equations (125)-(127) into Equation (103), dividing by the volume, and taking the limit as Δx , Δr , and $\Delta \theta$ approach zero yields:

$$\begin{aligned} & \frac{\partial}{\partial x} \left(K_x \frac{\partial T}{\partial x} \right) + \frac{1}{r} \frac{\partial}{\partial r} \left(K_r r \frac{\partial T}{\partial r} \right) + \frac{1}{r^2} \frac{\partial}{\partial \theta} \left(K_\theta \frac{\partial T}{\partial \theta} \right) \\ & = \rho c \frac{\partial T}{\partial t} \end{aligned} \tag{128}$$

The same techniques described earlier can be used to place Equation (128) into finite difference form and solve it for the temperature at the new time increment. This results in:

$$\begin{aligned} T'(I,J,K) = T(I,J,K) + \frac{\Delta t}{\rho c} & \left\{ K_x \frac{T(I+1,J,K) - 2 T(I,J,K) + T(I-1,J,K)}{(\Delta x)^2} \right. \\ & + \frac{\partial K_x}{\partial T} \left[\frac{T(I+1,J,K) - T(I-1,J,K)}{2 \Delta x} \right]^2 \\ & + K_r \frac{T(I,J+1,K) - 2 T(I,J,K) + [T(I,J-1,K)]}{(\Delta r)^2} \\ & + \frac{\partial K_r}{\partial T} \left[\frac{T(I,J+1,K) - T(I,J-1,K)}{2 \Delta r} \right]^2 \\ & + \frac{K_r}{r} \frac{T(I,J+1,K) - T(I,J-1,K)}{2 \Delta r} \\ & + \frac{K_\theta}{r^2} \frac{T(I,J,K+1) - 2 T(I,J,K) + T(I,J,K-1)}{(\Delta \theta)^2} \\ & \left. + \frac{1}{r^2} \frac{\partial K_\theta}{\partial T} \left[\frac{T(I,J,K+1) - T(I,J,K-1)}{2 \Delta \theta} \right]^2 \right\} \end{aligned} \tag{129}$$

Equation (129) was used to predict the interior node temperatures.

Boundary Condition Equation Development

The boundary condition at the axial centerline of the stator and rotor was taken to be adiabatic. This boundary condition accounts for 32 of the total of 196 boundary points shown in Figure 66. The remaining boundary points were divided into two basic groups, those containing a work input term and those not containing a work input term.

The boundary condition group without a work input term comprises 104 equations. A typical one of this group will be derived here. Consider the element at $I = 2$, $J = 8$, and $K = 5$. The heat transfer rate in is:

$$\dot{q}_{in} = \left(-K_{\theta} \frac{\Delta x}{2} \frac{\Delta r}{2} \frac{1}{r} \frac{\partial T}{\partial \theta} \right)_{\theta} - \left(K_r \frac{r \Delta \theta}{2} \frac{\Delta x}{2} \frac{\partial T}{\partial r} \right)_r \quad (130)$$

The heat transfer rate out is:

$$\dot{q}_{out} = \left(-K_x \frac{\Delta r}{2} \frac{r \Delta \theta}{2} \frac{\partial T}{\partial x} \right)_x + h \frac{\Delta x}{2} \frac{r \Delta \theta}{2} \left[T(2,8,5) - T_{\infty} \right] \quad (131)$$

The volume of the element is:

$$v = \frac{\Delta x}{2} \frac{\Delta r}{2} \frac{r \Delta \theta}{2} \quad (132)$$

Substituting Equations (130) - (132) into Equation (103) and dividing by the volume yields:

Contrails

$$\begin{aligned}
 & - \frac{2K_{\theta}}{r^2 \Delta \theta} \frac{\partial T}{\partial \theta} - \frac{2K_r}{r} \frac{\partial T}{\partial r} + \frac{2K_x}{\Delta x} \frac{\partial T}{\partial x} - \frac{2h}{\Delta r} \left[T(2,8,5) - T_{\infty} \right] \\
 & = \rho C \frac{\partial T}{\partial t}
 \end{aligned} \tag{133}$$

Expressing Equation (133) in finite difference form gives:

$$\begin{aligned}
 & - \frac{2K_{\theta}}{r^2 \Delta \theta} \frac{T(2,8,5) - T(2,8,4)}{\Delta \theta} - \frac{2K_r}{r} \frac{T(2,8,5) - T(2,7,5)}{\Delta r} \\
 & + \frac{2K_x}{\Delta x} \frac{T(3,8,5) - T(2,8,5)}{\Delta x} - \frac{2h}{\Delta r} \left[T(2,8,5) - T_{\infty} \right] \\
 & = \rho C \frac{T'(2,8,5) - T(2,8,5)}{\Delta t}
 \end{aligned} \tag{134}$$

Solving for $T'(2,8,5)$ results in:

$$\begin{aligned}
 T'(2,8,5) = T(2,8,5) + \frac{2\Delta t}{\rho C} \left\{ & - \frac{K_{\theta}}{r^2 \Delta \theta} \frac{T(2,8,5) - T(2,8,4)}{\Delta \theta} \right. \\
 & - \frac{K_r}{\Delta r} \frac{T(2,8,5) - T(2,7,5)}{\Delta r} + \frac{K_x}{\Delta x} \frac{T(3,8,5) - T(2,8,5)}{\Delta x} \\
 & \left. - \frac{h}{\Delta r} \left[T(2,8,5) - T_{\infty} \right] \right\}
 \end{aligned} \tag{135}$$

Equation (135) was used to predict the temperature at $I = 2$, $J = 8$, and $K = 5$.

The boundary condition group containing a work input term comprises 30 nodes on each disc. An additional complication arises in the development of the applicable equations due to the rotation of the

Contrails

rotor relative to the stator. Considering one node on the stator, at each increment of time, a different node from the rotor will be adjacent to this stator node. It is necessary to select the time increment such that at each point in time at which the equations are used, the nodes on the rotor exactly line up with the nodes on the stator. It is not desirable to apply a boundary condition equation when the rotor nodes are physically between the stator nodes. This lining-up problem can be solved by using a variable time step such that the rotation increment is a constant. The variable time step is necessitated by the fact that the rotor rotation speed is variable during a brake stop. The following equation shows the expression employed to calculate the variable time step value:

$$\Delta t = \frac{R_R \Delta \theta}{V_O \left(1 - \frac{t}{t_s}\right)} \quad (136)$$

Since the node numbers designated in Figure 66 are fixed to each disc, even during rotation, it is necessary to develop a technique for describing which rotor wear-surface node lines up with each stator wear-surface node. The circumferential direction is the only direction requiring this analysis since lines upon which K is constant are radial lines and since relative motion is only in the circumferential direction. A pictorial view of the rotor sector rotating past a stator sector at each time step is shown in Figure 67. At each time that the set of rotor nodes is directly adjacent to the stator nodes, an equation is desired that will predict the temperature of the nodes. In

order to avoid writing equations for eight rotor positions as well as for all wear-surface nodes, an equation can be written for each wear-surface node of the stator and a separate equation can be written for each wear-surface node of the rotor. Then, when a wear-surface node of the rotor lines up with a wear-surface node of the stator, the equations can be added and then solved for the new temperature. Note that the new temperature of the rotor wear-surface node will be identical to the new temperature of the stator wear-surface node since contact resistance is not used in this model. A typical equation for a rotor wear-surface node will now be derived. Consider the element at $I = 4$, $J = 5$, $K = 2$. (See Figure 66.) The heat transfer rate into this element is:

$$\begin{aligned} \dot{q}_{in} = & -K_x r \Delta \theta \Delta r \frac{T(4,5,2) - T(3,5,2)}{\Delta x} \\ & - \left(K_r \frac{\Delta x}{2} r \Delta \theta \frac{\partial T}{\partial r} \right)_r - \left(K_\theta \frac{\Delta x}{2} \Delta r \frac{1}{r} \frac{\partial T}{\partial \theta} \right)_\theta \end{aligned} \quad (137)$$

The heat transfer rate out of this element is:

$$\dot{q}_{out} = - \left(K_r \frac{\Delta x}{2} r \Delta \theta \frac{\partial T}{\partial r} \right)_{r+\Delta r} - \left(K_\theta \frac{\Delta x}{2} \Delta r \frac{1}{r} \frac{\partial T}{\partial \theta} \right)_{\theta+\Delta \theta} \quad (138)$$

Applying the first law of thermodynamics, as given in Equation (46), to the element being considered leads to:

Contrails

$$\begin{aligned}
 & - K_x r \Delta \theta \Delta r \frac{T(4,5,2) - T(3,5,2)}{\Delta x} - \left(K_r \frac{\Delta x}{2} r \Delta \theta \frac{\partial T}{\partial r} \right)_r \\
 & - \left(K_\theta \frac{\Delta x}{2} \Delta r \frac{1}{r} \frac{\partial T}{\partial \theta} \right)_\theta + \left(K_r \frac{\Delta x}{2} r \Delta \theta \frac{\partial T}{\partial r} \right)_{r+\Delta r} \\
 & + \left(K_\theta \frac{\Delta x}{2} \Delta r \frac{1}{r} \frac{\partial T}{\partial \theta} \right)_{\theta+\Delta \theta} - W_{i_4} = \rho \frac{\Delta x}{2} r \Delta \theta \Delta r C \frac{\partial T}{\partial t} \quad (139)
 \end{aligned}$$

where W_{i_4} is the rate at which work is input to this element. This work rate term is unknown but it will shortly be shown that it is not needed in this form.

If Equation (139) is now divided by $\frac{\Delta x}{2} r \Delta \theta \Delta r$ and the limit of each term is taken as $\Delta \theta$ and Δr approach zero, the following results:

$$\begin{aligned}
 & - \frac{2 K_x}{\Delta x} \frac{T(4,5,2) - T(3,5,2)}{\Delta x} + \frac{1}{r} \frac{\partial}{\partial r} \left(K_r r \frac{\partial T}{\partial r} \right) + \frac{1}{r^2} \frac{\partial}{\partial \theta} \left(K_\theta \frac{\partial T}{\partial \theta} \right) \\
 & - \dot{W}'_{i_4} = \rho C \frac{T'(4,5,2) - T(4,5,2)}{\Delta t} \quad (140)
 \end{aligned}$$

where \dot{W}'_{i_4} is still an unknown and the right-hand side of the equation has been expanded as described previously.

Consider the element at $I = 5$, $J = 5$, and $K = 4$. (See Figure 66.) The node of this element is a stator wear-surface node at $J = 5$ and will at various times during the brake stop, be adjacent to the rotor wear-surface node at $I = 4$, $J = 5$, and $K = 2$ (previously analyzed). For this stator node the heat transfer rate into the element is:

Contrails

$$\dot{q}_{in} = -\left(K_r \frac{\Delta x}{2} r \Delta \theta \frac{\partial T}{\partial r}\right)_r - \left(K_\theta \frac{\Delta x}{2} \Delta r \frac{1}{r} \frac{\partial T}{\partial \theta}\right)_\theta \quad (141)$$

The heat transfer rate out of this element is:

$$\begin{aligned} \dot{q}_{out} = & -K_x r \Delta \theta \Delta r \frac{T(6,5,4) - T(5,5,4)}{\Delta x} \\ & - \left(K_r \frac{\Delta x}{2} r \Delta \theta \frac{\partial T}{\partial r}\right)_{r+\Delta r} - \left(K_\theta \frac{\Delta x}{2} \Delta r \frac{1}{r} \frac{\partial T}{\partial \theta}\right)_{\theta+\Delta \theta} \end{aligned} \quad (142)$$

As before, if Equations (141) and (142) are substituted into Equation (46) the following results:

$$\begin{aligned} & K_x r \Delta \theta \Delta r \frac{T(6,5,4) - T(5,5,4)}{\Delta x} + \left(K_r \frac{\Delta x}{2} r \Delta \theta \frac{\partial T}{\partial r}\right)_{r+\Delta r} \\ & + \left(K_\theta \frac{\Delta x}{2} \Delta r \frac{1}{r} \frac{\partial T}{\partial \theta}\right)_{\theta+\Delta \theta} - \left(K_r \frac{\Delta x}{2} r \Delta \theta \frac{\partial T}{\partial r}\right)_r \\ & - \left(K_\theta \frac{\Delta x}{2} \Delta r \frac{1}{r} \frac{\partial T}{\partial \theta}\right)_\theta - \dot{W}_5 = \rho \frac{\Delta x}{2} r \Delta \theta \Delta r C \frac{\partial T}{\partial t} \end{aligned} \quad (143)$$

where \dot{W}_5 is the rate at which work is input into this element. At this point \dot{W}_5 is unknown and will be discussed later. Dividing Equation (143) by $\frac{\Delta x}{2} r \Delta \theta \Delta r$ and taking the limit of each term as $\Delta \theta$ and Δr approach zero yields:

Contrails

$$\begin{aligned} & \frac{2}{\Delta x} \frac{K_x}{\Delta x} \frac{T(6,5,4) - T(5,5,4)}{\Delta x} + \frac{1}{r} \frac{\partial}{\partial r} \left(K_r r \frac{\partial T}{\partial r} \right) \\ & + \frac{1}{r^2} \frac{\partial}{\partial \theta} \left(K_\theta \frac{\partial T}{\partial \theta} \right) - \dot{W}'_5 = \rho C \frac{T'(5,5,4) - T(5,5,4)}{\Delta t} \end{aligned} \quad (144)$$

where \dot{W}'_5 is an unknown and the right hand side of the equation has been expanded.

Considering Figure 67, it can be seen that at time increment number 2 the rotor $K = 2$ nodes are adjacent to the stator $K = 4$ nodes. Thus the rotor wear-surface node at $I = 4, J = 5, K = 2$ is adjacent to the stator wear-surface node at $I = 5, J = 5, K = 4$. In order to determine the temperature of these two nodes at this time increment, Equations (140) and (144) are added. As a shorthand notation all terms on the left-hand side of Equation (140) except the work rate term will be designated LHSR while all terms on the left-hand side of Equation (144) except the work rate term will be designated LHSS. In addition, the following definitions are used:

$$\text{RHSR} = \frac{\rho}{\Delta t} C_{4,5,2} \quad (145)$$

$$\text{RHSS} = \frac{\rho}{\Delta t} C_{5,5,4} \quad (146)$$

where the heat capacity is to be evaluated at the temperature at the node indicated by the subscripts. Using the above shorthand notations the sum of Equations (140) and (144) becomes:

$$\begin{aligned} \text{LHSR} + \text{LHSS} - \left(\dot{W}'_4 + \dot{W}'_5 \right) &= \text{RHSR} [T'(4,5,2) - T(4,5,2)] \\ &+ \text{RHSS} [T'(5,5,4) - T(5,5,4)] \end{aligned} \quad (147)$$

Note that the sum of the two fractional work rate terms is the total work rate input at the rubbing interface and has been previously derived as Equation (59). It is not necessary to know which portion of this term is associated with the rotor or stator. Note also that the temperature of the rotor and stator must be identical at each contact point, or:

$$T'(4,5,2) = T'(5,5,4) \quad (148)$$

Equation (147) can now be solved for $T'(4,5,2)$ [or $T'(5,5,4)$] to give:

$$T'(4,5,2) = \frac{\left[\text{RHSR } T(4,5,2) + \text{RHSS } T(5,5,4) + \text{LHSR} + \text{LHSS} - \left(\dot{W}'_4 + \dot{W}'_5 \right) \right]}{(\text{RHSR} + \text{RHSS})} \quad (149)$$

Equation (149) was used to predict the temperature at time step number 2 for the stator node at $I = 5, J = 5, K = 4$, and for the rotor node at $I = 4, J = 5, K = 2$.

All remaining boundary condition equations were developed similarly with areas and masses changed as applicable. These equations are given in Appendix Q. As was the case previously, radiative/convective heat transfer coefficients used in this development are given in Appendix J while the thermal conductivity and heat capacity values are given in Appendix K.

All equations developed for this three-dimensional model were incorporated into a computer program employing variable heat capacity,

variable thermal conductivity, variable radiative/convective heat transfer coefficient and variable work input. The program uses the equations derived above for the work input portion of the brake stop but uses a cooling scheme beginning at 1.25 times the stop time that lumps the entire mass of the rotor and stator into one mass at constant temperature and allows that mass to cool. The resulting computer program is given in Appendix R.

Three Dimensional Caliper

Interior Node Equation Development

The interior equation for the caliper brake is valid in the rotor, lining and housing. The model selected for the caliper brake is shown in Figure 68. The interior equation development is identical to that of the previous section. Thus Equation (129) is the applicable equation for predicting the interior node temperatures for the caliper brake.

Boundary Condition Equation Development

The boundary conditions are split into three groups; those at the lining and housing interface, those at the lining and rotor interface, and those open to the ambient air. Consider a node at the left lining and housing interface. If the node arrangement is selected as in Figure 69, it is noted that some nodes lie directly on the lining and housing interface. Considering the housing as Material 1 and the lining as Material 2, the heat transfer rate into an element at the lining and housing interface (small crosshatched element in Figure 69) is:

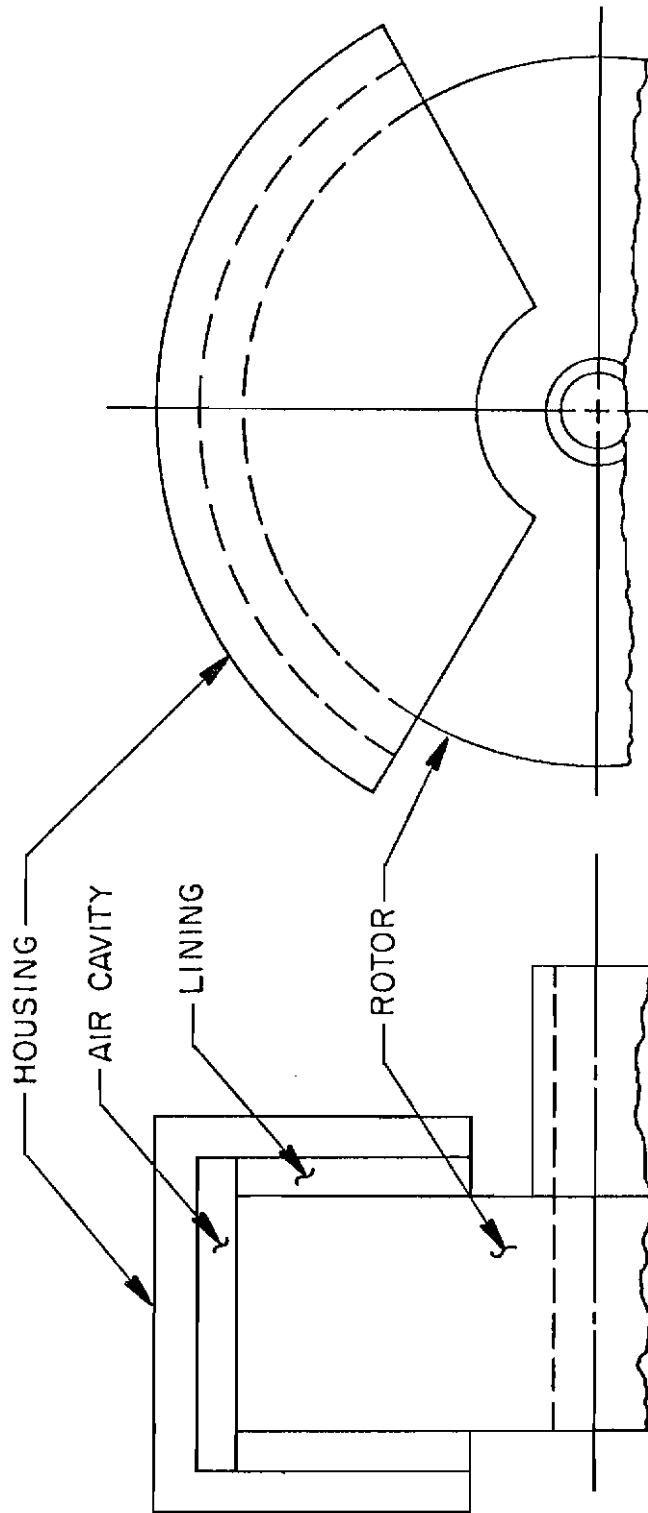


Figure 68. Caliper Brake Model

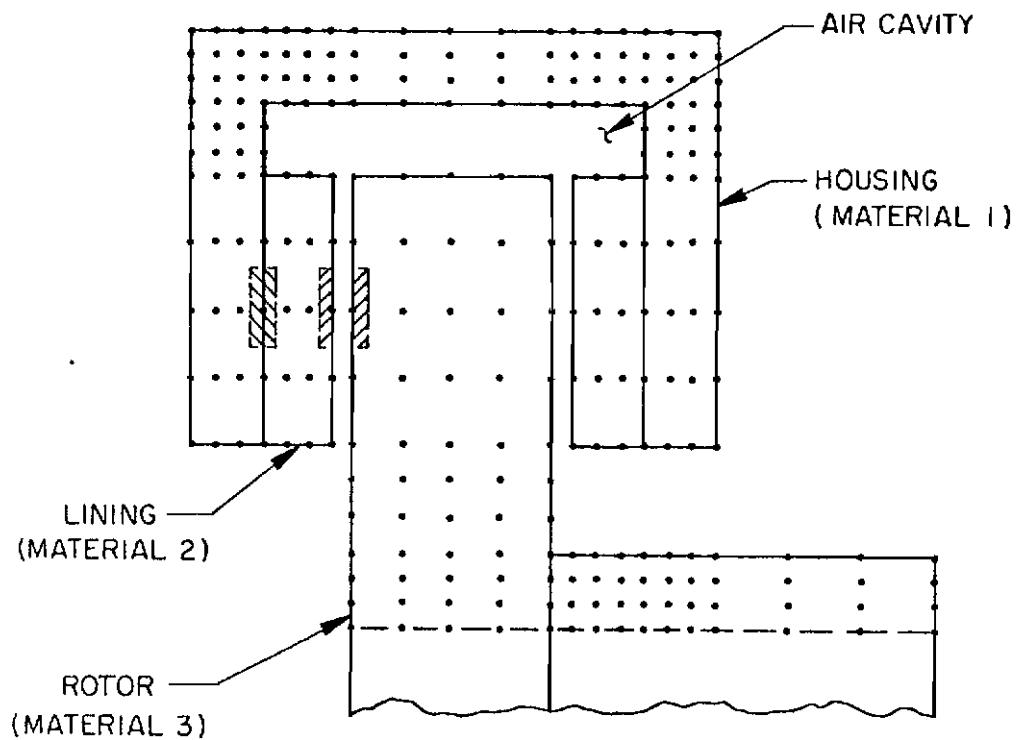


Figure 69. Caliper Brake Node Arrangement

Contrails

$$\begin{aligned}
 \dot{q}_{in} = & - \left(K_{\theta_1} \frac{\Delta x_1}{2} \Delta r \frac{1}{r} \frac{\partial T}{\partial \theta} \right)_{\theta} - \left(K_{\theta_2} \frac{\Delta x_2}{2} \Delta r \frac{1}{r} \frac{\partial T}{\partial \theta} \right)_{\theta} \\
 & - \left(K_{r_1} \frac{\Delta x_1}{2} r \Delta \theta \frac{\partial T}{\partial r} \right)_r - \left(K_{r_2} \frac{\Delta x_2}{2} r \Delta \theta \frac{\partial T}{\partial r} \right)_r \\
 & - \left(K_{x_1} \Delta r r \Delta \theta \frac{\partial T}{\partial x} \right)_x
 \end{aligned} \tag{150}$$

where the subscripts indicate the applicable material. Similarly, the heat transfer rate out of an element at the lining and housing interface is:

$$\begin{aligned}
 \dot{q}_{out} = & - \left(K_{\theta_1} \frac{\Delta x_1}{2} \Delta r \frac{1}{r} \frac{\partial T}{\partial \theta} \right)_{\theta+\Delta\theta} - \left(K_{\theta_2} \frac{\Delta x_2}{2} \Delta r \frac{1}{r} \frac{\partial T}{\partial \theta} \right)_{\theta+\Delta\theta} \\
 & - \left(K_{r_1} \frac{\Delta x_1}{2} r \Delta \theta \frac{\partial T}{\partial r} \right)_{r+\Delta r} - \left(K_{r_2} \frac{\Delta x_2}{2} r \Delta \theta \frac{\partial T}{\partial r} \right)_{r+\Delta r} \\
 & - \left(K_{x_2} \Delta r r \Delta \theta \frac{\partial T}{\partial x} \right)_{x+\Delta x}
 \end{aligned} \tag{151}$$

With \dot{q}_{in} and \dot{q}_{out} as shown in Equations (150) and (151), the first law of thermodynamics as given in Equation (103) yields:

$$\begin{aligned}
 \dot{q}_{in} - \dot{q}_{out} = & \rho_1 r \Delta \theta \Delta r \frac{\Delta x_1}{2} C_1 \frac{T' - T}{\Delta t} \\
 & + \rho_2 r \Delta \theta \Delta r \frac{\Delta x_2}{2} C_2 \frac{T' - T}{\Delta t}
 \end{aligned} \tag{152}$$

Contrails

Combining Equations (150) through (152), dividing by $\Delta\theta\Delta r$, and taking the limit of each term as $\Delta\theta$ and Δr approach zero gives:

$$\begin{aligned}
 & \frac{\Delta x_1}{2r} \frac{\partial}{\partial \theta} \left(K_{\theta_1} \frac{\partial T}{\partial \theta} \right) + \frac{\Delta x_2}{2r} \frac{\partial}{\partial \theta} \left(K_{\theta_2} \frac{\partial T}{\partial \theta} \right) + \frac{\Delta x_1}{2} \frac{\partial}{\partial r} \left(K_{r_1} r \frac{\partial T}{\partial r} \right) \\
 & + \frac{\Delta x_2}{2} \frac{\partial}{\partial r} \left(K_{r_2} r \frac{\partial T}{\partial r} \right) + \left(K_{x_2} r \frac{\partial T}{\partial x} \right)_2 - \left(K_{x_1} r \frac{\partial T}{\partial x} \right)_1 \\
 & = \left[\rho_1 \frac{\Delta x_1}{2} C_1 + \rho_2 \frac{\Delta x_2}{2} C_2 \right] r \frac{T' - T}{\Delta t} \tag{153}
 \end{aligned}$$

Placing Equation (153) in finite difference form, using techniques described earlier, and solving it for the new temperature results in:

$$\begin{aligned}
 T'(I,J,K) &= T(I,J,K) + \frac{2\Delta t}{r \left\{ \rho_1 \Delta x_1 C_1 + \rho_2 \Delta x_2 C_2 \right\}} \\
 & \left\{ \frac{\left(\Delta x_1 K_{\theta_1} + \Delta x_2 K_{\theta_2} \right)}{2r} \right. \\
 & \frac{T(I,J,K+1) - 2 T(I,J,K) + T(I,J,K-1)}{r^2(\Delta\theta)^2} \\
 & + \left[\frac{T(I,J,K+1) - T(I,J,K-1)}{2r\Delta\theta} \right]^2 \\
 & \left[\frac{\Delta x_1}{2r} \frac{\partial K_{\theta_1}}{\partial T} + \frac{\Delta x_2}{2r} \frac{\partial K_{\theta_2}}{\partial T} \right] \\
 & \left. \left(\frac{\Delta x_2}{2} r K_{r_2} + \frac{\Delta x_1}{2} r K_{r_1} \right) \right\}
 \end{aligned}$$

Contrails

$$\begin{aligned}
 & \frac{T(I, J+1, K) - 2 T(I, J, K) + T(I, J-1, K)}{(\Delta r)^2} \\
 & + \left(\frac{\Delta x_2}{2} r \frac{\partial K_{r_2}}{\partial T} + \frac{\Delta x_1}{2} r \frac{\partial K_{r_1}}{\partial T} \right) \\
 & \left[\frac{T(I, J+1, K) - T(I, J-1, K)}{2\Delta r} \right]^2 + \left(\frac{\Delta x_1}{2} K_{r_1} + \frac{\Delta x_2}{2} K_{r_2} \right) \\
 & \frac{T(I, J+1, K) - T(I, J-1, K)}{2\Delta r} \\
 & + K_{r_2} r \frac{T(I+1, J, K) - T(I, J, K)}{\Delta x_2} \\
 & - K_{r_1} r \frac{T(I, J, K) - T(I-1, J, K)}{\Delta x_1} \left. \right\} \quad (154)
 \end{aligned}$$

Equation (154) is the equation for predicting the temperature of a node between the left housing and the lining.

The crosshatched element at the interface of the lining and rotor (Figure 69) is shown in an expanded view in Figure 70 and will be used in the derivation of the equation predicting temperature for the two interface nodes. Two nodes are used in this case to allow a difference in temperature of the two surfaces. A contact resistance term will necessarily appear in the equations. The expression for the heat transfer rate into the lining element is:

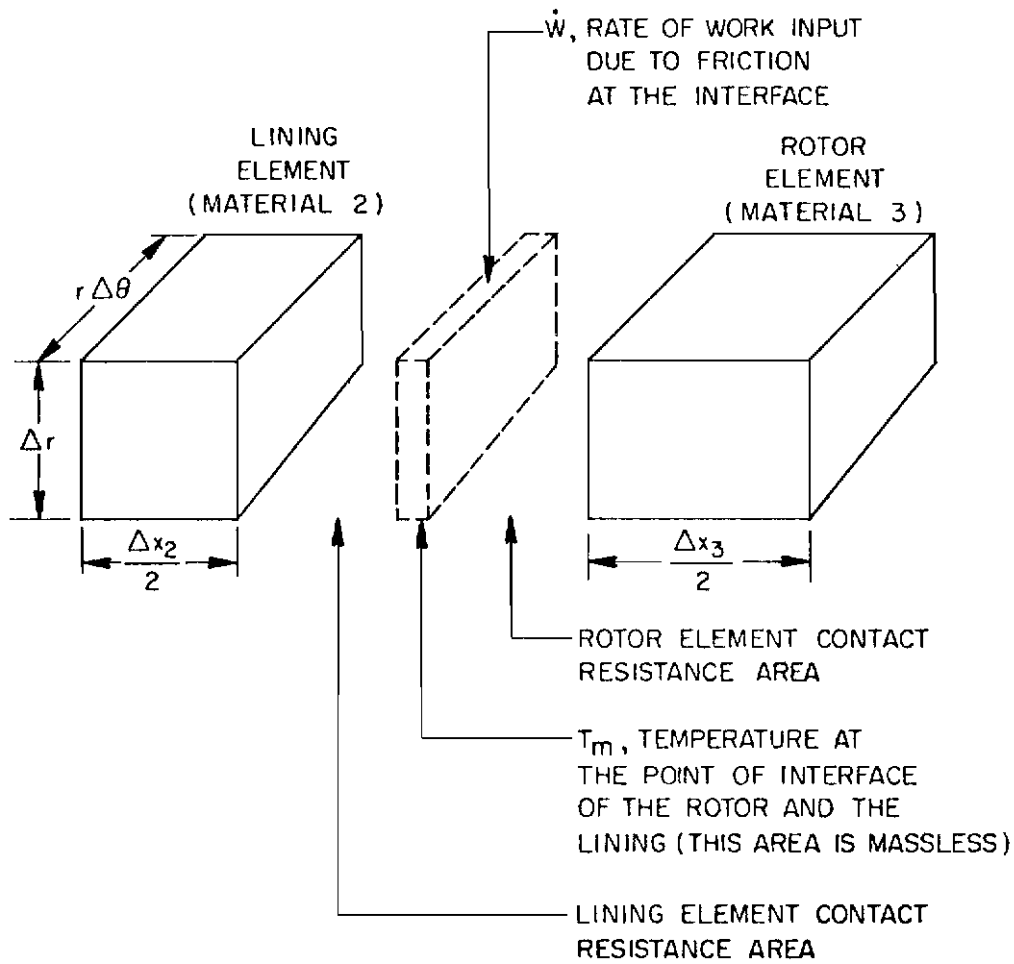


Figure 70. Expanded Lining/Rotor Interface

Contrails

$$\begin{aligned} \dot{q}_{in} = & - \left(K_{\theta 2} \frac{\Delta x_2}{2} \Delta r \frac{1}{r} \frac{\partial T_2}{\partial \theta} \right)_{\theta} - \left(K_{r 2} \frac{\Delta x_2}{2} r \Delta \theta \frac{\partial T_2}{\partial r} \right)_{r} \\ & - \left(K_{x 2} \Delta r r \Delta \theta \frac{\partial T_2}{\partial x} \right)_{x} + \frac{r \Delta \theta \Delta r}{RE} (T_m - T_2) \end{aligned} \quad (155)$$

where the subscript 2 refers to material 2. The heat transfer rate out of the lining element is:

$$\dot{q}_{out} = - \left(K_{\theta 2} \frac{\Delta x_2}{2} \Delta r \frac{1}{r} \frac{\partial T_2}{\partial \theta} \right)_{\theta + \Delta \theta} - \left(K_{r 2} \frac{\Delta x_2}{2} r \Delta \theta \frac{\partial T_2}{\partial r} \right)_{r + \Delta r} \quad (156)$$

The first law of thermodynamics (Equation 103) as applied to the lining element is:

$$\dot{q}_{in} - \dot{q}_{out} = \rho_2 \Delta r \frac{\Delta x_2}{2} r \Delta \theta C_2 \frac{T'_2 - T_2}{\Delta t} \quad (157)$$

Combining Equations (155) - (157), dividing by $\Delta \theta$ and Δr , and taking the limit as $\Delta \theta$ and Δr approach zero yields:

$$\begin{aligned} \frac{\Delta x_2}{2r} \frac{\partial}{\partial \theta} \left(K_{\theta 2} \frac{\partial T_2}{\partial \theta} \right) + \frac{\Delta x_2}{2} \frac{\partial}{\partial r} \left(K_{r 2} r \frac{\partial T_2}{\partial r} \right) \\ - \left(K_{x 2} r \frac{\partial T_2}{\partial x} \right)_{x} + \frac{r}{RE} (T_m - T_2) = r \rho_2 \frac{\Delta x_2}{2} C_2 \left(\frac{T'_2 - T_2}{\Delta t} \right) \end{aligned} \quad (158)$$

Contrails

Similarly the equation for the rotor element of Figure 70 is:

$$\begin{aligned} & \frac{\Delta x_3}{2r} \frac{\partial}{\partial \theta} \left(K_{\theta 3} \frac{\partial T_3}{\partial \theta} \right) + \frac{\Delta x_3}{2} \frac{\partial}{\partial r} \left(K_{r 3} r \frac{\partial T_3}{\partial r} \right) + \left(K_{x 3} r \frac{\partial T_3}{\partial x} \right)_{x+\Delta x} \\ & + \frac{r}{RE} \left(T_m - T_3 \right) = r \rho_3 \frac{\Delta x_3}{2} C_3 \frac{T'_3 - T_3}{\Delta t} \end{aligned} \quad (159)$$

For compactness designate all terms on the left-hand side of Equation (158) except the contact resistance term by SH1. Similarly designate all terms on the left-hand side of Equation (159) except the contact resistance term by SH2. Equation (46) or equivalently Equation (112) can now be applied to the combination of the lining and rotor elements (Figure 70) to give:

$$SH1 + SH2 - \frac{\dot{W}_e}{\Delta r \Delta \theta} = \rho_2 \frac{\Delta x_2}{2} r C_2 \frac{\partial T_2}{\partial t} + \rho_3 \frac{\Delta x_3}{2} r C_3 \frac{\partial T_3}{\partial t} \quad (160)$$

where the fact that Δr and $\Delta \theta$ have approached zero is no problem since \dot{W}_e is derived similarly and is:

$$\dot{W}_e = - \frac{\Delta \theta \Delta r T_t r V_o \left(1 - \frac{t}{t_s} \right)}{N \pi \left(r_{\ell o}^2 - r_{\ell i}^2 \right) R_R} \quad (161)$$

Contrails

Denoting the work term of Equation (160) by \dot{W}' and expanding the right-hand side leads to:

$$\begin{aligned} SH1 + SH2 - \dot{W}' = & \rho_2 \frac{\Delta x_2}{2} r C_2 \frac{T'_2 - T_2}{\Delta t} \\ & + \rho_3 \frac{\Delta x_3}{2} r C_3 \frac{T'_3 - T_3}{\Delta t} \end{aligned} \quad (162)$$

Subtract Equation (159) from Equation (158) to get:

$$\begin{aligned} SH1 - SH2 + \frac{r}{RE} (T_3 - T_2) = & \rho_2 \frac{\Delta x_2}{2} r C_2 \frac{T'_2 - T_2}{\Delta t} \\ & - \rho_3 \frac{\Delta x_3}{2} r C_3 \frac{T'_3 - T_3}{\Delta t} \end{aligned} \quad (163)$$

Equations (162) and (163) are now two equations with two unknowns, T'_3 and T'_2 . Substituting Equation (163) into Equation (162) and solving for T'_2 gives:

$$T'_2 = T_2 + \frac{\Delta t}{\rho_2 \Delta x_2 r C_2} \left\{ 2SH1 - \dot{W}' + \frac{r}{RE} (T_3 - T_2) \right\} \quad (164)$$

T'_3 can be calculated using either Equation (162) or Equation (163). Equations (162) through (164) are the equations for predicting the temperature at the interface of the left lining and the rotor. The equations for the right side of the brake are similar except for subscripts and the sign of the x-direction heat transfer rate term. Equations (162) through (164) must be applied to the brake with care since there exists relative motion between the rotor and lining. As in the previous development, a variable time step is desired so that the rotation increment during one time step will allow nodes on the rotor

to exactly line up with nodes on the lining. This variable time step is calculated by:

$$\Delta t = \frac{R_r \Delta \theta}{V_o \left(1 - \frac{t}{t_s}\right)} \quad (165)$$

In addition to the variable time step, Equations (162) through (164) must also contain a provision for determining the correct circumferential position when using the old (not primed) temperature values. This can be accomplished by subscripting the old temperature values such that the subscripts correspond to the angle traversed. The relation between the angle traversed and the time increment is Equation (165).

It should be noted that the somewhat involved procedure for equation addition within a computer program as developed in the previous section is not needed for this development since all elements are identical in the rubbing interface area. All boundaries not discussed above were taken to be adiabatic since previous results showed little cooling during the work input portion of the brake stop. Cooling of the brake after rotation is stopped can again be handled assuming a lumped mass cooling at constant temperature.

No computer program was developed for the caliper brake for a number of reasons. First, no tests were conducted within this effort to allow direct comparison of theory to experiment. Second, the experimental data from other authors is fairly limited. In addition, brake geometries and material properties of other authors are almost nonexistent. Last, but certainly not least, is the fact that the same techniques involved in the caliper brake equation development were used

in the multidisc brake equation development. This implies that the conclusions applying to the multidisc brake theory also apply to the caliper brake theory.

Two Dimensional (Entire Brake/Wheel/Tire)

This analysis is such that an axial temperature gradient can exist from stator to stator or rotor to rotor. The model selected for this two-dimensional multidisc analysis is shown in Figure 71. The numbered areas apply to the nodes assigned to that area. The torque tube is divided into six areas with node numbers 1, 9, 21, 22, 23, and 24. The rim is divided into seven areas with node numbers 3, 7, 8, 11, 12, 13, and 14. The tire is shown as two nodes, 4 and 6. The remaining two nodes are Number 5, the contained air and Number 2, the housing and hydraulic fluid node. The heat sink, all rotors and stators, is divided into eight areas bounded by the radial center lines of an adjacent rotor and stator. One of these eight areas is shown cross-hatched in Figure 71. Each of the eight heat sink areas is analyzed independently using primarily the equations derived in the two-dimensional radial/axial section of this report. The nodes utilized for each of the eight areas are necessarily the same as those used in the two-dimensional radial/axial section. The nodal pattern employed is shown in Figure 63. For brakes containing wear pads at the rotor/stator interface, the nodal pattern is shown in Appendix O as Figure O-2. Since each rotor and stator is in contact with either the rim or the torque tube, a heat transfer term was added to allow heat flow from the heat sink to the rim and torque tube.

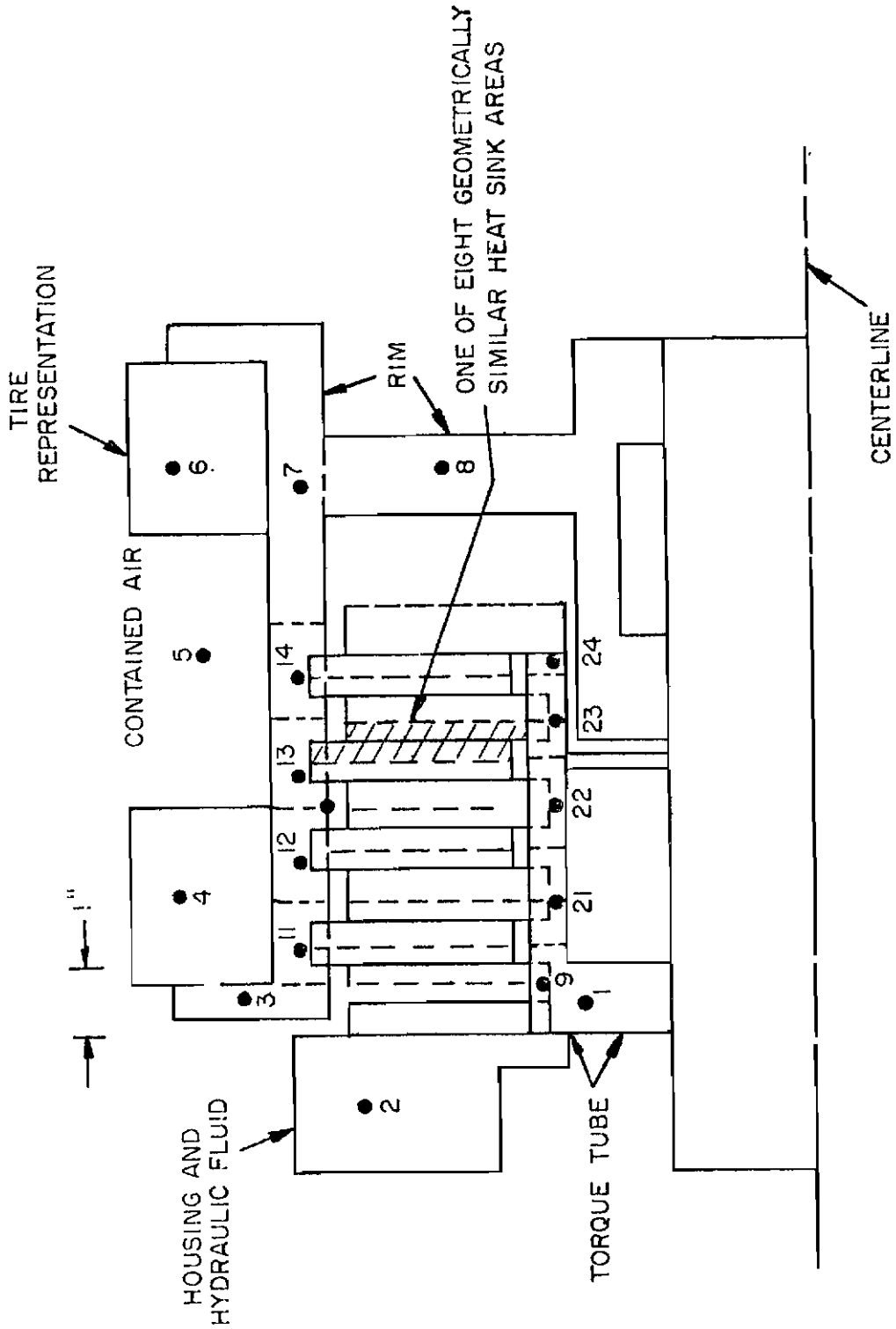


Figure 71. Multi-Disc Brake Model

Each numbered node shown in Figure 71 was treated as a constant temperature lump of mass with thermal properties based on the material being depicted. As an example of the method of equation development for each numbered node, consider Node 12. This node has been expanded and the heat transfer rates for the node have been identified in Figure 72. The convection-radiation heat transfer rate from Node 12 was obtained by:

$$QHR = h \times A12 (T12 - T_{\infty}) \quad (166)$$

where h is the convective-radiative heat transfer coefficient obtained as shown in Appendix J, $A12$ is the area of Node 12 open to the ambient air, $T12$ is the temperature of Node 12 and T_{∞} is the ambient air temperature. The conduction heat transfer rate from Node 12 to Node 4 is found by considering the internal resistances of the blocks of mass associated with Nodes 12 and 4. The resistance associated with Node 12 for this application is:

$$RE12 = \frac{LR10}{VKR(AR10)} \quad (167)$$

where $RE12$ is the resistance, $LR10$ is the length from the center of Node 12 to the contact point between the two masses, VKR is the thermal conductivity of the Node 12 (rim) material, and $AR10$ is the area of contact between the two masses. The resistance associated with Node 4 for this application is:

$$RE4 = \frac{LTT4}{VKT(AR10)} \quad (168)$$

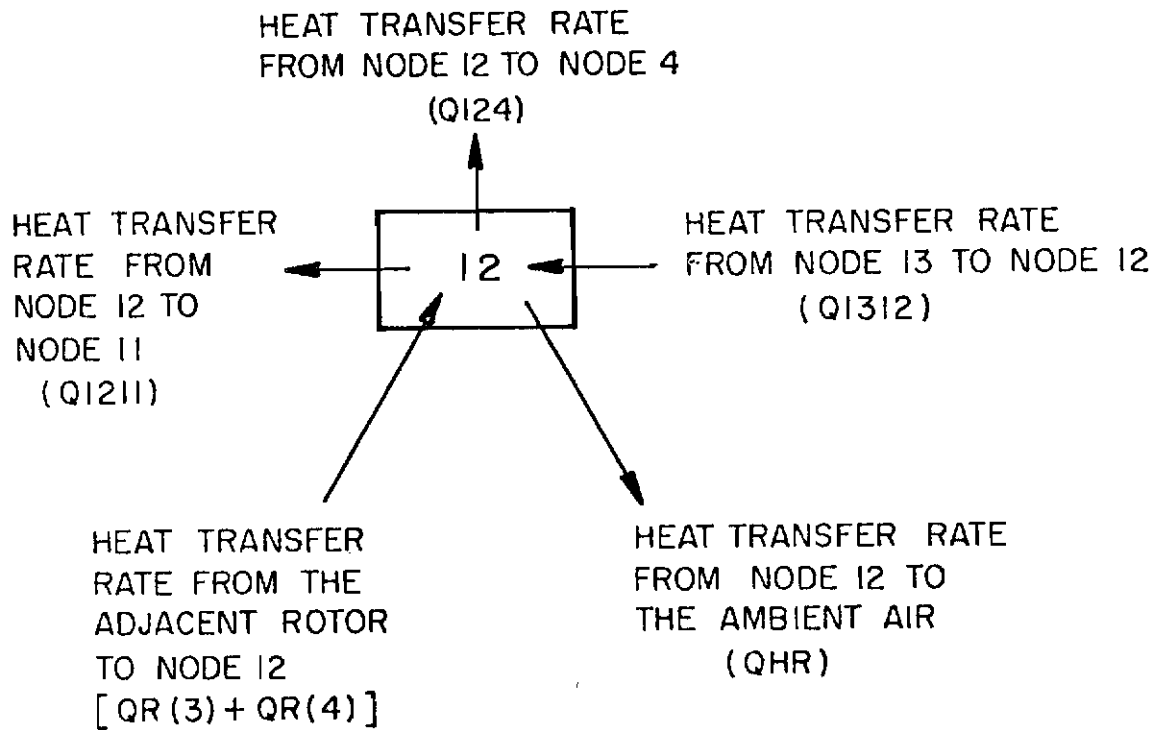


Figure 72. Node 12 Heat Transfer Rates

Contrails

where $RE4$ is the resistance, $LTT4$ is the length from the center of Node 4 to the contact point between the two masses, VKT is the thermal conductivity of the Node 4 (tire) material, and $ARIO$ is again the area of contact between the two masses. The heat transfer rate between Nodes 12 and 4 can now be written as:

$$Q_{124} = (T_{12} - T_4) \left(\frac{1}{RE4} + \frac{1}{RE12} \right) \quad (169)$$

Substituting Equations (167) and (168) into Equation (169) gives:

$$Q_{124} = (T_{12} - T_4) \frac{ARIO}{\frac{LRIO}{VKR} + \frac{LTT4}{VKT}} \quad (170)$$

The other heat transfer rates shown on Figure 72 are developed similarly. For Node 12, the first law of thermodynamics can be applied to give:

$$\begin{aligned} QR(3) + QR(4) + Q_{1312} - Q_{1211} - Q_{124} - Q_{HR} \\ = \rho VC \frac{T_{12}' - T_{12}}{\Delta t} \end{aligned} \quad (171)$$

Solving for the temperature at the time $t + \Delta t$, T_{12}' , in terms of the temperature at time t , T_{12} , yields:

$$\begin{aligned} T_{12}' = T_{12} + \frac{\Delta t}{\rho VC} [QR(3) + QR(4) + Q_{1312} - Q_{1211} \\ - Q_{124} - Q_{HR}] \end{aligned} \quad (172)$$

This equation, along with the similar equations for the other numbered nodes and the heat sink, was used to predict the temperatures within the entire brake, wheel, and tire.

Contrails

All remaining equations for the numbered nodes are shown in Appendix S. The radiative/convective heat transfer coefficients used are given in Appendix J while the thermal conductivity and the heat capacity values are given in Appendix K.

All equations developed for this two-dimensional model of the heat sink, tire, rim, torque tube, and brake housing were incorporated into a computer program employing variable heat capacity, variable thermal conductivity, variable work input and variable geometry. The program uses the equations derived above during the work input portion of the brake stop but uses a cooling scheme beginning at 1.25 times the stop time that lumps the entire heat sink mass into one mass at constant temperature and allows that mass to cool. During the heat sink cooling period, the masses of the numbered nodes in Figure 71 simultaneously absorb heat from the heat sink and lose heat to the surrounding air. The computer program resulting from the above equations is given in Appendix T.

CHAPTER VI CORRELATION OF RESULTS

Introduction

Five computer programs were used to predict the temperature at various locations within the brake and surrounding hardware. As a shorthand notation the programs and results are referred to as:

One-Dimensional Axial, 1-DA or 1-D Axial

One-Dimensional Radial, 1-DR or 1-D Radial

Two-Dimensional Radial/Axial (R/S Pair), 2-DRA or 2-D Radial/Axial

Two-Dimensional Entire Brake, 2-D

Three-Dimensional (R/S Pair), 3-D

Many of the required computer program inputs are given and explained in the program listings in the appendices and in the form of graphs within other appendices. For reference, Table 9 shows some selected program input values. The radii of the carbon heat sink are shown to be different than those of the beryllium heat sink even though they fit in the same brake housing and rim. The beryllium disc outside radii are smaller than the corresponding carbon disc outside radii and the beryllium disc inside radii are larger than the corresponding carbon disc inside radii. These values were used in the theoretical models to account for the fact that the beryllium discs had cutouts at various

TABLE 9
SELECTED COMPUTER PROGRAM INPUT VALUES

Variable	Stop 1.1-3	Stop 4.2-3	Stop 7.2-3	Stop 8.1-2
Heat Sink Initial Temperature (°F)	129.	120.	127.	127.
Area One Rotor to Rim (in. ²)	3.2 × RT	3.2 × RT	1.8 × RT	1.8 × RT
Area One Stator to Torque	5. × ST	5. × ST	3.8 × ST	3.8 × ST
Heat Sink Density (lbm/ft ³)	108.	108.	115.5	115.5
Stop Time (sec)	58.	41.	36.	124.
Initial Velocity (ft/sec)	207.	274.	212.	271.
Stator Half Thickness (in.)	.37	.37	.34/.29*	.34/.29*
Rotor Half Thickness (in.)	.34	.34	.29/.22	.29/.22
Rotor Outside Radius (in.)	7.2	7.2	6.8	6.8
Rotor Inside Radius (in.)	4.4	4.4	4.67	4.67
Stator Outside Radius (in.)	6.75	6.75	6.55	6.55
Stator Inside Radius (in.)	3.75	3.75	4.4	4.4
Ambient Temperature (°F)	80.	83.	76.	85.
Initial Temperatures for Nodes in Figure 71 (°F)				
1	105.	110.	83.	86.
2	92.	103.	77.	85.
3	112.	105.	83.	90.

TABLE 9---continued

Variable	Stop 1.1-3	Stop 4.2-3	Stop 7.2-3	Stop 8.1-2
4	112.	105.	83.	90.
5	100.	100.	90.	96.
6	112.	105.	83.	90.
7	112.	105.	83.	107.
8	112.	105.	83.	107.
9	105.	110.	83.	86.
11	112.	105.	88.	90.
12	112.	105.	88.	90.
13	112.	105.	82.	91.
14	108.	105.	77.	92.
21	105.	110.	83.	86.
22	105.	110.	83.	86.
23	105.	110.	83.	86.
24	105.	110.	83.	86.

*First number shown is half thickness including wear pad while second number shown is half thickness without the wear pad included.

locations around the circumference (see Figures 21 and 22); thus, in order to maintain the proper thickness and mass for a beryllium disc, the radii were modified.

Contact resistance was included in the boundary condition equations developed for predicting the temperature at the interface of a stator and rotor. This contact resistance term was included in developments 1-DA, 2-DRA and in the development for the caliper brake. No graphs or curves are presented showing this contact resistance effect because it was determined that less than a 1% difference in peak temperature occurred at the contact resistance values obtained from the disc surface measurements. Even when this contact resistance was multiplied by ten, the peak temperature changed by only about 2%. Thus for the models 2-D and 3-D the rubbing surface contact resistance was not used. Since the rubbing surface contact resistance does not take into account contact resistance between the wear pads and the actual disc material (see Figures 21 and 22), a separate development was employed to include this effect. This effect is significant and is discussed in more detail in a subsequent section.

Temperature-Time History, Experiment, 1-DA, 1-DR, 2-DRA

For the carbon brake, the thermocouple at a radial position of 5.5 in. and on the axial centerline of Stator 2 (see T/C No. 3 on Figures 30 and 32) was chosen as a typical heat sink temperature. Figure 73 shows a plot of temperature versus time comparing experiment with 1-DR, 1-DA, and 2-DRA. The time that the brake stops rotating is noted. In 1-DA there is no radial temperature gradient while in 1-DR there is no axial temperature gradient. The fact that a particular

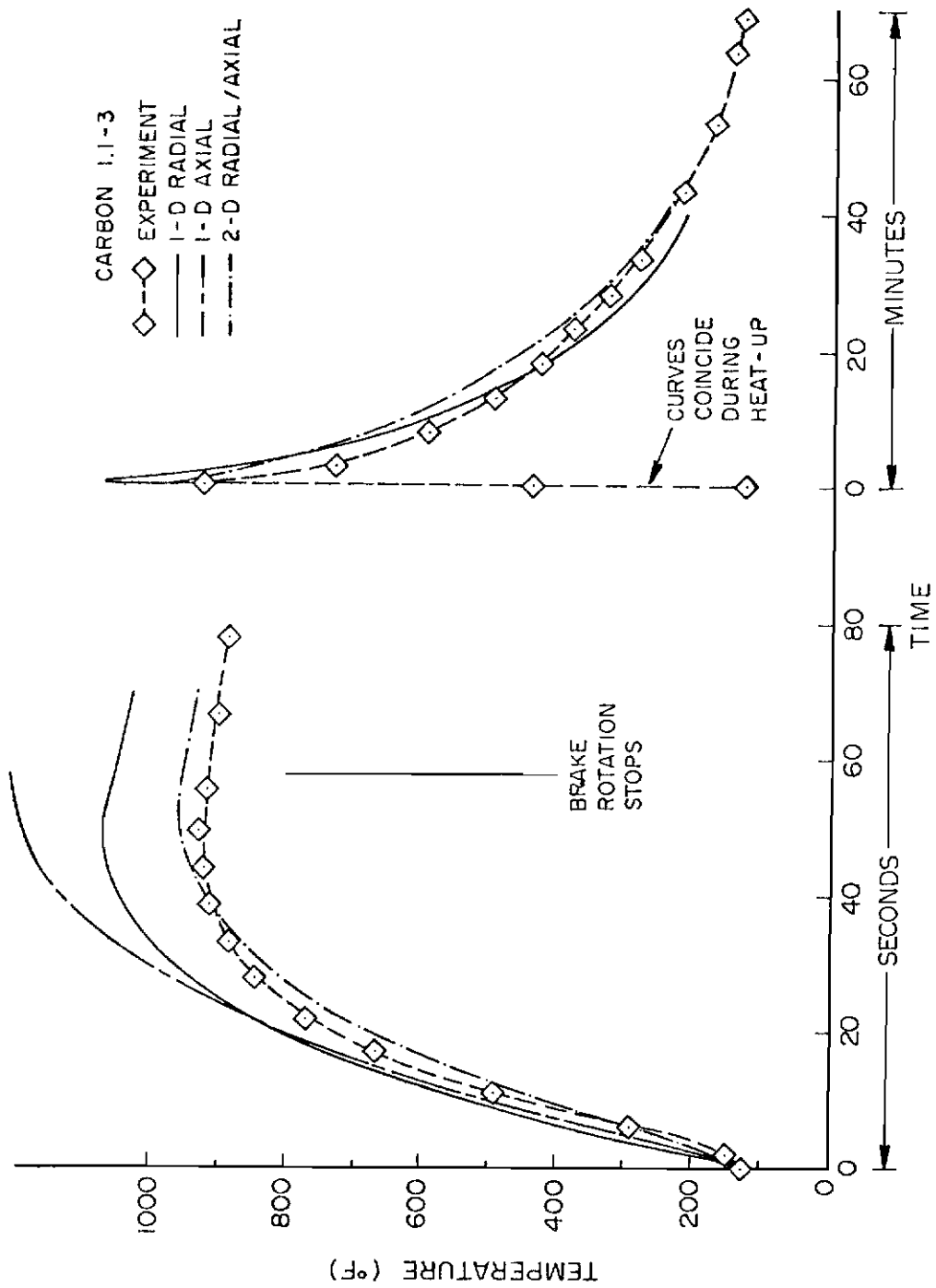


Figure 73. Temperature vs Time at R = 5.5. (Test 1.1-3, 1D vs 2 DRA)

Contrails

radius and axial position are specified by selecting the experimental location is neglected in the above two cases. The exact radial and axial locations can be determined for the 2-DRA model. As noted, the axial model overpredicts the temperature. This is the case since no provision for cooling is incorporated in the model. Since no cooling takes place, Figure 73 contains no cooling curve for the 1-DA model. The 1-DR model also overpredicts the temperature but is closer to experiment than the 1-DA model. For the 1-DR model cooling is provided at the outside and inside circumference of the disc. As discussed in the theoretical development section the 1-DR model predicts temperatures for the stator only. In addition to the circumferential cooling, cooling occurs at the face of the stator toward the inside radius at the area that is not in contact with the rotor. The reason for the temperature over prediction in the case of the 1-DR model is attributed to two things. First, the radial model work input term was treated as an internal heat generation since no boundary was present in the axial direction for work input. This insured no axial temperature gradient. On the other hand, the thermocouple was placed at the axial center of the disc which is the coolest axial position. Thus, a model without the axial gradient would predict a higher than measured temperature. The second reason that the 1-DR model could predict higher temperatures is because the 1-DR model is linked to the 1-DA model. This is true since the split of energy into the rotor/stator interface for the 1-DR model was taken to be that of the 1-DA model. Also shown on Figure 73 is the heating and cooling as predicted by the 2-DRA model. This model is much closer to experiment as it takes into account all required

convective/radiative cooling and accounts for temperature gradients in the radial and axial directions.

Figure 74 shows the predictions from the three models, 1-DA, 1-DR and 2-DRA for a brake stop that occurs in 41 seconds as compared to 58 seconds in Figure 73. Also the energy input into the brake on Figure 74 is 100 percent of normal kinetic energy (11.23×10^6 ft-lb) while that for Figure 73 was 60 percent. Again the 1-DA model gives the highest temperatures of the three models, followed by 1-DR and 2-DRA. The 2-DRA model again gives best results and shows a peak temperature difference from experiment of about 4% as compared with about 4% for Figure 73. The 2-DRA model does predict higher temperatures than experiment during the first 25 seconds of the stop. This lack of correlation is attributed to thermocouple lag time. The temperature gradient during the heat input for Figure 74 is about 32°F per second while that for Figure 73 is about 100°F per second.

Considering the beryllium heat sink, Figure 75 gives a 36-second stop and compares 1-DA, 1-DR, and 2-DRA to experiment. The energy input for this case is 60 percent of the normal kinetic energy. For the beryllium heat sink, the thermocouple at a radial position of 4.4 in. and on the axial centerline of Stator 2 (see T/C No. 3 on Figure 29) was chosen to compare to theory. Figure 76 shows a second stop with the beryllium heat sink. The stop time in this case is 124 seconds while the energy input is 100% of normal kinetic energy. Although the energy input levels correspond to those in Figures 73 and 74, the beryllium heat sink remains at a cooler temperature than the carbon due to the difference in thermal properties (see Appendix K)

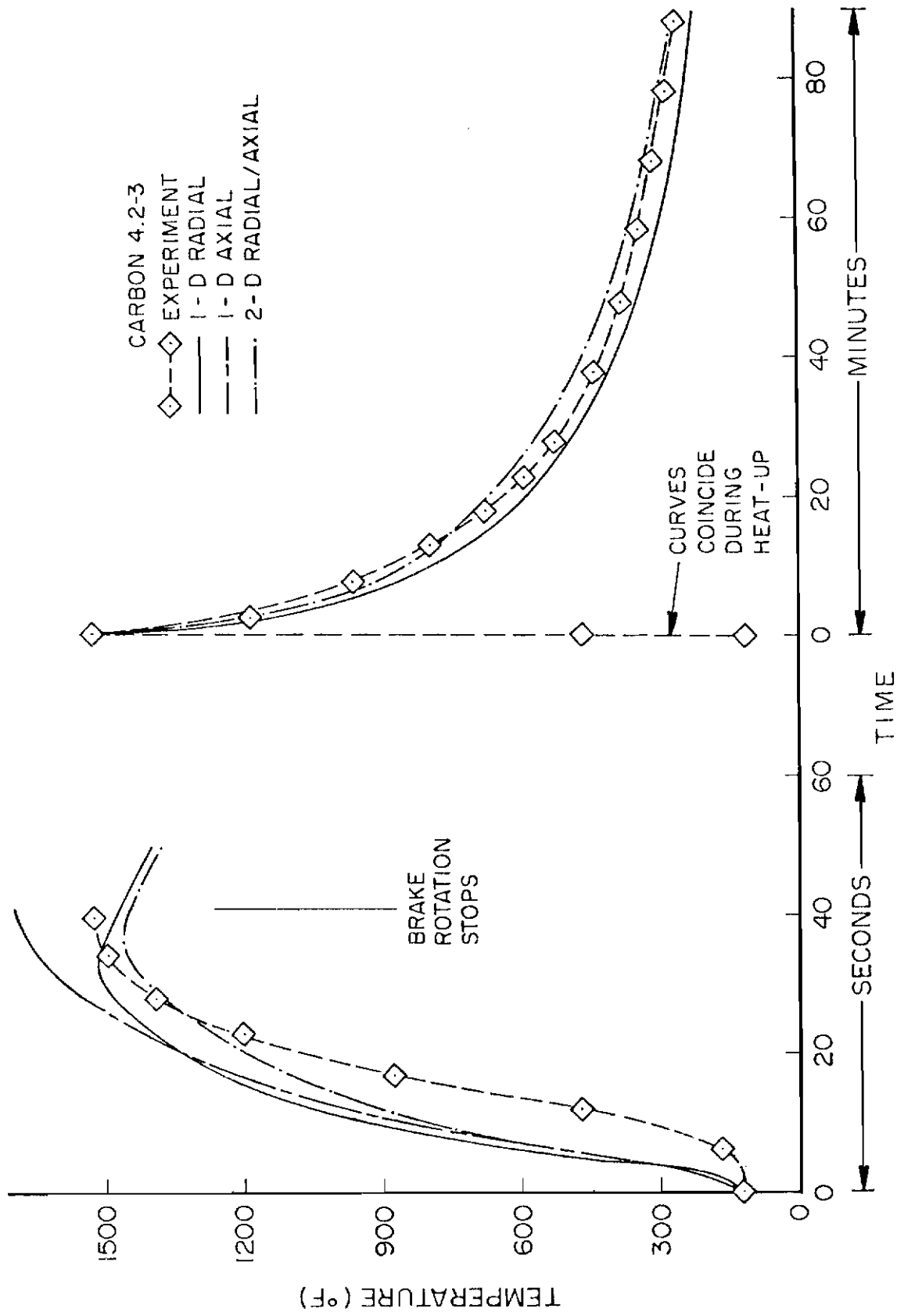


Figure 74. Temperature vs Time at R = 5.5 in. (Test 4.2-3, 1-D vs 2-DRA)

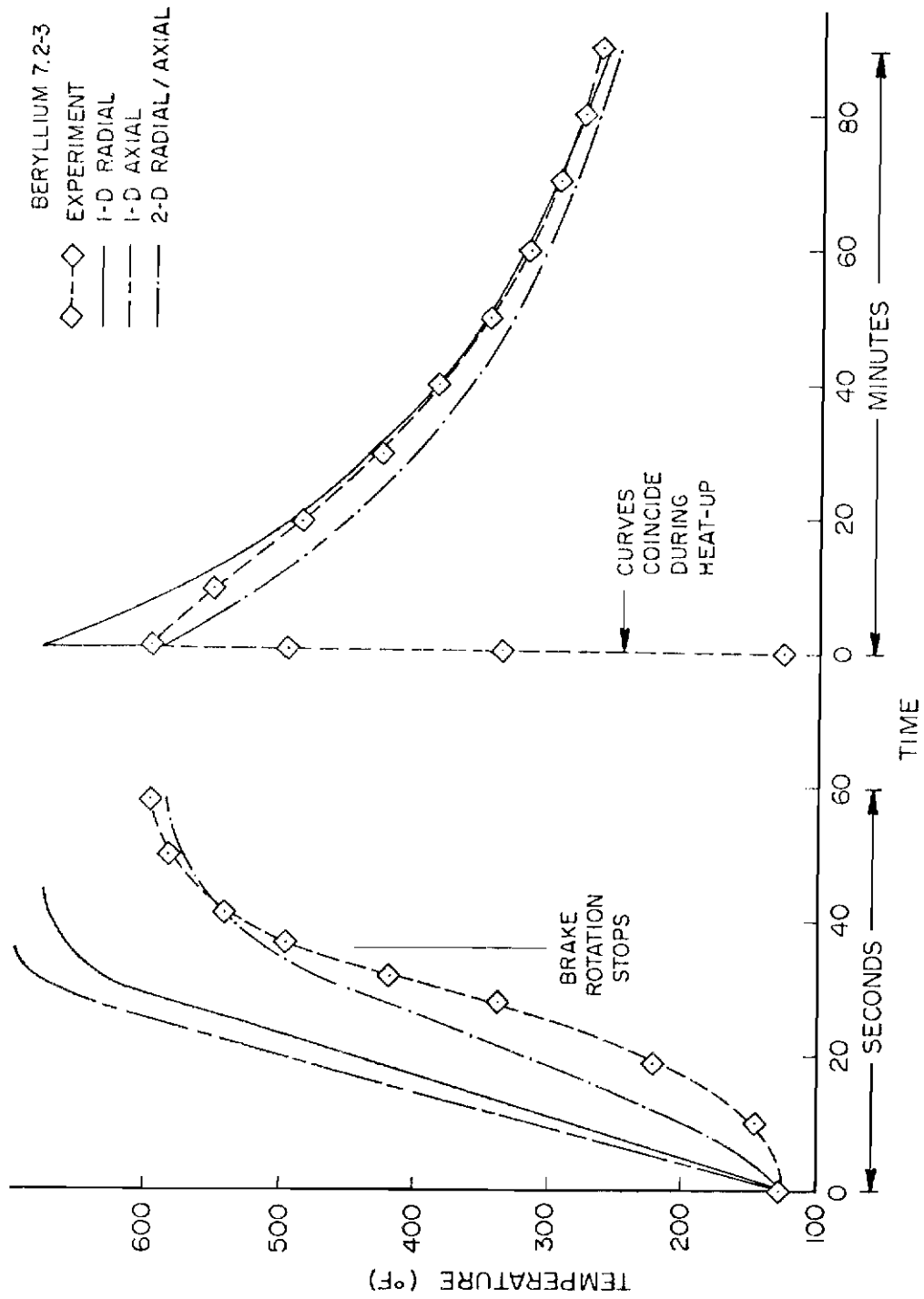


Figure 75. Temperature vs Time at R = 4.4 in. (Test 7.2-3)

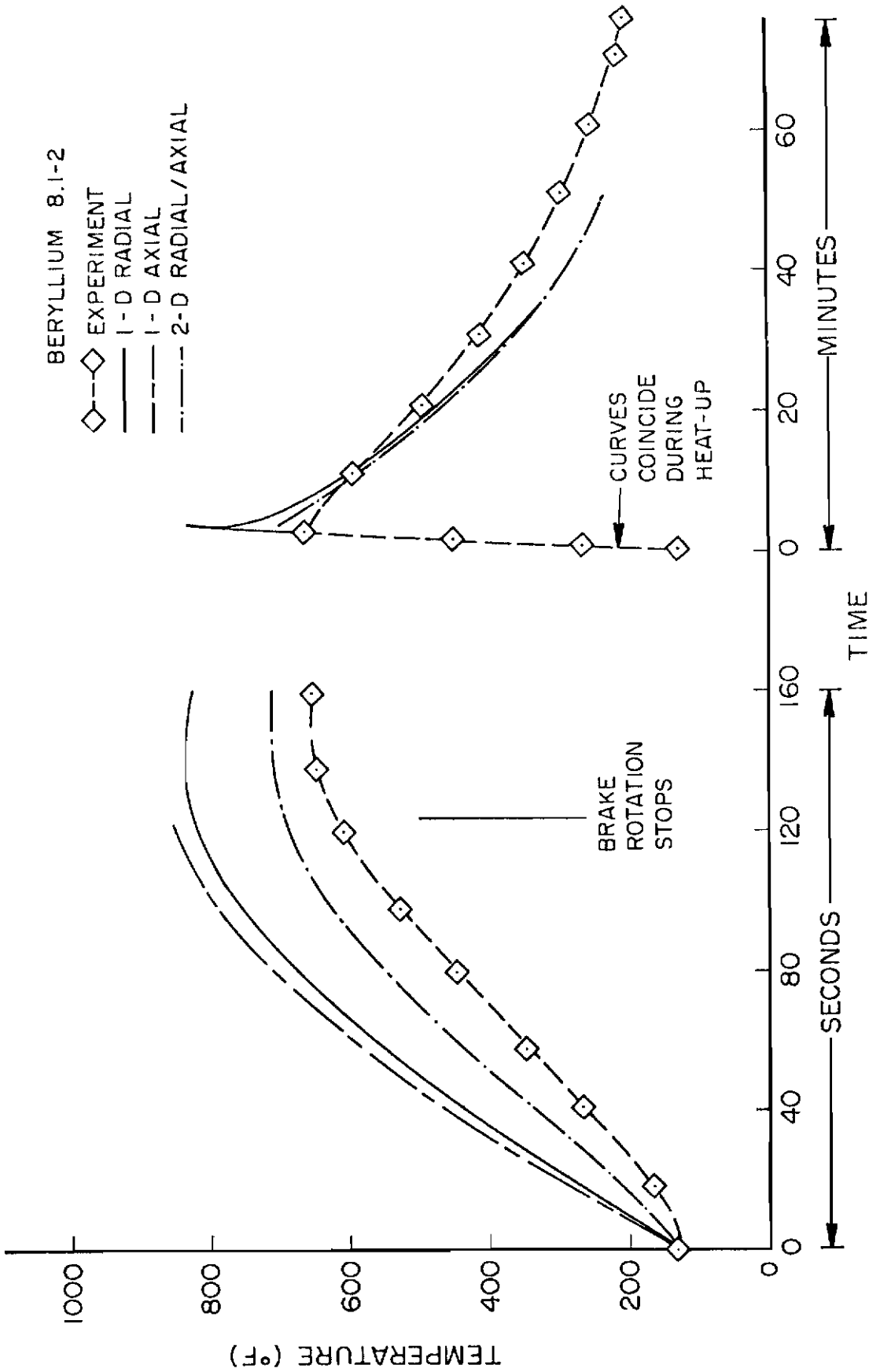


Figure 76. Temperature vs Time at R = 4.4 in. (Test 8.1-2 1D vs 2DRA)

Contrails

between the two. Again in both figures the 1-DA model predicts the highest temperatures, the 1-DR model predicts the next highest temperatures, and the 2-DRA model predicts temperatures closest to experiment. The peak temperature predicted by the 2-DRA model for Figure 75 is within 2% of experiment while for Figure 76 the peak temperature predicted is within 8% of experiment. The temperature gradient during the heat input is about 15°F per second in Figure 75 and about 8°F per second in Figure 76. The test with the highest temperature gradient during heat input, Figure 75, exhibits the same trend of the experimental temperatures lagging the 2-DRA predictions as was noted in Figure 74. Although the same trend is noted in Figures 74 and 75, the lag shown in Figure 75 cannot be solely attributed to thermocouple lag because of several differences between the 2-DRA model inputs for the two cases. The beryllium brake disc uses thin brake pads as the wearing surface and the use of these pads creates a contact resistance between the pad and the beryllium material. This contact resistance was assumed to be constant and was selected to be in the range normally found in this type application ($.005 \text{ HR-Ft}^2\text{-}^\circ\text{F/BTU}$). This contact resistance value used probably varies with temperature as the contact area between the wear pad and the beryllium material varies with temperature due to pad warpage. Another model input difference in the 2-DRA model for beryllium versus carbon is the thermal properties (Appendix K). Heat capacity of the beryllium material is about one-half that of the carbon. This means the beryllium is not able to store as much thermal energy as the carbon. Also the thermal conductivity of the beryllium is higher than that of the carbon so that the thermal

resistance is lower and the beryllium will therefore lose heat faster than the carbon.

The most important point to be made in this section is that for the 2-DRA model, the maximum temperature was predicted within 4% of experiment for three of the four stops studied and that the fourth was within 8%. It is this maximum temperature that must be accurate to be able to accurately predict the temperatures of any surrounding hardware. The precise temperature gradients during heating are not as important since these take place over about one minute compared with the approximately ten minutes required for the surrounding hardware to reach its maximum temperature.

Temperature-Time History, Constant/Variable Torque and Pads/No Pads

Recall from the theoretical development chapter that the work input term for each model was proportional to the torque generated by the brake during the brake stop. The torque can be calculated if brake pressure, deceleration, brake geometry, and coefficient of friction are known. This calculation results in a constant, average torque since brake pressure, deceleration and coefficient of friction are assumed constant. Unfortunately, brake test experience shows that the brake torque is not constant with time. Not only does torque vary with time but also it varies in different ways for different brake materials. Figure 77 is a comparison of average torque and typical torque curves for the carbon and beryllium brake (for actual torque curves of carbon and beryllium, see Appendix E). Also in Figure 77 with the same time scale, is a plot of flywheel energy versus time. It can be seen that

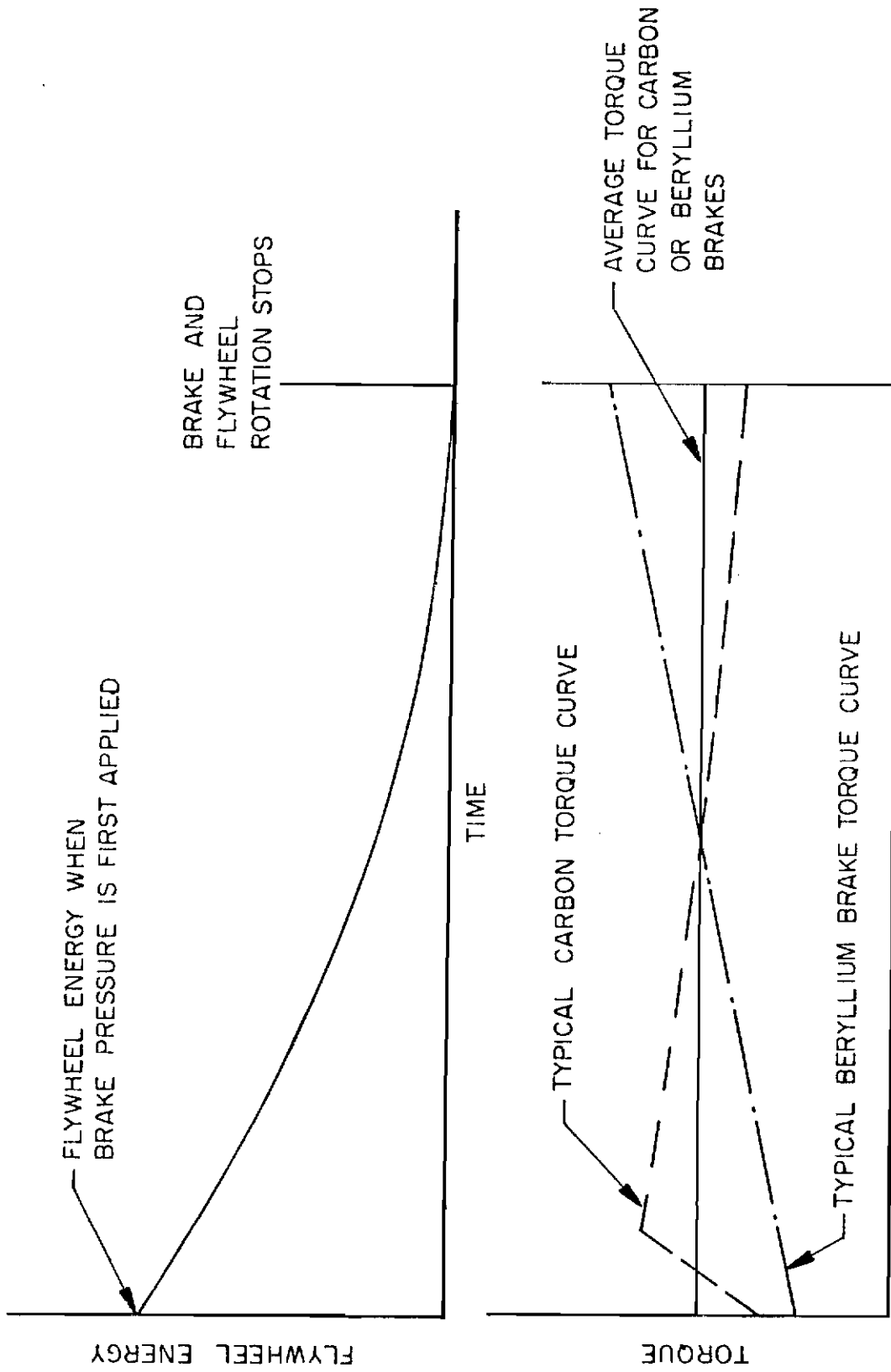


Figure 77. Torque and Flywheel Energy vs Time

Contrails

the highest energy of the flywheel and therefore the highest energy input into the brake occurs during the first portion of the stop and that after the midway point of the stop (at the stop time divided by 2), the vast majority of energy to be absorbed by the brake has already been absorbed. Thus, the shape of the torque curve is most important during the first half of the stop and use of an average torque for input into a thermal model would not produce an adequate simulation. The difference in temperatures resulting from the use of an average versus an exact torque curve in the 2-DRA model is depicted in Figure 78 for carbon. The constant torque maximum temperature is 7% lower than the variable torque maximum temperature of the 2-DRA model. Looking at Figure 77, it would be expected that use of the average torque curve for carbon would result in a prediction of lower temperatures but due to the actual torque beginning at a lower value than the average, the lower temperatures (7%) are not drastic. A more drastic difference should be noted for the case of beryllium since the actual torque curve is always lower than the average torque curve during the first half of the stop (note Figure 77). Figure 79 shows a beryllium experimental curve along with three curves from the 2-DRA model. The upper curve is the constant torque curve and gives a peak temperature 23% higher than the actual torque curve, the curve closest to the experimental curve.

Also shown in Figure 79 is a curve generated from the 2-DRA model assuming no wear pads on the beryllium disc but using the same equivalent disc thickness. Thus, the total disc thickness in this case is found by adding the wear pad thickness to the actual beryllium thickness. The entire resulting disc is assumed to be beryllium. The input

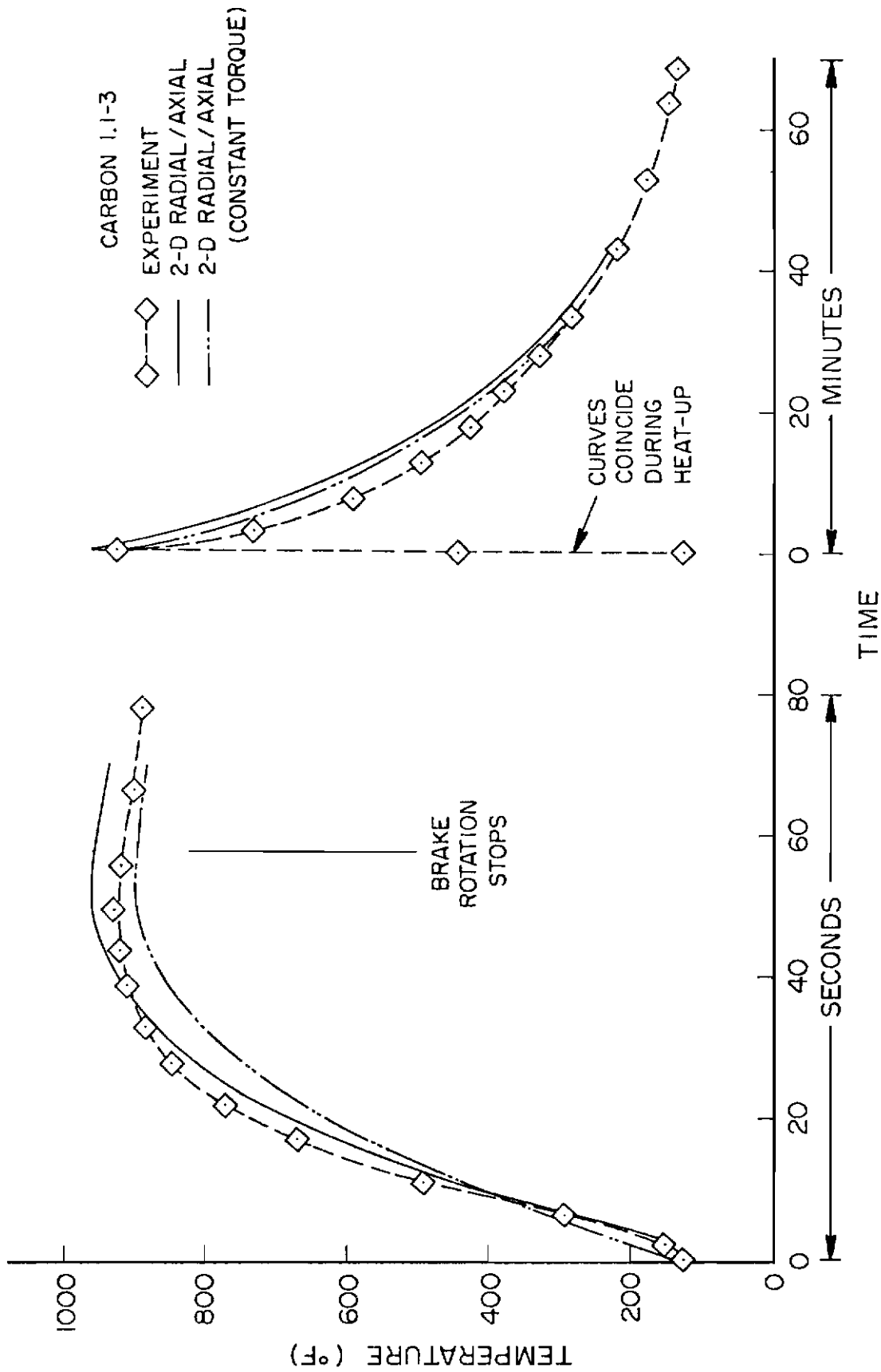


Figure 78. Temperature vs Time at R = 5.5 in. (Test 1.1-3 Constant Torque Effect)

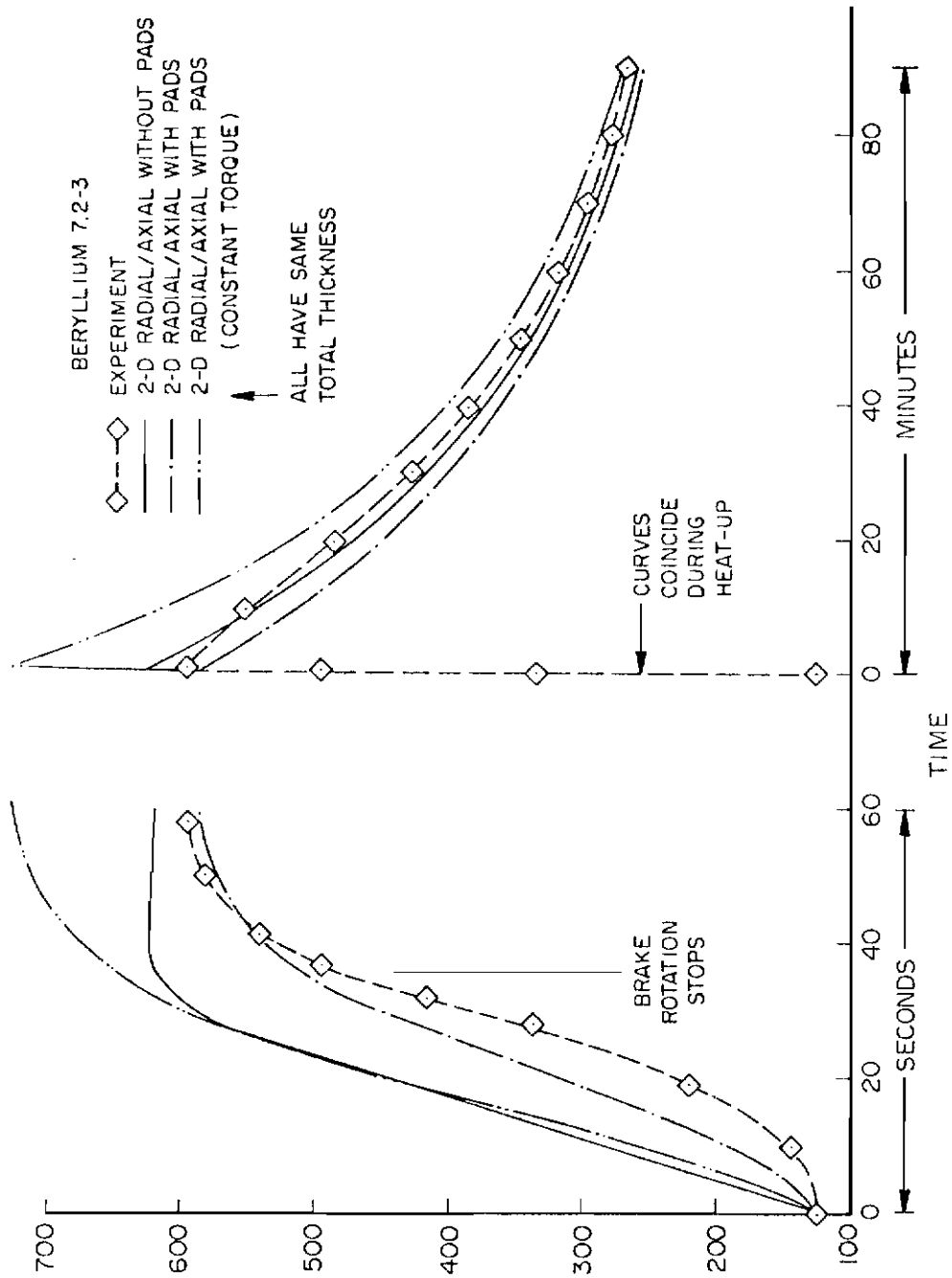


Figure 79. Temperature vs Time at R = 4.4 in. (Test 7.2-3, Wear Pad and Constant Torque Effect)

torque for this case was the actual torque curve. As can be seen in Figure 79, this type of 2-DRA model is not very accurate in that the temperature lag evident in the experimental data is not predicted and in that the peak temperature is 26°F different from experiment while the 2-DRA model including wear pads was only 10°F different from experiment.

Temperature-Time History, 2-DRA and 3-D

The three-dimensional temperature prediction model, 3-D, of a rotor and stator sector was shown in Figure 66. For the purposes of comparing experiment, 2-DRA and 3-D at the same physical location in the disc, and adequately representing the 3-D model, the 3-D model was modified somewhat. In order to simulate the conduction heat transfer out of the lug positions into the rim and torque tube, the nodes at (2,10,4), (2,9,4), (3,10,4), (3,9,4), (4,10,4), (4,9,4), for the rotor and at (5,1,4), (5,2,4), (6,1,4), (6,2,4), (7,1,4), (7,2,4) for the stator were forced at each time step to be a given percentage lower than the actual calculated value for that node. Also, during this time period the radiation convection heat transfer coefficient was taken to be zero. This coefficient was taken as zero since the primary heat loss mechanism for a disc during a stop is conduction through the lug areas. The actual percentage reduction in the temperatures of the nodes above was chosen so that the percentage reduction was the same for simulations of the carbon 1.1-3 test and the beryllium 7.2-3 test and so that the resultant peak temperatures of the simulations corresponded to the experimental values of the two tests. This temperature

reduction technique was used until 1.25 times the stop time at which time the conduction simulation was terminated and the disc was lumped into one mass and allowed to cool by convection/radiation. The result of this effort is shown in Figure 80 for the carbon disc. The 2-DRA and 3-D curves are within 1.5 percent of each other at the stop time and never are farther apart. Figure 81 shows the results for a beryllium disc. Since the primary objective of the 3-D model development was to look at circumferential temperature gradients, wear pads were not simulated. Thus, for the comparison of 2-DRA and 3-D in Figure 81, neither of the theoretical models used wear pads. The two theoretical curves are within 5% of each other at about 40 seconds and this is the largest deviation noted. This deviation is larger than that of the carbon and is attributed to the fact that the beryllium disc is not simulated as well as the carbon in the area of the wear pads or in the area of the radial cutouts (Figures 21 and 22).

Circumferential Direction Temperature Gradient, 3-D

To determine the relative importance of the circumferential temperature gradient in the brake application, the 3-D Model was used to generate temperatures in the circumferential direction. The conduction heat transfer out of the lugs was treated as previously discussed. The resulting temperatures were plotted for a carbon brake stop in Figure 82. The temperatures plotted occurred on the axial centerline of the stator and at the radial and circumferential positions shown in Figure 82. Three times during the brake stop were selected for plotting, namely .25, .5, and .75 times the stop time. At each time, a curve is shown of temperature versus circumferential

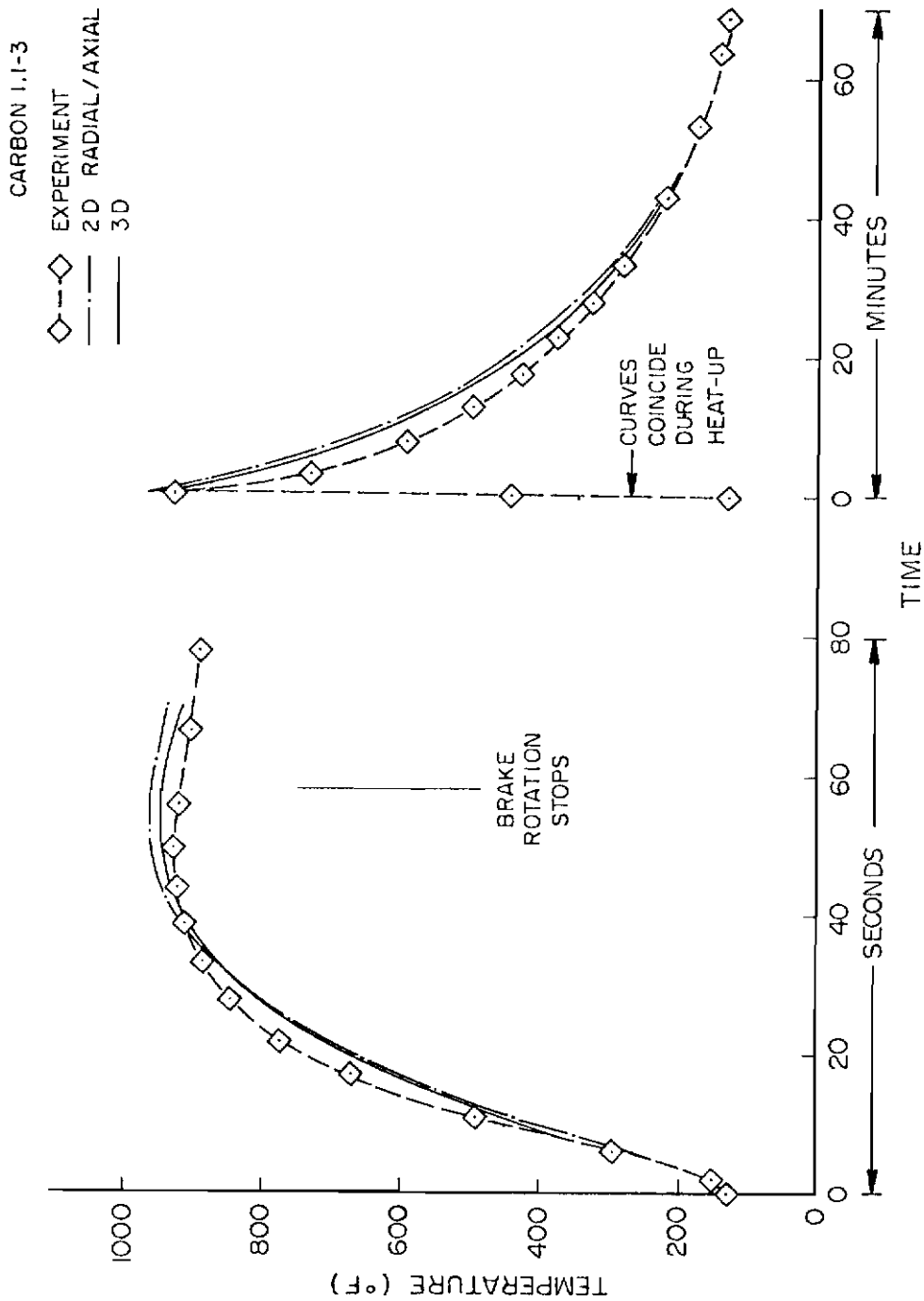


Figure 80. Temperature vs Time at 5.5 in. (Test 1.1-3, 2DRA vs 3D)

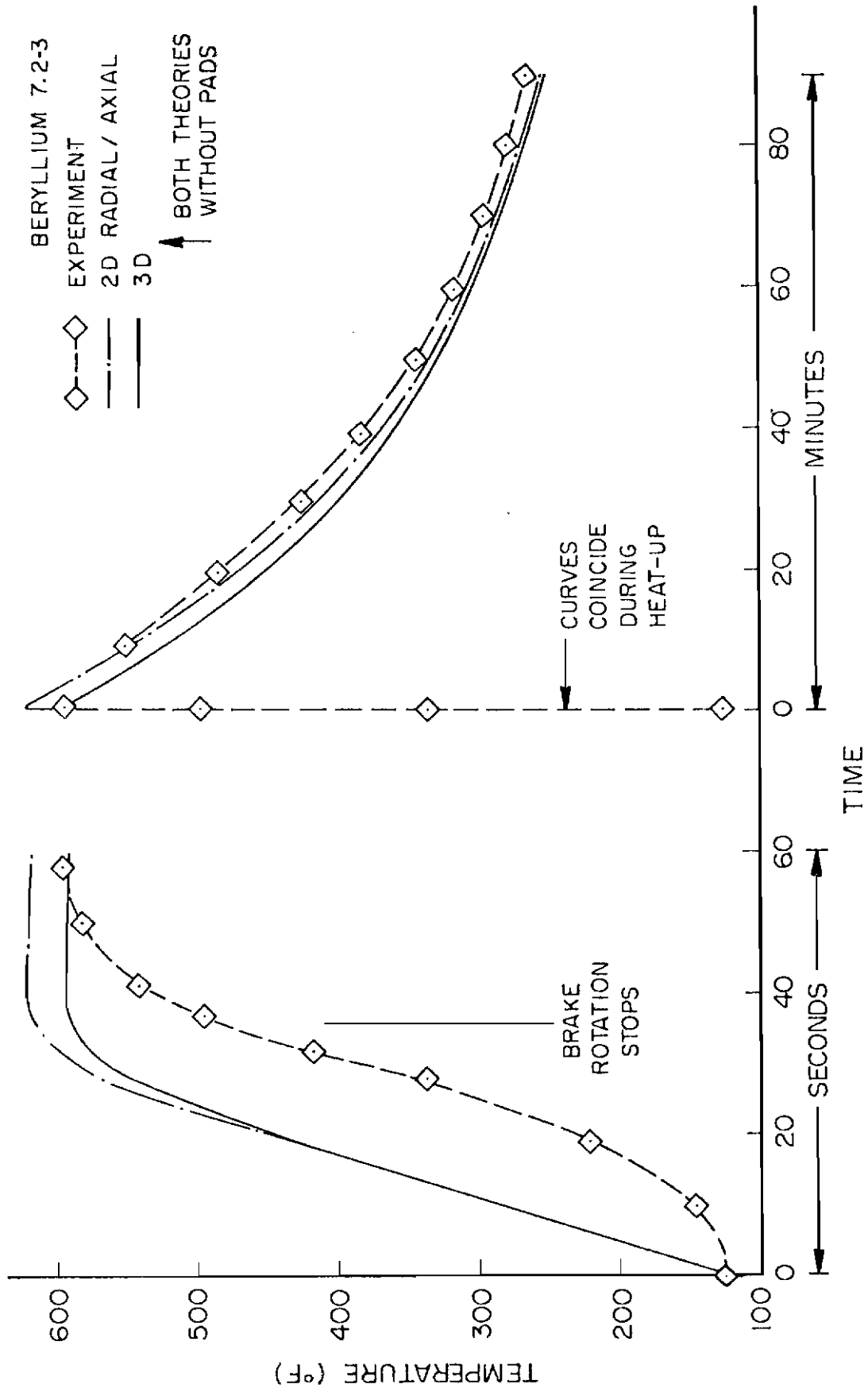


Figure 81. Temperature vs Time at 4.4 in. (Test 7.2-3, 2 DRA vs 3D)

Contrails

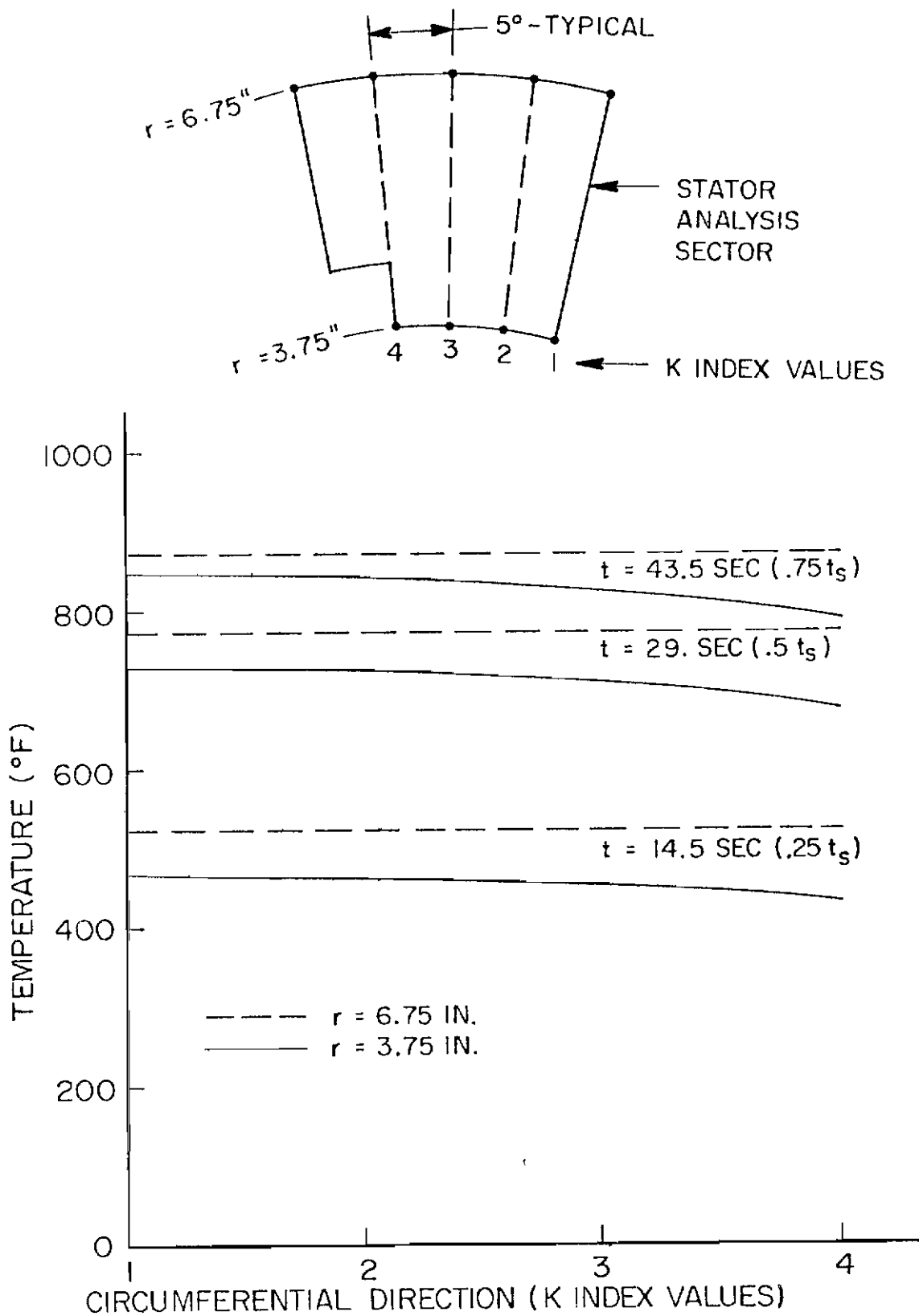


Figure 82. Temperature vs Circumferential Direction (Test 1.1-3)

direction at the inside and outside radii of the stator. The curves at the outside radius show no temperature variation in the circumferential direction but the curves at the inside radius do show a variation since the conduction occurs at the inside radius. Although the variation in temperature increases with time, the variation is at a constant 7%. The same type of analysis except for the beryllium brake, results in curves as shown in Figure 83. The variation at the inside radius is again a constant percentage but the percentage has increased to 14%. This occurs since the heat capacity of beryllium is about twice that of carbon. Although a temperature gradient does exist in the circumferential direction, it is not recommended that each disc of the brake be modeled in three directions since two-dimensional disc analysis is close to experiment and since computer time and storage dramatically increase when the third-dimension is added. If, on the other hand, information is desired in the lug area, then the three-dimensional model can be used for one disc pair only and the required information can be found.

Disc, Torque Tube, Rim and Contained Air Temperatures, 2-D

For disc temperature comparisons in the carbon, the thermocouple on the axial centerline of the stator at a radius of 5.5 inches was used, as before. The thermocouple in the beryllium stator was also selected as before, with a radius of 4.4 inches and on the axial centerline. Figures 84-87 show temperature versus time plots for the stator and torque tube of two tests using carbon and two tests using beryllium heat sink materials. The stator heating curves are similar

Contrails

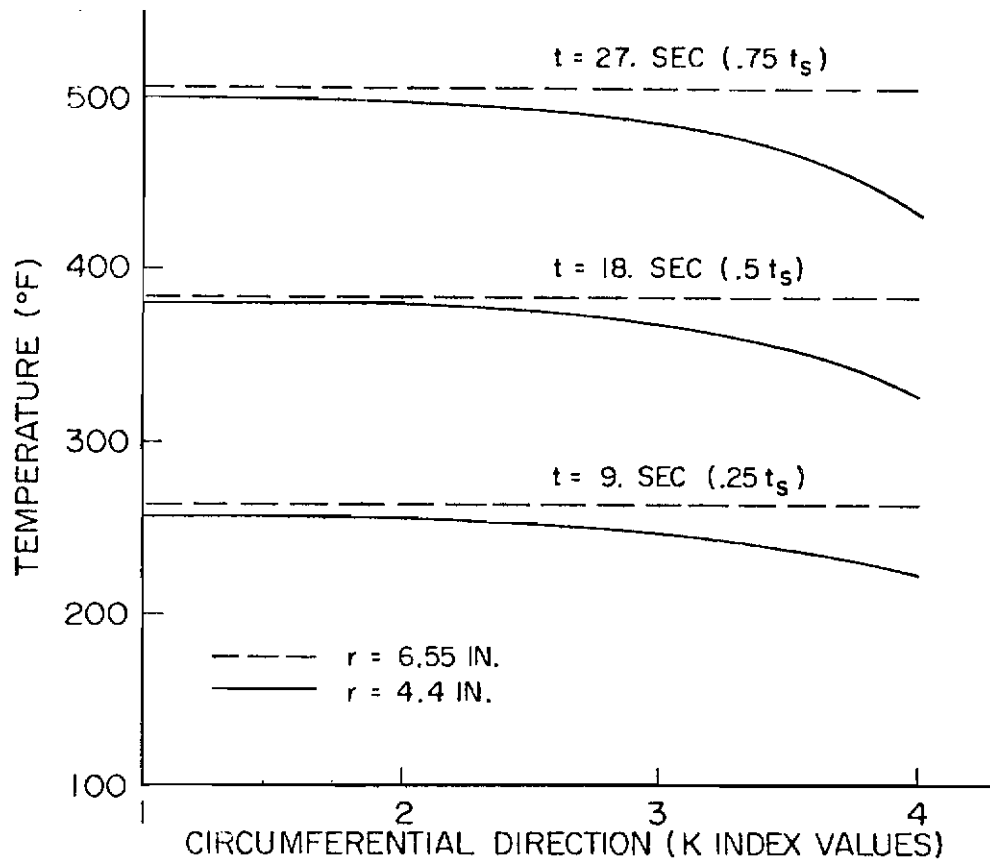
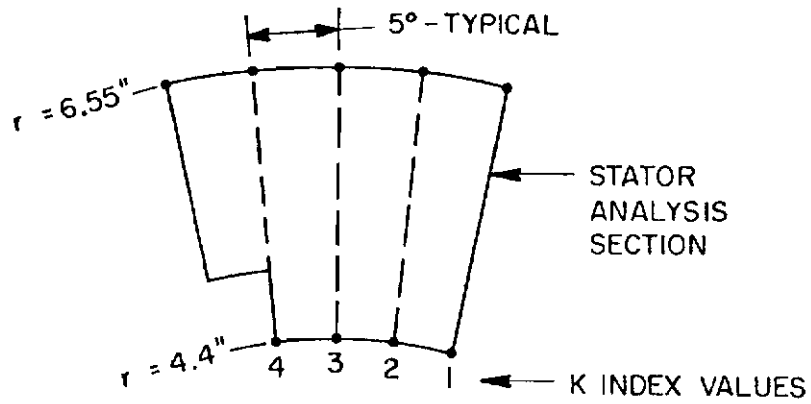


Figure 83. Temperature vs Circumferential Direction (Test 7.2-3)

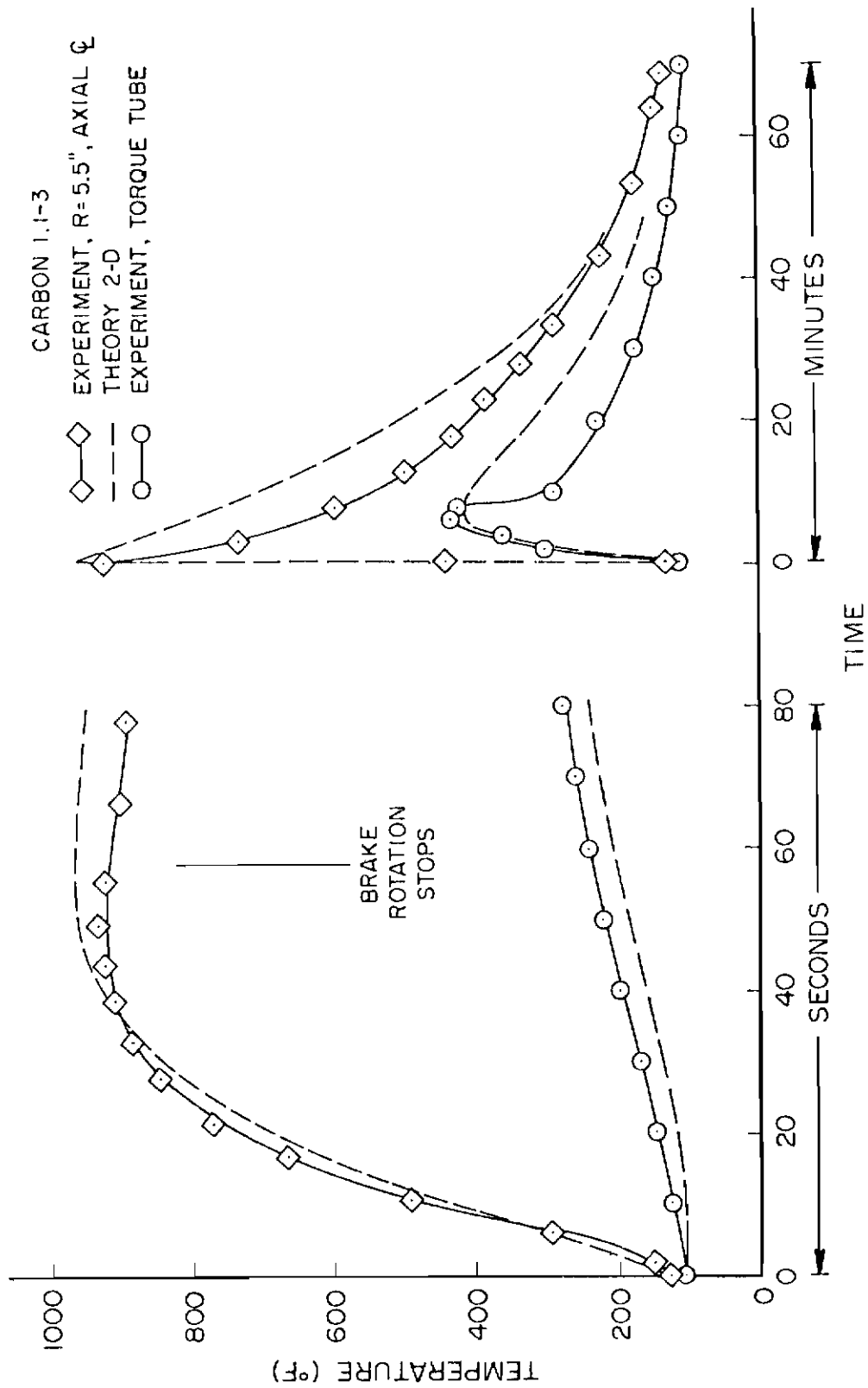


Figure 84. Temperature vs Time, Stator-Torque Tube (Test 1.1-3)

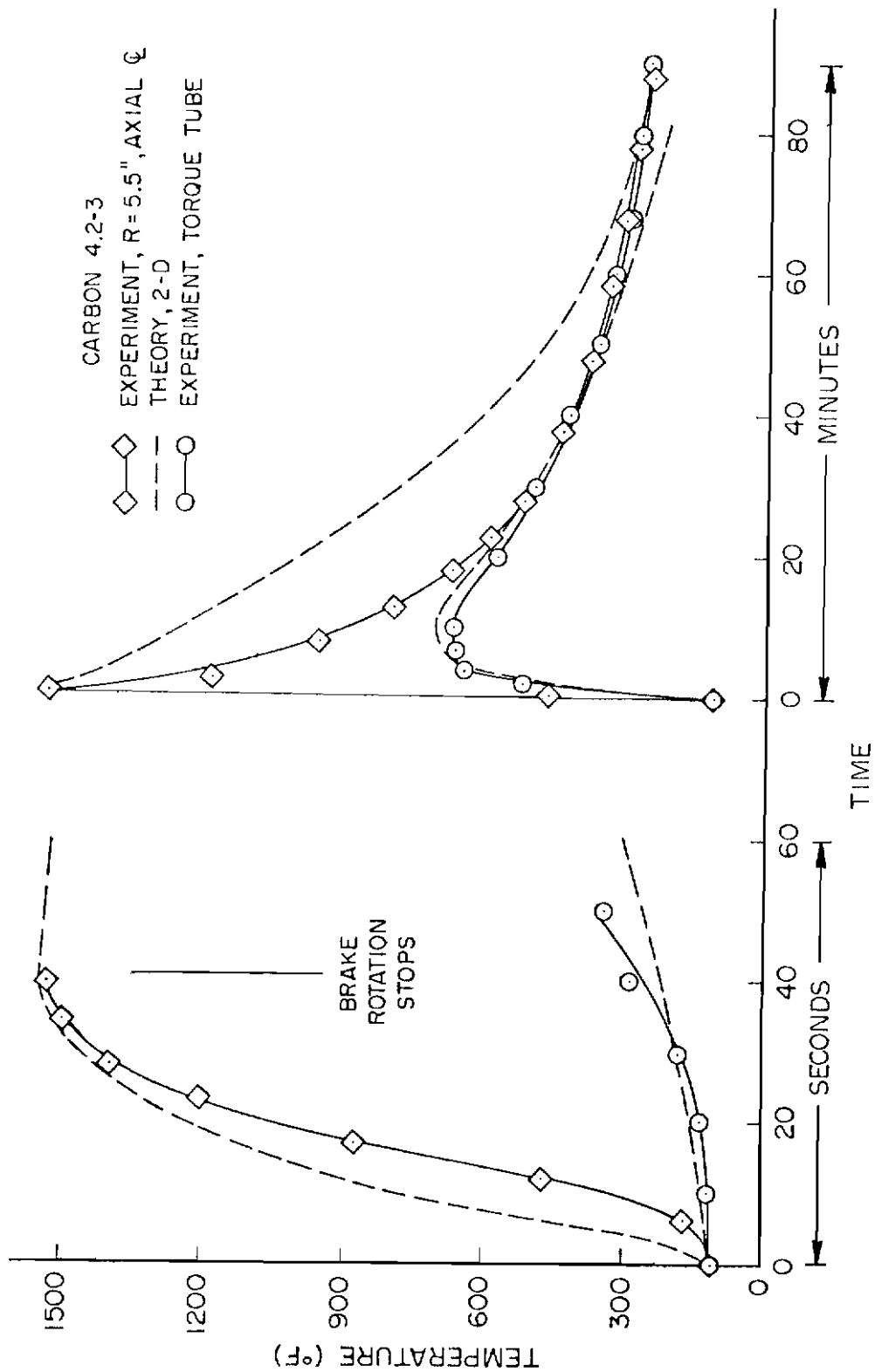


Figure 85. Temperature vs Time, Stator-Torque Tube (Test 4.2-3)

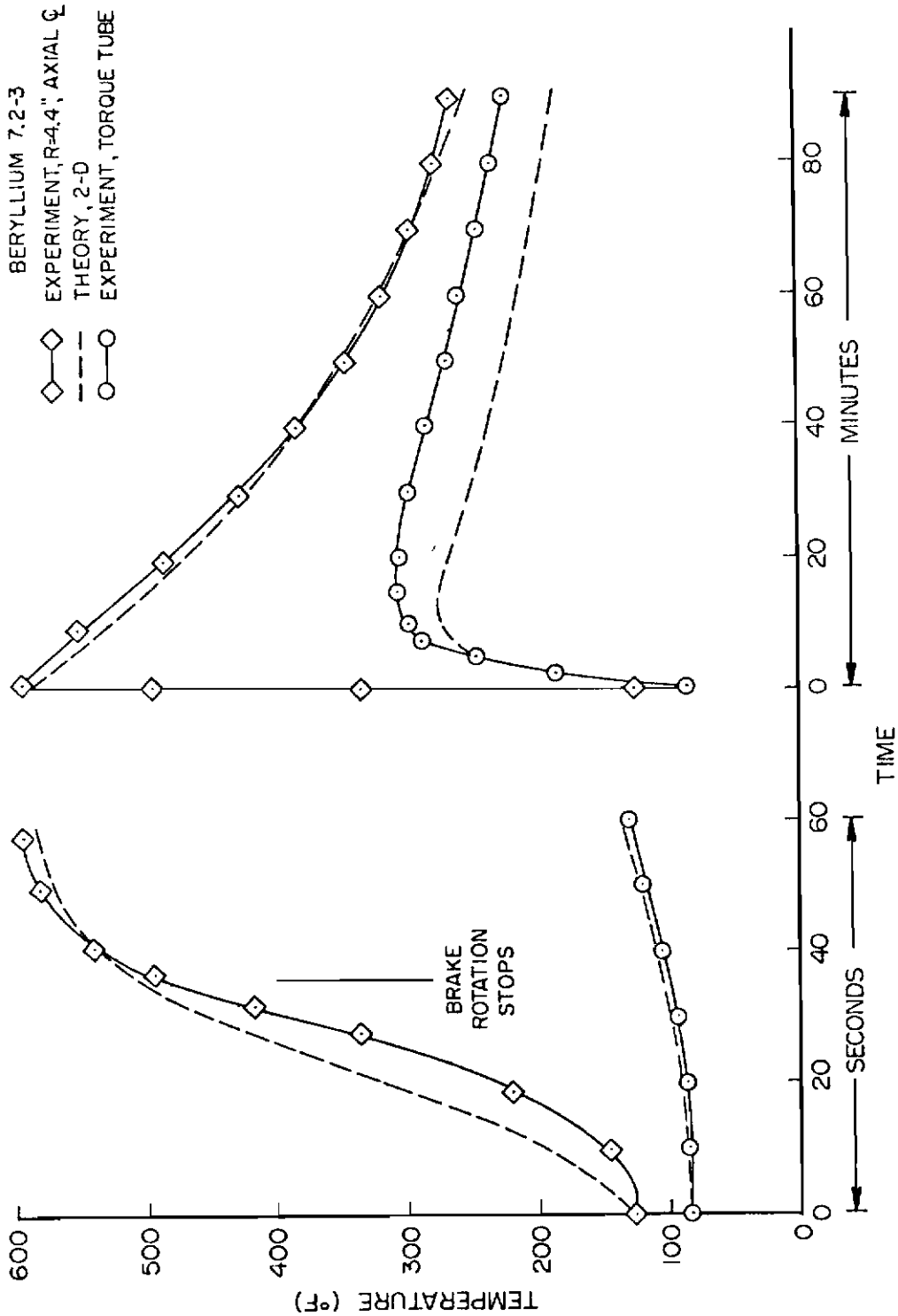


Figure 86. Temperature vs Time, Stator-Torque Tube (Test 7.2-3)

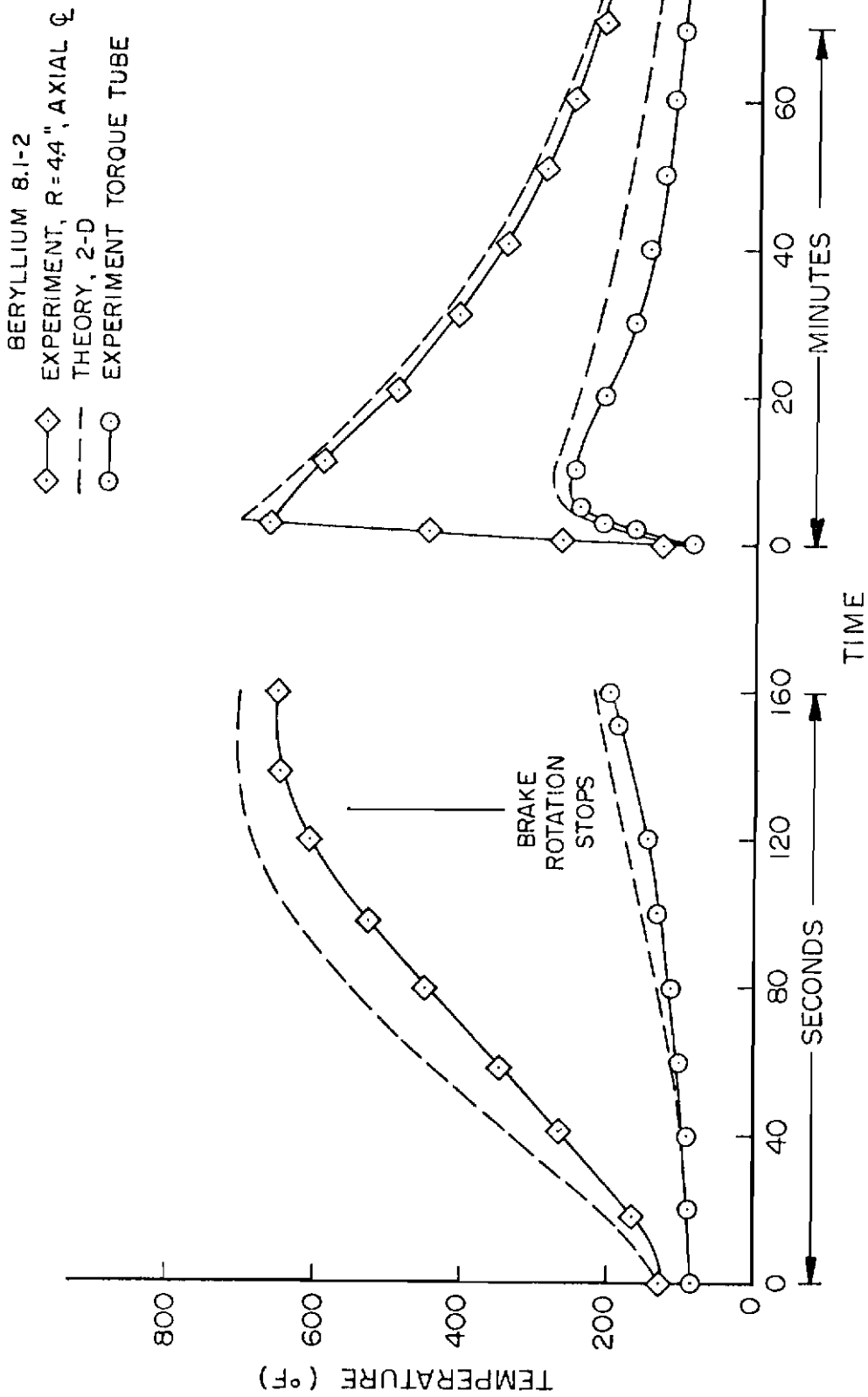


Figure 87. Temperature vs Time, Stator-Torque Tube (Test 8.1-2)

Contrails

to the heating curves of the 2-DRA model shown in Figures 73-76. This is necessarily so since the 2-DRA model is essentially a subroutine within the 2-D model. The difference between the two models is that cooling of the disc for the 2-DRA model is solely by convection/radiation and cooling for the 2-D model also includes heat conduction. The fact that the heating curves in all four cases do not change from model to model shows the relative unimportance of the cooling phenomenon during the work input portion of the stop. For the two carbon tests, the theory shows a higher temperature during cooling than is shown by the experimental curve. However the theoretical and experimental curves converge as time increases. In the case of beryllium the theoretical cooling curves are almost coincident with the experimental curves. A comparison of the torque tube temperature versus time curves in Figures 84-87 shows that the predicted peak temperatures are within about 6% of experimental peak temperatures for the carbon tests and within 10% for the two beryllium tests. The time at which the peak temperatures occur within the torque tube is predicted quite well for all four tests.

The relation between theory and experiment for the fuse plug and the drive lug for the four cases discussed above is depicted in Figures 88-91. It is to be expected that the thermal model will deviate from experiment more at greater distances from the work input than at the actual work input location. This is true since any model inaccuracies will be additive over distance and since contact at material interfaces is modeled as the same temperature for both materials (no contact resistance). For the carbon tests, Figures 88 and

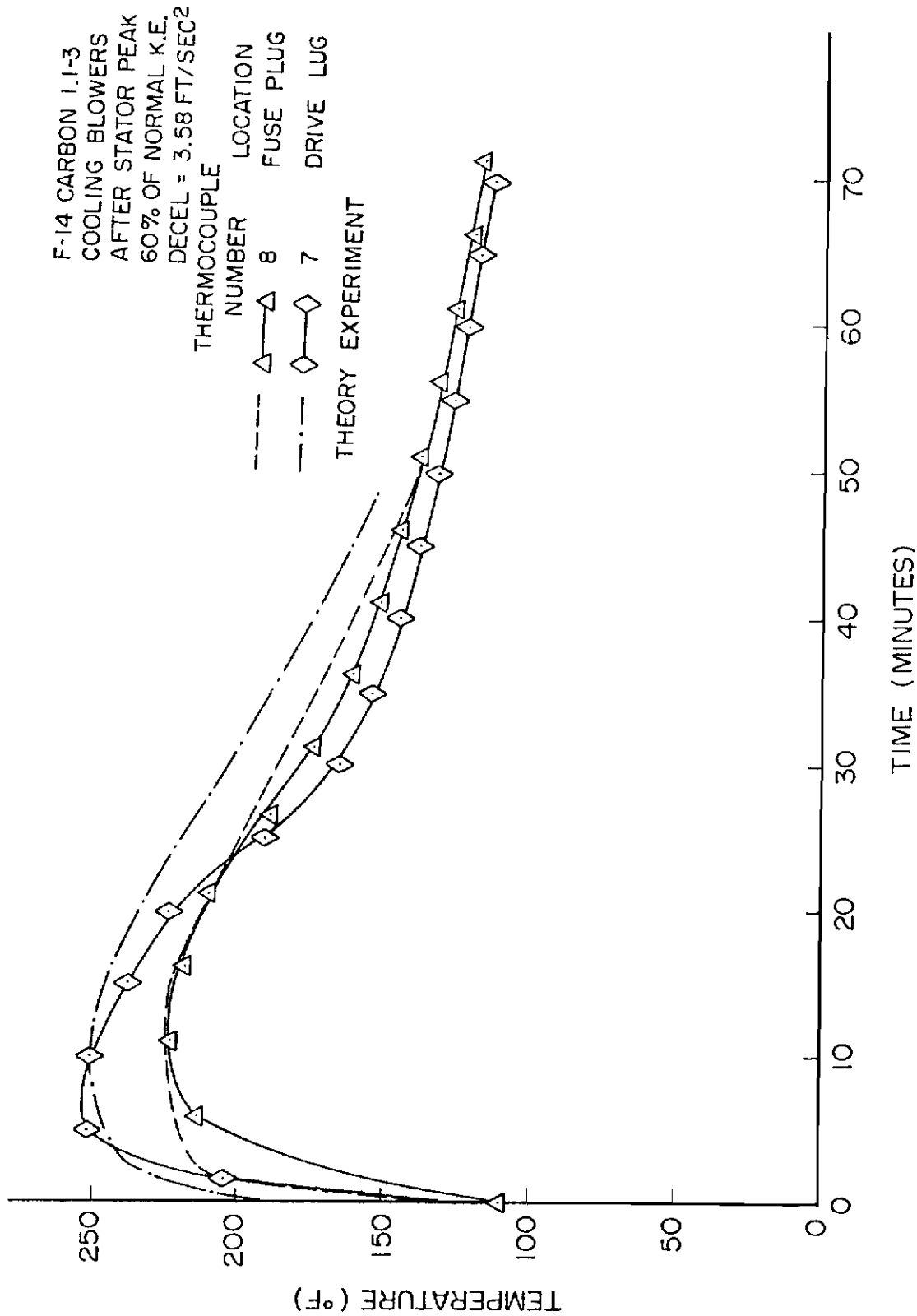


Figure 88. Temperature vs Time, Fuse Plug - Drive Lug (Test 1.1-3)

F-14 CARBON 4.2-3
NO COOLING BLOWERS
100% OF NORMAL K.E.
DECEL = 6.68 FT/SEC²

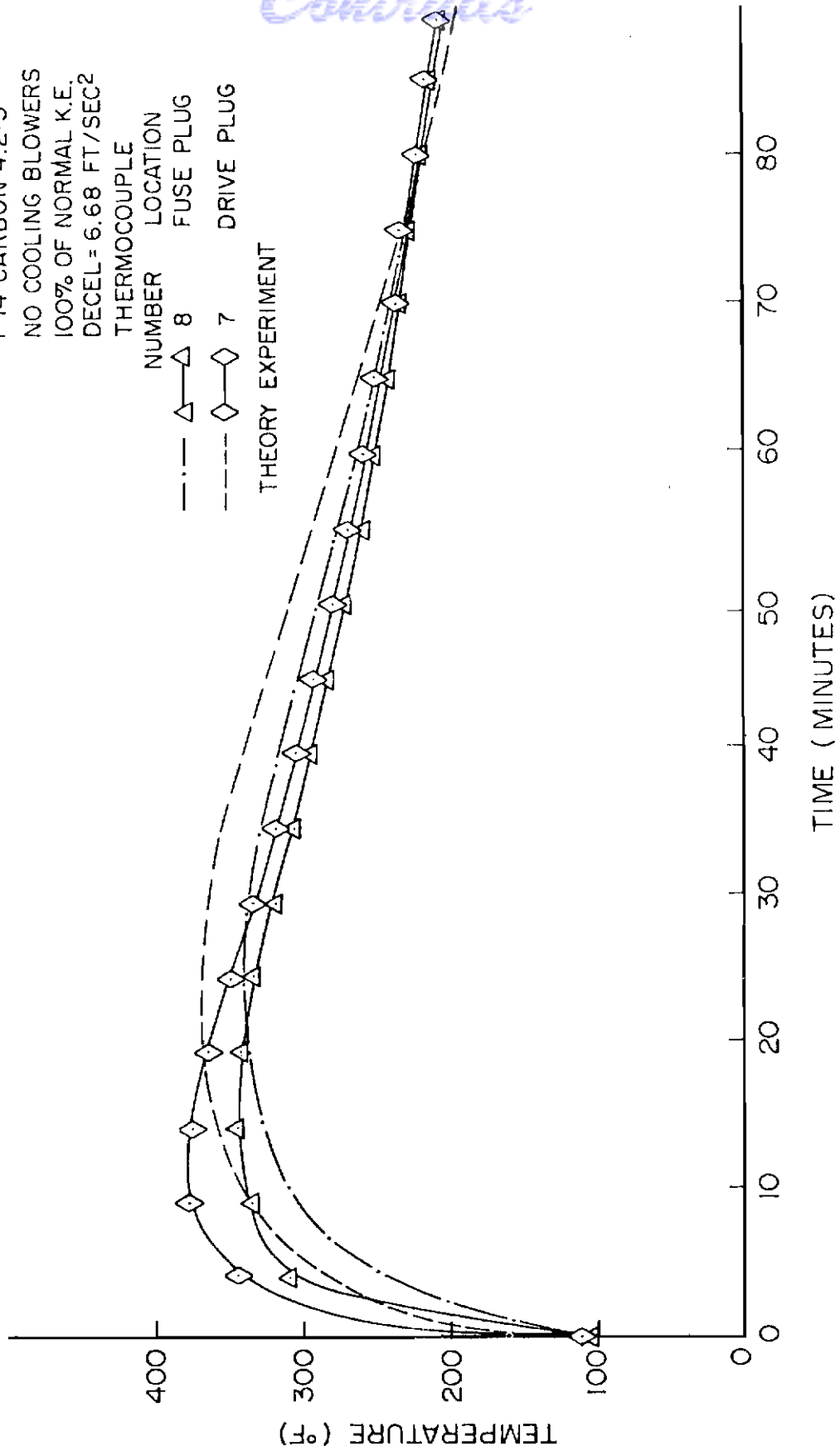


Figure 89. Temperature vs Time, Fuse Plug - Drive Lug (Test 4.2-3)

F-14 BERYLLIUM 7.2-3
 NO COOLING BLOWERS
 60% OF NORMAL K.E.
 DECEL = 5.89 FT/SEC²

THERMOCOUPLE
 NUMBER LOCATION
 8 FUSE PLUG
 7 DRIVE LUG

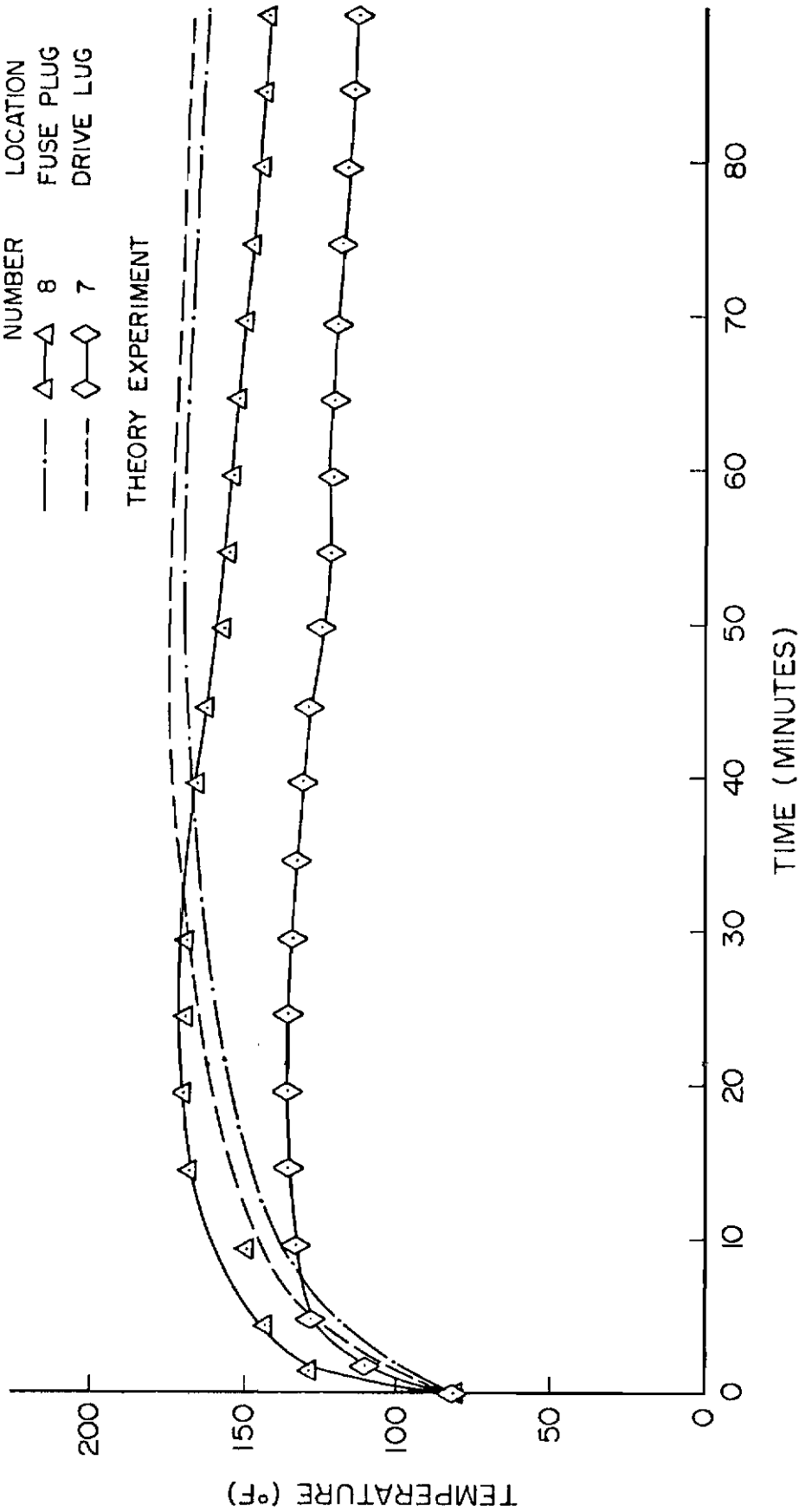


Figure 90. Temperature vs Time, Fuse Plug - Drive Lug (Test 7.2-3)

F-14 BERYLLIUM 8.1-2
COOLING BLOWERS
100% OF NORMAL K.E.
DECEL = 2.19 FT/SEC²

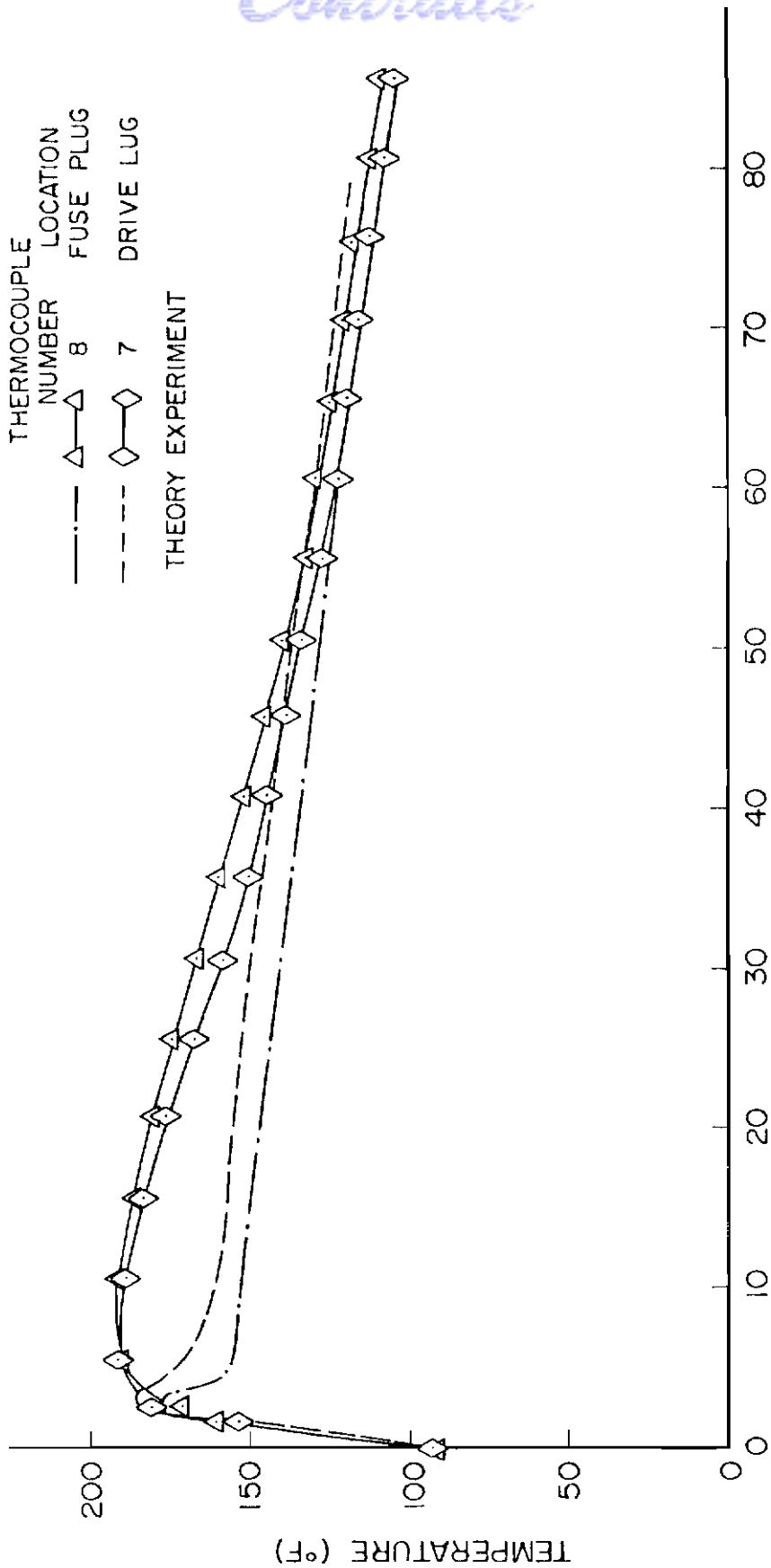


Figure 91. Temperature vs Time, Fuse Plug - Drive Lug (Test 8.1-2)

Contrails

89, the general shape of the predicted curves is the same as experiment. The maximum peak temperature difference from theory to experiment is less than 2%. The beryllium predictions, Figures 90 and 91, are not as close to experiment as are the carbon. One contributor to this fact is that the beryllium heat sink is not modeled, as exactly as is the carbon heat sink. The actual mass and volume of the beryllium was modeled, but the holes for the wear and attachment and other holes to allow for expansion were not modeled. Thus the fuse plug is within 7% of experiment while for the case in Figure 90, the drive lug is 29% higher than experiment. In three of the four figures shown, the drive lug predicted temperature is within 2% of the experiment.

The relation between the 2-D predictions for temperature in the bead seat and contained air is shown for four cases in Figures 92 through 95. Figures 92 and 93 are for carbon while Figures 94 and 95 are for beryllium. The bead seat peak temperature is within about 8% for three out of four cases and is 16% off for the fourth case, Figure 92. The contained air temperature is the node farthest from the work input and this fact helps explain why in three out of the four cases considered the predicted peak temperature is between 14% and 35% different from experiment. Another inaccuracy in the prediction of temperature within the contained air is that the interaction with the portion of the tire adjacent to the flywheel is neglected. The free convection effect of the hotter air rising within the tire cavity is also neglected.

As a summary of the comparison between experiment and the 2-D theory peak temperatures, Table 10 gives the percent variation of the

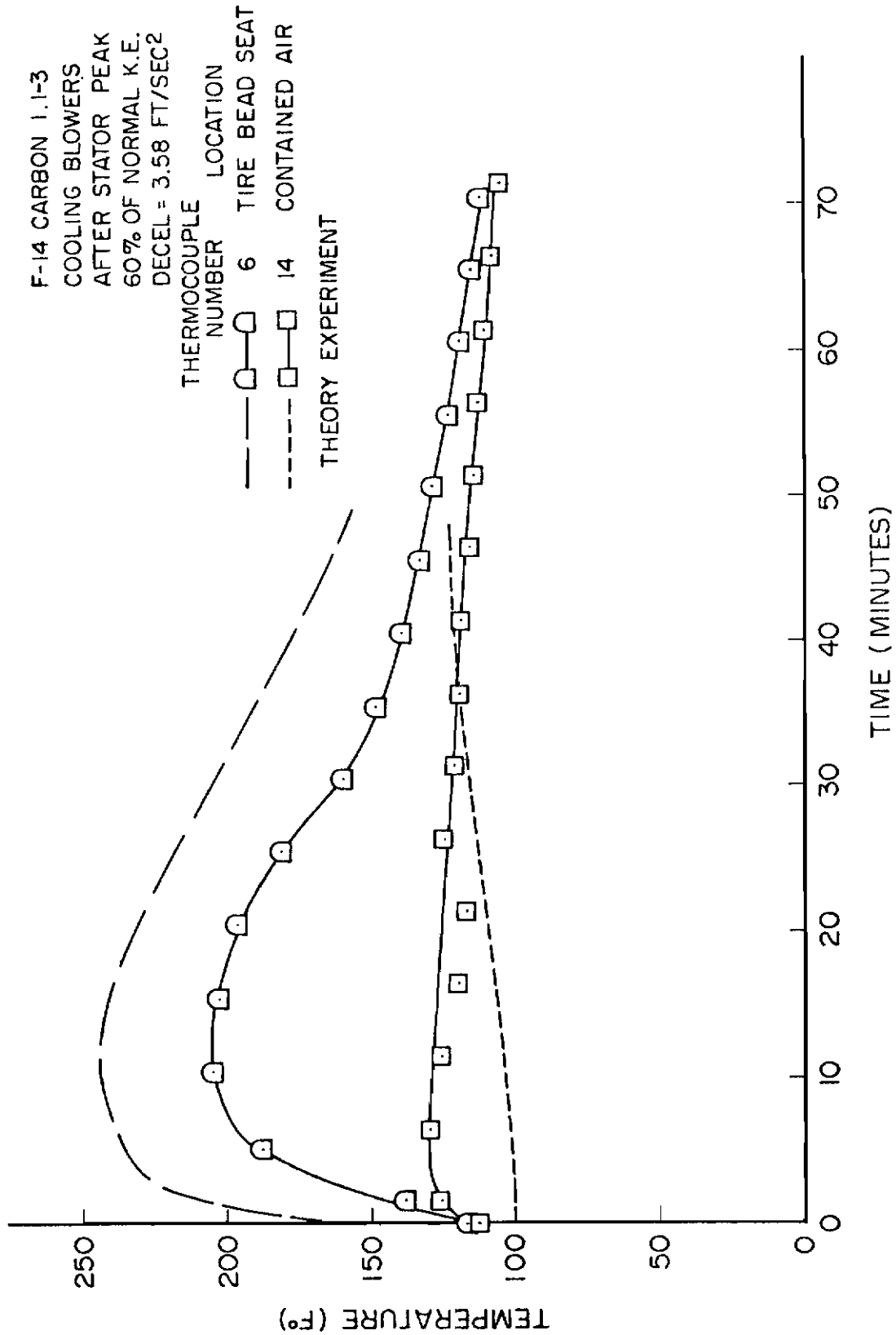


Figure 92. Temperature vs Time, Bead Seat - Contained Air (Test 1.1-3)

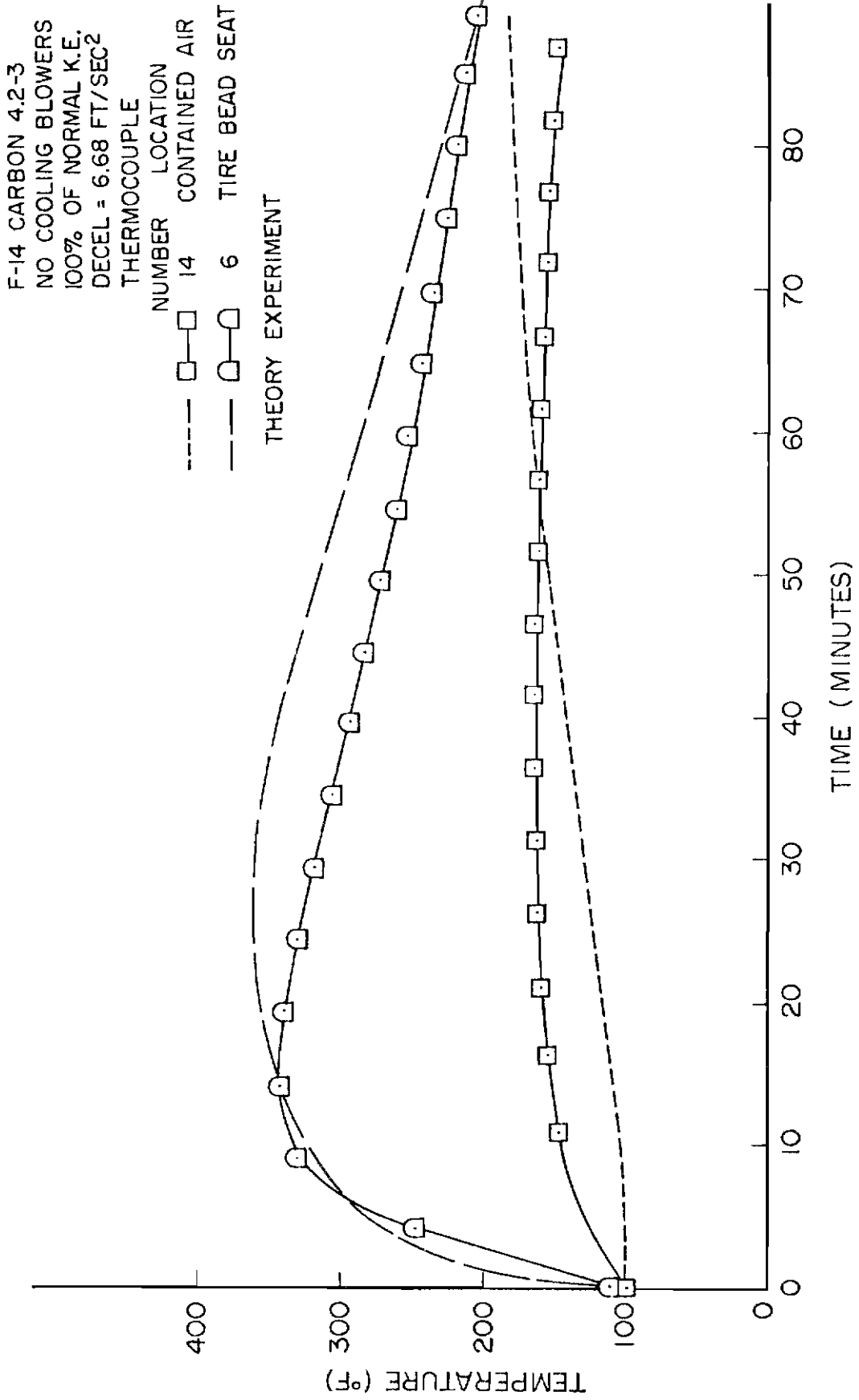


Figure 93. Temperature vs Time, Bead Seat - Contained Air (Test 4.2-3)

F-14 BERYLLIUM 7.2-3
NO COOLING BLOWERS
60% OF NORMAL K.E.
DECEL = 5.89 FT/SEC²
THERMOCOUPLE
NUMBER LOCATION

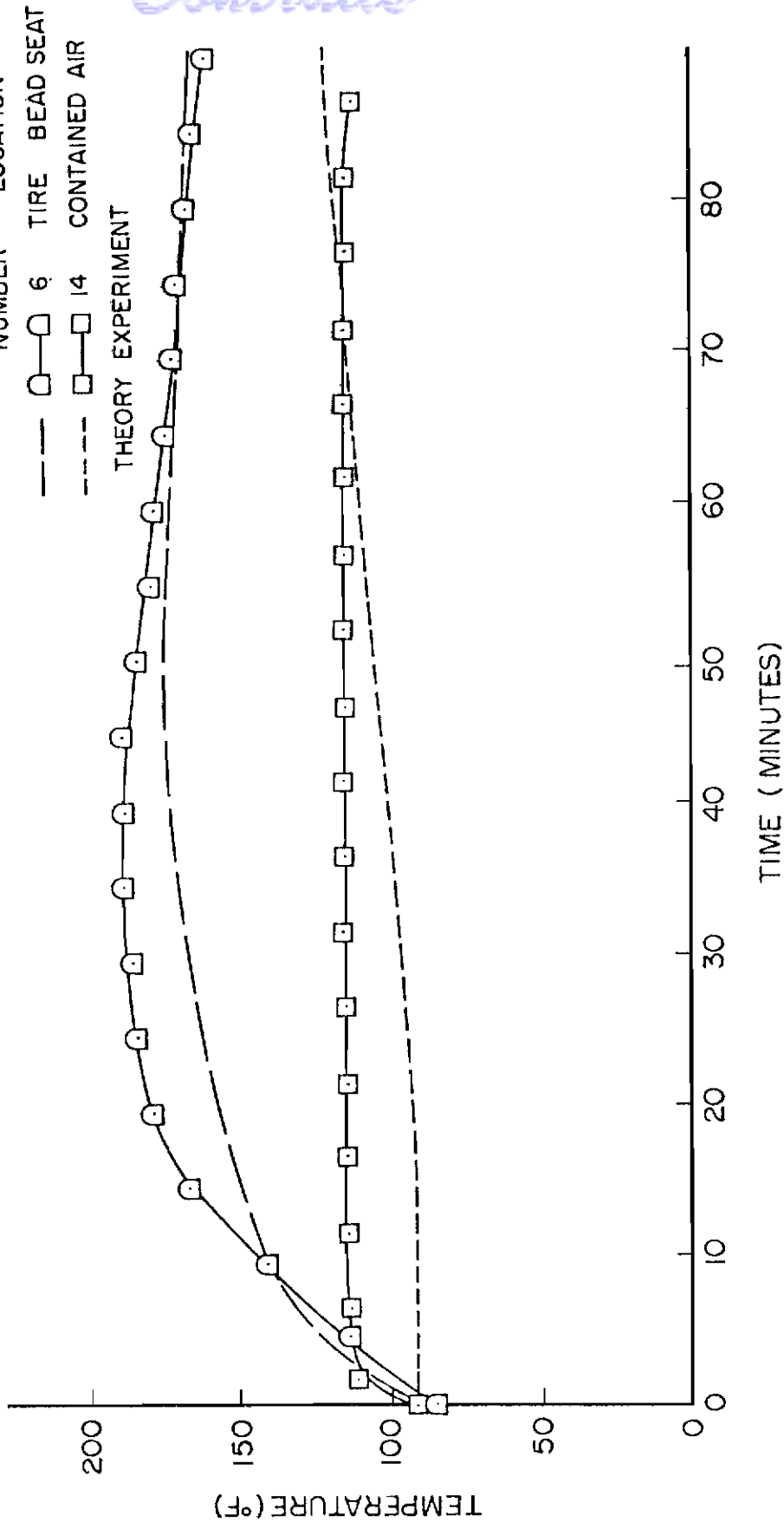


Figure 94. Temperature vs Time, Bead Seat - Contained Air (Test 7.2-3)

F-14 BERYLLIUM 8.1-2
COOLING BLOWERS
100% OF NORMAL K.E.
DECEL = 2.19 FT/SEC²
THERMOCOUPLE

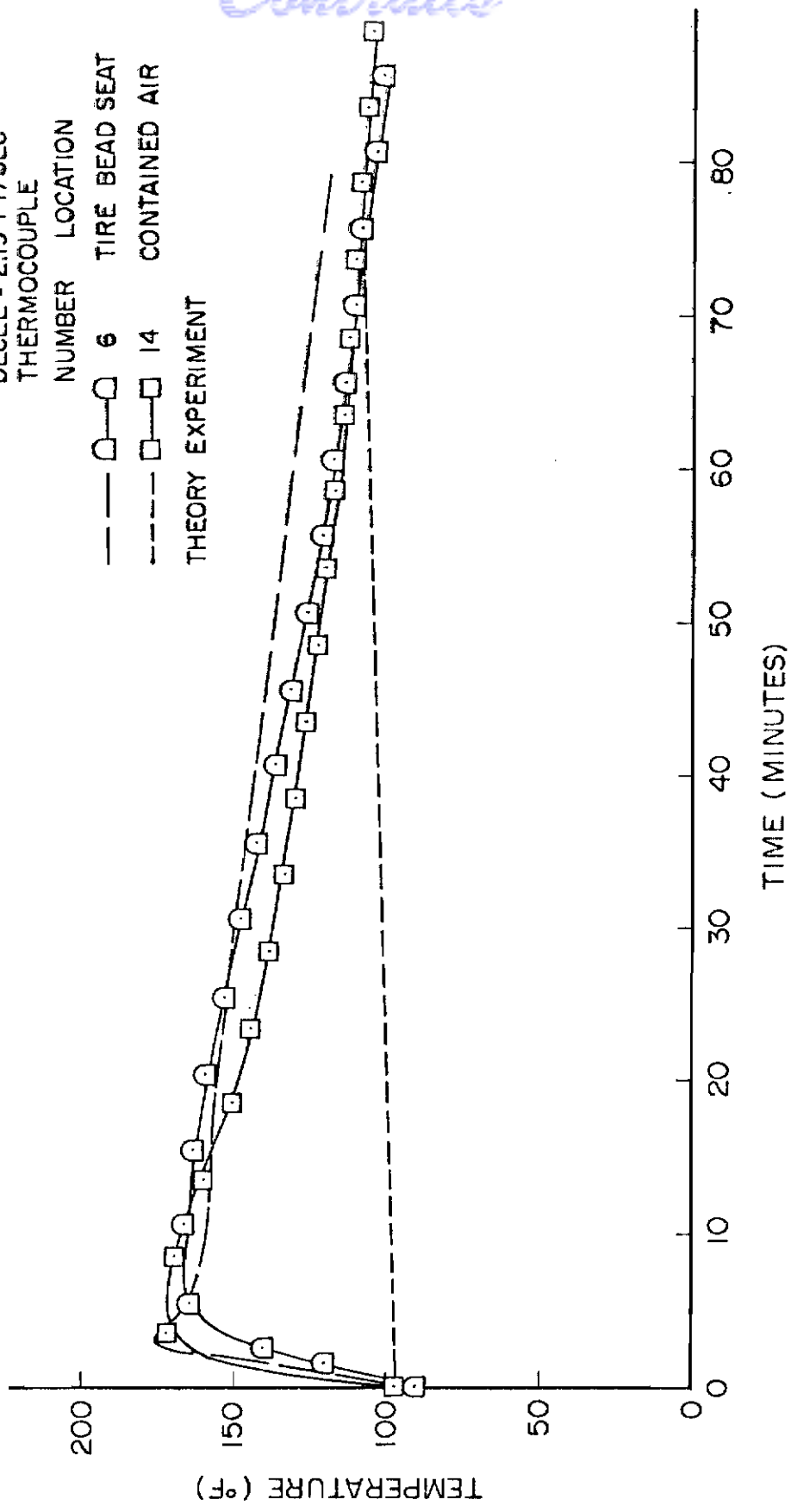


Figure 95. Temperature vs Time, Bead Seat - Contained Air (Test 8.1-2)

Contrails

2-D model from the experimental peak values. The six locations at which temperature was predicted are listed in order of expected accuracy beginning with the most accurate. As can be seen in Table 10, three out of four variations in the first five lines are less than 10%. Other than the contained air variation, only two of the 20 variation entries are substantially greater than 10%.

TABLE 10
EXPERIMENT VS THEORY PEAK TEMPERATURE COMPARISON*

Location	Stop 1.1-3	Stop 4.2-3	Stop 7.2-3	Stop 8.1-2
Stator Axial Centerline	4.9	.9	-2.2	7.9
Torque Tube	- 5.9	4.5	-10.5	9.6
Fuse Plug	1.3	.4	-1.2	-6.8
Drive Lug	-.8	-1.6	28.9	1.6
Bead Seat	16.2	6.8	-8.4	6.7
Contained Air	-5.4	14.2	14.8	-35.

*Table values are percent variation of the 2-D model from experimental peak values.

Two areas for which plots are not shown are in the hydraulic fluid location and in the axial direction from disc to disc. The theoretical model has the capability to predict the brake housing temperature which is not dramatically different from the fluid temperature but the capability to predict specifically the fluid temperature does not exist. This capability would require a more sophisticated model in the housing/fluid area and could require a specific model for each brake

simulated. On the other hand, the two-dimensional complete brake model does contain the capability of predicting the axial temperature variation from disc to disc. Although the capability exists, it was noted that the variation from stator to stator or from rotor to rotor was not predicted by the model. This phenomenon is not considered very important for this four rotor brake, since, of the ten temperature versus axial position plots in Appendix G, only one shows a definite axial temperature gradient and that is less than a 20% gradient through seven brake discs.

Conclusions

1. The one-dimensional axial model predicts temperatures up to 31% higher than experiment and no radial temperature gradient can be determined. No cooling exists and thus no cooldown curve could be predicted.
2. The one-dimensional radial model predicts temperatures up to 16% higher than experiment and no axial temperature gradient can be determined. The cooling curve is close to experiment.
3. Contact resistance at the rotor/stator interface produces a minimal effect in surface temperature difference, rotor to stator, even when 10 times the measured contact resistance is used.
4. The two-dimensional model predicted disc peak temperatures within less than 5% of experiment in three out of four cases, with the fourth case less than 8%.

Contrails

5. For brake discs with wear pads, it is important to explicitly include the wear pad in the thermal analysis and to include the contact resistance between the wear pad and the disc heat sink material.

6. In a thermal analysis it is necessary to use the variable torque versus time curve in lieu of an average torque curve. Failure to do this can result in deviations in the peak temperature of about 7% in carbon and about 23% in beryllium.

7. The three-dimensional program shows a circumferential temperature gradient of about 7% for carbon and about 14% for beryllium. It is not recommended that each disc of the entire brake be modeled in three directions since two-dimensional disc analysis is close to experiment and since computer time and storage dramatically increase with addition of the third dimension. For the same rotor/stator pair analysis section, 48 nodes are required for the two-dimensional analysis and 228 nodes are required for the three-dimensional analysis. If the exact temperatures and gradients are required at keyways, the use of the three-dimensional model for one rotor/stator becomes necessary.

8. Two-dimensional analysis of a rotor/stator pair gives good agreement with experiment as far as disc temperature, including cool-down, is concerned. A variable convective/radiative heat transfer coefficient is used in this case and compensates for the lack of heat conduction from the discs.

Contrails

9. A two-dimensional analysis of the stators, rotors, torque tube, fuse plug, drive lug, bead seat and contained air gives good (within 10%) correlation with experiment in most cases. A constant convective/radiative heat transfer coefficient is used in this case and does not compensate for the conduction from the discs. This is handled explicitly.

CHAPTER VII

UNIQUENESS AND OVERALL CONCLUSIONS

Uniqueness

The following items are unique to this effort:

1. The theoretical development includes six brake temperature prediction models ranging from one-dimensional to three-dimensional and the computer results are compared between models and to experiment. An extensive development such as this is not reported in the literature.
2. The thermal analysis includes caliper as well as multi-disc developments and thus is applicable to any vehicle employing disc type brakes (i.e., car, truck, aircraft, bus, etc.).
3. Contact resistance is considered not only at the sliding interface between a stator and rotor but also between the wear pads and primary heat sink material.
4. The capability exists not only to predict the temperature within the axial and radial directions of a stator and rotor but also to predict the axial temperature variations from stator to stator and rotor to rotor.
5. The heat transfer coefficient used in the boundary conditions is obtained from experimental data in two ways. The first assumes only convective and radiative heat transfer as the

Conclusions

cooling mechanisms (no conduction), while the second explicitly accounts for the heat conduction leaving a particular node.

6. The thermal conductivity is treated as a variable with temperature as well as with direction. The equations developed, therefore, contain the derivatives of thermal conductivity with respect to temperature and direction.
7. The estimate often made of the fraction of generated heat that flows into a rotor or stator is shown to be unnecessary. The particular fraction is a direct result of the correct application of the first law of thermodynamics and is not an input into the first law equation.
8. The importance of using a variable brake torque input instead of average torque to the computer model is clearly demonstrated and verified by comparison to experimental data.
9. In addition to the theoretical analysis uniqueness, extensive testing was accomplished in the area of thermocouple selection and in the area of full scale multi-disc brakes.

Overall Conclusions

The overall objective of this research is to develop a general model for accurately predicting temperatures within the stators, rotors, and brake housing of a typical disc brake. This objective is accomplished through the systematic development of six brake temperature prediction computer models. The validity of the models is demonstrated through comparison to experimental data collected specifically for this research.

Contrails

Specific conclusions regarding a particular portion of the research can be found on pages 60, 133, and 237. These pertain to the temperature measurement analysis, the theoretical development and the correlation of results chapters, respectively.

CHAPTER VIII

MODEL LIMITATIONS AND RECOMMENDATIONS

Model Limitations

The model selected from the six developed in this research as being the best design tool is the two-dimensional model with the capability of predicting rotor and stator temperatures as well as the surrounding brake hardware temperatures. This model has some limitations and those are listed below:

1. The farther the distance from the heat generation, the less accurate the model becomes. Thus, the predicted contained air temperature deviates from experiment in three out of the four cases considered by 15 to 35%.
2. The axle temperatures are not predicted by this model in that the torque tube/axle and rim/axle interfaces are treated as adiabatic.
3. The equations employed are programmed in such a way that the task of using experimental temperature data as inputs to the program in an attempt to calculate radiation/convection heat transfer coefficients cannot easily be accomplished.
4. The brake housing containing the hydraulic fluid is modeled as a lump of mass with the properties of the metallic housing. Since this area contains cavities of hydraulic fluid, retaining

Contrails

springs and pistons, the model is not as accurate here as in other areas such as the rotors, stators, rim, and torque tube.

5. The model is two-dimensional and thus does not give any information concerning circumferential temperature gradients. (This is obtainable from the three-dimensional model, however.)

Recommendations

The following items are recommended for follow-on efforts:

1. If more accurate information is desired in the brake housing and axle, the model should be modified to contain more nodes in these areas.
2. The present model employs experimentally determined heat transfer coefficients. It would be beneficial to conduct a research program using theoretical techniques to predict these coefficients and subsequently to compare the results to experimentally determined coefficients.
3. In this research, the finite difference numerical solution technique is used along with the Euler time marching technique. This is based on results from a finite difference, finite element, and exact solution to a one-dimensional transient heat transfer problem. Research should be conducted to compare the finite element technique to the finite difference technique in a transient, variable-property heat transfer problem in two and three dimensions. Other time marching techniques should also be employed. Emphasis should

Contrails

be placed on low computer run times, low computer storage, and model accuracy. Efficient computer programming should also be emphasized.

LIST OF REFERENCES

1. Evans, D. J. and Newcomb, T. P., Temperatures Reached in Braking When Thermal Properties of the Drum or Disk Vary in Temperature, *Journal of Mechanical Engineering Science*, v3, n4, Dec 1961, p 315-317.
2. Newcomb, T. P. and El-Sherbiny, Department of Technology, University of Loughborough, England, Liquid Cooled Disk Brakes (Friction Surface Temperature and Performance), *Wear*, v34, n3, Oct 1975, p 311-317.
3. Secrist, D. A. and Hornbeck, R. W., Carnegie-Mellon University, Analysis of Heat Transfer and Fade in Disk Brakes, *Journal of Engineering for Industry*, May 1976.
4. Limpert, Rudolph, Highway Safety Research Institute, Investigations of Thermal Conditions Leading to Surface Rupture of Cast Iron Rotors, SAE Paper 720447, May 22-26, 1972.
5. Hartter, L. L., Schwartz, H. W., and Rhee, S. K., Bendix Research Laboratory, Southfield, Michigan, Evaluating Copper Alloy Brake Disks by Thermal Modelling, SAE Paper 740560, Feb 25 - Mar 1, 1974.
6. Limpert, Rudolph, Temperature and Stress Analysis of Solid-Rotor Disk Brakes, University of Michigan Dissertation, 1972.
7. Rusnak, R. M., Schwartz, H. W., and Coleman, W. P., Bendix Corporation, Comparison by Thermal Analysis of Rotor Alloys for Automobile Disk Brakes, SAE Paper 700137, Jan 12-16, 1970.
8. Dike, G., Lund Technical University, On Optimum Design of Disk Brakes, *Journal of Engineering for Industry*, Aug 1974.
9. Santini, J. J. and Kennedy, F. E., Jr., Watervliet Arsenal, New York, An Experimental Investigation of Surface Temperatures and Wear in Disk Brakes, *Lubrication Engineering*, v31, n8, Aug 1975, p 402-404.
10. Santini, J. J., Kennedy, F. E., Jr., and Ling, F. F., Rensselaer Polytechnic Institute, New York, Effect of Design Parameters on Surface Temperature and Wear in Disk Brakes, NASA-CR-134923, May 1976.

Contrails

11. Schwartz, H. W., Hartter, L. L., Rhee, S. K., and Byers, J. E., Bendix Corporation, Evaluation of Gray Iron Brake Disks for Trucks by Thermal Modeling, SAE Paper 751013, Nov 10-13, 1975.
12. Sinclair, David and Gulick, W. F., The Dual Brake Inertia Dynamometer--A New Tool for Brake Testing, SAE Transactions, 1963, p 253.
13. Morgan, S. and Dennis, R. W., Theoretical Prediction of Disk Brake Temperatures and a Comparison With Experimental Data, SAE Paper 720090, Jan 10-14, 1972.
14. Parker, R. C. and Newcomb, T. P., The Performance and Characteristics of the Disk Brake, SAE Paper 836A, Mar 30-Apr 3, 1964.
15. Anderle, H. T., B. F. Goodrich Engineering Report No. 4062, A Numerical Method for Obtaining Transient Temperatures in the Thickness Direction of Heat Sink Elements, Sep 16, 1970.
16. Claridge, J. S., Dunlop Limited, Design and Simulation of an Aircraft Brake Using a Digital Computer, Aeronautical Journal, v77, n747, Mar 1973, p 136-146.
17. Scaringe, R. P., Ho, T. L., and Peterson, M. B., Rensselaer Polytechnic Institute, New York, The Design of Aircraft Brake Systems Employing Cooling to Increase Brake Life, NASA-CR-134980, Oct 1975.
18. Kennedy, F. E., Wu, J. J., and Ling, F. F., Rensselaer Polytechnic Institute, A Thermal, Thermoelastic, and Wear Analysis of High Energy Disk Brakes, NASA CR-134507, Jan 1974.
19. Mercer, J., USAF, Numerical Calculation of Temperature Distribution in an Aircraft Brake, to be published.
20. Ho, T. L. and Peterson, M. B., Rensselaer Polytechnic Institute, New York, Development of Aircraft Brake Materials, NASA-CR-134663, Mar 1974.
21. Peterson, M. B. and Ho, T. L., Rensselaer Polytechnic Institute, New York, Consideration of Materials for Aircraft Brakes, NASA-CR-121116, Apr 1972.
22. Ho, T. L., Kennedy, F. E., and Peterson, M. B., Evaluation of Materials and Design Modifications for Aircraft Brakes, NASA-CR-134896, Jan 1975.
23. Wagner, P. M., Evaluation of the Advanced Harrier Structural Carbon Heat Sink Brake, Air Force Flight Dynamics Laboratory TM-75-44, Mar 1975.

Contrails

24. Bender, J. R. and Han, C. P., Service Temperatures of Bendix Wheels and Brakes, Hill AFB Contract F42600-70-C-1301, Mar 1971.
25. Brewer, Jerry D., Experimental Investigation of Brake Characteristics Conducive to Strut Chatter, Air Force Institute of Technology Masters Thesis, GAW-MC74-2, AD780505, 1974.
26. Donaldson, J. O., Stocks, B. B., Teter, R. D., and Rebholz, M. J., Thermal Structural Analysis of F-14 Beryllium Brake Disks, Lockheed Missile and Space Company Report D128119, 31 Mar 1970.
27. Lee, Tom, Thermal and Stress Analysis of Ventilated Disk Brakes, UCLA Dissertation, 1974.
28. Nemeth, J. D. and Wieter, J. J., Computer Time-Temperature Study of Aircraft Wheel and Brake Components, Goodyear Aerospace Corporation, Hill AFB Contract F42600-71-C-1519, 2 Feb 1972.
29. Stout, Gilbert T., Development of Design Criteria for High Temperature Wheel, Brake, Tire and Related Bearings, Bendix Corporation, ASD-TDR-63-121, Nov 1963.
30. Arpaci, Vedat S., Conduction Heat Transfer, Addison-Wesley Publishing Company, 1966.
31. Carslaw, H. S. and Jaeger, J. C., Conduction of Heat in Solids, Oxford University Press, Second Edition, 1959.
32. Benedict, R. P., Fundamentals of Temperature, Pressure and Flow Measurements, John Wiley and Sons, Inc., 1969.
33. Kreith, Frank, Principles of Heat Transfer, 3rd Edition, Intext Educational Publishers, 1976.
34. Myers, Glen E., Analytical Methods in Conduction Heat Transfer, McGraw-Hill, 1971.
35. Lemmon, E. C. and Heaton, H. S., Accuracy Stability and Oscillation Characteristics of Finite Element Methods for Solving the Heat Conduction Equation, ASME Paper 69-WA/HT-35, 1969.
36. Huebner, Kenneth H., The Finite Element Method for Engineers, John Wiley and Sons, Inc., 1975.
37. Emery, A. F. and Carson, W. W., An Evaluation of the Use of the Finite Element Method in the Computation of Temperature, Journal of Heat Transfer, May 1971.
38. Schaaf, S. A., On the Superposition of a Heat Source and Contact Resistance, Quarterly of Applied Mathematics, Vol 5, 1947, p 107-111.

Contrails

39. Shlykov, Yu P. and Ganin, Ye A., Thermal Resistance of Metallic Contacts, International Journal of Heat and Mass Transfer, Vol 7, 1964, P 921-929.
40. Fontenot, J. E., Jr., Thermal Conductance of Contacts and Joints, Boeing Report No. D5-12206, Sep 2, 1964, p 43.

Contrails

APPENDIX A

PROGRAM LISTING FOR ONE-DIMENSIONAL
TRANSIENT TEMPERATURE
DISTRIBUTION OF
CHAPTER III

```

PROGRAM TA(INPUT,OUTPUT)
DIMENSION TT(10),TN(10)
PRINT 10
FORMAT(' Y TEMP(ACT) TIME(ACT) TEMP(ND)
6TIME(ND) ')
TP=1170.
C=.002
DT=.015625
TS=7.27
TS1=29.5
DY=.25
TO=119.
DO 1 I=1,10
TN(I)=0.
TT(I)=0.
K=0
J=0
K=K+1
J=J+1
IF(J.EQ.65) J=1
T=K*DT
TN(1)=T*(TP-T0)/(TS*T0)
DO 2 I=2,4
TN(I)=TT(I)*(1.-2.*DT/(DY*DY))+(TT(I+1)+TT(I-1))*DT/
6(DY*DY)
TN(5)=TN(4)/(1.+C)
DO 7 I=1,5
Y=(I-1)*DY
TIMEA=K*DT*TS1/TS
TEMPA=TN(I)*T0+T0
TIMEN=K*DT
TEMPN=TN(I)

```



```
7 IF (J.EQ.64) PRINT 9,Y,TEMPA,TIMEA,TEMPN,TIMEN  
9 FORMAT (5G12.6)  
6 DO 6 I=1,5  
TT(I)=TN(I)  
IF (TIMEN.LT.TS) GO TO 14  
STOP  
END  
..
```

APPENDIX B

PROGRAM LISTING FOR TWO-DIMENSIONAL
TRANSIENT TEMPERATURE
DISTRIBUTION OF
CHAPTER III

```

PROGRAM FDA (INPUT,OUTPUT)
DIMENSION T(10,10),TD(10,10)
PRINT 9
FORMAT( ' X TB TIME(ACT) TEMP(ACT) TIME(ND)
6TEMP(ND)
A=3.571
T0=119.
TP=1170.
TS=75.5
TS1=29.5
DX=.25
DY=.25
DT=.002
DO 2 I=1,5
DO 3 J=1,5
T(I,J)=0.
TD(I,J)=0.
CONTINUE
CONTINUE
K=0
K=K+1
JI=JI+1
IF(JI.EQ.2501) JI=1
DO 12 I=2,4
DO 13 J=2,4
TB=KXDX(TP-T0)/(TO*TS)
BOUNDARY CONDITIONS
T(2,5)=TB-27.5/TO
T(2,1)=T(2,5)
T(3,5)=TB-46.1/TO
T(3,1)=T(3,5)

```

```
T(4,5)=TB-49.9/T0
T(4,1)=T(4,5)
T(1,J)=TB
TB=TB*TO+TO
XT=(DT/(DX*DX))*T(I-1,J)-2.*T(I,J)+T(I+1,J)
YT=(DT*YA/(DY*DY))*T(I,J-1)-2.*T(I,J)+T(I,J+1)
TD(I,J)=T(I,J)+XT+YT
X=(I-1)*DX
TIMEN=K*XDT
TEMPN=TD(I,J)
TIMEA=K*XDT*TS1/TS
TEMPA=TD(I,J)*TO+TO
IF(JI.EQ.2500.AND.J.EQ.3) PRINT10,X,TIMEA,TEMPA,TIMEN,TEMPN,
6TB
10  FORMAT(6G12.6)
13  CONTINUE
12  CONTINUE
DO 114 I=2,4
DO 115 J=2,4
115 T(I,J)=TD(I,J)
CONTINUE
114 CONTINUE
IF(TIMEN.LT.TS) GO TO 14
STOP
END
```

APPENDIX C

PROGRAM LISTING FOR THERMOCOUPLE
BEAD TEMPERATURE ANALYSIS OF
CHAPTER III

```
PROGRAM FDC4(INPUT,OUTPUT)
PRINT 10
FORMAT(' TIME T(BEAD) QR(B/H) QCU(B/H) QCD(B/H)
6T(DESIRED) ')
QCD=0.0
QCU=0.0
QR=0.0
DT=.01
R=.02
TS=29.5
TP=1170.
TO=119.
T=TO
K=0
J=0
K=K+1
J=J+1
IF(J.EQ.301) J=1
TI=K*DT
TD=TO+TI*(TP-TO)/TS
TC=TO+TI*(TP-TO)/TS-14
TA=TC-13.
A=-51.56
IF(TI.LT.2.5)A=0.0
IF(TC.LT.TO)A=0.0
IF(TC.LT.TO)TC=TO
IF(TA.LT.TO)TA=TO
IF(T.GT.TC)PRINT 9, TI, T, QR, QCU, QCD, TA
IF(T.GT.TC)STOP
QCD=AXR XR
QR=1.4958E-10XR XR*(TC+460.)**4-(T+460.)**4)
QCU=.4364XR XR*(TA-T)
```

```
TN=T+(DT/(542.93*RR**3))*QCD+OCU+QR)
IF(J.EQ.300) PRINT 9,TI,TN,QR,OCU,QCD,TA
FORMAT(7G10.4)
T=TN
IF(TI.LT.TS) GO TO 14
STOP
END
```

9

..

APPENDIX D

THERMOCOUPLE CALIBRATION, CALIBRATION
CERTIFICATE, AND CHECKLIST FOR
RUNNING THERMOCOUPLE TESTS
OF CHAPTER III

Contrails

THERMOCOUPLE CALIBRATION

T/C Code	% Deviation At 750°F ³	% Deviation At 1100°F ³	Tests During Which Used ⁴
U. ¹	- .173	+ .054	24, 27
U2	- .08	+ .009	
E1	+ .173	+ .227	18, 19, 23
E2	+ .107	+ .136	
G1	0	- .036	Baseline
G2	+ .12	- .182	29, 30
2	- .413	- .600	
3	- .267	- .618	32, 34
4	- .333	- .682	
5	- .213	- .582	

¹Manufacturer tolerance is $\pm 75\%$ which is $\pm 5.6^\circ\text{F}$ at 750°F and 8.25°F at 1100°F .

²All data using the above thermocouples were corrected using the 750°F calibration point for temperatures below 925°F and using the 1100°F calibration point for temperatures above 925°F .

³A negative/positive deviation means that the deviation must be added/subtracted to/from the thermocouple reading to get the actual temperature.

⁴Thermocouples not used during testing were backup thermocouples.

Contrails

INSTRULAB, INC.
1205 Lamar Street
Dayton, Ohio 45404
513-223-2241

THERMOCOUPLE
CALIBRATION CERTIFICATE

Date 11-16-77
W.O.# 14790
Cust. PO# 04622

Systems Research Labs, Inc.
WPAFB, Bldg. 31, Area B
Dayton, Ohio 45433

CALIBRATION OF TEN (10) TYPE "K" THERMOCOUPLES (SUPPLIED BY SRL)

	750°F		1100°F	
	°F	mV	°F	mV
U1	-1.3	(.030)	+0.6	(.015)
U2	-0.6	(.014)	+0.1	(.002)
E1	+1.3	(.032)	+2.5	(.060)
E2	+0.8	(.018)	+1.5	(.037)
G1	0.0	(.000)	-0.4	(.010)
G2	0.9	(.022)	-2.0	(.048)
2	-3.1	(.075)	-6.6	(.159)
3	-2.0	(.049)	-6.8	(.131)
4	-2.5	(.059)	-7.5	(.180)
5	-1.6	(.038)	-6.4	(.154)

AMBIENT TEMP: 80° ± 5°F RELATIVE HUMIDITY: 45% ± 5%

To find correct temperatures when using above thermocouples, subtract plus (+) deviations and add negative (-) deviations from/to readings obtained.

Accuracy of results:

100 to 1600°F	--	±1.5°F
Above 1600°F	--	±2.5°F

Equipment Used: (All traceable to National Bureau of Standards)

Leeds & Northrup K-3 Potentiometer Ser. No. 1526510
Calibrated 6-2-77
Traceable to NBS Test No. 214726, 215102

Eppley Standard Cell Cat. 100 Ser. No. 841565
Calibrated 5-27-77
Traceable to NBS Test No. 214726, 215102

Contrails

Plat. 10% Rhod. Vs. Plat, Working Standard T/C

Calibrated 10-13-77

Standard Plat. 10% Rhod. Vs. Plat. T/C

Calibrated 10-14-76

Traceable to NBS Test No. 215470

INSTRULAB, INC.

(signed by): Robert A. Dudek

Contrails

PROCEDURE FOR THERMOCOUPLE EXPERIMENT

1. Mount carbon specimen between lamps.
2. Insert thermocouples as required.
3. Turn on main circuit breaker to power panel.
4. Turn on secondary circuit breaker to test machine.
5. Insert ice in thermocouple reference junction container.
6. Plug in lamp power "ready" circuit.
7. Plug in and turn on x-y-y' plotter and time base. Allow to warm up one half hour prior to use.
8. Zero both temperature channels on the plotter.
9. Turn lamp control to full power on the manual setting.
10. Move test machine control lever to left and wait for ready light to activate.
11. Turn on compressor in machine shop.
12. Turn on lamp cooling air making sure not to exceed 12 psig downstream of the regulator.
13. Turn on lamp cooling water until valve is fully open.
14. Energize lamps for about three seconds, then push stop button. This allows the carbon sample to heat to about 150°F so that a constant starting temperature can be reached. Allow baseline thermocouple temperature to reach 100°F.
15. Immediately start time base on x-y-y' plotter and energize lamps until the baseline thermocouple reaches 1500°F.
16. Depress stop button on test machine.
17. Allow plotter to record cooling curves until one sheet of plotter paper is used, then turn off time base and move to new sheet.
18. Change test thermocouples when carbon is sufficiently cool and repeat 14-18 until desired thermocouples are tested.
19. Turn off all equipment, cooling air, cooling water, and the compressor making sure to turn off the cooling air prior to turning off the compressor.

APPENDIX E
RECORDED TEST PARAMETERS
VERSUS TIME FROM
CHAPTER IV

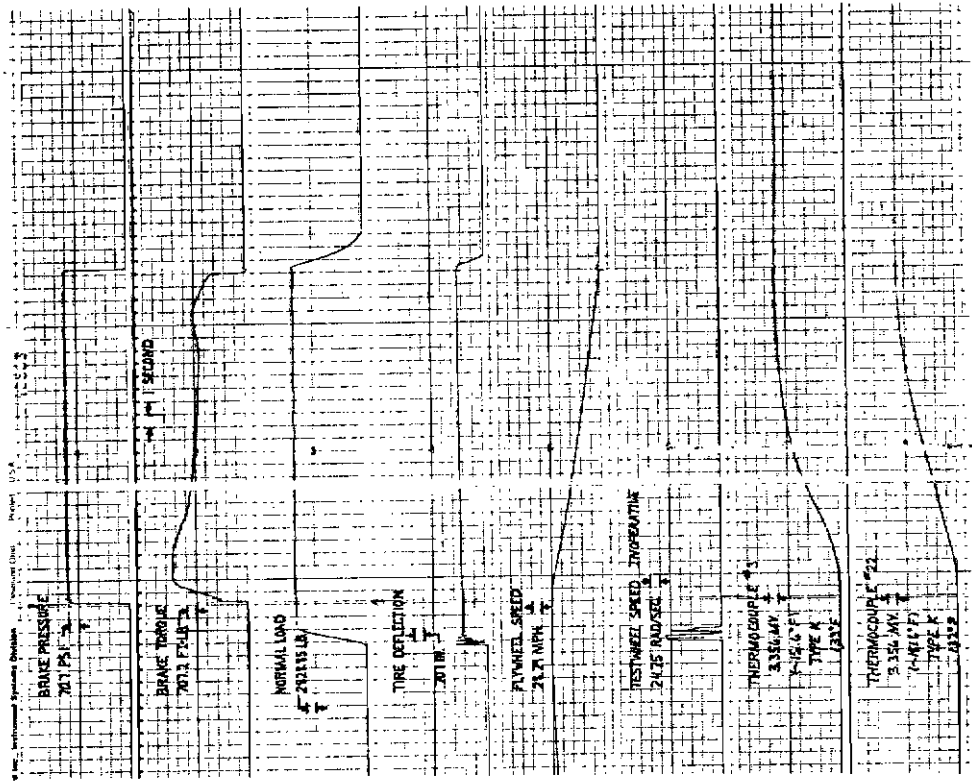


Figure E-2. Test Parameters vs Time (Test 2.1-2)

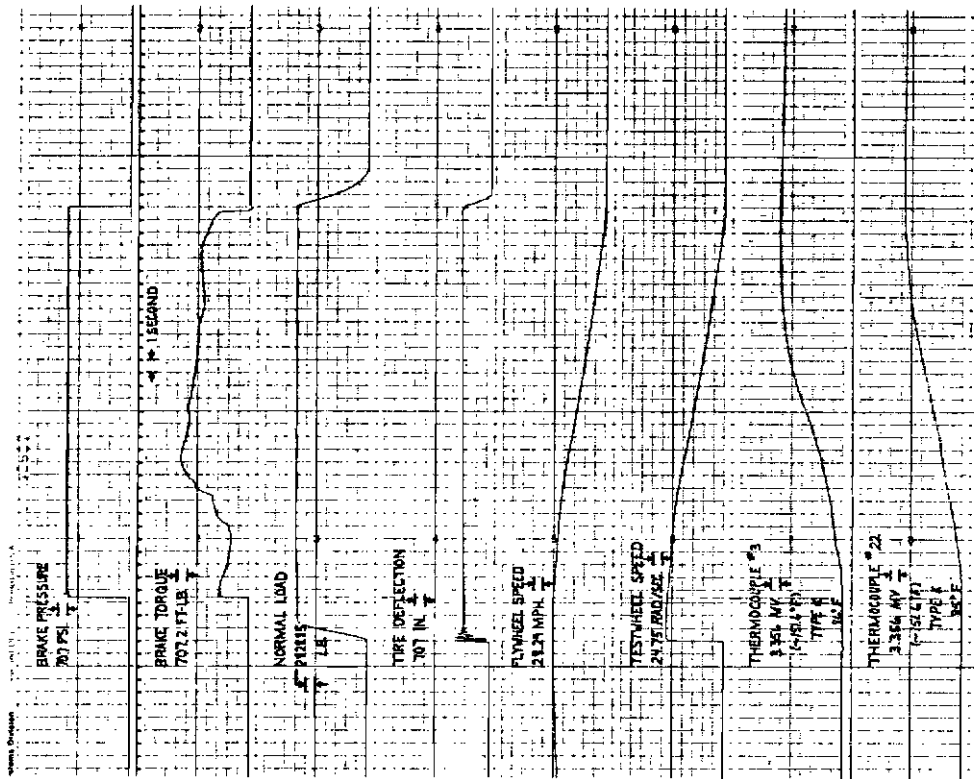


Figure E-3. Test Parameters vs Time (Test 2.2-3)

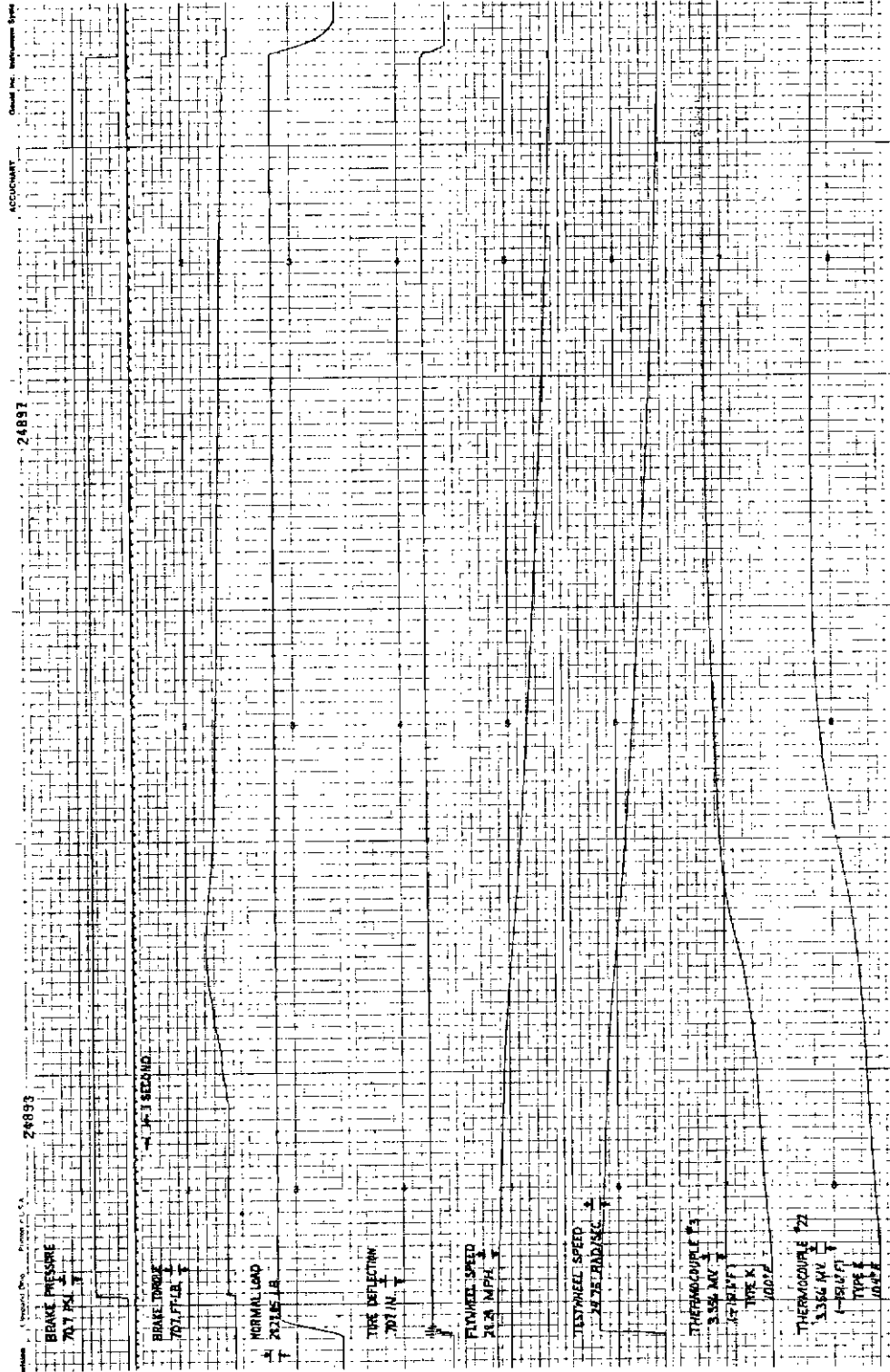


Figure E-4. Test Parameters vs Time (Test 3.1-2)

Controls

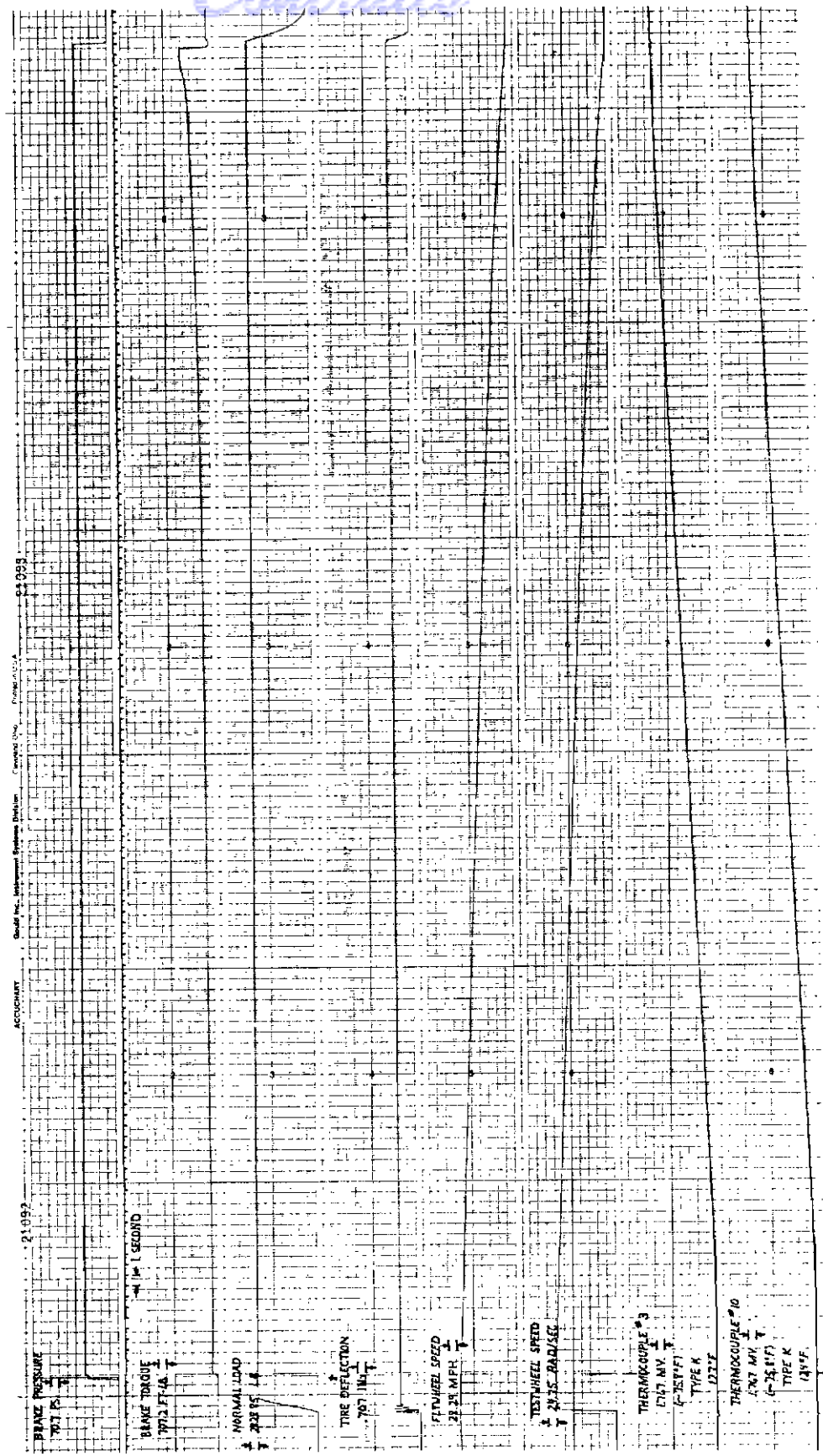


Figure E-6. Test Parameters vs Time (Test 6.1-3)

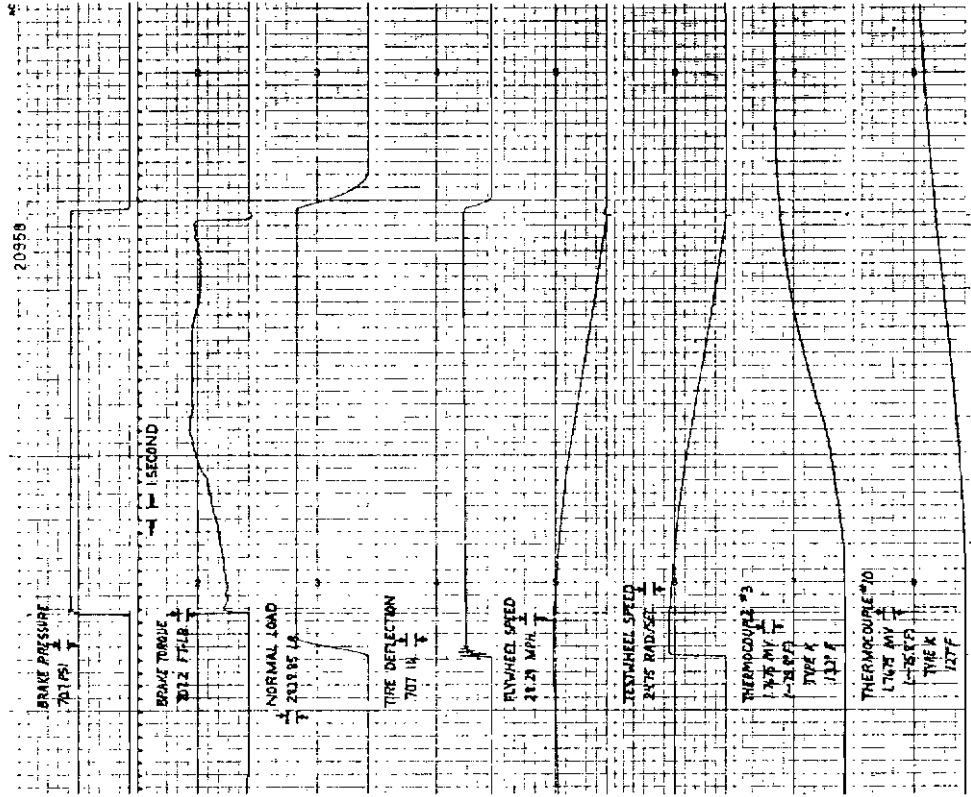


Figure E-7. Test Parameters vs Time (Test 7.1-2)

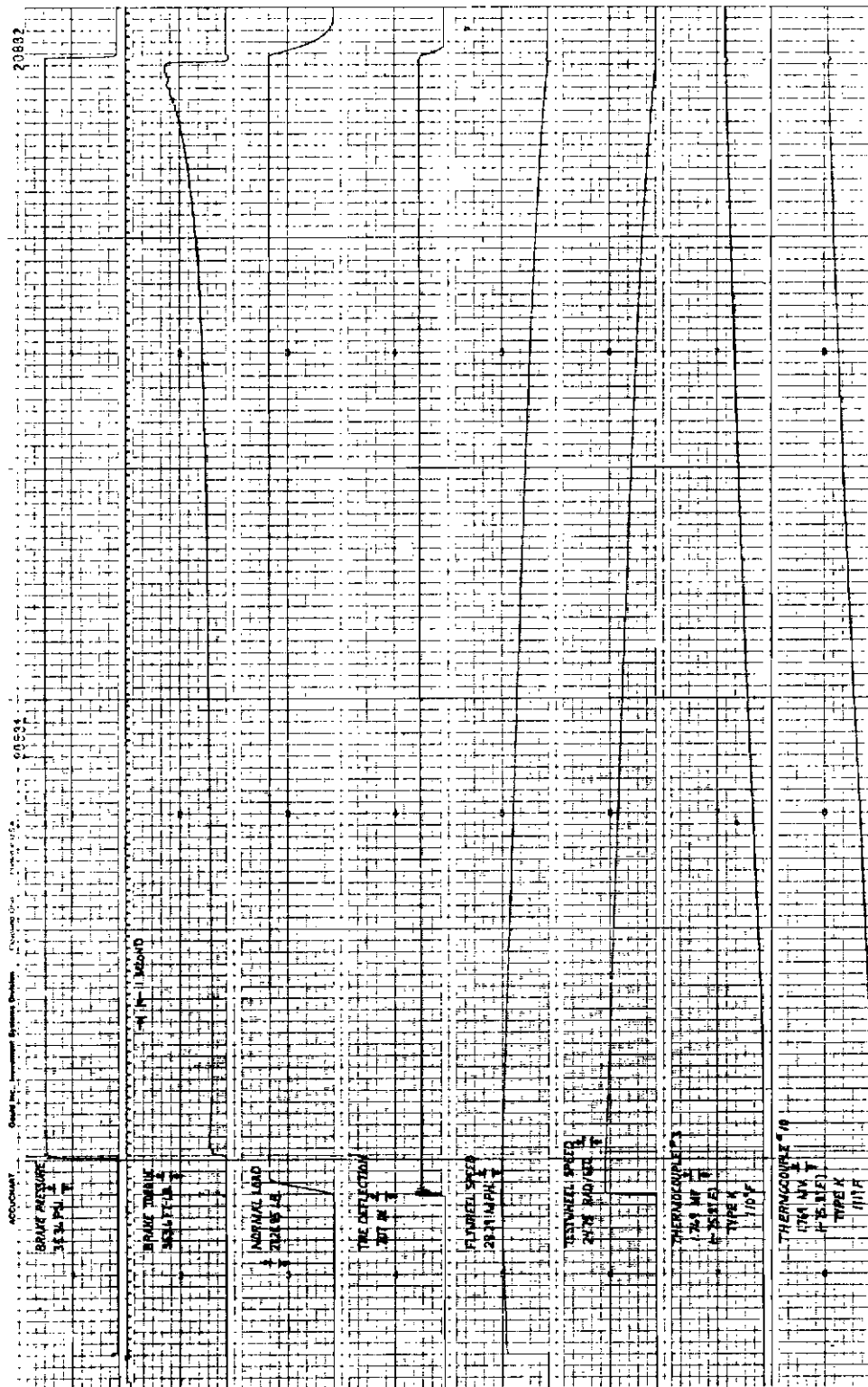


Figure E-9. Test Parameters vs Time (Test 8.1-2)

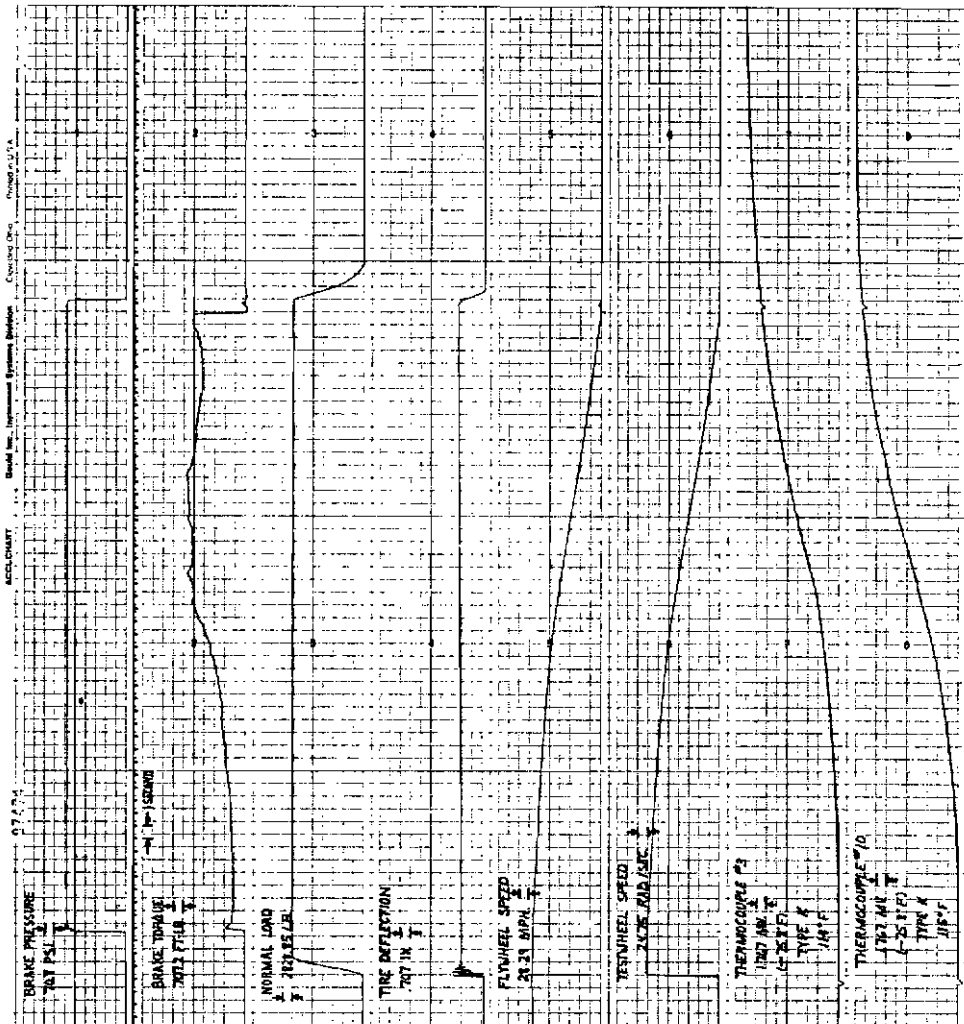


Figure E-10. Test Parameters Vs Time (Test 9.2-2)

APPENDIX F
TEMPERATURE VERSUS TIME PLOTS
FOR STATOR 2, ROTOR 2
AND TORQUE TUBE

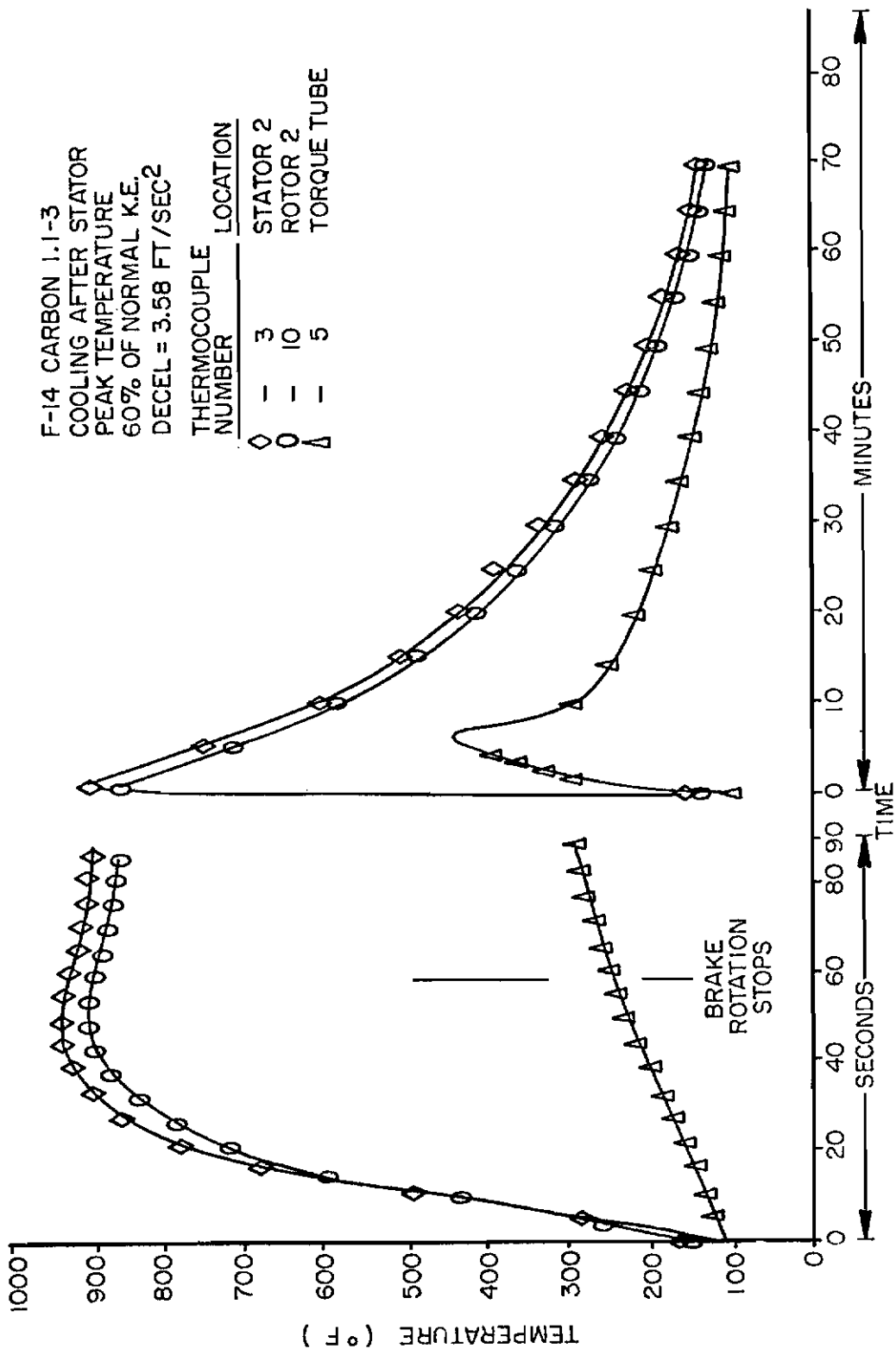


Figure F-1. Temperature vs Time for Stator 2, Rotor, Torque Tube (Test 1.1-3)

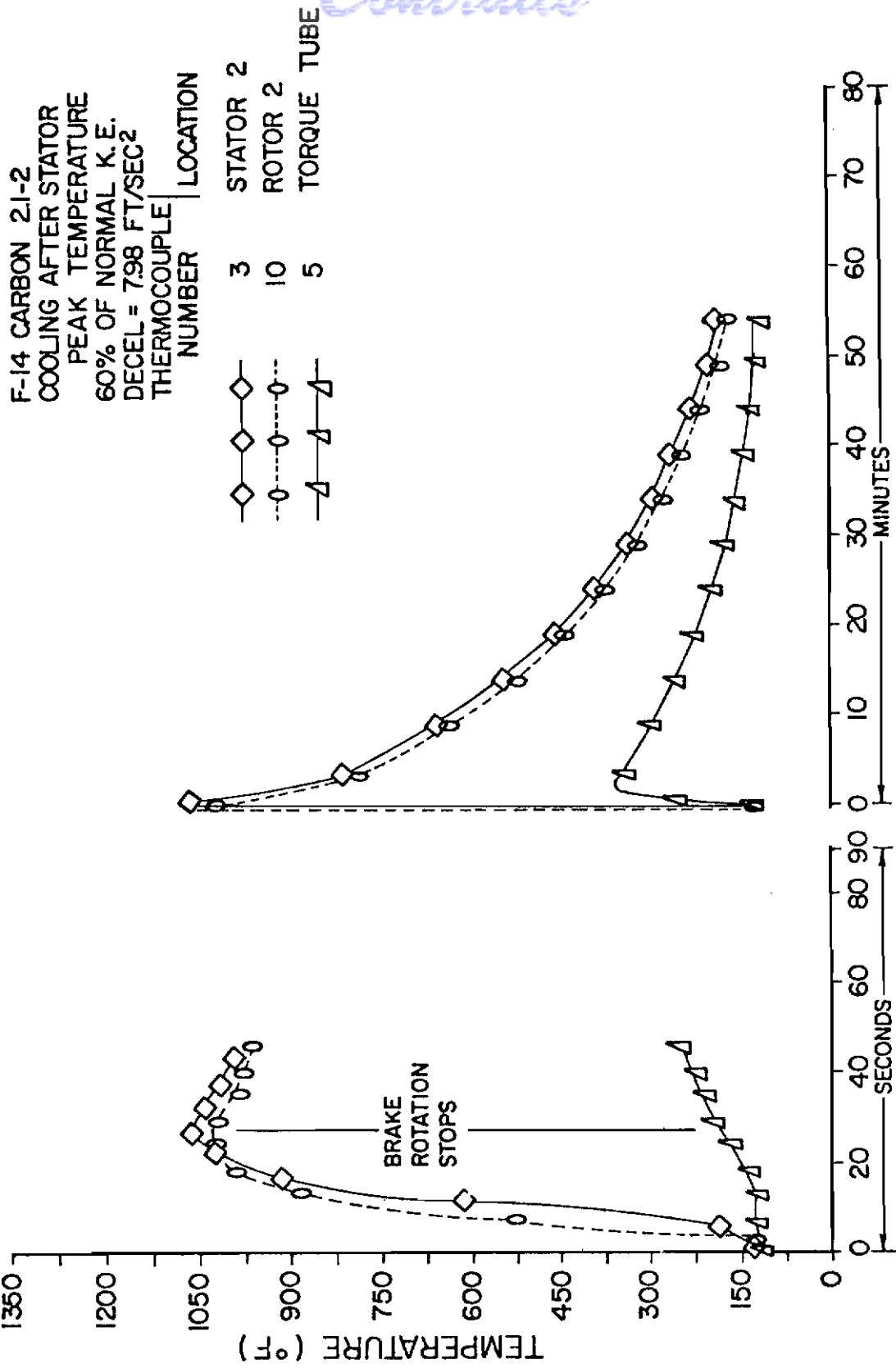


Figure F-2. Temperature vs Time for Stator 2, Rotor 2, Torque Tube (Test 2.1.1-2)

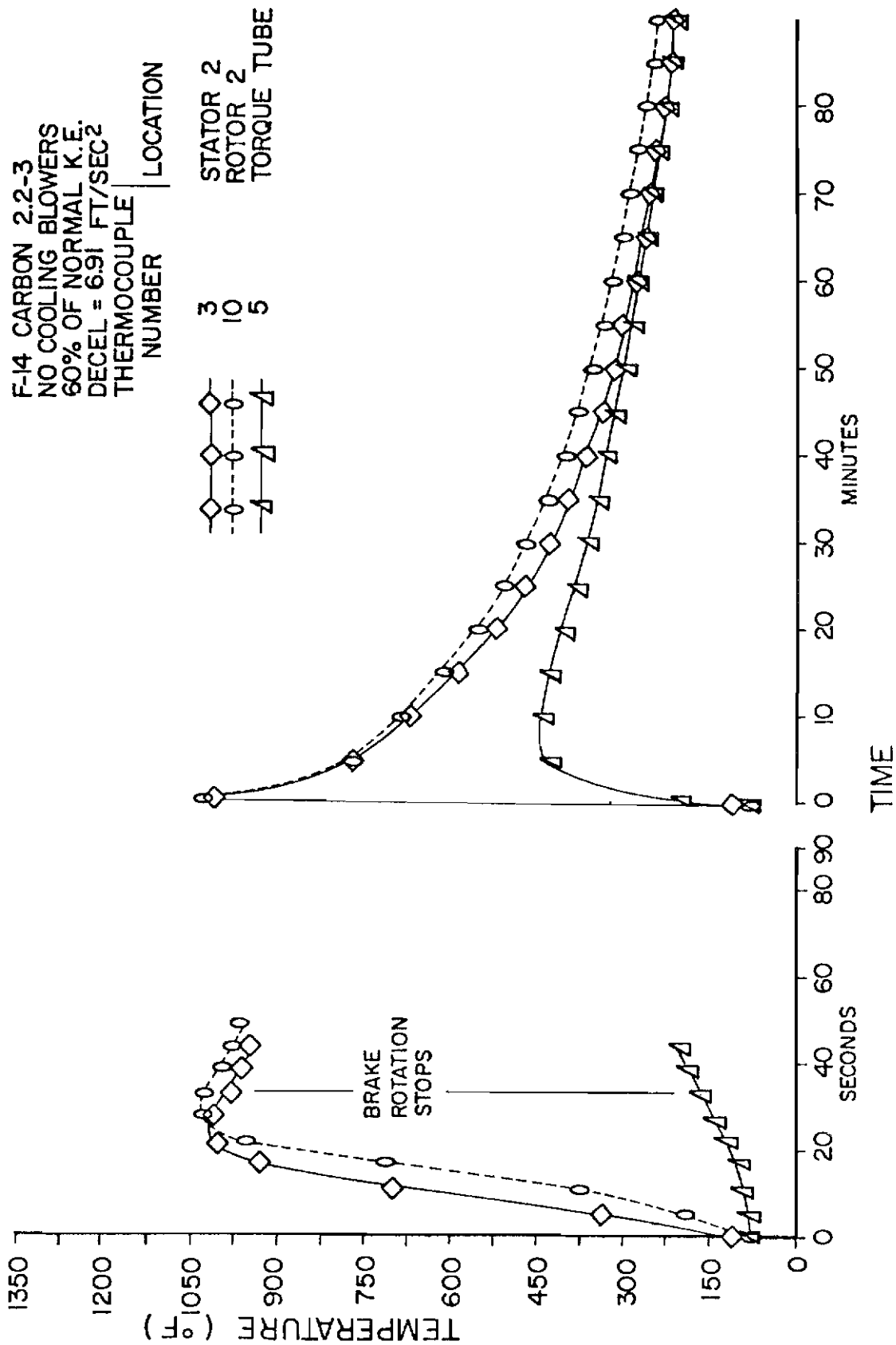


Figure F-3. Temperature vs Time for Stator 2, Rotor 2, Torque Tube (Test 2.2-3)

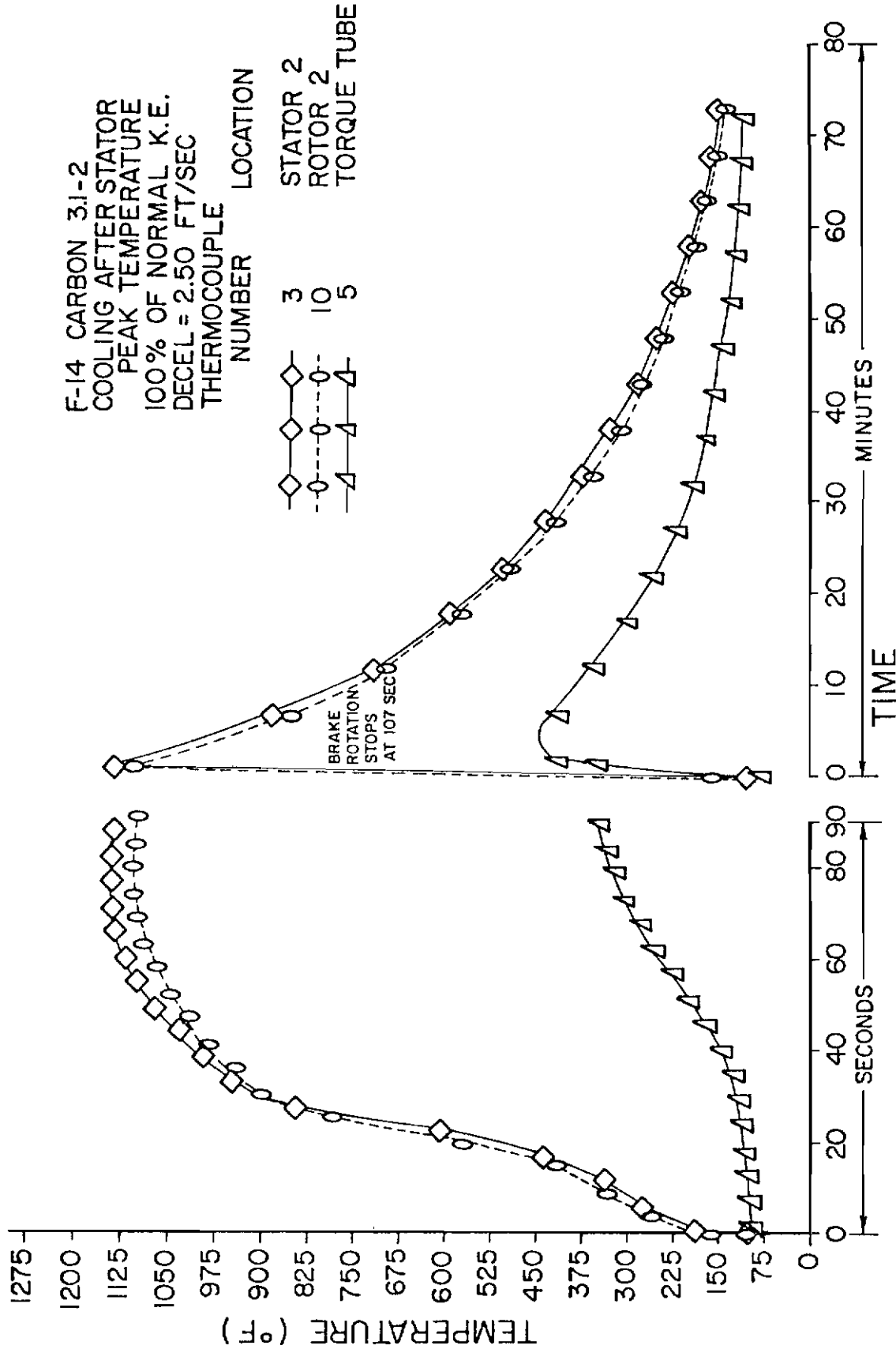


Figure F-4. Temperature vs Time for Stator 2, Rotor 2, Torque Tube (Test 3.1-2)

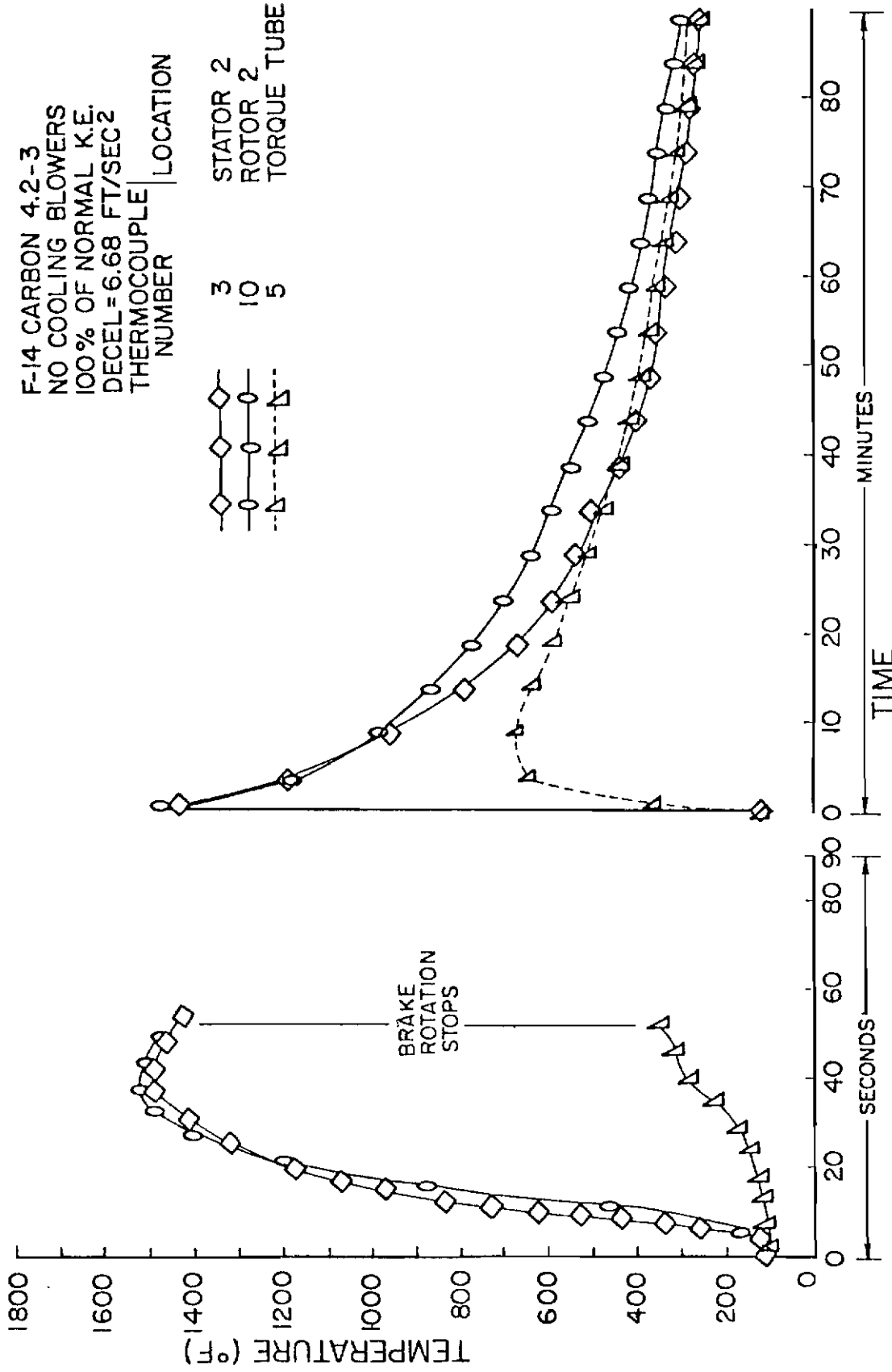


Figure F-5. Temperature vs Time for Stator 2, Rotor 2, Torque Tube (Test 4.2-3)

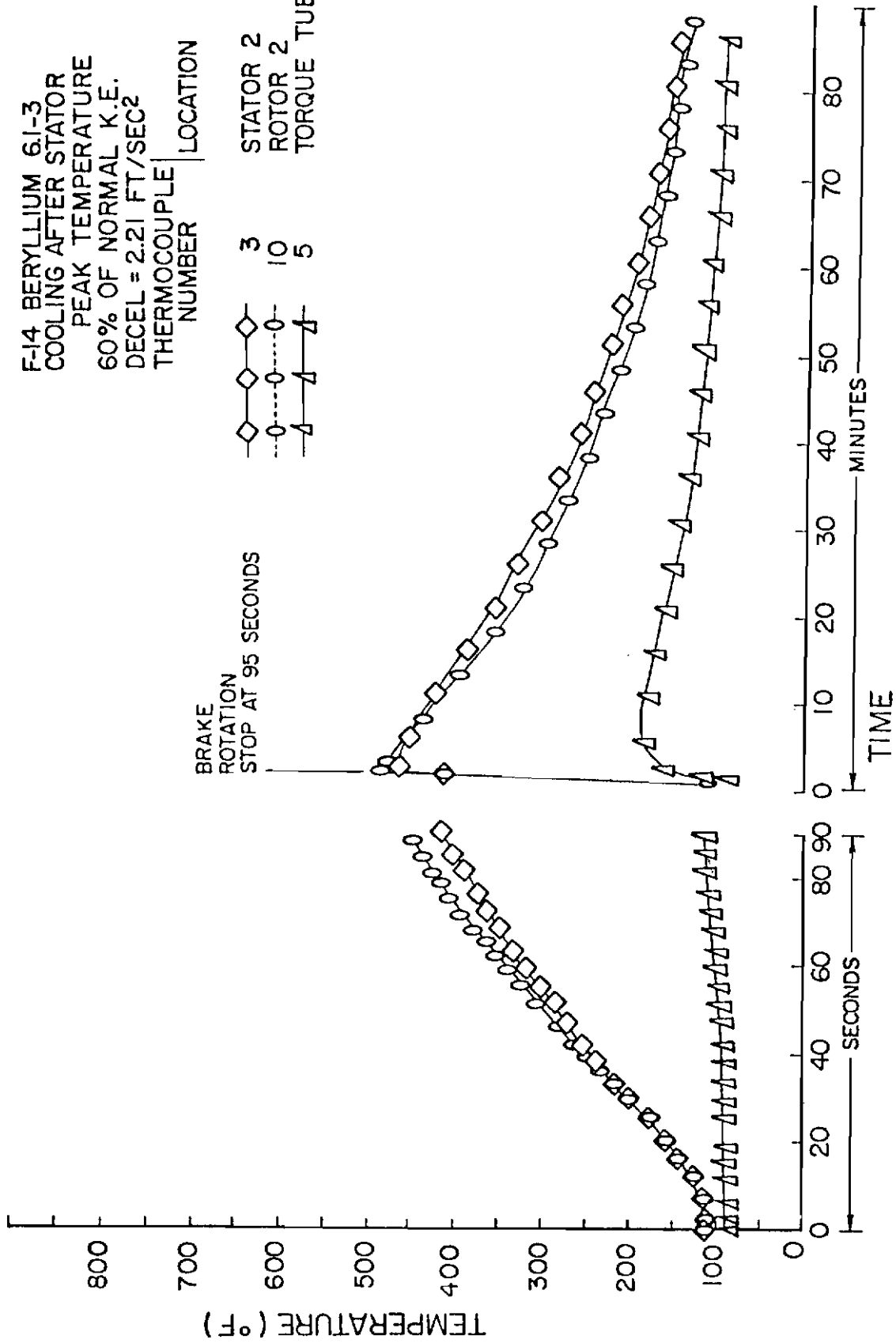


Figure F-6. Temperature vs Time for Stator 2, Rotor 2, Torque Tube (Test 6.1-3)

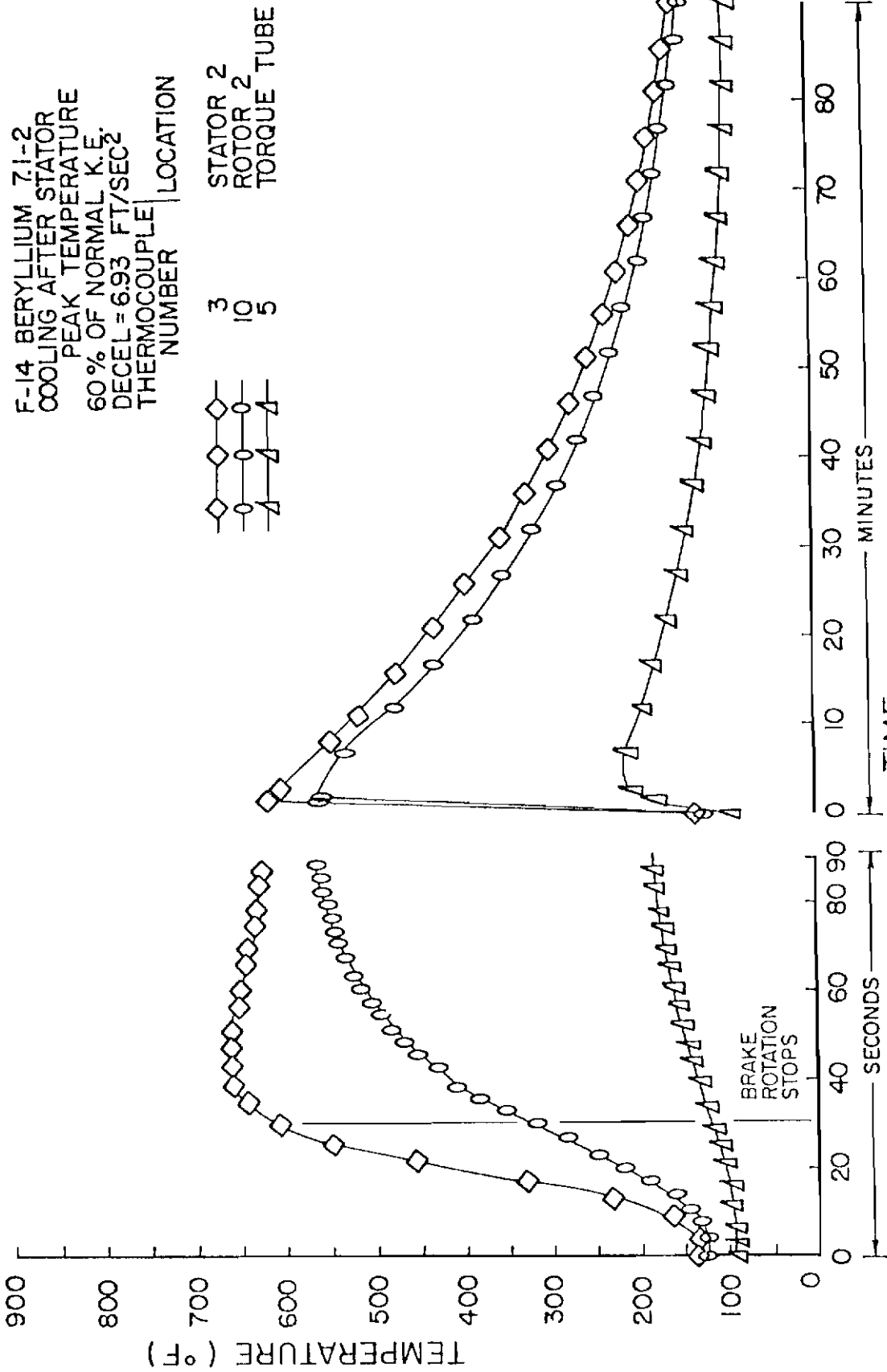


Figure F-7. Temperature vs Time for Stator 2, Rotor 2, Torque Tube (Test 7.1-2)

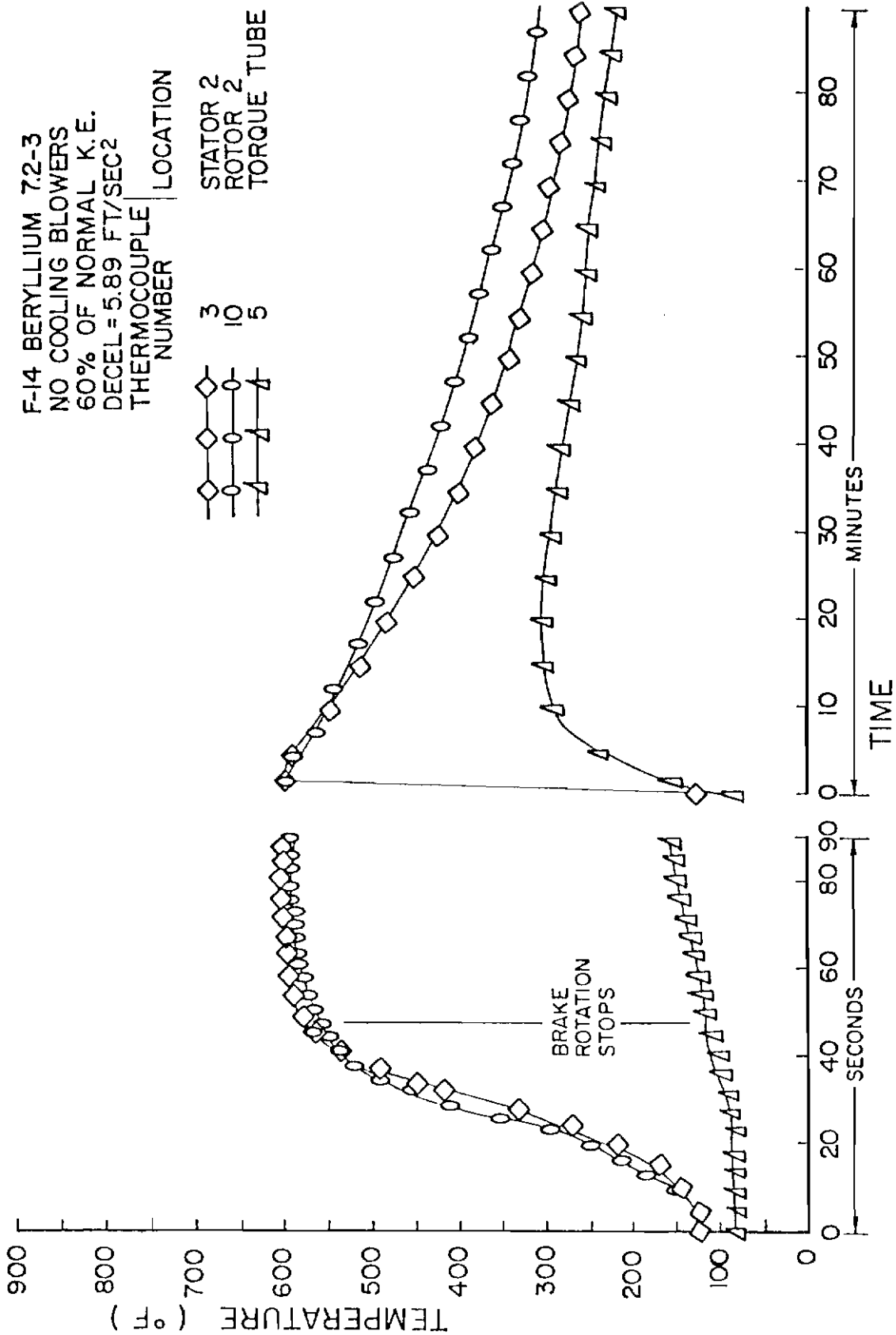


Figure F-8. Temperature vs Time for Stator 2, Rotor 2, Torque Tube (Test 7.2-3)

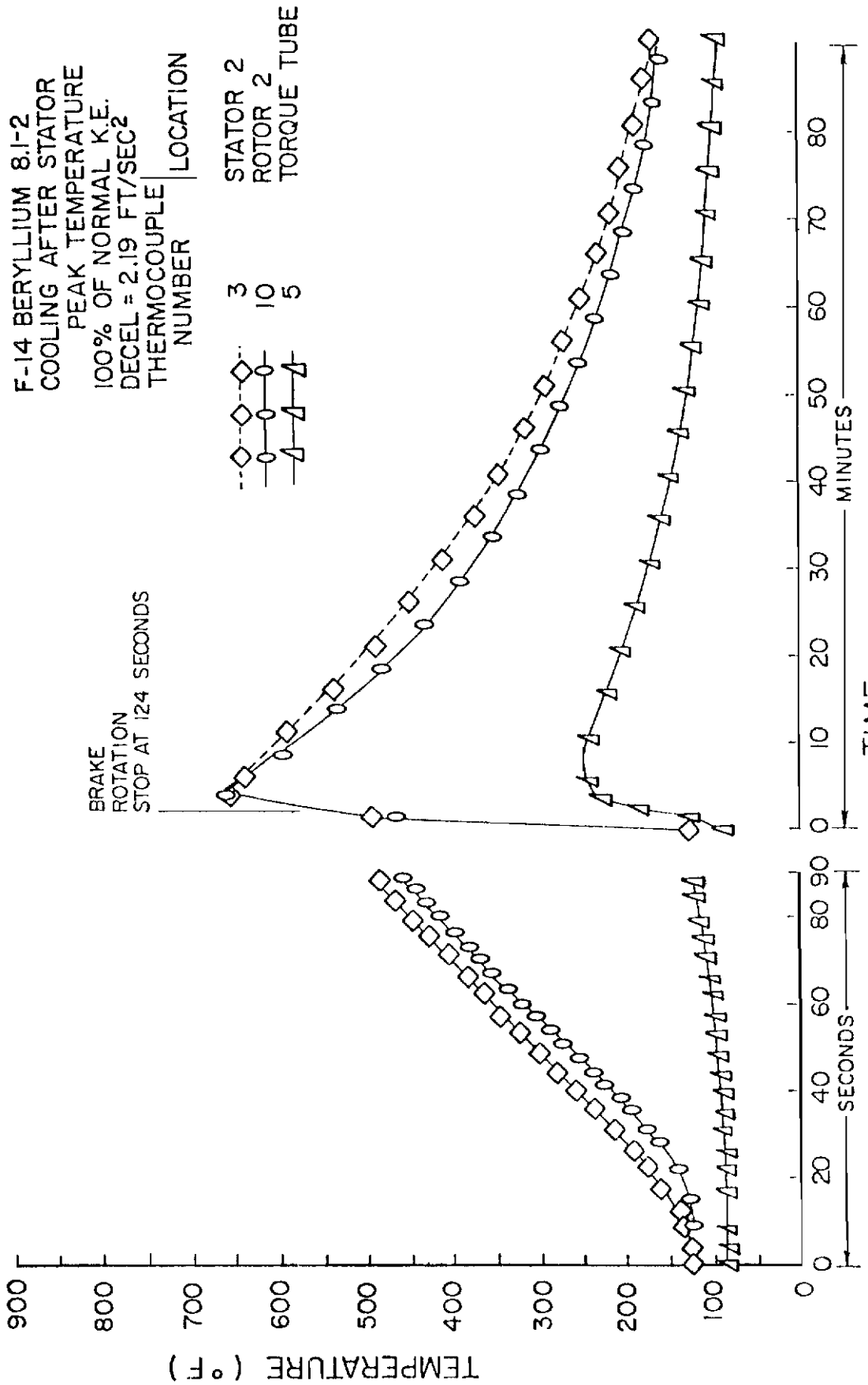


Figure F-9. Temperature vs Time for Stator 2, Rotor 2, Torque Tube (Test 8.1-2)

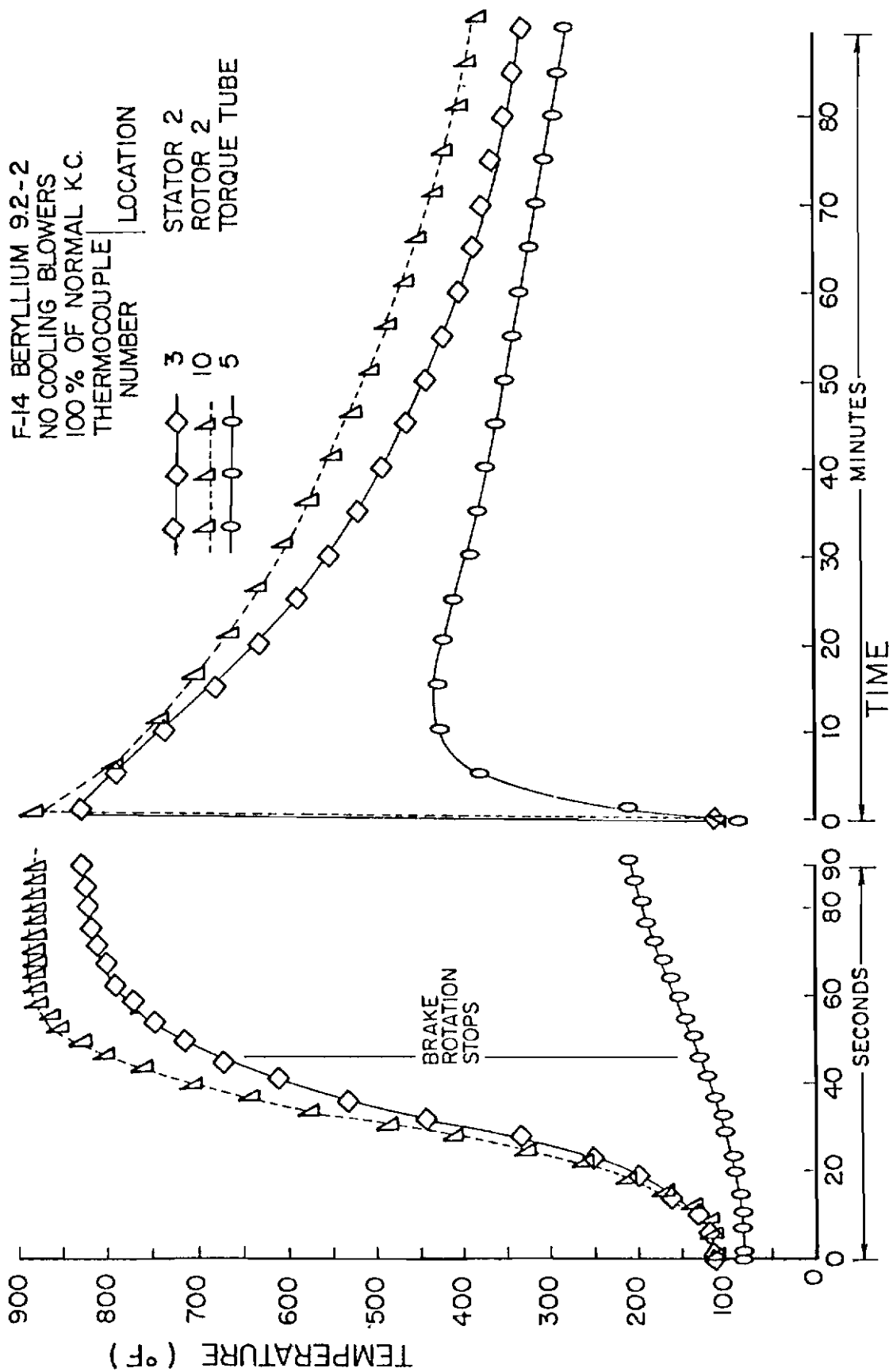


Figure F-10. Temperature vs Time for Stator 2, Rotor 2, Torque Tube (Test 9.2-2)

APPENDIX G

TEMPERATURE VERSUS AXIAL
POSITION PLOTS AT
VARIOUS TIMES

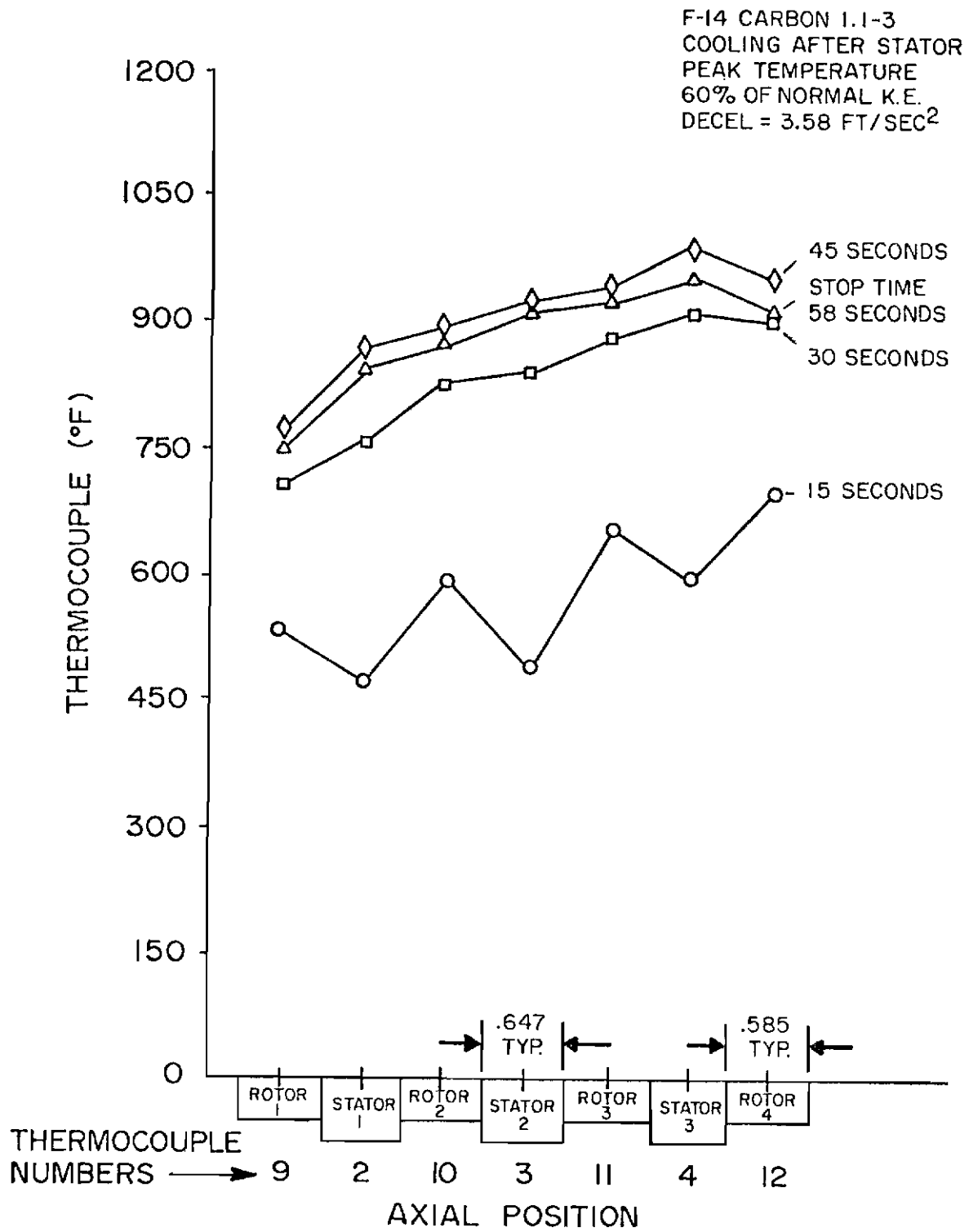


Figure G-1. Temperature vs Axial Position (Test 1.1-3)

Contrails

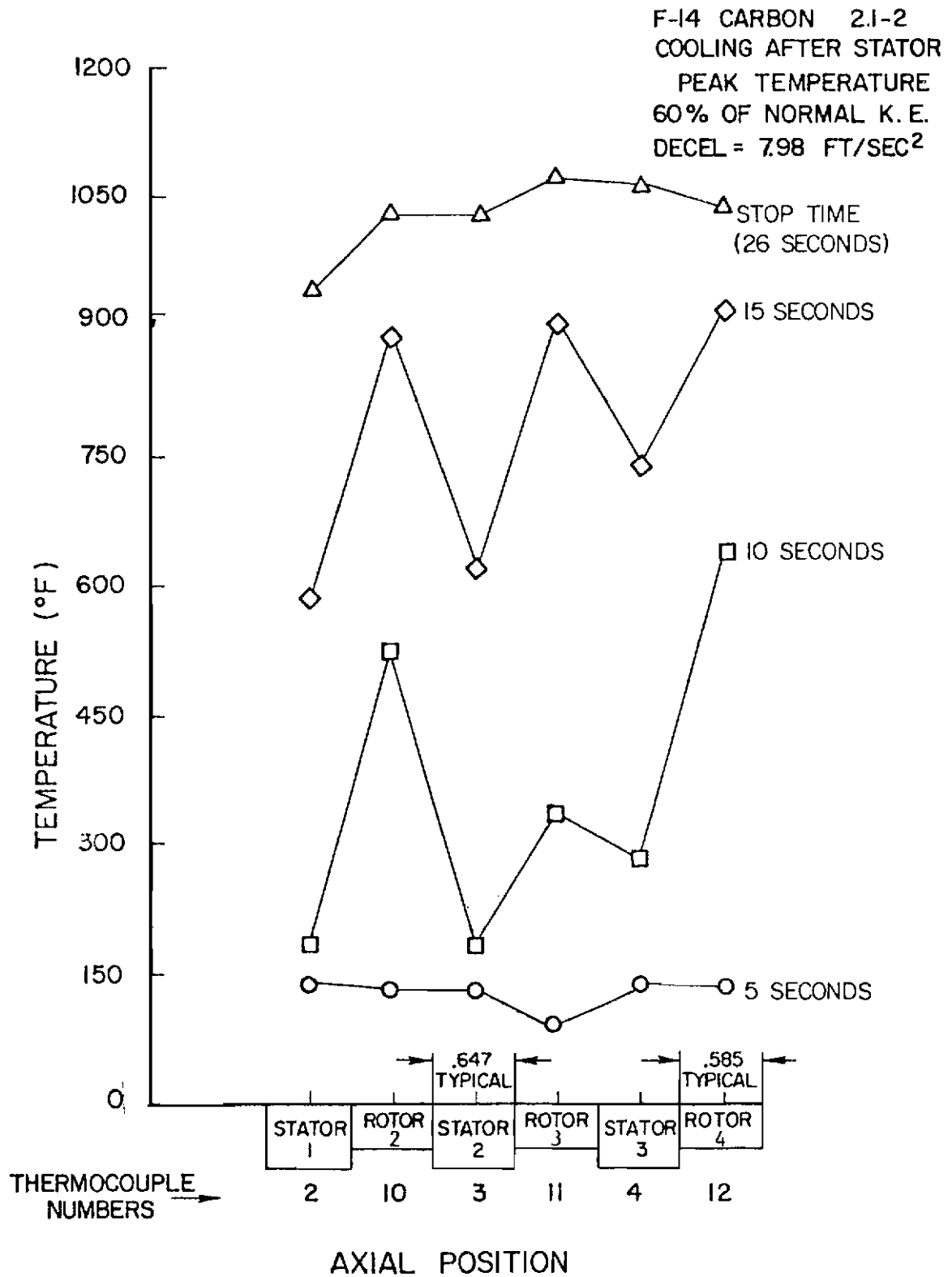


Figure G-2. Temperature vs Axial Position (Test 2.1-2)

Contrails

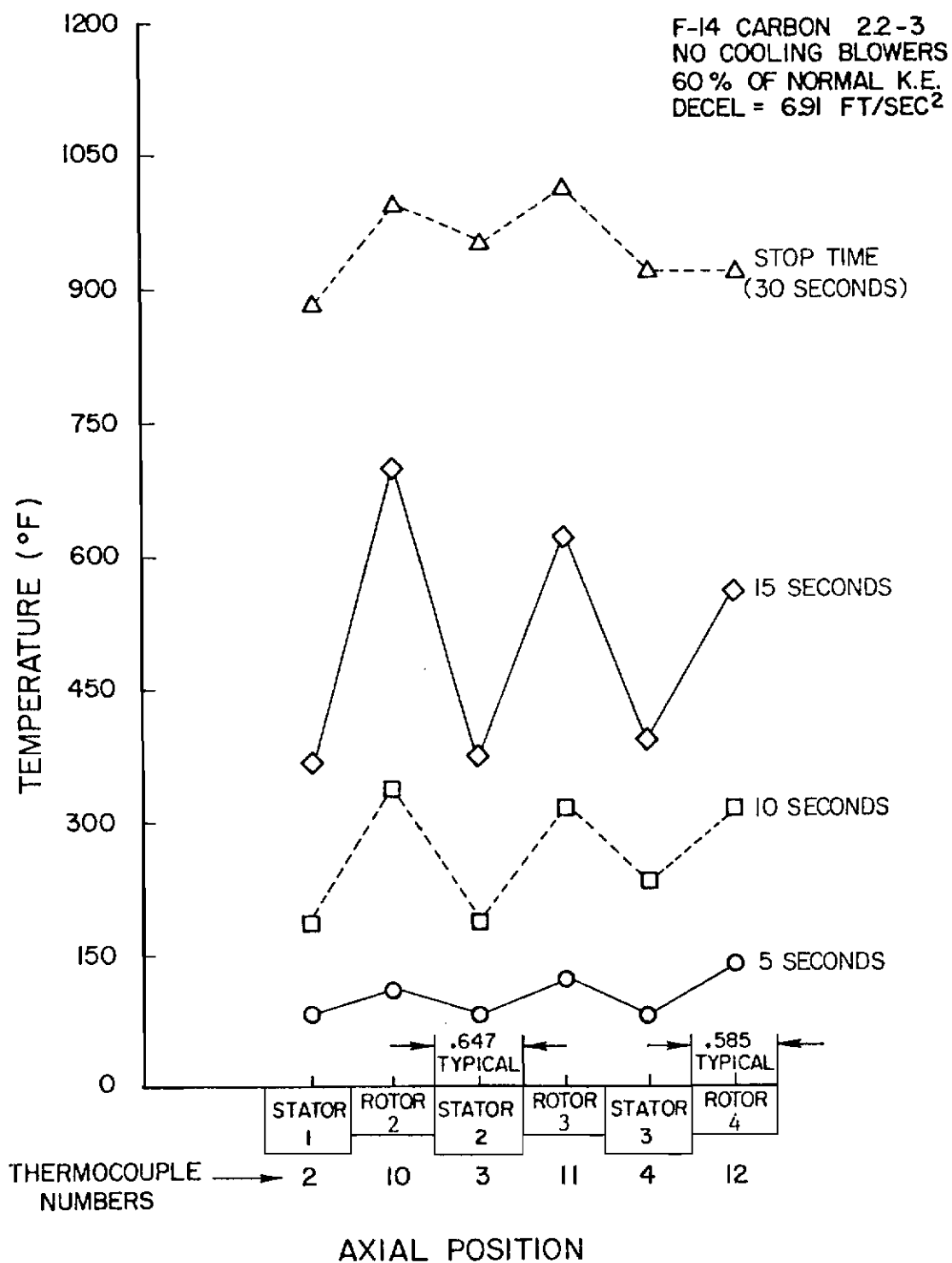


Figure G-3. Temperature vs Axial Position (Test 2.2-3)

Contrails

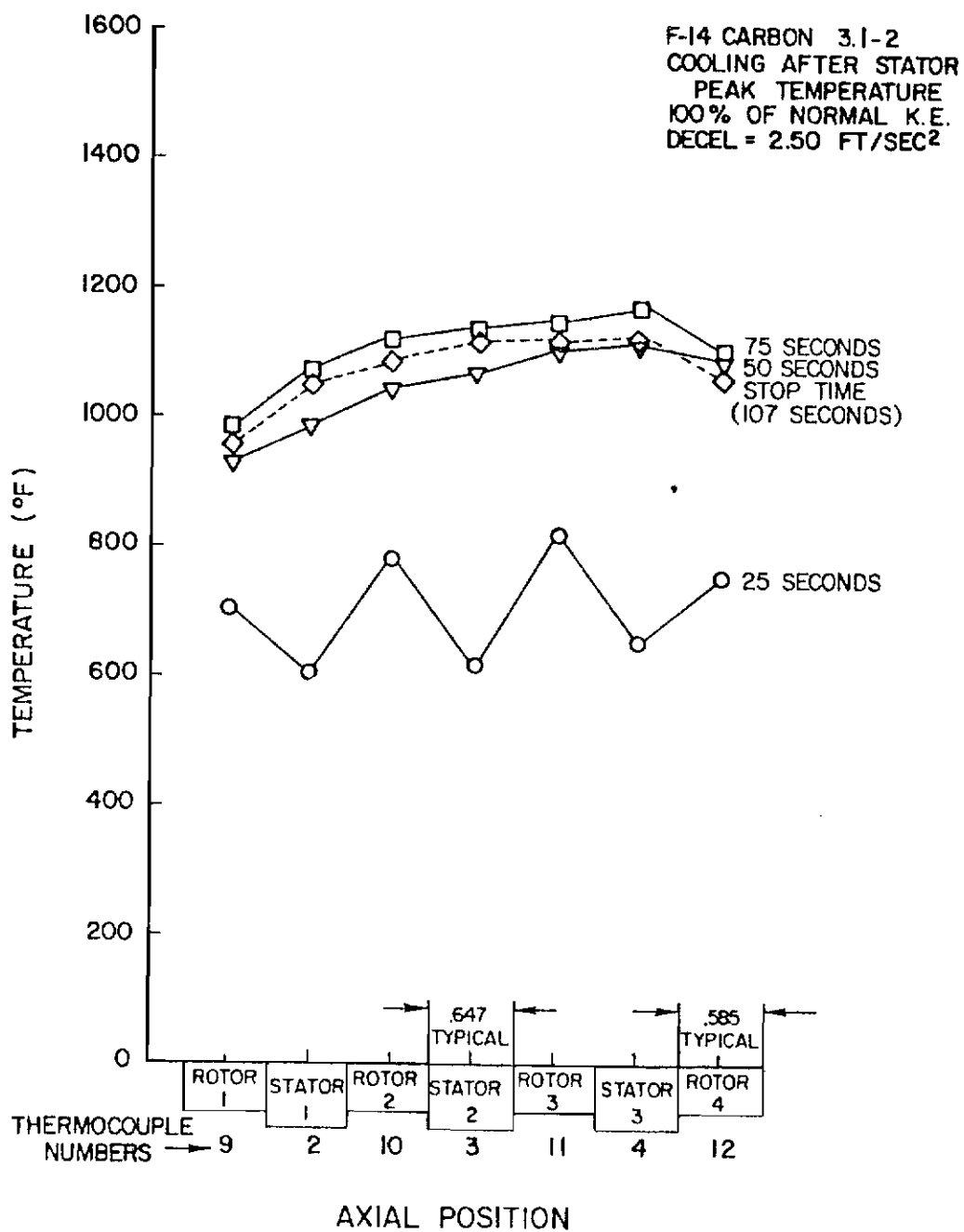


Figure G-4. Temperature vs Axial Position (Test 3.1-2)

Contrails

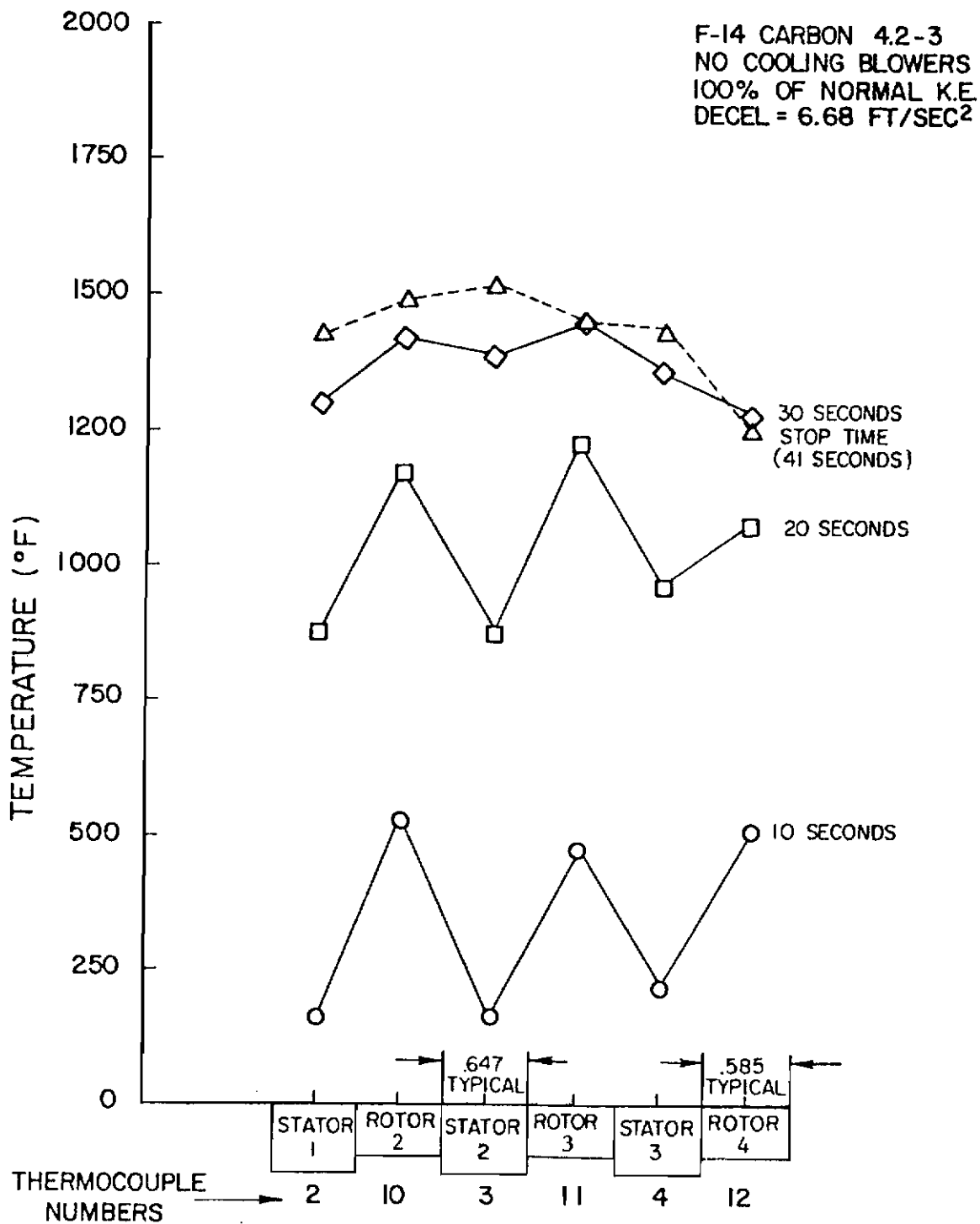


Figure G-5. Temperature vs Axial Position (Test 4.2-3)

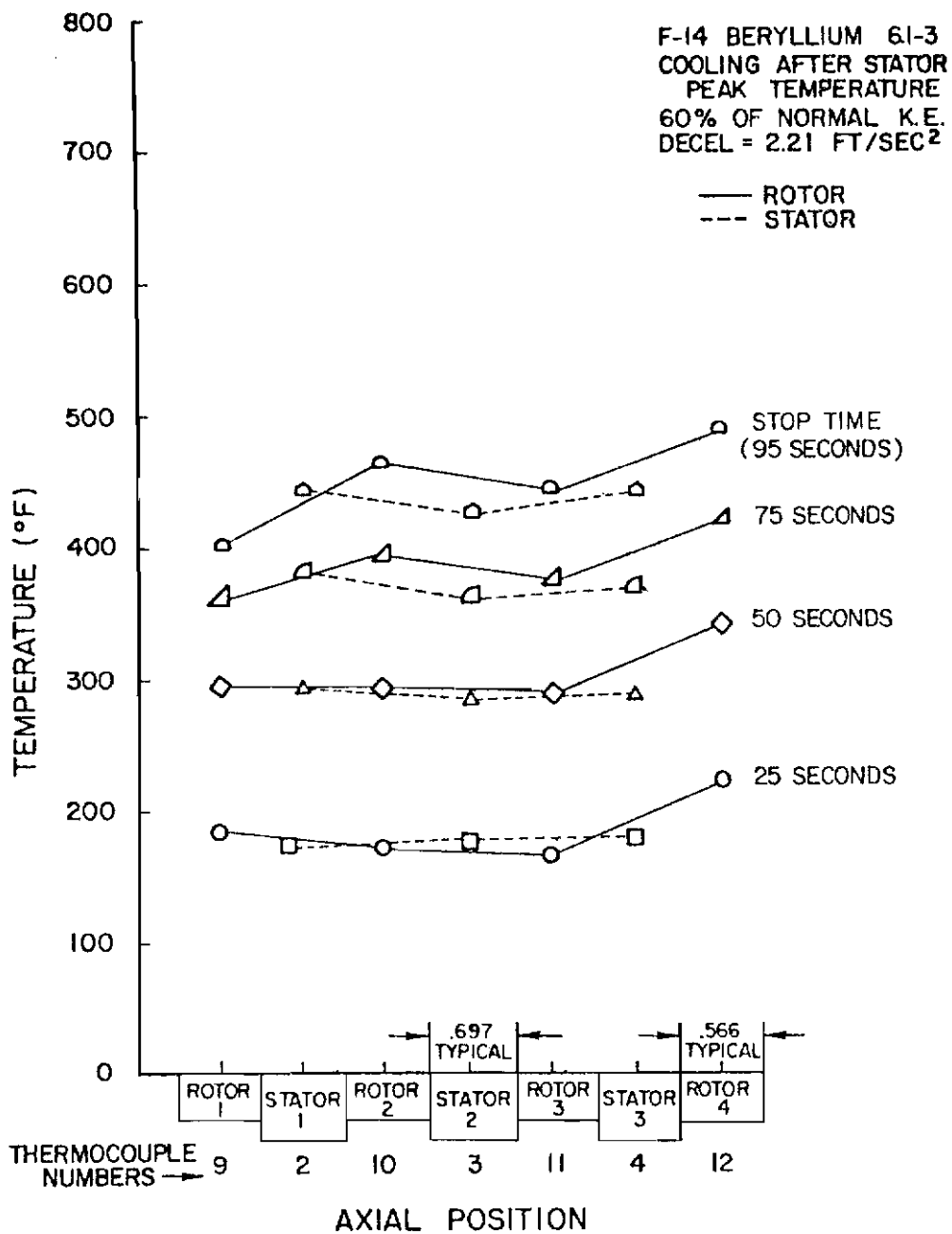


Figure G-6. Temperature vs Axial Position (Test 6.1-3)

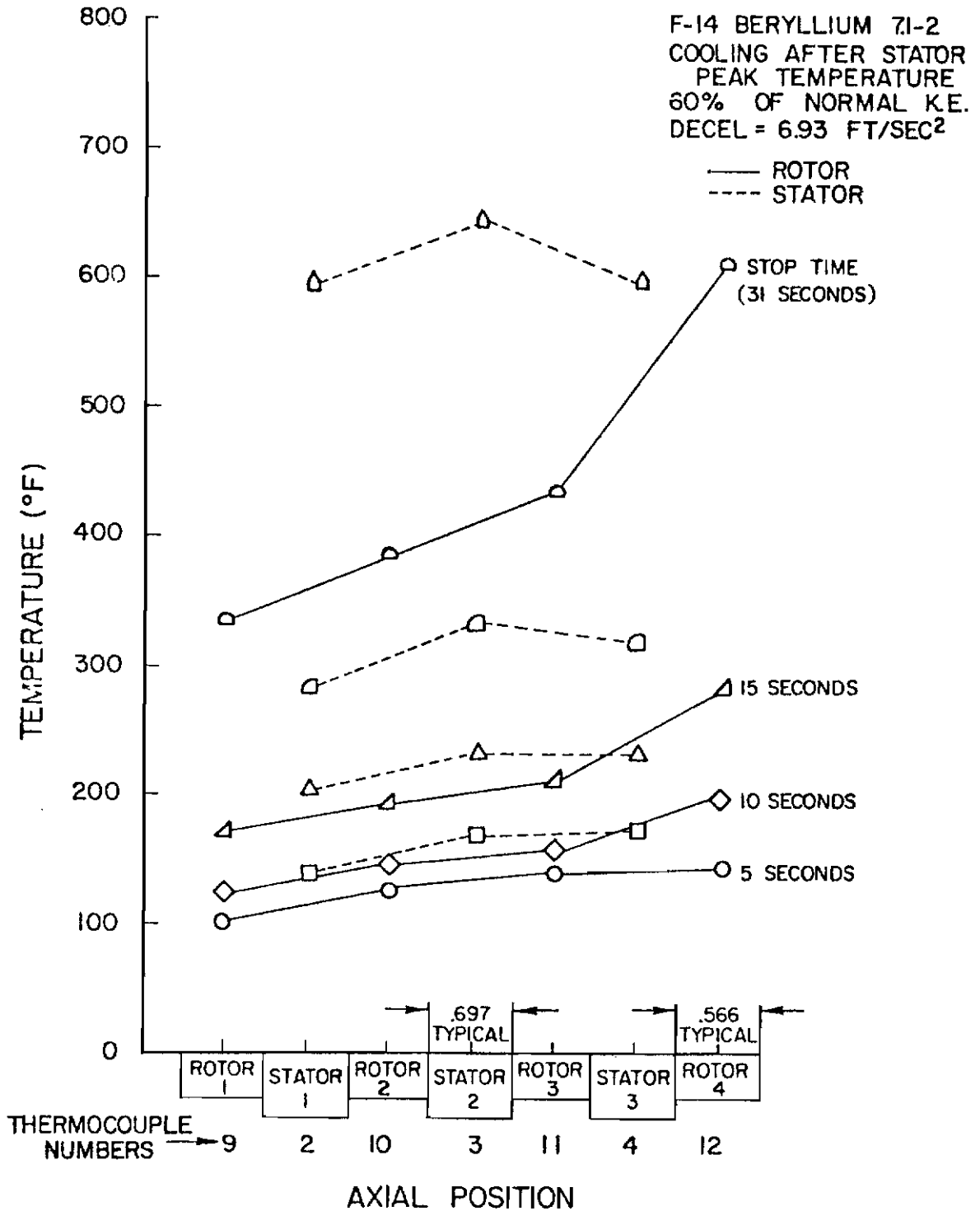
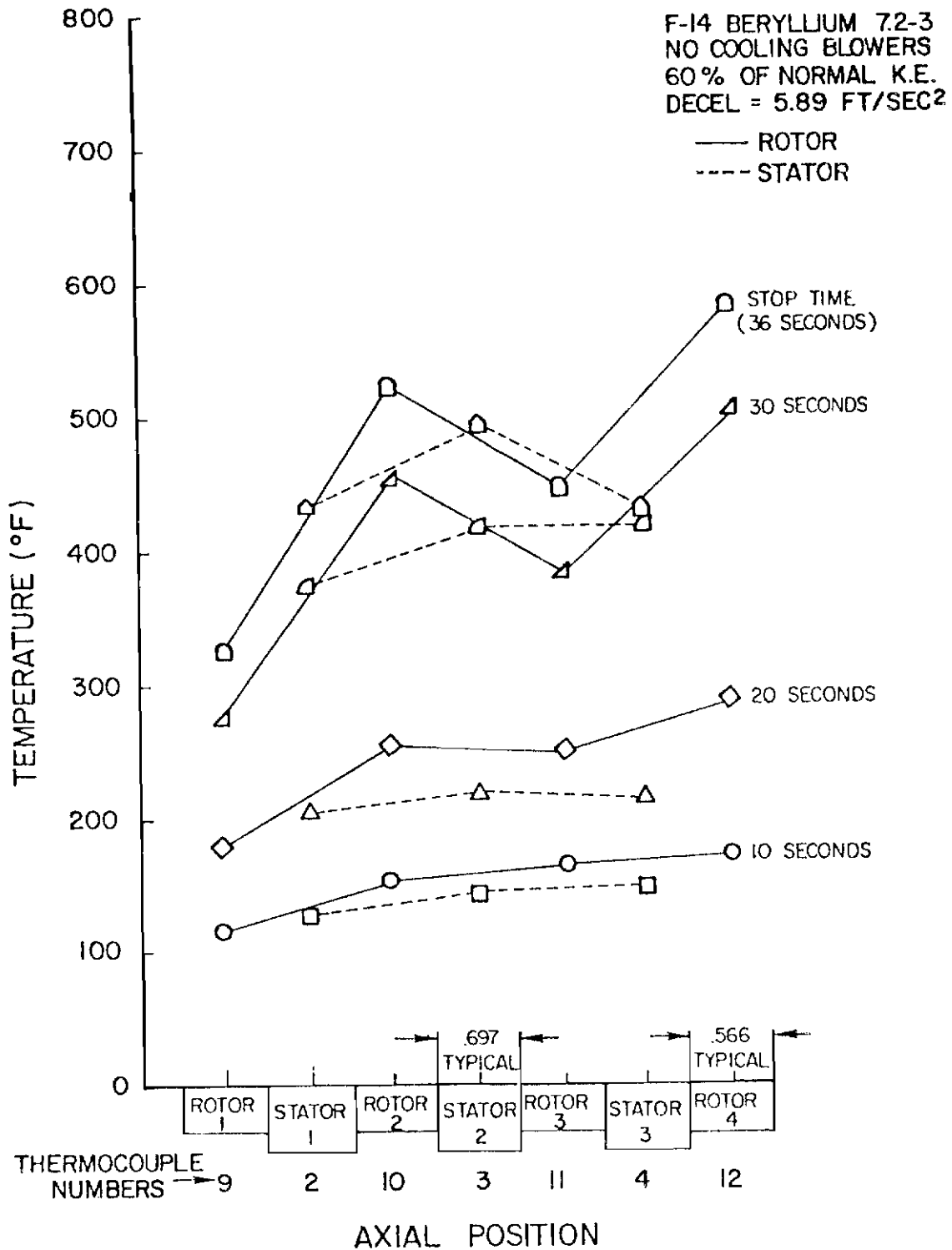


Figure G-7. Temperature vs Axial Position (Test 7.1-2)

Contrails



Contrails

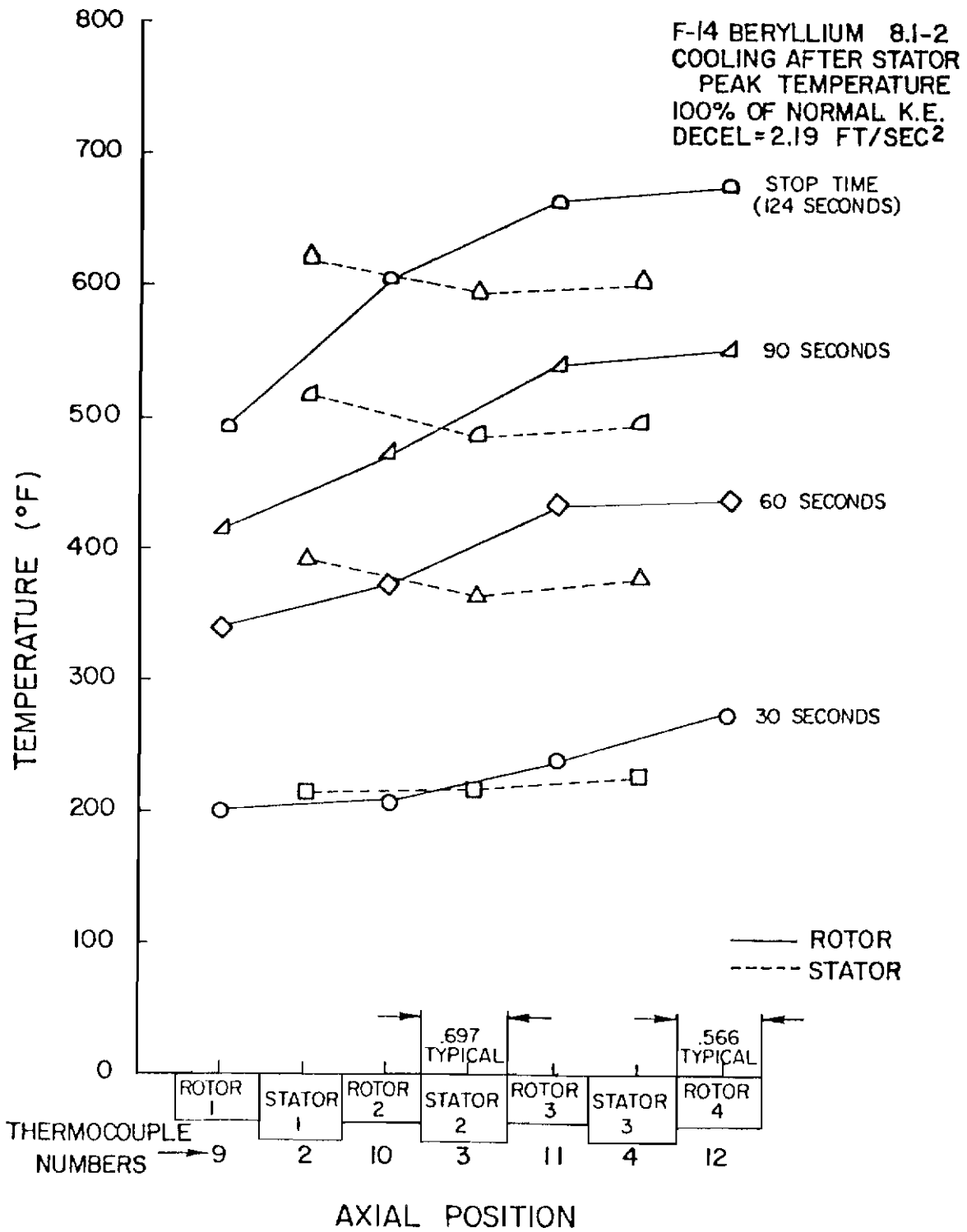


Figure G-9. Temperature vs Axial Position (Test 8.1-2)

Contrails

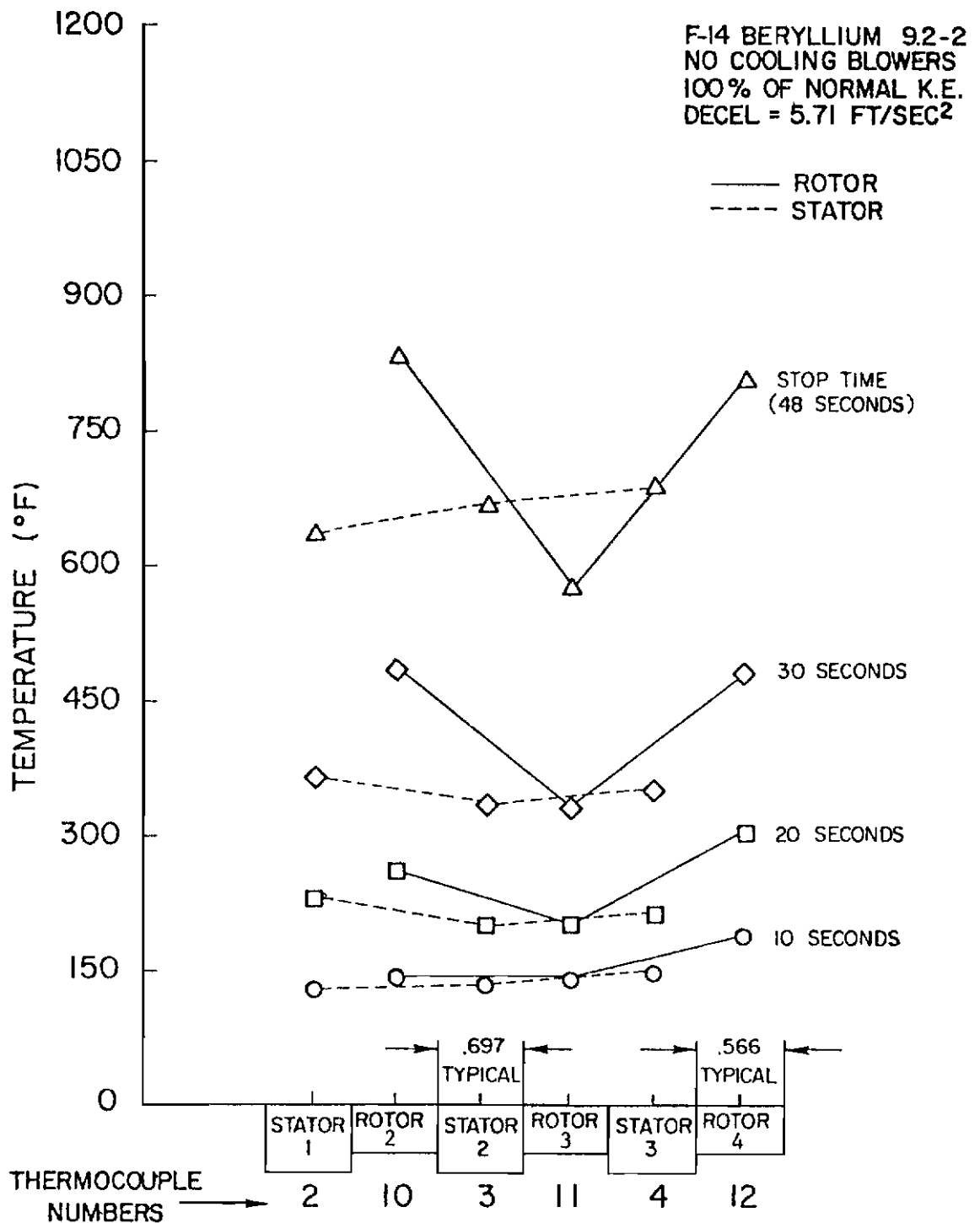


Figure G-10. Temperature vs Axial Position (Test 9.2-2)

APPENDIX H
TEMPERATURE VERSUS TIME PLOTS
FOR RADIALLY LOCATED
THERMOCOUPLES

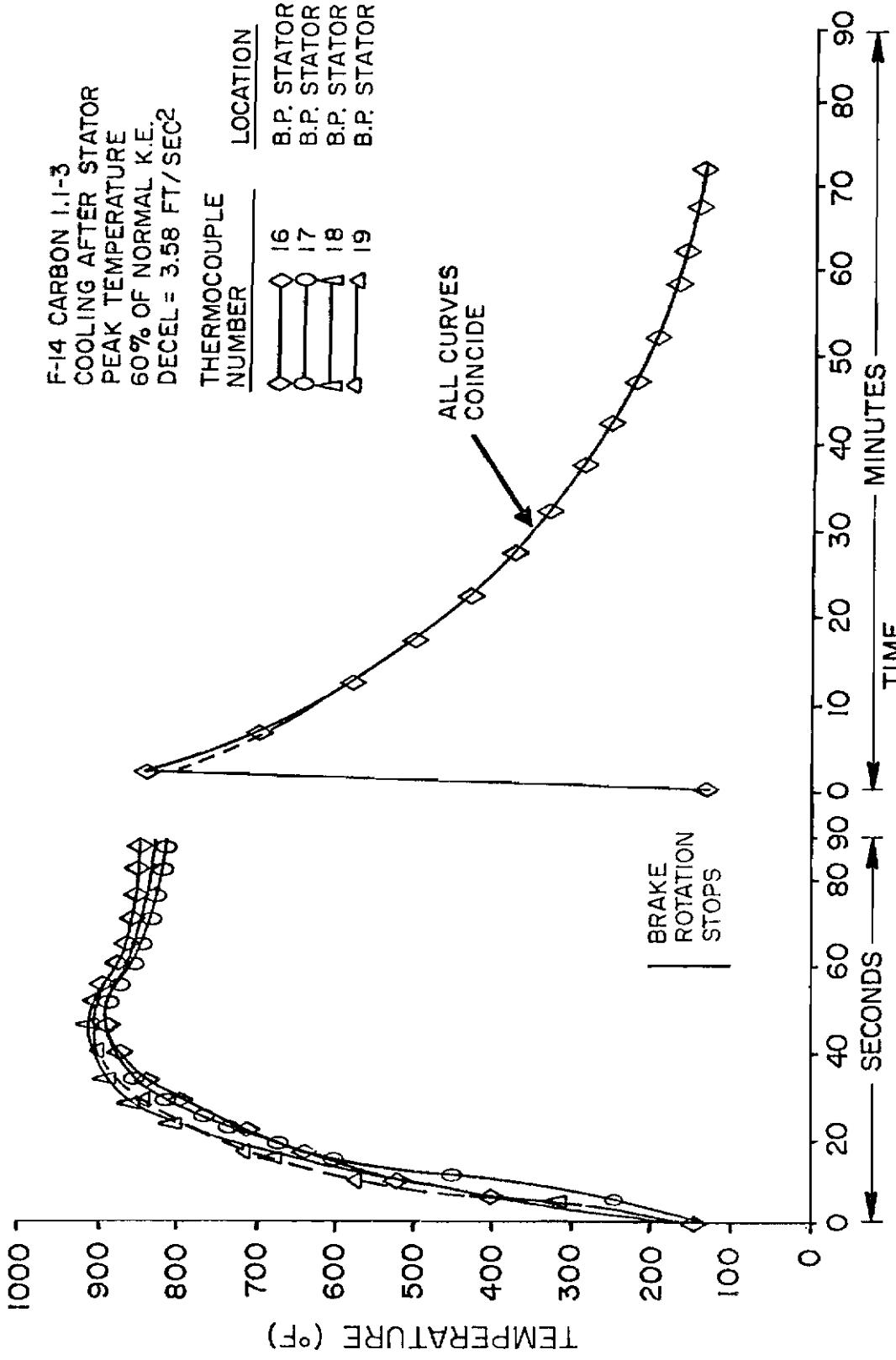


Figure H-1. Temperature vs Time for Radial Thermocouples (Test 1.1-3)

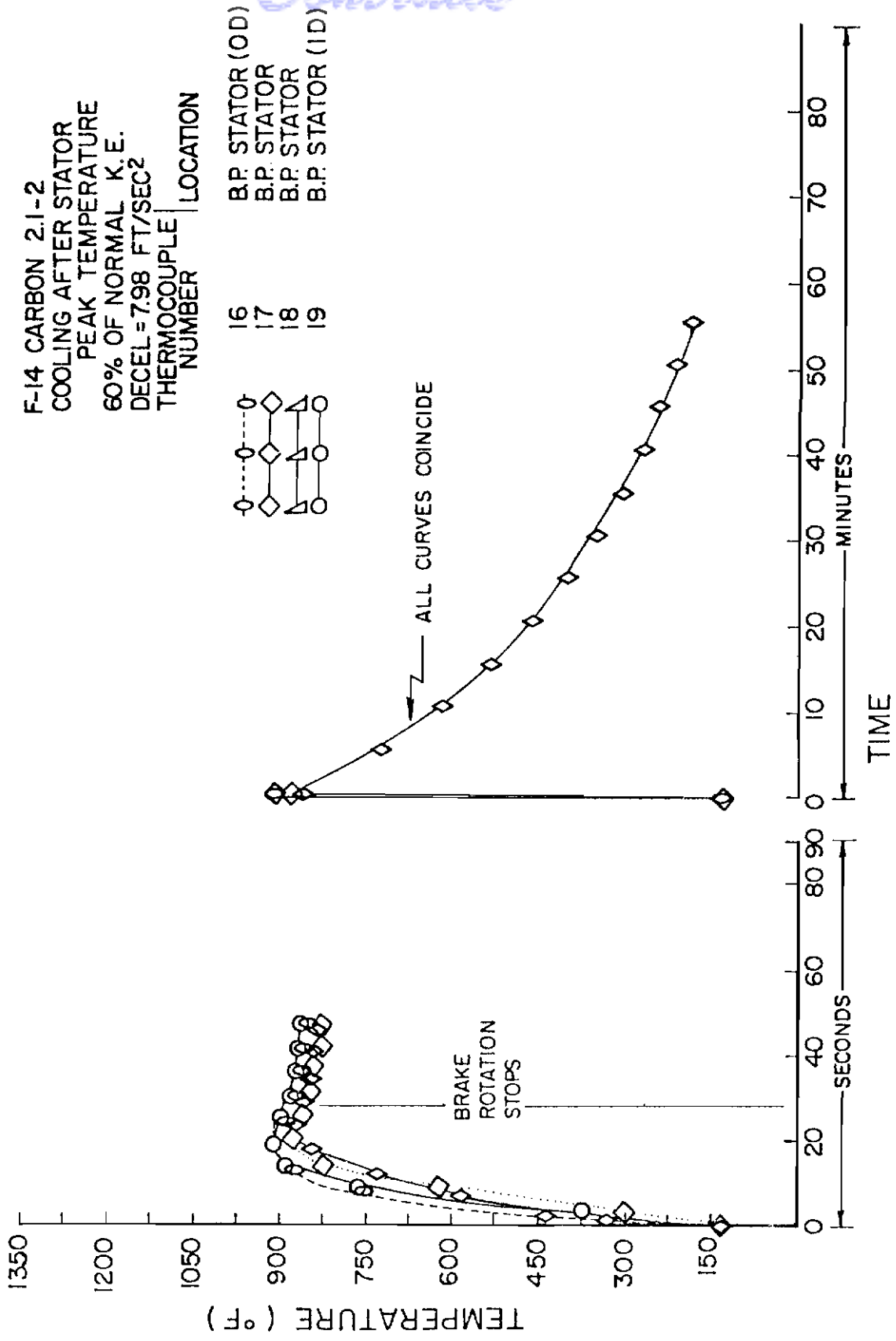


Figure H-2. Temperature vs Time for Radial Thermocouples (Test 2.1-2)

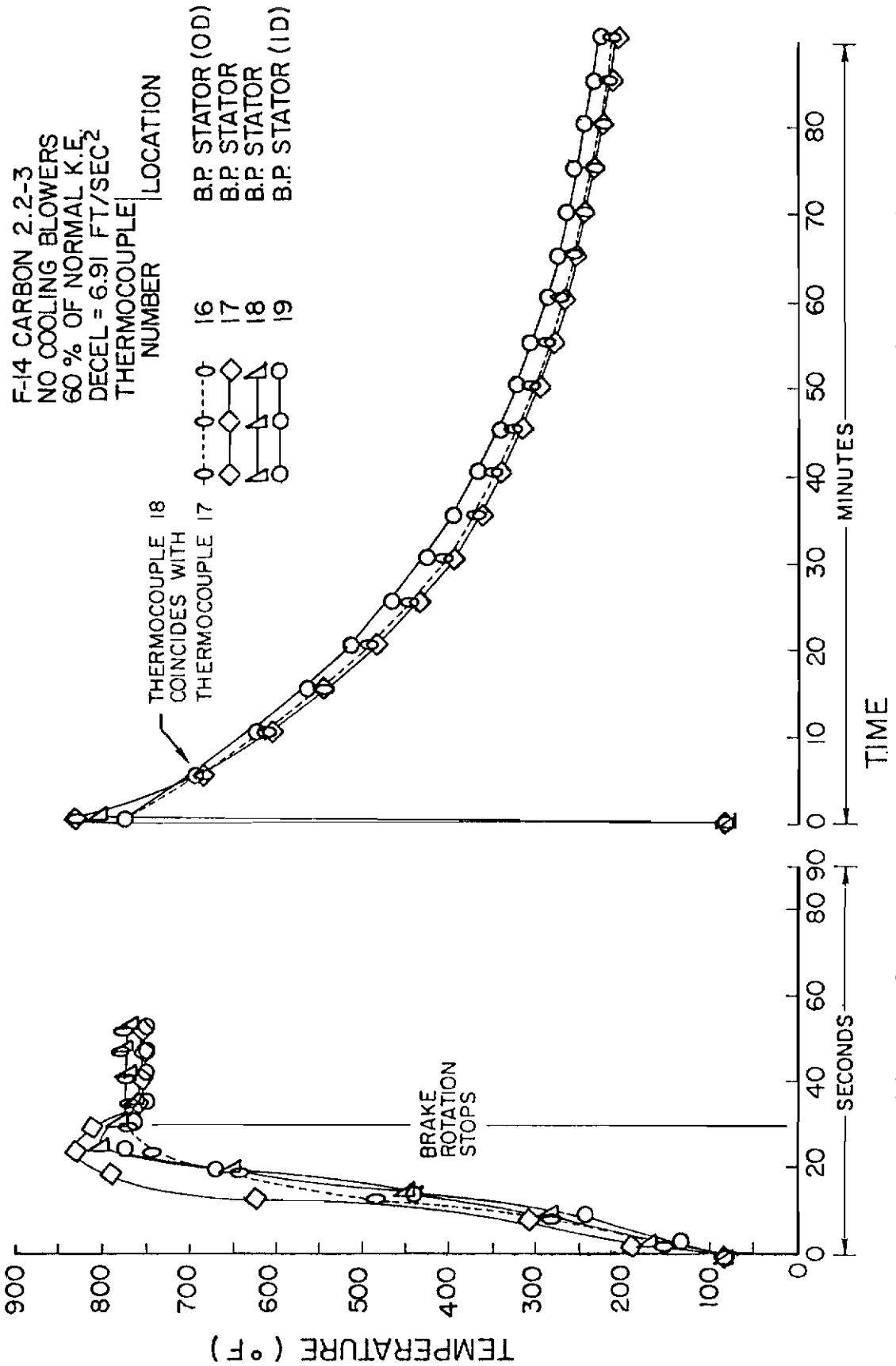


Figure H-3. Temperature vs Time for Radial Thermocouples (Test 2.2-3)

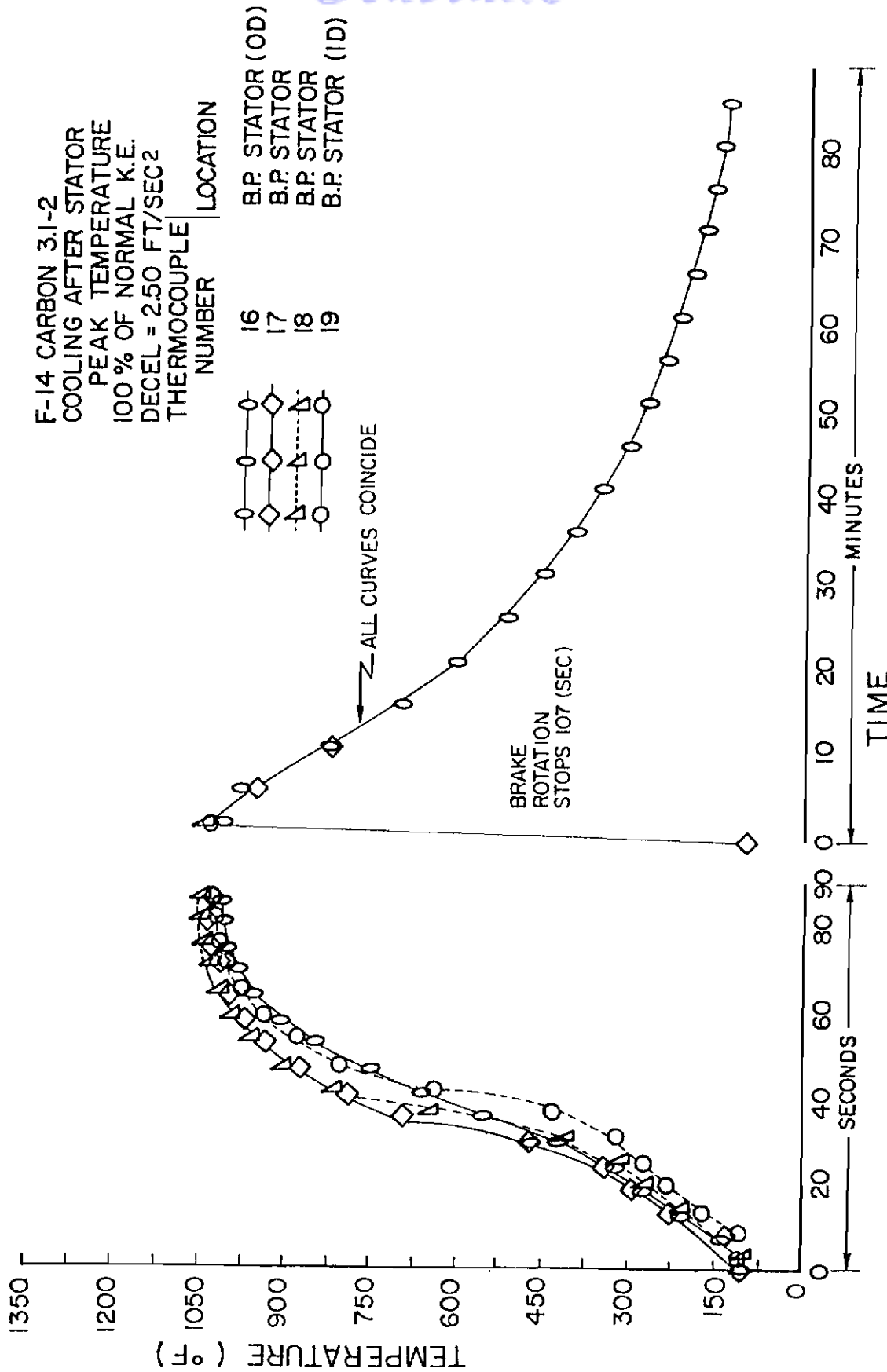


Figure H-4. Temperature vs Time for Radial Thermocouples (Test 3.1-2)

F-14 CARBON 4.2-3
 NO COOLING BLOWERS
 100% OF NORMAL KE.
 DECEL = 6.68 FT/SEC²

THERMOCOUPLE NUMBER	LOCATION
16	B.P. STATOR (OD)
17	B.P. STATOR
18	B.P. STATOR
19	B.P. STATOR (ID)

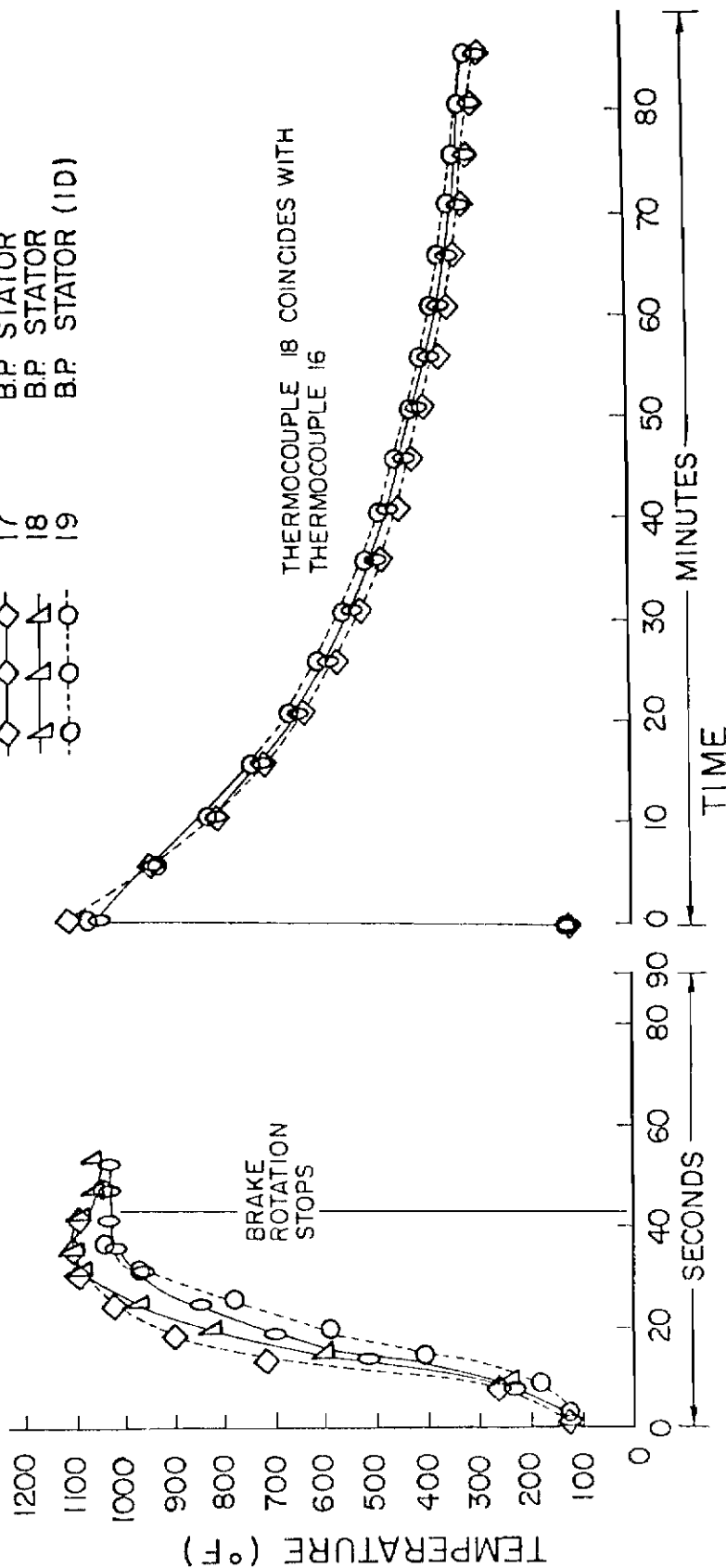


Figure H-5. Temperature vs Time for Radial Thermocouples (Test 4.2-3)

APPENDIX I

TEMPERATURE VERSUS RADIAL
POSITION PLOTS AT
VARIOUS TIMES

F-14 CARBON 1.1-3
 COOLING AFTER STATOR
 PEAK TEMPERATURE
 60% OF NORMAL K.E.
 DECEL = 3.58 FT/SEC²

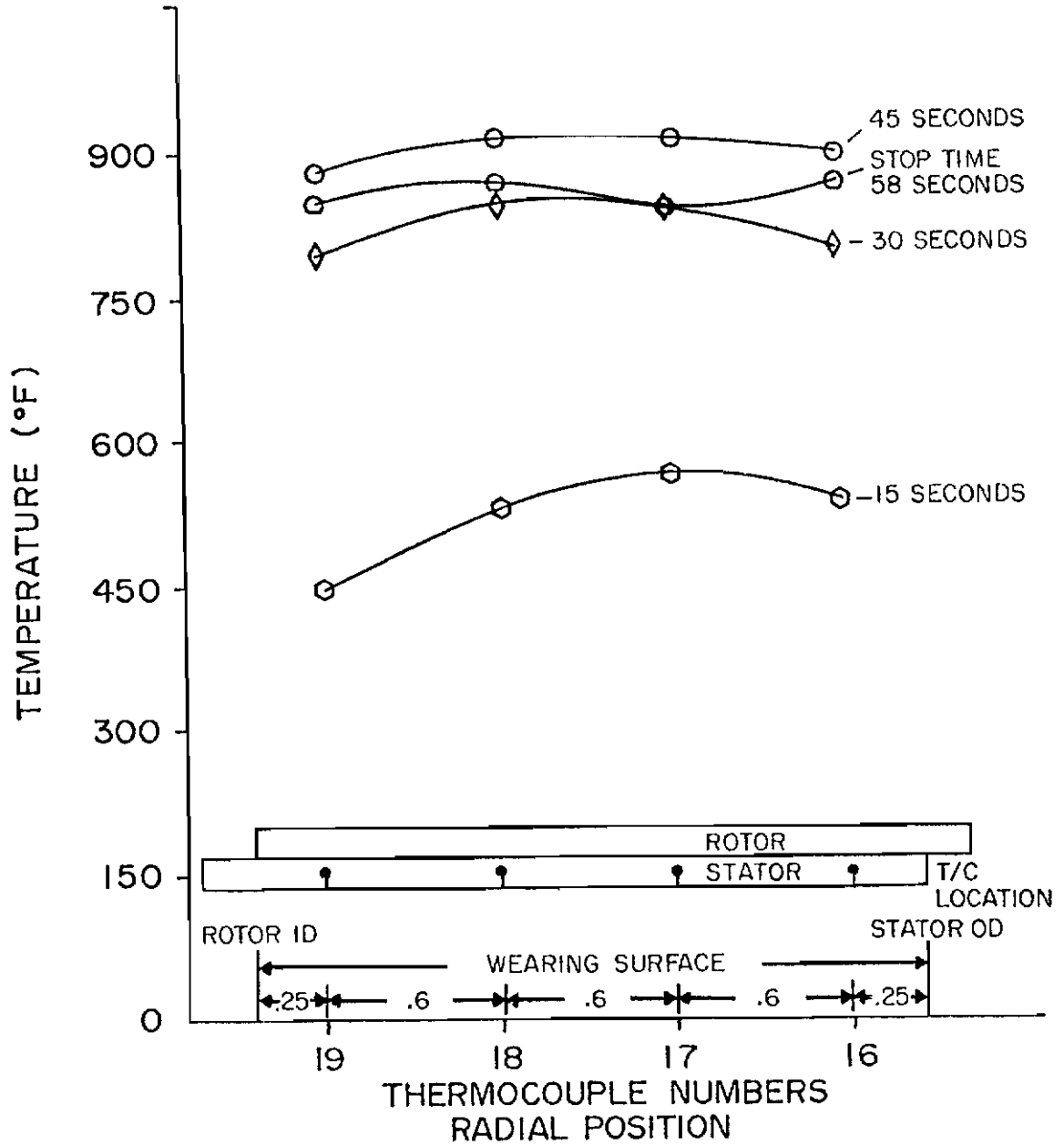


Figure I-1. Temperature vs Radial Position (Test 1.1-3)

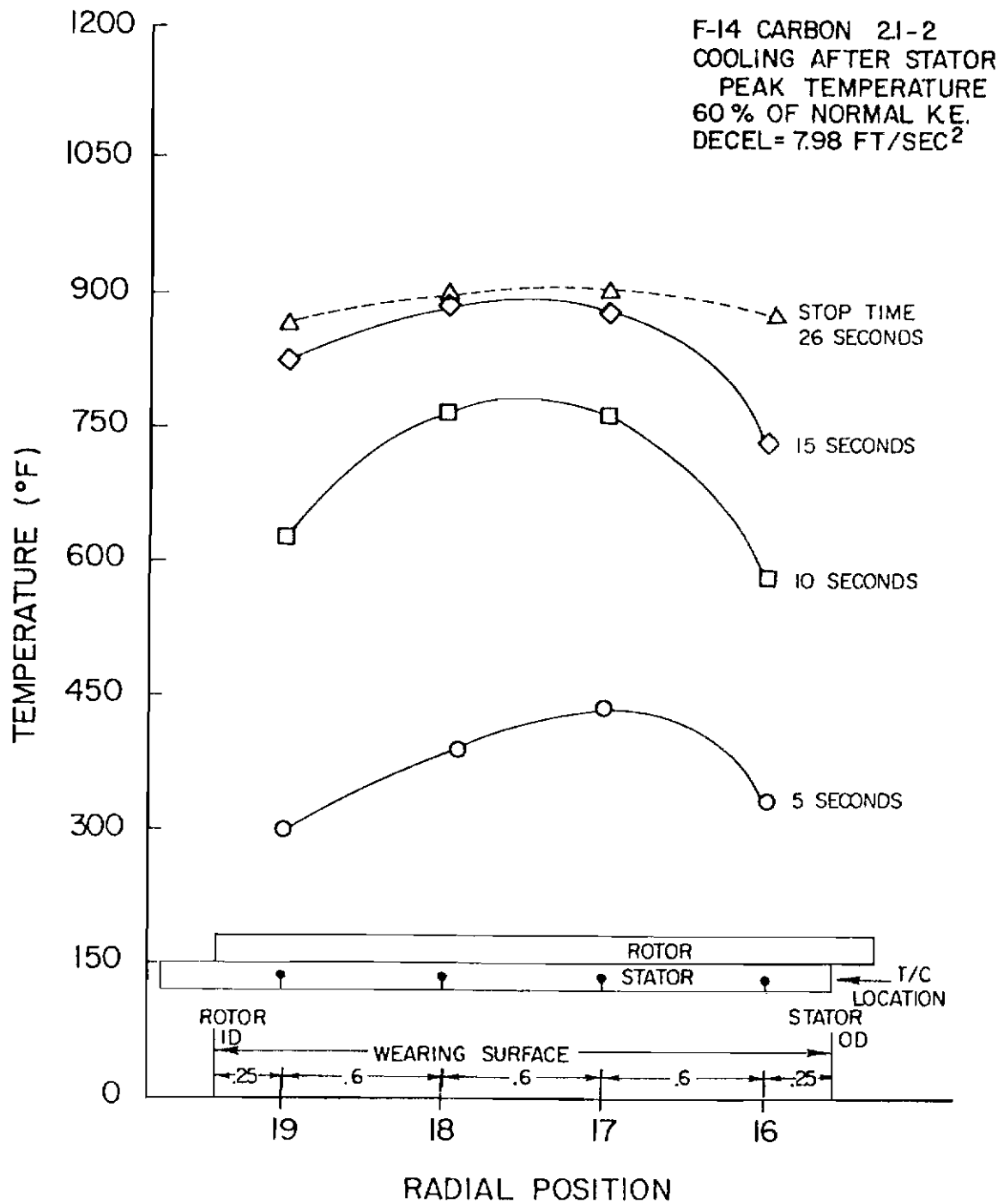


Figure I-2. Temperature vs Radial Position (Test 2.1-2)

Contrails

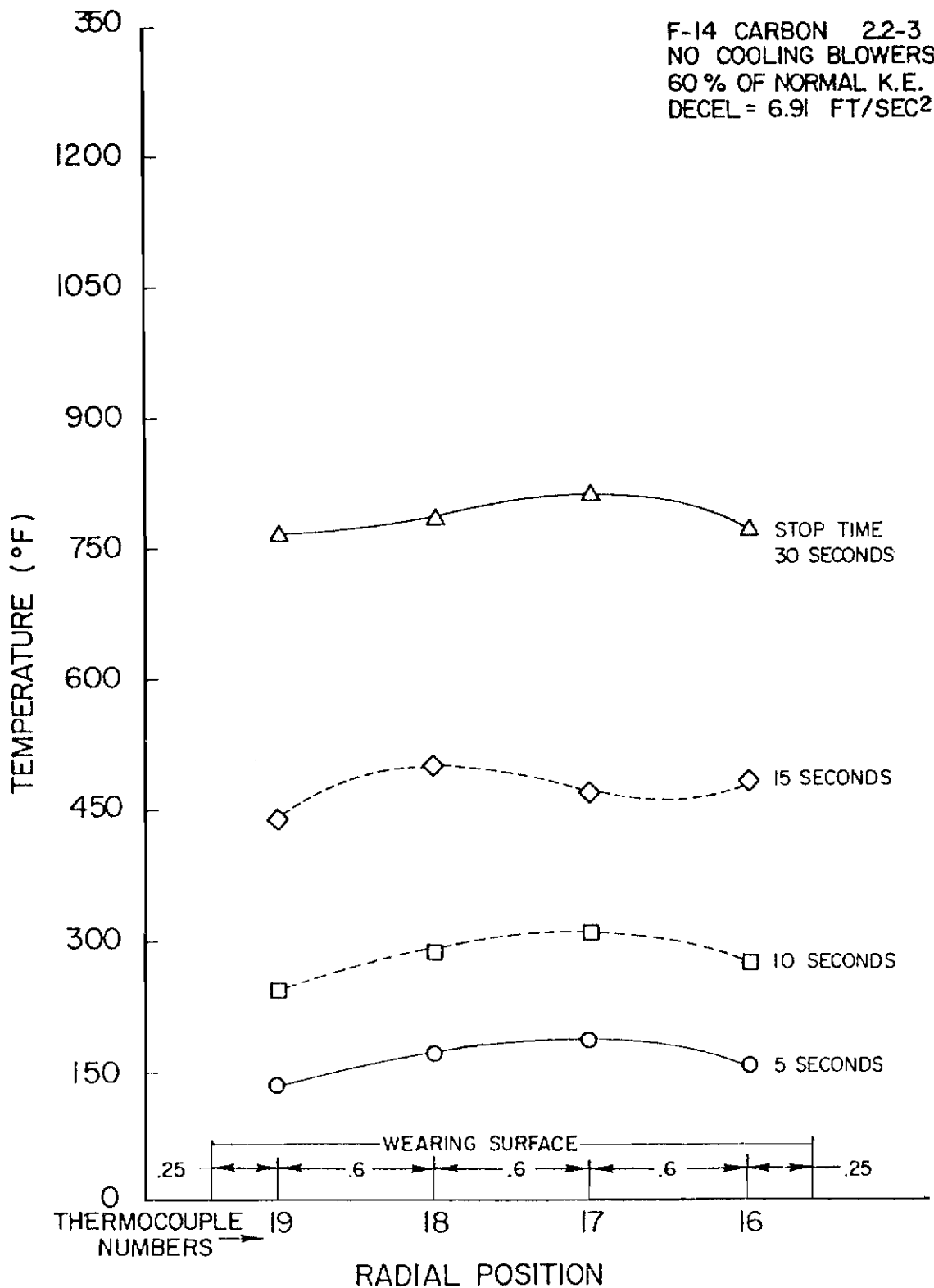


Figure I-3. Temperature vs Radial Position (Test 2.2-3)

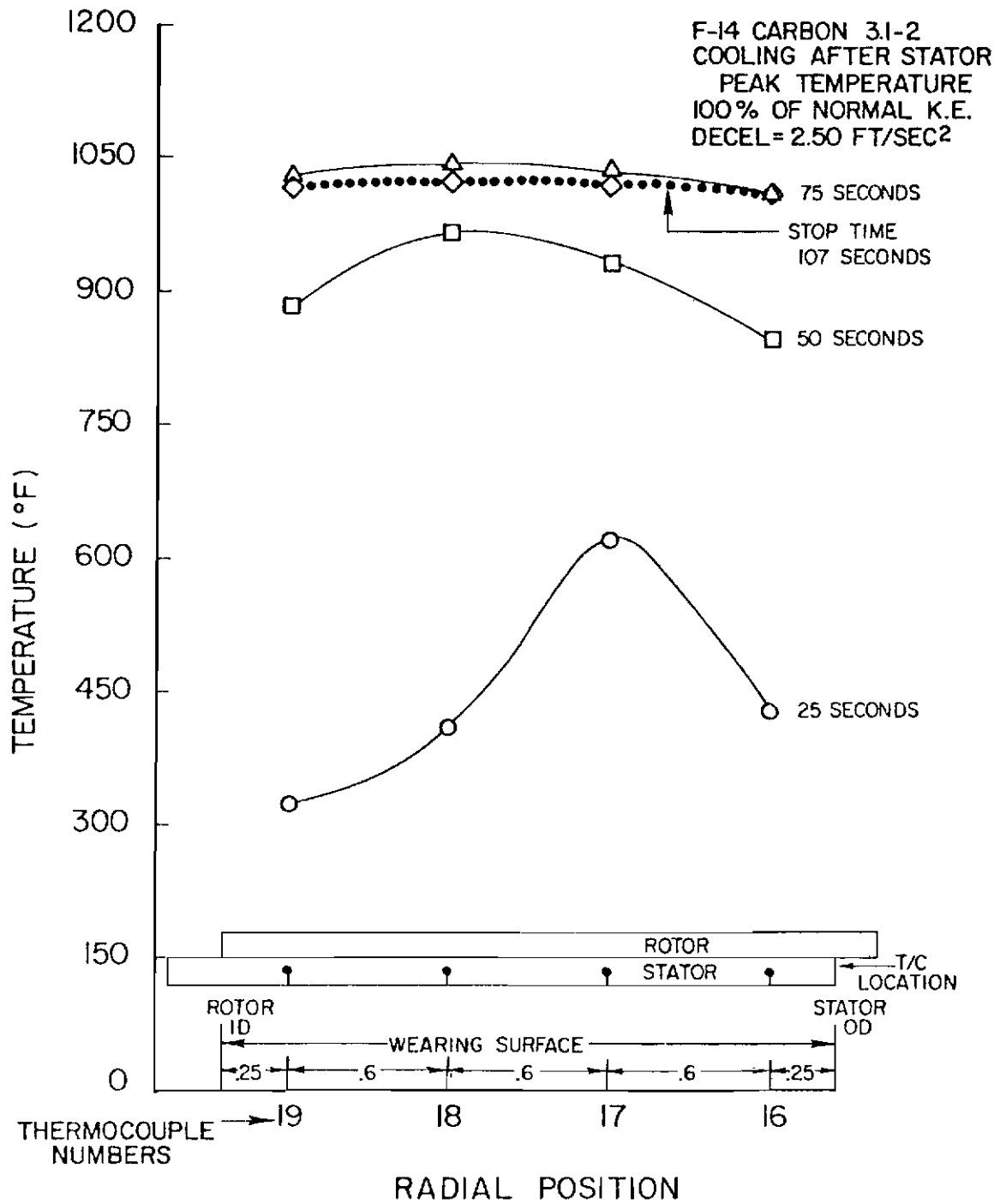


Figure I-4. Temperature vs Radial Position (Test 3.1-2)

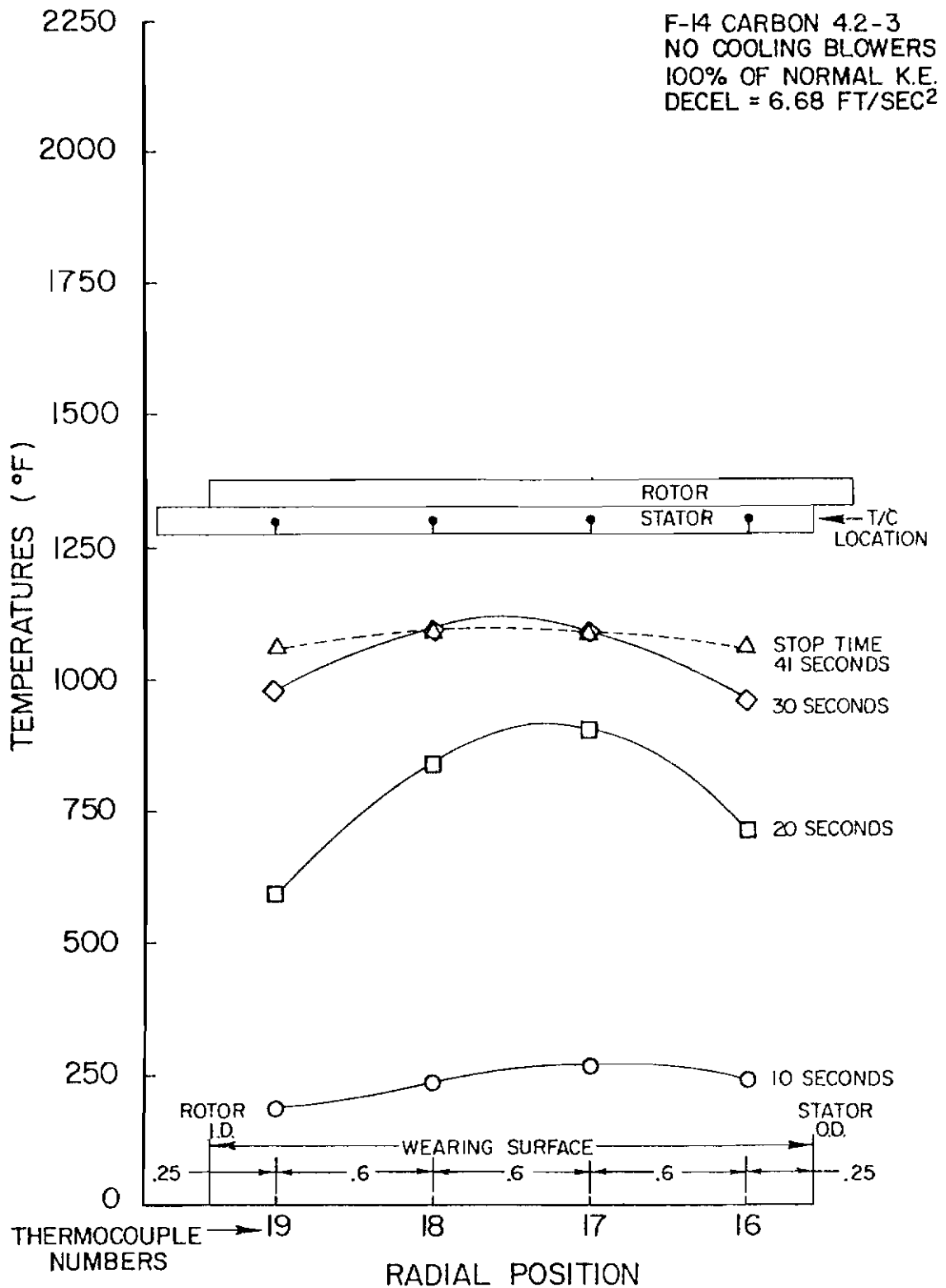


Figure I-5. Temperature vs Radial Position (Test 4.2-3)

APPENDIX J

CONVECTIVE/RADIATIVE HEAT TRANSFER
COEFFICIENT CALCULATION
PROCEDURE

Contrails

Two methods were used to calculate convective/radiative heat transfer coefficients. The first involved using the classical approach of assuming no heat conduction from the stators or rotors to the rim, torque tube or any other surrounding brake hardware. The following equation is applied to the heat sink, all rotors and stators:

$$h A (T - T_{\infty}) = \rho C V \frac{dT}{dt} \quad (J-1)$$

Using experimental cooling data in the form of temperature versus time plots, the temperature and time increment can be found. This information along with the material properties and disc geometry allow all quantities in Equation (J-1) to be known except for the h value. Using the Euler time marching technique and solving Equation (J-1) for h results in:

$$h = \frac{\rho C V (T' - T)}{A (T - T_{\infty}) \Delta t} \quad (J-2)$$

where T' is the temperature of the heat sink at a time increment, Δt , from the temperature, T. Evaluation of the convection/radiation heat transfer coefficient in this way assumes only convective/radiative cooling, thus the resulting values were used only in theoretical models that did not contain conduction from the heat sink. These models were one-dimensional radial, two-dimensional radial/axial and the cooldown portion of the three-dimensional model. The resulting convective/radiative heat transfer coefficients plotted versus temperature are shown in Figure J-1 for carbon and in Figure J-2 for beryllium. The h-values are different for beryllium and carbon due to disc geometry differences and due to the fact that heat shields were used during

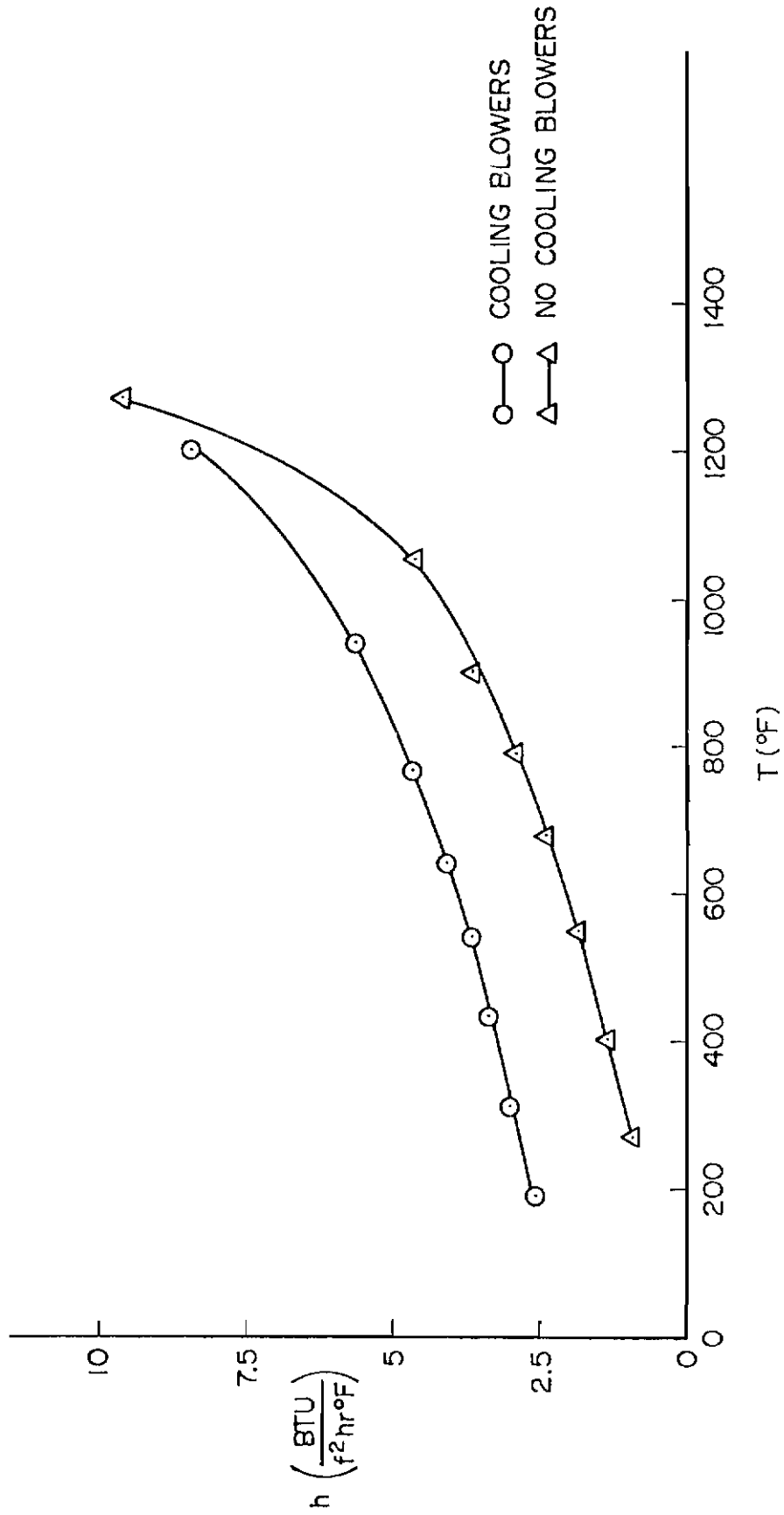


Figure J-1. Carbon Combined Heat Transfer Coefficient

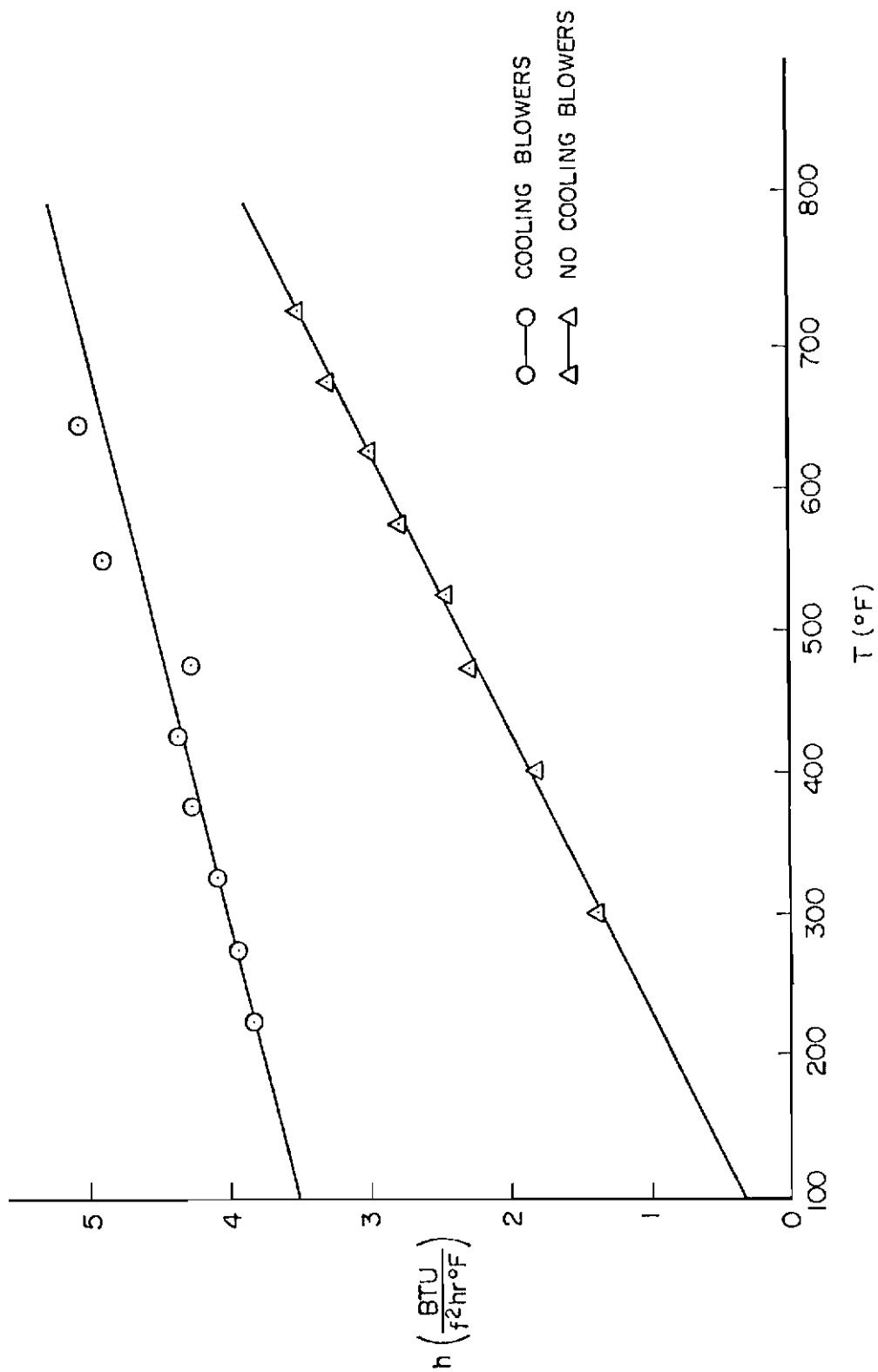


Figure J-2. Beryllium Combined Heat Transfer Coefficient

Contrails

carbon tests but not during beryllium tests. On each figure two curves are shown, one for which no exterior cooling was provided and one for which the cooling blowers on the test dynamometer were used.

The second method employed for calculating convective/radiative heat transfer coefficients involved including the conduction heat transfer from the disc to surrounding brake hardware. Thus the first law equation for the heat sink would appear as:

$$\dot{q}_{SR} + \dot{q}_{ST} + \dot{q}_{SH} + h A (T - T_{\infty}) = \rho C V \frac{dT}{dt} \quad (J-3)$$

where \dot{q} terms are the conduction heat transfer rate terms and the subscripts are defined as: SR - sink to rim, ST - sink to torque tube, and SH - sink to housing. The first law was also applied to the housing, rim, wheel, torque tube, and tire including the conduction terms from adjacent brake hardware (see Figure 33). In this way a different value of h could be found not only at different temperatures but also for each separate piece of brake hardware. To obtain h for the heat sink, Equation (J-3) was solved for h to give:

$$h = \frac{1}{A(T-T_{\infty})} \left(\rho C V \frac{T' - T}{\Delta t} - \dot{q}_{SR} - \dot{q}_{ST} + \dot{q}_{SH} \right) \quad (J-4)$$

The \dot{q} terms were calculated by setting them equal to a temperature difference divided by a thermal resistance. The temperature difference was obtained from experimental data, and the resistance was calculated based on the thermal conductivity, area through which heat was transferred, and the distance from the area through which heat was conducted to the geometrical center of the heat sink. The results of calculating

Contrails

h in this fashion was that each piece of brake hardware had almost the same coefficient as any other piece and that this value did not change significantly with temperature. The radiative/convective heat transfer coefficients calculated in this way are:

$$\text{Carbon with Blowers,} \quad h = 2. \frac{\text{BTU}}{\text{HR-FT-FT-}^\circ\text{F}}$$

$$\text{Carbon without Blowers,} \quad h = 1. \frac{\text{BTU}}{\text{HR-FT-FT-}^\circ\text{F}}$$

$$\text{Beryllium with Blowers,} \quad h = 2.2 \frac{\text{BTU}}{\text{HR-FT-FT-}^\circ\text{F}}$$

$$\text{Beryllium without Blowers,} \quad h = .4 \frac{\text{BTU}}{\text{HR-FT-FT-}^\circ\text{F}}$$

APPENDIX K
HEAT CAPACITY AND THERMAL
CONDUCTIVITY CURVES

Contrails

The following three graphs show thermal conductivity, heat capacity, and thermal diffusivity for beryllium and carbon as a function of temperature. The carbon thermal conductivity is shown in both the radial (with ply) direction and the axial (across ply) direction. The beryllium data was obtained from Brush-Beryllium Company while the carbon data was measured specifically for this effort by Southern Research Institute.

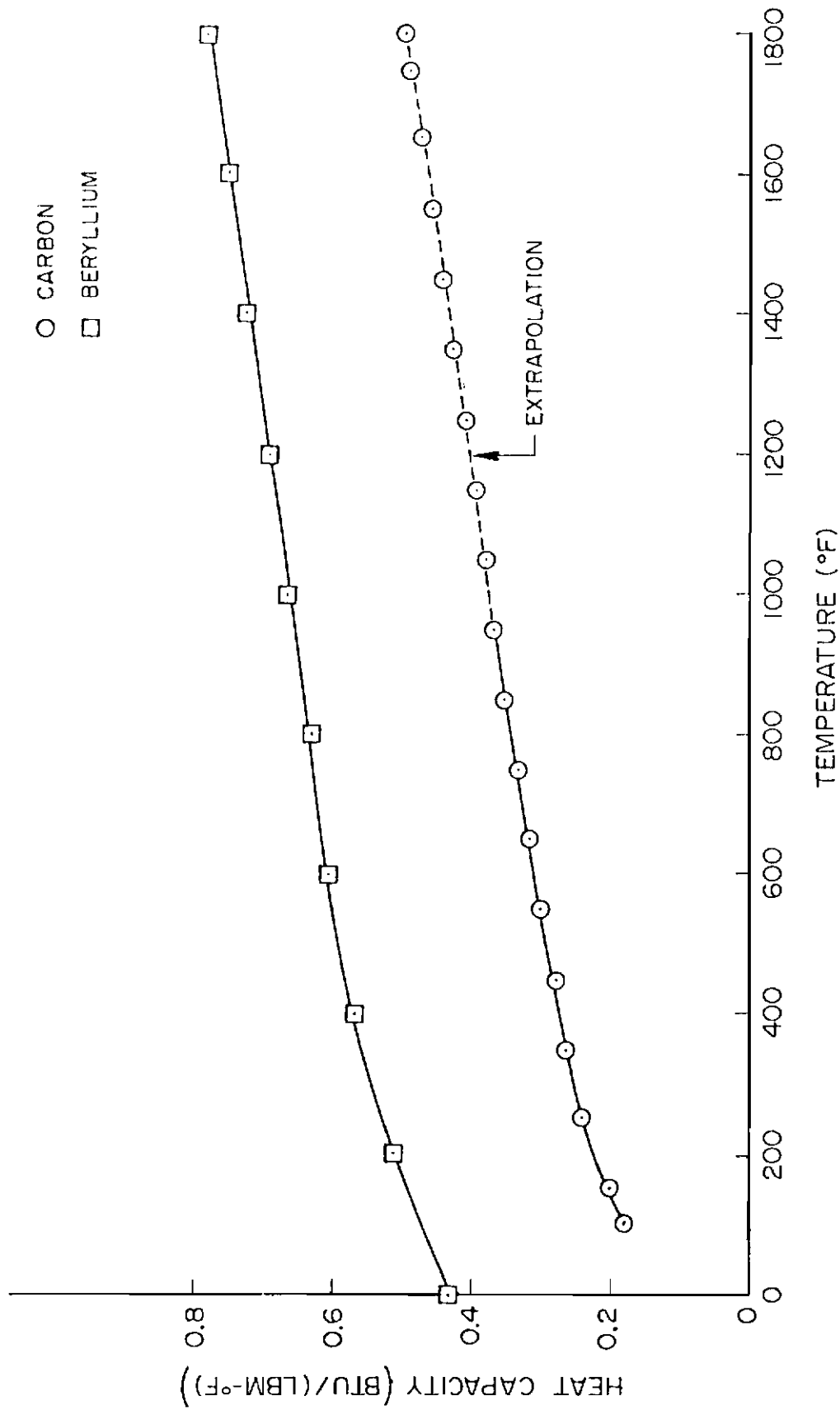


Figure K-1. Heat Capacity vs Temperature

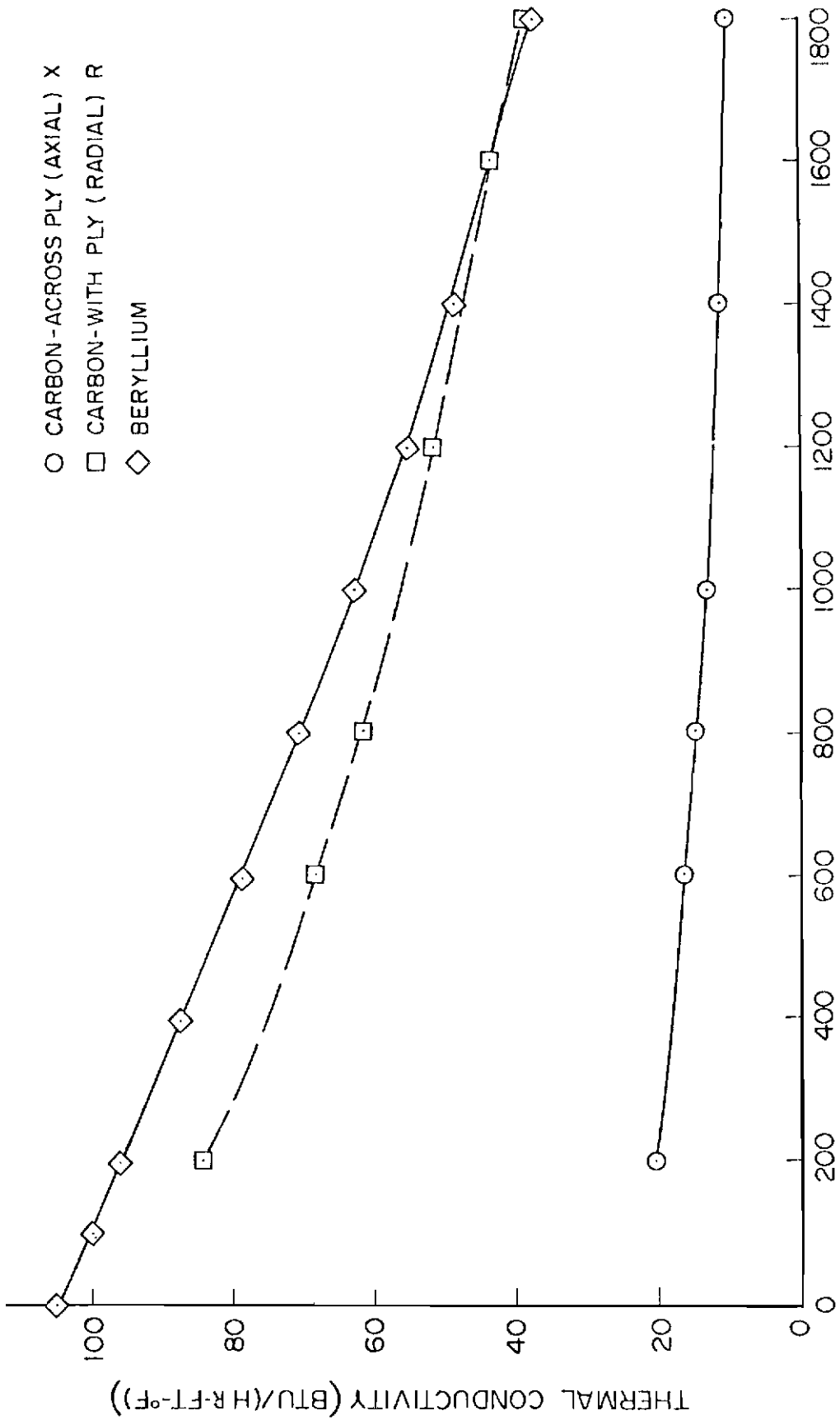


Figure K-2. Thermal Conductivity vs Temperature

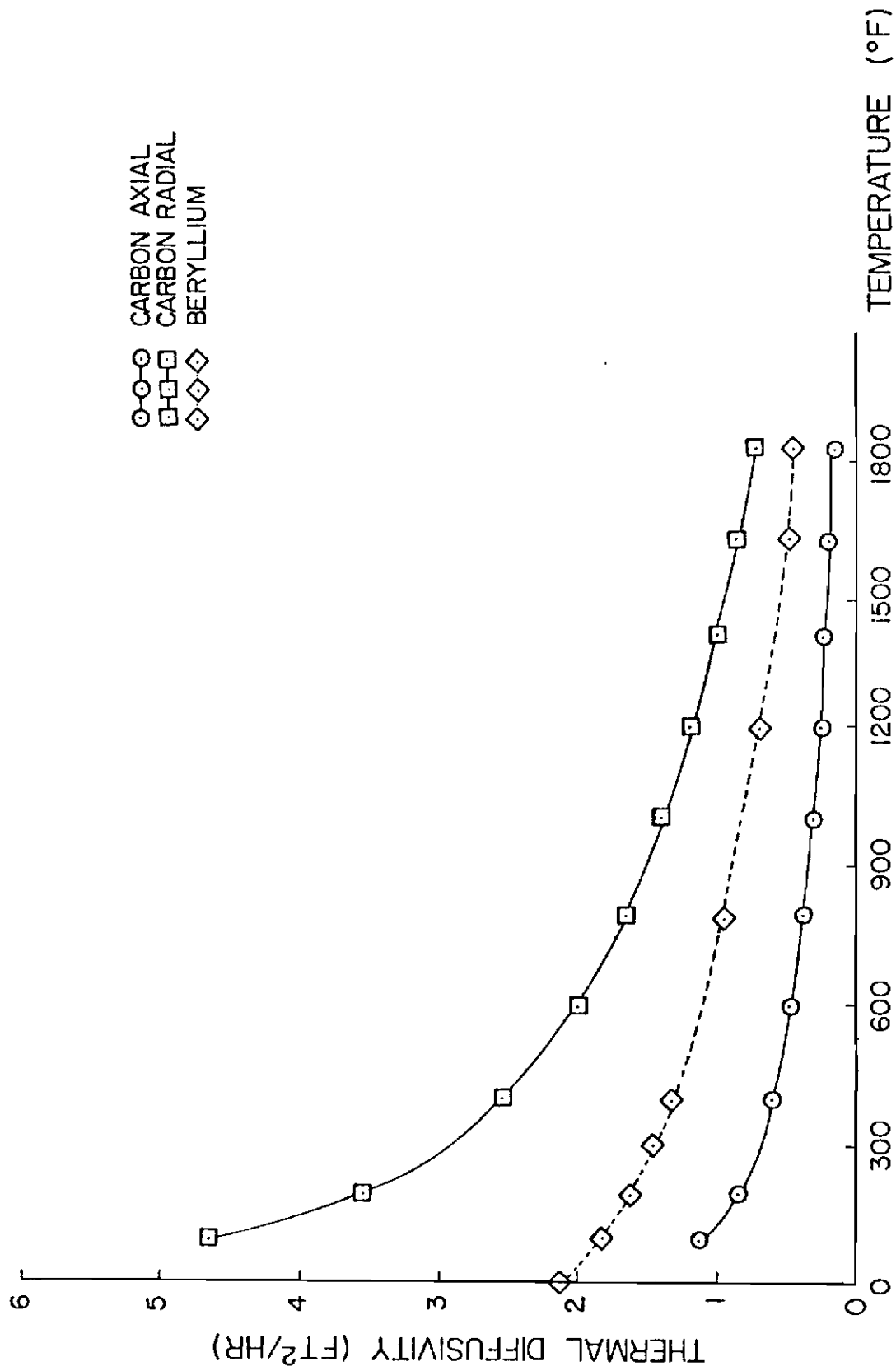


Figure K-3. Thermal Diffusivity vs Temperature

APPENDIX L

PROGRAM LISTING FOR ONE-DIMENSIONAL
RADIAL (IDR) TEMPERATURE
PREDICTION MODEL

```
PROGRAM IDR (INPUT,OUTPUT)
THIS PROGRAM SOLVES THE TRANSIENT ONE DIMENSIONAL
RADIAL HEAT TRANSFER EQUATION ASSUMING A WORK INPUT
DUE TO BRAKE FRICTION UNTIL THE STOP TIME IS REACHED.
AT 1.25* THE STOP TIME THE BRAKE IS
LUMPED INTO ONE MASS AT CONSTANT TEMPERATURE AND
ALLOWED TO COOL.
DIMENSION TN(61), T(61), TE(10), CVAL(10)
DIMENSION VALK(10), HVAL(10)
PRINT 100
FORMAT ("      RADIUS      TEMP      TIME")
INITIAL TEMPERATURE(F)
TO=129.
DELTA TIME(SEC)
DT=.02
DT2=DT/2.
INITIAL TEMPERATURE SET, T IS TEMP(F), TN IS NEW TEMP(F)
DO 1 I=1,61
TN(I)=TO
T(I)=TO
CONTINUE
DENSITY(LBM/CUBIC FEET)
RHO=108.
STOP TIME(SECONDS)
TS=56.
INITIAL VELOCITY(FT/SEC)
VO=207.
TEMPERATURE,TE(F), HEAT CAPACITY,CVAL (BTU/LBM-F), AND THERMAL
CONDUCTIVITY,KVAL,(BTU/HR-FT-F)
```

Contrails

TE(1)=100.
TE(2)=200.
TE(3)=400.
TE(4)=600.
TE(5)=800.
TE(6)=1000.
TE(7)=1200.
TE(8)=1400.
TE(9)=1600.
TE(10)=1800.
CVAL(1)=.18
CVAL(2)=.222
CVAL(3)=.275
CVAL(4)=.311
CVAL(5)=.343
CVAL(6)=.37
CVAL(7)=.401
CVAL(8)=.432
CVAL(9)=.464
CVAL(10)=.496
VALK(1)=89.9
VALK(2)=84.5
VALK(3)=75.1
VALK(4)=68.5
VALK(5)=61.2
VALK(6)=56.
VALK(7)=51.3
VALK(8)=47.2

```
VALK(9)=43.1
VALK(10)=38.9
CONVECTIVE/RADIATIVE HEAT TRANSFER COEFFICIENT (BTU/HR-FT-FT-F)
HVAL(1)=2.4
HVAL(2)=2.65
HVAL(3)=3.25
HVAL(4)=3.90
HVAL(5)=4.88
HVAL(6)=6.10
HVAL(7)=8.45
HVAL(8)=26.5
HVAL(9)=32.
HVAL(10)=37.
NDIM=NUMBER OF VALUES OF TE INSERTED INTO PROGRAM
NDIM=10
IDIM=NUMBER OF NODES IN RADIAL DIRECTION
IDIM=31
SIR=STATOR INSIDE RADIUS(IN)
SIR=3.75
SOR=STATOR OUTSIDE RADIUS(IN)
SOR=6.75
DR=DELTA RADIUS (IN)
DR=(SOR-SIR)/(FLOAT(IDIM-1))
CON=RHO*DR*DR*3600./144.
RIR=ROTOR INSIDE RADIUS
RIR=4.4
A=HALF OF STATOR THICKNESS
A=.34
RR=ROLLING RADIUS OF THE TIRE(IN)
```



```

RR=16.5
N=THE NUMBER OF FRICTION PAIRS
N=8
TINF IS AMBIENT TEMPERATURE(F)
TINF=80.
TI=0.
TIME(TI) INCREASED BY DELTA TIME
TI=TI+DT
IF(TI.LE.1.)TT=(18.*TI/1.5+6.)*70.72
IF(TI.GT.1..AND.TI.LE.9.)TT=(11.*TI/9.+17.)*70.72
IF(TI.GT.9..AND.TI.LE.TS)TT=(-14.*TI/58.+31.)*70.72
IF(TI.GT.TS)TT=0.
TH IS A HOLD TEMPERATURE FOR ENTRY INTO K,C SUBROUTINE
TH=T(1)
CALL INT(TE,VALK,TH,VK,DK,NDIM)
CALL INT(TE,CVAL,TH,C,DC,NDIM)
CALL INT(TE,HVAL,TH,H,DH,NDIM)
TN(1)=T(1)+(2.*DT*VK*(T(2)-T(1)))/(
6RHO*DR*DR*C)-2.*DT*H*(T(1)-TINF)/(RHO*12.*DR*C)*144./3600.
DTC1=CON*C/(2.*(VK+H*DR/12.))
DTC4=CON*C/VK
IDIMI=IDIM-1
DO 4 I=2,IDIMI
TH=T(I)
CALL INT(TE,VALK,TH,VK,DK,NDIM)
CALL INT(TE,CVAL,TH,C,DC,NDIM)
R=DR*(I-1)+SIR
A2=.552*TT*V0*(144.*3600/778.)*R*(1.-TI/TS)/(A+3.14159

```

```

6*RR*N*(SOR*SOR-RIR*RIR)
IF(TI.GE.TS) A2=0.
IF(R.LT.RIR) A2=0.
TN(I)=T(I)+(DT/(R*RHO*C))*((VK*R*(T(I+1)-2.*T(I))+T(I-1))
6/(OR*DR))+VK*(T(I+1)-T(I-1))/(2.*DR)+R*DK*((T(I+1)-T(I-1)))/(
62.*OR))*2.*A2)*144./3600.
R2=R+DR
IF(R.EQ.5.5)I445=I
IF(R.LT.5.5.AND.R2.GT.5.5)I445=I
DO 83 KK=1,40
TEST=FLOAT(KK-1)*5.
IF(ABS(TI-TEST).LT.DT2.AND.I.EQ.I445) PRINT 9,R,TN(I445),TI
IF(ABS(TI-TEST).LT.DT2.AND.I.EQ.I445) GO TO 84
CONTINUE
CONTINUE
CONTINUE
A1=.552*TT*R*/O*(1.-TI/TS)*(144.*3600./778.)/(N*RR*
62.*3.14159*A*(SOR*SOR-RIR*RIR))
TH=T(IDIM)
CALL INT(TE,VALK,TH,VK,DK,NDIM)
CALL INT(TE,CVAL,TH,C,DC,NDIM)
R=SOR
CALL INT(TE,HVAL,TH,H,DH,NDIM)
TN(IDIM)=T(IDIM)+(144./3600.)*(2.*DT/(RHO*R*C
6))*(-R*H*(T(IDIM)-TINF)/DR-VK*R*(T(IDIM)-T(IDIM-1
6))/(OR*DR)+A1)
DTC2=CON*C/VK
DTC3=CON*C/(2.*(VK+H*DR/12.))
TPI=TS/2.

```

83
84
4

```
IF (ABS(TI-TPI).GT.DT2) GO TO 10
DO 7 I=1, IOIM, 2
R=SIR+DR*(I-1)
PRINT 9, R, TN(I), II
CONTINUE
CONTINUE
FORMAT(1X, 6G12.6)
REPLACE OLD TEMPERATURE VALUES WITH NEW TEMPERATURES
DT=10.
IF (DTC1.LT.DT) DT=DTC1
IF (DTC2.LT.DT) DT=DTC2
IF (DTC3.LT.DT) DT=DTC3
IF (DTC4.LT.DT) DT=DTC4
DT=DT/2.
DT2=DT/2.
DO 11 I=1, IOIM
T(I)=TN(I)
IT=0
DO 77 II=1, IOIM
R=DR*(II-1)+SIR
IF (R.EQ.5.5) I445=II
R2=R+DR
IF (R.LT.5.5.AND.R2.GT.5.5) I445=II
CONTINUE
FORMAT(1X, 3G10.4, I5)
TS15=TS*1.25
IF (TI.LT. TS15) GO TO 78
PRINT 14
```

7
10
9
C

11

77
99

```

14  FORMAT ( "  TIME(MIN)    TEMP ")
    T4=TN(I445)
    IF(H.EQ.0.) PRINT 13,T4
    IF(H.EQ.0.) STOP
13  FORMAT(IX,3HT4=,G10.4,33HH=0. NO COOLING BEYOND THIS VALUE)
    T4=TN(I445)
    TII=TI/60.
    CONTINUE
    AA=1+(RIR*RIR-SIR*SIR)/(A*(SOR+SIR))
    CALL INT(TE,CVAL,T4,C,DC,NDIM)
    DTC5=RHO*(SOR-SIR)*60.*C/(2.*H*12.*(1+AA))
    DT=1.
    IF(DT.GT.DTC5)DT=DT/2.
    IF(DT.GT.DTC5) GO TO 79
    CALL INT(TE,HVAL,T4,H,DH,NDIM)
    TN4=T4-2.*H*DT*(12./60.)*(T4-TINF)*(1+AA)/(RHO*(SOR-SIR)*C
6)
    IF(IT.EQ.0)PRINT 9,II,T4
    IF(IT.EQ.5)IT=0
    II=II+1
    IF(IT.EQ.5) PRINT 9,TII,T4
    T4=TN4
    TII=TII+DT
    IF(T4.LT.200.) STOP
    GO TO 80
    CONTINUE
    GO TO 3
    END
78

```

```

SUBROUTINE INT(TE,CVAL,T,C,DC,NDIM)
DIMENSION TE(10),CVAL(10)
THE NEXT 10 STATEMENTS ASSIGN ENDPOINT C,DC, VALUES FOR TE
OUTSIDE OF CURVE ENDPOINTS
IF(T.LE.TE(NDIM)) GO TO 5
C=CVAL(NDIM)
DC=(CVAL(NDIM)-CVAL(NDIM-1))/(TE(NDIM-1))
RETURN
CONTINUE
IF(T.GE.TE(1)) GO TO 6
C=CVAL(1)
DC=(CVAL(2)-CVAL(1))/(TE(2)-TE(1))
RETURN
CONTINUE
DO 1 I=1,NDIM
IF(T.NE.TE(I)) GO TO 2
C=CVAL(I)
IF(I.EQ.10) DC=(CVAL(NDIM)-CVAL(NDIM-1))/(TE(NDIM)-TE(NDIM-1))
IF(I.EQ.10) GO TO 4
DC=(CVAL(I+1)-CVAL(I))/(TE(I+1)-TE(I))
CONTINUE
RETURN
CONTINUE
IF(T.LE.TE(I).OR.T.GE.TE(I+1)) GO TO 3
DC=(CVAL(I+1)-CVAL(I))/(TE(I+1)-TE(I))
C=CVAL(I)+(CVAL(I+1)-CVAL(I))*(T-TE(I))/(TE(I+1)-TE(I))
RETURN
CONTINUE
CONTINUE
CONTINUE
RETURN
END

```

APPENDIX M
CONTACT RESISTANCE VALUES
AND CALCULATION
PROCEDURE

Contrails

The procedure used to calculate the contact resistance at the rotor/stator sliding interface was to employ the empirical formula developed by Yu P. Shlykov and Ye A. Ganin.³⁹ The formula developed was compared to experimental data from other authors as well as to experimental data on four materials as tested by Shlykov and Ganin. The empirical formula is:

$$\frac{1}{RE} = \frac{K_A}{h} + \frac{.7 P K_M 10^4}{\sigma_B} \quad (M1)$$

where RE is the interface contact resistance, K_A is the thermal conductivity of the air trapped between the two surfaces in contact, h is the roughness (arithmetic average) of the contacting material surface (assuming identical materials), P is the pressure between the two surfaces, K_M is the thermal conductivity of the contacting material, σ_B is the yield strength of the contacting material and .7 is an empirical constant given in meters⁻¹. The air thermal conductivity was taken at the average interface temperature and the actual values were taken from the work of J. E. Fontenot, Jr.⁴⁰ The graph given by Fontenot was linearized to give:

$$K_A = (.00045 T + .335) \times 10^{-6} \text{ BTU}/(\text{IN-SEC-}^\circ\text{F}) \quad (M2)$$

The thermal conductivity of the contacting material, K_M , was also selected at the average interface temperature and was permitted to vary with temperature. The yield strength, σ_B was taken to be 14,000 psi for carbon and 10,000 psi for beryllium. The value of the roughness, h, was measured for both the carbon and the beryllium using a profilometer. The arithmetic roughness value for the carbon was

Contrails

.00137 in. while the value for beryllium was .00101 in. The final expression used to calculate the contact resistance of the beryllium heat sink was:

$$R_E = \frac{1}{513,270,000 \times K_A + .2134 \times P \times K_M} \quad (M3)$$

where K_A is found from Equation (M2), K_M is found from an interpolating subroutine and P , an input parameter, is the pressure between the two surfaces. Similarly, the final expression for calculating the contact resistance of the carbon material was:

$$R_E = \frac{1}{374,000,000 \times K_A + .1524 \times P \times K_M} \quad (M4)$$

Equations (M3) and (M4) require the following units:

$$K_A - \frac{\text{BTU}}{(\text{IN-SEC-}^\circ\text{F})}$$

$$K_M - \frac{\text{BTU}}{(\text{FT-HR}^\circ\text{F})}$$

$$P - \text{psig}$$

$$R_E - \frac{(\text{HR FT-FT-}^\circ\text{F})}{\text{BTU}}$$

APPENDIX N

PROGRAM LISTING FOR ONE-DIMENSIONAL
AXIAL (IDA) TEMPERATURE
PREDICTION MODEL

```

PROGRAM IDA (INPUT,OUTPUT)
THIS PROGRAM SOLVES THE TRANSIENT ONE DIMENSIONAL
AXIAL HEAT TRANSFER EQUATION ASSUMING A WORK INPUT
DUE TO BRAKE FRICTION UNTIL THE STOP TIME IS REACHED.
THE BRAKE WILL NOT COOL DOWN SINCE THERE IS NO HEAT
TRANSFERRED FROM THE BOUNDARIES.
DIMENSION TN(61), T(61), TE(10), CVAL(10)
DIMENSION JALK(10)
PRINT 101
101 FORMAT ( "      TIME      T (2)      T (7)      T (12)      T (13)
100      T (18)      X      T (23)      " )
C      INITIAL TEMPERATURE(F)      TEMP      TIME" )
TO=127.
C      DELTA TIME(SEC)
DT=.61
DT2=DT/2.
C      INITIAL TEMPERATURE SET, T IS TEMP(F), TN IS NEW TEMP(F)
DO 1 I=1,25
TN(I)=TO
T(I)=TO
CONTINUE
C      DENSITY(LBM/CUBIC FEET)
RHO=115.5
C      STOP TIME(SECONDS)
TS=36.
C      INITIAL VELOCITY(FT/SEC)
VO=212.
C      TEMPERATURE,TE(F), HEAT CAPACITY,CVAL(BTU/LBM-F), AND THERMAL

```

C CONDUCTIVITY, KVAL, (BTU/HR-FT-F)
TE(1)=0.
TE(2)=100.
TE(3)=200.
TE(4)=300.
TE(5)=400.
TE(6)=600.
TE(7)=1200.
TE(8)=1600.
TE(9)=2000.
TE(10)=2400.
CVAL(1)=.43
CVAL(2)=.47
CVAL(3)=.509
CVAL(4)=.54
CVAL(5)=.569
CVAL(6)=.63
CVAL(7)=.691
CVAL(8)=.751
CVAL(9)=.812
CVAL(10)=.872
VALK(1)=105.
VALK(2)=100.
VALK(3)=96.
VALK(4)=92.
VALK(5)=88.
VALK(6)=71.
VALK(7)=56.

```
VALK(8)=43.  
VALK(9)=33.  
VALK(10)=24.  
RT=HALF OF ROTOR THICKNESS(IN)  
RT=.27  
ST=HALF OF STATOR THICKNESS(IN)  
ST=.34  
RE=CONTACT RESISTANCE(HR-FT-FT-F/BTU)  
RE=.00078  
IF(RE.NE.0.)GO TO 13  
H=1.  
GO TO 14  
CONTINUE  
H=2./RE  
CONTINUE  
DXR=DISTANCE INCREMENT IN ROTOR(IN)  
DXR=RT/10.  
DXS=DISTANCE INCREMENT IN STATOR(IN)  
DXS=ST/10.  
DXA=(DXS+DXR)/2.  
NDIM=NUMBER OF VALUES OF TE INSERTED INTO PROGRAM  
NDIM=10  
IDIM=NUMBER OF NODES IN AXIAL DIRECTION  
IDIM=24  
SIR=STATOR INSIDE RADIUS(IN)  
SIR=4.4  
SOR=STATOR OUTSIDE RADIUS(IN)  
SOR=6.55  
RIR=ROTOR INSIDE RADIUS
```

```

RIR=4.67
RR=ROLLING RADIUS OF THE TIRE(IN)
RR=16.5
N=THE NUMER OF FRICTION PAIRS
N=8
TINF IS AMBIENT TEMPERATURE(F)
TINF=76.
TI=0.
TIME(TI) INCREASED BY DELTA TIME
TI=TI+DT
IF(TI.LE.9.5)TT=141.4*9.
IF(TI.GT.9.5.AND.TI.LE.28.5)TT=(TI-.5)*141.4
IF(TI.GT.28.5.AND.TI.LE.TS)TT=28.*141.4
TH IS A HOLD TEMPERATURE FOR ENTRY INTO K,C SUBROUTINE
IDIMI=IDIM-1
OO 4 I=2, IDIMI
TH=T(I)
CALL INT(TE,JALK,TH,VK,DK,NDIM)
CALL INT(TE,CVAL,TH,C,DC,NDIM)
A=DT/(RHO*C)
DX=DXR
IF(I.GT.13) DX=DXS
TN(I)=T(I)+A*((VK/(DX*DX))*(T(I+1)-2.*T(I)+T(I-1))+DK*((T(I+1)
6 -T(I-1))/(2.*DX))*(T(I+1)-T(I-1))/(2.*DX))*144./3600.
IF(I.EQ.2) DTC1=RHO*C*DX*DX*3600./(2.*144.*VK)
IF(I.EQ.23) DTC2=RHO*C*DX*DX*3600./(2.*144.*VK)
CONTINUE
4 TN(1)=TN(3)

```

```

IN(24)=TN(22)
DO 83 KK=1,40
TEST=FLOAT(KK-1)*5.
IF (ABS(TI-TEST).LT.DT2) PRINT 9, TI, T(2), T(7), T(12), T(13), T(18
6), T(23)
IF (ABS(TI-TEST).LT.DT2) GO TO 84
CONTINUE
CONTINUE
TH=T(12)
CALL INT(TE, VALK, TH, VK12, DK12, NDIM)
CALL INT(TE, CVAL, TH, C12, DC12, NDIM)
TH=T(13)
CALL INT(TE, VALK, TH, VK13, DK13, NDIM)
CALL INT(TE, CVAL, TH, C13, DC13, NDIM)
CA=(C12+C13)/2.
W=-1728.*TT*V0*(1.-TI/TS)/(N*RR*3.14159*(SOR*SOR-RIR)*778.)
IF(TI.GE.TS) W=0.
B=DXS*VK12/(DXR*VK13)
CZ=VK13*(T(14)-T(13))-B*T(12)+8*T(11))*12./(DXS*3600.)
CZZ=(VK13*(T(14)-T(13))+B*T(12)-8*T(11))*12./(DXS*3600.)
D=RHO*CA*OXA/(2.*DT*12.)
E=1.
F=RHO*C12*DXR/(2.*DT*12.)
G=1.
P=RHO*C13*OXS/(2.*DT*12.)
Q=1.
CALL INT(TE, VALK, T(12), VK12, DK12, NDIM)
CALL INT(TE, VALK, T(13), VK13, DK13, NDIM)
TRE=(T(12)+T(13))/2.

```

83
84

```
VKRE=(VK12+VK13)/2.  
PRESS=210.1  
JKA=.000452*TRF+.335  
RE=1/(513.3*VKA+.2134*PRESS*VKRE)  
H=2./RE  
TN(13)=(CZ+H*(T(12)-T(13))/3600.+F*G*((CZ-W)/(E*0))+T(13))+  
6T(13)*P*Q)/(F*G+P*Q)  
TN(12)=T(12)+T(13)-TN(13)+(CZ-W)/(E*0)  
IF(RE.NE.0.) GO TO 12  
TN(13)=T(13)+.5*((CZ-W)/(E*0))  
TN(12)=TN(13)  
CONTINUE  
DTC3=RHO*C*DX*DX*3600./(2.*144.*JK13)  
TPI=TS  
TPI2=TS/2.  
IF (ABS(TPI2-TI).LT.DT2) GO TO 17  
IF (ABS(TI-TPI).GT.DT2) GO TO 10  
CONTINUE  
PRINT 100  
X=-DXR  
DO 7 I=2, IOIMI  
DX=DXR  
IF(I.GT.12) DX=DXS  
IF(I.EQ.13) GO TO 16  
X=X+DX  
C XND=X NONDIMENSIONAL  
XND=X/(RT+ST)  
CONTINUE  
16
```

12

17

C

16

```
7 PRINT 9,X,XND,TN(I),TI  
10 CONTINUE  
9 CONTINUE  
C FORMAT(1X,7G12.6)  
11 REPLACE OLD TEMPERATURE VALUES WITH NEW TEMPERATURES  
DO 11 I=1, IDIM  
T(I)=TN(I)  
DT=10.  
IF(OTC1.LT.DT) DT=DTC1  
IF(OTC2.LT.DT) DT=DTC2  
IF(OTC3.LT.DT) DT=DTC3  
OT=DT/1.2  
OT2=OT/2.  
IF(TI.LE.TPI) GO TO 3  
STOP  
END
```



```

SUBROUTINE INT(TE,CVAL,T,C,DC,NDIM)
DIMENSION TE(10),CVAL(10)
THE NEXT 10 STATEMENTS ASSIGN ENDPOINT C,DC, VALUES FOR TE
OUTSIDE OF CURVE ENDPOINTS
IF(T.LE.TE(NDIM)) GO TO 5
C=CVAL(NDIM)
DC=(CVAL(NDIM)-CVAL(NDIM-1))/(TE(NDIM-1))
RETURN
CONTINUE
5 IF(T.GE.TE(1)) GO TO 6
C=CVAL(1)
DC=(CVAL(2)-CVAL(1))/(TE(2)-TE(1))
RETURN
CONTINUE
6 DO 1 I=1,NDIM
IF(T.NE.TE(I)) GO TO 2
C=CVAL(I)
IF(I.EQ.10) DC=(CVAL(NDIM)-CVAL(NDIM-1))/(TE(NDIM)-TE(NDIM-1))
IF(I.EQ.10) GO TO 4
DC=(CVAL(I+1)-CVAL(I))/(TE(I+1)-TE(I))
CONTINUE
4 RETURN
CONTINUE
2 IF(T.LE.TE(I).OR.T.GE.TE(I+1)) GO TO 3
DC=(CVAL(I+1)-CVAL(I))/(TE(I+1)-TE(I))
C=CVAL(I)+(CVAL(I+1)-CVAL(I))*(T-TE(I))/(TE(I+1)-TE(I))
RETURN
CONTINUE
3 CONTINUE
1 CONTINUE
RETURN
END
```

APPENDIX O

BOUNDARY CONDITION EQUATIONS FOR
TWO-DIMENSIONAL RADIAL/AXIAL
(R/S PAIR) MODEL

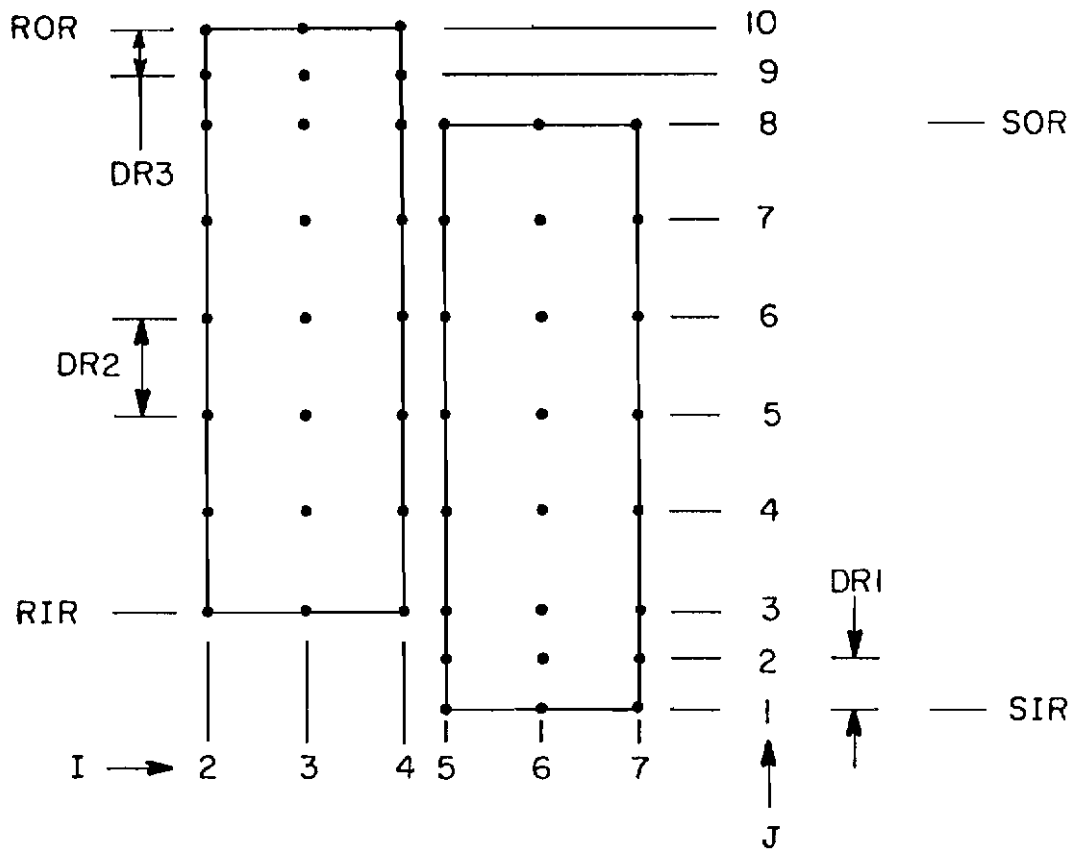


Figure 0-1. Two-Dimensional Grid Numbering Scheme

Contrails

BOUNDARY CONDITION EQUATIONS FOR IIDRA

$$\begin{aligned}
 T'(2,3) = T(2,3) + \frac{2\Delta t}{\rho DR2 DXR C} & \left\{ K_r DXR \frac{T(2,4) - T(2,3)}{DR2} \right. \\
 & \left. + K_x DR2 \frac{T(3,3) - T(2,3)}{DXR} - h DXR [T(2,3) - T_\infty] \right\} \quad (0-1)
 \end{aligned}$$

$$\begin{aligned}
 T'(2,10) = T(2,10) + \frac{2\Delta t}{\rho DR3 DXR C} & \left\{ K_x DR3 \frac{T(3,10) - T(2,10)}{DXR} \right. \\
 & \left. - K_r DXR \frac{T(2,10) - T(2,9)}{DR3} - h DXR [T(2,10) - T_\infty] \right\} \quad (0-2)
 \end{aligned}$$

$$\begin{aligned}
 T'(3,3) = T(3,3) + \frac{\Delta t}{\rho C} & \left\{ K_x \frac{T(4,3) - 2T(3,3) + T(2,3)}{DXR^2} \right. \\
 & + \frac{\partial K_x}{\partial T} \left[\frac{T(4,3) - T(2,3)}{2 DXR} \right]^2 + \frac{2K_r}{DR2} \frac{T(3,4) - T(3,3)}{DR2} \\
 & \left. - \frac{2h}{DR2} [T(3,3) - T_\infty] \right\} \quad (0-3)
 \end{aligned}$$

$$\begin{aligned}
 T'(3,10) = T(3,10) + \frac{\Delta t}{\rho C} & \left\{ K_x \frac{T(4,10) - 2T(3,10) + T(2,10)}{DXR^2} \right. \\
 & + \frac{\partial K_x}{\partial T} \left[\frac{T(4,10) - T(2,10)}{2 DXR} \right]^2 - \frac{2K_r}{DR3} \frac{T(3,10) - T(3,9)}{DR3} - \frac{2h}{DR3} \\
 & \left. [T(3,10) - T_\infty] \right\} \quad (0-4)
 \end{aligned}$$

Contrails

$$\begin{aligned}
 T'(4,10) = T(4,10) + \frac{2 \Delta t}{\rho \text{ DXR DR3 C}} & - \left\{ K_x \text{ DR3 } \frac{T(4,10) - T(3,10)}{\text{DXR}} \right. \\
 & \left. - K_r \text{ DXR } \frac{T(4,10) - T(4,9)}{\text{DR3}} - h (\text{DXR} + \text{DR3}) \left[T(4,10) - T_\infty \right] \right\} \quad (0-5)
 \end{aligned}$$

$$\begin{aligned}
 T'(5,1) = T(5,1) + \frac{2\Delta t}{\rho \text{ DXS DR1 C}} & \left\{ K_x \text{ DR1 } \frac{T(6,1) - T(5,1)}{\text{DXS}} \right. \\
 & \left. + K_r \text{ DXS } \frac{T(5,2) - T(5,1)}{\text{DR1}} - h (\text{DR1} + \text{DXS}) \left[T(5,1) - T_\infty \right] \right\} \quad (0-6)
 \end{aligned}$$

$$\begin{aligned}
 T'(5,2) = T(5,2) + \frac{2\Delta t}{\rho C} & \left\{ K_r \frac{T(5,3) - 2T(5,2) + T(5,1)}{\text{DR1}^2} \right. \\
 & + \frac{K_r}{r} \frac{T(5,3) - T(5,1)}{2 \text{ DR1}} + \frac{\partial K_r}{\partial T} \left[\frac{T(5,3) - T(5,1)}{2 \text{ DR1}} \right]^2 \\
 & \left. + \frac{2K_x}{\text{DXS}} \frac{T(6,2) - T(5,2)}{\text{DXS}} - \frac{2h}{\text{DXS}} \left[T(5,2) - T_\infty \right] \right\} \quad (0-7)
 \end{aligned}$$

$$\begin{aligned}
 T'(7,1) = T(7,1) + \frac{2\Delta t}{\rho \text{ DXS DR1 C}} & \left\{ -K_x \text{ DR1 } \frac{T(7,1) - T(6,1)}{\text{DXS}} \right. \\
 & \left. + K_r \text{ DXS } \frac{T(7,2) - T(7,1)}{\text{DR1}} - h (\text{DR1} + \text{DXS}) \left[T(7,1) - T_\infty \right] \right\} \quad (0-8)
 \end{aligned}$$

Contrails

$$\begin{aligned}
 T'(4,9) = T(4,9) + \frac{\Delta t}{\rho C} & \left\{ K_r \frac{T(4,10) - 2T(4,9) + T(4,8)}{DR3^2} \right. \\
 & + \frac{K_r}{r} \frac{T(4,10) - T(4,8)}{2 DR3} + \frac{\partial K_r}{\partial T} \left[\frac{T(4,10) - T(4,8)}{2 DR3} \right]^2 \\
 & \left. - \frac{2K_x}{DXR} \frac{T(4,9) - T(3,9)}{DXR} - \frac{2h}{DXR} \left[T(4,9) - T_\infty \right] \right\} \quad (0-9)
 \end{aligned}$$

$$\begin{aligned}
 T'(6,1) = T(6,1) + \frac{\Delta t}{\rho C} & \left\{ K_x \frac{T(7,1) - 2T(6,1) + T(5,1)}{DXS^2} \right. \\
 & + \frac{\partial K_x}{\partial T} \left[\frac{T(7,1) - T(5,1)}{2 DXS} \right]^2 + \frac{2K_r}{DR1} \frac{T(6,2) - T(6,1)}{DR1} \\
 & \left. - \frac{2h}{DR1} \left[T(6,1) - T_\infty \right] \right\} \quad (0-10)
 \end{aligned}$$

$$\begin{aligned}
 T'(6,8) = T(6,8) + \frac{\Delta t}{\rho C} & \left\{ K_x \frac{T(7,8) - 2T(6,8) + T(5,8)}{DXS^2} \right. \\
 & + \frac{\partial K_x}{\partial T} \left[\frac{T(7,8) - T(5,8)}{2 DXS} \right]^2 - \frac{2K_r}{DR2} \frac{T(6,8) - T(6,7)}{DR2} \\
 & \left. - \frac{2h}{DR2} \left[T(6,8) - T_\infty \right] \right\} \quad (0-11)
 \end{aligned}$$

$$\begin{aligned}
 T'(7,8) = T(7,8) + \frac{2\Delta t}{\rho DXS DR2 C} & \left\{ -K_x DR2 \frac{T(7,8) - T(6,8)}{DXS} \right. \\
 & \left. - K_r DXS \frac{T(7,8) - T(7,7)}{DR2} - h (DXS + DR2) \left[T(7,8) - T_\infty \right] \right\} \quad (0-12)
 \end{aligned}$$

Contrails

$$\begin{aligned}
 T'(5,8) = T(5,8) + \frac{2\Delta t}{\rho \text{ DR2 DXS C58}} & \left\{ \frac{T_T V_O \text{ DR2} \left(1 - \frac{t}{t_s}\right)}{N\pi 2 R_R (\text{SOR}^2 - \text{RIR}^2)} \right. \\
 + \frac{\text{DR2}}{2\text{RE}} [T(4,8) - T(5,8)] + \text{DR2 KX58} & \frac{T(6,8) - T(5,8)}{\text{DXS}} \\
 - h \text{ DXS } T(5,8) - T_\infty - \text{DXS KR58} & \left. \frac{T(5,8) - T(5,7)}{\text{DR2}} \right\} \quad (0-13)
 \end{aligned}$$

$$\begin{aligned}
 T'(4,8) = T(4,8) + \frac{4\Delta t}{\rho \text{ DXR (DR2+DR3)} \text{ C48}} & \left\{ - \frac{\rho \text{ DR2 DXS C58}}{4\Delta t} \right. \\
 [T'(5,8) - T(5,8)] + \frac{T_T \text{ DR2 } V_O}{N\pi 2 R_R} & \left(1 - \frac{t}{t_s}\right) \\
 - \text{KX48} \frac{\text{DR2} + \text{DR3}}{2} \frac{T(4,8) - T(3,8)}{\text{DXR}} & \\
 - \frac{h \text{ DR3}}{2} T(4,8) - T_\infty + \frac{\text{KR48 DXR}}{2} & \frac{T(4,9) - T(4,8)}{\text{DR3}} \\
 - \frac{\text{KR48 DXR}}{2} \frac{T(4,8) - T(4,7)}{\text{DR2}} & \left. \right\} \quad (0-14)
 \end{aligned}$$

Contrails

$$T'(4,3) = T(4,3) + \frac{\Delta t}{\rho \text{ DXR}} \left\{ \frac{T(5,3) - T(4,3)}{\text{RE}} \right.$$

$$+ \frac{T_T V_o \left(1 - \frac{t}{t_s}\right)}{N \pi R_R (\text{SOR}^2 - \text{SIR}^2)} - 2 \text{ KX43} \frac{T(4,3) - T(3,3)}{\text{DXR}}$$

$$\left. - \frac{2h \text{ DXR}}{\text{DR2}} [T(4,3) - T_\infty] + \frac{2\text{KR43} \text{ DXR}}{\text{DR2}} \frac{T(4,4) - T(4,3)}{\text{DR2}} \right\} \quad (0-15)$$

$$T'(5,3) = T(5,3) + \frac{2\Delta t \text{ DR2}}{\rho \text{ DXS} (\text{DR1} + \text{DR2})} \left\{ - \frac{\rho \text{ DXR}}{2\Delta t} [T'(4,3) - T(4,3)] \text{ C43} \right.$$

$$+ \frac{T_T V_o \left(1 - \frac{t}{t_s}\right)}{N (\text{SOR}^2 - \text{RIR}^2) \pi R_R} - \text{KX43} \frac{T(4,3) - T(3,3)}{\text{DXR}}$$

$$- \frac{h \text{ DXR}}{\text{DR2}} [T(4,3) - T_\infty] + \frac{\text{KR43} \text{ DXR}}{\text{DR2}} \frac{T(4,4) - T(4,3)}{\text{DR2}}$$

$$- \frac{\text{KR53} \text{ DXS}}{\text{DR2}} \frac{T(5,3) - T(5,2)}{\text{DR1}} + \frac{\text{KR53} \text{ DXS}}{\text{DR2}} \frac{T(5,4) - T(5,3)}{\text{DR2}}$$

$$\left. + \text{KX53} \frac{\text{DR1} + \text{DR2}}{\text{DR2}} \frac{T(6,3) - T(5,3)}{\text{DXS}} - \frac{h \text{ DR1}}{\text{DR2}} [T(5,3) - T_\infty] \right\} \quad (0-16)$$

The following two equations are for $T'(4,8) = T'(5,8)$ and $T'(4,3) = T'(5,3)$ when contact resistance is zero.

Contrails

$$T'(4,8) = T(4,8) + \frac{4\Delta t}{\rho [DXR (DR2+DR3) + DR2 DXS]} C48$$

$$\left\{ \begin{aligned} & - \frac{K_x (DR2+DR3)}{2} \frac{T(4,8) - T(3,8)}{DXR} + \frac{K_x DR2}{2} \frac{T(6,8) - T(5,8)}{DXS} \\ & - \frac{K_r (DXR+DXS)}{2} \frac{T(4,8) - T(4,2)}{DR2} + \frac{K_r DXR}{2} \frac{T(4,9) - T(4,8)}{DR3} \\ & - \frac{h (DR3+DXS)}{2} [T(4,8) - T_\infty] - \frac{\dot{W}_e}{2\pi r DR2} \end{aligned} \right\} \quad (0-17)$$

$$T'(4,3) = T(4,3) + \frac{4\Delta t}{\rho [DR2 DXR + DXS (DR1+DR2)]} C43$$

$$\left\{ \begin{aligned} & - \frac{K_x DR2}{2} \frac{T(4,3) - T(3,3)}{DXR} + \frac{K_x (DR2+DR1)}{2} \frac{T(6,3) - T(5,3)}{DXS} \\ & - \frac{K_r DXS}{2} \frac{T(5,3) - T(5,2)}{DR1} + \frac{K_r (DXS+DXR)}{2} \frac{T(4,4) - T(4,3)}{DR2} \\ & - \frac{h (DXR+DR1)}{2} [T(4,3) - T_\infty] + \frac{\dot{W}_e}{2\pi r DR2} \end{aligned} \right\} \quad (0-18)$$

Boundary condition equations derived for taking into account the wear pads that exist in some brakes are based on Figure 0-2. The temperature of the pad is designated TP(J) while the pad thickness is designated PT. The resulting equations for this interface condition are:

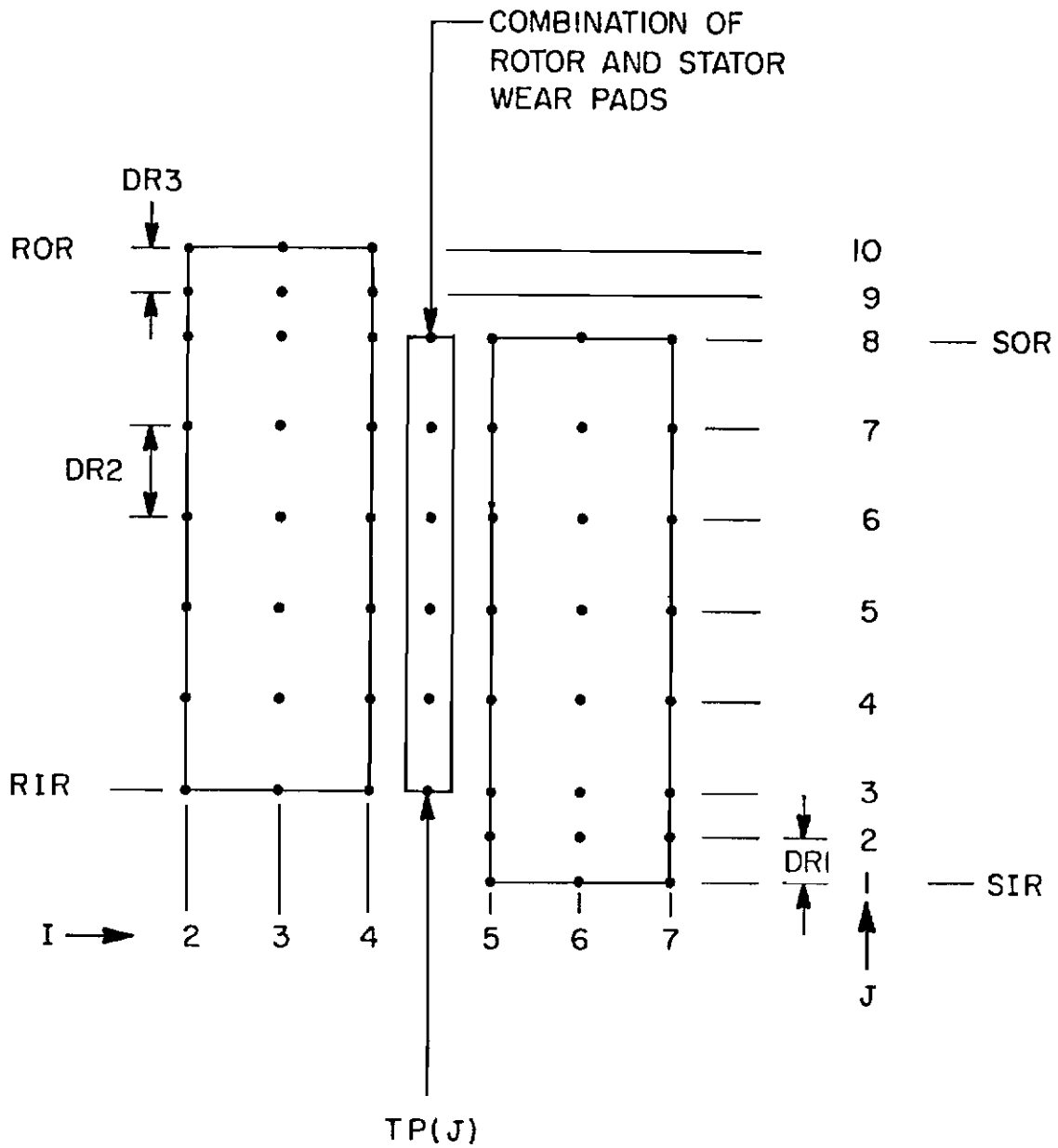


Figure O-2. Two-Dimensional Grid Numbering Scheme (with Wear Pads)

$$\begin{aligned}
 TP'(3) = TP(3) + \frac{\Delta t}{\rho C} & \left\{ \frac{2K_r}{DR^2} \frac{TP(4) - TP(3)}{DR^2} \right. \\
 & - \frac{2TP(3) - T(5,3) - T(4,3)}{PT RE} - \frac{2h}{DR^2} [TP(3) - T_\infty] \\
 & \left. + \frac{T_T V_o \left(1 - \frac{t}{t_s}\right)}{\pi N R_R PT (SOR^2 - RIR^2)} \right\} \quad (0-19)
 \end{aligned}$$

$$\begin{aligned}
 TP'(8) = TP(8) + \frac{\Delta t}{\rho C} & \left\{ - \frac{2K_r}{DR^2} \frac{TP(8) - TP(7)}{DR^2} \right. \\
 & - \frac{2h}{DR^2} [TP(8) - T_\infty] - \frac{2TP(8) - T(4,8) - T(5,8)}{RE PT} \\
 & \left. + \frac{T_T V_o \left(1 - \frac{t}{t_s}\right)}{\pi N R_R PT (SOR^2 - RIR^2)} \right\} \quad (0-20)
 \end{aligned}$$

$$\begin{aligned}
 TP'(J) = TP(J) + \frac{\Delta t}{\rho PT C} & \left\{ PT K_r \frac{TP(J+1) - 2TP(J) + TP(J-1)}{DR^2} \right. \\
 & + \frac{\partial K_r}{\partial T} \frac{TP(J+1) - TP(J-1)}{2 DR^2} + \frac{K_r}{r} \frac{TP(J+1) - TP(J-1)}{2 DR^2} \\
 & \left. - \frac{2TP(J) - T(5,J) - T(4,J)}{RE} + \frac{T_T V_o \left(1 - \frac{t}{t_s}\right)}{\pi N (SOR^2 - RIR^2) R_R} \right\} \quad (0-21)
 \end{aligned}$$

Contrails

$$\begin{aligned}
 T'(4, J) = T(4, J) + \frac{2\Delta t}{DXR \rho C} & \left\{ \frac{DXR}{2} \left[K_r \frac{T(4, J+1) - 2 T(4, J) + T(4, J-1)}{DR2^2} \right. \right. \\
 & + \frac{\partial K_r}{\partial T} \left(\frac{T(4, J+1) - T(4, J-1)}{2 DR2} \right)^2 + \frac{K_r}{r} \frac{T(4, J+1) - T(4, J-1)}{2 DR2} \left. \right] \\
 & - K_x \frac{T(4, J) - T(3, J)}{DXR} + \frac{TP(J) - T(4, J)}{RE} \left. \right\} \quad (0-22)
 \end{aligned}$$

$$\begin{aligned}
 T'(5, J) = T(5, J) + \frac{2\Delta t}{DXS \rho C} & \left\{ \frac{DXS}{2} \right. \\
 & \left[K_r \frac{T(4, J+1) - T(4, J-1)}{2 DR2} + \frac{\partial K_r}{\partial T} \left(\frac{T(5, J+1) - T(5, J-1)}{2 DR2} \right)^2 \right. \\
 & + \frac{K_r}{r} \frac{T(4, J+1) - T(4, J-1)}{2 DR2} \left. \right] + K_x \frac{T(6, J) - T(5, J)}{DXS} \\
 & + \frac{TP(J) - T(5, J)}{RE} \left. \right\} \quad (0-23)
 \end{aligned}$$

$$\begin{aligned}
 T'(4, 3) = T(4, 3) + \frac{4\Delta t}{\rho DXR DR2 C} & \left\{ \frac{K_r DXR}{2} \frac{T(4, 4) - T(4, 3)}{DR2} \right. \\
 & - \frac{K_x DR2}{2} \frac{T(4, 3) - T(3, 3)}{DXR} - \frac{h DXR}{2} [T(4, 3) - T_\infty] \\
 & + \frac{DR2 [TP(3) - T(4, 3)]}{2 RE} \left. \right\} \quad (0-24)
 \end{aligned}$$

Contrails

$$\begin{aligned}
 T'(5,3) = T(5,3) + \frac{4\Delta t}{\rho(DR1+DR2)DXS C} & \left\{ \frac{K_r DXS}{2} \frac{T(5,4) - T(5,3)}{DR2} \right. \\
 - \frac{K_r DXS}{2} \frac{T(5,3) - T(5,2)}{DR1} & + \frac{K_x (DR1+DR2)}{2} \frac{T(6,3) - T(5,3)}{DXS} \\
 + \frac{DR2 [TP(3) - T(5,3)]}{2 RE} & \left. - \frac{h DR1}{2} [T(5,3) - T_\infty] \right\} \quad (0-25)
 \end{aligned}$$

$$\begin{aligned}
 T'(4,8) = T(4,8) + \frac{4\Delta t}{\rho(DR2+DR3)(DXR)C} & \left\{ - \frac{K_x (DR2+DR3)}{2} \frac{T(4,8) - T(3,8)}{DXR} \right. \\
 - \frac{K_r DXR}{2} \frac{T(4,8) - T(4,7)}{DR2} & \\
 + \frac{K_r DXR}{2} \frac{T(4,9) - T(4,8)}{DR3} & - \frac{h DR3}{2} [T(4,8) - T_\infty] \\
 + \frac{DR2 [TP(8) - T(4,8)]}{2 RE} & \left. \right\} \quad (0-26)
 \end{aligned}$$

$$\begin{aligned}
 T'(5,8) = T(5,8) + \frac{4\Delta t}{\rho DXS DR2 C} & \left\{ - \frac{K_r DXS}{2} \frac{T(5,8) - T(5,7)}{DR2} \right. \\
 + \frac{K_x DR2}{2} \frac{T(6,8) - T(5,8)}{DXS} & - \frac{h DXS}{2} [T(5,8) - T_\infty] \\
 + \frac{DR2 [TP(8) - T(5,8)]}{2 RE} & \left. \right\} \quad (0-27)
 \end{aligned}$$

APPENDIX P

PROGRAM LISTING FOR TWO-DIMENSIONAL
RADIAL/AXIAL (R/S PAIR) (TIDRA)
TEMPERATURE PREDICTION MODEL

```

PROGRAM IIDRA (INPUT,OUTPUT)
THIS PROGRAM SOLVES THE TRANSIENT TWO DIMENSIONAL RADIAL/
AXIAL HEAT TRANSFER EQUATION ASSUMING A WORK INPUT
DUE TO BRAKE FRICTION UNTIL THE STOP TIME IS REACHED.
AT 1.25* THE STOP TIME THE BRAKE IS
LUMPED INTO ONE MASS AT CONSTANT TEMPERATURE AND
ALLOWED TO COOL.
DIMENSION TN(8,10), T(8,10), TE(10), CVAL(10)
DIMENSION VALKX(10), VALKR(10), HVAL(10),TP(10),TPN(10)
PRINT 100
100 FORMAT (" R TN(7,3) TN(4,5) TN(5,5) T(6,5) T(6,5)
65) TIME ")
C INITIAL TEMPERATURE(F)
TD=127.
C DELTA TIME(SEC)
DT=.001
DT2=DT/2.
C INITIAL TEMPERATURE SET, T IS TEMP(F), TN IS NEW TEMP(F)
DO 1 I=1,8
DO 2 J=1,10
TN(I,J)=TC
T(I,J)=TO
TP(J)=TO
TPN(J)=TO
2 CONTINUE
1 CONTINUE
C DENSITY (LBM/CUBIC FOOT)
RHO=115.5
C*****IF IPAD = 1 , THIS PROGRAM ASSUMES THAT WEAR PADS EXIST &

```

USES APPLICABLE EQUATIONS.....IF IPAD=0 NO WEAR PADS ARE ASSUMED
AND DIFFERENT EQUATIONS ARE SOLVED.

IPAD=1
PT=TOTAL PAD THICKNESS FOR ONE INTERFACE (IN)

PT=.1
PRHO=PAD DENSITY (LBM/CUBIC FT)

PRHO=100.

STOP TIME(SECONDS)

TS=36.

PRESS=EFFECTIVE BRAKE PRESSURE (LB/IN-IN)

PRESS=210.1

INITIAL VELOCITY(FT/SEC)

V0=212.

TEMPERATURE,TE(F), HEAT CAPACITY,CVAL(BTU/LBM-F), X-THERMAL

CONDUCTIVITY,VALKX(BTU/HR-FT-F), AND R-THERMAL CONDUCTIVITY,

VALKR(BTU/HR-FT-F)

TE(1)=0.

TE(2)=100.

TE(3)=200.

TE(4)=300.

TE(5)=400.

TE(6)=800.

TE(7)=1200.

TE(8)=1600.

TE(9)=2000.

TE(10)=2400.

CVAL(1)=.43

CVAL(2)=.47

CVAL(3)=.509
CJAL(4)=.540
CVAL(5)=.569
CVAL(6)=.63
CJAL(7)=.691
CVAL(8)=.751
CVAL(9)=.812
CVAL(10)=.872
JALKR(1)=105.
VALKR(2)=100.
VALKR(3)=96.
JALKR(4)=92.
VALKR(5)=88.
VALKR(6)=71.
VALKR(7)=56.
JALKR(8)=43.
VALKR(9)=33.
VALKR(10)=24.
VALKX(1)=105.
VALKX(2)=100.
VALKX(3)=96.
VALKX(4)=92.
JALKX(5)=88.
VALKX(6)=71.
VALKX(7)=56.
JALKX(8)=43.
VALKX(9)=33.
VALKX(10)=24.
CONVECTIVE/RADIATIVE HEAT TRANSFER COEFFICIENT (BTU/HR-FT-FT-F)

C

```
HVAL(1)=0.  
HVAL(2)=.31  
HVAL(3)=.81  
HVAL(4)=1.32  
HVAL(5)=1.8  
HVAL(6)=3.86  
HVAL(7)=5.89  
HVAL(8)=7.92  
HVAL(9)=9.95  
HVAL(10)=11.98  
C NDIM=NUMBER OF VALUES OF IE INSERTED INTO PROGRAM  
NDIM=10.  
C PRESS=EFFECTIVE BRAKE PRESSURE(LBF/IN-IN)  
PRESS=210.1  
C SIR=STATOR INSIDE RADIUS(IN)  
SIR=4.4  
C SOR=STATOR OUTSIDE RADIUS(IN)  
SOR=6.55  
C ROR=ROTOR OUTSIDE RADIUS(IN)  
ROR=6.8  
C RIR=ROTOR INSIDE RADIUS(IN)  
RIR=4.67  
C ST=HALF OF STATOR THICKNESS(IN)  
ST=.29  
C RT=HALF OF ROTOR THICKNESS(IN)  
RT=.22  
DKR=RT/2.  
DXS=ST/2.
```

```

DR1=(RIR-SIR)/2.
DR2=(SOR-RIR)/5.
DR3=(ROR-SOR)/2.
DXA=(DXS+DXR)/2.
C   RK=ROLLING RADIUS OF THE TIRE(IN)
RR=16.5
C   N=THE NUMBER OF FRICTION PAIRS
N=8
C   TINF IS AMBIENT TEMPERATURE(F)
TINF=76.
TI=0.
C   A=COOLING AREA DURING COOL DOWN(IN-IN)
A=2.*3.14159*PI*(ROR+RIR)+2.*3.14159*ST*(SOR+SIR)+3.14159*
6 (ROR+ROR-SOR+SOR)+3.14159*(RIR+RIR-SIR+SIR)
IF(IPAD.EQ.1)A=A+3.14159*PI*2.*(RIR+SOR)
C   V=VOLUME OF ROTOR AND STATOR FOR USE IN COOL DOWN(IN-IN)
V=3.14159*(ROR+ROR-RIR+RIR)*RT+3.14159*(SOR+SOR-SIR+SIR)*ST
IF(IPAD.EQ.1)V=V+PI*3.14159*(SOR**2-RIR**2)
C   TIME(TI) INCREASED BY DELTA TIME
TI=TI+DT
C   TT=TORQUE (FT-LB)
TT=TORQUE (FT-LB)
IF(TI.LE.9.5)TT=141.4*9.
IF(TI.GT.9.5.AND.TI.LE.28.5)TT=(TI-.5)*141.4
IF(TI.GT.28.5.AND.TI.LE.TS)TT=28.*141.4
IF(TI.GT.TS)TT=0.
C   TH IS A HOLD TEMPERATURE FOR ENTRY INTO K,C SUBROUTINE
C   SUTC=SAVE VALUE FOR DT CRITICAL CALCULATION
SDTC=10.
III=0

```

```
DO 4 I=2,7
DO 5 J=2,9
IF (I.EQ.4.OR.I.EQ.5) GO TO 4
IF (J.LT.4.AND.J.LE.5) GO TO 5
IF (J.GT.7.AND.I.GT.5) GO TO 5
CALL INT(TE,VALKX,T(I,J),VKX,DKX,NDIM)
CALL INT(TE,VALKR,T(I,J),VKR,OKR,NDIM)
IF (I.LT.4) DX=DXR
IF (I.GT.5) DX=DXS
IF (J.EQ.2) R=SIR+DR1
IF (J.EQ.3) R=RIR
IF (J.EQ.4) R=RIR+DR2
IF (R.LT.RIR) DR=DR1
IF (R.GE.RIR.AND.R.LT.SOR) DR=DR2
IF (R.GE.SOR) DR=DR3
IF (J.GT.4) R=R+DR
IF (R.GE.RIR.AND.R.LT.SOR) DRP=DR2
IF (R.GE.SOR) DRP=DR3
IF (R.LT.RIR) DRP=DR1
IF (R.LE.RIR) DRM=DR1
IF (R.GT.RIR.AND.R.LE.SOR) DRM=DR2
IF (R.GT.SOR) DRM=DR3
A1=(T(I+1,J)-T(I-1,J))/(2.*DX)
A2=(T(I+1,J)-2.*T(I,J)+T(I-1,J))/(DX*DX)
A3=(T(I,J+1)-T(I,J-1))/(DRP+DRM)
A4=((T(I,J+1)-T(I,J))/DRP)-(T(I,J)-T(I,J-1))/DRM)/((DRP+DRM)*.5)
CALL INT(TE,CVAL,T(I,J),C,DC,NDIM)
DTC1=RHO*C*3600./(144.*(2.*VKR/(DRP*DRM)+2.*VKX/(DX*DX)))
```

```

IF (QTC1.LT.SDTC) SDTC=DTC1
TN(I,J)=T(I,J)+((DT*(144./3600.))/(RHO*C))*((VKR*A4)+(DKR*A3
6*A3)+((VKR*A3)/R)+(VKX*A2)+(DKX*A1*A1))
5 CONTINUE
4 CONTINUE
DO 6 J=2,9
TN(3,J)=TN(6,J)
TN(1,J)=TN(3,J)
6 CONTINUE
CALL INT(TE,VALKX,T(2,3),VKX,DKX,NDIM)
CALL INT(TE,VALKR,T(2,3),/KR,DKR,NDIM)
CALL INT(TE,CVAL,T(2,3),C,DC,NDIM)
CALL INT(TE,HVAL,T(2,3),H,DH,NDIM)
TN(2,3)=T(2,3)+((2.*DT*(144./3600.))/(RHO*DR2*DXR*C
6))*((/KR*DXR)/DR2)*((T(2,4)-T(2,3))-((H*DXR)/12.))
6*(T(2,3)-TINF))+VKX*DR2*(T(3,3)-T(2,3))/DXR)
CALL INT(TE,VALKX,T(2,10),VKX,DKX,NDIM)
CALL INT(TE,/ALKR,T(2,10),/KR,DKR,NDIM)
CALL INT(TE,CVAL,T(2,10),C,DC,NDIM)
CALL INT(TE,HVAL,T(2,10),H,DH,NDIM)
TN(2,10)=T(2,10)+((2.*DT*(144./3600.))/(RHO*DR3*DXR*C
6))*((/KX*DR3)/DXR)*((T(3,10)-T(2,10))-((VKR*DXR)/DR3)*((T(2,
610)-T(2,9))-((H*DXR)/12.))*((T(2,10)-TINF))
CALL INT(TE,VALKX,T(3,3),VKX,DKX,NDIM)
CALL INT(TE,/ALKR,T(3,3),/KR,DKR,NDIM)
CALL INT(TE,CVAL,T(3,3),C,DC,NDIM)
CALL INT(TE,HVAL,T(3,3),H,DH,NDI
TN(3,3)=T(3,3)+((DT*(144./3600.))/(RHO*C))*((VKX*(T(4,3)
6-2.*T(3,3)+T(2,3))/(DXR*DXR)+DKX*((T(4,3)-T(2,3))/(2.*DXR))*

```

```

6*2.+2.*DKR*(T(3,4)-T(3,3))/(DR2*DR2)-2.*H*(T(3,3)-TINF)/(12.*
6DR2)
CALL INT(TE,VALKX,T(3,10),JKX,DKX,NDIM)
CALL INT(TE,VALKR,T(3,10),VKR,DKR,NDIM)
CALL INT(TE,CVAL,T(3,10),C,DC,NDIM)
CALL INT(TE,HVAL,T(3,10),H,DH,NDIM)
TN(3,10)=T(3,10)+((DT*(144./3600.))/(RHO*C))
6*((VKX/(DXR*DXR))*T(4,10)-(2.*T(3,10))+T(2,10))+(DKX*
6((T(4,10)-T(2,10))/(2*DXR))*2)-((2.*VKR)/(DR3**2))*((
6T(3,10)-T(3,9))-((2.*H)/(DR3*12.))*T(3,10)-TINF))
CALL INT(TE,VALKX,T(4,10),VKX,DKX,NDIM)
CALL INT(TE,VALKR,T(4,10),VKR,DKR,NDIM)
CALL INT(TE,CVAL,T(4,10),C,DC,NDIM)
CALL INT(TE,HVAL,T(4,10),H,DH,NDIM)
TN(4,10)=T(4,10)+((2.*DT*(144./3600.))/(RHO*DXR*DR3*C
6))*((-VKX*DR3)/DXR)*T(4,10)-T(3,10))-((VKR*DXR)/DR3)*T(4
6,10)-T(4,9))-((H*(DXR+DR3))/12.)*T(4,10)-TINF))
CALL INT(TE,VALKX,T(5,1),VKX,DKX,NDIM)
CALL INT(TE,VALKR,T(5,1),VKR,DKR,NDIM)
CALL INT(TE,CVAL,T(5,1),C,DC,NDIM)
CALL INT(TE,HVAL,T(5,1),H,DH,NDIM)
TN(5,1)=T(5,1)+((2.*DT*(144./3600.))/(RHO*DXS*DR1*C))
6*((VKX*DR1)/DXS)*T(6,1)-T(5,1))+((VKR*DXS)/DR1)*T(5,2)-T(
65,1))-((H*(DR1+DXS))/12.)*T(5,1)-TINF))
CALL INT(TE,VALKX,T(7,1),VKX,DKX,NDIM)
CALL INT(TE,VALKR,T(7,1),VKR,DKR,NDIM)
CALL INT(TE,CVAL,T(7,1),C,DC,NDIM)
CALL INT(TE,HVAL,T(7,1),H,DH,NDIM)

```

```

TN(7,1)=T(7,1)+((2.*DT*(144./3600.))/(RHO*DXS*DR1*C))
6*(((-VKX*DR1)/DXS)*T(7,1)-T(6,1))+((VKR*DXS)/DR1)*T(7,2)-T
6(7,1))-((H*(OXS))/12.)*T(7,1)-TINF))
CALL INT(TE,JALKX,T(7,8),JKX,DKX,NDIM)
CALL INT(TE,VALKR,T(7,8),VKR,DKR,NDIM)
CALL INT(TE,CVAL,T(7,8),C,DC,NDIM)
CALL INT(TE,HVAL,T(7,8),H,DH,NDIM)
TN(7,8)=T(7,8)+((2.*DT*(144./3600.))/(RHO*DXS*DR2*C))
6*(((-VKX*DR2)/DXS)*T(7,8)-T(6,8))-VKR*(DXS/DR2)*T(7,8)-T(7
6,7))-((H*(DXS+DR2)/12.)*T(7,8)-TINF))
CALL INT(TE,JALKX,T(5,2),JKX,DKX,NDIM)
CALL INT(TE,VALKR,T(5,2),VKR,DKR,NDIM)
CALL INT(TE,CVAL,T(5,2),C,DC,NDIM)
CALL INT(TE,HVAL,T(5,2),H,DH,NDIM)
R=SIR+DR1
TN(5,2)=T(5,2)+((DT*(144./3600.))/(RHO*C))*(VKR*(T(
65,3)-2.*T(5,2)+T(5,1))/(DR1**2))+((VKR/(2.*R*DR1))*T(5,3)-
6T(5,1)))+(DKR*(T(5,3)-T(5,1))/(2.*DR1)**2)+((2.*VKX)/(DXS*
6*2))*T(6,2)-T(5,2))+((-2.*H)/(12.*DXS))*T(5,2)-TINF))
CALL INT(TE,VALKR,T(4,9),VKX,DKX,NDIM)
CALL INT(TE,JALKR,T(4,9),JKR,DKR,NDIM)
CALL INT(TE,CVAL,T(4,9),C,DC,NDIM)
CALL INT(TE,HVAL,T(4,9),H,DH,NDIM)
R=SOR+DR3
TN(4,9)=T(4,9)+((DT*(144./3600.))/(RHO*C))*(VKR/(DR3
6*DR3))*T(4,10)-2.*T(4,9)+T(4,8))+((VKR/(2.*R*DR3))*T(4,10)
6-T(4,8)))+(DKR*(T(4,10)-T(4,8))/(2.*DR3)**2))-((2.*VKX)/
6(OXR*DXR))*T(4,9)-T(3,9))-((2.*H)/(12.*DXR))*T(4,9)-TINF
6))

```

```

CALL INT(TE, VALKX, T(6, 1), VKX, DKX, NDIM)
CALL INT(TE, VALKR, T(6, 1), VKR, DKR, NDIM)
CALL INT(TE, CVAL, T(6, 1), C, DC, NDIM)
CALL INT(TE, HVAL, T(6, 1), H, DH, NDIM)
TN(6, 1) = T(5, 1) + (DT*(144./3600.)) / (RHO*C) * ((VKX)/(DXS
6 *DXS)) * (T(7, 1) - 2.*T(6, 1) + T(5, 1)) + (DKX*((T(7, 1) - T(5, 1)) / (2.
6 *DXS)) **2) + (((2.*VKR)/(DR1*DR1)) * (T(6, 2) - T(6, 1))) - (((2.*H)/
6 (12.*DR1)) * (T(6, 1) - TINF))
CALL INT(TE, VALKX, T(6, 8), VKX, DKX, NDIM)
CALL INT(TE, VALKR, T(6, 8), VKR, DKR, NDIM)
CALL INT(TE, CVAL, T(6, 8), C, DC, NDIM)
CALL INT(TE, HVAL, T(6, 8), H, DH, NDIM)
TN(6, 8) = T(6, 8) + (DT*(144./3600.)) / (RHO*C) * ((VKX)/(D
6XS *DXS)) * (T(7, 8) - 2.*T(6, 8) + T(5, 8)) + (DKX*((T(7, 8) - T(5, 8)) / (
62.*DXS)) **2) - (((2.*VKR)/(DR2*DR2)) * (T(6, 8) - T(6, 7))) - (((2.*H
6)/DR2)) * ((T(6, 8) - TINF) / 12.))
DO 8 J=4, 7
P=RIR+DR2*(J-3)
T3=(T(6, J) - T(5, J)) / DXS
T4=(T(4, J+1) - 2.*T(4, J) + T(4, J-1)) / (DR2*DR2)
T5=(T(4, J+1) - T(4, J-1)) / (2.*DR2)
T6=(T(4, J) - T(3, J)) / DXR
CALL INT(TE, CVAL, T(4, J), C4, DC4, NDIM)
CALL INT(TE, VALKR, T(4, J), VKR4J, DKR4J, NDIM)
CALL INT(TE, VALKX, T(4, J), VKX4J, DKX4J, NDIM)
W=TT*VO*(1.-TI/TS)*666.1/(3.14159*N*RR*(SOR**2-RIR**2))
TN(4, J) = T(4, J) + (2.*DT*(144./3600.)) / (RHO*(DXR+DXS)*C4) * (-VKX4J*T6
6+VKX4J*T3+(DXR+DXS)*(VKR4J*T4+DKR4J*T5+VKR4J*T5/R).5+W)

```



```

TN(5,J)=TN(4,J)
IF(IPAD.NE.1) GO TO 300
T1=(T(5,J+1)-2.*T(5,J)+T(5,J-1))/DR2**2
T2=(T(5,J+1)-T(5,J-1))/(2.*DR2)
T3=(T(6,J)-T(5,J))/DXS
CALL INT(TE,CVAL,T(5,J),C5,DC5,NDIM)
CALL INT(TE,VALKR,T(5,J),VKR5J,DKR5J,NDIM)
CALL INT(TE,VALKX,T(5,J),VKX5J,DKX5J,NDIM)
DC=0.
CALL INT(TE,VALKX,TP(J),PK,DK,NDIM)
PK=.426*PK
PC=.12
RE=.005
TPN(J)=TP(J)+(.04*DT/(PRHO*PC))*(PT*(PK*(TP(J+1)-2.*TP(
6 J)+TP(J-1))/DR2**2+OK*((TP(J+1)-TP(J-1))/(2.*DR2))**2+PK*(TP(J+1)
6 -TP(J-1))/(2.*R*DR2))-(2.*TP(J)-T(5,J)-T(4,J))/(RE*12.))+W)
TN(4,J)=T(4,J)+(DT*.04*2./(RHO*DXR*C4))*(DXR/2.)*(VKR4J*T4+DKR4J
6 *T5**2+VKR4J*T5/R)-VKX4J*T6+(TP(J)-T(4,J))/(RE*12.))
TN(5,J)=T(5,J)+(DT*.04*2./(RHO*DXS*C5))*(DXS/2.)*(VKR5J*T1+DKR5J*
6 T2**2+VKR5J*T2/R)+VKX5J*T3+(TP(J)-T(5,J))/(RE*12.))
CONTINUE
CONTINUE
T7=(T(4,8)-T(4,7))/DR2
T8=(T(4,9)-T(4,8))/DR3
T9=(T(4,8)-T(3,8))/DXR
T10=(T(6,8)-T(5,8))/DXS
T12=(T(5,3)-T(5,2))/DR1
T14=(T(6,3)-T(5,3))/DXS
T15=(T(4,3)-T(3,3))/DXR

```

300
8

```
T16=(T(4,4)-T(4,3))/DR2
CALL INT(TE,CVAL,T(4,8),C48,OC48,NDIM)
CALL INT(TE,CJAL,T(4,3),C43,DC43,NDIM)
CALL INT(TE,VALKX,T(4,8),VKX48,DKX48,NDIM)
CALL INT(TE,VALKX,T(4,3),VKX43,DKX43,NDIM)
CALL INT(TE,JALKR,T(4,8),JKR48,DKR48,NDIM)
CALL INT(TE,VALKR,T(4,3),VKR43,DKR43,NDIM)
W=W*DR2/2.
CALL INT(TE,HVAL,T(4,8),H4,DH,NDIM)
TN(4,8)=T(4,8)+(4.*DT*(144./3600.)/(RHO*(DXR*(DR2+DR3)+DR2*DXS)*C
648))*(-VKX48*T9*(DR2+DR3)/2.+VKX48*T10*DR2/2.-VKR48*(DXR+DXS)*
6T7/2.+VKR48*DXR*T8/2.-H4*(DR3+DXS)*(T(4,8)-TINF)/2.+W)
TN(5,8)=TN(4,8)
CALL INT(TE,HVAL,T(4,3),H,OH,NDIM)
TN(4,3)=T(4,3)+(4.*DT*(144./3600.)/(RHO*(DR2*DXR+DXS*(DR1+DR2))*C
643))*(-VKX43*T15*DR2/2.+VKX43*(DR2+DR1)*T14/2.-VKR43*DXS*T12/2.
6+VKR43*(DXS+DXR)*T16/2.-H*(DXR+DR1)*(T(4,3)-TINF)/2.+W)
TN(5,3)=TN(4,3)
IF(IPAD.NE.1) GO TO 301
CALL INT(TE,VALKX,T(5,3),VKX53,DKX53,NDIM)
CALL INT(TE,VALKR,T(5,3),VKR53,DKR53,NDIM)
CALL INT(TE,CJAL,T(5,3),C53,DC53,NDIM)
CALL INT(TE,VALKX,T(5,8),VKX58,DKX58,NDIM)
CALL INT(TE,JALKR,T(5,8),JKR58,DKR58,NDIM)
CALL INT(TE,CVAL,T(5,8),C58,DC58,NDIM)
CALL INT(TE,VALKX,TP(3),PK,DK,NDIM)
DC3=0.
PK3=.425*PK
```

```

PC3=.12
CALL INT(TE, VALKX, TP(8), PK, DK, NDIM)
DC8=0.
PK3=.425*PK
PC8=.12
RE3=.005
RE8=.005
CALL INT(TE, HVAL, T(4,3), H, DH, NDIM)
TN(4,3)=T(4,3)+(4.*.04*DT/(RHO*C43*DXR*DR2))*(VKR43*DXR*T16/2.-VKX
643*DK2*T15/2.-H*DXR*(T(4,3)-TINF)/(2.*12.))+DR2*(TP(3)-T(4,3))/
6(2.*RE3*12.)
CALL INT(TE, HVAL, T(5,3), H, DH, NDIM)
TN(5,3)=T(5,3)+(4.*.04*DT/(RHO*C53*DXS*(DR1+DR2)))*(VKR53*DXS*(T(5
6,4)-T(5,3))/(2.*DR2)-JKR53*DXS*(T(5,3)-T(5,2))/(2.*DR1)+JKX53
6*(DR2+DR1)*(T(6,3)-T(5,3))/(2.*DXS)+
6DR2*(TP(3)-T(5,3))/(2.*RE3*12.)-H*DR1*(T(5,3)-TINF)/(2.*12.)
TN(4,8)=T(4,8)+(DT*.04*4./(RHO*C48*DXR*(DR2+DR3)))*(-JKX48*T9*(
6DR2+DR3)/2.-VKR48*DXR*T7/2.+VKR48*DXR*T8/2.-H4*DR3*(T(4,8)-TINF
6)/(2.*12.))+DR2*(TP(8)-T(4,8))/(2.*RE8*12.)
CALL INT(TE, HVAL, T(5,8), H, DH, NDIM)
TN(5,8)=T(5,8)+(4.*.04*DT*4./(RHO*C58*DXS*DR2))*(-VKR58*DXS*(T(5,8)-T
6(5,7))/(2.*DR2)+VKX58*DR2*(T(6,8)-T(5,8))/(2.*DXS)-H*DXS*(T(5,8)
6-TINF)/(2.*12.))+DR2*(TP(6)-T(5,8))/(2.*RE8*12.)
W=666.1*TT*VO*(1.-TI/T5)/(RR*N*3.14159*PT*(SOR**2-RIR**2))
CALL INT(TE, HVAL, TP(3), H, DH, NDIM)
TPN(3)=TP(3)+(DT*.04/(PRHO*PC3))*(2.*PK3*(TP(4)-TP(3)
5)/DR2**2-(2.*TP(3)-T(5,3)-T(4,3))/(PT*RE3*12.)-2.*H*(TP(3)-TINF
6)/(DR2*12.)+W)
CALL INT(TE, HVAL, TP(8), H, DH, NDIM)

```

```

301  TPN(8)=TP(8)+(DT*.04/(PRHO*PC8))*(-2.*PK8*(TP(8)-TP(7))
      6/DR2**2-2.*H*(TP(8)-TINF)/(DR2*12.)-(2.*TP(8)-T(4,8)-T(5,8))/(
      6RE8*PT*12.)*W)
      CONTINUE
      DO 83 KK=1,40
      T55=TN(7,5)+.207*(TN(7,6)-TN(7,5))
      TEST=FLOAT(KK-1)*5.
      IF (ABS(TI-TEST).LT.DT2) PRINT 9,RIR,TN(7,3),TN(4,5),TN(5,5),T55
      6,II
      IF(ABS(TI-TEST).GE.DT2) GO TO 141
      DO 140 J=1,10
      K=11-J
      CONTINUE
      CONTINUE
      14c  IF (ABS(TI-TEST).LT.DT2) GO TO 84
      14d  CONTINUE
      83   TPI=TS/2.
      34   IF (ABS(TI-TPI).GT.DT2) GO TO 10
      101  PRINT 101
      6    FORMAT ("      R      TN(4,J)      TN(5,J)      TN(6,J)      TN(7,J)
          6      TIME      ")
      DO 7 J=1,8
      IF (J.EQ.1) R=SIR
      IF (J.EQ.2) R=SIR+DR1
      IF (J.GE.3) R=RIR+FLOAT(J-3)*DR2
      PRINT 9,R,TN(4,J),TN(5,J),TN(6,J),TN(7,J),TI
      CONTINUE
      7

```

```
10 PRINT 100
CONTINUE
9 FORMAT(1X,6G12.6)
C REPLACE OLD TEMPERATURE VALUES WITH NEW TEMPERATURES
DT=10.
IF(SDTC.LT.DT)DT=SDTC
DT=DT/2.
DT2=DT/2.
DO 11 I=1,8
DO 12 J=1,10
TP(J)=TPN(J)
T(I,J)=TN(I,J)
12 CONTINUE
11 IT=0
99 FORMAT(1X,3G10.4,I5)
TS15=TS*2.
IF(TI.LT.TS15) GO TO 78
PRINT 14
FORMAT ( " TIME(MIN) TEMP ")
TT4=T(7,3)
IF(H.EQ.0.) PRINT 13,TT4
IF(H.EQ.0.)STOP
13 FORMAT(1X,4HTT4=,G10.4,33HH=0. NO COOLING BEYOND THIS VALUE)
TTI=TT/50.
C IN THIS SECTION OF THE PROGRAM, ALL NODES ARE LUMPED AND
C ALLOWED TO COOL AS ONE MASS.
30 CONTINUE
CALL INT(TE,CJAL,TT4,C,DC,NDIM)
CALL INT(TE,HVAL,TT4,H,OH,NDIM)
```

```
79      DTC5=RHO*V*C*60./(H*A*12.)  
        DT=1.  
        IF(DT.GT.DTC5)DT=DT/2.  
        IF(DT.GT.DTC5) GO TO 79  
        TN4=TT4+DT*(12./60.)*H*A*(TINF-TT4)/(RHO*V*C)  
        IF(IT.EQ.0) PRINT 9,II,TT4  
        IF(IT.EQ.5) IT=0  
        IT=IT+1  
        IF(IT.EQ.5) PRINT 9,TII,TT4  
        TT4=TN4  
        TII=TII+DT  
        IF(TT4.LT.200.) STOP  
        GO TO 80  
78      CONTINUE  
        IF(TI.LT.TS.OR.TI.GT.(TS+DT)) GO TO 3  
        DO 130 J=1,10  
        K=11-J  
        PRINT 131,K,T(2,K),T(3,K),T(4,K),T(5,K),T(6,K),T(7,K)  
        CONTINUE  
131     FORMAT (1X,I5,6F10.3)  
        GO TO 3  
        END
```

```

SUBROUTINE INT(TE,CVAL,T,C,DC,NDIM)
DIMENSION TE(10),CVAL(10)
THE NEXT 10 STATEMENTS ASSIGN ENDPOINT C,DC, VALUES FOR TE
C
C OUTSIDE OF CURVE ENDPOINTS
IF(T.LE.TE(NDIM)) GO TO 5
C=CVAL(NDIM)
DC=(CVAL(NDIM)-CVAL(NDIM-1))/(TE(NDIM-1))
RETURN
5 CONTINUE
IF(T.GE.TE(1)) GO TO 6
C=CVAL(1)
DC=(CVAL(2)-CVAL(1))/(TE(2)-TE(1))
RETURN
6 CONTINUE
DO 1 I=1,NDIM
IF(T.NE.TE(I)) GO TO 2
C=CVAL(I)
IF(I.EQ.10) DC=(CVAL(NDIM)-CVAL(NDIM-1))/(TE(NDIM)-TE(NDIM-1))
IF(I.EQ.10) GO TO 4
DC=(CVAL(I+1)-CVAL(I))/(TE(I+1)-TE(I))
CONTINUE
RETURN
2 CONTINUE
IF(T.LE.TE(I).OR.T.GE.TE(I+1)) GO TO 3
DC=(CVAL(I+1)-CVAL(I))/(TE(I+1)-TE(I))
C=CVAL(I)+(CVAL(I+1)-CVAL(I))*(T-TE(I))/(TE(I+1)-TE(I))
RETURN
3 CONTINUE
1 CONTINUE
RETURN
END

```

APPENDIX Q
BOUNDARY CONDITION EQUATIONS
FOR THREE-DIMENSIONAL
(R/S PAIR) MODEL

Contrails

BOUNDARY CONDITIONS WITHOUT A WORK RATE TERM

For the boundary conditions in this section the following 13 equations are used to allow the remaining equations to be condensed.

$$THO = \frac{K_{\theta} [T(I,J,K+1) - T(I,J,K)]}{(r\Delta\theta)^2} \quad (Q-1)$$

$$THI = \frac{-K_{\theta} [T(I,J,K) - T(I,J,K-1)]}{(r\Delta\theta)^2} \quad (Q-2)$$

$$THIO = \left\{ \frac{K_{\theta} [T(I,J,K+1) - 2 T(I,J,K) + T(I,J,K-1)]}{(\Delta\theta)^2} + \frac{\partial K_{\theta}}{\partial T} \left[\frac{[T(I,J,K+1) - T(I,J,K-1)]}{(2\Delta\theta)} \right]^2 \right\} / r^2 \quad (Q-3)$$

$$RO = \frac{K_r [T(I,J+1,K) - T(I,J,K)]}{(\Delta r)^2} \quad (Q-4)$$

$$RI = \frac{-K_r [T(I,J,K) - T(I,J-1,K)]}{(\Delta r)^2} \quad (Q-5)$$

$$RIO = \frac{K_r [T(I,J+1,K) - 2 T(I,J,K) + T(I,J-1,K)]}{(\Delta r)^2} + \frac{K_r [T(I,J+1,K) - T(I,J-1,K)]}{(2r\Delta r)} + \frac{\partial K_r}{\partial T} \left[\frac{[T(I,J+1,K) - T(I,J-1,K)]}{(2\Delta r)} \right]^2 \quad (Q-6)$$

$$XO = \frac{K_x [T(I+1, J, K) - T(I, J, K)]}{(\Delta x)^2} \quad (Q-7)$$

$$XI = \frac{-K_x [T(I, J, K) - T(I-1, J, K)]}{(\Delta x)^2} \quad (Q-8)$$

$$XIO = \frac{K_x [T(I+1, J, K) - 2 T(I, J, K) + T(I-1, J, K)]}{(\Delta x)^2} + \frac{\partial K_x}{\partial T} \left[\frac{[T(I+1, J, K) - T(I-1, J, K)]^2}{(2\Delta x)} \right]^2 \quad (Q-9)$$

$$THH = \frac{-h [T(I, J, K) - T_\infty]}{(r\Delta\theta)} \quad (Q-10)$$

$$RH = \frac{-h [T(I, J, K) - T_\infty]}{\Delta r} \quad (Q-11)$$

$$XH = \frac{-h [T(I, J, K) - T_\infty]}{\Delta x} \quad (Q-12)$$

$$W = \frac{\Delta t}{\rho C} \quad (Q-13)$$

$$T'(2, 10, 4) = T(2, 10, 4) + 2 W(THI+RI+THH+RH+XO) \quad (Q-14)$$

$$T'(3, 10, 4) = T(3, 10, 4) + \left(\frac{XIO}{2} + THI+RI+THH+RH \right) \quad (Q-15)$$

$$T'(4, 10, 4) = T(4, 10, 4) + 2 W(THI+THH+RI+RH+XI+XH) \quad (Q-16)$$

$$T'(4, 10, 2-3) = T(4, 10, 2-3) + W (THIO+RI+RH+XI+XH) \quad (Q-17)$$

Contrails

$$T'(2,4-7,5) = T(2,4-7,5) + 2W \left(\frac{RIO}{2} + THI + XO \right) \quad (Q-18)$$

$$T'(2,10,2-3) = T(2,10,2-3) + 2W \left(RI + RH + \frac{THIO}{2} + XO \right) \quad (Q-19)$$

$$T'(3,4-7,5) = T(3,4-7,5) + W(XIO + RIO + 2THI) \quad (Q-20)$$

$$T'(3,10,2-3) = T(3,10,2-3) + W(XIO + THIO + 2RI + 2RH) \quad (Q-21)$$

$$T'(2,3,5) = T(2,3,5) + 2W(RO + RH + XO + THI) \quad (Q-22)$$

$$T'(2,10,1) = T(2,10,1) + 2W(RI + RH + THO + XO) \quad (Q-23)$$

$$T'(3,10,1) = T(3,10,1) + 2W(RI + RH + XIO + THO) \quad (Q-24)$$

$$T'(4,10,1) = T(4,10,1) + 2W(XI + XH + RI + RH + THO) \quad (Q-25)$$

$$T'(2,9,4) = T(2,9,4) + 2W \left(\frac{RIO}{2} + THI + THH + XO \right) \quad (Q-26)$$

$$T'(3,9,4) = T(3,9,4) + W(RIO + XIO + 2THI + 2THH) \quad (Q-27)$$

$$T'(4,9,4) = T(4,9,4) + 2W \left(\frac{RIO}{2} + XI + XH + THI + THH \right) \quad (Q-28)$$

$$T'(4,9,2-3) = T(4,9,2-3) + W(RIO + THIO + 2XI + 2XH) \quad (Q-29)$$

$$T'(3,3,5) = T(3,3,5) + 2W \left(\frac{XIO}{2} + RO + RH + THI \right) \quad (Q-30)$$

$$T'(4,9,1) = T(4,9,1) + 2W \left(\frac{RIO}{2} + XI + XH + THO \right) \quad (Q-31)$$

$$T'(2,8,4) = T(2,8,4) + \frac{2}{3} W (2THI + THO + THH + 2RI + RO + RH + 3XO) \quad (Q-32)$$

Contrails

$$T'(3,8,4) = T(3,8,4) + \frac{2}{3} W(1.5XIO+2THI+THO+THH+2RI+RO+RH) \quad (Q-33)$$

$$T'(2,8,5) = T(2,8,5) + 2W(RI+RH+THI+XO) \quad (Q-34)$$

$$T'(3,8,5) = T(3,8,5) + 2W\left(\frac{XIO}{2} + RI+RH+THI\right) \quad (Q-35)$$

$$T'(6,8,1) = T(6,8,1) + 2W\left(\frac{XIO}{2} + RI+RH+THO\right) \quad (Q-36)$$

$$T'(6,8,2-4) = T(6,8,2-4) + W\left(\frac{XIO}{2} + 2RI+2RH+THIO\right) \quad (Q-37)$$

$$T'(7,8,1) = T(7,8,1) + 2W(RI+RH+XI+THI) \quad (Q-38)$$

$$T'(7,8,2-4) = T(7,8,2-4) + 2W\left(\frac{THIO}{2} + RI+RH+XI\right) \quad (Q-39)$$

$$T'(6,8,5) = T(6,8,5) + 2W\left(\frac{XIO}{2} + RI+RH+THI\right) \quad (Q-40)$$

$$T'(7,8,5) = T(7,8,5) + 2W(RI+RH+XI+THI) \quad (Q-41)$$

$$T'(6,4-7,5) = T(6,4-7,5) + W(XIO+RIO+2THI) \quad (Q-42)$$

$$T'(7,4-7,5) = T(7,4-7,5) + 2W\left(\frac{RIO}{2} + XI+THI\right) \quad (Q-43)$$

$$T'(6,3,5) = T(6,3,5) + 2W\left(\frac{XIO}{2} + RO+RH+THI\right) \quad (Q-44)$$

$$T'(7,3,5) = T(7,3,5) + 2W(RO+RH+XI+THI) \quad (Q-45)$$

$$T'(7,1,4) = T(7,1,4) + 2 W(RO+RH+XI+THI) \quad (Q-46)$$

$$T'(7,2,4) = T(7,2,4) + 2W\left(\frac{RIO}{2} + XI+THI\right) \quad (Q-47)$$

Contrails

$$T'(7,3,4) = T(7,3,4) + \frac{2}{3} W(RI+3XI+2RO+RH+2THI+THO+THH) \quad (Q-48)$$

$$T'(6,3,4) = T(6,3,4) + \frac{2}{3} W(1.5XIO+2THI+THO+THH+RI+RH+2RO) \quad (Q-49)$$

$$T'(6,1,4) = T(6,1,4) + 2W \left(\frac{XIO}{2} + THI+THH+RO+RH \right) \quad (Q-50)$$

$$T'(7,1,2-3) = T(7,1,2-3) + 2W \left(RO+RH+ \frac{THIO}{2} + XI \right) \quad (Q-51)$$

$$T'(7,1,1) = T(7,1,1) + 2 W(RO+RH+THO+XI) \quad (Q-52)$$

$$T'(7,2-7,1) = T(7,2-7,1) + 2W \left(\frac{RIO}{2} + THO+XI \right) \quad (Q-53)$$

$$T'(5,1,4) = T(5,1,4) + 2 W(XO+XH+RO+RH+THI+THH) \quad (Q-54)$$

$$T'(5,2,4) = T(5,2,4) + 2W \left(\frac{RIO}{2} + XO+XH+THI+THH \right) \quad (Q-55)$$

$$T'(6,2,4) = T(6,2,4) + 2W \left(\frac{XIO}{2} + \frac{RIO}{2} + THI+THH \right) \quad (Q-56)$$

$$T'(6,2-7,1) = T(6,2-7,1) + W(XIO+RIO+2THO) \quad (Q-57)$$

$$T'(6,1,1) = T(6,1,1) + 2W \left(\frac{XIO}{2} + RO+RH+THO \right) \quad (Q-58)$$

$$T'(5,1,2-3) = T(5,1,2-3) + 2W \left(\frac{THIO}{2} + RO+RH+XO+XH \right) \quad (Q-59)$$

$$T'(5,1,1) = T(5,1,1) + 2 W(XO+XH+RO+RH+THO) \quad (Q-60)$$

Contrails

$$T'(5,2,1) = T(5,2,1) + 2W \left(\frac{RIO}{2} + XO+XH+THO \right) \quad (Q-61)$$

$$T'(5,2,2-3) = T(5,2,2-3) + W(2XO+2XH+THIO+RIO) \quad (Q-62)$$

$$T'(3,3,1) = T(3,3,1) + 2W \left(\frac{XIO}{2} + RO+RH+THO \right) \quad (Q-63)$$

$$T'(3,4-9,1) = T(3,4-9),1) + W(XIO+RIO+2THO) \quad (Q-64)$$

$$T'(2,3,1) = T(2,3,1) + 2W (THO+RO+RH+XO) \quad (Q-65)$$

$$T'(2,4-9,1) = T(2,4-9,1) + 2W \left(\frac{RIO}{2} + XO+THO \right) \quad (Q-66)$$

$$T'(2,3,2-4) = T(2,3,2-4) + 2W \left(\frac{THIO}{2} + RO+RH+XO \right) \quad (Q-67)$$

$$T'(3,3,2-4) = T(3,3,2-4) + W(THIO+XIO+2RO+2RH) \quad (Q-68)$$

$$T'(6,1,2-3) = T(6,1,2-3) + W(THIO+XIO+2RO+2RH) \quad (Q-69)$$

BOUNDARY CONDITIONS CONTAINING A WORK RATE TERM

Figure Q-1 shows the way in which the rotor and stator wear-surface elements were identified. The rotor and the stator each have 10 different kinds of elements. For instance, all rotor elements numbered 6 have five heat flow paths (r-direction in, r-direction out, θ -direction in, θ -direction out, x-direction in). The rotor elements numbered 5 are different since they have four heat flow paths (r-direction in, r-direction out, θ -direction in, x-direction in). As discussed in Chapter V, equations were developed for the rotor independently from the stator and the two added at the applicable time

Contrails

increment. The following 20 equations are those developed for the different numbered elements as shown on Figure Q-1. Equations (Q-1) through (Q-13) are again utilized so that the equations will be shorter. The stator elements are identified with the letter S while the rotor elements are identified with the letter R.

$$S1; RI + THI + RH + XO - \dot{W}_5 = \frac{[T'(5,J,K) - T(5,J,K)]}{W} \quad (Q-70)$$

$$S2; RI + THIO + RH + XO - \dot{W}_5 = \frac{[T'(5,J,K) - T(5,J,K)]}{W} \quad (Q-71)$$

$$S3; RI + THO + RH + XO - \dot{W}_5 = \frac{[T'(5,J,K) - T(5,J,K)]}{W} \quad (Q-72)$$

$$S4; \frac{RIO}{2} + THO + XO - \dot{W}_5 = \frac{[T'(5,J,K) - T(5,J,K)]}{W} \quad (Q-73)$$

$$S5; \frac{RIO}{2} + THI + XO - \dot{W}_5 = \frac{[T'(5,J,K) - T(5,J,K)]}{W} \quad (Q-74)$$

$$S6; \frac{RIO}{2} + \frac{THIO}{2} + XO - \dot{W}_5 = \frac{[T'(5,J,K) - T(5,J,K)]}{W} \quad (Q-75)$$

$$S7; RO + THI + XO + RH - \dot{W}_5 = \frac{[T'(5,J,K) - T(5,J,K)]}{W} \quad (Q-76)$$

$$S8; RO + THI + 1.5 XO$$

$$+ \frac{(RH+RI+THH+THO+XH5)}{2} - \dot{W}_5 = \frac{1.5 [T'(5,J,K) - T(5,J,K)]}{W} \quad (Q-77)$$

$$S9; 2XO + THIO + RIO + XH - \dot{W}_5 = \frac{2 [T'(5,J,K) - T(5,J,K)]}{W} \quad (Q-78)$$

$$S10; RIO + 2THO + 2XO + XH5 - \dot{W}_5 = \frac{2 [T'(5,J,K) - T(5,J,K)]}{W} \quad (Q-79)$$

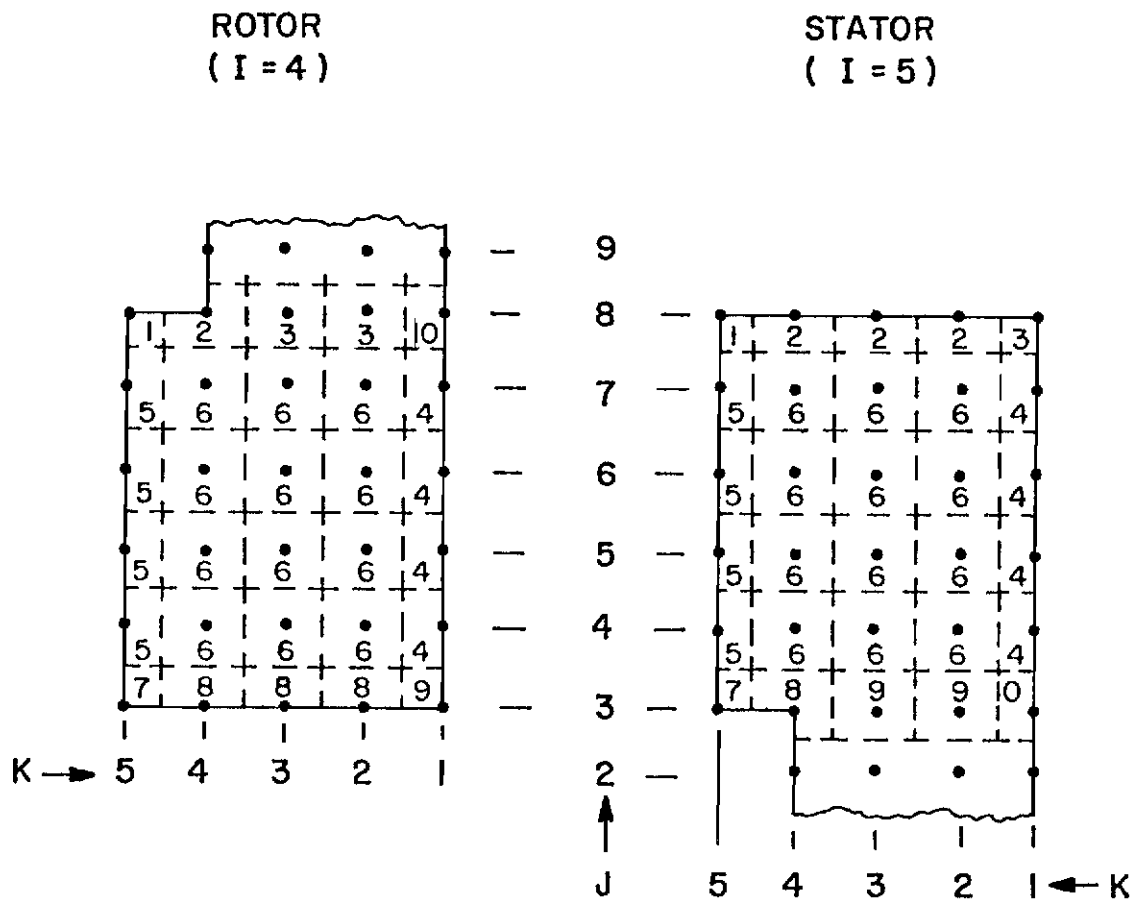


Figure Q-1. Wear-Surface Element Identification

Contrails

$$R1; RI + THI + RH + XI - \dot{W}_4 = \frac{[T'(4,J,K) - T(4,J,K)]}{W} \quad (Q-80)$$

$$R2; RI + THI + \frac{(RO+THO+RH+TTH+1.5XI+XH)}{2} - \dot{W}_4 = 1.5 \frac{[T'(4,J,K) - T(4,J,K)]}{W} \quad (Q-81)$$

$$R3; XH + THIO + RIO + 2XI - \dot{W}_4 = \frac{2 [T'(4,J,K) - T(4,J,K)]}{W} \quad (Q-82)$$

$$R4; \frac{RIO}{2} + THO + XI - \dot{W}_4 = \frac{[T'(4,J,K) - T(4,J,K)]}{W} \quad (Q-83)$$

$$R5; \frac{RIO}{2} + THI + XI - \dot{W}_4 = \frac{[T'(4,J,K) - T(4,J,K)]}{W} \quad (Q-84)$$

$$R6; \frac{RIO}{2} + \frac{THIO}{2} + XI - \dot{W}_4 = \frac{[T'(4,J,K) - T(4,J,K)]}{W} \quad (Q-85)$$

$$R7; RO + THI + XI + RH - \dot{W}_4 = \frac{[T'(4,J,K) - T(4,J,K)]}{W} \quad (Q-86)$$

$$R8; RO + THIO + RH + XI - \dot{W}_4 = \frac{[T'(4,J,K) - T(4,J,K)]}{W} \quad (Q-87)$$

$$R9; RO + THO + RH + XI - \dot{W}_4 = \frac{[T'(4,J,K) - T(4,J,K)]}{W} \quad (Q-88)$$

$$R10; RIO + 2THO + XH + XI - \dot{W}_4 = \frac{2 [T'(4,J,K) - T(4,J,K)]}{W} \quad (Q-89)$$

APPENDIX R

PROGRAM LISTING FOR THREE-DIMENSIONAL
(R/S PAIR) TEMPERATURE
PREDICTION MODEL

```

PROGRAM I110 (INPUT,OUTPUT)
THIS PROGRAM SOLVES THE TRANSIENT THREE DIMENSIONAL
HEAT TRANSFER EQUATION ASSUMING A WORK INPUT
DUE TO BRAKE FRICTION UNTIL THE STOP TIME IS REACHED.
AT 1.25* THE STOP TIME THE BRAKE IS
LUMPED INTO ONE MASS AT CONSTANT TEMPERATURE AND
ALLOWED TO COOL.
DIMENSION TN(3,10,5), T(8,10,5), TE(10), CVAL(10)
DIMENSION VALKX(10), VALKR(10), HVAL(10)
PRINT 100
FORMAT ("      TN(7,3,1)      TN(4,5,1)      TN(5,5,1)      T(7,R=5.
65,1)      TIME      ",)
C INITIAL TEMPERATURE(F)
T0=129.
C DENSITY(LBM/CUBIC FEET)
RHO=108.
C STOP TIME(SECONDS)
TS=58.
C INITIAL VELOCITY(FT/SEC)
V0=207.
C TEMPERATURE,TE(F), HEAT CAPACITY,CVAL(BTU/LBM-F), X-THERMAL
CONDUCTIVITY,VALKX(BTU/HR-FT-F), AND R-THERMAL CONDUCTIVITY,
VALKR(BTU/HR-FT-F)
TE(1)=100.
TE(2)=200.
TE(3)=400.
TE(4)=600.
TE(5)=800.
TE(6)=1000.

```

TE(7)=1200.
TE(8)=1400.
TE(9)=1600.
TE(10)=1800.
CVAL(1)=.18
CVAL(2)=.222
CVAL(3)=.275
CVAL(4)=.311
CVAL(5)=.343
CVAL(6)=.37
CVAL(7)=.401
CVAL(8)=.432
CVAL(9)=.464
CVAL(10)=.496
VALKR(1)=89.9
VALKR(2)=84.5
VALKR(3)=75.1
VALKR(4)=66.5
VALKR(5)=61.2
VALKR(6)=56.
VALKR(7)=51.3
VALKR(8)=47.2
VALKR(9)=43.1
VALKR(10)=38.9
VALKX(1)=21.8

```
VALKX(2)=20.5  
VALKX(3)=18.1  
VALKX(4)=16.7  
VALKX(5)=15.  
VALKX(6)=13.2  
VALKX(7)=12.1  
VALKX(8)=11.  
VALKX(9)=10.6  
VALKX(10)=10.  
C CONVECTIVE/RADIATIVE HEAT TRANSFER COEFFICIENT(BTU/HR-FT-FT-F)  
HVAL(1)=2.4  
HVAL(2)=2.65  
HVAL(3)=3.25  
HVAL(4)=3.90  
HVAL(5)=4.88  
HVAL(6)=6.10  
HVAL(7)=8.45  
HVAL(8)=26.5  
HVAL(9)=32.  
HVAL(10)=37.  
C NDIM=NUMBER OF VALUES OF IE INSERTED INTO PROGRAM  
NDIM=10.  
C SIR=STATOR INSIDE RADIUS(IN)  
SIR=3.75  
C SOR=STATOR OUTSIDE RADIUS(IN)  
SOR=6.75  
C ROR=ROTOR OUTSIDE RADIUS(IN)  
ROR=7.2  
C RIR=ROTOR INSIDE RADIUS(IN)
```

```
RIR=.4.4
ST=HALF OF STATOR THICKNESS(IN)
ST=.37
RT=HALF OF ROTOR THICKNESS(IN)
RT=.34
DXR=RT/2.
DXS=ST/2.
DR1=(RIR-SIR)/2.
DR2=(SOR-RIR)/5.
DR3=(ROR-SOR)/2.
DXA=(DXS+DXR)/2.
RR=ROLLING RADIUS OF THE TIRE(IN)
RR=16.5
N=THE NUMBER OF FRICTION PAIRS
N=8
TINF IS AMBIENT TEMPERATURE(F)
TINF=8C.
TI=0.
A=COOLING AREA DURING COOL DOWN(IN-IN)
A=2.*3.14159*RT*(ROR+RIR)+2.*3.14159*(SOR+SIR)+3.14159*
6 (ROR*ROR-SOR*SOR)+3.14159*(RIR*RIR-SIR*SIR)
V=VOLUME OF ROTOR AND STATOR FOR USE IN COOL DOWN(IN-IN)
V=3.14159*(ROR*ROR-RIR*RIR)*RT+3.14159*(SOR*SOR-SIR*SIR)*ST
NTH=5
INITIAL TEMPERATURE SET,T IS TEMP(F),TN IS NEW TEMP(F)
DO 1 I=1,8
DO 2 J=1,10
DO 300 K=1,NTH
```

```

307 IN(I,J,K)=IC
2 T(I,J,K)=TO
CONTINUE
CONTINUE
1 CONTINUE
0 SDTC=SAVE VALUE FOR DT CRITICAL CALCULATION
SDTC=10.
KKH=0
3 CONTINUE
0 DTH=MINIMUM ANGLE THROUGH WHICH ROTOR ROTATES DURING EACH TIME
0 STEP (RADIANS)
0 DTH=.08725546
0 THE FOLLOWING STATEMENTS CALCULATE THE NEW DT VALUE AND
0 CALCULATE THE VALUE OF KK (THE RELATIVE POSITION OF THE
0 ROTOR AND STATOR FOR BOUNDARY CONDITION APPLICATION)
DT=10.
IF (SDTC.LT.DT) DT=SDTC/2.
IF (DT.GT.2.)DT=.01
IF (ABS(TI-TS).LT..1.OR.TI.GT.TS) GO TO 99
DTH1=DT*10*12.*(1.-TI/TS)/RR
DTHC=DTH1/DTH
CH1=DTHC/8.
ICH1=CH1
CH2=CH1-ICH1
KK=CH2*8.
KK=KK+1
DTH2=(FLOAT(KK)/8.+FLOAT(ICH1))*8.*DTH
KKH=KKH+KK
IF (KKH.GT.8) KKH=KKH-8

```

```

99      KK=KKH
        DT=DTH2*RR/(V0*(1.-II/TS)*12.)
        CONTINUE
        DT2=DT/2.
        SDTC=10.
        TI=TI+DT
        PRINT 20
        C
        20      FORMAT ( " 20 " )
            IF(TI.LE.1.)TT=(18.*TI/1.5+6.)*70.72
            IF(TI.GT.1..AND.TI.LE.9.)TT=(11.*TI/9.+17.)*70.72
            IF(TI.GT.9.)TT=(-14.*TI/58.+31.)*70.72
            IF(TI.GT.TS)TT=0.
        C      TH IS A HOLD TEMPERATURE FOR ENTRY INTO K,C SUBROUTINE
        C      SDTC=SAVE VALUE FOR DT CRITICAL CALCULATION
            SDTC=10.
            III=0
            DO 302 K=2,4
            DO 4 I=2,7
            DO 5 J=2,9
            IF (I.EQ.4.OR.I.EQ.5) GO TO 44
            IF (J.LT.4.AND.I.LE.5) GO TO 55
            IF (J.GT.7.AND.I.GT.5) GO TO 55
            IF(K.NE.4) GO TO 3113
            IF(I.LT.4.AND.J.GT.7) GO TO 55
            IF(I.GT.5.AND.J.LT.4) GO TO 55
            CONTINUE
            CALL INT(TE,VALKX,T(I,J,K),VKX,DKX,NDIM)
            CALL INT(TE,VALKR,T(I,J,K),VKR,DKR,NDIM)
        C
        3113

```



```

IF (I.LT.4) OX=DXR
IF (I.GT.5) OX=DXS
IF (J.EQ.2) R=SIR+DR1
IF (J.EQ.3) R=RIR
IF (J.EQ.4) R=RIR+DR2
IF (R.LT.RIR) DR=DR1
IF (R.GE.RIR.AND.R.LT.SOR) DR=DR2
IF (R.GE.SOR) DR=DR3
IF (J.GT.4) R=R+DR
IF (R.GE.RIR.AND.R.LT.SOR) DRP=DR2
IF (R.GE.SOR) DRP=DR3
IF (R.LT.RIR) DRP=DR1
IF (R.LE.RIR) DRM=DR1
IF (R.GT.RIR.AND.R.LE.SOR) DRM=DR2
IF (R.GT.SOR) DRM=DR3
A1=(T(I+1,J,K)-T(I-1,J,K))/(2.*DX)
A2=(T(I+1,J,K)-2.*T(I,J,K)+T(I-1,J,K))/(DX*DX)
A3=(T(I,J+1,K)-T(I,J-1,K))/(DRP+DRM)
A4=((T(I,J+1,K)-T(I,J,K))/DRP)-(T(I,J,K)-T(I,J-1,K))/DRM)/(.5*(D
6RP+DRM))
CALL INT(TE,CVAL,T(I,J,K),C,DC,NDIM)
A6=(T(I,J,K+1)-T(I,J,K-1))/(2.*DTH)
A7=(T(I,J,K+1)-2.*T(I,J,K)+T(I,J,K-1))/DTH**2
DTC1=RHO*C*3600./(144.*2.*(VKR/(DRP*DRM)+VKX/(DX*DX)
6+VKR/(R*R*0TH*DTH)))
IF (DTC1.LT.SDTC) SDTC=DTC1
TN(I,J,K)=T(I,J,K)+((DT*(144./3600.))/(RHO*C))*((VKR*A4)+(DKR*A3
6*A3)+((VKR*A3)/R)+(VKX*A2)+(DKX*A1*A1)
6+VKR*A7/(R*R)+A6*A6*DKR/(R*R))

```

```
35 CONTINUE
36 CONTINUE
37 CONTINUE
38 CONTINUE
39 CONTINUE
40 FORMAT ( " 21 " )
41 DO 6 J=2,9
42 DO 66 K=2,4
43 TN(8,J,K)=TN(6,J,K)
44 TN(1,J,K)=TN(3,J,K)
45 CONTINUE
46 CONTINUE
47 IF(KK.EQ.5) JJ=4
48 IF(KK.GT.5) JJ=9-KK
49 IF(KK.LT.5) JJ=KK+1
50 DO 310 I=2,7
51 IF(I.LT.4) DX=DXR
52 IF(I.GT.5) DX=DXS
53 DO 311 J=1,10
54 IF(I.LE.4.AND.J.LE.2) GO TO 3111
55 IF(I.GE.5.AND.J.GE.9) GO TO 3111
56 IF(J.EQ.1) R=SIR
57 IF(J.EQ.1) DRP=DR1
58 IF(J.EQ.3) F=RIR
59 IF(J.EQ.2) R=SIR+DR1
60 IF(J.EQ.4) R=RIR+DR2
61 IF(R.LT.RIR) DR=DR1
62 IF(R.GE.RIR.AND.R.LT.SOR) DR=DR2
```

```

IF(R.GE.SOR) JR=DR3
IF(J.GT.4) R=R+DR
IF(R.GE.RIR.AND.R.LT.SOR) DRP=DR2
IF(R.GE.SOR) DRP=DR3
IF(R.LT.RIR) DRP=DR1
IF(R.LE.RIR) DRM=DR1
IF(R.GT.RIR.AND.R.LE.SOR) DRM=DR2
IF(R.GT.SOR) DRM=DR3
DC 312 K=1,5
C ROTOR ROTATION ALGORITHM, THE K1 VALUE IS THE THETA NOOE OF THE
C ROTOR CORRESPONDING TO THE K VALUE ON THE STATOR AT EACH TIME STEP
IF((K-1).GE.KK)K1=K-KK
IF((K-1).LT.KK.AND.KK.LE.4) K1=JJ-(K-1)
IF(KK.GE.5.AND.(K+3).GE.KK) K1=KK-(K-2)
IF(KK.GE.5.AND.(K+3).LE.KK) K1=JJ+K-1
DRA=(DRP+DRM)/2.
IF(I.EQ.4.AND.J.LT.9) GO TO 3112
IF(I.EQ.5.AND.J.GT.2) GO TO 3112
CALL INT(TE,CVAL,T(I,J,K),C,DC,NDIM)
CALL INT(TE,HVAL,T(I,J,K),H,OH,NDIM)
CALL INT(TE,ALKR,T(I,J,K),JKR,DKR,NDIM)
CALL INT(TE,VALKX,T(I,J,K),VKX,DKX,NDIM)
IF(K.EQ.5) GO TO 90
THO=VKR*(T(I,J,K+1)-T(I,J,K))/(OTH*OTH*R)
CONTINUE
IF(K.EQ.1) GO TO 91
THI=-VKR*(T(I,J,K)-T(I,J,K-1))/(OTH*OTH*R)
IF(K.EQ.5) GO TO 91
THIO=(JKR*(T(I,J,K+1)-2.*T(I,J,K)+T(I,J,K-1)))/(OTH*OTH)

```

C C

90

```

6+DKR*((T(I,J,K+1)-T(I,J,K-1))/(2.*DTH))**2)/(R*R)
CONTINUE
91 IF(J.EQ.10) GO TO 92
R0=VKR*(T(I,J+1,K)-T(I,J,K))/(DRA*DRP)
CONTINUE
92 IF(J.EQ.1) GO TO 93
R1=-VKR*(T(I,J,K)-T(I,J-1,K))/(DRA*DRM)
IF(J.EQ.10) GO TO 93
R10=VKR*(T(I,J+1,K)-2.*T(I,J,K)+T(I,J-1,K))/(DRA*DRA)+JKR*(T(I,J+1
6,K)-T(I,J-1,K))/(2.*DRA*R)+DKR*((T(I,J+1,K)-T(I,J-1,K))/(2.*DRA
6))**2
CONTINUE
93 X0=VKX*(T(I+1,J,K)-T(I,J,K))/(DX*DX)
XI=-VKX*(T(I,J,K)-T(I-1,J,K))/(DX*DX)
X10=VKX*(T(I+1,J,K)-2.*T(I,J,K)+T(I-1,J,K))/(DX*DX)
6+DKX*((T(I+1,J,K)-T(I-1,J,K))/(2.*DX))**2
IF(R.LE.RIR) DR=DRM
H=H/12.
THH=-H*DR*(T(I,J,K)-TINF)/(R*DRA*DTH)
RH=-H*(T(I,J,K)-TINF)/DRA
XH=-H*DR*(T(I,J,K)-TINF)/(DX*DRA)
W=144.*DT/(3600.*RHO*C)
CONTINUE
3112 IF(I.NE.4.AND.I.NE.5) GO TO 2
CALL INT(TE,CVAL,T(4,J,K),C4,DC4,NDIM)
CALL INT(TE,CVAL,T(5,J,K1),C5,DC5,NDIM)
CALL INT(TE,HVAL,T(4,J,K),H4,DH,NDIM)
CALL INT(TE,HVAL,T(5,J,K1),H5,DH,NDIM)

```

```

CALL INT(TE, VALKR, T(4, J, K), VKR4, DKR4, NDIM)
CALL INT(TE, VALKX, T(4, J, K), VKX4, DKX4, NDIM)
CALL INT(TE, VALKR, T(5, J, K1), /KR5, DKR5, NDIM)
CALL INT(TE, VALKX, T(5, J, K1), VKX5, DKX5, NDIM)
XI4=-VKX4*(T(4, J, K)-T(3, J, K))/DXR
IF(J.EQ.10.OR.J.EQ.1) GO TO 94
RI04=DXR*(JKR4*(T(4, J+1, K)-2.*T(4, J, K)+T(4, J-1, K))/(DRA*DRA)+VKR4
6*(T(4, J+1, K)-T(4, J-1, K))/(2.*DRA*R)+DKR4*((T(4, J+1, K)
6-T(4, J-1, K))/(2.*DRA))*2)
RI05=DXS*(JKR5*(T(5, J+1, K1)-2.*T(5, J, K1)+T(5, J-1, K1))/(DRA*DRA)
6+VKR5*(T(5, J+1, K1)-T(5, J-1, K1))/(2.*DRA*R)+DKR5*((T(5, J+1, K1)
6-T(5, J-1, K1))/(2.*DRA))*2)
94 CONTINUE
IF(K.EQ.1.OR.K.EQ.5) GO TO 95
THI04=DXR*((VKR4*(T(4, J, K+1)-2.*T(4, J, K)+T(4, J, K-1))/(DTH*DTH)
6+DKR4*((T(4, J, K+1)-T(4, J, K-1))/(2.*DTH))*2)/(R*R))
95 CONTINUE
IF(K1.EQ.1.OR.K1.EQ.5) GO TO 96
THI05=DXS*((VKR5*(T(5, J, K1+1)-2.*T(5, J, K1)+T(5, J, K1-1))/(DTH*DTH)
6+DKR5*((T(5, J, K1+1)-T(5, J, K1-1))/(2.*DTH))*2)/(R*R))
96 CONTINUE
X05=VKX5*(T(6, J, K1)-T(5, J, K1))/DXS
IF(J.EQ.1) GO TO 97
RI4=DXR*(-VKR4*(T(4, J, K)-T(4, J-1, K))/(DRA*DRM))
RI5=DXS*(-VKR5*(T(5, J, K1)-T(5, J-1, K1))/(DRA*DRM))
97 CONTINUE
IF(J.EQ.10) GO TO 98
R04=DXR*(VKR5*(T(4, J+1, K)-T(4, J, K))/(DRA*DRP))
R05=DXS*(VKR5*(T(5, J+1, K1)-T(5, J, K1))/(DRA*DRP))

```

```

48 CONTINUE
   IF(K.EQ.1) GO TO 50
   TH14=-VKR4*DXR*(T(4,J,K)-T(4,J,K-1))/(DTH*DTH*R*R)
50 CONTINUE
   IF(K1.EQ.1) GO TO 51
   TH15=-VKR5*DXS*(T(5,J,K1)-T(5,J,K1-1))/(DTH*DTH*R*R)
51 CONTINUE
   IF(K.EQ.5) GO TO 52
   TH04=VKR4*DXR*(T(4,J,K+1)-T(4,J,K))/(DTH*DTH*R*R)
52 CONTINUE
   IF(K1.EQ.5) GO TO 53
   TH05=VKR5*DXS*(T(5,J,K1+1)-T(5,J,K1))/(DTH*DTH*R*R)
53 CONTINUE
   H4=H4/12.
   H5=H5/12.
   RH4=-DXR*H4*(T(4,J,K)-TINF)/DRA
   RH5=-DXS*H5*(T(5,J,K1)-TINF)/DRA
   XH4=-DXR*H4*(T(4,J,K)-TINF)*DR/(DRA*DX)
   XH5=-DXS*H5*(T(5,J,K1)-TINF)*DR/(DRA*DX)
   THH4=-DXR*DR*H4*(T(4,J,K)-TINF)/(R*DTH*DRA)
   THH5=-DXS*DR*H5*(T(5,J,K1)-TINF)/(R*DTH*DRA)
   DR=DRP
   CONTINUE
   IF((I.EQ.4.OR.I.EQ.5).AND.J.GE.3.AND.J.LE.8) GO TO 403
   E=T(I,J,K)
   IF(I.EQ.2.AND.J.EQ.10.AND.K.EQ.4)TN(I,J,K)=E+2.*W*(THI+RI+THH+RH
6+X0)
   IF(I.EQ.3.AND.J.EQ.10.AND.K.EQ.4)TN(I,J,K)=E+W*2.*(X10/2.+THI+RI+T

```

```
6HH+RH)
IF(I.EQ.4.AND.J.EQ.10.AND.K.EQ.4)TN(I,J,K)=E+W*2.*(THI+THH+RI+RH+X
6I+XH)
IF(I.EQ.4.AND.J.EQ.10.AND.K.EQ.3)TN(I,J,K)=E+W*(THIO+XI+XH+1.*(RI+
6RH))
IF(I.EQ.4.AND.J.EQ.10.AND.K.EQ.2)TN(I,J,K)=E+W*(THIO+XI+XH+1.*(RI+
6RH))
IF(I.EQ.2.AND.J.EQ.10.AND.K.EQ.3)TN(I,J,K)=E+W*2.*(RI+RH+XO+THIO/2
6.)
IF(I.EQ.2.AND.J.EQ.10.AND.K.EQ.2)TN(I,J,K)=E+W*2.*(RI+RH+XO+THIO/2
6.)
IF(I.EQ.3.AND.J.EQ.10.AND.K.EQ.3)TN(I,J,K)=E+W*(XIO+THIO+2.*(RI+RH
6))
IF(I.EQ.3.AND.J.EQ.10.AND.K.EQ.2)TN(I,J,K)=E+W*(XIO+THIO+2.*(RI+RH
6))
IF(I.EQ.2.AND.J.EQ.10.AND.K.EQ.1)TN(I,J,K)=E+W*2.*(RI+RH+THO+XO)
IF(I.EQ.3.AND.J.EQ.10.AND.K.EQ.1)TN(I,J,K)=E+W*2.*(RI+RH+XIO*.5+TH
6O)
IF(I.EQ.4.AND.J.EQ.10.AND.K.EQ.1)TN(I,J,K)=E+W*2.*(XI+XH+RI+RH+THO
6)
IF(I.EQ.2.AND.J.EQ.9.AND.K.EQ.4)TN(I,J,K)=E+W*2.*(RIO/2.+THI+THH+X
6O)
IF(I.EQ.3.AND.J.EQ.9.AND.K.EQ.4)TN(I,J,K)=E+W*(RIO+XIO+2.*(THI+THH
6))
IF(I.EQ.4.AND.J.EQ.9.AND.K.EQ.4)TN(I,J,K)=E+W*2.*(RIO/2.+XI+XH+THH
6+THI)
IF(I.EQ.4.AND.J.EQ.9.AND.K.EQ.3)TN(I,J,K)=E+W*(RIO+THIO+2.*(XI+XH)
6)
IF(I.EQ.4.AND.J.EQ.9.AND.K.EQ.2)TN(I,J,K)=E+W*2.*(RIO/2.+THIO/2.+X
```

```
6I+XH)
IF(I.EQ.4.AND.J.EQ.9.AND.K.EQ.1)TN(I,J,K)=E+W*(RIO/2.+XI+XH+THO)*2
6)
IF(I.EQ.2.AND.J.EQ.8.AND.K.EQ.4)TN(I,J,K)=E+W*.667*(2.*THI+2.*RI+T
6HO+THH+R
50+RH+3.*XO)
IF(I.EQ.3.AND.J.EQ.8.AND.K.EQ.4)TN(I,J,K)=E+W*.667*(1.5*XIO+2.*THI
6+THO+THH
6+2.*RI+RO+RH)
IF(I.EQ.2.AND.J.EQ.8.AND.K.EQ.5)TN(I,J,K)=E+W*2.*(RI+RH+THI+XO)
IF(I.EQ.3.AND.J.EQ.8.AND.K.EQ.5)TN(I,J,K)=E+W*2.*(XIO/2.+RI+RH+THI
6)
EE=2.*(RIO/2.+THI+XO)
IF(I.EQ.2.AND.J.EQ.7.AND.K.EQ.5)TN(I,J,K)=E+W*EE
IF(I.EQ.2.AND.J.EQ.6.AND.K.EQ.5)TN(I,J,K)=E+W*EE
IF(I.EQ.2.AND.J.EQ.5.AND.K.EQ.5)TN(I,J,K)=E+W*EE
IF(I.EQ.2.AND.J.EQ.4.AND.K.EQ.5)TN(I,J,K)=E+W*EE
EE=(XIO+RIO+2.*THI)
IF(I.EQ.3.AND.J.EQ.7.AND.K.EQ.5)TN(I,J,K)=E+W*EE
IF(I.EQ.3.AND.J.EQ.6.AND.K.EQ.5)TN(I,J,K)=E+W*EE
IF(I.EQ.3.AND.J.EQ.5.AND.K.EQ.5)TN(I,J,K)=E+W*EE
IF(I.EQ.3.AND.J.EQ.4.AND.K.EQ.5)TN(I,J,K)=E+W*EE
IF(I.EQ.2.AND.J.EQ.3.AND.K.EQ.5)TN(I,J,K)=E+W*2.*(RO+RH+XO+THI)
IF(I.EQ.3.AND.J.EQ.3.AND.K.EQ.5)TN(I,J,K)=E+W*2.*(XIO/2.+RO+RH+THI
6)
IF(I.EQ.6.AND.J.EQ.8.AND.K.EQ.1)TN(I,J,K)=E+W*2.*(XIO/2.+RI+RH+THO
6)
EE=2.*(XIO/2.+THIO/2.+RI+RH)
```



```

IF(I.EQ.5.AND.J.EQ.8.AND.K.EQ.2)TN(I,J,K)=E+W*EE
IF(I.EQ.5.AND.J.EQ.8.AND.K.EQ.3)TN(I,J,K)=E+W*EE
IF(I.EQ.6.AND.J.EQ.8.AND.K.EQ.4)TN(I,J,K)=E+W*EE
IF(I.EQ.7.AND.J.EQ.8.AND.K.EQ.1)TN(I,J,K)=E+W*2.*(RI+RH+XI+THO)
EE=2.*(THIO/2.+RI+RH+XI)
IF(I.EQ.7.AND.J.EQ.8.AND.K.EQ.2)TN(I,J,K)=E+W*EE
IF(I.EQ.7.AND.J.EQ.8.AND.K.EQ.3)TN(I,J,K)=E+W*EE
IF(I.EQ.7.AND.J.EQ.8.AND.K.EQ.4)TN(I,J,K)=E+W*EE
IF(I.EQ.5.AND.J.EQ.8.AND.K.EQ.5)TN(I,J,K)=E+W*2.*(XIO/2.+RI+RH+THI
6) IF(I.EQ.7.AND.J.EQ.8.AND.K.EQ.5)TN(I,J,K)=E+W*2.*(RI+RH+XI+THI)
EE=XIO+RIO+2.*THI
IF(I.EQ.6.AND.J.EQ.7.AND.K.EQ.5)TN(I,J,K)=E+W*EE
IF(I.EQ.5.AND.J.EQ.6.AND.K.EQ.5)TN(I,J,K)=E+W*EE
IF(I.EQ.5.AND.J.EQ.5.AND.K.EQ.5)TN(I,J,K)=E+W*EE
IF(I.EQ.6.AND.J.EQ.4.AND.K.EQ.5)TN(I,J,K)=E+W*EE
EE=2.*(RIO/2.+XI+THI)
IF(I.EQ.7.AND.J.EQ.7.AND.K.EQ.5)TN(I,J,K)=E+W*EE
IF(I.EQ.7.AND.J.EQ.6.AND.K.EQ.5)TN(I,J,K)=E+W*EE
IF(I.EQ.7.AND.J.EQ.5.AND.K.EQ.5)TN(I,J,K)=E+W*EE
IF(I.EQ.7.AND.J.EQ.4.AND.K.EQ.5)TN(I,J,K)=E+W*EE
IF(I.EQ.5.AND.J.EQ.3.AND.K.EQ.5)TN(I,J,K)=E+W*2.*(XIO/2.+RO+RH+THI
6) IF(I.EQ.7.AND.J.EQ.3.AND.K.EQ.5)TN(I,J,K)=E+W*2.*(RO+RH+XI+THI)
IF(I.EQ.7.AND.J.EQ.1.AND.K.EQ.4)TN(I,J,K)=E+W*2.*(RO+RH+XI+THI)
IF(I.EQ.7.AND.J.EQ.2.AND.K.EQ.4)TN(I,J,K)=E+W*2.*(RIO/2.+XI+THI
6+THH)
IF(I.EQ.7.AND.J.EQ.3.AND.K.EQ.4)TN(I,J,K)=E+W*.667*(3.*XI+RI+2.*RO
6+RH+2.*T

```

```

6HI+THO+THH)
IF(I.EQ.6.AND.J.EQ.3.AND.K.EQ.4)TN(I,J,K)=E+W*.667*(1.5*XIO+2.*THI
6+2.*RO+T
6HO+THH+RI+RH)
IF(I.EQ.6.AND.J.EQ.1.AND.K.EQ.4)TN(I,J,K)=E+W*2.*(XIO/2.+THI+THH+R
6O+RH)
EE=2.*(THIO/2.+RO+RH+XI)
IF(I.EQ.7.AND.J.EQ.1.AND.K.EQ.2)TN(I,J,K)=E+W*EE
IF(I.EQ.7.AND.J.EQ.1.AND.K.EQ.3)TN(I,J,K)=E+W*EE
IF(I.EQ.7.AND.J.EQ.1.AND.K.EQ.1)TN(I,J,K)=E+2.*W*(RO+RH+THO+XI)
EE=2.*(RIO/2.+THO+XI)
IF(I.EQ.7.AND.J.EQ.2.AND.K.EQ.1)TN(I,J,K)=E+W*EE
IF(I.EQ.7.AND.J.EQ.3.AND.K.EQ.1)TN(I,J,K)=E+W*EE
IF(I.EQ.7.AND.J.EQ.4.AND.K.EQ.1)TN(I,J,K)=E+W*EE
IF(I.EQ.7.AND.J.EQ.5.AND.K.EQ.1)TN(I,J,K)=E+W*EE
IF(I.EQ.7.AND.J.EQ.6.AND.K.EQ.1)TN(I,J,K)=E+W*EE
IF(I.EQ.7.AND.J.EQ.7.AND.K.EQ.1)TN(I,J,K)=E+W*EE
IF(I.EQ.5.AND.J.EQ.1.AND.K.EQ.4)TN(I,J,K)=E+W*2.*(XO+XH+RO+RH+THI+
6THH)
IF(I.EQ.5.AND.J.EQ.2.AND.K.EQ.4)TN(I,J,K)=E+W*2.*(RIO/2.+XO+XH+THI
6+THH)
IF(I.EQ.5.AND.J.EQ.2.AND.K.EQ.4)TN(I,J,K)=E+W*(XIO+RIO+2.*(THI+THH
6))
EE=XIO+RIO+2.*THO
IF(I.EQ.5.AND.J.EQ.2.AND.K.EQ.1)TN(I,J,K)=E+W*EE
IF(I.EQ.6.AND.J.EQ.3.AND.K.EQ.1)TN(I,J,K)=E+W*EE
IF(I.EQ.6.AND.J.EQ.4.AND.K.EQ.1)TN(I,J,K)=E+W*EE
IF(I.EQ.6.AND.J.EQ.5.AND.K.EQ.1)TN(I,J,K)=E+W*EE

```

IF(I.EQ.6.AND.J.EQ.6.AND.K.EQ.1)TN(I,J,K)=E+W*EE
IF(I.EQ.6.AND.J.EQ.7.AND.K.EQ.1)TN(I,J,K)=E+W*EE
IF(I.EQ.6.AND.J.EQ.1.AND.K.EQ.1)TN(I,J,K)=E+W*2.*(XIO/2.+RO+RH+THO)

6)

EE=2.*(THIO/2+RO+RH+XO+XH)
IF(I.EQ.5.AND.J.EQ.1.AND.K.EQ.2)TN(I,J,K)=E+W*EE
IF(I.EQ.5.AND.J.EQ.1.AND.K.EQ.3)TN(I,J,K)=E+W*EE
IF(I.EQ.5.AND.J.EQ.1.AND.K.EQ.1)TN(I,J,K)=E+W*2.*(XO+XH+RO+RH+THO)
IF(I.EQ.5.AND.J.EQ.2.AND.K.EQ.1)TN(I,J,K)=E+W*2.*(RIO/2.+XO+XH+THO)

6)

EE=2.*(XO+XH)+THIO+RIO
IF(I.EQ.5.AND.J.EQ.2.AND.K.EQ.2)TN(I,J,K)=E+W*EE
IF(I.EQ.5.AND.J.EQ.2.AND.K.EQ.3)TN(I,J,K)=E+W*EE
IF(I.EQ.3.AND.J.EQ.3.AND.K.EQ.1)TN(I,J,K)=E+W*2.*(XIO/2.+RO+RH+THO)

6)

EE=XIO+RIO+2.*THO
IF(I.EQ.3.AND.J.EQ.4.AND.K.EQ.1)TN(I,J,K)=E+W*EE
IF(I.EQ.3.AND.J.EQ.5.AND.K.EQ.1)TN(I,J,K)=E+W*EE
IF(I.EQ.3.AND.J.EQ.6.AND.K.EQ.1)TN(I,J,K)=E+W*EE
IF(I.EQ.3.AND.J.EQ.6.AND.K.EQ.1)TN(I,J,K)=E+W*EE
IF(I.EQ.3.AND.J.EQ.7.AND.K.EQ.1)TN(I,J,K)=E+W*EE
IF(I.EQ.3.AND.J.EQ.8.AND.K.EQ.1)TN(I,J,K)=E+W*EE
IF(I.EQ.3.AND.J.EQ.9.AND.K.EQ.1)TN(I,J,K)=E+W*EE
IF(I.EQ.2.AND.J.EQ.3.AND.K.EQ.1)TN(I,J,K)=E+W*2.*(RO+RH+XO+THO)

EE=RIO+2.*(XO+THO)

IF(I.EQ.2.AND.J.EQ.4.AND.K.EQ.1)TN(I,J,K)=E+W*EE
IF(I.EQ.2.AND.J.EQ.5.AND.K.EQ.1)TN(I,J,K)=E+W*EE
IF(I.EQ.2.AND.J.EQ.6.AND.K.EQ.1)TN(I,J,K)=E+W*EE
IF(I.EQ.2.AND.J.EQ.7.AND.K.EQ.1)TN(I,J,K)=E+W*EE

```

IF(I.EQ.2.AND.J.EQ.8.AND.K.EQ.1)TN(I,J,K)=E+W*EE
IF(I.EQ.2.AND.J.EQ.9.AND.K.EQ.1)TN(I,J,K)=E+W*EE
EE=2.*(THIO/2.+RO+RH+XO)
IF(I.EQ.2.AND.J.EQ.3.AND.K.EQ.2)TN(I,J,K)=E+W*EE
IF(I.EQ.2.AND.J.EQ.3.AND.K.EQ.3)TN(I,J,K)=E+W*EE
IF(I.EQ.2.AND.J.EQ.3.AND.K.EQ.4)TN(I,J,K)=E+W*EE
EE=THIO+XIO+2.*(RO+RH)
IF(I.EQ.3.AND.J.EQ.3.AND.K.EQ.2)TN(I,J,K)=E+W*EE
IF(I.EQ.3.AND.J.EQ.3.AND.K.EQ.3)TN(I,J,K)=E+W*EE
IF(I.EQ.3.AND.J.EQ.3.AND.K.EQ.4)TN(I,J,K)=E+W*EE
IF(I.EQ.6.AND.J.EQ.1.AND.K.EQ.2)TN(I,J,K)=E+W*EE
IF(I.EQ.6.AND.J.EQ.1.AND.K.EQ.3)TN(I,J,K)=E+W*EE
CONTINUE
IF(I.NE.4) GO TO 402
THE FOLLOWING STATEMENTS THROUGH 402 ARE THE BOUNDARY
CONDITIONS INVOLVING WORK INPUT , AT EACH TIME STEP
DX5=2.*DT*144./(DXS*RH0+C5*3600.)
DX4=2.*DT*144./(DXR*RH0+C4*3600.)
W1=666.1*VO*TT*(1.-TI/TS)/(N*RR+3.14159*(SOR**2-RIR**2))
S1=RI5+THI5+RH5+XO5
S2=RI5+RH5+THI05+XO5
S3=RI5+THO5+RH5+XO5
S4=RI05/2.+THO5+XO5
S5=RI05/2.+THI5+XO5
S6=RI05/2.+THI05/2.+XO5
S7=R05+THI5+XO5+RH5
S8=R05+THI5+2.*(RH5+RI5+THH5+THO5+XH5)
S9=2.*XO5+THI05+RI05+XH5

```

403

C
C

```
S10=RI05+XH5+2.*(TH05+X05)
R1=RI4+RH4+THI4+XI4
R2=RI4+THI4+2.*(R04+TH04+RH4+THH4+3.*XI4+XH4)
R3=XH4+THI04+RI04+2.*XI4
R4=RI04/2.+TH04+XI4
R5=RI04/2.+THI4+XI4
R6=RI04/2.+THI04/2.+XI4
R7=R04+THI4+RH4+XI4
R8=R04+THI04/2.+RH4+XI4
R9=R04+TH04+RH4+XI4
R10=RI04+TH04/2.+XH4+XI4/2.
AS=1.
AR=1.
IF(J.NE.3)GO TO 400
SS=S9
AS=2.
IF(K.EQ.1)SS=S10
IF(K.EQ.4)SS=S8
IF(K.EQ.4)AS=1.5
IF(K.EQ.5)SS=S7
IF(K.EQ.5)AS=1.
PRR=R8
IF(KK.EQ.1.AND.K.EQ.2)RRR=R9
IF(KK.EQ.2.AND.K.EQ.3)RRR=R9
IF(KK.EQ.3.AND.K.EQ.4)RRR=R9
IF(KK.EQ.4.AND.K.EQ.5)RRR=R9
IF(KK.EQ.4.AND.K.EQ.1)RRR=R7
IF(KK.EQ.5.AND.K.EQ.2)RRR=R7
IF(KK.EQ.6.AND.K.EQ.3)RRR=R7
```

```
IF(KK.EQ.7.AND.K.EQ.4) RRR=R7
IF(KK.EQ.8.AND.K.EQ.5) RRR=R7
IF(KK.EQ.9.AND.K.EQ.1) RRR=R7
TN(4,3,K)=DX4*DX5*(W1+RRR+SS+AS*T(5,3,K1)/DX5+AR*T(4,3,K)/DX4)/
6(AS*DX4+AR*DX5)
TN(5,3,K1)=TN(4,3,K)
CONTINUE
IF(J.LT.4.OR.J.GT.7) GO TO 401
SS=S6
IF(K.EQ.1) SS=S4
IF(K.EQ.5) SS=S5
RRR=R6
IF(KK.EQ.1.AND.K.EQ.2) RRR=R4
IF(KK.EQ.2.AND.K.EQ.3) RRR=R4
IF(KK.EQ.3.AND.K.EQ.4) RRR=R4
IF(KK.EQ.4.AND.K.EQ.5) RRR=R4
IF(KK.EQ.4.AND.K.EQ.1) RRR=R5
IF(KK.EQ.5.AND.K.EQ.2) RRR=R5
IF(KK.EQ.6.AND.K.EQ.3) RRR=R5
IF(KK.EQ.7.AND.K.EQ.4) RRR=R5
IF(KK.EQ.8.AND.K.EQ.5) RRR=R5
IF(KK.EQ.8.AND.K.EQ.1) RRR=R4
TN(4,J,K)=DX4*DX5*(W1+RRR+SS+AS*T(5,J,K1)/DX5+AR*T(4,J,K)/
6DX4)/(AS*DX4+AR*DX5)
TN(5,J,K1)=TN(4,J,K)
CONTINUE
IF(J.NE.8) GO TO 402
SS=S2
401
```

```
IF(K.EQ.1)SS=S1
IF(K.EQ.5)SS=S3
RRR=R3
IF(KK.EQ.1.AND.K.EQ.2)RRR=R10
IF(KK.EQ.1.AND.K.EQ.1)RRR=R2
IF(KK.EQ.2.AND.K.EQ.3)RRR=R10
IF(KK.EQ.3.AND.K.EQ.1)RRR=R2
IF(KK.EQ.3.AND.K.EQ.4)RRR=R10
IF(KK.EQ.4.AND.K.EQ.1)RRR=R1
IF(KK.EQ.4.AND.K.EQ.2)RRR=R2
IF(KK.EQ.4.AND.K.EQ.5)RRR=R10
IF(KK.EQ.5.AND.K.EQ.1)RRR=R2
IF(KK.EQ.5.AND.K.EQ.2)RRR=R1
IF(KK.EQ.5.AND.K.EQ.3)RRR=R2
IF(KK.EQ.6.AND.K.EQ.2)RRR=R2
IF(KK.EQ.6.AND.K.EQ.3)RRR=R1
IF(KK.EQ.6.AND.K.EQ.4)RRR=R2
IF(KK.EQ.7.AND.K.EQ.3)RRR=R2
IF(KK.EQ.7.AND.K.EQ.4)RRR=R1
IF(KK.EQ.7.AND.K.EQ.5)RRR=R2
IF(KK.EQ.8.AND.K.EQ.1)RRR=R10
IF(KK.EQ.8.AND.K.EQ.4)RRR=R2
IF(KK.EQ.8.AND.K.EQ.5)RRR=R1
IF(ABS(RRR-R10).LT..01.OR.ABS(RRR-R3).LT..01)AR=2.
IF(ABS(RRR-R2).LT..01)AR=1.5
TN(4,8,K)=DX4*DX5*(W1+RRR+SS+AS*T(5,8,K1)/DX5+AR*T(4,8,K)/DX4)/
6(AS*DX4+AR*DX5)
TN(5,8,K1)=TN(4,8,K)
CONTINUE
```

402

```

998 CONTINUE
312 CONTINUE
3111 CONTINUE
311 CONTINUE
310 CONTINUE
22  FORMAT ( " 22 " )
    DO 83 KK2=1,40
      T55=TN(7,5,1)+.3333*(TN(7,6,1)-TN(7,5,1))
      TEST=FLOAT(KK2-1)*2.
      IF (ABS(TI-TEST).LT.DT2) PRINT 9,TN(7,3,1),TN(4,5,1),TN(5,5,1),T55
6, TI
      IF (ABS(TI-TEST).GE.DT2) GO TO 141
140 CONTINUE
141 CONTINUE
      IF (ABS(TI-TEST).LT.DT2) GO TO 84
83 CONTINUE
84 CONTINUE
      TPI1=TS/4.*$TPI2=.75*TS
      TPI=TS/2.
      IF (ABS(TI-TPI).GT.DT2.AND.ABS(TI-TPI1).GT.DT2.AND.ABS(TI-TPI2).GT.
6 DT2) GO TO 10
102 PRINT 102
      FORMAT ( " R TN(7,J,1) TN(7,J,2) TN(7,J,3) TN(7,J)
5,4) TN(7,J,5) " ;
      DO 77 J=1,8,7
        IF (J.EQ.1) K=SIR
        IF (J.EQ.3) R=SOR
        PRINT 9,R,TN(7,J,1),TN(7,J,2),TN(7,J,3),TN(7,J,4),TN(7,J,5)

```



```
77 CONTINUE
PRINT 100
CONTINUE
FORMAT(1X,5G12.6)
REPLACE OLD TEMPERATURES WITH NEW TEMPERATURES
DO 11 I=1,8
DO 12 J=1,16
DO 317 K=1,5
T(I,J,K)=TN(I,J,K)
CONTINUE
CONTINUE
CONTINUE
11 CONTINUE
IT=0
TS15=TS*1.25
IF(TI.LI.TS15) GO TO 78
PRINT 14
FORMAT ( " TIME(MIN) TEMP ")
TT4=TT55
IF(H.EQ.0.) PRINT 13,TT4
IF(H.EQ.0.) STOP
FORMAT(1X,4HT4=,G10.4,33HH=0. NO COOLING BEYOND THIS VALUE)
TTI=TI/60.
IN THIS SECTION OF THE PROGRAM, ALL NODES ARE LUMPED AND
ALLOWED TO COOL AS ONE MASS.
CONTINUE
CALL INT(TE,CVAL,TT4,C,DC,NDIM)
CALL INT(TE,HVAL,TT4,H,DH,NDIM)
DTC5=RHO*V*C*60./(H*A*12.)
DT=1.

14
13
C
C
80
```

```

79  IF(DT.GT.DTC5)DT=DT/2.
    IF(DT.GT.DTC5) GO TO 79
    TN4=TT4+DT*(12./60.)*H*A*(TINF-TT4)/(RHO*V*C)
    IF(IT.EQ.0)PRINT 9,II,TT4
    IF(II.EQ.5)II=0
    IT=IT+1
    IF(II.EQ.5) PRINT 9,III,TT4
    TT4=TN4
    TII=TII+DT
    IF(TT4.LT.200.) STOP
    GO TO 80
78  CONTINUE
    IF(TI.LT.TS.OR.TI.GT.(TS+DT)) GO TO 3
    PRINT 991
    FORMAT ( "ATS> J T(2,J,1) T(3,J,1) T(4,J,1) T(5,
6J,1) T(6,J,1) T(7,J,1) " )
    DO 130 J=1,10
    K=11-J
    PRINT 131,K,T(2,K,1),T(3,K,1),T(4,K,1),T(5,K,1),T(6,K,1),T(7,K,1)
130 CONTINUE
131 FORMAT (1X,15,6F10.3)
    GO TO 3
    END

```

```

SUBROUTINE INT(TE,CVAL,T,C,DC,NDIM)
DIMENSION TE(10),CVAL(10)
C THE NEXT 10 STATEMENTS ASSIGN ENDPOINT C,DC, VALUES FOR TE
C OUTSIDE OF CURVE ENDPOINTS
IF(T.LE.TE(NDIM)) GO TO 5
C=CVAL(NDIM)
DC=(CVAL(NDIM)-CVAL(NDIM-1))/(TE(NDIM-1))
RETURN
5 CONTINUE
IF(T.GE.TE(1)) GO TO 6
C=CVAL(1)
DC=(CVAL(2)-CVAL(1))/(TE(2)-TE(1))
RETURN
6 CONTINUE
DC 1 I=1,NDIM
IF(T.NE.TE(I)) GO TO 2
C=CVAL(I)
IF(I.EQ.10) DC=(CVAL(NDIM)-CVAL(NDIM-1))/(TE(NDIM)-TE(NDIM-1))
IF(I.EQ.10) GO TO 4
DC=(CVAL(I+1)-CVAL(I))/(TE(I+1)-TE(I))
CONTINUE
RETURN
CONTINUE
IF(T.LE.TE(I).OR.T.GE.TE(I+1)) GO TO 3
DC=(CVAL(I+1)-CVAL(I))/(TE(I+1)-TE(I))
C=CVAL(I)+(CVAL(I+1)-CVAL(I))*(T-TE(I))/(TE(I+1)-TE(I))
RETURN
CONTINUE
CONTINUE
RETURN
END

```

APPENDIX S
EQUATIONS FOR TWO-DIMENSIONAL
(ENTIRE BRAKE/WHEEL/
TIRE) MODEL

Contrails

The heat transfer rates from one node of Figure 71 to another node are:
(The definition of all symbols is shown as comment statements in Appendix T).

$$Q78 = \frac{(T7-T8) A7T8}{\frac{L7T8}{VKR} + \frac{LRT7}{VKR}} \quad (S-1)$$

$$Q76 = \frac{(T7-T6) A6T7}{\frac{L7T6}{VKR} + \frac{L6T7}{VKT}} \quad (S-2)$$

$$Q75 = \frac{(T7-T5) A5T7}{\frac{L7T5}{VKR} + \frac{L5T7}{VK5}} \quad (S-3)$$

$$Q65 = \frac{(T6-T5) A5T6}{\frac{LTT5}{VKT} + \frac{L5TT}{VK5}} \quad (S-4)$$

$$Q45 = \frac{(T4-T5) A5T6}{\frac{LTT5}{VKT} + \frac{L5TT}{VK5}} \quad (S-5)$$

$$Q34 = \frac{(T3-T4) A3T4}{\frac{L3T4}{VKR} + \frac{L4T3}{VKT}} \quad (S-6)$$

$$Q113 = \frac{(T11-T3) ARITI}{\frac{L3T11}{VKR} + \frac{(RT+ST)}{VKR}} \quad (S-7)$$

$$Q91 = \frac{(T9-T1) A1T9}{\frac{L9T1}{VKTT} + \frac{L1T9}{VKTT}} \quad (S-8)$$

$$Q92 = \frac{(T9-T2) A2T9}{\frac{L9T2}{VKTT} + \frac{L2T9}{VK2}} \quad (S-9)$$

Contrails

$$Q1211 = \frac{(T12-T11) \text{ ARITI}}{\left(\frac{2 \text{ L11T3}}{\text{VKR}}\right)} \quad (\text{S-10})$$

$$Q1312 = \frac{(T13-T12) \text{ ARITI}}{\left(\frac{2 \text{ L11T3}}{\text{VKR}}\right)} \quad (\text{S-11})$$

$$Q1413 = \frac{(T14-T13) \text{ ARITI}}{\left(\frac{2\text{L11T3}}{\text{VKR}}\right)} \quad (\text{S-12})$$

$$Q147 = \frac{(T14-T7) \text{ ARITI}}{\frac{\text{L11T3}}{\text{VKR}} + \frac{\text{L7T14}}{\text{VKR}}} \quad (\text{S-13})$$

$$Q145 = \frac{(T14-T5) \text{ ARI0}}{\frac{\text{LRIO}}{\text{VKR}} + \frac{\text{L5TR}}{\text{V5}}} \quad (\text{S-14})$$

$$Q135 = \frac{(T13-T5) \text{ ARI0}}{\frac{\text{LRIO}}{\text{VKR}} + \frac{\text{L5TR}}{\text{V5}}} \quad (\text{S-15})$$

$$Q124 = \frac{(T12-T14) \text{ ARI0}}{\frac{\text{LRIO}}{\text{VKR}} + \frac{\text{LTTR}}{\text{VKT}}} \quad (\text{S-16})$$

$$Q114 = \frac{(T11-T4) \text{ ARI0}}{\frac{\text{LRIO}}{\text{VKR}} + \frac{\text{LTTR}}{\text{VKT}}} \quad (\text{S-17})$$

$$Q219 = \frac{(T21-T9) \text{ ATITI}}{\frac{\text{L11T3}}{\text{VKTT}} + \frac{\text{L9T21}}{\text{VKTT}}} \quad (\text{S-18})$$

$$Q2221 = \frac{(T22-T21) \text{ ATITI}}{\left(\frac{2 \text{ L11T3}}{\text{VKTT}}\right)} \quad (\text{S-19})$$

Contrails

$$Q2322 = \frac{(T23-T22) ATITI}{\left(\frac{2L11T3}{VKTT}\right)} \quad (S-20)$$

$$Q2423 = \frac{(T24-T23)ATITI}{\left(\frac{2L11T3}{VKTT}\right)} \quad (S-21)$$

$$Q238 = \frac{(T23-T8) A23T8}{\frac{L23T8}{VKTT} + \frac{L8T23}{VKR}} \quad (S-22)$$

$$QH1 = H A1 (T1-TINF) \quad (S-23)$$

$$QH2 = H A2(T2-TINF) \quad (S-24)$$

$$QH3 = H A3(T3-TINF) \quad (S-25)$$

$$QH4 = H A4(T4-TINF) \quad (S-26)$$

$$QH5 = H A5(T5-TINF) \quad (S-27)$$

$$QH6 = H A6 (T6-TINF) \quad (S-28)$$

$$QH7 = H A7(T7-TINF) \quad (S-29)$$

$$QH8 = H A8(T8-TINF) \quad (S-30)$$

$$QHR = H AR(TR(I)-TINF) \quad (S-31)$$

$$QHT = H AT(TSS(I)-TINF) \quad (S-32)$$

$$QR(I) = \frac{.5 [TRA-TR(I)] ARTR}{\frac{LRITR}{.5VKR} + \frac{LRTRI}{.5VKKR}} \quad (S-33)$$

Contrails

$$QS(I) = \frac{.5[TSA-TSS(I)] ATTS}{\frac{LTTS}{VKTT} + \frac{LSTT}{VKKS}} \quad (S-34)$$

The temperature at the new time step in terms of the temperature at the previous time step is:

$$TN1 = T1 + \frac{\Delta t}{\rho VC} (Q91-QH1) \quad (S-35)$$

$$TN2 = T2 + \frac{\Delta t}{\rho VC} (Q92-QH2) \quad (S-36)$$

$$TN3 = T3 + \frac{\Delta t}{\rho VC} (Q113-Q34-QH3) \quad (S-37)$$

$$TN4 = T4 + \frac{\Delta t}{\rho VC} (Q34+Q114+Q124-Q45-QH4) \quad (S-38)$$

$$TN5 = T5 + \frac{\Delta t}{\rho VC} (Q45+Q135+Q65+Q145+Q75-QH5) \quad (S-39)$$

$$TN6 = T6 + \frac{\Delta t}{\rho VC} (Q76-Q65-QH6) \quad (S-40)$$

$$TN7 = T7 + \frac{\Delta t}{\rho VC} (Q147-Q76-Q78-QH7-Q75) \quad (S-41)$$

$$TN8 = T8 + \frac{\Delta t}{\rho VC} (Q78-QH8+Q238) \quad (S-42)$$

$$TN9 = T9 + \frac{\Delta t}{\rho VC} [QS(1)-Q92-Q91-QHT(1)] \quad (S-43)$$

$$TN11 = T11 + \frac{\Delta t}{\rho VC} [QR(1)+QR(2)-Q113+Q1211-QHR(1)-QHR(2)-Q114] \quad (S-44)$$

Contrails

$$\text{TN12} = \text{T12} + \frac{\Delta t}{\rho VC} [\text{QR}(3)+\text{QR}(4)+\text{Q1312}-\text{Q1211}-\text{QHR}(3)-\text{QHR}(4) \\ -\text{Q124}] \quad (\text{S-45})$$

$$\text{TN13} = \text{T13} + \frac{\Delta t}{\rho VC} [\text{QR}(5)+\text{QR}(6)+\text{Q1413}-\text{Q1312}-\text{Q135}-\text{QHR}(5)-\text{QHR}(6)] \quad (\text{S-46})$$

$$\text{TN14} = \text{T14} + \frac{\Delta t}{\rho VC} [\text{QR}(7)+\text{QR}(8)-\text{Q1413}-\text{Q147}-\text{Q145}-\text{QHR}(7)-\text{QHR}(8)] \quad (\text{S-47})$$

$$\text{TN21} = \text{T21} + \frac{\Delta t}{\rho VC} [\text{QS}(2)+\text{QS}(3)+\text{Q2221}-\text{Q219}-\text{QHT}(2)-\text{QHT}(3)] \quad (\text{S-48})$$

$$\text{TN22} = \text{T22} + \frac{\Delta t}{\rho VC} [\text{QS}(4)+\text{QS}(5)+\text{Q2322}-\text{Q2221}-\text{QHT}(4)-\text{QHT}(5)] \quad (\text{S-49})$$

$$\text{TN23} = \text{T23} + \frac{\Delta t}{\rho VC} [\text{QS}(6)+\text{QS}(5)+\text{Q2423}-\text{Q2322}-\text{QHT}(6)-\text{QHT}(7)-\text{Q238}] \quad (\text{S-50})$$

$$\text{TN24} = \text{T24} + \frac{\Delta t}{\rho VC} [\text{QS}(8)-\text{Q2423}-\text{QHT}(8)] \quad (\text{S-51})$$

APPENDIX T

PROGRAM LISTING FOR TWO-DIMENSIONAL
(ENTIRE BRAKE/WHEEL
TIRE) MODEL

```

PROGRAM IID (INPUT, OUTPUT)
THIS PROGRAM SOLVES THE TRANSIENT TWO DIMENSIONAL RADIAL/
AXIAL HEAT TRANSFER EQUATION FOR ALL ROTORS AND STATORS.
A LUMPED MASS APPROACH IS USED FOR THE TIRE(2 LUMPS),
HOUSING(1 LUMP), RIM((# OF ROTORS + 3)LUMPS)
AND THE TORQUE TUBE ((# OF ROTORS + 2)LUMPS). AT 1.25
TIMES THE STOP TIME THE HEAT SINK IS LUMPED INTO 1
MASS AND ALL LUMPS ARE THEN ALLOWED TO COOL.
DIMENSION TT1(8,10),TT2(8,10),TT3(8,10),TT4(8,10),
6TT5(8,10),TT6(8,10),TT7(8,10),TT8(8,10),TP1(10),TP2(10),
6TP3(10),TP4(10),TP5(10),TP6(10),TP7(10),TP8(10),TR(8),
6TSS(8),QR(8),QS(8),QHR(8),QHT(8)
REAL L2T9,L9T2,L1T9,L9T1,L3T4,L4T3,L3T11,L11T3,LRITR,
6LTT5,L6T7,L7T6,L7T8,L8T7,LTT5,L5T1,L7T14,LRTRI,LSIT,
6L9T21,L5T7,L7T5,LTTR,LRI0,L5TR,L8T23,L23T6,L2T
6S
P=3.14159
NF=# OF ROTORS
NR=4
TIME IS AMBIENT TEMPERATURE(F)
TINF=80.
ST IS HALF OF STATOR THICKNESS(IN)
ST=.37
RT IS HALF OF ROTOR THICKNESS(IN)
RT=.34
TS IS STOP TIME
TS=58.
H IS RADIATIVE/CONVECTIVE HEAT TRANSFER COEFFICIENT
(BTU/HR-FT-FT-F)

```

C H=2.
A#-AREA FOR CONVECTION(IN-IN)
A1=25.9
A2=467.
A3=137.4
A4=109.3
A5=0.0
A5=109.3
A7=201.2
A8=4596.0
AR=27.5
AT=32.2
A#1T#2-CONTACT AREA BETWEEN#1(IN-IN)
A1T9=11.0
A2T9=57.2
A3T4=2367.
A3T11=59.9
A4T12=32.4
A5T13=32.4
A5T14=32.4
A5T7=36.9
A5T6=107.5
A6T7=2367.
A7T8=653.
A23T8=2.8
C AREA-RIM INCREMENT AT OUTSIDE RADIUS(IN)
AKI0=30.6
C AREA-RIM TO 1 ROTOR

C ARTR=3.2*RT
C AREA-TORQUE TUBE TO 1 STATOR
C ATTS=5.*ST
C AREA-RIM INCREMENT TO NEXT RIM INCREMENT
C AFITI=37.2
C AREA-TORQUE TUBE INCREMENT TO NEXT TORQUE TUBE INCREMENT (IN-IN)
C ATITI=14.3
C SOR=6.75
C SIR=3.75
C KOR=7.2
C RIR=4.4
C AZTS=AREA 2 TO STATOR
C A2TS=0.
C L#1T#2-LENGTH FROM CENTER OF #1 TO CONTACT POINT BETWEEN
C #1(IN)
L2T9=1.
L9T2=.4
L1T9=.7
L9T1=.17
L3T4=.25
L4T3=1.2
L3T11=.5
L11T3=.6
L8T23=2.
L23T8=.17
C LRIO-LENGTH ROTOR INCREMENT TO OUTSIDE RADIUS
LRIO=.35
C LFITR-LENGTH RIM TO ROTOR CONTACT POINT
LRITR=.35

C L1TS-LENGTH TORQUE TUBE TO STATOR CONTACT POINT
L1TS=.3
L6T7=1.0
L7T6=.35
L7T8=.35
L8T7=2.
C L1TR-LENGTH TIRE TO ROTOR CONTACT POINT
L1TR=1.
C L5TR-LENGTH AIR C.G. TO ROTOR CONTACT POINT
L5TR=10.5
C L1T5-LENGTH TIRE TO AIR C.G. CONTACT POINT
L1T5=1.2
C L5TT-LENGTH AIR C.G. TO TIRE CONTACT POINT
L5TT=6.
L7T14=2.3
L9T21=1.25
L5T7=11.
L7T5=.5
C L2TS-LENGTH 2 TO STATOR CONTACT POINT
L2TS=1.4
L V#-VOLUME OF # (IN-IN-IN)
V1=22.4
V2=150.
V3=56.
V4=266.
V5=7512.
V6=268.
V7=204.8

V6=140.
V9=(5.5-7.*(RT+ST))*5.22
C VRI-VOLUME OF 1 RIM INCREMENT ABOVE 1 ROTOR
C JRI=(ST+RT)*2.*.75*2.*P*7.37
C VTI-VOLUME OF 1 TORQUE TUBE INCREMENT BELOW 1 STATOR
C VTI=(ST+RT)*10.44
C C#-HEAT CAPACITY OF # (BTU/LBM-F)
C2=.23
C5=.24
C CT-C OF TIRE
C CT=.37
C CR-C OF RIM
C CK=.23
C CTT-C OF TORQUE TUBE
C CTT=.13
C R#-DENSITY OF # (LBM/FT-FT-FT)
R2=170.
R5=.0808
C ROI-R OF TIRE
ROI=94.
C RORI-R OF RIM
RORI=170.
C RII-R OF TORQUE TUBE
RII=303.
C VK#-VALUE OF THERMAL CONDUCTIVITY (BTU/HR-FT-F)
VK2=90.
VK5=.0165
C JKT-K OF TIRE
VKT=.1

C VKR-VK OF RIM
VKR=90.
C JKTT-JK OF TORQUE TUBE
VKTT=4.3
C INITIAL TEMPERATURES ARE:
T1=105.
T2=92.
T3=112.
T4=112.
T5=100.
T6=112.
T7=112.
T8=112.
T9=105.
T11=112.
T12=112.
T13=112.
T14=108.
T21=105.
T22=105.
T23=105.
T24=105.
SOTC1=.012
TI=0.
T0=129.
TRA=TO
TSA=TO
QS2=0.


```

DD 18 I=1,8
QK(I)=0.
QS(I)=0.
CONTINUE
ICNT-PRINT COUNTER
ICNT=5
DT-DELTA TIME (SEC)
DT=1000.
Q78=(T7-T8)*A7T8/(L7T8/JKR+L8T7/JKR)
Q76=(T7-T6)*A6T7/(L7T6/VKR+L6T7/VKT)
Q75=(T7-T5)*A5T7/(L7T5/VKR+L5T7/VK5)
Q65=(T6-T5)*A5T6/(L7T5/VKT+L5T7/VK5)
Q45=(T4-T5)*A5T6/(L7T5/VKT+L5T7/VK5)
Q34=(T3-T4)*A3T4/(L3T4/VKR+L4T3/VKT)
Q113=(T11-T3)*ARIT1/(L3T11/VKR+(RT+ST)/VKR)
Q91=(T9-T1)*A1T9/(L9T1/JKT+L1T9/JKT)
Q92=(T9-T2)*A2T9/(L9T2/VKT+L2T9/VK2)
Q1211=(T12-T11)*ARIT1/(2.*L11T3/VKR)
Q1312=(T13-T12)*ARIT1/(2.*L11T3/JKR)
Q1413=(T14-T13)*ARIT1/(2.*L11T3/VKR)
Q147=(T14-T7)*ARIT1/(L11T3/VKR+L7T14/VKR)
Q145=(T14-T5)*ARIO/(LRI0/VKR+L5TR/VK5)
Q135=(T13-T5)*ARIO/(LRI0/JKR+L5TR/JK5)
Q124=(T12-T4)*ARIO/(LRI0/VKR+L1TR/VKT)
Q114=(T11-T4)*ARIO/(LRI0/VKR+L1TR/VKT)
Q219=(T21-T9)*ATIT1/(L11T3/JKT+L9T21/JKT)
Q2221=(T22-T21)*ATIT1/(2.*L11T3/VKT)
Q2322=(T23-T22)*ATIT1/(2.*L11T3/VKT)
Q2423=(T24-T23)*ATIT1/(2.*L11T3/VKT)

```

```

18
C
C
C
1

```

Q238=(T23-T8)*A23T8/(L23T8/VKTT+L8T23/VKR)
QH1=H*A1*(T1-TINF)/12.
QH2=H*A2*(T2-TINF)/12.
QH3=H*A3*(T3-TINF)/12.
QH4=H*A4*(T4-TINF)/12.
QH5=H*A5*(T5-TINF)/12.
QH6=H*A6*(T6-TINF)/12.
QH7=H*A7*(T7-TINF)/12.
QH8=H*A8*(T8-TINF)/12.
TR(1)=T11
TR(2)=T11
TR(3)=T12
TR(4)=T12
TR(5)=T13
TR(6)=T13
TR(7)=T14
TR(8)=T14
TSS(1)=T9
TSS(2)=T21
TSS(3)=T21
TSS(4)=T22
TSS(5)=T22
TSS(6)=T23
TSS(7)=T23
TSS(8)=T24
00 77 I=1,5
QHR(I)=H*AR*(TR(I)-TINF)/12.
QHT(I)=H*AT*(TSS(I)-TINF)/12.

77

```

CONTINUE
IF(SDTC1.LT.DT) DT=SDTC1/1.2
DT2=DT/2.
TI=TI+DT
SDTC=1000.
SDTC1=1000.
TS15=TS
IF(TI.GT.TS15) GO TO 7
DO 4 I=1,8
IF(I.EQ.1.AND.TI.LT.TS) QS(I)=QS(I)+QS2
IF(I.EQ.1) CALL IIDRA(TRA,TSA,TT1,TP1,DT,TI,SDTC,QR(1),QS(1),VKKR,
6 VKKS,LRTRI,LSTT)
IF(I.EQ.2) CALL IIDRA(TRA,TSA,TT2,TP2,DT,TI,SDTC,QR(2),QS(2),VKKR,
6 VKKS,LRTRI,LSTT)
IF(I.EQ.3) CALL IIDRA(TRA,TSA,TT3,TP3,DT,TI,SDTC,QR(3),QS(3),VKKR,
6 VKKS,LRTRI,LSTT)
IF(I.EQ.4) CALL IIDRA(TRA,TSA,TT4,TP4,DT,TI,SDTC,QR(4),QS(4),VKKR,
6 VKSS,LRTRI,LSTT)
IF(I.EQ.5) CALL IIDRA(TRA,TSA,TT5,TP5,DT,TI,SDTC,QR(5),QS(5),VKKR,
6 VKSS,LRTRI,LSTT)
IF(I.EQ.6) CALL IIDRA(TRA,TSA,TT6,TP6,DT,TI,SDTC,QR(6),QS(6),VKKR,
6 VKSS,LRTRI,LSTT)
IF(I.EQ.7) CALL IIDRA(TRA,TSA,TT7,TP7,DT,TI,SDTC,QR(7),QS(7),VKKR,
6 VKSS,LRTRI,LSTT)
IF(I.EQ.8) CALL IIDRA(TRA,TSA,TT8,TP8,DT,TI,SDTC,QR(8),QS(8),VKKR,
6 VKSS,LRTRI,LSTT)
IF(SDTC.LT.SDTC1) SDTC1=SDTC
QR(I)=(TRA-TR(I))*5+ARTR/(LRITR/VKR+LRTRI/VKKR)
QS(I)=(TSA-TSS(I))*5+ATTS/(LITTS/VKTT+LSTT/VKKS)

```

IF (I.EQ.1) QS2 = (TSA-T2) * 42TS / (L2TS / VK2 + LSTT / VKKS)

CONTINUE

DO 17 J=2,9

TT1(1,J) = TT2(3,J)

TT2(1,J) = TT1(3,J)

TT3(1,J) = TT4(3,J)

TT4(1,J) = TT3(3,J)

TT5(1,J) = TT6(3,J)

TT6(1,J) = TT5(3,J)

TT7(1,J) = TT8(3,J)

TT8(1,J) = TT7(3,J)

TT2(8,J) = TT3(6,J)

TT3(8,J) = TT2(6,J)

TT4(8,J) = TT5(6,J)

TT5(6,J) = TT4(6,J)

TT6(8,J) = TT7(6,J)

TT7(6,J) = TT6(6,J)

TT1(2,J) = (TT1(2,J) + TT2(2,J)) / 2.

TT2(2,J) = TT1(2,J)

TT3(2,J) = (TT3(2,J) + TT4(2,J)) / 2.

TT4(2,J) = TT3(2,J)

TT5(2,J) = (TT5(2,J) + TT6(2,J)) / 2.

TT6(2,J) = TT5(2,J)

TT7(2,J) = (TT7(2,J) + TT8(2,J)) / 2.

TT8(2,J) = TT7(2,J)

TT2(7,J) = (TT2(7,J) + TT3(7,J)) / 2.

TT3(7,J) = TT2(7,J)

TT4(7,J) = (TT4(7,J) + TT5(7,J)) / 2.

```

TI5(7,J)=TI4(7,J)
TI6(7,J)=(TI6(7,J)+TT7(7,J))/2.
TI7(7,J)=TI6(7,J)
CONTINUE
CONTINUE
TN1=TI1+.04*DT*(Q91-QH1)/(RORI*V1*CR)
IF(TI.GT.TS) QS2=0.
TN2=I2+.04*DT*(Q92-QH2+QS2)/(R2*V2*C2)
TN3=I3+.04*DT*(Q113-Q34-QH3)/(RORI*V3*CR)
TN4=I4+.04*DT*(Q34+Q114+Q124-Q45-QH4)/(ROT*V4*CT)
TN5=I5+.04*DT*(Q45+Q65+Q135+Q145+Q75-QH5)/(R5*V5*C5)
TN6=I6+.04*DT*(Q76-Q65-QH6)/(ROT*V6*CT)
TN7=I7+.04*DT*(Q147-Q76-Q78-QH7-Q75)/(RORI*V7*CR)
TN8=I8+.04*DT*(Q78-QH8+Q238)/(RORI*V8*CR)
TN9=I9+.04*DT*(QS(1)-Q91-Q92-QHT(1))/(RTT*V9*CTT)
AA=.04*DT/(RORI*VRI*CR)
TN11=I11+AA*(QR(1)+QR(2)-Q113+Q1211-QHR(1)-Q114-QHR(2))
TN12=I12+AA*(QR(3)+QR(4)+Q1312-Q1211-QHR(3)-QHR(4)-Q124)
TN13=I13+AA*(QR(5)+QR(6)+Q1413-Q1312-Q135-QHR(5)-QHR(6))
TN14=I14+AA*(QR(7)+QR(8)-Q1413-Q147-Q145-QHR(7)-QHR(8))
BB=.04*DT/(RTT*VTI*CTT)
TN21=I21+BB*(QS(2)+QS(3)+Q2221-Q219-QHT(2)-QHT(3))
TN22=I22+BB*(QS(4)+QS(5)+Q2322-Q2221-QHT(4)-QHT(5))
TN23=I23+BB*(QS(6)+QS(7)+Q2423-Q2322-QHT(6)-QHT(7)-Q238)
TN24=I24+BB*(QS(8)-Q2423-QHT(8))
IF(TI.GT.TS15) GO TO 8
TTT4=(TT1(7,6)+TT2(7,6)+TT3(7,6)+TT4(7,6)+TT5(7,6)+TT6(7,6)
+TT7(7,6)+TT8(7,6))/8.
CONTINUE

```

17
7

8

```

IF (TI.LE.TS15) GO TO 10
LHSTR=(SOR-KIR)/2.*(ROR-SOR)
LHSTT=(SOF-RIR)/2.*(RIR-SIR)
QHOLD=0.
DO 11 I=1,2
QY(I)=(TTT4-TR(I))*ARTR*.5/(LRITR/VKR+LHSTR/VKKR)
QS(I)=(TTT4-TSS(I))*ATTS*.5/(LTTS/VKTT+LHSTT/VKKS)
QHOLD=QHOLD+QR(I)+QS(I)
CONTINUE
CALL IIDRA(TTT4,QHOLD,TT5,TP5,DT,TI,SDTC,QR(5),QS(5),VKKR,
6/VKKS,LKTRI,LSSTT)
A=2.*P*RT*(ROR+RIR)+2.*P*(SOR+SIR)*ST+P*(ROR+ROR-SOR*SOR)+
6P*(RIR+RIR-SIR*SIR)
DENO=H*A*8./12.+4.*ARTR/(LRITR/VKR+LHSTR/VKKR)+4.*ATTS*
6(LTTS/VKTT+LHSTT/VKKS)
DTCTT4=SDTC/DENO
CONTINUE
TS15=TS
IF (ABS(TI-FLOAT(ICNT)).GE.DT) GO TO 82
ITEST=5
IF (ABS(TI-60.)*LI.DT2) ITEST=30
IF (TI.GT.60.) ITEST=30
IF (ABS(TI-300.)*LI.DT2) ITEST=120
IF (TI.GT.300.) ITEST=120
ICNT=ICNT+ITEST
TI=TI/60.
IF (TI.LT.TS15) PRINT 94,TI,T2,T3,T5,T8,T12,T14,T22,TT4(7,5)
IF (TI.LT.TS15) PRINT 94,TT2(2,5),TT3(7,5),TT4(2,5),TT5(7,5),TT6(2,

```

```

65),TT7(7,5),TT8(2,5)
IF(TI.GT.TS15) PRINT 94,TTI,T2,T3,T5,T8,T12,T14,T22,TTT4
FORMAT(1X,1FF7.1)
CONTINUE
CONTINUE
FORMAT(1X,6G12.6)
T1=TN1
T2=TN2
T3=TN3
T4=TN4
T5=TN5
T6=TN6
T7=TN7
T8=TN8
T9=TN9
T11=TN11
T12=TN12
T13=TN13
T14=TN14
T21=TN21
T22=TN22
T23=TN23
T24=TN24
OTC1=25.*RORI*J1*CR/(JKTT*A1T9/(L9T1+L1T9)+H*A1/12.)
ADD2=A2TS/(L2TS/VK2+LSTT/VKKS)
IF(TI.GT.TS) ADD2=0.
OTC2=25.*R2*J2*C2/(A2T9/(L9T2/JKT+L2T9/JK2)+H*A2/12.+ADD2)
OTC3=25.*RORI*V3*CR/(ARIT1*VKR/(L3T11+RT+ST)+H*A3/12.+A3T4/
6(L3T4/VKR+L4T3/VKT))

```

94
62
64
3

DE4=A3T+/(L3T4/VKR+L4T3/VKT)+ARIO/(LRIO/VKR+LTTR/JKT)+ARIO/
6 (LRIO/VKR+LTTR/VKT)+A5T6/(LTT5/VKT+L5TT/VK5)+H*A4/12.
DTC4=25.*R0T*V4*CT/DE4
DE5=2.*A5T6/(LTT5/VKT+L5TT/VK5)+ARIO
6/(LRIO/JKR+L5TR/JK5)+ARIO/(LRIO/JKR+L5TR/JK5)+A5T7/
6 (LTT5/VKR+L5T7/VK5)+H*A5/12.
DTC5=25.*R5*V5*CS/DE5
DE6=A6T7/(L7T6/VKR+L6T7/JKT)+A5T6/(LTT5/JKT+L5TT/VK5)+H*A6/12.
DTC6=25.*R0T*V6*CT/DE6
DE7=ARITII/(L11T3/VKR+L7T14/VKR)+A6T7/(L7T6/VKR+L6T7/VKT)+A7T8/
6 (L7T8/VKR+L6T7/VKR)+A5T7/(L7T5/VKR+L5T7/VK5)+H*A7/12.
DTC7=25.*R0RI*J7*CR/DE7
ADD8=A23T8/(L23T8/VKTT+L6T23/VKR)
DTC8=25.*R0RI*V8*CR/(A7T8/(L7T8/VKR+L8T7/VKR)+H*A8/12.+ADD8)
DF9=.5*ATTS/(LTT5/VKT+LSTT/JKKS)+A2T9/(L9T2/JKTT+L2T9/JK2)+
6A1T9/(L9T1/VKTT+L1T9/VKTT)+H*AT/12.
DTC9=25.*RTT*V9*CTT/DE9
DE11=ARTR/(LRITR/VKR+LRTRI/VKKR)+ARITII/(L3T11/VKR+(RT+ST)/VKR)
6+ARITII/(2.*L11T3/VKR)+ARIO/(LRIO/VKR+LTTR/VKT)+2.*H*AR/12.
DTC11=25.*R0RI*VRI*CR/DE11
DE13=ARTR/(LRITR/VKR+LRTRI/VKKR)+ARITII/(L11T3/VKR)+ARIO/(LRIO/VKR
6+L5TR/VK5)+2.*H*AR/12.
DTC13=25.*R0RI*VRI*CR/DE13
DE14=ARTR/(LRITR/VKR+LRTRI/VKKR)+ARITII/(2.*L11T3/VKR)+ARITII/(L11T3
6/VKR+L7T14/VKR)+ARIO/(LRIO/VKR+L5TR/VK5)+2.*H*AR/12.
DTC14=25.*R0RI*VRI*CR/DE14
DE21=ATTS/(LTT5/VKTT+LSTT/VKKS)+ATITII/(2.*L11T3/VKTT)
6+ARITII/(L11T3/VKTT+L9T21/VKTT)+2.*H*AT/12.


```
DTC21=25.*RTI*VTI*CTI/OE21
DE23=ATTS/(LITS/JKTI+LSTI/JKKS)+ATIII/(L11T3/VKTI)
6+2.*H*AT/12.*A23T8/(L23T8/VKTI+L8T23/VKR)
DTC23=25.*RTI*VTI*CTI/OE23
IF(DTC1.LT.SDTC1)SDTC1=DTC1
IF(DTC2.LT.SDTC1)SDTC1=DTC2
IF(DTC3.LT.SDTC1)SDTC1=DTC3
IF(DTC4.LT.SDTC1)SDTC1=DTC4
IF(DTC5.LT.SDTC1)SDTC1=DTC5
IF(DTC6.LT.SDTC1)SDTC1=DTC6
IF(DTC7.LT.SDTC1)SDTC1=DTC7
IF(DTC8.LT.SDTC1)SDTC1=DTC8
IF(DTC9.LT.SDTC1)SDTC1=DTC9
IF(DTC11.LT.SDTC1)SDTC1=DTC11
IF(DTC13.LT.SDTC1)SDTC1=DTC13
IF(DTC14.LT.SDTC1)SDTC1=DTC14
IF(DTC21.LT.SDTC1)SDTC1=DTC21
IF(DTC23.LT.SDTC1)SDTC1=DTC23
TS15=TS
IF(TI.LE.TS15) GO TO 1
IF(TI.GT.TS15.AND.DTCTT4.LT.SDTC1)SDTC1=DTCTT4
IF(TTT4.GT.200.) GO TO 1
STOP
END
```

```

SUBROUTINE IIDRA(TRA,TSA,I,TP,DT,II,SDTC,QR,QS,VKKR,VKKS,LRTRI,LS
6TT)
C THIS SUBROUTINE SOLVES THE TRANSIENT TWO DIMENSIONAL RADIAL/
C AXIAL HEAT TRANSFER EQUATION FOR 1 ROTOR & STATOR ASSUMING A WORK
C INPUT DUE TO BRAKE FRICTION UNTIL THE STOP TIME IS REACHED.
DIMENSION TN(8,10), T(8,10), TE(10), CVAL(10)
DIMENSION VALXX(10), VALKR(10), HVAL(10), TP(10), TPN(10)
C INITIAL TEMPERATURE(F)
TO=129.
IF(TI.GT.DT) GO TO 990
C INITIAL TEMPERATURE SET, T IS TEMP(F), TN IS NEW TEMP(F)
DO 1 I=1,8
DO 2 J=1,10
TN(I,J)=TO
T(I,J)=TO
TP(J)=TO
TPN(J)=TO
CONTINUE
CONTINUE
990 CONTINUE
C DENSITY (LBM/CUBIC FOOT)
RHO=100.
C*****IF IPAD = 1, THIS PROGRAM ASSUMES THAT WEAR PADS EXIST &
C USES APPLICABLE EQUATIONS.....IF IPAD=0 NO WEAR PADS ARE ASSUMED
C AND DIFFERENT EQUATIONS ARE SOLVED.
IPAD=C
PT=TOTAL PAD THICKNESS FOR ONE INTERFACE (IN)
PT=.1
PRHO=PAD DENSITY (LBM/CUBIC FT)

```

PRHO=100.
C STOP TIME(SECONDS)
TS=56.
C INITIAL VELOCITY(FT/SEC)
VO=207.
C TEMPERATURE,TE(F), HEAT CAPACITY,CVAL(BTU/LBM-F), X-THERMAL
C CONDUCTIVITY,JALKX(BTU/HR-FT-F), AND R-THERMAL CONDUCTIVITY,
C VALKR(BTU/HR-FT-F)
TE(1)=100.
TE(2)=200.
TE(3)=400.
TE(4)=600.
TE(5)=800.
TE(6)=1000.
TE(7)=1200.
TE(8)=1400.
TF(9)=1600.
TL(10)=1800.
C/JAL(1)=.18
CVAL(2)=.222
CVAL(3)=.275
CVAL(4)=.311
CVAL(5)=.343
CVAL(6)=.37
CVAL(7)=.401
C/JAL(8)=.432
CVAL(9)=.464
CVAL(10)=.495

VALKR(1)=89.9
VALKR(2)=84.5
VALKR(3)=75.1
VALKR(4)=68.5
VALKR(5)=61.2
VALKR(6)=56.
VALKR(7)=51.3
VALKR(8)=47.2
VALKR(9)=43.1
VALKR(10)=38.9
VALKX(1)=21.8
VALKX(2)=20.5
VALKX(3)=18.1
VALKX(4)=16.7
VALKX(5)=15.
VALKX(6)=13.2
VALKX(7)=12.1
VALKX(8)=11.
VALKX(9)=10.6
VALKX(10)=10.
CONVECTIVE/RADIATIVE HEAT TRANSFER COEFFICIENT (BTU/HR-FT-FT-F)

HH=2.
HVAL(1)=HH
HVAL(2)=HH
HVAL(3)=HH
HVAL(4)=HH
HVAL(5)=HH
HVAL(6)=HH
HVAL(7)=HF

C

```
HVAL(8)=HH
HVAL(9)=HH
HVAL(10)=HH
C NDIM=NUMBER OF VALUES OF TE INSERTED INTO PROGRAM
C NDIM=10.
C SIR=STATOR INSIDE RADIUS(IN)
C SIR=3.75
C SCR=STATOR OUTSIDE RADIUS(IN)
C SOR=6.75
C ROR=ROTOR OUTSIDE RADIUS(IN)
C ROR=7.2
C RIR=ROTOR INSIDE RADIUS(IN)
C RIR=4.4
C ST=HALF OF STATOR THICKNESS(IN)
C ST=.37
C RT=HALF OF ROTOR THICKNESS(IN)
C RT=.34
C DXR=RT/2.
C DXS=ST/2.
C DR1=(RIR-SIR)/2.
C DR2=(SOR-RIR)/5.
C DR3=(ROR-SOR)/2.
C LPTRI=DR3/4.
C LSTT=DR1/4.
C DXA=(DXS+DXR)/2.
C RP=ROLLING RADIUS OF THE TIRE(IN)
C RR=16.5
C N=THE NUMBER OF FRICTION PAIRS
```

```

N=8
C   TINF IS AMBIENT TEMPERATURE(F)
    TINF=8C.
C   A=COOLING AREA DURING COOL DOWN(IN-IN)
    A=2.*3.14159*RT*(ROR+RIR)+2.*3.14159*ST*(SOR+SIR)+3.14159*
6   (ROR*ROR-SOR*SOR)+3.14159*(RIR*RIR-SIR*SIR)
C   IF(IPAD.EQ.1)A=A+3.14159*PT*2.*(RIR+SOR)
    V=VOLUME OF ROTOR AND STATOR FOR USE IN COOL DOWN(IN-IN)
    V=3.14159*(KOR*ROR-RIR*RIR)*RT+3.14159*(SOR*SOR-SIR*SIR)*ST
    IF(IFAD.EQ.1)V=V+PT*3.14159*(SOR**2-RIR**2)
    TS15=TS
    IF(TI.LE.TS15) GO TO 888
    CALL INT(TE,CVAL,TRA,C,DC,NDIM)
    CALL INT(TE,HVAL,TRA,H,DH,NDIM)
    TTN4=TRA-.04*DT*(TSA+H*A*3.*(TRA-TINF)/12.)/(8.*RHO*C*V)
    TRA=TTN4
    CALL INT(TE,VALKR,TRA,VKKR,DK,NDIM)
    CALL INT(TE,VALKR,TRA,VKKS,DK,NDIM)
    SDTC=25.*RHO*C*V*8.
    RETURN
C88
C   CONTINUE
    TT=TORQUE (FT-LB)
    IF(TI.LE.1.) TT=(18.*TI/1.5+6.)*70.72
    IF(TI.GT.1. AND.TI.LE.9.) TT=(11.*TI/9.+17.)*70.72
    IF(TI.GT.9.) TT=(-14.*TI/53.+31.)*70.72
    IF(TI.GT.TS)TT=0.
    SDTC=SAVE VALUE FOR DT CRITICAL CALCULATION
    SCIC=1000.
    III=0

```

```
DO 4 I=2,7
DO 5 J=2,9
IF (I.EQ.4.OR.I.EQ.5) GO TO 4
IF (J.LI.4.AND.I.LE.5) GO TO 5
IF (J.GT.7.AND.I.GT.5) GO TO 5
CALL INT(TE,VALKX,T(I,J),VKX,DKX,NDIM)
CALL INT(TE,VALKR,T(I,J),VKR,DKR,NDIM)
IF (I.LI.4) OX=DXR
IF (I.GT.5) OX=OX5
IF (J.FA.2) R=SIR+DR1
IF (J.EQ.3) R=RIR
IF (J.EQ.4) R=RIR+DR2
IF (R.LI.RIR) DR=DR1
IF (R.GE.FIR.AND.R.LT.SOR) DR=DR2
IF (R.GE.SOR) DR=DR3
IF (J.GT.4) R=R+DR
IF (R.GE.RIR.AND.R.LT.SOR) DRP=DR2
IF (R.GE.SOR) DRP=DR3
IF (R.LT.RIR) DRP=DR1
IF (R.LE.RIR) DRM=DR1
IF (R.GT.RIR.AND.R.LE.SOR) DRM=DR2
IF (R.GT.SOR) DRM=DR3
A1=(T(I+1,J)-T(I-1,J))/(2.*DX)
A2=(T(I+1,J)-2.*T(I,J)+T(I-1,J))/(DX*DX)
A3=(T(I,J+1)-T(I,J-1))/(DRP+DRM)
A4=((T(I,J+1)-T(I,J))/DRP)-(T(I,J)-T(I,J-1))/DRM)/((DRP+DRM)*.5)
CALL INT(TE,CVAL,T(I,J),C,DC,NDIM)
DTC1=RHDC*3600./(144.*(2.*VKR/(DRP*DRM)+2.*VKX/(DX*DX)))
```

```

IF (DT(1,LT,SDTC) SDTC=DT(1,
TN(I,J)=T(I,J)+(DT*(144./3600.)/(RHO*C))*((JKR*A4)+(DKR*A3
6*A3)+((VKR*A3)/R)+(VKX*A2)+(DKX*A1*A1))
CONTINUE
CONTINUE
DO 6 J=2,9
TN(8,J)=TN(6,J)
TN(1,J)=TN(3,J)
CONTINUE
CALL INT(TE,VALKX,T(2,3),VKX,DKX,NDIM)
CALL INT(TE,VALKR,T(2,3),VKR,DKR,NDIM)
CALL INT(TE,CJAL,T(2,3),C,DC,NDIM)
CALL INT(TE,HVAL,T(2,3),H,DH,NDIM)
TN(2,3)=T(2,3)+(2.*DT*(144./3600.)/(RHO*DR2*DXR*C
6))*((VKR*DXR)/DR2)*T(2,3)-T(2,3)-((H*DXR)/12.)
6*(T(2,3)-TINF)+VKX*DR2*(T(3,3)-T(2,3))/DXR)
CALL INT(TE,VALKX,T(2,10),VKX,DKX,NDIM)
CALL INT(TE,VALKR,T(2,10),VKR,DKR,NDIM)
CALL INT(TE,CJAL,T(2,10),C,DC,NDIM)
CALL INT(TE,HVAL,T(2,10),H,DH,NDIM)
TN(2,10)=T(2,10)+(2.*DT*(144./3600.)/(RHO*DR3*DXR*C
6))*((VKX*DR3)/DXR)*T(3,10)-T(2,10)-((JKR*DXR)/DR3)*T(2,
610)-T(2,9)-((H*DXR)/12.)*T(2,10)-TINF)
CALL INT(TE,VALKX,T(3,3),VKX,DKX,NDIM)
CALL INT(TE,VALKR,T(3,3),VKR,DKR,NDIM)
CALL INT(TE,CJAL,T(3,3),C,DC,NDIM)
CALL INT(TE,HVAL,T(3,3),H,DH,NDIM)
TN(3,3)=T(3,3)+(DT*(144./3600.)/(RHO*C))*((VKX*(T(4,3)
6-2.*T(3,3)+T(2,3))/(DXR*DXR)+DKX*(T(4,3)-T(2,3))/(2.*DXR))*

```

5 4

6


```

6*2.+2.*DKR*(T(3,4)-T(3,3))/(OR2*DR2)-2.*H*(T(3,3)-TINF)/(12.*
6DR2)
  CALL INT(TE,VALKX,T(3,10),VKX,DKX,NDIM)
  CALL INT(TE,VALKR,T(3,10),VKR,DKR,NDIM)
  CALL INT(TE,CVAL,T(3,10),C,DC,NDIM)
  CALL INT(TE,HVAL,T(3,10),H,DH,NDIM)
  TN(3,10)=T(3,10)+(DT*(144./3600.))/(RHO*C)
  6*((VKX/(DXR*DXR))*T(4,10)-(2.*T(3,10))+T(2,10))+DKX*
  6*((T(4,10)-T(2,10))/(2*DXR))*2)-((2.*VKR)/(DR3**2))*
  6T(3,10)-T(3,9))-QR/(DXR*DR3*2.*3.14159*ROR)
  CALL INT(TE,VALKX,T(4,10),VKX,DKX,NDIM)
  CALL INT(TE,VALKR,T(4,10),VKR,DKR,NDIM)
  CALL INT(TE,CVAL,T(4,10),C,DC,NDIM)
  CALL INT(TE,HVAL,T(4,10),H,DH,NDIM)
  TN(4,10)=T(4,10)+(2.*DT*(144./3600.))/(RHO*DXR*DR3*C
  6))*((-VKX*DR3)/DXR)*(T(4,10)-T(3,10))-((VKR*DXR)/DR3)*T(4
  6,10)-T(4,9))-((H*DR3)/12.)*T(4,10)-TINF)-QR/(4.*3.14159*ROR
  6)
  CALL INT(TE,VALKX,T(5,1),VKX,DKX,NDIM)
  CALL INT(TE,VALKR,T(5,1),VKR,DKR,NDIM)
  CALL INT(TE,CVAL,T(5,1),C,DC,NDIM)
  CALL INT(TE,HVAL,T(5,1),H,DH,NDIM)
  TN(5,1)=T(5,1)+(2.*DT*(144./3600.))/(RHO*DXS*DR1*C)
  6*((VKX*DR1)/DXS)*(T(6,1)-T(5,1))+((VKR*DXS)/DR1)*(T(5,2)-T(
  6,1))-((H*DR1)/12.)*T(5,1)-TINF)-QS/(4.*3.14159*SIR)
  CALL INT(TE,VALKX,T(7,1),VKX,DKX,NDIM)
  CALL INT(TE,VALKR,T(7,1),VKR,DKR,NDIM)
  CALL INT(TE,CVAL,T(7,1),C,DC,NDIM)

```

```

CALL INT(TE,HVAL,T(7,1),H,DH,NDIM)
TN(7,1)=T(7,1)+((2.*DT*(144./3600.))/(RHO*DXS*DR1*C))
6*((-VKX*DR1)/DXS)*T(7,1)-T(6,1)+((VKR*DXS)/DR1)*T(7,2)-T
6(7,1)-QS/(4.*3.14159*SIR))
CALL INT(TE,VALKX,T(7,8),VKX,DKX,NDIM)
CALL INT(TE,VALKR,T(7,8),VKR,DKR,NDIM)
CALL INT(TE,CVAL,T(7,8),C,DC,NDIM)
CALL INT(TE,HVAL,T(7,8),H,DH,NDIM)
TN(7,8)=T(7,8)+((2.*DT*(144./3600.))/(RHO*DXS*DR2*C))
6*((-VKX*DR2)/DXS)*T(7,8)-T(6,8)-V KR*(DXS/DR2)*T(7,8)-T(7
6,7))-((H*(DXS+DR2)/12.)*T(7,8)-TINF)))
CALL INT(TE,VALKX,T(5,2),JKX,DKX,NDIM)
CALL INT(TE,VALKR,T(5,2),VKR,DKR,NDIM)
CALL INT(TE,CVAL,T(5,2),C,DC,NDIM)
CALL INT(TE,HVAL,T(5,2),H,DH,NDIM)
R=SIR+DR1
TN(5,2)=T(5,2)+((DT*(144./3600.))/(RHO*C))*(VKR*((T(
65,3)-2.*T(5,2)+T(5,1))/(DR1**2))+((VKR/(2.*R*DR1))*T(5,3)-
6T(5,1)))+(DKR*((T(5,3)-T(5,1))/(2.*DR1)**2)+((2.*VKX)/(DXS*
6*2))*T(5,2)-T(5,2))+((-2.*H)/(12.*DXS))*T(5,2)-TINF)))
CALL INT(TE,VALKX,T(4,9),VKX,DKX,NDIM)
CALL INT(TE,VALKR,T(4,9),VKR,DKR,NDIM)
CALL INT(TE,CVAL,T(4,9),C,DC,NDIM)
CALL INT(TE,HVAL,T(4,9),H,DH,NDIM)
R=SOR+DR3
TN(4,9)=T(4,9)+((DT*(144./3600.))/(RHO*C))*((VKR/DR3
6*DR3))*T(4,10)-2.*T(4,9)+T(4,8))+((VKR/(2.*R*DR3))*T(4,10)
6-T(4,8)))+(DKR*((T(4,10)-T(4,8))/(2.*DR3)**2))-((2.*VKX)/
6(DXR*DXR))*T(4,9)-T(3,9))-((2.*H)/(12.*DXR))*T(4,9)-TINF

```

```

6)))
CALL INT(TE, VALKX, T(6,1), VKX, DKX, NDIM)
CALL INT(TE, VALKR, T(6,1), VKR, DKR, NDIM)
CALL INT(TE, CVAL, T(6,1), C, DC, NDIM)
CALL INT(TE, HVAL, T(6,1), H, DH, NDIM)
TN(5,1)=T(5,1)+((DT*(144./3600.))/(RHO*C))*(((VKX)/(DXS
6*DXS))*(T(7,1)-2.*T(6,1)+T(5,1))+DKX*((T(7,1)-T(5,1))/(2.
6*DXS))*(2.*VKR)/(DR1**2))*(T(6,2)-T(6,1))-QS/(2.*3.14
6159*SIR*DXS*DR1))
CALL INT(TE, VALKX, T(6,8), VKX, DKX, NDIM)
CALL INT(TE, VALKR, T(6,8), VKR, DKR, NDIM)
CALL INT(TE, CVAL, T(6,8), C, DC, NDIM)
CALL INT(TE, HVAL, T(6,8), H, DH, NDIM)
TN(6,8)=T(6,8)+((DT*(144./3600.))/(RHO*C))*(((VKX)/(D
6XS*DXS))*(T(7,8)-2.*T(6,8)+T(5,8))+DKX*((T(7,8)-T(5,8))/(
62.*DXS))*(2.*VKR)/(DR2*DR2))*(T(6,8)-T(6,7))-(((2.*H
5)/DR2))*((T(6,8)-TINF)/12.))
DO 3 J=4,7
R=RIR+DR2*(J-3)
T3=(T(6,J)-T(5,J))/DXS
T4=(T(4,J+1)-2.*T(4,J)+T(4,J-1))/(DR2*DR2)
T5=(T(4,J+1)-T(4,J-1))/(2.*DR2)
T6=(T(4,J)-T(3,J))/DXR
CALL INT(TE, CVAL, T(4,J), C4, DC4, NDIM)
CALL INT(TE, VALKR, T(4,J), VKR4J, DKR4J, NDIM)
CALL INT(TE, VALKX, T(4,J), VKX4J, OKX4J, NDIM)
W=TT*VC*(1.-TI/TS)*666.1/(3.14159*N*RR*(SOR**2-RIR**2))
TN(4,J)=T(4,J)+(2.*DT*(144./3600.))/(RHO*(DXR+DXS)*C4))*((-VKX4J*T6

```

```

6+VKX4J*T3+(DXR+DXS)*(VKR4J*T4+DKR4J*T5+VKR4J*T5/R)*.5+W)
TN(5,J)=TN(4,J)
IF(IPAD.NE.1) GO TO 300
T1=(T(5,J+1)-2.*T(5,J)+T(5,J-1))/DR2**2
T2=(T(5,J+1)-T(5,J-1))/(2.*DK2)
T3=(T(6,J)-T(5,J))/DXS
CALL INT(TE,CVAL,T(5,J),C5,DC5,NDIM)
CALL INT(TE,VALKR,T(5,J),VKR5J,OKR5J,NDIM)
CALL INT(TE,VALKX,T(5,J),VKX5J,OKX5J,NDIM)
CALL INT(TE,VALKX,TP(J),PK,DK,NDIM)
PK=.426*PK
PC=.12
RE=.005
TPN(J)=TP(J)+(.04*DT/(PRHO*PC))*(PT*(PK*(TP(J+1)-2.*TP(
5J)+TP(J-1))/DR2**2+DK*(TP(J+1)-TP(J-1))/(2.*DR2))**2+PK*(TP(J+1)
6-TP(J-1))/(2.*R*DR2))- (2.*TP(J)-T(5,J)-T(4,J))/(RE*12.)+W)
TN(4,J)=T(4,J)+(DT*.04*2./(RHO*DXR*C4))*(DXR/2.)*(VKR4J*T4+DKR4J
6*T5**2+VKR4J*T5/R)-VKX4J*T6+(TP(J)-T(4,J))/(RE*12.)
TN(5,J)=T(5,J)+(DT*.04*2./(RHO*DXS*C5))*(DXS/2.)*(VKR5J*T1+OKR5J*
6T2**2+VKR5J*T2/R)+VKX5J*T3+(TP(J)-T(5,J))/(RE*12.)
CONTINUE
CONTINUE
T7=(T(4,8)-T(4,7))/DR2
T8=(T(4,9)-T(4,8))/DR3
T9=(T(4,8)-T(3,8))/DXR
T10=(T(6,8)-T(5,8))/DXS
T12=(T(5,3)-T(5,2))/DR1
T14=(T(6,3)-T(5,3))/DXS
T15=(T(4,3)-T(3,3))/DXR

```

39C
8

```
T16=(T(4,4)-T(4,3))/DR2
CALL INT(TE,CVAL,T(4,8),C+8,DC48,NDIM)
CALL INT(TE,CVAL,T(4,3),C+3,DC43,NDIM)
CALL INT(TE,VALKX,T(4,8),VKX+8,DKX48,NDIM)
CALL INT(TE,JALKX,T(4,3),JKX43,DKX43,NDIM)
CALL INT(TE,VALKR,T(4,8),VKR48,DKR48,NDIM)
CALL INT(TE,VALKR,T(4,3),VKR43,DKR43,NDIM)
W=W*DR2/2.
CALL INT(TE,HVAL,T(4,8),H4,DH,NDIM)
TN(4,8)=T(4,8)+(4.*DT*(14./3600.)/(RHO*(DR2+DR3)+DR2*DXS)*C
648)*(-VKX48*T9*(DR2+DR3)/2.+VKX48*T10*DR2/2.-VKR48*(DXR+DXS)*
6T7/2.+JKR48*DXR*T8/2.-H4*(DR3+DXS)*(T(4,8)-TINF)/2.+W)
TN(5,8)=TN(4,8)
CALL INT(TE,HVAL,T(4,3),H,DH,NDIM)
TN(4,3)=T(4,3)+(4.*DT*(14./3600.)/(RHO*(DR2+DXR+DXS*(DR1+DR2))*C
643)*(-VKX43*T15*DR2/2.+VKX43*(DR2+DR1)*T14/2.-VKR43*DXS*T12/2.
6+VKR43*(DXS+DXR)*T16/2.-H*(DXR+DR1)*(T(4,3)-TINF)/2.+W)
TN(5,3)=TN(4,3)
IF(IPAD.NE.1) GO TO 301
CALL INT(TE,VALKX,T(5,3),VKX53,DKX53,NDIM)
CALL INT(TE,VALKR,T(5,3),VKR53,DKR53,NDIM)
CALL INT(TE,CVAL,T(5,3),C+3,DC53,NDIM)
CALL INT(TE,VALKX,T(5,8),VKX58,DKX58,NDIM)
CALL INT(TE,VALKR,T(5,8),VKR58,DKR58,NDIM)
CALL INT(TE,CVAL,T(5,8),C+8,DC58,NDIM)
CALL INT(TE,JALKX,TP(3),PK,DK,NDIM)
PK3=.426*PK
PC3=.12
```

```
CALL INT(TE,VALKX,TP(8),PK,DK,NDIM)
PK8=.426*PK
PC8=.12
RE3=.005
RF8=.005
CALL INT(TE,HVAL,T(4,3),H,DH,NDIM)
TN(4,3)=T(4,3)+(4.*.04*DT/(RHO*C43*DXR*DR2))*(VKR43*DXR*T16/2.-VKX
643*DR2*T15/2.-H*DXR*(T(4,3)-TINF)/(2.*12.)+DR2*(TP(3)-T(4,3)))/
6(2.*RE3*12.)
CALL INT(TE,HVAL,T(5,3),H,DH,NDIM)
TN(5,3)=T(5,3)+(.04*4.*DT/(RHO*C53*DXS*(DR1+DR2)))*(VKR53*DXS*(T(5
6,1)-T(5,3))/(2.*DR2)-VKR53*DXS*(T(5,3)-T(5,2))/(2.*DR1)+VKX53
6*(DR2+DR1)*T(6,3)-T(5,3))/(2.*DXS)+
6DR2*(TP(3)-T(5,3))/(2.*RE3*12.)-H*DR1*(T(5,3)-TINF)/(2.*12.)
TN(4,8)=T(4,8)+(DT*.04*4./(RHO*C43*DXR*(DR2+DR3)))*(-JKX+8*T9*(
6DR2+DR3)/2.-VKR48*DXR*T7/2.+VKR48*DXR*T8/2.-H+*DR3*(T(4,8)-TINF
6)/(2.*12.)+DR2*(TP(8)-T(4,8)))/(2.*RE8*12.)
CALL INT(TE,HVAL,T(5,8),H,DH,NDIM)
TN(5,8)=T(5,8)+(4.*DT*(RHO*C58*DXS*DR2))*(-VKR58*DXS*(T(5,8)-T
```

```
6(5,7))/(2.*DR2)+VKX58*DR2*(T(6,8)-T(5,8))/(2.*DXS)-H*DXS*(T(5,8)
6-TINF)/(2.*12.)+DR2*(TP(8)-T(5,8))/(2.*RE8*12.)
W=55E.1*TT*70*(1.-II/TS)/(RR*N*3.14159*PT*(SOR**2-RIR**2))
CALL INT(TE,HVAL,TP(3),H,OH,NDIM)
TPN(3)=TP(3)+(DT*.04/(PRHD*PC3))*(2.*PK3*(TP(4)-TP(3)
6)/DR2**2-(2.*TP(3)-T(5,3)-T(4,3))/(PT*RE3*12.)-2.*H*(TP(3)-TINF
6)/(DR2*12.)+W)
CALL INT(TE,HVAL,TP(8),H,OH,NDIM)
TPN(8)=TP(8)+(DT*.04/(PRHD*PC8))*(-2.*PK8*(TP(8)-TP(7))
6/DR2**2-2.*H*(TP(8)-TINF)/(DR2*12.)-(2.*TP(8)-T(4,8)-T(5,8))/(
6RE8*PT*12.)+W)
301 CONTINUE
TRA=(T(2,10)+T(3,10)+T(4,10))/3.
TSA=(T(5,1)+T(6,1)+T(7,1))/3.
CALL INT(TE,VALKR,TRA,VKKR,DK,NDIM)
CALL INT(TE,VALKR,TSA,VKKS,DK,NDIM)
00 11 I=1,8
00 12 J=1,10
TP(J)=TPN(J)
7(I,J)=TN(I,J)
12 CONTINUE
11 RETURN
END
```

```

SUBROUTINE INT(TE,CVAL,T,C,DC,NDIM)
DIMENSION TE(10),CVAL(10)
THE NEXT 10 STATEMENTS ASSIGN ENDPOINT C,DC, VALUES FOR TE
OUTSIDE OF CURVE ENDPOINTS
IF(T.LE.TE(NDIM)) GO TO 5
C=CVAL(NDIM)
DC=(CVAL(NDIM)-CVAL(NDIM-1))/(TE(NDIM-1))
RETURN
CONTINUE
IF(T.GE.TE(1)) GO TO 6
C=CVAL(1)
DC=(CVAL(2)-CVAL(1))/(TE(2)-TE(1))
RETURN
CONTINUE
DO 1 I=1,NDIM
IF(T.NE.TE(I)) GO TO 2
C=CVAL(I)
IF(I.EQ.10) DC=(CVAL(NDIM)-CVAL(NDIM-1))/(TE(NDIM)-TE(NDIM-1))
IF(I.EQ.10) GO TO 4
DC=(CVAL(I+1)-CVAL(I))/(TE(I+1)-TE(I))
CONTINUE
RETURN
CONTINUE
CONTINUE
IF(T.LE.TE(I).OR.T.GE.TE(I+1)) GO TO 3
DC=(CVAL(I+1)-CVAL(I))/(TE(I+1)-TE(I))
C=CVAL(I)+(CVAL(I+1)-CVAL(I))*(T-TE(I))/(TE(I+1)-TE(I))
RETURN
CONTINUE
CONTINUE
CONTINUE
RETURN
END
```